

U N I V E R S I T Y   O F   S T U T T G A R T

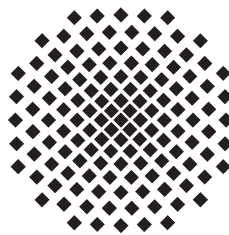
Institute for Theoretical Physics III

Master thesis

**Phase transitions and topological phases  
by driven dissipation**

Nicolai Lang

October 14, 2013



Supervised by  
Prof. Dr. H. P. Büchler

Secondary Corrector  
Prof. Dr. U. Seifert



### **Statutory Declaration**

I herewith formally declare that I have written the submitted thesis independently. I did not use any outside support except for the quoted literature and other sources mentioned in the paper.

I clearly marked and separately listed all of the literature and all of the other sources which I employed when producing this academic work, either literally or in content.

Stuttgart, October 14, 2013

Nicolai Lang



# Abstract

One of the most fascinating phenomena in nature surely is the emergence of long range order in initially disordered systems caused by simple *local* interactions. Transitions between such qualitatively distinct *phases* are often accompanied by sharp changes in particular quantities of the system when specific parameters are varied. Such collective phenomena that can be triggered by small changes of the system's configuration are usually referred to as *phase transitions*.

Whereas statistical physics accounts for the latter in the general framework of classical mechanics, there has also been intense interest in the emergence of phase transitions in *quantum mechanical systems*. There the critical fluctuations that are responsible for the appearance of collective order can be caused by *quantum fluctuations* only — at zero temperature! In this context one speaks of *quantum phases* and *quantum phase transitions*.

In recent years it was realised by the scientific community that there are quantum phases that elude a characterisation by *local* properties. There the order is “hidden” in more intricate structures that are features of the incredible complexity that characterises various sectors of the system Hilbert spaces. Such systems are referred to as *topologically ordered*.

Another aspect of topology that has found broad acceptance in condensed matter physics is concerned with systems that exhibit a remarkable resilience about local disorder. Their ground states feature *long range entanglement* and their Hamiltonians are characterised by *topological invariants* that account for the aforementioned stability. This outlines the field of *topological phases* which has been (and is still) a vivid area of research.

A few years ago it was realised that both — topologically ordered systems and topological phases — may be applicable to the great quest of quantum engineering, namely the search for scalable and stable *quantum memories* that prevent coherent states from decoherence. The emergence of *topological quantum memories* bridged the domains of quantum information theory and condensed matter physics.

All these concepts are usually treated as part of the *Hamiltonian framework* of *closed* quantum systems. Originally promoted by the quantum optics community, the mathematical description and physical investigation of *open* quantum systems has seen considerable progress in the last decades. Only lately physicists started to think about combining features of dissipatively driven systems and topology related properties [1].

This thesis is concerned with *various* topics, all of which relate to the outlined subject matters above. The major structure is two-part: In the first and most comprehensive part, constituted by Chapter 2 and 3, we deal with quantum phases and their dissipative counterparts. In particular, we construct dissipative versions of the paradigmatic *transverse field Ising model* and a more sophisticated instance, the  $\mathbb{Z}_2$ -*Gauge-Higgs model* [2] which is related to topological order.

In the additional second part, namely Chapter 4 and 5, we deal once more with the dissipative counterpart of a well-known Hamiltonian theory: the *Majorana chain* [3] which is a paradigmatic example for a topological phase. We discuss and criticise recent results [1] regarding the dissipative realisation of the Majorana chain and subsequently investigate a possible *dissipatively driven, self-correcting quantum memory*. We conclude that the straightforward dissipative implementation of the Majorana chain does *not* yield a self-stabilising quantum memory.



# Zusammenfassung

Eines der faszinierendsten Phänomene in der Natur ist sicher das Auftreten von langreichweitiger Ordnung in vormals ungeordneten Systemen auf Grund einfacher *lokaler* Wechselwirkungen. Diese Übergänge zwischen qualitativ unterschiedlichen *Phasen* werden oft von deutlichen Änderungen bestimmter Größen begleitet. Solche kollektiven Phänomene, die durch kleine Veränderungen der Systemparameter ausgelöst werden können, werden als *Phasenübergänge* bezeichnet.

Die statistische Physik befasst sich mit solchen Übergängen im Rahmen der klassischen Mechanik. Es ist aber auch äußerst interessant das Auftreten von Phasenübergängen in *quantenmechanischen Systemen* zu betrachten. Am absoluten Nullpunkt werden die für den Übergang zur kollektiven Ordnung charakteristischen kritischen Fluktuationen ausschließlich durch *Quantenfluktuationen* hervorgerufen. Solche Systeme werden durch *Quantenphasen* und *Quantenphasenübergänge* charakterisiert.

In den letzten Jahren hat man erkannt, dass die Theorie Quantenphasen erlaubt, die sich der Identifikation durch *lokale* Eigenschaften entziehen. In solchen Phasen ist die vorhandene Ordnung in komplizierteren Strukturen der Zustände "versteckt". Die dafür nötige Komplexität der Zustände wird von den oft unanschaulichen Eigenschaften des Hilbertraums ermöglicht, der das System beschreibt. Solche Systeme bezeichnet man als *topologisch geordnet*.

Eine andere Anwendung der Topologie, die im Bereich der kondensierten Materie mit Begeisterung begrüßt wurde, betrifft Systeme die eine erstaunliche Robustheit gegen lokale Unordnung aufweisen. Deren Grundzustände sind durch *langreichweitige Verschränkungen* charakterisiert und ihre Beschreibung mittels Hamiltonoperatoren erlaubt die Definition *topologischer Invarianten* die wiederum eine Erklärung für die genannte Stabilität liefern. Solche Systeme werden weithin als *topologische Phasen* bezeichnet und sind bis zum heutigen Tag ein Feld intensiver Forschung.

Vor einigen Jahren hat man erkannt, dass beide Konzepte — topologisch geordnete Systeme und topologische Phasen — auf eines der drängendsten Probleme von Quantencomputern angewandt werden können: Skalierbare und stabile *Quantenspeicher* sollen die zur Dekohärenz neigende Quanteninformation schützen, konnten aber bis heute nicht im benötigten Umfang realisiert werden. Der neue Ansatz *topologischer Quantenspeicher* verspricht mögliche Lösungen dieses Problems und schlägt eine Brücke zwischen Physik der kondensierten Materie und Quanteninformationstheorie.

Alle zuvor angerissenen Konzepte werden normalerweise im Rahmen *abgeschlossener* Quantensysteme behandelt, deren Dynamik üblicherweise durch Hamiltonoperatoren beschrieben wird. Das ursprünglich von der Quantenoptik vorangetriebene Feld *offener* Quantensysteme hat in den letzten Jahrzehnten große Fortschritte erfahren, sowohl im Rahmen der mathematischen Beschreibung als auch im Hinblick auf die zugrunde liegende Physik. Es ist allerdings noch nicht allzu lange her, dass versucht wurde die Möglichkeiten dissipativer Systeme mit den oben erwähnten, faszinierenden topologischen Eigenschaften zu kombinieren [1].

Diese Masterarbeit behandelt *verschiedene* Themen, die alle im ein oder anderen Zusammenhang mit den oben erläuterten Konzepten stehen. Sie besteht aus zwei Teilen: Im ersten und größten Abschnitt, der von den Kapiteln 2 und 3 gebildet wird, befassen wir uns mit Quantenphasen und ihren dissipativen Gegenstücken. Dort konstruieren wir eine dissipative Version des paradigmatischen Ising-Modells mit transversalem Magnetfeld. Als Beispiel für eine weitaus komplexere Theorie übersetzen wir die  $\mathbb{Z}_2$ -Gittereichtheorie mit gekoppeltem Higgs-Feld [2] in ihr dissipatives Analogon. Letztere steht im Zusammenhang mit topologisch geordneten Systemen.

Im zusätzlichen, zweiten Teil dieser Arbeit, d.h. in Kapitel 4 und 5, untersuchen wir ein weiteres dissipatives Gegenstück zu einem bekannten Modell: Kitaevs *Majorana Kette* [3], die man als Paradebeispiel einer topologischen Phase betrachten kann. Wir diskutieren und üben Kritik an neueren Resultaten [1] die auf eine dissipative Realisierung der Majorana Kette abzielen. Anschließend untersuchen wir einen möglichen *dissipativen, selbst korrigierenden Quantenspeicher* und kommen zu dem Schluss, dass die direkte dissipative Implementierung der Majorana Kette *nicht* als selbst korrigierender Quantenspeicher genutzt werden kann.



# Contents

<b>Abstract</b>	<b>5</b>
<b>Zusammenfassung</b>	<b>7</b>
<b>Contents</b>	<b>9</b>
<b>Preface</b>	<b>13</b>
<b>Acknowledgements</b>	<b>17</b>
<b>1 Theoretical basics</b>	<b>19</b>
1.1 A short note on the mathematical framework . . . . .	20
1.1.1 Quantum states and their transformations . . . . .	20
1.1.2 Open quantum systems: The Lindblad equation . . . . .	22
1.1.3 The quantum trajectory approach to Markovian dynamics . . . . .	23
1.2 Quantum phases and phase transitions . . . . .	34
1.2.1 Quantum phases in Hamiltonian systems . . . . .	34
1.2.2 Quantum phases in dissipatively driven systems . . . . .	35
1.3 Topological quantum error correction . . . . .	36
1.3.1 Quantum error correction codes . . . . .	36
1.3.2 Self-correcting and topological quantum memories . . . . .	37
1.3.3 The Toric Code model . . . . .	37
1.3.4 The Majorana chain . . . . .	41
1.4 Lattice gauge theories and Higgs fields . . . . .	69
1.4.1 The $\mathbb{Z}_2$ -Ising gauge theory . . . . .	69
1.4.2 The $\mathbb{Z}_2$ -Gauge-Higgs model . . . . .	75
1.5 The overall picture . . . . .	83
<b>2 Spontaneous symmetry breaking by dissipation</b>	<b>85</b>
2.1 The Setting . . . . .	86
2.2 Symmetry considerations . . . . .	89
2.2.1 General definitions . . . . .	89
2.2.2 Symmetries of the TIM master equation . . . . .	90
2.3 A mean field approach . . . . .	94
2.3.1 Derivation of the mean field Lindblad superoperator . . . . .	94
2.3.2 Static solutions . . . . .	99

2.3.3	Dynamic evolution . . . . .	122
2.4	Comparing the mean field theories of $\mathcal{L}^{\text{mf}}$ , $H^{\text{mf}}$ and $H_p^{\text{mf}}$ . . . . .	146
2.4.1	Mean field results & Short summary . . . . .	146
2.4.2	Comparison of phase transitions . . . . .	153
2.5	Exact solutions of a minimal instance . . . . .	156
2.5.1	The system in superoperator language . . . . .	156
2.5.2	Solutions for steady states . . . . .	157
2.5.3	Relaxation to steady states . . . . .	165
2.6	Quantum trajectory Monte Carlo simulation . . . . .	168
2.6.1	Technical remarks . . . . .	168
2.6.2	Comparison with exact evolution: A consistency check . . . . .	170
2.6.3	Dissipative transverse field Ising model in one and two dimension(s) . . . . .	176
<b>3</b>	<b>A dissipative <math>\mathbb{Z}_2</math>-Gauge-Higgs model</b> . . . . .	<b>187</b>
3.1	Mean field theory for the unitary theory . . . . .	188
3.1.1	Two mean fields and unphysical degrees of freedom . . . . .	188
3.1.2	A single mean field in unitary gauge . . . . .	190
3.2	The Setting . . . . .	193
3.2.1	Dissipative interpretation of a unitary theory . . . . .	193
3.2.2	Steady states . . . . .	195
3.3	A short mean field analysis . . . . .	203
3.3.1	Derivation of the mean field Lindblad superoperator . . . . .	203
3.3.2	Static solutions . . . . .	208
<b>4</b>	<b>The dissipative Majorana chain</b> . . . . .	<b>217</b>
4.1	The Setting . . . . .	218
4.2	Steady states of the number conserving jump operators . . . . .	219
4.2.1	Notation and some preliminary notes . . . . .	219
4.2.2	Dark states . . . . .	225
4.2.3	Steady states . . . . .	227
4.2.4	A parent Hamiltonian for the dark states . . . . .	236
4.3	A mean field theory for late times . . . . .	239
4.3.1	Derivation of the mean field theory . . . . .	239
4.3.2	Some properties of the quadratic mean field theory . . . . .	246
4.4	Topology as local indistinguishability . . . . .	251
4.5	Some concluding remarks . . . . .	257
<b>5</b>	<b>Dissipatively driven topological quantum error correction</b> . . . . .	<b>259</b>
5.1	Algorithmic error correction and locality . . . . .	260
5.1.1	Classical error correction: An abstract point of view . . . . .	260
5.1.2	Classical local error correction . . . . .	261
5.1.3	Local quantum error correction . . . . .	264
5.2	Error correction and the dissipative Majorana chain . . . . .	265
5.2.1	A naïve approach: Dissipative dynamics with parity violation . . . . .	265
5.2.2	A second approach: Dissipative dynamics with parity conservation . . . . .	266
5.2.3	QTMC simulation . . . . .	272
5.3	Some asides: QCA and localisation of observables . . . . .	277

5.3.1	A physically motivated definition of quantum cellular automata . . . . .	277
5.3.2	An new concept: Localisable observables . . . . .	280
<b>Conclusion</b>		<b>283</b>
<b>A Non-equilibrium steady states in mean field approximation</b>		<b>285</b>
<b>B Dissipative TIM: Mean field jump operators</b>		<b>293</b>
<b>C QTMC simulation: Implementation</b>		<b>301</b>
<b>D Auxiliary calculations</b>		<b>305</b>
<b>E Some Asides: Locality in lattice systems</b>		<b>307</b>
E.1	Templates and instances . . . . .	307
E.2	Realisability and locality . . . . .	310
E.2.1	Spatial structures . . . . .	310
E.2.2	An application: Local quantum circuits and quantum complexity theory .	323
<b>List of Figures</b>		<b>326</b>
<b>Bibliography</b>		<b>330</b>
<b>Corrigenda</b>		<b>341</b>



# Preface

This is a work on physics; on theoretical physics, to be precise. But there are other realms of expertise within the vast field of modern physics which are of equal significance, both, in a practical and a philosophical perception.

Until quite recently the footing of physics was twofold: Knowledge about nature entered the stage by experiments, intricate instruments and ingenious setups opened windows to the smallest and largest structures of our world. This knowledge was condensed by theoreticians into creations of mathematical beauty, formulas and calculi describing all facets of nature without the misleading connotations of natural languages. Once in a while theories called for effects which have never been observed or been expected before; and if they proved real, one could not avoid the impression that *truth* has been found: It is not remarkable that one could fit a smooth curve through any given number of points, but it is truly intriguing when all future points fall onto the very same curve.

This circle of experiment, condensation and prediction lies at the very heart of physics (and any other natural science) for it is the origin of scientific insight. While theories where simple, condensation and prediction where both subsumed under the term *theoretical physics*. However, it is much simpler to contrive an elegant theory than expanding it into concrete predictions which are, evidently, crucial for scientific verification. Consequently, called forth by the proliferating complexity of theoretical constructs, a new pillar of physics emerged to bridge the imminent chasm ripping apart theory and experiment: Computational physics.

The advent of computers changed the way physicists work fundamentally – how they deal with theories and their implications: On the one hand, powerful computers allow for predictions based on highly complex theories which could have never been derived by hand. On the other hand, simulating theories on a chip is much less demanding than doing experiments in the lab. Hence one is tempted to supersede the hard and often unrewarding work in the lab by *computer experiments*.

It is crucial to be fully aware of the epistemological implications, for computer experiments do not probe nature but *theories*. In a nutshell, there is one and only one way to gain *knowledge* of our world: By doing experiments. And there is just one way to gain *insight* into our world: By contriving theories.

This is *the big picture* I want the reader to be aware of; especially in the context of this purely theoretical and computational piece of work. There are a few other aspects which I deem important in general and which give direction to the contentual structure and layout of this thesis.

There are two prevalent reasons for writing scientific literature: The first is *documentation*. This aspect is based upon the requirement of verifiability. Good documentation demands for detailed explanations, calculations and results. At this point I want to stress that there is *no justification whatsoever* for omitting details in documentations of scientific endeavours – except one intends to conceal inconsistencies deliberately or prevent fellow scientists to catch up and raise inconvenient questions.

The second reason is *didactics*. Unfortunately a great number of scientific papers (at least in the physics community) seem to propagate a notion of “didactics-free science” where *explaining* the physics and gauging its relevance with respect to *the big picture* is considered beneath the scientists dignity. But explaining physics is *not* a mere side issue – it is the *crux* of the scientific endeavour in its entirety. Failing in teaching physics means failing in doing physics, for there is no sense in the gain of knowledge and insight if it cannot be passed on.

Nicolai Lang  
Stuttgart, October 2013







# Acknowledgements

As stated in the statutory declaration, this thesis has been written by a single author, that is, by *me*. Science, however, is not a solitary endeavour and there are always people who contributed indirectly one way or another. This prominent page is dedicated to these silent contributors — the remaining 340 pages deal with physics and physics only.

Above all I would like to express my gratitude to my supervisor Prof. Hans Peter Büchler who kept me busy for a whole year. He provided the seeds for this work and served as a guide whenever my physical intuition faltered. I am especially thankful that he didn't held me back when I once again wandered from one topic to another following the trail of exciting thoughts. I would also like to thank my secondary corrector, Prof. Udo Seifert, for two stimulating discussions about my projects and results. Explaining the very own lines of thought to a questioning opponent is especially useful to shed light on the crucial points of an argument.

I would also like to acknowledge the hospitality of Prof. P. Zoller and his group at the IQOQI at the University of Innsbruck where three days of interesting and intense discussions on various topics broadened my horizons.

Thanks are also due to my office roommate David Peter for interesting discussions on the mathematics of Lindblad dynamics, gauge theories and other stuff more or less related to physics; there are still some riddles I put aside that wait for a solution.

In addition I would like to acknowledge financial support by the German National Academic Foundation (Studienstiftung des deutschen Volkes e.V.) due to which my personal library of textbooks grew considerably.

There is more to a master thesis than the science it is concerned with. For instance the everyday financial and non-material support by one's family. In that regard I would particularly like to thank my mother Karin, my father Manfred and my brother Robin who is just following me on my path to a better understanding of this world.

Nicolai Lang  
*Stuttgart, October 2013*



# Theoretical basics

*“Ordinary language is totally unsuited for expressing what physics really asserts, since the words of everyday life are not sufficiently abstract. Only mathematics and mathematical logic can say as little as the physicist means to say.”*

Bertrand Russell

This is a work on *theoretical* physics. As such there is a considerable amount of mathematics involved. This preliminary section is *not* dedicated to this mathematical framework of physics, though there are some remarks in this regard. To make use of the discussions and calculations that are described in the following, the reader is assumed to be familiar with the fundamental concepts of analysis, linear algebra and abstract algebra as well as notions from condensed matter physics and quantum information theory.

I tried hard to explain my findings and concepts as comprehensibly as possible, with enough details to provide eager readers with the tools for recalculations. To set the scene for these explanations, this preliminary chapter is mainly focused on two models and their analysis, namely the Majorana chain and the  $\mathbb{Z}_2$ -Gauge-Higgs model. I want to stress that these discussions are a bit more than mere outlines of well-known facts: They represent my own learning progress at the beginning of my master studies and are based on the results I computed during this period. The main purpose is to convey the knowledge I accumulated in a condensed form, in the hope that it might be useful for one or two who seek for understanding of this special subject.

This preliminary chapter is structured as follows. In Section 1.1 we start with some remarks on the mathematical framework of quantum physics and open quantum systems. In particular, we introduce the Lindblad equation and its interpretation in terms of quantum trajectories in Subsection 1.1.2 and illustrate the latter by means of a simple example. In Section 1.2 we review shortly the field of quantum phases and phase transitions with asides on non-equilibrium phase transitions. In Section 1.3 follows a brief review of quantum error correction. We use this as an opportunity to give a detailed analysis of the *Majorana chain*, both as a topological quantum phase and as a quantum memory. In Section 1.4 follows a detailed discussion of the  *$\mathbb{Z}_2$ -Gauge-Higgs model*, the second pivotal theory of this thesis. We conclude this chapter in Section 1.5 with an outline of the various relations between the aforementioned models to provide an *overall picture*.

## 1.1 A short note on the mathematical framework

Let us start this chapter with some brief remarks on the mathematical framework of quantum theory. First we address the description of quantum states and their transformations. Subsequently we introduce the Lindblad master equation as an effective description of open quantum systems with Markovian coupling to the environment. Since the Lindbladian evolution of quantum systems is applied throughout this thesis, we provide a detailed discussion of a simple example to illustrate the time evolution and the quantum trajectory interpretation.

### 1.1.1 Quantum states and their transformations

Here we outline the mathematical framework of quantum theory to smooth the way for Lindbladian superoperators or the like. Quantum mechanical systems in *pure* quantum states are described by a system Hilbert space  $\mathcal{H}$ . For the spin- $\frac{1}{2}$  systems that we consider in Chapter 2 and 3 this is just the tensor product  $\mathcal{H} = \bigotimes_{i=1}^N \mathbb{C}_i^2$  for  $N$  spins with (complex) dimension  $2^N$ . For the fermionic systems in Chapter 4 and 5 this is an *antisymmetric* Fock space  $F_N^{(a)}$  which can be thought of as a direct sum of antisymmetrised tensor products of single particle Hilbert spaces. In the framework of second quantisation, this definition is usually omitted in favour of a direct introduction as the abstract Hilbert space spanned by the fermionic number states  $|n_1, \dots, n_L\rangle$  where  $L$  denotes the number of fermionic sites in the system.

Physical operations and quantities are then described by bounded operators<sup>1</sup>  $\mathcal{B}(\mathcal{H})$  on the Hilbert space. The latter forms a non-abelian operator algebra via composition and addition of the linear operators. For finite systems we may always think of complex matrices (provided the basis is evident).

Physical *observables* are required to yield real expectation values and therefore identified with *self-adjoint* or *Hermitian* operators  $\mathcal{O}(\mathcal{H}) = \{A \in \mathcal{B}(\mathcal{H}) \mid A^\dagger = A\}$ . The expectation value of an observable  $A$  in a state describe by the state vector  $|\Psi\rangle \in \mathcal{H}$  is then given by  $\langle A \rangle = \langle \Psi \mid A \mid \Psi \rangle$  where the Bra-Ket notation  $\langle \bullet \mid \bullet \rangle = \langle \bullet | \bullet \rangle$  is motivated by the RIESZ representation theorem. Let us stress that  $\mathcal{O}(\mathcal{H})$  is *not* an algebra with respect to composition of operators since  $(AB)^\dagger = BA \neq AB$  in general (it becomes an algebra if one chooses the anticommutator  $\{\bullet, \bullet\}$  as product, though).

The above framework (observables as operators, states as vectors of a Hilbert space) is not the most general one as it not suited to describe *ensembles* of quantum states, that is *mixed* quantum states. To this end it is enlightening to consider the expectation value  $\langle A \rangle = \langle \Psi \mid A \mid \Psi \rangle$  as a *linear functional* on the observable space  $\mathcal{O}(\mathcal{H})$ . This can be achieved by the introduction of the (pure) *density matrix*  $\rho_\Psi \equiv |\Psi\rangle \langle \Psi|$  (which is a bounded, Hermitian trace class operator with trace one) and defining a *state*  $\hat{\rho}_\Psi$  as

$$\hat{\rho}_\Psi : \mathcal{O}(\mathcal{H}) \rightarrow \mathbb{R}, \quad A \mapsto \hat{\rho}_\Psi[A] := \text{Tr}[\rho_\Psi A] = \langle \Psi \mid A \mid \Psi \rangle. \quad (1.1)$$

In this perception a quantum state is represented by a *positive linear functional with norm one*, that is  $\hat{\rho}_\Psi[\mathbb{1}] = 1$  which corresponds to the statement that the density matrix  $\rho_\Psi$  itself has *trace* one and is positive-semidefinite. The benefit from this algebraic and more general point of view is that it accounts for a more general class of *states* than the above mentioned pure states. Since

<sup>1</sup>As we consider only finite dimensional spin-systems and fermionic theories in this thesis, it is reasonable to restrict this discussion to *bounded* operators.

the only requirements for a density matrix  $\rho$  (which defines a *state*  $\hat{\rho}$  via  $\hat{\rho}[\bullet] = \text{Tr}[\rho\bullet]$ ) are (1) (semi)positivity, (2) Hermiticity and (3) the normalisation constraint  $\text{Tr}[\rho] = 1$ , there is a (non-unique) orthonormal basis  $\{|n\rangle\}$  so that the spectral decomposition of the density matrix reads

$$\rho = \sum_n p_n |n\rangle \langle n| \quad (1.2)$$

with the additional constraints  $0 \leq p_n \leq 1$  and  $\sum_n p_n = 1$  due to (1) and (3). Then observables can be computed via

$$\hat{\rho}[A] = \text{Tr}[\rho A] = \sum_n p_n \text{Tr}[|n\rangle \langle n| A] = \sum_n p_n \langle n| A |n\rangle \quad (1.3)$$

which illustrates the interpretation of  $\rho$  as a *classical* mixture of states  $\{|n\rangle\}$  with probabilities  $\{p_n\}$ . However note that  $\rho$  does *not* describe a classical probability density on  $\mathcal{H}$  as it is not normalised on the *whole* Hilbert space but on a orthonormal subset. This relates to the fact that the decomposition of a density matrix is not unique and thus the *interpretation* as a mixture of *distinct* quantum states is somewhat misleading.

Before we conclude with some remarks on the *transformations* of density matrices (and therefore, states) let us point out that the family of all density operators in  $\mathcal{B}(\mathcal{H})$  constitutes a *convex set*. This is easy to see since any two given density matrices  $\rho_1$  and  $\rho_2$  can be combined via

$$\rho_t = t \cdot \rho_1 + (1 - t) \cdot \rho_2 \quad \text{where} \quad 0 \leq t \leq 1 \quad (1.4)$$

to form a new state  $\rho_t$  which is the *convex combination* of  $\rho_1$  and  $\rho_2$ . To show that  $\rho_t$  is a valid density matrix recall that (1) the real linear combination of Hermitian operators is Hermitian, (2) the sum of positive operators remains positive, and (3) the normalisation is preserved due to the convex combination. This is used, for instance, in Section 2.5 where we solve the dissipative dynamics of a two-spin system analytically.

The quantum mechanics of pure states describes the coherent transformation of quantum states by unitary operations  $U$ ,  $U \in \mathcal{B}(\mathcal{H})$  and  $U^\dagger U = \mathbb{1} = U U^\dagger$ , as they correspond to rotations in complex Hilbert spaces and therefore preserve the normalisation of states:  $\langle \Psi | U^\dagger U | \Psi \rangle = \langle \Psi | \Psi \rangle = 1$ . In the more general framework of (potentially) mixed states, described by density matrices  $\rho$ , the requirements for the most general description of *physical transformations* read differently: Let  $\Phi : \mathcal{B}(\mathcal{H}) \rightarrow \mathcal{B}(\mathcal{H})$  be a linear *superoperator* on the set of bounded operators. If  $\Phi$  describes a *physical transformation*, we have to demand that  $\Phi$  maps the convex set  $\mathcal{D}(\mathcal{H})$  of density matrices into itself, i.e. the restriction

$$\Phi : \mathcal{D}(\mathcal{H}) \rightarrow \mathcal{D}(\mathcal{H}) \quad (1.5)$$

has to be well defined. This is implied by the following requirements: (1)  $\Phi$  has to be *linear* and *Hermiticity preserving*; (2) it has to preserve the positivity of density matrices, that is, it has to be a *positive map*; (3) it has to preserve the normalisation of density matrices, meaning it has to be *trace preserving*; (4) if one adds an arbitrary finite dimensional ancilla system described by  $\mathcal{H}_a$ , the tensor product  $\mathbb{1}_a \otimes \Phi$  must remain a positive map on the enlarged Hilbert space  $\mathcal{H}_a \otimes \mathcal{H}$ . Maps with this property are termed *completely positive*. Requirement (4) has a *physically* motivated origin: The description of a physical operation must not be influenced by any *non-interacting* ancilla system  $\mathcal{H}_a$ .

Superoperators  $\Phi$  that satisfy these four properties map density matrices to density matrices and are consequently considered a description of physical operations. Such superoperators are called *completely positive trace preserving* (CPTP) maps. In the realm of quantum information, CPTP maps are often referred to as *quantum channels*.

This was a *very* brief outline of the algebraic foundations of quantum physics. For more detailed discussions and definitions I refer the reader to one of the many textbooks on algebraic quantum theory. A comprehensive review of the topic is given in the lecture notes by Wolf [4].

### 1.1.2 Open quantum systems: The Lindblad equation

Here we review important mathematical tools that will be used throughout this thesis. The unitary time evolution of pure quantum states is described by the Schrödinger equation

$$i\partial_t |\Psi\rangle = H |\Psi\rangle \quad (1.6)$$

where  $H$  denotes the system Hamiltonian and the reduced Planck constant  $\hbar$  is set to 1. In the previous paragraph, we generalised pure states to density matrices who describe the very same state. This generalisation must be parallelized by a new equation which describes the time evolution of the Schrödinger equation in the framework of density matrices. This equation is called Von Neumann equation and reads

$$\partial_t \rho = -i[H, \rho] \quad (1.7)$$

which is, in fact, equivalent to Eq. (1.6). The formal time evolution is then easily derived and one finds  $\rho(t) = e^{-iHt} \rho_0 e^{iHt}$ . This describes a *unitary* time evolution and may be considered as a parametrised family of superoperators (quantum channels), meaning  $\mathcal{U}(t)[\bullet] = e^{-iHt} \bullet e^{iHt}$  is a CPTP map for each  $t \in \mathbb{R}$ . Unitary evolution describes quantum systems that interact only *coherently* with their environment (if at all). *Open* quantum systems are much harder to describe due to the multitude of possible interactions with the environment. In this thesis we consider systems that interact incoherently with *Markovian* environments (termed *baths* henceforth).

The *most general* time-homogeneous evolution of a density matrix that describes a system which is coupled to a Markovian environment in terms of a *master equation* is given by the *Lindblad equation*<sup>2</sup> [5]:

$$\partial_t \rho = -i[H, \rho] + \sum_{i,j} \tilde{\kappa}_{i,j} \left( \tilde{L}_i \rho \tilde{L}_j^\dagger - \frac{1}{2} \{ \tilde{L}_j^\dagger \tilde{L}_i, \rho \} \right) \quad (1.8)$$

which clearly generalises the time evolution described by Eq. (1.7). The Hamiltonian  $H$  describes the unitary evolution of the system whereas the *jump operators*  $\{\tilde{L}_i\}$  describe the incoherent operations of the environment on the system; the matrix  $\tilde{\kappa}_{i,j}$  describes the dissipative dynamics and must be positive (see below). There are various derivations of the Lindblad master equation [6–8]. It requires several approximations to infer the Lindbladian jump operators  $\{\tilde{L}_i\}$  from a *microscopic model*. This thesis is *not* concerned with such derivations. Here we consider the jump operators as mere “mathematical degrees of freedom”. The jump operators that we are concerned with are nevertheless *physically motivated*. This becomes clear in Chapter 2 where we contrive reasonable jump operators for a dissipative transverse field Ising model.

<sup>2</sup>Equivalent terms are “Master equation in Lindblad form” and “Lindblad master equation”.

Eq. (1.8) is the most general form of the Lindblad master equation. Since  $\tilde{\kappa}_{i,j}$  is required to be positive, there is always a unitary transformation which yields the *diagonal* form of the Lindblad equation:

$$\partial_t \rho = -i [H, \rho] + \sum_i \kappa_i \left( L_i \rho L_i^\dagger - \frac{1}{2} \{L_i^\dagger L_i, \rho\} \right) \quad (1.9)$$

Here the new jump operators  $\{L_i\}$  and the new couplings  $\kappa_i$  are related to  $\{\tilde{L}_i\}$  and  $\tilde{\kappa}_{i,j}$  via a unitary transformation. This is the most common form of the Lindblad equation and in the following only such diagonal Lindblad equations are considered.

The mathematics of the Lindblad equation is quite interesting but goes beyond the scope of this thesis. To cut the matter short: The right-hand side of Eq. (1.9) is obviously linear in the density matrix  $\rho$ . It is then straightforward to see that the right-hand side can be considered a *superoperator*  $\mathcal{L}[\rho]$  on the convex set of density matrices  $\mathcal{D}(\mathcal{H})$ . The curious structure of the Lindblad equation is responsible for the fact that the superoperator  $\exp[\mathcal{L}t]$  is a CPTP map (that is, a quantum channel) for  $0 \leq t \leq \infty$ . The latter describes the time evolution described by Eq. (1.9). This is formally derived in the next section by means of an appropriate vectorisation in the superoperator language. Since  $\exp[\mathcal{L}t_1] \cdot \exp[\mathcal{L}t_2] = \exp[\mathcal{L}(t_1 + t_2)]$  remains a CPTP map for non-negative  $t_1$  and  $t_2$ , we are led to the conclusion that the set  $\{\exp[\mathcal{L}t]\}$  features the structure of a *semigroup* (actually, a monoid). Hence we ended up in the realm of *quantum dynamical semigroups*. In this reading, the Lindblad superoperator  $\mathcal{L}$  is the *generator* of a quantum dynamical semigroup, that is a continuous family of quantum channels.

For further information regarding Lindblad master equations and quantum dynamical semigroups I refer the reader to [9] and [10]. In the next subsection we recast the Lindblad equation in a more convenient form by a vectorisation of density matrices.

### 1.1.3 The quantum trajectory approach to Markovian dynamics

Here we recast the Lindblad master equation in a vectorised form: Density *matrices* (operators) become *vectors* and *superoperators* become *matrices* that act on these vectors. In this framework the formal solution of the Lindblad equation along the lines of  $\mathcal{U}(t)[\bullet] = e^{-iHt} \bullet e^{iHt}$  (see the previous discussions) becomes trivial.

Vectorisation and the superoperator formalism

Let  $\mathcal{H}$  be a Hilbert space and  $\mathcal{B}(\mathcal{H})$  the  $C^*$ -algebra of bounded (trace class) operators on  $\mathcal{H}$ . We will adopt the following notation: Symbols with hats, e.g.  $\hat{\rho}$ , denote abstract operators on  $\mathcal{H}$  whereas hat-less symbols, e.g.  $\rho$ , denote matrices, i.e. basis-dependent representations of an abstract operator. By a slight abuse of notation, we will nevertheless write  $\rho \in \mathcal{B}(\mathcal{H})$ . Consider now the well-known operation of *vectorisation* defined via

$$\text{vec} : \mathbb{C}^{n \times m} \rightarrow \mathbb{C}^{nm} \quad A = \begin{bmatrix} a_1 & a_2 & \dots & a_m \end{bmatrix} \mapsto \text{vec}(A) = \begin{bmatrix} a_1 \\ a_2 \\ \vdots \\ a_m \end{bmatrix}. \quad (1.10)$$

There are some well-known relations which will be useful in the following:

$$\text{vec}(ABC) = (\mathbf{C}^T \otimes \mathbf{A}) \text{vec}(\mathbf{B}) \quad (1.11a)$$

$$\text{vec}(\mathbf{AB}) = (\mathbf{1} \otimes \mathbf{A}) \text{vec}(\mathbf{B}) = (\mathbf{B}^T \otimes \mathbf{1}) \text{vec}(\mathbf{A}) \quad (1.11b)$$

Furthermore it is straightforward to show that  $\text{Tr}[\mathbf{A}^\dagger \mathbf{B}] = \langle \text{vec}(\mathbf{A}) | \text{vec}(\mathbf{B}) \rangle$  where  $\langle \bullet | \bullet \rangle$  denotes the usual complex inner product.

We proceed with the following notation

$$|\mathbf{O}\rangle\rangle \equiv \text{vec}(\mathbf{O}) \quad \text{and write} \quad |\mathbf{O}\rangle\rangle \in \mathcal{B}(\mathcal{H}) \quad (1.12)$$

which is just an extension of the common Dirac notation to the more general framework of  $C^*$ -algebraic quantum mechanics [11]. An isomorphism between  $\mathcal{B}(\mathcal{H})$  and its dual space  $\mathcal{B}^*(\mathcal{H})$  is established via the Hilbert-Schmidt inner product, i.e. for  $\hat{\mathbf{O}} \in \mathcal{B}(\mathcal{H})$  we define the linear functional  $\hat{\mathbf{O}}^*[\bullet] \equiv \text{Tr}[\hat{\mathbf{O}}^\dagger \bullet]$ . In combination with the notation introduced above this yields the appealing notation

$$|\mathbf{O}\rangle\rangle \in \mathcal{B}(\mathcal{H}) \quad \Rightarrow \quad \langle\langle \mathbf{O} | = |\mathbf{O}\rangle\rangle^\dagger \in \mathcal{B}^*(\mathcal{H}) \quad (1.13)$$

for dual operators and, consistently, we find

$$\text{Tr}[\mathbf{A}^\dagger \mathbf{B}] = \langle\langle \mathbf{A} | \mathbf{B} \rangle\rangle \quad \text{Hilbert-Schmidt inner product} \quad (1.14a)$$

$$\text{Tr}[\mathbf{A}] = \langle\langle \mathbf{1} | \mathbf{A} \rangle\rangle \quad \text{Trace} \quad (1.14b)$$

$$\gamma[\rho] = \langle\langle \rho | \rho \rangle\rangle \quad \text{Purity} \quad (1.14c)$$

where  $\rho$  denotes a density operator. ■

The quantum trajectory approach

The Lindblad equation (1.9) describes the time evolution of a density matrix  $\rho = \rho(t)$ . As in the case of unitary dynamics, described by the Von Neumann equation (1.7), there are different approaches to evolve states in time. The formal solution  $\mathcal{U}(t)[\bullet]$  for unitary dynamics propagates states in time. It is well-known that this propagation can be unravelled by a Dyson series and interpreted in terms of Feynman diagrams. A similar method can be applied to the time evolution of a dissipative system that is governed by a Lindblad master equation. This method expands the time evolution superoperator in terms of *quantum trajectories*.

In the next paragraphs we first derive the formal time evolution superoperator and subsequently expand it by means of a Dyson series to end up with the quantum trajectory interpretation of Lindbladian dynamics. We start with the master equation in Lindblad form

$$\partial_t \rho = -i[H, \rho] + \sum_j \left[ L_j \rho L_j^\dagger - \frac{1}{2} \{L_j^\dagger L_j, \rho\} \right] \equiv \mathcal{H}[\rho] + \mathcal{D}[\rho] \equiv \mathcal{L}[\rho] \quad (1.15)$$



where  $\mathcal{H}$  describes the unitary evolution and the jump operators  $\{L_j\}$  describe the effective coupling to the environment via the dissipator  $\mathcal{D}$ . Application of the vectorisation  $|\bullet\rangle\rangle$  on both sides yields

$$\partial_t |\rho\rangle\rangle = -i[|H\rho\rangle\rangle - |\rho H\rangle\rangle] + \sum_j |L_j \rho L_j^\dagger\rangle\rangle - \frac{1}{2}[|H_P \rho\rangle\rangle + |\rho H_P\rangle\rangle]$$

where we introduced the parent Hamiltonian  $H_P = \sum_j L_j^\dagger L_j$ . Application of the rules in (1.11) yields

$$\partial_t |\rho\rangle\rangle = -i[\mathbb{1} \otimes H - \bar{H} \otimes \mathbb{1}] |\rho\rangle\rangle + \sum_j \bar{L}_j \otimes L_j |\rho\rangle\rangle - \frac{1}{2}[\mathbb{1} \otimes H_P + \bar{H}_P \otimes \mathbb{1}] |\rho\rangle\rangle.$$

If we now introduce the quantum jump matrices  $L_j \equiv \bar{L}_j \otimes L_j$ ,  $\mathbf{L} \equiv \sum_j L_j$  and the effective (non-Hermitian) Hamiltonian  $H_{\text{eff}} \equiv H - \frac{i}{2}H_P$ , the master equation takes the form

$$\partial_t |\rho\rangle\rangle = -i[\mathbb{1} \otimes H_{\text{eff}} - \bar{H}_{\text{eff}} \otimes \mathbb{1}] |\rho\rangle\rangle + \mathbf{L} |\rho\rangle\rangle = (\mathbf{H}_{\text{eff}} + \mathbf{L}) |\rho\rangle\rangle = \mathcal{L} |\rho\rangle\rangle$$

where we introduced  $\mathbf{H}_{\text{eff}} \equiv -i[\mathbb{1} \otimes H_{\text{eff}} - \bar{H}_{\text{eff}} \otimes \mathbb{1}]$  and  $\mathcal{L} \equiv \mathbf{H}_{\text{eff}} + \mathbf{L}$ .

That is, in this framework the Lindblad master equation reads

$$\partial_t |\rho\rangle\rangle = \mathcal{L} |\rho\rangle\rangle \quad \Leftrightarrow \quad \partial_t \langle\langle \rho | = \langle\langle \rho | \mathcal{L}^* \quad (1.16)$$

where  $\mathcal{L}^*$  denotes the adjoint Lindbladian. The formal solution is then clearly

$$|\rho(t)\rangle\rangle = \exp(\mathcal{L}t) |\rho_0\rangle\rangle \quad \Leftrightarrow \quad \langle\langle \rho(t) | = \langle\langle \rho_0 | \exp(\mathcal{L}^*t) \quad (1.17)$$

and the Heisenberg picture is easily derived since  $\langle\langle \mathcal{O} \rangle\rangle(t) = \langle\langle \rho(t) | \mathcal{O} \rangle\rangle = \langle\langle \rho_0 | e^{\mathcal{L}^*t} | \mathcal{O} \rangle\rangle = \langle\langle \rho_0 | \mathcal{O}(t) \rangle\rangle$ , thus  $|\mathcal{O}(t)\rangle\rangle = \exp(\mathcal{L}^*t) |\mathcal{O}_0\rangle\rangle$ . Therefore the time evolution of operators in the Heisenberg picture is governed by the adjoint master equation

$$\partial_t |\mathcal{O}\rangle\rangle = \mathcal{L}^* |\mathcal{O}\rangle\rangle \quad \Leftrightarrow \quad \partial_t \mathcal{O} = i[H, \mathcal{O}] + \sum_j \left[ L_j^\dagger \mathcal{O} L_j - \frac{1}{2} \{L_j^\dagger L_j, \mathcal{O}\} \right]. \quad (1.18)$$

Non-equilibrium steady states (NESS) are characterised by

$$\mathcal{L} |\text{NESS}\rangle\rangle = 0 \quad \text{or} \quad \langle\langle \text{NESS} | \mathcal{L}^* = 0 \quad (1.19)$$

whereas, due to the non-Hermiticity of the Lindbladian, the left-vacuum is *not* the dual of a NESS but rather encodes the trace-preserving property of the semi-group evolution, meaning  $\langle\langle \mathbb{1} | \mathcal{L} = 0$  which states just that  $\partial_t \text{Tr}[\rho] = \partial_t \langle\langle \mathbb{1} | \rho \rangle\rangle = 0$  under  $\partial_t |\rho\rangle\rangle = \mathcal{L} |\rho\rangle\rangle$ .

In order to obtain an unravelling of the time evolution superoperator  $\exp(\mathcal{L}t)$  in terms of quantum jumps  $\{L_j\}$  (or rather  $\{\bar{L}_j\}$ ), one defines the superoperators

$$\mathbb{A} \equiv e^{(\mathbf{H}_{\text{eff}} + \mathbf{L})t} \quad \text{and} \quad \mathbb{B} \equiv e^{-\mathbf{H}_{\text{eff}}t} \mathbb{A}. \quad (1.20)$$

It follows easily  $\partial_t \mathbb{B} = -\mathbf{H}_{\text{eff}} e^{-\mathbf{H}_{\text{eff}} t} \mathbb{A} + e^{-\mathbf{H}_{\text{eff}} t} (\mathbf{H}_{\text{eff}} + \mathbf{L}) \mathbb{A} = e^{-\mathbf{H}_{\text{eff}} t} \mathbf{L} e^{\mathbf{H}_{\text{eff}} t} \mathbb{B}$ . If we take into account that  $\mathbb{B}(0) = \mathbb{1}$ , we can write

$$\mathbb{B}(t) = \mathbb{1} + \int_0^t \partial_s \mathbb{B}(s) ds = \mathbb{1} + \int_0^t e^{-\mathbf{H}_{\text{eff}} s} \mathbf{L} e^{\mathbf{H}_{\text{eff}} s} \mathbb{B}(s) ds \quad (1.21)$$

and consequently

$$\exp(\mathcal{L}t) = \mathbb{A}(t) = e^{\mathbf{H}_{\text{eff}} t} + e^{\mathbf{H}_{\text{eff}} t} \int_0^t e^{-\mathbf{H}_{\text{eff}} s} \mathbf{L} e^{\mathbf{H}_{\text{eff}} s} \mathbb{B}(s) ds. \quad (1.22)$$

Reinserting Eq. (1.21) recursively yields a Dyson series

$$\exp(\mathcal{L}t) = \sum_{m=0}^{\infty} \int_0^t dt_m \int_0^{t_m} dt_{m-1} \dots \int_0^{t_2} dt_1 \left\{ e^{\mathbf{H}_{\text{eff}}(t-t_m)} \mathbf{L} e^{\mathbf{H}_{\text{eff}}(t_m-t_{m-1})} \mathbf{L} \dots \mathbf{L} e^{\mathbf{H}_{\text{eff}} t_1} \right\} \quad (1.23)$$

If we introduce the functional integral

$$\int_{[0,t],\{L_j\}} \mathcal{D}[\mathbf{L}] \bullet = \sum_{m=0}^{\infty} \sum_{j_1} \dots \sum_{j_m} \int_0^t dt_m \int_0^{t_m} dt_{m-1} \dots \int_0^{t_2} dt_1 \bullet \quad (1.24)$$

and the short-hand notation

$$\prod_{l \in \mathbf{L}} l \equiv L_{j_1}(t_1) \dots L_{j_m}(t_m), \quad (1.25)$$

and recall that the time-ordering operator  $\mathcal{T}$  [12] yields the intermittence by time labeled quantum jumps, meaning

$$\mathcal{T} \left[ \exp(\mathbf{H}_{\text{eff}} t) \prod_{l \in \mathbf{L}} l \right] = e^{\mathbf{H}_{\text{eff}}(t-t_m)} L_{j_m} e^{\mathbf{H}_{\text{eff}}(t_m-t_{m-1})} L_{j_{m-1}} \dots L_{j_1} e^{\mathbf{H}_{\text{eff}}(t_1-0)}, \quad (1.26)$$

we can write the dissipative time evolution operator in a compact form as

$$\exp(\mathcal{L}t) = \int_{[0,t],\{L_j\}} \mathcal{D}[\mathbf{L}] \mathcal{T} \left[ \exp(\mathbf{H}_{\text{eff}} t) \prod_{l \in \mathbf{L}} l \right]. \quad (1.27)$$

Let now the system be in initial state  $|\rho_0\rangle\rangle$ . If we define the probability density

$$P[\mathbf{L}; t] \equiv \langle\langle \mathbb{1} | \mathcal{T} \left[ \exp(\mathbf{H}_{\text{eff}} t) \prod_{l \in \mathbf{L}} l \right] | \rho_0 \rangle\rangle \quad (1.28)$$

$$= \langle\langle \mathbb{1} | e^{\mathbf{H}_{\text{eff}}(t-t_m)} L_{j_m} e^{\mathbf{H}_{\text{eff}}(t_m-t_{m-1})} L_{j_{m-1}} \dots L_{j_1} e^{\mathbf{H}_{\text{eff}}(t_1-0)} | \rho_0 \rangle\rangle \quad (1.29)$$

and the *conditioned density matrix*

$$|\rho_c[\mathbf{L}; t]\rangle\rangle \equiv (P[\mathbf{L}; t])^{-1} \mathcal{T} \left[ \exp(\mathbf{H}_{\text{eff}} t) \prod_{l \in \mathbf{L}} l \right] |\rho_0\rangle\rangle \quad (1.30)$$

one can write for the unravelling of the dissipative dynamics (starting from  $|\rho_0\rangle\rangle$ )

$$|\rho(t)\rangle\rangle = \exp(\mathcal{L}t) |\rho_0\rangle\rangle = \int_{[0,t],\{\mathbf{L}_j\}} \mathcal{D}[\mathbf{L}] P[\mathbf{L}; t] |\rho_c[\mathbf{L}; t]\rangle\rangle . \quad (1.31)$$

That is, the state at time  $t$  is given as convex combination of all possible quantum jump trajectories  $\mathbf{L}$  weighted with homogeneous coordinates  $P[\mathbf{L}; t]$  which determine the probability for  $\mathbf{L}$  to occur. Note that the trace-preserving property of the quantum-dynamical semigroup reads

$$\int_{[0,t],\{\mathbf{L}_j\}} \mathcal{D}[\mathbf{L}] P[\mathbf{L}; t] = 1 \quad \text{for all } 0 \leq t \leq \infty \quad (1.32)$$

in this perception.

A straightforward expansion of the time evolution superoperator  $\exp(\mathcal{L}t)$  is in terms of jump trajectories  $\mathcal{E}_N(\tau)$  with fixed number of jumps  $N$ . I.e. define the fixed number functional integral

$$\int_{[0,t],\{\mathbf{L}_j\}} \mathcal{D}^N[\mathbf{L}] \bullet = \sum_{j_1} \cdots \sum_{j_N} \int_0^t dt_N \int_0^{t_N} dt_{N-1} \cdots \int_0^{t_2} dt_1 \bullet \quad (1.33)$$

and the *fixed number channel*

$$\mathcal{E}_N(t) := \int_{[0,t],\{\mathbf{L}_j\}} \mathcal{D}^N[\mathbf{L}] \mathcal{T} \left[ \exp(\mathbf{H}_{\text{eff}} t) \prod_{l \in \mathbf{L}} l \right] \quad (1.34)$$

which describes all possible trajectories between 0 and  $t$  with exactly  $N$  jumps occurring. The complete evolution is then given by

$$\exp(\mathcal{L}t) = \sum_{N=0}^{\infty} \mathcal{E}_N(t) . \quad (1.35)$$

We will give an example of this expansion in the next subsection. ■

Example: Unravelling of the Lindblad equation

To convey a sense of the insights we gained in the former subsection, let us unravel the dynamics of a very simple system in terms of quantum jump trajectories.

### ■ A simple system & Exact solution

Consider a single spin described by  $\mathcal{H} = \mathbb{C}^2$  and coupled to two competing baths

$$A = \sqrt{a} \sigma_x^+ = \frac{\sqrt{a}}{2} (\sigma^z - i\sigma^y) \quad \text{and} \quad B = \sqrt{b} \sigma_z^+ = \frac{\sqrt{b}}{2} (\sigma^x + i\sigma^y) \quad (1.36)$$

with bath strengths  $a$  and  $b$ . In the following we consider the parameters  $(a, b) = (t, 1-t)$  for  $t \in [0, 1]$ . Clearly the dark state for  $t = 0$  ( $t = 1$ ) is the completely  $z$ -polarised state  $|\uparrow\rangle$  (completely  $x$ -polarised state  $|\rightarrow\rangle$ ). For  $0 < t < 1$  we do not expect a pure steady state.

In this special case we find

$$H_P = a \sigma_x^- \sigma_x^+ + b \sigma_z^- \sigma_z^+ = \frac{1}{2} \begin{bmatrix} a & -a \\ -a & a + 2b \end{bmatrix} \quad (1.37)$$

and consequently

$$\mathbf{H}_{\text{heff}} = \frac{1}{4} \begin{bmatrix} -2a & a & a & 0 \\ a & -2(a+b) & 0 & a \\ a & 0 & -2(a+b) & a \\ 0 & a & a & -2a-4b \end{bmatrix}. \quad (1.38)$$

For the jumps follows

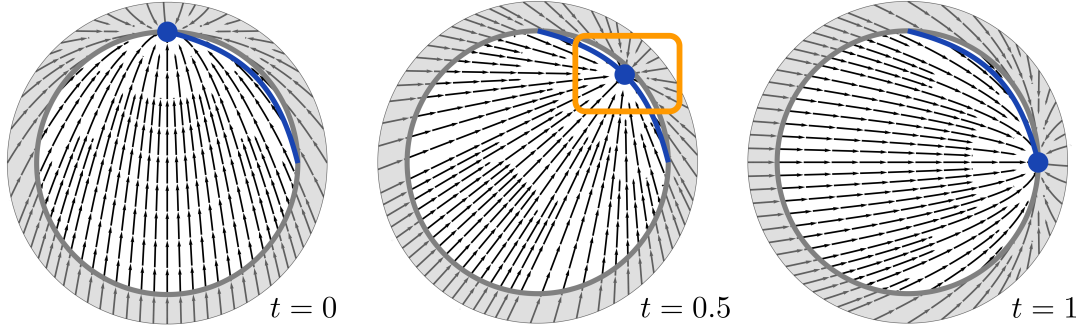
$$\mathbf{L} = a \overline{\sigma_x^+} \otimes \sigma_x^+ + b \overline{\sigma_z^+} \otimes \sigma_z^+ = \frac{1}{4} \begin{bmatrix} a & -a & -a & a+4b \\ a & -a & -a & a \\ a & -a & -a & a \\ a & -a & -a & a \end{bmatrix} \quad (1.39)$$

which leads us to the Lindblad superoperator

$$\mathcal{L} = \mathbf{H}_{\text{eff}} + \mathbf{L} = \frac{1}{4} \begin{bmatrix} -a & 0 & 0 & a+4b \\ 2a & -3a-2b & -a & 2a \\ 2a & -a & -3a-2b & 2a \\ a & 0 & 0 & -a-4b \end{bmatrix}. \quad (1.40)$$

It is straightforward to calculate the spectrum and the eigenvectors of  $\mathcal{L}$  which yields a single vanishing eigenvalue (for  $a \cdot b \neq 0$ ). The corresponding (devectorised) eigenvector reads

$$\rho_{\text{NESS}} = \begin{bmatrix} \frac{1}{2} + \frac{b}{2b+a} & \frac{a}{b+2a} \\ \frac{a}{b+2a} & \frac{1}{2} \cdot \frac{a}{2b+a} \end{bmatrix} = \begin{bmatrix} \frac{3}{2} - \frac{1}{2-t} & \frac{t}{1+t} \\ \frac{t}{1+t} & \frac{1}{2} \cdot \frac{t}{2-t} \end{bmatrix} \quad (1.41)$$



■ **Figure 1.1:** Cross-sections of the Bloch sphere in the  $a_x$ - $a_z$ -plane at  $a_y = 0$ . Physical states are described by points in the white regions; pure states lie on the (thick grey) border and mixed ones inside the Bloch sphere. The stream lines illustrate the vector field  $\dot{\mathbf{a}}(a_x, a_y, a_z)$  which describes the dynamics of a state coupled to bath  $A$  and  $B$  with relative strength  $t$ . There is a unique steady state for all parameters which becomes a (pure) dark state for  $t = 0$  ( $|\uparrow\rangle$ ) and  $t = 1$  ( $|+\rangle$ ). Note that in-between these two limiting cases the steady states is (slightly) mixed as highlighted by the orange box. The “path” of the steady state for  $0 \leq t \leq 1$  is depicted as thick blue line whereas the steady state for the shown vector field is marked as blue dot.

where we inserted  $(a, b) = (t, 1 - t)$ . Note that one has to normalise the eigenvector so that  $\text{Tr}[\rho_{\text{NESS}}] = 1$ . This is the non-equilibrium steady state of the Lindblad equation  $\dot{\rho} = \mathcal{L}[\rho]$  in dependence of the bath couplings  $a$  and  $b$ . As a consistency check we point out that  $\rho_{\text{NESS}}(t = 0) = |\uparrow\rangle\langle\uparrow|$  and  $\rho_{\text{NESS}}(t = 1) = |+\rangle\langle+|$ .

Since our system comprises a single spin, it is advantageous to describe its (mixed) states as points on and in the Bloch sphere. Therefore parametrise the density matrix  $\rho = \frac{1}{2}(\mathbb{1} + \mathbf{a}\sigma)$  with the Bloch vector  $\mathbf{a} = [a_x, a_y, a_z]^T \in \mathbb{R}^3$ ,  $|\mathbf{a}| \leq 1$ . By using  $a_i = \text{Tr}[\sigma^i \rho]$  the Lindblad equation can be recast in the form

$$\dot{a}_i = \dot{\mathbf{a}}(a_x, a_y, a_z) \equiv \text{Tr} \left[ \sigma^i \mathcal{L} \left[ \frac{1}{2} (\mathbb{1} + \mathbf{a}\sigma) \right] \right] \quad \text{for } i = x, y, z \quad (1.42)$$

which describes a *dynamical system* in  $\mathbb{R}^3$  with the vector field  $\dot{\mathbf{a}}(a_x, a_y, a_z)$ . In the superoperator framework this reads

$$\dot{a}_i = \langle\langle \mathbb{1} | [\sigma^0 \otimes \sigma^i] \mathcal{L} | 1/2 (\mathbb{1} + \mathbf{a}\sigma) \rangle\rangle \quad \text{for } i = x, y, z. \quad (1.43)$$

For our system this yields

$$\begin{aligned} \dot{a}_x &= t - \frac{1+t}{2} a_x \\ \dot{a}_y &= -\frac{1}{2} a_y \\ \dot{a}_z &= 1 - t + \frac{t-2}{2} a_z \end{aligned}$$

and the corresponding steady state clearly reads  $\mathbf{a}_{\text{NESS},x} = \frac{2t}{1+t}$ ,  $\mathbf{a}_{\text{NESS},y} = 0$  and  $\mathbf{a}_{\text{NESS},z} = \frac{2t-2}{t-2}$  which is consistent with our findings above. The vector field  $\dot{\mathbf{a}}(a_x, a_y, a_z)$  and the steady states are illustrated in Fig. 1.1 for three parameters  $t = 0, 0.5, 1$ . Note that the vector field flows invariably *into* the Bloch sphere which is a consequence of the fact that  $\exp(\mathcal{L}\tau)$  is a CPTP map

for all  $0 \leq \tau \leq \infty$ . The time evolution – which is formally given as  $\rho(\tau) = \exp(\mathcal{L}\tau)\rho_0$  – can now be obtained by solving the dynamical system above. One finds

$$a_x(\tau) = \frac{2t}{1+t} + \left( a_x(0) - \frac{2t}{1+t} \right) e^{-\frac{1+t}{2}\tau} \quad (1.44a)$$

$$a_y(\tau) = a_y(0) e^{-\frac{1}{2}\tau} \quad (1.44b)$$

$$a_z(\tau) = \frac{2t-2}{t-2} + \left( a_z(0) - \frac{2t-2}{t-2} \right) e^{-\frac{2-t}{2}\tau} \quad (1.44c)$$

with the initial state  $\rho_0 = \frac{1}{2}(\mathbb{1} + \mathbf{a}(0)\sigma)$ .

### ■ Approximation by jump histories

To get a sense of the previously derived unravelling of  $\exp(\mathcal{L}t)$  in terms of quantum jump trajectories (see Eq. (1.27)), we calculate the contributions for fixed jump numbers as given in Eq. (1.35). To this end we summon the operator norm

$$\|A\| := \max_{x \neq 0} \frac{\|Ax\|_2}{\|x\|_2} \quad \text{for } A \in \mathbb{C}^{n \times n} \quad (1.45)$$

(which equals the spectral norm of  $A$ ). Here  $\|\bullet\|_2$  denotes the Euclidean norm on  $\mathbb{R}^n$ . To get a feeling for the importance of each channel at a given time  $t$  we compute the relative norm

$$\Delta_N(t) := \frac{\|\mathcal{E}_N(t)\|}{\|e^{\mathcal{L}t}\|} \quad (1.46)$$

for each channel  $\mathcal{E}_N(t)$  where  $\|\bullet\|$  denotes the operator norm as introduced above. To quantify the deviation of a fixed number expansion up to  $N_{\max}$  jumps from the *steady state*, we introduce the relative norm deviation

$$\delta_{N_{\max}}[\rho_{\text{NESS}}](t) := \frac{\|\sum_{N=0}^{N_{\max}} \mathcal{E}_N(t) - \lim_{\tau \rightarrow \infty} e^{\mathcal{L}\tau}\|}{\|\lim_{\tau \rightarrow \infty} e^{\mathcal{L}\tau}\|}. \quad (1.47)$$

Analogously, the deviation from the *current evolution operator* is given by

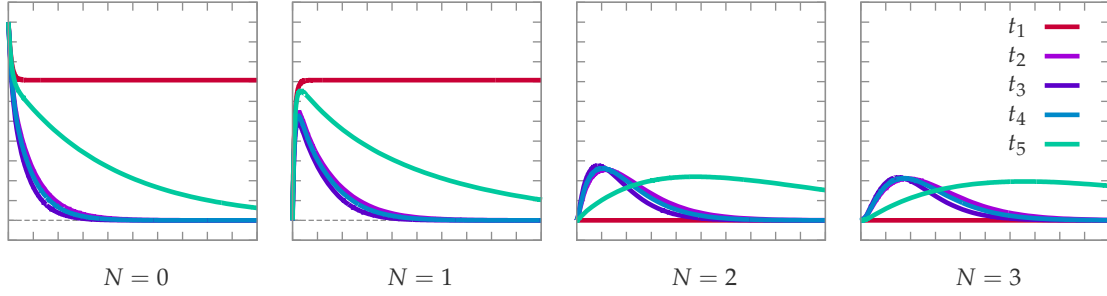
$$\delta_{N_{\max}}[\rho(t)](t) := \frac{\|\sum_{N=0}^{N_{\max}} \mathcal{E}_N(t) - e^{\mathcal{L}t}\|}{\|e^{\mathcal{L}t}\|}. \quad (1.48)$$

Recall the recursive structure of the Dyson series which becomes apparent in Eq. (1.21) and (1.22). This structure suggest the following computation scheme:

$$\tilde{\mathcal{E}}_0(t) := \mathbb{1} \quad \text{and} \quad \tilde{\mathcal{E}}_{N+1}(t) := \int_0^t e^{-\mathbf{H}_{\text{eff}}s} \mathbf{L} e^{\mathbf{H}_{\text{eff}}s} \tilde{\mathcal{E}}_N(s) ds \quad (1.49)$$

Where the channels for fixed jump numbers can be retrieved via

$$\mathcal{E}_N(t) = e^{\mathbf{H}_{\text{eff}}t} \tilde{\mathcal{E}}_N(t). \quad (1.50)$$



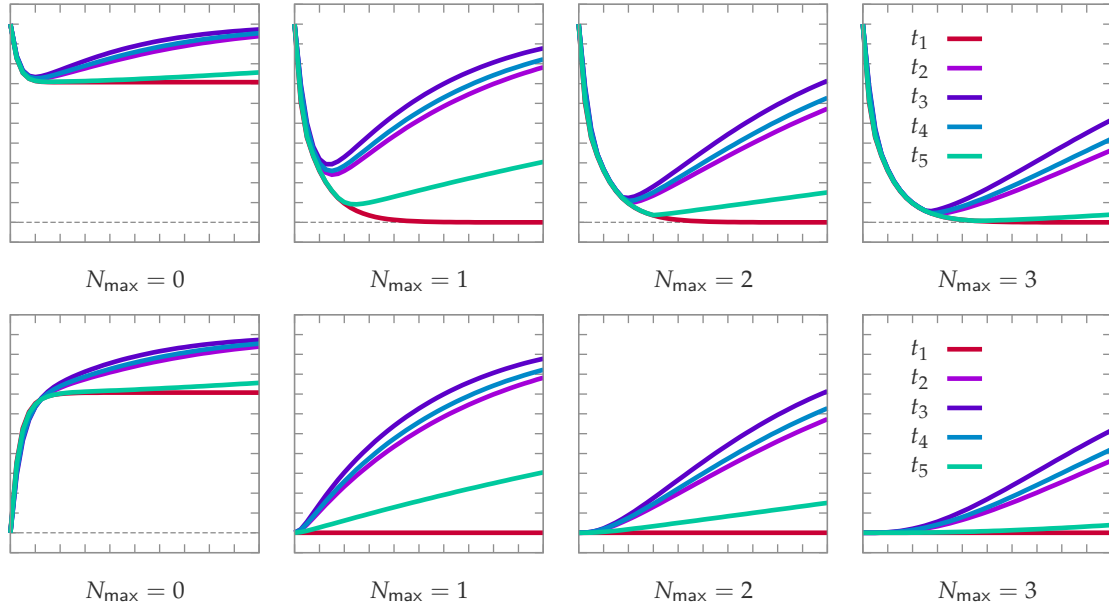
■ **Figure 1.2:** Contributions of finite jump trajectories to the time evolution channel  $\exp(\mathcal{L}\tau)$  over time  $\tau$ . The norm contributions  $\Delta_{N_{\max}}$  for the  $N = 0, 1, 2, 3$  jump channels  $\mathcal{E}_N(\tau)$  are shown for five relative couplings  $(t_1, t_2, t_3, t_4, t_5) = (0, 0.25, 0.50, 0.75 - 0.05, 1.00 - 0.05)$ . Note that for the case of a pure steady state ( $t_1 = 0$  with dark state  $|\uparrow\rangle$ ) the only contributions stem from the zero- and one-jump trajectories whereas for mixed systems ( $0 < t < 1$ ) channels with more jumps become important at specific times depending on the relative coupling  $t$ . The closer the system's steady state is to a pure dark state the lower is the frequency of jumps; as a consequence, trajectories with large number of jumps become important at later times. See  $t_5$  for instance.

This recursion can easily be computed by *Mathematica* analytically up to  $N = 3$  jumps. The results are shown in Fig. 1.2 and Fig. 1.3. There are some remarks in order:

- Consider the four plots of Fig. 1.2. The plots show the rescaled norm of  $\mathcal{E}_N(\tau)$ , namely  $\Delta_{N_{\max}}(\tau)$ , in dependence of time  $\tau$  for  $N = 0, 1, 2, 3$  and different parameters  $(t_1, t_2, t_3, t_4, t_5) = (0, 0.25, 0.50, 0.75 - 0.05, 1.00 - 0.05)$ . If there is a pure steady state (dark state) – which is the case for  $t_1 = 0$ , namely  $|\uparrow\rangle$  – there are only contributions from zero- and one-jump trajectories. The zero-jump trajectory dominates in the beginning but becomes less important for later times. This is easy to understand since in our simple system there are only two possible ways to reach the pure steady state  $|\uparrow\rangle$ : Either the initial state is already the dark state – then there is no jump necessary. Or the state differs from the dark state – then a single jump  $B$  is sufficient to reach  $|\uparrow\rangle$ . At the beginning the probability that this single jump already occurred is low; thus the zero-jump channel  $\mathcal{E}_0$  dominates this region. At later times the probability that the single jump occurred converges to 1 and consequently the one-jump channel  $\mathcal{E}_1$  contributes significantly.

If the steady state is mixed (which is the case for the remaining parameters) we cannot expect the jumps to cease at some finite time since the steady state is a true (classical) ensemble of quantum states. The system is therefore characterised by a  $t$ -dependent jump rate in  $\rho_{\text{NESS}}$ . So we expect  $\mathcal{E}_N(\tau)$  be important for times  $\tau$  after which one expects  $N$  jumps (on average) – which certainly depends on the  $t$ -dependent jump rate. This can be observed in the diagrams for  $N = 1, 2, 3$  where the maximum is shifted towards later times for increasing  $N$ . Furthermore note that the system with parameter  $t_5$  has a *nearly pure* steady state close to  $|\uparrow\rangle$ . The jump frequency is quite low which causes the large shift of the  $N = 2$  and  $N = 3$  channels to the right. The  $\mathcal{E}_0$  channel becomes unimportant for mixed steady states at late times since the probability that no jump occurred vanishes. Clearly this is not true for dark states where the bath decouples completely from the system once a dark state is reached.

- Consider the plots in the upper row of Fig. 1.3. The plots show the rescaled norm of  $\sum_{N=0}^{N_{\max}} \mathcal{E}_N(\tau) - \lim_{s \rightarrow \infty} e^{\mathcal{L}s}$ , namely  $\delta_{N_{\max}}[\rho_{\text{NESS}}](\tau)$ , in dependence of the time  $\tau$  for the same param-



■ **Figure 1.3:** Relative deviations of finite number jump trajectories from exact steady state solutions and dynamical states. In the upper row the normalised deviations  $\delta_{N_{\max}}[\rho_{\text{NESS}}]$  from the steady state are plotted for expansion with contributions of up to  $N_{\max} = 0, 1, 2, 3$  jumps over the time  $\tau$ . The evolutions are shown for five relative couplings  $(t_1, t_2, t_3, t_4, t_5) = (0, 0.25, 0.50, 0.75 - 0.05, 1.00 - 0.05)$ . Note that for the case  $t_1 = 0$  the steady state is the dark state  $|\uparrow\rangle$ . In this case the sum of zero- and one-jump trajectories is sufficient to end up at the steady state projector  $|\rho_{\text{NESS}}\rangle\rangle\langle\langle\mathbb{1}|$ . For the other couplings the steady state is mixed and thus finite jump trajectories approximate the steady state best in a time interval which is determined by the coupling strength  $t$ . Note that the minimum of  $\delta_{N_{\max}}[\rho_{\text{NESS}}]$  shifts to larger times  $\tau$  if more jumps are included. In the lower row the normalised deviations  $\delta_{N_{\max}}[\rho(\tau)]$  from the current state are plotted for the same expansions and parameters. For  $t_1$  the contributions of zero and one jumps are sufficient to get the full evolution operator  $\exp(\mathcal{L}\tau)$ . Depending on the purity of the current state, more jumps are needed to provide a reasonable approximation for  $\exp(\mathcal{L}\tau)$ .

eters as above. If the steady state is unique (as in our case), one can write  $\lim_{s \rightarrow \infty} e^{\mathcal{L}s} = |\rho_{\text{NESS}}\rangle\rangle\langle\langle\mathbb{1}|$  where  $|\rho_{\text{NESS}}\rangle\rangle\langle\langle\mathbb{1}|$  maps any initial state to the steady state  $|\rho_{\text{NESS}}\rangle\rangle$ . Therefore the plots quantify an approximation of the steady state superoperator  $|\rho_{\text{NESS}}\rangle\rangle\langle\langle\mathbb{1}|$  (which is a quantum channel) by partial sums of the fixed number channels  $\mathcal{E}_N(\tau)$  at finite times  $\tau$ . As expected, the dark state superoperator  $|\uparrow\rangle\rangle\langle\langle\uparrow|$  for  $t_1 = 0$  can be expressed exactly for  $\tau \rightarrow \infty$  in terms of zero- and one-jump channels. For mixed steady states an approximation by finite sums of channels  $\mathcal{E}_N(\tau)$  cannot be expected for  $\tau \rightarrow \infty$ . However, there is a chance of an intermediate time interval where, on the one hand, the number of jumps is low enough such that a finite partial sum of fixed number channels provides a reasonable approximation for  $\exp(\mathcal{L}\tau)$ , and, on the other hand, the time evolution is already close to the steady state  $|\rho_{\text{NESS}}\rangle\rangle\langle\langle\mathbb{1}|$ . Then one indeed ends up with an approximation for the steady state superoperator in terms of fixed number channels. These time intervals can be identified as pronounced minima in the plots. Note that the minima are smaller and occur later for larger  $N_{\max}$ .

- Consider the plots in the lower row of Fig. 1.3. The plots show the rescaled norm of  $\sum_{N=0}^{N_{\max}} \mathcal{E}_N(\tau) - e^{\mathcal{L}\tau}$ , namely  $\delta_{N_{\max}}[\rho(\tau)](\tau)$ , in dependence of the time  $\tau$  for the same parameters. For the parameter  $t_1 = 0$  with pure steady state the sum of  $\mathcal{E}_0(\tau)$  and  $\mathcal{E}_1(\tau)$  equals the time evolu-



tion superoperator  $\exp(\mathcal{L}\tau)$  for all times. This is due to the arguments we mounted in part (i). For mixed steady states with non-vanishing jump rate for all times the approximation with small numbers of fixed number channels is only valid at the beginning. At late times the contributions to  $\exp(\mathcal{L}\tau)$  are shifted towards channels with increasing numbers of jumps which manifests itself in the positive slope of the curves for parameters  $0 < t < 1$ .

We conclude that for generic cases (where the steady state is mixed) it is not possible to approximate either the time evolution superoperator or the steady state by finite sums of fixed number channels – although they occur as the canonical contributors in the Dyson series. However, for systems where the only steady states are dark states, finite sums *can be* sufficient if the number of concatenated jumps is bounded from above. We will see later that this not true in general, e.g. if jump operators generate free trajectories of charges. We note that there are ingenious resummation techniques for the quantum trajectory representation of Markovian quantum systems which lead to reasonable approximations for some systems, see Ref. [13] for details.

## 1.2 Quantum phases and phase transitions

In this section we present a brief outline of the wide field of quantum phases and phase transitions, as well as their extensions to dynamical phase transitions by driven dissipation. For further details I refer the reader to the given references and the two textbooks [14] by Sachdev and [15] by Wen.

### 1.2.1 Quantum phases in Hamiltonian systems

Quantum phases and phase transitions describe order phenomena at zero temperature that are purely quantum mechanical in origin. The critical fluctuations that are responsible for the phase transition are due to *quantum* fluctuations and not driven by *thermal* fluctuations as in the case of classical phase transitions.

The paradigmatic example for a quantum phase transition is the Ising model in a transverse magnetic field [14] with a symmetric paramagnetic phase for strong magnetic field and a symmetry-broken ferromagnetic phase for strong spin-spin couplings. See paragraph 1.3.4 for an analytical solution of the one-dimensional model by means of a Jordan-Wigner transformation and the additional remarks in Section 2.1 where we introduce our dissipative model.

The classification of quantum phases is closely related to the concept of *topological phases* and both a young and active field of research [16–21]. Introductions and comprehensible explanations for the concept of quantum phases can be found in [19, 22]. Let me sketch the basic idea: The classification comprises only *gapped* quantum phases which are characterised as ground states of gapped quasilocal Hamiltonians. As an example for a gapped quantum phase, consider the ground state manifold of Kitaev’s Majorana chain which is discussed in Subsec. 1.3.4. Then it is reasonable to introduce an equivalence relation on the set of all states of a given system that are ground states of some gapped Hamiltonian. Two *states* are termed equivalent if there is a smooth path in the space of *Hamiltonians* (think of varying parameters) such that (1) the Hamiltonians remain gapped along the path and (2) the two states correspond to the ground states at the *endpoints* of this path in the operator space. According to this definition the set of all gapped quantum phases separates into a union of disjoint equivalence classes. These classes are called *quantum phases*. The motivation for the above definition is the following: Quantum phase transitions of one gapped phase to another are indicated by a *vanishing* gap at the phase boundary. If two phases can *in principle* be connected by a deformation of their Hamiltonians without a vanishing gap, there are no *fundamental* differences between observables to be expected since there is no non-analytical behaviour present.

This is the *formal* definition — however, it is not a very handy one. To this end the authors of [22] show that the equivalence relation is closely related to the concept of *quasilocal unitary equivalence*. To cut the matter short: They apply facts known from quantum information theory to show that the definition above in terms of Hamiltonians can be probed by the existence of quantum circuits with constant depth. Meaning, there is an equivalent but operationally more convenient method to check whether two ground states belong to the same quantum phase or not. From this point of view, the classification of quantum phases becomes a classification of *long range entanglement*. To find representatives for each quantum phase, the technique of *quantum state renormalisation* [22–24] can be applied which drives the quantum state under scrutiny

towards a renormalisation fixed point (i.e. another quantum state) *in the same phase*. Two states that are driven towards the same fixed point belong to the same phase.

Note that the equivalence relation can be tightened by requiring the Hamiltonians to obey specific *symmetries*. If one allows only for Hamiltonian paths with prescribed symmetries, this restricts the set of possible paths and “fractionalises” the equivalence classes further.

Let us conclude this brief review of quantum phases by a definition of *topological phases*. As stated above, quantum phases are characterised by their pattern of long range entanglement. Phases that can be transformed to trivial, unentangled product states are termed *topologically trivial*. They do not feature patterns of long range entanglement that cannot be resolved by quasilocal unitary operations. *Topological phases* comprise all remaining phases, namely all phases that feature non-trivial long range entanglement that *cannot* be destroyed by quasilocal unitaries. If one inflicts additional symmetries on the classification, this yields the concept of *symmetry protected topological phases*. Such phases cannot be transformed to trivial product states by quasilocal unitaries *given* the latter obey the prescribed symmetries. For instance, fermionic systems require parity symmetry due to superselection (see paragraph 1.3.4); it is therefore reasonable to classify fermionic topological phases (such as the Majorana chain, see 1.3.4) with the additional constraint of parity symmetry.

### 1.2.2 Quantum phases in dissipatively driven systems

The above discussion related to *pure* quantum phases. At finite temperature  $T > 0$  the density matrix is in thermal equilibrium and given by  $\rho = \mathcal{Z}^{-1} \exp(-\beta H)$  with the partition function  $\mathcal{Z} = \text{Tr}[\exp(-\beta H)]$ . Classical phase transitions (driven by thermal fluctuations) can be triggered by variations of the (inverse) temperature  $\beta$  (in the thermodynamic limit). But there are other possibilities to drive phase transitions actively by Markovian environments which compete either with a given Hamiltonian dynamics or with other dissipative baths. The states  $\rho$  of such *dissipative* phases are generally mixed. However, these states are *not* in thermal equilibrium and one speaks of *non-equilibrium phase transitions*.

As of this writing, the field of dissipatively driven and dynamical phase transitions is an active area of research [12, 25–35]. In this thesis we contribute to this field by the introduction of a purely dissipative transverse field Ising model and a purely dissipative  $\mathbb{Z}_2$ -Gauge-Higgs model. We point out that dissipatively driven versions of the quantum Ising model have been scrutinised quite recently [12, 30]. However, to the best of my knowledge, our proposed jump operators (see Chapter 2) have not been considered before. Furthermore, we are not aware of any dissipative counterpart of a lattice gauge theory as introduced in Chapter 3.

This concludes our review of quantum phases and dissipatively driven phase transitions. Further references and remarks are given throughout the thesis — whenever they are required. The next section leaves the realm of pure condensed matter physics and approaches the interesting field of quantum information theory in general and quantum error correction in particular.

## 1.3 Topological quantum error correction

Quantum error correction is, as the term suggests, the quantum mechanical analogue of classical error correction techniques. One of the most crucial components for any computing machine is its memory; usually divided into volatile and non-volatile components. Classical computers use their Random Access Memory (RAM) as volatile and a hard disc drive (HDD) or solid state drive (SSD) as non-volatile components. Independent of the type, none of the mentioned memory devices would be usable if there was not a sophisticated machinery of error correction procedures running all the time to keep track of errors and launch countermeasures. The necessity for error correction is mainly caused by a noisy environment at finite temperatures. As quantum states are notoriously unstable in the presence of unknown interactions due to the environment and tend to decohere rapidly, the need for *quantum* error correction is at the heart of the whole endeavour to build a universal and scalable quantum computer. Without scalable quantum memories of high fidelity, there will be no full-fledged quantum computer.

### 1.3.1 Quantum error correction codes

The groundbreaking result by Peter Shor showed that quantum error correction is possible *in principle* [36]. The *Shor Code* provided a paradigmatic example how to store a logical qubit in the subspace  $\mathcal{C}$  (the *code space*) of a larger Hilbert space spanned by the states of several *physical* qubits. Today there is a variety of quantum codes that allow for the correction of arbitrary bit-flip ( $\sigma^x$ ) and phase errors ( $\sigma^z$ ). A mathematical framework that proved hugely useful for the work with and classification of quantum codes is the so called *stabiliser formalism*. We will use this framework now and then and I assume that the reader is familiar with its basic aspects. If not: detailed explanations can be found in [37] and a nice review of its application to quantum codes in the preliminaries of [38]. A comprehensive review of quantum codes and the stabiliser formalism is given in [39].

Ever since the invention of the Shor Code, new and more sophisticated concepts of quantum error correction were contrived. For instance, it was realised that there are quantum mechanical systems with subspaces in their Hilbert space that are *decoupled* from non-unitary interactions with the environment (that is, noise), so called *decoherence free subspaces* [40]. There is also research to exploit such subspaces for fault tolerant quantum operations [41].

A more general notion than encoding quantum information in *subspaces* of a Hilbert space is subsumed under the term *subsystem codes*. Subsystem codes encode quantum information in a subsystem Hilbert space  $\mathcal{C}$  where  $\mathcal{H} = (\mathcal{C} \otimes \mathcal{P}) \oplus \mathcal{E}$  is the full Hilbert space. A good explanation is given in the preliminaries of [42]. The stabiliser formalism can also be applied in this generalised notion if one introduces gauge degrees of freedom [43].

Although it is now a well established fact that stable quantum memories are possible *in theory*, it remains one of the most demanding fields of quantum engineering to actually tailor systems that can be controlled with a high fidelity; which usually is required for quantum error correction schemes that are based on active algorithms. This creates the impression that nature “tries to prevent” coherent quantum information from being stored reliably. This fragility inherent to quantum information spurred the investigation of various concepts that relate quantum memories to much more fundamental properties [44–47].

Another subdomain of quantum error correction is currently one of the most vibrant areas of research in the realm of quantum information theory and condensed matter physics; it may be tagged by the terms *self-correcting quantum memories* and *topological quantum memories* [38, 48–69]. Let us have a closer look at this fascinating concept to protect quantum information from decoherence.

### 1.3.2 Self-correcting and topological quantum memories

The central idea of *self-correcting quantum memories* is to encode the information in code spaces which can be realised as the ground state space of a Hamiltonian with logical operators that are energetically penalised by the latter. To put it in another way: One tries to merge the concepts of abstract quantum codes with the features of condensed matter systems to get rid of *active* quantum error correction schemes (which usually include complex measurement and correction processes). One aims at Hamiltonian theories that protect quantum information by simple, local interactions *without* active error correction.

Today it is believed that there is a close relation between the existence of topological order at finite temperatures and self-correcting quantum memories [54, 57]. Typical candidates for self-correcting quantum memories are systems with *topological ordered phases* [49–51, 60, 64–67] such as the toric code [70] that we discuss in the next paragraph. But there are also *topological phases* that yield potentially stable quantum memories due to their topological properties and additional symmetries. The paradigmatic example for a system with topologically protected code space is the Majorana wire [3] and generalisations thereof [52, 53]. We give a detailed discussion of the Majorana wire in the course of this section.

But even in the field of self-correcting systems, it remains notoriously hard to contrive Hamiltonians that retain both their topological order and their ability for error self-correction [48]. However, there are some promising results that suggest that topological order and self-correction may be realised in three dimensional systems [50, 64].

Instead of talking about some abstract concepts, let us review two simple but paradigmatic topological quantum memories: We start with the *toric code* that features a topologically ordered phase with an underlying string-net structure of its ground states. Subsequently we proceed with the *Majorana chain* as a prototypical example for a topological phase with a topologically (and symmetry) protected ground state space.

### 1.3.3 The Toric Code model

We start with *the* paradigmatic example of topological quantum error correction and topologically ordered phases, namely the Toric Code Model (TCM) as proposed by Kitaev in [70]. What follows is a brief outline of the important facts. For a more detailed discussion we refer the reader to the original proposal [70] or the review [51]. We do *not* deal with the toric code explicitly in this thesis. However, there are multiple references in context of the  $\mathbb{Z}_2$ -Gauge-Higgs model (see Section 1.4 and Chapter 3) and even in Appendix E. This short introduction provides the basis for these references. We assume that the reader is familiar with the stabiliser formalism, a comprehensible introduction of which can be found in [37].

Start with a two-dimensional square lattice with  $L \times L$  faces and periodic boundary conditions (that is, embedded into the torus). Attach a spin- $\frac{1}{2}$  to each edge  $e \in \mathbb{E}$  and define the system Hilbert space as  $\mathcal{H}_{\text{TCM}} \equiv \otimes_{e \in \mathbb{E}} \mathbb{C}_e^2$ . To define a quantum code space, we have to provide its stabilising operators.

For the toric code these read

$$A_s = \prod_{e \in s} \sigma_e^x \quad \text{and} \quad B_p = \prod_{e \in p} \sigma_e^z \quad (1.51)$$

where  $e \in s$  and  $e \in p$  denotes the edges  $e$  adjacent to site  $s$  or plaquette  $p$ .  $A_s$  and  $B_p$  are termed *star* and *plaquette* operators, respectively. Their non-trivial support is illustrated by the left plot in Fig. 1.4. It is easy to see that all star and plaquette operators commute and therefore they define a stabiliser group

$$\mathcal{S} := \text{span} \{A_s, B_p \mid s \in \mathcal{S}, p \in \mathcal{P}\} \quad (1.52)$$

which is an abelian subgroup of the Pauli group. Here  $\mathcal{S}$  and  $\mathcal{P}$  denotes the sets of sites and faces, respectively. The code space, that is, the *toric code*, is defined as the  $\mathcal{S}$ -invariant linear subspace

$$\mathcal{PS} := \{|\Psi\rangle \in \mathcal{H}_{\text{TCM}} \mid \mathcal{S}|\Psi\rangle = |\Psi\rangle\} \quad (1.53)$$

which is characterised by all states in  $\mathcal{H}_{\text{TCM}}$  that are invariant with respect to all star and plaquette operators. Stabiliser theory provides a simple method to determine the dimension of  $\mathcal{PS}$ : It holds  $\dim \mathcal{PS} = 2^{N-S}$  where  $N = 2L^2$  denotes the number of spins (i.e. number of edges) and  $S$  is the rank of the stabiliser group  $\mathcal{S}$ , that is, the number of independent generators. There are  $L^2$  star operators and  $L^2$  plaquette operators. However, the products of all star and plaquette operators read

$$\prod_{s \in \mathcal{S}} A_s = \mathbb{1} \quad \text{and} \quad \prod_{p \in \mathcal{P}} B_p = \mathbb{1}. \quad (1.54)$$

Hence there are only  $2L^2 - 2$  independent generators of  $\mathcal{S}$  which yields for its dimension  $\dim \mathcal{PS} = 2^{2L^2 - 2L^2 + 2} = 2^2 = 4$ . We conclude that the stabiliser subspace  $\mathcal{PS}$  encodes *two logical qubits*. The dimension of the code space is actually dependent on the *genus*  $g$  (the number of “holes”) of the compact and orientable 2-manifold on which the system lives. An application of EULER’S formula for graph embeddings yields a general dimension of  $\dim \mathcal{PS} = 2^{2g} = 4^g$ , meaning there are two logical qubits encoded per hole of the underlying manifold.

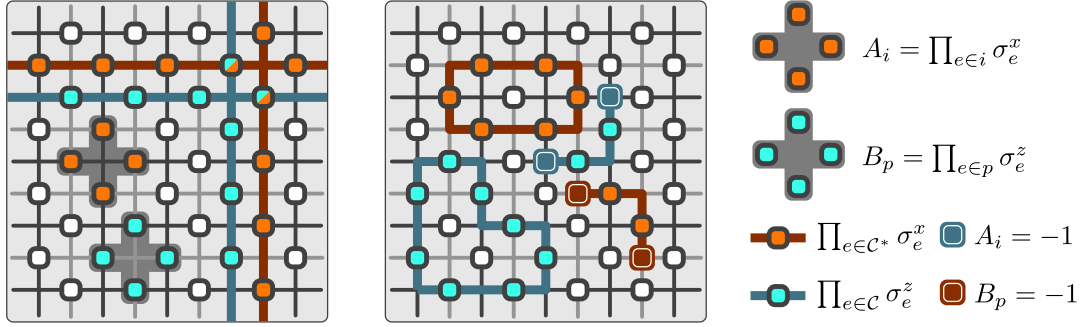
Let  $\mathcal{C}_{s,t}$  and  $\mathcal{C}'_{p,q}$  denote two paths on the lattice and the dual lattice with endpoints on sites  $s,t$  and plaquettes  $p,q$ , respectively. Then define the *string operators*

$$Z[\mathcal{C}_{s,t}] := \prod_{e \in \mathcal{C}_{s,t}} \sigma_e^x \quad \text{and} \quad X[\mathcal{C}'_{p,q}] := \prod_{e' \in \mathcal{C}'_{p,q}} \sigma_{e'}^z \quad (1.55)$$

where edges  $e$  and dual edges  $e'$  refer to the same spins, see Fig. 1.4. It is easy to see that all stabilisers commute with the strings *except* for their endpoints: Star operators anticommute with  $\sigma^z$ -endpoints on the lattice and plaquette operators anticommute with  $\sigma^x$ -endpoints on the dual lattice. This is illustrated on the centred lattice of Fig. 1.4. Note that *closed* string operators, termed *loop operators*, with loops that are *homologously trivial*<sup>3</sup> act trivially on the code space  $\mathcal{S}$  as they equal products of plaquettes (loops) and star operators (dual loops). Two such trivial loop operators are shown in Fig. 1.4 close to the open strings.

The question is now how one operates on the logical qubits stored in  $\mathcal{PS}$ . To this end consider the four closed but homologously *non-trivial* loops depicted on the left lattice of Fig. 1.4.

<sup>3</sup>A loop (dual loop) is homologously trivial if it is the boundary of a set of faces (dual faces).



■ **Figure 1.4:** Setup for the toric code as proposed by Kitaev. We show a two-dimensional square lattice with periodic boundary conditions. The dual lattice is illustrated by grey edges. Spins are attached to the edges. On the left-hand side we illustrate the action of the star  $A_s$  and plaquette operators  $B_p$  as described in the text (see the key to the right). The logical string operators are drawn with red and cyan lines. The crossing of corresponding logical operators which is responsible for their (anti)commutation relations is bicoloured. The centred lattice illustrates (1) topologically trivial loops of  $\sigma^x$  (red) and  $\sigma^z$  operators (cyan) that act trivially on the code space and (2) pairs of electric charges  $\blacksquare$  and magnetic vortices  $\blacksquare$  with possible (topologically hidden) strings connecting them.

Denote the vertical loop (dual loop) by  $\mathcal{C}_2$  ( $\mathcal{C}'_1$ ) and the horizontal loop (dual loop) by  $\mathcal{C}_1$  ( $\mathcal{C}'_2$ ). The corresponding loop operators are labeled as follows

$$X_i \equiv X[\mathcal{C}'_i] \quad \text{and} \quad Z_i \equiv Z[\mathcal{C}_i] \quad (1.56)$$

where  $i = 1, 2$ . It is easily seen that these operators obey the Pauli algebra of two qubits, that is

$$[Z_i, X_j] = 0, \quad \{Z_i, X_i\} = 0, \quad [X_i, X_j] = 0, \quad [Z_i, Z_j] = 0 \quad (1.57)$$

where  $i \neq j$ . The reason for the anticommutation relation between  $X$  and  $Z$  operators of the same index is the topologically unavoidable odd number of intersections of the corresponding string and dual string. These intersections are bicoloured in Fig. 1.4 (left lattice).

We are almost done. Recall that all star and plaquette operators together with two loop (dual loop) operators of the same type commute with each other. Consequently they can be diagonalised simultaneously with eigenvalues  $\pm 1$  since all operators are given as products of Pauli matrices. We chose an eigenbasis for the two  $Z$ -loop operators in the protected space  $\mathcal{PS}$  (which is the  $+1$ -eigenspace of all star and plaquette operators after all) and label them by the eigenvalues of  $Z_1$  and  $Z_2$ :  $|v_1, v_2\rangle$  with *topological quantum numbers*  $v_1, v_2 \in \{-1, +1\}$ . Due to the Pauli algebra of the four loop operators we immediately find

$$Z_j |v_1, v_2\rangle = v_j |v_1, v_2\rangle \quad \text{and} \quad X_1 |v_1, v_2\rangle = |-v_1, v_2\rangle, \quad X_2 |v_1, v_2\rangle = |v_1, -v_2\rangle. \quad (1.58)$$

We conclude that the *logical qubits* of the quantum code are labeled by topological quantum numbers  $v_1$  and  $v_2$  and the *non-local* loop operator algebra  $\text{span}\{X_1, X_2, Z_1, Z_2\}$  yields a four dimensional representation of the Pauli algebra on the code space

$$\mathcal{PS} = \text{span}\{|v_1, v_2\rangle \mid v_1, v_2 \in \{-1, +1\}\}. \quad (1.59)$$

This is a paradigmatic example for both a *topological code* and a *stabiliser code*. Note that logical operations require non-trivial operations on  $\mathcal{O}(L)$  physical spins and therefore are protected

against *local* and *uncorrelated* noise, at least in principle. Local  $\sigma^x$ -errors (bit-flip errors) and  $\sigma^z$ -errors (phase errors) correspond to open and closed string operators, depending on their distribution. As long as they do not form closed strings that wind around the torus, they cannot cause *logical errors*. Trivial closed strings are no errors at all as mentioned above. Open strings have endpoints that can be detected either by star or by plaquette operators. Such a measurement does not destroy the encoded quantum information and is called an *error syndrome*. The subsequent error correction uses minimum-weight perfect matching algorithms to *pair* the endpoints of strings (detected by stabilisers with eigenvalue  $-1$ ) with appropriately chosen string operators to form closed loops that map the state back to the protected code space  $\mathcal{PS}$ . A similar error correction scheme will be discussed in paragraph 1.3.4 for the Majorana chain.

To conclude this discussion of the toric code, let us introduce the Hamiltonian

$$H_{TCM} = -J_A \sum_{s \in S} A_s - J_B \sum_{p \in \mathbb{P}} B_p \quad (1.60)$$

with the parameters  $J_A, J_B \geq 0$ . This is a frustration free Hamiltonian with ground state space  $\mathcal{PS}$ . *The ground state space of  $H_{TCM}$  is a quantum code!* Elementary excitations correspond to single sites  $s$  with  $A_s = -1$  and faces  $p$  with  $B_p = -1$ . Their excitation energy is obviously  $2J_A$  and  $2J_B$ . In the above context this reads: The endpoints of error chains carry energetically penalised excitations of the toric code Hamiltonian  $H_{TCM}$ . Sites with  $A_s = -1$  are termed *electric charges* whereas faces with  $B_p = -1$  are called *magnetic vortices*. This bridges between the abstract quantum code that we introduced above and a condensed matter realisation as the ground state space of a gapped Hamiltonian. That the occurrence of errors is energetically penalised is the basic concept of *self-correcting quantum memories*. Unfortunately, the toric code does not penalise the *diffusion* of excitations. This leads to the conclusion that the toric code is completely unstable at *finite temperatures* in two spatial dimensions [71, 72]. A generalisation becomes partially stable in three dimensions [73] and the four-dimensional toric code is completely stable at finite temperatures [49]. In contrast, for finite *magnetic fields* the *topologically ordered phase* — which makes error correction possible — remains stable [74]. This aspect provides a link to lattice gauge theories, namely the  $\mathbb{Z}_2$ -Gauge-Higgs model that we discuss in Subsec. 1.4.2. Let us now finish this treatment of a topologically ordered phase and quantum memory and proceed with a *topological phase* which can also be used as a quantum memory, namely the *Majorana chain*.



### 1.3.4 The Majorana chain

Majorana fermions are well known to particle physicists as, for instance, neutrinos may be fermions of this type. However, their recurrent appearance in condensed matter physics made it seem more convenient to probe Majorana fermions in solid state setups than in high energy physics [75]. Their peculiar properties will become clear in the following.

Basic properties of the model

The Majorana chain was introduced by Kitaev in [3] as a toy model for unpaired Majorana modes in superconducting quantum wires and is arguably the simplest model with this properties. The Hamiltonian for the Majorana chain reads

$$H = - \sum_{i=1}^{L-1} \left[ w a_i^\dagger a_{i+1} - \Delta a_i a_{i+1} + \text{h.c.} \right] - \mu \sum_{i=1}^L \left( a_i^\dagger a_i - \frac{1}{2} \right) \quad (1.61)$$

with the chemical potential  $\mu \in \mathbb{R}$ , the hopping amplitude  $w \in \mathbb{R}$  and the superconducting gap  $\Delta = |\Delta|e^{i\theta} \in \mathbb{C}$ , where  $\theta \in [0, 2\pi)$  denotes the superconducting phase.  $a_i$  and  $a_i^\dagger$  are the usual fermionic annihilation and creation operators. The setup can be thought of as a linear chain of  $L$  fermionic sites as depicted in the upper part of Fig. 1.5. The Hamiltonian in Eq. (1.61) describes a system with open boundary conditions (OBC) as can be seen from the fact that the first sum runs from 1 to  $L - 1$ .

To analyse the Hamiltonian in Eq. (1.61) for certain parameter configurations it proves useful to write it in terms of so called *Majorana operators* or *modes*:

#### ► Definition 1.1: Majorana operators

Let  $\mathfrak{F}_L$  be the fermionic algebra generated by creation and annihilation operators  $\{a_i, a_i^\dagger \mid i = 1, \dots, L\}$  and characterised by the anticommutation relations

$$\{a_i, a_j\} = 0 = \{a_i^\dagger, a_j^\dagger\} \quad \text{and} \quad \{a_i, a_j^\dagger\} = \delta_{i,j} \quad \text{for all } i, j = 1, \dots, L. \quad (1.62)$$



Splitting the fermionic degrees of freedom into real and imaginary parts yields the **Majorana operators**

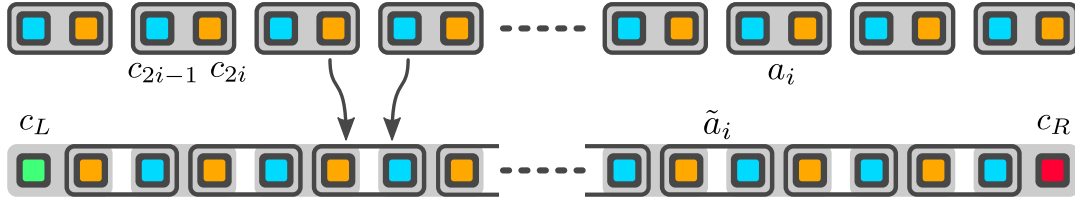
$$c_{2i-1} \equiv a_i + a_i^\dagger \quad \text{and} \quad c_{2i} \equiv i(a_i^\dagger - a_i) \quad \text{for } i = 1, \dots, L \quad (1.63)$$

which obey the CLIFFORD algebra

$$\{c_l, c_m\} = 2\delta_{l,m} \quad \text{for } l, m = 1, \dots, 2L \quad (1.64)$$

and are self-adjoint, i.e.  $c_l = c_l^\dagger$ .

We adopt the notation introduced in [3] for the sake of consistency. Note that by some authors the Majorana operators are denoted as  $\gamma_{L,i}$  and  $\gamma_{R,i}$  where the  $L$  refers to the *left-hand mode*  $c_{2i-1}$  of physical site  $i$  and  $R$  to the *right-hand mode*  $c_{2i}$ . In figure 1.5 the left and right hand modes are depicted as  and , respectively.



■ **Figure 1.5:** The Majorana chain as proposed by Kitaev in [3]. In the upper part the original chain with physical sites (grey rectangles) is shown. Each physical fermion, described by  $a_i$  and  $a_i^\dagger$ , can be split into two independent Majorana modes  $c_{2i-1}$  and  $c_{2i}$  denoted by  $\blacksquare$  and  $\blacksquare$ . At the distinct parameter combination  $|\Delta| = w$  and  $\mu = 0$  the Hamiltonian (1.61) reduces to (1.71) where the Majorana modes are regrouped to fermionic quasiparticles described by  $\tilde{a}_i$  and  $\tilde{a}_i^\dagger$ . Due to this regrouping the utter left and right Majorana modes  $c_L$  and  $c_R$ , denoted by  $\blacksquare$  and  $\blacksquare$ , remain unpaired. They correspond to a highly delocalised quasiparticle located at the ends of the wire.

The Majorana modes  $c_l$  are often termed *Majorana fermions* although they *do not* obey fermionic statistics but (non-abelian) *anyonic statistics* – which makes them potentially useful for topological quantum computation. However, we will use the terms “Majorana mode” and “Majorana fermion” synonymously and ask the reader to keep this subtlety in mind.

A distinctive feature is the fact that Majorana fermions are their own antiparticles since  $c_l = c_l^\dagger$  (which is more or less their defining property). Another point of view is that Majorana fermions (as defined above) constitute “half a fermion” as two of them can be recombined to form a purely fermionic mode

$$a_i = \frac{1}{2} (c_{2i-1} + ic_{2i}) \quad \text{and} \quad a_i^\dagger = \frac{1}{2} (c_{2i-1} - ic_{2i}). \quad (1.65)$$

Note the resemblance of this procedure to the decomposition of complex numbers into real and imaginary parts. Therefore Majorana modes may be considered as real ( $c_{2i-1}$ ) and imaginary ( $c_{2i}$ ) parts of fermions. The reality condition on real and imaginary parts corresponds in this case to the Majorana condition  $c_l = c_l^\dagger$ .

It is now straightforward to recast Eq. (1.61) in terms of Majorana modes. However, to get rid of any complex coefficients in the Hamiltonian (namely the superconducting gap  $\Delta = |\Delta|e^{i\theta} \in \mathbb{C}$ ) it is useful to perform a simple unitary transformation of the fermionic modes

$$a_j \longrightarrow \hat{a}_j = e^{i\theta/2} a_j \quad \text{and} \quad a_j^\dagger \longrightarrow \hat{a}_j^\dagger = e^{-i\theta/2} a_j^\dagger. \quad (1.66)$$

Note that on the level of the Fock space (which is a *module* or *representation* of the fermionic and Majorana algebra) this corresponds to a unitary transformation of the number state basis where each number state is multiplied by a phase factor depending on its occupancy. Physically nothing interesting happened up to this point – we just changed the basis of the underlying Fock space.

In this new basis the Hamiltonian reads

$$H = - \sum_{i=1}^{L-1} \left[ w \hat{a}_i^\dagger \hat{a}_{i+1} - |\Delta| \hat{a}_i \hat{a}_{i+1} + \text{h.c.} \right] - \mu \sum_{i=1}^L \left( \hat{a}_i^\dagger \hat{a}_i - \frac{1}{2} \right) \quad (1.67)$$

where we got rid of the complex phase of the superconducting gap. For the sake of simplicity we do not write the hat in the following, i.e.  $\hat{a}_i \rightarrow a_i$ .

Inserting the Majorana operators as defined in Def. 1.1 yields

$$H = \frac{i}{2} \sum_{i=1}^{L-1} [(|\Delta| + w)c_{2i}c_{2i+1} + (|\Delta| - w)c_{2i-1}c_{2i+2}] - \mu \frac{i}{2} \sum_{i=1}^L c_{2i-1}c_{2i} \quad (1.68)$$

where the left most mode is  $c_{2 \cdot 1 - 1} = c_1 = c_L$  and the right most mode is  $c_{2 \cdot (L-1) + 2} = c_{2L} = c_R$ , denoted by ■ and ■ in Fig. 1.5.

There are two special cases which correspond to perfect pairings of Majorana modes, as shown in Fig. 1.5:

►  $w = 0 = |\Delta|$  and  $\mu < 0$

In this case the Hamiltonian reads

$$H = -\mu \frac{i}{2} \sum_{i=1}^L c_{2i-1}c_{2i} = -\mu \sum_{i=1}^L \left( a_i^\dagger a_i - \frac{1}{2} \right) \quad (1.69)$$

where we used the relation

$$n_i \equiv a_i^\dagger a_i = \frac{1}{2} (1 + ic_{2i-1}c_{2i}) \quad (1.70)$$

for the number operator  $n_i$ . The elementary excitations therefore are just original fermions  $a_i^\dagger$  on the *physical* site  $i$ , i.e. the Majorana modes are paired on physical sites as shown in the upper part of Fig. 1.5. Thus there are no non-local elementary excitations – each fermion is located on a single physical site. ◀

►  $w = |\Delta| > 0$  and  $\mu = 0$

This is the most interesting case, and we will shortly see why. Now the Hamiltonian takes the form

$$H = (|\Delta| + w) \frac{i}{2} \sum_{i=1}^{L-1} c_{2i}c_{2i+1} = iw \sum_{i=1}^{L-1} c_{2i}c_{2i+1} \quad (1.71)$$

where it is important to realise that  $c_{2i}$  and  $c_{2i+1}$  belong to *different* physical sites (namely,  $i$  and  $i + 1$ ). We already realised that one can re-pair Majorana modes to “full-fledged fermions”. From a purely algebraic point of view, there is *no difference* between, say,  $c_{2i}$  and  $c_{2j}$  or  $c_{2i-1}$  and  $c_{2j}$ . Therefore we can pair *any* two Majorana modes to get a valid fermionic mode. However, in most of the cases the resulting fermions (called *quasiparticles* since they do not correspond to physical fermions) are highly delocalised with respect to the spatial meta-structure of the Fock space (which stemmed from the original physical fermionic modes).

Nonetheless there is a straightforward way to create fermionic quasiparticles that remain (up to one exception) quasilocal:

$$\tilde{a}_i \equiv \frac{1}{2} (c_{2i} + ic_{2i+1}) \quad \text{and} \quad \tilde{a}_i^\dagger \equiv \frac{1}{2} (c_{2i} - ic_{2i+1}) . \quad (1.72)$$

It is straightforward to show that  $\tilde{a}_i$  and  $\tilde{a}_i^\dagger$  obey a fermionic algebra and thus represent valid fermionic modes. To see that they do not correspond to physical fermions rewrite them in the original fermion operators by inserting the definitions of the Majorana operators:

$$\tilde{a}_i = \frac{i}{2} \left( a_i^\dagger - a_i + a_{i+1} + a_{i+1}^\dagger \right) \quad \text{and} \quad \tilde{a}_i^\dagger = \frac{i}{2} \left( a_i^\dagger - a_i - a_{i+1}^\dagger - a_{i+1} \right) \quad (1.73)$$

So the new quasiparticles correspond to quasilocal superpositions of physical fermions. It is now easy to show that

$$\tilde{n}_i \equiv \tilde{a}_i^\dagger \tilde{a}_i = \frac{1}{2} (\mathbb{1} + ic_{2i}c_{2i+1}) \quad (1.74)$$

and consequently we find for the Hamiltonian in the new quasiparticle basis

$$H = 2w \sum_{i=1}^{L-1} \left( \tilde{a}_i^\dagger \tilde{a}_i - \frac{1}{2} \right). \quad (1.75)$$

That is, in this parameter regime the elementary excitations are no longer physical fermions but quasiparticles which are localised “between” two physical sites. This situation is depicted in the lower part of Fig. 1.5. However, there is a crucial difference between Eq. (1.75) and Eq. (1.69): In the quasiparticle Hamiltonian only  $L - 1$  fermionic degrees of freedom show up whereas in the other case all  $L$  fermionic degrees of freedom are part of the Hamiltonian.

Clearly, in Eq. (1.75) the fermionic mode

$$b \equiv \tilde{a}_L = \frac{1}{2} (c_{2L} + ic_1) = \frac{1}{2} (c_R + ic_L) \quad (1.76)$$

is missing. It is formed out of the two remaining unpaired Majorana modes at the endpoints of the chain, denoted by ■ and ■ in Fig. 1.5. If we imposed periodic boundary conditions (PBC), this would just be another local quasiparticle. But due to the open boundary conditions, this fermionic mode represents a macroscopically delocalised fermion. One “half” sitting on the left boundary, the other “half” on the right boundary of the wire. Since this mode is not probed by the Hamiltonian in Eq. (1.75), its ground state space is two-fold degenerate

$$|\tilde{0}\rangle = \prod_{i=1}^L \tilde{a}_i |0\rangle \quad \text{and} \quad |\tilde{1}\rangle = b^\dagger |\tilde{0}\rangle \quad (1.77)$$

where  $|\tilde{1}\rangle$  and  $|\tilde{0}\rangle$  denote the ground states<sup>4</sup> with and without occupied boundary mode  $b$ . ◀

Exact solution for OBC: Diagonalisation of the Hamiltonian

We aim at an exact diagonalisation of the Hamiltonian in Eq. (1.61) for arbitrary values of  $\omega$ ,  $\Delta$  and  $\mu$ .

<sup>4</sup>Note that the *quasiparticle vacuum*  $|\tilde{0}\rangle$  (defined by  $\tilde{a}_i |\tilde{0}\rangle = 0$  for all  $i = 1, \dots, L$ ) is not the same as the *physical vacuum*  $|0\rangle$  (defined by  $a_i |0\rangle = 0$  for all  $i = 1, \dots, L$ ). They do not even have the same parity!

### ■ General treatment

To this end, we start with a general treatment of quadratic fermionic Hamiltonians of the most generic form (up to some constant)

$$H = \sum_{i,j=1}^L \left[ a_i^\dagger A_{ij} a_j + \frac{1}{2} (a_i^\dagger B_{ij} a_j^\dagger + \text{h.c.}) \right] \quad (1.78)$$

where  $A_{ij} \in \mathbb{C}$  is an element of the Hermitian matrix  $A$  and  $B_{ij} \in \mathbb{C}$  of the skew-symmetric matrix  $B$ , that is

$$\bar{A}_{ij} = A_{ji} \quad \text{and} \quad B_{ij} = -B_{ji} \quad (1.79)$$

which is necessary<sup>5</sup> to be consistent with the fermionic algebra of  $a_i$  and  $a_i^\dagger$ . Now express the fermionic operators in real Majorana modes, i.e.

$$H = \frac{1}{4} \sum_{i,j=1}^L \left[ (c_{2i-1} - ic_{2i}) A_{ij} (c_{2j-1} + ic_{2j}) + \frac{1}{2} ((c_{2i-1} - ic_{2i}) B_{ij} (c_{2j-1} - ic_{2j}) + \text{h.c.}) \right] \quad (1.80)$$

and regroup the Majorana modes so that (dropping constants)

$$H = \frac{i}{4} \sum_{l,m=1}^{2L} c_l \Lambda_{lm} c_m = \frac{i}{4} \mathbf{c}^\dagger \mathbf{\Lambda} \mathbf{c} \quad (1.81)$$

where  $\mathbf{c} = [c_1, c_2, \dots, c_{2L}]^T$  is a column vector of Majorana modes. Hermiticity of  $H$  demands that  $\mathbf{\Lambda}$  is a real, skew-symmetric matrix, i.e.  $\Lambda_{lm} = -\Lambda_{ml}$  and  $\bar{\Lambda}_{lm} = \Lambda_{ml}$ . Now recall the following statement from basic linear algebra:

#### ► Lemma 1.1: Spectral theory of skew-symmetric matrices

Let  $\mathbf{\Lambda} \in \mathbb{R}^{2L \times 2L}$  be a real,  $2L$  by  $2L$  skew-symmetric matrix. Then there is a real, orthogonal matrix  $\mathbf{\Xi} = [\boldsymbol{\zeta}_1, \dots, \boldsymbol{\zeta}_{2L}]^T \in \mathbb{R}^{2L \times 2L}$  such that

$$\mathbf{\Xi} \mathbf{\Lambda} \mathbf{\Xi}^T = \mathbf{\Gamma} = \begin{bmatrix} \varepsilon_1 & \mathbf{0} & \cdots & \mathbf{0} \\ \mathbf{0} & \varepsilon_2 & \cdots & \mathbf{0} \\ \vdots & \vdots & \ddots & \vdots \\ \mathbf{0} & \mathbf{0} & \cdots & \varepsilon_L \end{bmatrix} \quad (1.82)$$

where  $\mathbf{0}$  is the  $2 \times 2$  zero matrix and

$$\varepsilon_i = \begin{bmatrix} 0 & \varepsilon_i \\ -\varepsilon_i & 0 \end{bmatrix} \quad (1.83)$$

is a real ( $\varepsilon_i \in \mathbb{R}$ )  $2 \times 2$  block matrix. The eigenvalues are purely imaginary and given by  $\pm i\varepsilon_j$  for  $j = 1, \dots, L$ .

*Proof.* See any basic linear algebra textbook. ■

<sup>5</sup>Actually, the requirement for  $B$  is not *necessary* since any symmetric part of  $B$  would just drop out.

So let us apply this transformation to our Hamiltonian

$$H = \frac{i}{4} \mathbf{c}^\dagger \Xi^T \Xi \Lambda \Xi^T \Xi \mathbf{c} = \frac{i}{4} \mathbf{d}^\dagger \Gamma \mathbf{d} \quad (1.84)$$

where we introduced new Majorana operators  $\mathbf{d} = \Xi \mathbf{c}$ . Indeed, we find

$$d_i = \Xi_{ij} c_j \quad \Rightarrow \quad d_i^\dagger = \Xi_{ij} c_j^\dagger = \Xi_{ij} c_j = d_i \quad (1.85)$$

$$\Rightarrow \quad \{d_i, d_j\} = \Xi_{il} \Xi_{jm} \{c_l, c_m\} = 2\Xi_{il} \Xi_{jm} \delta_{lm} = 2\Xi_{im} \Xi_{jm} = 2\delta_{ij} \quad (1.86)$$

where we used Einstein's convention and the fact that  $\Xi$  is real and orthogonal. Due to the block diagonal form of  $\Gamma$  the Hamiltonian expands to

$$H = \frac{i}{4} \mathbf{d}^\dagger \Gamma \mathbf{d} = \frac{i}{4} \sum_{i=1}^L \varepsilon_i [d_{2i-1} d_{2i} - d_{2i} d_{2i-1}] = \frac{i}{2} \sum_{i=1}^L \varepsilon_i d_{2i-1} d_{2i} \quad (1.87)$$

and if we introduce the new fermionic quasiparticles

$$\tilde{a}_j \equiv \frac{1}{2} (d_{2j-1} + i d_{2j}) \quad \text{and} \quad \tilde{a}_j^\dagger \equiv \frac{1}{2} (d_{2j-1} - i d_{2j}) \quad (1.88)$$

and use the relation  $\tilde{a}_i^\dagger \tilde{a}_i = \frac{1}{2} (\mathbb{1} + i d_{2i-1} d_{2i})$  we finally end up with

$$H = \frac{i}{2} \sum_{i=1}^L \varepsilon_i d_{2i-1} d_{2i} = \sum_{i=1}^L \varepsilon_i \left( \tilde{a}_i^\dagger \tilde{a}_i - \frac{1}{2} \right). \quad (1.89)$$

Finally, we are lead to the question how to get by the transformation matrix  $\Xi$ . As introduced above the columns of  $\Xi^T$  are real vectors  $\xi_l$  of size  $2L$ . Clearly these are *no* eigenvectors of  $\Lambda$ . However, they are closely related to the latter via

$$\xi_{2i-1} = \frac{1}{2} (\Phi_i + \Psi_i) \quad (1.90)$$

$$\xi_{2i} = \frac{1}{2i} (\Phi_i - \Psi_i) \quad (1.91)$$

where  $\Lambda \Phi_i = i\varepsilon_i \Phi_i$  and  $\Lambda \Psi_i = -i\varepsilon_i \Psi_i$  are the eigenvectors of  $\Lambda$ . Conversely we find

$$\Phi_i = \xi_{2i-1} + i\xi_{2i} \quad (1.92)$$

$$\Psi_i = \xi_{2i-1} - i\xi_{2i} \quad (1.93)$$

which is nothing else than the coordinate version of Eq. (1.65). In this sense the  $\xi_l$  correspond to Majorana modes whereas  $\Psi_i$  corresponds to fermionic holes ( $\tilde{a}_i$ ) and  $\Phi_i$  to the fermions themselves ( $\tilde{a}_i^\dagger$ ). Note that  $\xi_l \in \mathbb{R}^{2L}$  but  $\Psi_i, \Phi_i \in \mathbb{C}^{2L}$ . The relations above can be proved easily

$$\Lambda \Phi_i = \Xi^T \Xi \Lambda \Xi^T \Xi \Phi_i = \Xi^T \Gamma (e_{2i-1} + i e_{2i}) = i\varepsilon_i \Xi^T (e_{2i-1} + i e_{2i}) = i\varepsilon_i (\xi_{2i-1} + i\xi_{2i}) = i\varepsilon_i \Phi_i$$

where  $e_l$  denotes the  $l$ th standard basis vector.

In the end we find the following expressions for the new quasiparticles in Majorana representation

$$\tilde{a}_i^\dagger = \frac{1}{2} \mathbf{\Psi}_i^T \mathbf{c}, \quad \tilde{a}_i = \frac{1}{2} \mathbf{\Phi}_i^T \mathbf{c} \quad \text{and} \quad d_l = \boldsymbol{\zeta}_l^T \mathbf{c}. \quad (1.94)$$

Let us now express the modes in the original (physical) fermionic degrees of freedom. To this end, recall that  $c_{2i-1} = a_i + a_i^\dagger$  and  $c_{2i} = i(a_i^\dagger - a_i)$ . Therefore

$$\begin{aligned} \tilde{a}_i^\dagger &= \frac{1}{2} \mathbf{\Psi}_i^T \mathbf{c} \\ &= \frac{1}{2} \left[ \Psi_i^{2j-1} c_{2j-1} + \Psi_i^{2j} c_{2j} \right] \\ &= \frac{1}{2} \left[ \Psi_i^{2j-1} (a_j + a_j^\dagger) + i \Psi_i^{2j} (a_j^\dagger - a_j) \right] \\ &= \frac{1}{2} \left[ \Psi_i^{2j-1} - i \Psi_i^{2j} \right] a_j + \frac{1}{2} \left[ \Psi_i^{2j-1} + i \Psi_i^{2j} \right] a_j^\dagger \\ &= \eta_{i,j}^- a_j + \eta_{i,j}^+ a_j^\dagger \end{aligned}$$

where we introduced the new matrices

$$\eta_{i,j}^- \equiv \frac{1}{2} \left[ \Psi_i^{2j-1} - i \Psi_i^{2j} \right] \quad \text{and} \quad \eta_{i,j}^+ \equiv \frac{1}{2} \left[ \Psi_i^{2j-1} + i \Psi_i^{2j} \right] \quad (1.95)$$

that describe the quasiparticles in terms of physical fermions. To get a feeling for the new quasiparticles, let us plot the probability of finding a *physical* fermion (hole) on site  $l$  provided the  $i$ th quasiparticle is present in the system. That is, we calculate

$$\langle 0 | \tilde{a}_i a_l^\dagger a_l \tilde{a}_i^\dagger | 0 \rangle = \langle 0 | \left( \bar{\eta}_{i,j}^- a_j^\dagger + \bar{\eta}_{i,j}^+ a_j \right) a_l^\dagger a_l \left( \eta_{i,k}^- a_k + \eta_{i,k}^+ a_k^\dagger \right) | 0 \rangle = \bar{\eta}_{i,j}^+ \eta_{i,k}^+ \langle 0 | a_j a_l^\dagger a_l a_k^\dagger | 0 \rangle = \left| \eta_{i,l}^+ \right|^2.$$

for fermions and

$$\langle L | \tilde{a}_i a_l a_l^\dagger \tilde{a}_i^\dagger | L \rangle = \langle L | \left( \bar{\eta}_{i,j}^- a_j^\dagger + \bar{\eta}_{i,j}^+ a_j \right) a_l a_l^\dagger \left( \eta_{i,k}^- a_k + \eta_{i,k}^+ a_k^\dagger \right) | L \rangle = \bar{\eta}_{i,j}^- \eta_{i,k}^- \langle L | a_j^\dagger a_l a_l^\dagger a_k | L \rangle = \left| \eta_{i,l}^- \right|^2.$$

for holes. Here  $|0\rangle$  denotes the physical vacuum and  $|L\rangle = |1, \dots, 1\rangle$  the completely filled state.

To point out the central result:

### ► Result 1.1: Quasiparticles

The distribution of physical fermions (holes) of the  $i$ th quasiparticle is given by

$$\text{Fermions:} \quad \left| \eta_{i,l}^+ \right|^2 = \frac{1}{4} \left| \Psi_i^{2l-1} + i \Psi_i^{2l} \right|^2 \quad (1.96)$$

$$\text{Holes:} \quad \left| \eta_{i,l}^- \right|^2 = \frac{1}{4} \left| \Psi_i^{2l-1} - i \Psi_i^{2l} \right|^2 \quad (1.97)$$

where  $l$  runs over all physical sites  $l = 1, \dots, L$ .

This concludes our general treatment. ■

### ■ Application to the Majorana chain

Let us now apply our findings of the previous paragraph to the Majorana chain. To this end, recall the Hamiltonian in Majorana representation:

$$H = \frac{i}{2} \sum_{i=1}^{L-1} [(|\Delta| + w)c_{2i}c_{2i+1} + (|\Delta| - w)c_{2i-1}c_{2i+2}] - \mu \frac{i}{2} \sum_{i=1}^L c_{2i-1}c_{2i} \quad (1.98)$$

So here the  $\Lambda$ -matrix reads

$$\Lambda_{l,m} = \begin{cases} |\Delta| + w & \text{for } l = 2i \wedge m = 2i + 1 \\ -|\Delta| - w & \text{for } m = 2i \wedge l = 2i + 1 \\ |\Delta| - w & \text{for } l = 2i - 1 \wedge m = 2i + 2 \\ -|\Delta| + w & \text{for } m = 2i - 1 \wedge l = 2i + 2 \\ -\mu & \text{for } l = 2j - 1 \wedge m = 2j \\ \mu & \text{for } m = 2j - 1 \wedge l = 2j \\ 0 & \text{otherwise} \end{cases} \quad (1.99)$$

where  $i = 1, \dots, L - 1$  and  $j = 1, \dots, L$ . Note that we chose the matrix *skew-symmetric*, which is always possible and necessary for our former calculations to apply.

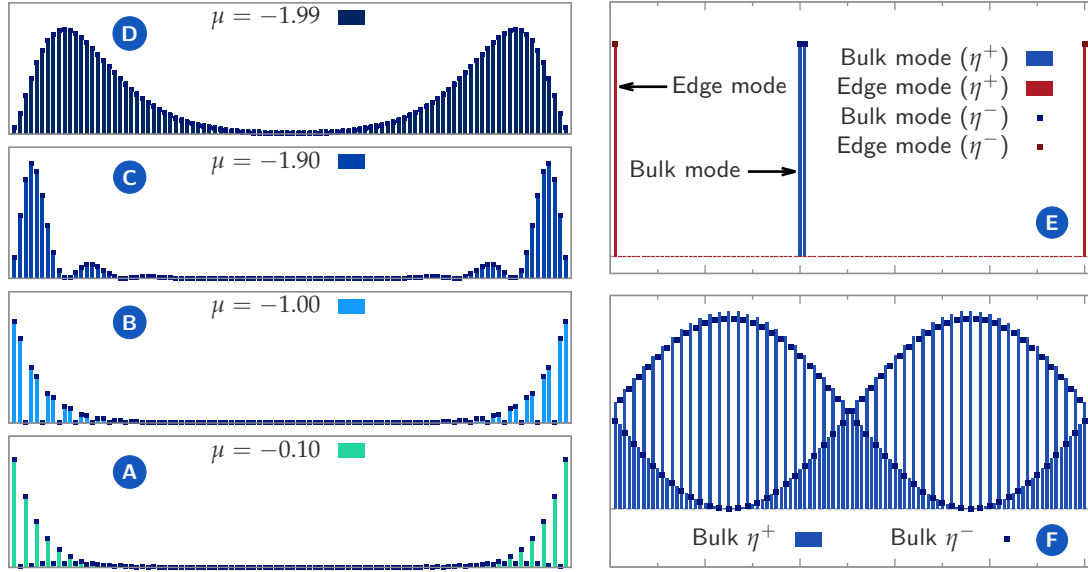
This matrix can easily be implemented by means of a CAS such as `Mathematica`. Diagonalisation yields the spectrum  $\varepsilon_i$  as well as the eigenvectors  $\Psi_i$  and  $\Phi_i$ . There are some points worth mentioning:

#### ► Localisation of Majorana modes

In Fig. 1.6 we illustrate the fermion density  $|\eta_{i,l}^+|^2$  (bars) and the hole density  $|\eta_{i,l}^-|^2$  (points) as a function of site  $l$  for some characteristic modes  $i$  and a chain with  $L = 100$  sites. At the ideal point  $\Delta = \omega$  and  $\mu = 0$  the fermionic quasiparticles are localised on the lattice of physical fermions and each bulk mode  $\tilde{a}_i$ ,  $i = 1, \dots, L - 1$ , occupies *two* physical sites, this can be seen in plot (E). The edge mode  $\tilde{a}_L$  however is macroscopically delocalised between the two endpoints of the chain, see also (E).

Away from the critical point, this “splitting” of a physical fermion into one “half” fermion at the leftmost and the other “half” at the rightmost site becomes less clear as the sequence of plots (A)-(D) illustrates. There we set  $\Delta = 0.1$  and  $\omega = 1$  and vary the chemical potential from  $\mu = -0.1$  (A) to  $\mu = -1.99$  (B); please note that the topological phase transition occurs at  $\mu = 2$  since  $\omega = 1$ . We observe that the formerly localised boundary modes leak into the bulk the stronger the chemical potential gets. As we will see below, this lifts the degeneracy of states with and without occupied edge mode as the leftmost and rightmost Majoranas interact (in finite systems). In contrast to the ideal point  $\Delta = \omega$  and  $\mu = 0$  were the bulk modes are strictly localised (E), a slight deviation of the chemical potential results in strongly delocalised bulk modes, as can be seen in (F) were we show a characteristic mode for  $\Delta = 1 = \omega$  and  $\mu = 0.1$ .



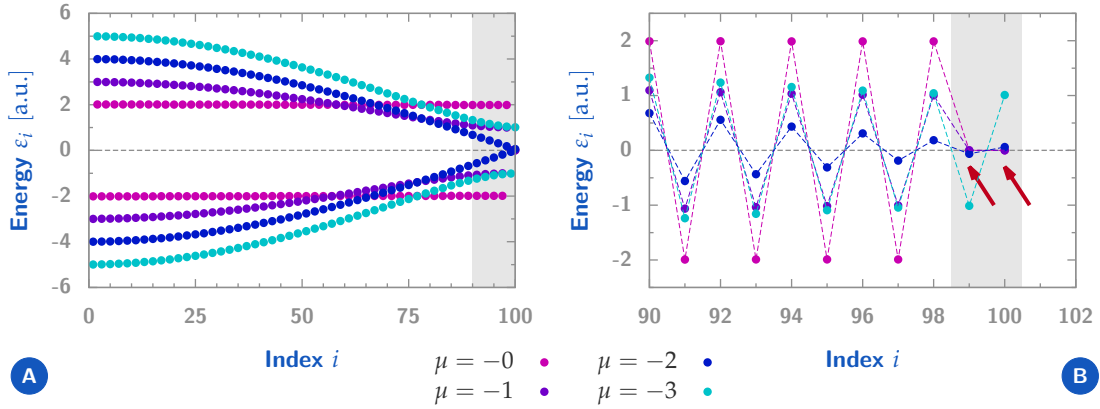


■ **Figure 1.6:** We show spatial distributions of fermion ( $|\eta_{i,l}^+|^2$ , denoted by bars) and hole densities ( $|\eta_{i,l}^-|^2$ , denoted by points) for some characteristic modes  $i$  and a Majorana chain with  $L = 100$  sites. The horizontal axes represent the spatial extension of the chain for  $l = 1, 2, \dots, 100$ . (A)-(D) illustrate the edge mode for fixed gap  $\Delta = 0.1$  and tunneling amplitude  $\omega = 1$  and varying chemical potential  $\mu$ . At the ideal point  $\Delta = \omega$  and  $\mu = 0$  all bulk modes are localised on two adjacent *physical* fermionic sites. Only the edge mode corresponds to a physical fermion which is macroscopically delocalised between the two endpoints of the chain, see (E). For increasing chemical potential  $|\mu|$ , the localised edge mode (E) starts leaking into the bulk of the chain, see (A)-(D). In contrast to the localised modes at the ideal point (E) for  $\mu = 0$ , typical bulk modes for  $\mu = 0.1$  look like (F).

### ► Spectrum of Majorana modes

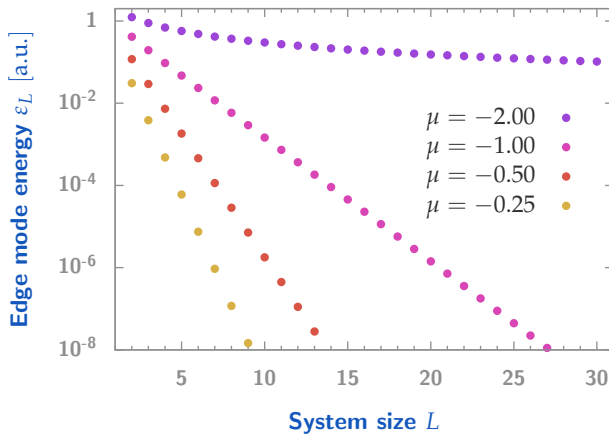
In Fig. 1.7 we show the spectrum of a Majorana chain with  $L = 50$  sites, that is the spectrum of the corresponding matrix  $\Lambda$ . More precisely, the imaginary part of its spectrum; which is purely imaginary as we pointed out earlier. The double structure of the spectrum is related to the skew-symmetry of  $\Lambda$  which implies that there are  $L$  pairs of eigenvalues  $\pm i\varepsilon_k$ ,  $k = 1, \dots, L$ . The eigenvalues are indexed by  $i$  with decreasing absolute values where  $i$  runs from 1 to  $2L = 100$ . This gives rise to the characteristic double spectrum in (A). The spectra shown were computed for  $\Delta = 1 = \omega$  and varying chemical potential  $\mu = 0, -1, -2, -3$ . The highlighted region in (A) is shown in (B) to emphasise the zero modes marked by red arrows. Away from the topological phase transition at  $|\mu| = 2$  the spectrum is gapped. For  $|\mu| \rightarrow 2$  the gap closes — a typical feature of a quantum phase transition. As (B) reveals, there are two Majorana modes with zero energy in the (topological) phase for  $|\mu| < 2$ . Both of them gain finite energy in the (trivial) phase for  $|\mu| > 2$ . We conclude that in the topological phase the fermionic boundary mode  $\tilde{a}_L$  (which is constructed from the *two* Majorana zero modes) is not penalised by the Hamiltonian. The ground state is two-fold degenerate: The boundary mode may be occupied or unoccupied. This is no longer true in the trivial phase where there is no fermionic zero mode and the ground state is the unique quasiparticle vacuum.

If one examines the two highlighted “zero” modes in Fig. 1.7 (B) in detail, it turns out that their energy is not *exact* zero. This is only true in the thermodynamic limit as Fig. 1.8 reveals:

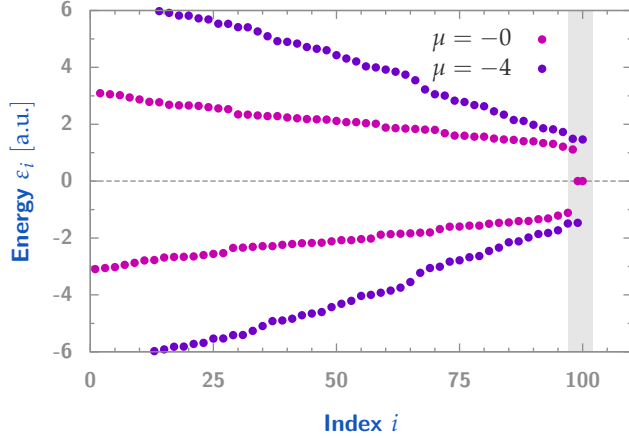


■ **Figure 1.7:** We show the spectrum of a Majorana chain with  $L = 50$  sites for fixed parameters  $\Delta = 1 = \omega$  and varying chemical potential  $\mu$ . Details of the grey region in (A) are illustrated in (B). Please note that the spectrum is gapped away from the topological phase transition at  $\mu = 2$ . As (B) reveals, there are two zero energy modes in the topological phase  $|\mu| < 2$ . These modes are no longer zero energy modes in the trivial phase for  $|\mu| > 2$ . In the topological phase, the shown degeneracy is resilient with respect to spatially varying parameters, see Fig. 1.9.

There we plot the minimum of the absolute values  $\{\varepsilon_i\}$  (which is the zero mode energy) as a function of the system size  $L$  for varying chemical potentials  $\mu = -0.25, -0.50, -1, -2$ . In the topological phase ( $|\mu| < 2$ ), the zero mode energy vanishes exponentially with  $L$ . This decrease becomes slower the closer the system is to the phase transition at  $|\mu| = 2$ . In the trivial phase for  $|\mu| > 2$  the energy no longer goes to zero as there are no zero modes left. This finite energy lifts the degeneracy of the occupied and unoccupied edge mode in *finite systems* and away from the ideal point. It is caused by the aforementioned interaction of the two delocalised Majorana modes which manifests in the leakage of the modes into the bulk as observed in Fig. 1.6 (A)-(D). It becomes clear from the fermion density distribution in (A) that the overlap between leftmost and rightmost Majorana mode is already negligible for the shown  $L = 100$  chain and vanishes in the thermodynamic limit  $L \rightarrow \infty$  completely. Therefore the two edge Majorana modes are usually referred to as *Majorana zero modes* even though the system is not exactly degenerate for finite chains (away from the ideal point).



■ **Figure 1.8:** We show the ground state energy of the Majorana edge modes for fixed parameters  $\Delta = 1 = \omega$  and varying chemical potential  $\mu$  with respect to the system size  $L$ . In the topological phase for  $\mu < 2$ , the edge mode energy vanishes exponentially with the system size. This changes at the topological phase transition  $\mu = 2$  beyond which these modes no longer have zero energy. The non-vanishing energy for *finite systems* at *non-ideal* parameter points  $\mu \neq 0$  is a consequence of the overlap (and thus interaction) of the two left and right boundary Majorana modes, see Fig. 1.6 (A)-(D).



■ **Figure 1.9:** We show the spectrum of a Majorana chain with  $L = 50$  sites for static disorder and varying chemical potential  $\mu$ . Here the parameters are chosen site-dependent, that is  $\Delta_l = \Delta + p_l^\Delta \cdot \delta\Delta$  (analogously for  $\omega$  and  $\mu$ ) where  $p_l^{\Delta,\omega,\mu}$  is a uniformly distributed random variate in  $\mathcal{U}(-1,1)$  and we set  $\Delta = 1 = \omega$ ,  $\delta\Delta = \delta\omega = \delta\mu = 0.5$ . Note that the degeneracy of the zero modes (grey region) in the topological phase for  $\mu = 0$  remains unaffected by the disorder. Compare these results with the unperturbed ones in Fig. 1.7.

### ► Stability of Majorana modes

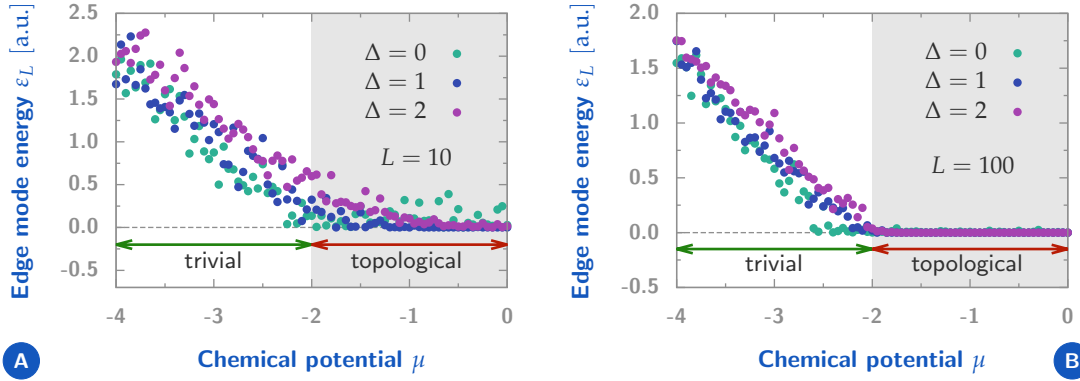
Let us now have a look at one of the most striking features that characterise Hamiltonians with a hidden topological invariant (we come to that later, see 1.3.4). In Fig. 1.9 we show the same spectrum as in Fig. 1.7 (A) for an  $L = 50$  site chain. In contrast to the previous systems, we introduced static disorder in the form of *site dependent parameters*

$$\begin{aligned}\Delta_l &= \Delta + p_l^\Delta \cdot \delta\Delta \\ \omega_l &= \omega + p_l^\omega \cdot \delta\omega \\ \mu_l &= \mu + p_l^\mu \cdot \delta\mu\end{aligned}$$

with the mean values  $\Delta = 1$ ,  $\omega = 1$ ,  $\mu = 0, -4$  and the disorder parameters  $\delta\Delta = \delta\omega = \delta\mu = 0.5$ .  $p_l^{\Delta,\omega,\mu}$  are uniformly distributed random variables in  $\mathcal{U}(-1,1)$  for all  $l = 1, \dots, L$ . The spectrum of these disordered systems is depicted in Fig. 1.9. As a result of the disorder, the spectrum is no longer smooth but features dents and jags, cf. Fig. 1.7 (A). The crucial point is, that the Majorana zero modes in the topological phase ( $\mu = 0 < 2$ ) seem to be completely unaffected by the perturbations. Their energy is not lifted and the ground state degeneracy is conserved. This is a characteristic feature of *topological phases*: The ground state degeneracy is resilient against local perturbations of the system.

In Fig. 1.10 we demonstrate this startling phenomenon in a different way: Both plots show the edge mode energy of disordered systems as a function of  $\mu$  (we set  $\delta\mu = 0$  but  $\delta\Delta = 0.5 = \delta\omega$ ). Obviously the gap closes for  $|\mu| \rightarrow 2$  where the phase transition occurs. But this is not the point. The point is, that we used *different* parameter sets  $\{\Delta_l, \omega_l, \mu_l\}$  for each value of  $\mu$ . In the trivial phase, the effect is not really surprising: The points scatter around an average value that depends on  $\mu$  and  $\Delta = 0, 1, 2$  (we set  $\omega = 1$ ). But the moment the system enters the topological phase, the effect of the disorder ceases almost completely for the larger system with  $L = 100$  and becomes smaller for the short chain with  $L = 10$ . The edge mode energy does not “know” about the disorder in the bulk if the system is in the topological phase. This statement becomes exact in the thermodynamic limit. That this effect is non-trivial becomes evident in the phase for  $|\mu| > 2$  where such resilience against disorder cannot be observed. ◀

<sup>6</sup>In the topological phase, the system is gapped as well. The gap closes at the topological phase transition. However, there are no zero energy modes in the trivial phase which explains the behaviour of the energy shown in the plots.



■ **Figure 1.10:** We show the edge mode energy of Majorana chains with  $L = 10$  (A) and  $L = 100$  (B) sites as a function of the chemical potential. For each value of  $\mu$  we chose an independent, random parameter set  $\{\Delta_l, \omega_l, \mu_l\}$  for  $\delta\Delta = 0.5 = \delta\omega$  and  $\delta\mu = 0$ , see the caption of Fig. 1.9, and computed the ground state energy. We set  $\omega = 1$  and  $\Delta = 0, 1, 2$ . Whereas in the trivial phase for  $|\mu| > 2$  the system is gapped and the gap<sup>6</sup> itself depends on both the mean value  $\Delta$  and the static disorder, in the topological phase for  $|\mu| < 2$  (grey region) this dependence ceases almost completely for large systems (B). This independence with respect to spatial disorder and the mean values of the parameters becomes exact in the thermodynamic limit and characterises the topological phase.

Exact solution for PBC: Bogoliubov-de Gennes transformation

In the following we are going to derive the exact spectrum of the Majorana chain for arbitrary parameters  $\mu$ ,  $w$  and  $\Delta$  by a BOGOLIUBOV-DE GENNES transformation in momentum space. The result was originally derived by Kitaev in [3] and can be “reused” for the exact diagonalisation of the transverse field Ising model (see 1.3.4).

A BOGOLIUBOV-DE GENNES transformation can be thought of as an algebra isomorphism mapping the representation of some fermionic (Dirac) algebra over a given Fock space onto an isomorphic representation over the same Fock space. The original representations are usually referred to as *physical fermions* whereas the new representations are called *quasiparticles*. These are the fundamental excitations of the theory under investigation and the Hamiltonian becomes diagonal in terms of the new fermionic degrees of freedom.

Let us recall the Majorana chain Hamiltonian in terms of fermionic modes (see Eq. 1.61):

$$H_{\text{OBC}} = - \sum_{i=1}^{L-1} \left[ w a_i^\dagger a_{i+1} - \Delta a_i a_{i+1} + \text{h.c.} \right] - \mu \sum_{i=1}^L \left( a_i^\dagger a_i - \frac{1}{2} \right) \quad (1.100)$$

Since we are interested in the *Bulk properties* of the theory there is no point in demanding open boundary conditions. Thus we close the chain by adding the missing summands which connect sites 1 and  $L$  and end up with

$$H_{\text{PBC}} = - \sum_{i=1}^L \left[ w a_i^\dagger a_{i+1} - \Delta a_i a_{i+1} + \text{h.c.} + \mu \left( a_i^\dagger a_i - \frac{1}{2} \right) \right] \quad (1.101)$$

where all indices are integers modulo  $L$  (for convenience  $i$  runs from 1 to  $L$  and not from 0 to  $L - 1$ ).

The Hamiltonian with periodic boundary conditions can now be efficiently written in terms of momentum degrees of freedom. Therefore introduce

$$\hat{a}_m := \frac{1}{\sqrt{L}} \sum_{j=1}^L a_j e^{-i\frac{2\pi}{L}m \cdot j} \quad \text{where } m \in \{1, \dots, L\} \quad (1.102a)$$

$$a_j = \frac{1}{\sqrt{L}} \sum_{m=1}^L \hat{a}_m e^{i\frac{2\pi}{L}m \cdot j} \quad \text{where } j \in \{1, \dots, L\} \quad (1.102b)$$

For the sake of simplicity write  $a_k \equiv \hat{a}_m$  with  $k = \frac{2\pi}{L}m$  and define the abbreviation  $\sum_k \equiv \sum_{k=\frac{2\pi}{L}}^{2\pi} = \sum_{m=1}^L$ . It is easy to show that  $a_k$  is another representation of the Dirac algebra, meaning they satisfy the fermionic anticommutation relations. Expressing  $H_{\text{PBC}}$  in  $k$ -modes yields

$$\begin{aligned} H_{\text{PBC}} &= - \sum_{j=1}^L \left[ w \frac{1}{L} \sum_k \sum_q a_k^\dagger a_q e^{-ikj} e^{iq(j+1)} - \Delta \frac{1}{L} \sum_k \sum_q a_k a_q e^{ikj} e^{iq(j+1)} + \text{h.c.} \right. \\ &\quad \left. + \mu \left( \frac{1}{L} \sum_k \sum_q a_k^\dagger a_q e^{-ikj} e^{iqj} - \frac{1}{2} \right) \right] \\ &= - \sum_k \left[ w e^{ik} a_k^\dagger a_k - \Delta e^{-ik} a_k a_{-k} + \text{h.c.} + \mu a_k^\dagger a_k \right] + \frac{\mu L}{2} \end{aligned}$$

where we used the orthogonality relation  $\sum_{j=1}^L e^{-ikj} e^{iqj} = L \delta_{k=q \bmod 2\pi}$ . We subtract the constant offset  $\frac{\mu L}{2}$  to the other side and find

$$\tilde{H}_{\text{PBC}} = - \sum_k \left[ 2w \cos k a_k^\dagger a_k + \mu a_k^\dagger a_k - \Delta \left( e^{-ik} a_k a_{-k} + e^{ik} a_{-k}^\dagger a_k^\dagger \right) \right]$$

where we introduced  $\tilde{H}_{\text{PBC}} = H_{\text{PBC}} - \frac{\mu L}{2}$ . The substitutions  $a_k a_{-k} = \frac{1}{2} (a_k a_{-k} - a_{-k} a_k)$  and  $a_{-k}^\dagger a_k^\dagger = \frac{1}{2} (a_{-k}^\dagger a_k^\dagger - a_k^\dagger a_{-k}^\dagger)$  yields

$$\begin{aligned} \tilde{H}_{\text{PBC}} &= - \sum_k \left[ 2w \cos k a_k^\dagger a_k + \mu a_k^\dagger a_k - \frac{\Delta}{2} \left( e^{-ik} a_k a_{-k} - e^{-ik} a_{-k} a_k + e^{ik} a_{-k}^\dagger a_k^\dagger - e^{ik} a_k^\dagger a_{-k}^\dagger \right) \right] \\ &= - \sum_k \left[ 2w \cos k a_k^\dagger a_k + \mu a_k^\dagger a_k - \frac{\Delta}{2} \left( e^{-ik} a_k a_{-k} - e^{ik} a_k a_{-k} + e^{ik} a_{-k}^\dagger a_k^\dagger - e^{-ik} a_{-k}^\dagger a_k^\dagger \right) \right] \\ &= - \sum_k \left[ 2w \cos k a_k^\dagger a_k + \mu a_k^\dagger a_k + \frac{i\Delta}{2i} \left( e^{ik} - e^{-ik} \right) a_k a_{-k} - \frac{i\Delta}{2i} \left( e^{ik} - e^{-ik} \right) a_{-k}^\dagger a_k^\dagger \right] \end{aligned}$$

Where we used that the substitution  $k \rightarrow -k$  can be applied to each summand separately since the summation over the full Brillouin zone can be shifted by any multiple of  $\frac{2\pi}{L}$ . Therefore the Hamiltonian takes the simple form

$$\tilde{H}_{\text{PBC}} = \sum_k \left[ -2w \cos k a_k^\dagger a_k - \mu a_k^\dagger a_k - i\Delta \sin k a_k a_{-k} + i\Delta \sin k a_{-k}^\dagger a_k^\dagger \right]. \quad (1.103)$$

Let us expand this Hamiltonian by the substitution  $a_k^\dagger a_k \rightarrow \frac{1}{2} (a_k^\dagger a_k + a_{-k}^\dagger a_{-k})$  in the sum (note that cosine is an even function!):

$$\tilde{H}_{\text{PBC}} = \frac{1}{2} \sum_k \left[ -(2w \cos k + \mu) a_k^\dagger a_k - (2w \cos k + \mu) a_{-k}^\dagger a_{-k} - i2\Delta \sin k a_k a_{-k} + i2\Delta \sin k a_{-k}^\dagger a_k^\dagger \right].$$

If we apply the relations  $a_{-k}^\dagger a_{-k} = \mathbb{1} - a_{-k} a_{-k}^\dagger$  and  $\sum_k (2w \cos k + \mu) = L\mu$ , the constant  $\frac{\mu L}{2}$  drops out and we find

$$H_{\text{PBC}} = \frac{1}{2} \sum_k \left[ -(2w \cos k + \mu) a_k^\dagger a_k + (2w \cos k + \mu) a_{-k} a_{-k}^\dagger - i2\Delta \sin k a_k a_{-k} + i2\Delta \sin k a_{-k}^\dagger a_k^\dagger \right].$$

Now introduce the Nambu spinor  $\Psi_k := [a_k, a_{-k}^\dagger]^T$ ; then this Hamiltonian can be rewritten as

$$H_{\text{PBC}} = \frac{1}{2} \sum_k \Psi_k^\dagger \mathbf{H}_k \Psi_k \quad \text{where} \quad \mathbf{H}_k := \begin{bmatrix} -(2w \cos k + \mu) & -2\Delta i \sin k \\ 2\Delta i \sin k & (2w \cos k + \mu) \end{bmatrix}. \quad (1.104)$$

### ■ Spectrum

We note that  $\mathbf{H}_k$  is Hermitian,  $\mathbf{H}_k^\dagger = \mathbf{H}_k$ , and thus can be diagonalised by a unitary transformation  $T$ . To this end, let us calculate the spectrum of  $\mathbf{H}_k$  via  $\det[\mathbf{H}_k - \varepsilon(k)\mathbb{1}] \stackrel{!}{=} 0$  which is easily evaluated to

$$\varepsilon(k) = \pm \sqrt{(2w \cos k + \mu)^2 + 4\Delta^2 \sin^2 k} \quad (1.105)$$

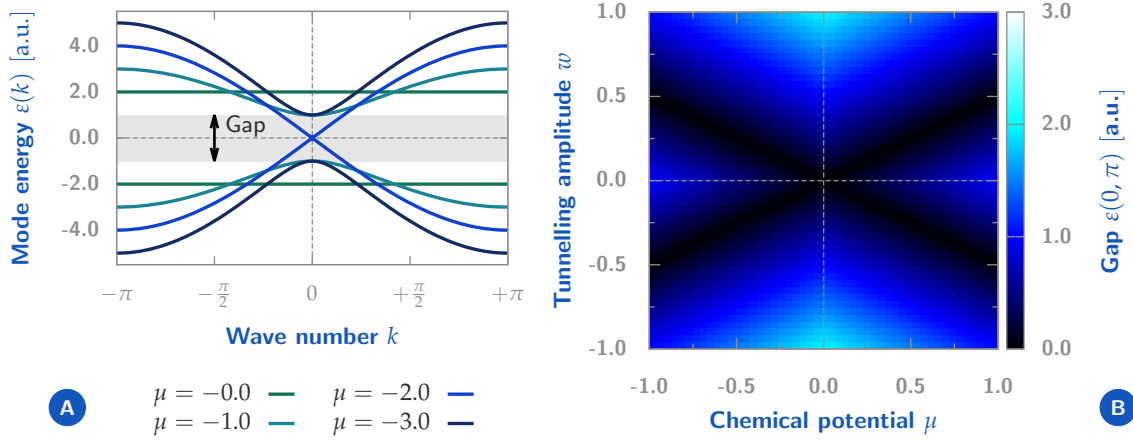
which is Eq. (13) in Ref. [3]. The only possibilities for a gapless spectrum ( $\Delta \neq 0$ ) are  $k = 0, \pi$ :

$$\varepsilon(0) = \pm |\pm 2w + \mu| \stackrel{!}{=} 0 \quad \Rightarrow \quad 2|w| = |\mu| \quad (1.106)$$

We therefore expect a quantum phase transition at  $2|w| = |\mu|$  and two distinct quantum phases in the parameter regimes  $2|w| > |\mu|$  and  $2|w| < |\mu|$ , respectively. Fig. 1.11 illustrates these findings. Note that we already found two representatives of these phases: The parameters  $w = |\Delta| > 0$  and  $\mu = 0$  with  $H = 2w \sum_{i=1}^{L-1} (\tilde{a}_i^\dagger \tilde{a}_i - 1/2)$  represent the first phase since  $2|w| > |\mu|$  and the parameters  $w = 0 = |\Delta|$  and  $\mu < 0$  with  $H = -\mu \sum_{i=1}^L (a_i^\dagger a_i - 1/2)$  represent the second phase since  $2|w| < |\mu|$ . We furthermore found that the first phase is characterised by a degenerate ground state manifold *in the thermodynamic limit*  $L \rightarrow \infty$  whereas the second phase has as unique ground state the fermion vacuum. This hints at a quantum phase transition where the spectral gap of  $H$  closes – exactly what we found above for  $2|w| = |\mu|$ . ■

### ■ Bogoliubov quasiparticles

To complete this analysis, let us calculate the eigenvectors of  $\mathbf{H}_k$  which determine the Bogoliubov quasiparticles of the theory. We will restrict ourselves to the ideal case  $w = |\Delta|$  and  $\mu = 0$  in



■ **Figure 1.11:** We illustrate the spectrum (A) and the gap (B) of the Majorana chain as derived in the text, see Eq. 1.105. In (A) the spectrum is shown in  $k$ -space for  $\Delta = 1 = \omega$  and varying  $\mu$ . The system is gapped for all parameters but  $\mu = 2$  where the topological phase transition occurs. Then the gap closes at  $k = 0$  and the discrete topological invariant jumps discontinuously, see Fig. 1.13. In (B) we illustrate the gap  $\varepsilon$  at  $k = 0, \pi$  colour-coded in the  $\mu$ - $\omega$ -plane. The upper and lower blue regions denote the topological phase for  $|\mu| < 2|\omega|$  whereas the trivial phase corresponds to the blue regions on the left and right hand side. The topological phase transition occurs in the black regions where the gap vanishes.

the topological phase since then one can expect nice solutions in momentum space as well as in real space. The Hamiltonian matrix in the NAMBU basis reads

$$\mathbf{H}_k := 2\omega \begin{bmatrix} -\cos k & -i \sin k \\ i \sin k & \cos k \end{bmatrix} \quad (1.107)$$

and the eigenvectors are easily derived

$$\mathbf{g}_1(k) = \phi_1 \begin{bmatrix} -i \sin \frac{k}{2} \\ \cos \frac{k}{2} \end{bmatrix}, \quad \mathbf{g}_2(k) = \phi_2 \begin{bmatrix} i \cos \frac{k}{2} \\ \sin \frac{k}{2} \end{bmatrix} \quad \text{and} \quad \mathbf{T}_k = \begin{bmatrix} -i\phi_1 \sin \frac{k}{2} & i\phi_2 \cos \frac{k}{2} \\ \phi_1 \cos \frac{k}{2} & \phi_2 \sin \frac{k}{2} \end{bmatrix} \quad (1.108)$$

where  $\mathbf{T}_k$  is the unitary transformation matrix such that  $\mathbf{T}_k^\dagger \mathbf{H}_k \mathbf{T}_k = \text{diag}[\varepsilon(k), -\varepsilon(k)]$ . Here we used the trigonometric identities  $\cos^2 \frac{k}{2} = \frac{1}{2}(1 + \cos k)$ ,  $\sin^2 \frac{k}{2} = \frac{1}{2}(1 - \cos k)$  and  $\sin k = 2 \sin \frac{k}{2} \cos \frac{k}{2}$ . We kept the phases  $\phi_1 \equiv \phi_1(k) = e^{i\varphi_1(k)}$  and  $\phi_2 \equiv \phi_2(k) = e^{i\varphi_2(k)}$  as a free parameters since they cannot be determined at this stage and we need them to obtain a new Dirac algebra (see below). Now calculate

$$\mathbf{\Psi}_k^\dagger \mathbf{H}_k \mathbf{\Psi}_k = \mathbf{\Psi}_k^\dagger \mathbf{T}_k \mathbf{T}_k^\dagger \mathbf{H}_k \mathbf{T}_k \mathbf{T}_k^\dagger \mathbf{\Psi}_k \equiv \tilde{\mathbf{\Psi}}_k^\dagger \text{diag}[\varepsilon(k), -\varepsilon(k)] \tilde{\mathbf{\Psi}}_k \quad (1.109)$$

where we introduced the new spinors

$$\tilde{\mathbf{\Psi}}_k \equiv \begin{bmatrix} \tilde{a}_k \\ \tilde{a}_{-k}^\dagger \end{bmatrix} := \mathbf{T}_k^\dagger \mathbf{\Psi}_k = \begin{bmatrix} i\phi_1^* \sin \frac{k}{2} & \phi_1^* \cos \frac{k}{2} \\ -i\phi_2^* \cos \frac{k}{2} & \phi_2^* \sin \frac{k}{2} \end{bmatrix} \cdot \begin{bmatrix} a_k \\ a_{-k}^\dagger \end{bmatrix} = \begin{bmatrix} i\phi_1^* \sin \frac{k}{2} a_k + \phi_1^* \cos \frac{k}{2} a_{-k}^\dagger \\ -i\phi_2^* \cos \frac{k}{2} a_k + \phi_2^* \sin \frac{k}{2} a_{-k}^\dagger \end{bmatrix}$$

which describe the quasiparticles of the theory. Clearly, to recover a consistent Dirac algebra it is necessary (but not sufficient) to choose  $\phi_2(k) = -i\phi_1^*(-k)$ , i.e.

$$\tilde{\Psi}_k = \begin{bmatrix} \tilde{a}_k \\ \tilde{a}_{-k}^\dagger \end{bmatrix} = \begin{bmatrix} i\phi_1^*(k) \sin \frac{k}{2} a_k + \phi_1^*(k) \cos \frac{k}{2} a_{-k}^\dagger \\ \phi_1(-k) \cos \frac{k}{2} a_k + i\phi_1(-k) \sin \frac{k}{2} a_{-k}^\dagger \end{bmatrix}. \quad (1.110)$$

Choose now  $\phi_1(k) = e^{-i\frac{k}{2}}$ . That the  $\tilde{a}_k$  and  $\tilde{a}_k^\dagger$  indeed obey a fermionic algebra and thus represent fermionic quasiparticles can easily be checked:

$$\begin{aligned} \{\tilde{a}_k, \tilde{a}_q\} &= ie^{\frac{i}{2}(k+q)} \sin \frac{k}{2} \cos \frac{q}{2} \{a_k, a_{-q}^\dagger\} + ie^{\frac{i}{2}(k+q)} \sin \frac{q}{2} \cos \frac{k}{2} \{a_{-k}^\dagger, a_q\} \\ &= ie^{\frac{i}{2}(k+q)} \sin \frac{k}{2} \cos \frac{q}{2} \delta_{k=-q \pmod{2\pi}} + ie^{\frac{i}{2}(k+q)} \sin \frac{q}{2} \cos \frac{k}{2} \delta_{-k=q \pmod{2\pi}} \\ &= ie^{i\pi m} \sin \frac{k}{2} (-1)^m \cos \frac{k}{2} \delta_{k=-q \pmod{2\pi}} - ie^{i\pi m} (-1)^m \sin \frac{k}{2} \cos \frac{k}{2} \delta_{-k=q \pmod{2\pi}} \\ &= i \sin \frac{k}{2} \cos \frac{k}{2} \left( \delta_{k=-q \pmod{2\pi}} - \delta_{-k=q \pmod{2\pi}} \right) = 0 \end{aligned}$$

Here we set  $k = -q + 2\pi m \Leftrightarrow -k = q - 2\pi m$  for some  $m \in \mathbb{Z}$ .  $\{\tilde{a}_k^\dagger, \tilde{a}_q^\dagger\} = 0$  follows immediately. Similarly we show

$$\begin{aligned} \{\tilde{a}_k, \tilde{a}_q^\dagger\} &= e^{\frac{i}{2}(k-q)} \sin \frac{k}{2} \sin \frac{q}{2} \{a_k, a_q^\dagger\} + e^{\frac{i}{2}(k-q)} \cos \frac{q}{2} \cos \frac{k}{2} \{a_{-k}^\dagger, a_{-q}\} \\ &= e^{\frac{i}{2}(k-q)} \sin \frac{k}{2} \sin \frac{q}{2} \delta_{k=q \pmod{2\pi}} + e^{\frac{i}{2}(k-q)} \cos \frac{q}{2} \cos \frac{k}{2} \delta_{-k=-q \pmod{2\pi}} \\ &= e^{i\pi m} \sin \frac{k}{2} (-1)^m \sin \frac{k}{2} \delta_{k=q \pmod{2\pi}} + e^{i\pi m} (-1)^m \cos \frac{k}{2} \cos \frac{k}{2} \delta_{-k=-q \pmod{2\pi}} \\ &= \sin^2 \frac{k}{2} \delta_{k=q \pmod{2\pi}} + \cos^2 \frac{k}{2} \delta_{-k=-q \pmod{2\pi}} = \delta_{k=q \pmod{2\pi}}. \end{aligned}$$

We conclude that  $T_k^\dagger$  (due to our choice of  $\phi_1$  and  $\phi_2$ ) preserves the Dirac algebra which makes it a *canonical transformation*. Note that if we chose  $\phi_1(k) = 1$  this would lead us to  $\{\tilde{a}_k, \tilde{a}_{k+2\pi}^\dagger\} = -1$  which certainly is not consistent with a Dirac algebra! The eigenmodes in momentum space therefore read

$$\tilde{a}_k = ie^{i\frac{k}{2}} \sin \frac{k}{2} a_k + e^{i\frac{k}{2}} \cos \frac{k}{2} a_{-k}^\dagger. \quad (1.111)$$

The Hamiltonian is diagonal in this modes and reads

$$H_{\text{PBC}} = \frac{1}{2} \sum_k \tilde{\Psi}_k^\dagger \text{diag} [\varepsilon(k), -\varepsilon(k)] \tilde{\Psi}_k = \frac{1}{2} \sum_k \left( \varepsilon(k) \tilde{a}_k^\dagger \tilde{a}_k - \varepsilon(k) \tilde{a}_{-k} \tilde{a}_{-k}^\dagger \right) \quad (1.112)$$

Note that  $\varepsilon(-k) = \varepsilon(k)$  and  $\tilde{a}_{-k} \tilde{a}_{-k}^\dagger = \mathbb{1} - \tilde{a}_{-k}^\dagger \tilde{a}_{-k}$  which leads to

$$H_{\text{PBC}} = \sum_k \varepsilon(k) \left( \tilde{a}_k^\dagger \tilde{a}_k - \frac{1}{2} \right). \quad (1.113)$$



To close the circle, let us recast the modes and the Hamiltonian in real space:

$$\begin{aligned}\tilde{a}_j &= \frac{1}{\sqrt{L}} \sum_k e^{ikj} \tilde{a}_k = \frac{1}{\sqrt{L}} \sum_k e^{ikj} \left[ i e^{i\frac{k}{2}} \sin \frac{k}{2} a_k + e^{i\frac{k}{2}} \cos \frac{k}{2} a_{-k}^\dagger \right] \\ &= \frac{1}{2\sqrt{L}} \sum_k e^{ikj} \left[ e^{ik} a_k - a_k + e^{ik} a_{-k}^\dagger + a_{-k}^\dagger \right] \\ &= \frac{1}{2} \left[ a_{j+1} - a_j + a_{j+1}^\dagger + a_j^\dagger \right]\end{aligned}$$

And we find the localised quasiparticles

$$\tilde{a}_j = \frac{1}{2} \left( a_{j+1} - a_j + a_{j+1}^\dagger + a_j^\dagger \right) \quad (1.114)$$

which we already derived (up to a global phase) in the previous analysis of this special case. Recall that for  $w = |\Delta|$  and  $\mu = 0$  we have  $\varepsilon(k) = 2w$  and thus by PARSEVAL'S theorem  $H_{\text{PBC}} = 2w \sum_j \left( a_j^\dagger a_j - \frac{1}{2} \right)$ . ■

#### ■ Dynamics of quasiparticles for non-ideal parameters

Up to now we mostly were concerned with the ideal Majorana chain, i.e. the parameters  $|\Delta| = w > 0$  and  $\mu = 0$ , where the Hamiltonian takes a simple form in terms of *localised* quasiparticles with flat spectrum,  $\varepsilon(k) = 2w$ . Due to this band structure there is no dynamics for the elementary excitations  $\tilde{a}_j^\dagger$ . In an experiment this ideal case cannot be prepared *exactly*, meaning there will inevitably be small perturbations due to  $|\Delta| \approx w > 0$  and  $\mu \approx 0$ .

To get an intuition for the effect of such perturbations on the quasiparticles it is enlightening to express the full Hamiltonian (see Eq. (1.61))

$$H = - \sum_{i=1}^{L-1} \left[ w a_i^\dagger a_{i+1} - \Delta a_i a_{i+1} + \text{h.c.} \right] - \mu \sum_{i=1}^L \left( a_i^\dagger a_i - \frac{1}{2} \right) \quad (1.115)$$

in terms of quasiparticle operators  $\tilde{a}_j$  and  $\tilde{a}_j^\dagger$ . To this end, recall that the Hamiltonian can be recast in Majorana modes

$$H = \frac{i}{2} \sum_{i=1}^{L-1} \left[ (|\Delta| + w) c_{2i} c_{2i+1} + (|\Delta| - w) c_{2i-1} c_{2i+2} \right] - \mu \frac{i}{2} \sum_{i=1}^L c_{2i-1} c_{2i} \quad (1.116)$$

(see Eq. (1.68)). This is some kind of *universal* form from which the Majorana modes can now be repaired arbitrarily to yield fermionic degrees of freedom. Clearly, we combine them according to

$$\tilde{a}_i = \frac{1}{2} (c_{2i} + i c_{2i+1}) \quad \text{and} \quad \tilde{a}_i^\dagger = \frac{1}{2} (c_{2i} - i c_{2i+1}) . \quad (1.117)$$

We already derived the form of the first part in these modes. If we introduce  $J = w + |\Delta|$  the Hamiltonian reads

$$H = J \sum_{j=1}^{L-1} \left( \tilde{a}_j^\dagger \tilde{a}_j - \frac{1}{2} \right) + (|\Delta| - w) \frac{i}{2} \sum_{i=1}^{L-1} c_{2i-1} c_{2i+2} - \mu \frac{i}{2} \sum_{i=1}^L c_{2i-1} c_{2i} \quad (1.118)$$

where the part proportional to  $J$  describes the ideal Majorana chain and the subsequent parts are perturbations proportional to  $|\Delta| - w$  and  $\mu$ , respectively. A cumbersome but straightforward calculation yields

$$\frac{i}{2} \sum_{i=1}^{L-1} c_{2i-1} c_{2i+2} = H_{\text{NNN,BND}} + H_{\text{NNN,BLK}} \quad \text{and} \quad \frac{i}{2} \sum_{i=1}^L c_{2i-1} c_{2i} = H_{\text{NN,BND}} + H_{\text{NN,BLK}}.$$

The perturbation in  $|\Delta| - w$  gives rise to the *next-nearest neighbour* (NNN) dynamics for quasiparticles in the *bulk* (BLK)

$$H_{\text{NNN,BLK}} = \frac{1}{2} \sum_{j=2}^{L-2} \left( \tilde{a}_{j-1} \tilde{a}_{j+1}^\dagger - \tilde{a}_{j-1}^\dagger \tilde{a}_{j+1} \right) + \text{h.c.} \quad (1.119)$$

and the coupling of the boundary (BND) mode  $\tilde{b} \equiv \tilde{a}_L$  to the bulk via

$$H_{\text{NNN,BND}} = \frac{1}{2} \left( \tilde{a}_2^\dagger \tilde{b}^\dagger + \tilde{a}_2 \tilde{b}^\dagger + \tilde{b}^\dagger \tilde{a}_{L-2}^\dagger + \tilde{a}_{L-2} \tilde{b}^\dagger \right) + \text{h.c.} \quad (1.120)$$

$H_{\text{NNN,BLK}}$  leads to next-nearest neighbour hopping and pair creation & annihilation of quasiparticles in the bulk. Hence the quasiparticles obtain a non-trivial dynamics which lets them diffuse coherently through the system. Note that although the *number* of quasiparticles is not conserved, their *parity* is. This is true since it was true for the physical fermions  $a_i^\dagger$  in the original formulation of the theory. The most interesting novelty is due to  $H_{\text{NNN,BND}}$  which couples the delocalised (!) boundary mode to the excitations of the bulk. Namely, excitations from the bulk can hop into the boundary mode or pairs of quasiparticles can be created where one partner is directly inserted into the boundary mode.

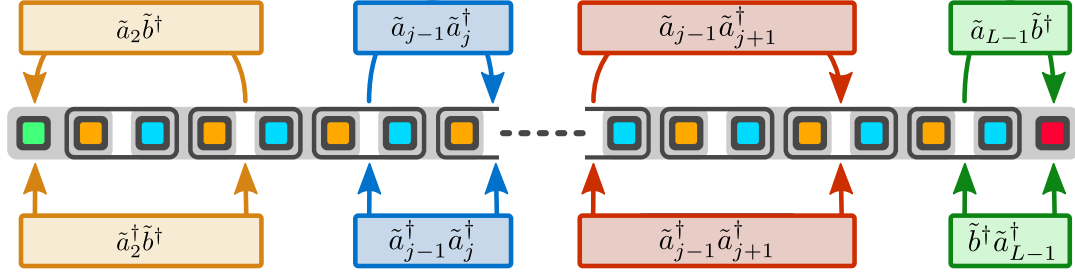
Analogously, the perturbation in  $\mu$  gives rise to the *nearest neighbour* (NN) dynamics for quasiparticles in the *bulk*

$$H_{\text{NN,BLK}} = \frac{1}{2} \sum_{j=2}^{L-1} \left( \tilde{a}_{j-1} \tilde{a}_j^\dagger - \tilde{a}_{j-1}^\dagger \tilde{a}_j \right) + \text{h.c.} \quad (1.121)$$

and the coupling of the boundary mode to the bulk via

$$H_{\text{NN,BND}} = \frac{1}{2} \left( \tilde{a}_1^\dagger \tilde{b}^\dagger + \tilde{a}_1 \tilde{b}^\dagger + \tilde{b}^\dagger \tilde{a}_{L-1}^\dagger + \tilde{a}_{L-1} \tilde{b}^\dagger \right) + \text{h.c.} \quad (1.122)$$

The effects of  $H_{\text{NN,BLK}}$  and  $H_{\text{NN,BND}}$  are comparable to the ones discussed above – besides the fact that the hopping and pair creation & annihilation affects nearest-neighbour sites. It is important to realise that the hopping into the boundary mode provides quasiparticles with a *tunnelling mechanism* between the two ends of the chain – which are *macroscopically* far apart! This leads to new, macroscopically delocalised eigenmodes of the system, as can be seen for example in Fig. 1.6 (c).



■ **Figure 1.12:** Emergent dynamics for quasiparticles away from the ideal Majorana chain at  $|\Delta| = w > 0$ ,  $\mu = 0$ . The ideal Majorana chain features a *flat* band structure  $\varepsilon(k) = J = |\Delta| + w$ . As a consequence, elementary excitations remain stationary and do not show any dynamics. This behaviour changes for  $|\Delta| \neq w$  and  $\mu \neq 0$  as can be formally seen in Eq. (1.123). In the bulk,  $|\Delta| \neq w$  leads to next-nearest neighbour (NNN) hopping ( $\tilde{a}_{j-1}\tilde{a}_{j+1}^\dagger$ ) and pair creation & annihilation ( $\tilde{a}_{j-1}^\dagger\tilde{a}_{j+1}$ ) of quasiparticles. Similarly  $\mu \neq 0$  induces nearest-neighbour (NN) hopping ( $\tilde{a}_{j-1}\tilde{a}_j^\dagger$ ) and pair creation & annihilation ( $\tilde{a}_{j-1}^\dagger\tilde{a}_j$ ) of quasiparticles. It is important to realise that now the delocalised boundary mode  $\tilde{b} = \tilde{a}_L$  shows up in the perturbations which is a result of the leakage of the edge modes into the bulk. The bulk couples via hopping ( $\tilde{a}_2\tilde{b}^\dagger, \tilde{a}_{L-2}\tilde{b}^\dagger, \tilde{a}_1\tilde{b}^\dagger, \tilde{a}_{L-1}\tilde{b}^\dagger$ ) and pair creation & annihilation ( $\tilde{a}_2^\dagger\tilde{b}, \tilde{a}_{L-2}^\dagger\tilde{b}, \tilde{b}^\dagger\tilde{a}_2, \tilde{b}^\dagger\tilde{a}_{L-2}$ ) to the boundary mode. Note that the interaction with the boundary mode is *symmetric* between both ends of the chain (albeit the figure suggests otherwise) as  $\tilde{b}$  is delocalised.

To conclude, one finally ends up with

$$H_{\text{OBC}} = H_{\text{MJ}} + (|\Delta| - w) [H_{\text{NNN,BND}} + H_{\text{NNN,BLK}}] - \mu [H_{\text{NN,BND}} + H_{\text{NN,BLK}}]. \quad (1.123)$$

where  $H_{\text{MJ}} = J \sum_{j=1}^{L-1} (\tilde{a}_j^\dagger \tilde{a}_j - 1/2)$  describes the ideal Majorana chain with localised quasiparticles as fundamental excitations whereas the additional terms impose non-trivial dynamics and pair creation & annihilation on these excitations. As a consequence, the disturbed ground state is not void of quasiparticles anymore. We illustrate our findings in Fig. 1.12. ■

Topological invariants: The Majorana chain as a topological phase

Let us now derive one of the most intriguing properties of the Majorana chain which is, by the way, responsible for the very existence and stability of the edge modes with respect to static disorder. The basic idea is to define a partial<sup>7</sup>, continuous *functional*  $\varphi$  on the space  $\mathbb{H}$  of Hamiltonians (which feature certain symmetries) that maps on a space with discrete topology, usually some subset of  $\mathbb{Z}$ . By construction, these functionals often have a *topological character* since they are defined as a topological invariant of (continuous) mappings from the Brillouin zone (which is a smooth, compact manifold after all) into some other topological space.

As a paradigmatic example let  $\mathbb{H} = \{H(\mu, w, \Delta) \mid \mu, w, \Delta \in \mathbb{R}\}$  be the set of Majorana chain Hamiltonians  $H(\mu, w, \Delta)$  which can be identified with  $\mathbb{R}^3$ . Then all considered Hamiltonians can be cast in the Nambu representation of Eq. (1.104). Note that  $H_k$  is Hermitian and traceless

<sup>7</sup>The domain is usually a proper *subset* of  $\mathbb{H}$ . I.e. there are Hamiltonians  $H$  in  $\mathbb{H}$  such that  $\varphi(H)$  is undefined. In most cases,  $\varphi$  is well defined on Hamiltonians with spectral gap in the thermodynamic limit.

and thus can be written as  $\mathbf{H}_k = \mathbf{h}_k \sigma$  where  $\sigma$  is a column vector of Pauli matrices. More precisely:

$$\mathbf{H}_k = \begin{bmatrix} -(2w \cos k + \mu) & -2\Delta i \sin k \\ 2\Delta i \sin k & (2w \cos k + \mu) \end{bmatrix} = -(2w \cos k + \mu)\sigma^z + 2\Delta \sin k \sigma^y \quad (1.124)$$

and therefore

$$\mathbf{h}_k = \begin{bmatrix} 0 \\ 2\Delta \sin k \\ -(2w \cos k + \mu) \end{bmatrix}. \quad (1.125)$$

The norm of  $\mathbf{h}_k$  is given by the energy spectrum  $\varepsilon(k)$ . That is, as long as  $H(\mu, w, \Delta)$  is gapped,  $\mathbf{h}_k$  can be normalised to  $\hat{\mathbf{h}}_k := \varepsilon(k)^{-1} \mathbf{h}_k$  for all  $k \in [0, 2\pi)$ . If we drop the vanishing  $x$ -component and consider  $\hat{\mathbf{h}}_k$  as a vector in  $S^1 = \{x \in \mathbb{R}^2 \mid |x| = 1\}$  we can write

$$\hat{\mathbf{h}}_k : [0, 2\pi) \longrightarrow S^1; \quad k \mapsto \hat{\mathbf{h}}_k. \quad (1.126)$$

Note that due to the periodicity of  $\hat{\mathbf{h}}_k$  the domain  $[0, 2\pi)$  can be equipped with the topology of a circle<sup>8</sup> while preserving the continuity of  $\hat{\mathbf{h}}_k$ . So we actually get a continuous mapping of the form

$$\hat{\mathbf{h}}_k : S^1 \longrightarrow S^1; \quad k \mapsto \hat{\mathbf{h}}_k \quad (1.127)$$

whose homotopy classes are described by the homotopy group  $\pi_1(S^1) \cong \mathbb{Z}$ . If we denote by  $\Gamma[\hat{\mathbf{h}}_k]$  the *winding number* of  $\hat{\mathbf{h}}_k$  with respect to the origin (which is just a label for the homotopy classes in  $\pi_1(S^1)$ ) we end up with the following continuous functional

$$\varphi : \mathbb{H} \longrightarrow \mathbb{Z}; \quad H \mapsto \Gamma[\hat{\mathbf{h}}_k] \quad (1.128)$$

which classifies our Hamiltonians by topological numbers  $\varphi[H] \in \mathbb{Z}$ . Since  $\varphi[H]$  is constant on connected components of  $\mathbb{H}$  as long as the Hamiltonian remains gapped, it can only change when the spectral gap closes; this is the signature of a *topological phase transition*.

As it turns out, in the present case the winding numbers are restricted to 0 and 1. Thus  $\varphi$  is called a  $\mathbb{Z}_2$ -topological invariant. In Fig. 1.13 the behaviour of  $\mathbf{h}_k$  and  $\hat{\mathbf{h}}_k$  is illustrated.

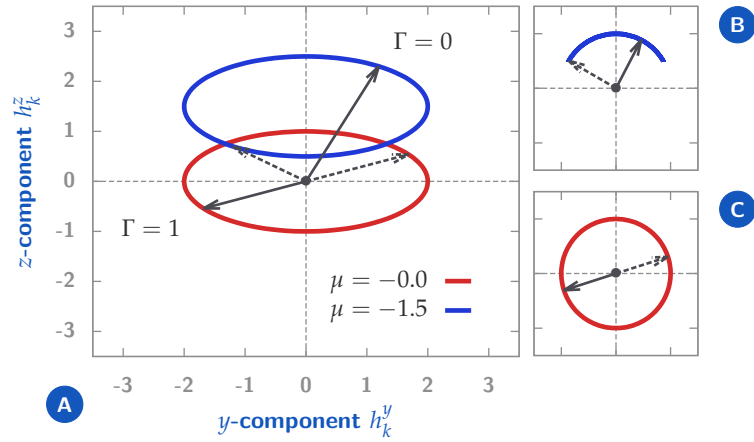
Clearly  $\Gamma[\mathbf{h}_k] = \Gamma[\hat{\mathbf{h}}_k]$  since normalisation does not effect winding numbers. A decomposition of  $\mathbf{h}_k$  reads

$$\mathbf{h}_k = \begin{bmatrix} h_k^y \\ h_k^z \end{bmatrix} = 2 \begin{bmatrix} \Delta \sin k \\ -w \cos k \end{bmatrix} + \begin{bmatrix} 0 \\ -\mu \end{bmatrix}. \quad (1.129)$$

It is therefore trivial to see that

$$\varphi[H(\mu, w, \Delta)] = \Gamma[\hat{\mathbf{h}}_k] = \begin{cases} 0 & \text{for } 2|w| < |\mu| \\ \text{undef.} & \text{for } 2|w| = |\mu| \\ 1 & \text{for } 2|w| > |\mu| \end{cases} \quad (1.130)$$

<sup>8</sup>Which is math speak for the physicists notion of a Brillouin zone in one dimension.



■ **Figure 1.13:** Illustration of the winding number  $\Gamma$  as topological invariant of the Majorana chain in the trivial ( $\Gamma = 0$ ) and topological phase ( $\Gamma = 1$ ). In (A) we show the path of  $\mathbf{h}_k$  in the  $y$ - $z$ -plane as  $0 \leq k < 2\pi$  runs through the Brillouin zone. We set  $\Delta = 1$  and  $\omega = 0.5$ . In the trivial phase for  $\mu = -1.5$  the path of  $\mathbf{h}_k$  does not enclose the origin and the winding number is  $\Gamma = 0$ . However, in the topological phase for  $\mu = 0$  the path encloses the origin and we find  $\Gamma = 1$ . In (B) and (C) we show the normalised vector  $\hat{\mathbf{h}}_k$  for both cases separately. There the winding numbers  $\Gamma = 0$  (B) and  $\Gamma = 1$  (C) become evident. Note that for both shown systems the spectrum is *gapped* as the paths do not cross the origin. Hence the winding numbers are well defined.

which tells us that there is a topological phase transition at  $2|w| = |\mu|$  for  $\Delta \neq 0$ . In Fig. 1.13 these two cases are shown for  $\Delta = 1$  and  $w = 0.5$ . Thus the critical chemical potential is  $\mu_c = -2w = -1$ . Note how the winding numbers differ for  $\mu = 0$  and  $\mu = -1.5$ .

Note that Kitaev's original work employs another functional  $\varphi'$  to characterise the topological phase transition. In [3] the *Majorana number* defined in terms of the Pfaffian  $\text{Pf}[\Lambda]$  is introduced as an algebraic property of the Hamiltonian  $H$ . The equivalence of these two approaches is a well-known fact [76].

Jordan-Wigner transformation: We just solved the 1D Ising model in transverse field

As we will be concerned with a dissipative version of the Ising model in transverse field (see Chapter 2), let us elaborate a nice connection between the topological phase transition we found above and the exemplary quantum phase transition of the one dimensional quantum Ising chain with transverse magnetic field. What follows exemplifies the power of formal mappings between seemingly different theories in general and the usefulness of the famous Jordan-Wigner transformation in this particular case [14,77].

The basic idea behind the Jordan-Wigner transformation (JWT) is to find a representation of the Dirac algebra  $\mathfrak{F}_L$  (describing a system of spinless fermions) on the Hilbert space of  $L$  spin- $\frac{1}{2}$  degrees of freedom  $\mathcal{H}_L = \otimes_{i=1}^L \mathbb{C}_i^2$ . Usually the JWT is applied to systems in one spatial dimension since then it is possible to map *quasilocal* fermionic theories on *quasilocal* theories with spin degrees of freedom. In higher dimensions the JWT can be applied formally as well – however, if the interactions of one system are truly high-dimensional, the transformed system will exhibit *non-local* interactions; which is considered not only unphysical but (in most cases) does not help from a mathematical point of view whatsoever.

To define the algebra representation of  $\mathfrak{F}_L$  consider  $\mathcal{H}_L = \otimes_{i=1}^L \mathbb{C}_i^2$  with the standard basis  $\{|\uparrow\rangle, |\downarrow\rangle\}$  for each spin. Within this basis, the representation  $\rho_L$  reads

$$\rho_L : \mathfrak{F}_L \longrightarrow \text{End } \mathcal{H}_L \cong \text{Mat}(\mathbb{C}, 2^L) \quad (1.131a)$$

$$a_j \mapsto \rho_L(a_j) = \left[ \prod_{k=1}^{j-1} \sigma_k^z \right] \sigma_j^+ \quad (1.131b)$$

$$a_j^\dagger \mapsto \rho_L(a_j^\dagger) = \left[ \prod_{k=1}^{j-1} \sigma_k^z \right] \sigma_j^- \quad (1.131c)$$

which is easily confirmed to carry the Dirac algebra. Here  $\sigma^\pm = \frac{1}{2}(\sigma^x \pm i\sigma^y)$  denote the usual ladder operators for spin- $\frac{1}{2}$  representations of  $\mathfrak{su}(2)$ . It is important to realise that the original *local* fermionic operators  $a_i$  and  $a_i^\dagger$  are mapped to *non-local* string-operators in the spin-system where the strings are responsible for the Fermi statistics<sup>9</sup>.

Now let us start from the Majorana chain Hamiltonian with the restriction that  $|\Delta| = w$  ( $\mu \in \mathbb{R}$  is arbitrary):

$$\begin{aligned} H_{\text{MJ}} &= -w \sum_{i=1}^{L-1} [a_i^\dagger a_{i+1} - a_i a_{i+1} + \text{h.c.}] - \mu \sum_{i=1}^L \left( a_i^\dagger a_i - \frac{1}{2} \right) \\ &= w \sum_{i=1}^{L-1} (a_i - a_i^\dagger) (a_{i+1} + a_{i+1}^\dagger) - \mu \sum_{i=1}^L \left( a_i^\dagger a_i - \frac{1}{2} \right) \end{aligned}$$

By means of Eq. (1.131) it follows easily

$$\rho_L(a_i^\dagger a_i) = \sigma_i^- \sigma_i^+ = \frac{1}{2}(\mathbb{1} - \sigma_i^z) \quad (1.132a)$$

$$\rho_L(a_i - a_i^\dagger) = \left[ \prod_{k=1}^{i-1} \sigma_k^z \right] i\sigma_i^y \quad (1.132b)$$

$$\rho_L(a_{i+1} + a_{i+1}^\dagger) = \left[ \prod_{k=1}^i \sigma_k^z \right] \sigma_{i+1}^x \quad (1.132c)$$

and subsequently

$$\rho_L(H_{\text{MJ}}) = w \sum_{i=1}^{L-1} i\sigma_i^y \sigma_i^z \sigma_{i+1}^x + \frac{\mu}{2} \sum_{i=1}^L \sigma_i^z = -w \sum_{i=1}^{L-1} \sigma_i^x \sigma_{i+1}^x + \frac{\mu}{2} \sum_{i=1}^L \sigma_i^z. \quad (1.133)$$

An additional unitary  $-\pi/2$ -rotation  $U = \prod_j \exp\left(i\frac{\pi}{4}\sigma_j^y\right)$  about the  $y$ -axis yields  $U\sigma^z U^\dagger = -\sigma^x$  and  $U\sigma^x U^\dagger = \sigma^z$  and therefore

$$H_{\text{TIM}} = U\rho_L(H_{\text{MJ}})U^\dagger = -w \sum_{i=1}^{L-1} \sigma_i^z \sigma_{i+1}^z - \frac{\mu}{2} \sum_{i=1}^L \sigma_i^x \quad (1.134)$$

which is just the Ising model in a transverse magnetic field with open boundary conditions.

<sup>9</sup>Whereas in this case the strings are mere formal artefacts, there are two dimensional systems where strings or string-nets give rise to *emergent* fermions or even *anyons* [78,79]. An example would be the toric code in 1.3.3.

So we conclude

► **Result 1.2: Majorana chain and transverse field Ising model**

The one dimensional quantum Ising model with transverse magnetic field is mathematically equivalent to the Majorana chain with open boundary conditions and restriction  $\Delta = w$ . The corresponding parameters are

$$w \hat{=} J \quad \text{and} \quad \mu \hat{=} 2h_x \quad (1.135)$$

with the nearest-neighbour (ferromagnetic) interaction  $J$  and the  $x$ -magnetic field  $h_x$ .

One can use this mapping to derive the exact spectrum of the transverse field Ising model in one spatial dimension. However, be aware that we used *open boundary conditions* to avoid non-local interactions and to end up with an exact mapping to the TIM. Indeed, if the Majorana chain is closed, the JWT of the additional hopping and pairing terms yield

$$\rho_L \left( (a_L - a_L^\dagger) (a_1 + a_1^\dagger) \right) = \left[ \prod_{k=1}^{L-1} \sigma_k^z \right] i\sigma_L^y \sigma_1^x = -\sigma_1^y \left[ \prod_{1 < k < L} \sigma_k^z \right] \sigma_L^y \quad (1.136)$$

which is a highly non-local interaction and thus unphysical (additionally it destroys the exact equivalence connecting the two models!).

Note on superselection rules

The Majorana chain Hamiltonian features only contributions with an even numbers of fermionic creation and annihilation operators (if we count creation operators as  $+1$  and annihilation operators on the same site as  $-1$ ). This is equivalent to say that  $H_{MJ}$  preserves the *fermionic parity*  $P = \prod_j (-1)^{a_j^\dagger a_j}$ . This parity conservation proves crucial in the application of the Majorana chain as a quantum memory, see the following paragraph 1.3.4. Moreover, the existence of the Majorana edge modes is closely related to the parity conservation of the theory.

The prototypical realisation of the Majorana chain is based on superconductor-semiconductor hybrid structures where the proximity of a semiconducting nanowire to a superconducting bulk induces pairing of electrons in the wire. Cooper pairs can tunnel from the wire into the bulk and vice versa; but this interaction preserves the parity of the wire [3, 80]. It is a well-known experimental fact that the parity of a system can be preserved reasonably well — in contrast to many other quantities.

It seems that parity is a particularly “strong” symmetry of nature. Such “strong” symmetries are called *superselection rules*. Superselection rules were first introduced by Wick, Wightman and Wigner for the parity of elementary particles [81]; a historical review on superselection rules can be found in [82]. The basic idea of superselection is that the Hilbert space of *physically realisable states* decays into disjoint parts called *superselection sectors*. States from different superselection sectors *cannot* form coherent superpositions. To put it more algebraically: Not all self-adjoint operators in  $\mathcal{B}(\mathcal{H})$  correspond to physically realisable observables. That is, there is no physical observable that detects the relative phase between two states from different superselection sectors. There are various reasons for superselection rules and some of them are just empirically motivated.

For instance, *parity superselection* expresses the fact that there are no stable coherent superpositions of states with different (fermionic) parities. If one tried to do so, the prepared state would immediately decohere into a mixture of parity eigenstates. This accounts for the empirical fact that all observable states in nature are parity eigenstates. Therefore all the *coherent physics* of fermions takes place in one of the two (even or odd) *parity superselection sectors*. As Hamiltonians describe the unitary (that is, coherent) evolution of physical systems, fermionic Hamiltonians are only considered a description of the latter if they are parity conserving; then any coherent evolution takes place in a parity superselection sector.

As stated above, the reasons for superselection are various and their discussion is way beyond the scope of this thesis. Let me give just a few references for this intriguing topic: Another important superselection rule was discussed by Aharonov in [83], namely *charge superselection* which expresses the impossibility of superimposing states with different electrical charge. An algebraic treatment of superselection is given in [84] and in the introductory paragraphs of [85]. There are also abstract arguments involving measurement theory to define the concept of superselection more precisely [86]. Superselection is also an important concept in quantum information theory [85]. In this connection, one of the most fascinating approaches is to view superselection as lack of “reference frames”, see Ref. [87] for an illuminating review.

Let us now return to the Majorana chain and its application as quantum error correction code; but keep in mind that there is a lot more to it than meets the eye if we claim that parity is conserved.

The Majorana chain as a quantum error correction code

In the following we are going to review the algorithmic error correction procedure along the lines of [52]. To this end, the two-fold degenerate ground state space of the Hamiltonian

$$H = iw \sum_{j=1}^{L-1} c_{2j}c_{2j+1}, \quad (1.137)$$

which is Kitaev’s Majorana chain for ideal parameters  $|\Delta| = w > 0$  and  $\mu = 0$ , is reformulated as a quantum code within a (generalised) stabiliser framework. If we define

$S_j \equiv -ic_{2j}c_{2j+1}$	Stabiliser
$E_j \equiv -ic_{2j-1}c_{2j}$	Elementary (phase) error

the Hamiltonian reads  $H = -w \sum_{j=1}^{L-1} S_j$ . Since  $S_j^\dagger = S_j$ ,  $S_j^2 = \mathbb{1}$  and  $[S_i, S_j] = 0$ , the ground state space is the protected space of the stabiliser  $\mathcal{S} = \text{span} \{S_j \mid 1 \leq j \leq L-1\}$ , that is

$$\mathcal{PS} = \{|\Psi\rangle \in \mathcal{H} \mid \mathcal{S}|\Psi\rangle = |\Psi\rangle\}. \quad (1.138)$$

Since there are  $L$  fermionic sites but only  $L-1$  independent stabiliser generators  $S_j$ , we find  $\dim \mathcal{PS} = 2^{L-(L-1)} = 2$ , which corresponds to the degeneracy due to the boundary mode. Note that  $S_j = -ic_{2j}c_{2j+1} = 1 - 2\tilde{a}_j^\dagger \tilde{a}_j = (-1)^{\tilde{a}_j^\dagger \tilde{a}_j}$  measures the fermionic parity (or occupancy) of quasiparticle site  $j$ . In contrast, the elementary error  $E_j = -ic_{2j-1}c_{2j} = 1 - 2a_j^\dagger a_j = (-1)^{a_j^\dagger a_j}$



measures the fermionic parity on the *physical* site  $j$ . It is easy to see that  $[E_l, E_m] = 0$  and  $[E_i, S_j] = 0$  if  $i \neq j \wedge i \neq j + 1$  but

$$\{E_i, S_j\} = 0 \quad \text{iff} \quad i = j \vee i = j + 1. \quad (1.139)$$

Thus the *boundaries* of error strings  $E_{i_1} \dots E_{i_n}$  carry elementary excitations of the Hamiltonian  $H$ . The latter occur in pairs due to the even number of fermionic modes in  $E_j$ , i.e.  $E_j = \tilde{a}_j^\dagger \tilde{a}_{j-1} + \tilde{a}_j \tilde{a}_{j-1} + \tilde{a}_{j-1}^\dagger \tilde{a}_j^\dagger + \tilde{a}_{j-1}^\dagger \tilde{a}_j$  conserves the quasiparticle parity.

To point out which errors can be corrected (and which not) it is convenient to recast the code in terms of spin- $\frac{1}{2}$  operators  $\{\sigma_i^x, \sigma_i^y, \sigma_i^z\}$ , i.e. Pauli matrices. This can be done by the Jordan-Wigner transformation

$$\rho(c_{2j}) = \left[ \prod_{i=1}^{j-1} \sigma_i^z \right] \sigma_j^y \quad \text{and} \quad \rho(c_{2j-1}) = \left[ \prod_{i=1}^{j-1} \sigma_i^z \right] \sigma_j^x \quad (1 \leq j \leq L) \quad (1.140)$$

which yields a representation  $\rho$  of the Majorana algebra on  $\mathcal{H}_L = \bigotimes_{i=1}^L \mathbb{C}_i^2$ .

In this representation we find

$$\begin{aligned} S_j &= -i\sigma_j^y \sigma_j^z \sigma_{j+1}^x = \sigma_j^x \sigma_{j+1}^x && \text{Stabiliser} \\ E_j &= -i\sigma_j^x \sigma_j^y = \sigma_j^z && \text{Elementary (phase) error.} \end{aligned}$$

If we consider the system as  $L$  qubit register, it is now obvious that  $E_j$  acts as single-qubit *phase flip error* whereas  $S_j$  represents the product of two adjacent *bit-flip errors*. Now consider an arbitrary error  $E = E^x E^z$  where  $E^x$  is an even combination of bit-flip errors  $\sigma_j^x$  and  $E^z$  is an arbitrary combination of phase errors  $\sigma_j^z$ <sup>10</sup>. Then it is clear that  $E$  may be written as product of elementary errors  $E_j$  and stabilisers  $S_j$  (up to a global phase).

Before we proceed with the correction of  $E$ , we should explain why the assumption that  $E^x$  is an even product of bit-flip errors is legit. To this end recall that the parity operator can be written as

$$P = \prod_{j=1}^L (-1)^{a_j^\dagger a_j} = \prod_{j=1}^L (-ic_{2j-1} c_{2j}) = - \prod_{j=1}^{L-1} (-ic_{2j} c_{2j+1}) \cdot (-ic_{2L} c_1) = - \prod_{j=1}^L (-1)^{\tilde{a}_j^\dagger \tilde{a}_j} = \prod_{j=1}^L \sigma_j^z.$$

Please note that the *quasiparticle vacuum*  $|\text{Vac}\rangle$  obeys  $\prod_{j=1}^L (-1)^{\tilde{a}_j^\dagger \tilde{a}_j} |\text{Vac}\rangle = |\text{Vac}\rangle$  and therefore has *odd* parity! The superselection rule for fermionic parity demands that  $[P, A] = 0$  for any admissible observable  $A$ , that is, any physically realisable error  $E$  *commutes* with the parity operator  $P$ . This is only possible if  $E^x$  contains an even number of bit-flip errors.

Therefore it is legit to claim that  $E = E^x E^z$  contains an even number of bit-flip errors and consequently can be written in the form

$$E \propto E_{i_1} \dots E_{i_n} S_{j_1} \dots S_{j_m} \quad (1.141)$$

<sup>10</sup>Due to linearity, this is a sufficient condition for the correctability of arbitrary single-qubit errors with even bit-flip operators.

where the proportionality takes account of the global phase due to (potential) reordering. If we start from a logical state in the code space,  $|\Psi\rangle \in \mathcal{PS}$ , the corrupted state reads

$$|\Psi\rangle^E = E_{i_1} \dots E_{i_n} S_{j_1} \dots S_{j_m} |\Psi\rangle = E_{i_1} \dots E_{i_n} |\Psi\rangle \quad (1.142)$$

and we can just *ignore* the bit-flip errors completely! To correct this error we have to perform a *syndrome measurement*, that is, we measure all stabilisers  $S_j$  and obtain for each (dual) site  $j$  an eigenvalue  $s_j = \pm 1$ . These measurements cause projections of the corrupted state on  $S_j$ -eigenspaces, namely

$$|\Psi\rangle^E [\{s_j\}] \propto \prod_{j=1}^{L-1} \left[ \frac{1}{2} (\mathbb{1} + s_j \cdot S_j) \right] |\Psi\rangle^E. \quad (1.143)$$

The crucial point of a quantum error correction code is that such syndrome measurements cannot destroy *logical* coherences. To map  $|\Psi\rangle^E [\{s_j\}]$  back to the code space  $\mathcal{PS}$  (which corresponds to the error syndrome  $s_j = 1$  for all  $j$ ), the elementary error  $E_{i_1} \dots E_{i_n}$  must be reverted. The problem is that we cannot infer  $\{i_1, \dots, i_n\}$  from the error syndrome  $\{s_j\}$  with certainty since  $S_j$  detects only *endpoints* of error chains. Then it is clear that there are exactly *two* complementary operators that map  $|\Psi\rangle^E [\{s_j\}]$  back to the code space:  $\mathcal{C}[\{s_j\}]$  and  $\bar{\mathcal{C}}[\{s_j\}]$  are complementary chains of error strings  $\{E_{k_i}\}$  such that their ends coincide with the (dual) sites where  $s_j = -1$ . It is easy to see that there are exactly two of these strings and that it follows

$$\mathcal{C}[\{s_j\}] |\Psi\rangle^E [\{s_j\}] = |\Psi\rangle \quad \text{and} \quad \bar{\mathcal{C}}[\{s_j\}] |\Psi\rangle^E [\{s_j\}] = \prod_{j=1}^L E_j |\Psi\rangle = P |\Psi\rangle \quad (1.144)$$

or vice versa. In both cases we find that  $\mathcal{C}[\{s_j\}] |\Psi\rangle^E [\{s_j\}] \in \mathcal{PS}$  and  $\bar{\mathcal{C}}[\{s_j\}] |\Psi\rangle^E [\{s_j\}] \in \mathcal{PS}$ . How to choose the correct operator? Usually one assumes that the error rate is small; hence the error chain with a minimum number of elementary errors is the correct choice *in most cases*. This is called *minimum weight decoding* as we choose the correction operator with the *smaller* total length of the error chain. If we can ensure that there occurred at most  $\lfloor \frac{L-1}{2} \rfloor$  errors, then the above procedure yields the correct result  $|\Psi\rangle$  with certainty. If there are more than  $\lfloor \frac{L-1}{2} \rfloor$  errors, the above procedure fails as we choose the complementary error string and thereby introduce a *logical* phase error  $P$ . This *pairing of excitations* ( $s_j = -1$  denotes a site where a quasiparticle  $\tilde{a}_j^\dagger$  resides) is typical for topological quantum error correction codes; recall the pairing of anyons during the correction procedure of the toric code in that regard.

Here we considered the ideal Majorana chain with parameters  $|\Delta| = \omega$  and  $\mu = 0$ . In the last paragraph of 1.3.4 we showed that  $|\Delta| \neq \omega$  causes next-nearest neighbour tunnelling and pair creation & annihilation of quasiparticles  $\tilde{a}_j^\dagger$  and  $\mu \neq 0$  is responsible for nearest-neighbour hopping and pair creation & annihilation. In the language of the quantum code this reads: Away from the ideal point, pairs of errors are created & annihilated coherently and their dispersion is non-trivial, that is, they *diffuse* through the system. This diffusion causes *logical* errors whenever a pair of excitations is created and the partners reach *different* ends of the chain.

To sum it up: The abstract quantum code *cannot* correct odd bit-flip errors. However, due to the implementation as the ground state space of a *fermionic* Hamiltonian, parity superselection inhibits potentially uncorrectable errors. In this sense, the Majorana chain is a full-fledged quantum error correction code. There are two additional points worth mentioning: First, the Majorana chain is often called a *topological* quantum memory. Where is the topology? It is important to distinguish between topological quantum memories such as the toric code which are based

on *topologically ordered phases* with a topology dependent ground state degeneracy, and topological quantum memories such as the Majorana chain which are basically “non-topological” error correction codes that can be implemented as the ground state space of a Hamiltonian which is protected by a topological invariant (i.e. a winding number). In a nutshell: The *existence* of the code space and its resilience against disorder in the chain is based on topological effects. The error correction code makes use of this topologically protected code space *and* of parity superselection to provide a single logical qubit which can be restored by an active error correction scheme.

The second point is that a *single* Majorana chain cannot be used as a quantum memory for the same reason that there cannot occur odd bit-flip errors: The two logical qubit states  $|\bar{0}\rangle$  (quasiparticle vacuum) and  $|\bar{1}\rangle = b^\dagger |\bar{0}\rangle$  (occupied boundary mode) clearly belong to different superselection sectors. It is therefore physically impossible to create coherent superpositions of these states, which after all is the whole point of a *quantum* memory. An actual implementation would require a reference system which compensates for the parity change so that the total parity of the chain and the reference system remains unaltered. Usually one thinks of a second, parallel Majorana chain as this reference system so one can use four unpaired Majorana modes to create two fermionic zero modes. Then a logical bit-flip corresponds to an even parity operation on *both* modes. In most cases it is nevertheless possible to think of a *single* chain and allow coherent superpositions of the occupied and unoccupied edge mode without complications; we just have to keep in mind that actual implementations require more sophisticated setups.

#### Experimental realisations

So far the Majorana chain was presented as a purely theoretical model that supports unpaired Majorana fermions at the edges of a quantum wire. There are two main reasons why there have been tremendous efforts towards experimental realisations in last years after Kitaev’s ground breaking proposal [3]: First, Majorana fermions have been proposed to play a crucial role in high energy physics, namely in neutrino physics. Unless there are convincing experimental results that support the neutrinoless double beta decay (or related effects), there is no evidence that Majorana fermions actually exist in nature — at least as fundamental particles. With the Majorana chain as a starting point, condensed matter physicists may be the first to see actual Majorana fermions in the lab. Even though the Majoranas in condensed matter systems are not fundamental in the perception of particle physicists (they are quasiparticles after all), its remains an intriguing task to create and *observe* these bizarre particles.

The second reason was given in the previous paragraph: The Majorana chain is a quantum memory that combines topological protection with protection by superselection, that is, parity conservation. Furthermore, the Majoranas exhibit non-abelian braiding statistics (they are non-abelian anyons) which makes them possible constituents of a topological quantum computer [88].

Mostly driven by the promising applications to quantum information<sup>11</sup>, there has been a variety of proposals for the implementation and detection of unpaired Majorana fermions in quantum wires. See e.g. Refs. [89–92] for some of the most recent publications. There were also proposals to extend the notion of Majorana *wires* to higher spatial dimensions in terms of

<sup>11</sup>At least it is well received by the public audience if one claims to “built a quantum computer”. To tell people that one badly wants to see a “fermion that is its own antiparticle” usually doesn’t produce the same effect.

“Majorana fermion codes” [52] or to improve the resilience of the stored quantum information by static disorder [53].

This is all theory *about* experimental realisations. As of this writing and to the best of my knowledge there is no realisation of a working quantum memory based on Majorana fermions. There are, however, most recent experiments that suggest the observation of signatures which might be caused by Majorana fermions [80, 93]. Nevertheless, the experimental results merely *support* the existence of these elusive particles; an unarguable verification remains to be done.

## 1.4 Lattice gauge theories and Higgs fields

In this section we introduce two paradigmatic examples of *lattice gauge theories* in condensed matter physics as we will be concerned with the second one in Chapter 3. A comprehensible outline of such theories can be found in Kogut's review [94] and Wen's textbook on quantum field theory of many body systems [15]. We start our discussions below with the pure  $\mathbb{Z}_2$ -Ising gauge theory originally introduced by Wegner in [95] and comprehensibly discussed by Fradkin and Susskind in [96]. This is done mainly due to didactical purposes and in view of the subsequent discussion of the more complex  $\mathbb{Z}_2$ -Gauge-Higgs model which was originally introduced by Fradkin and Shenker in [2].

### 1.4.1 The $\mathbb{Z}_2$ -Ising gauge theory

To convey a feeling for quantum lattice gauge theories we start with a paradigmatic model that already played its part in this thesis: The Ising model in a transverse magnetic field which we mimicked dissipatively in chapter 2. This is *not* a gauge theory as it describes an ordinary quantum mechanical many-body system on a lattice in  $D$  dimensions with a *global*  $\mathbb{Z}_2$  symmetry and equal numbers of physical and mathematical degrees of freedom<sup>12</sup>. The Hamiltonian reads

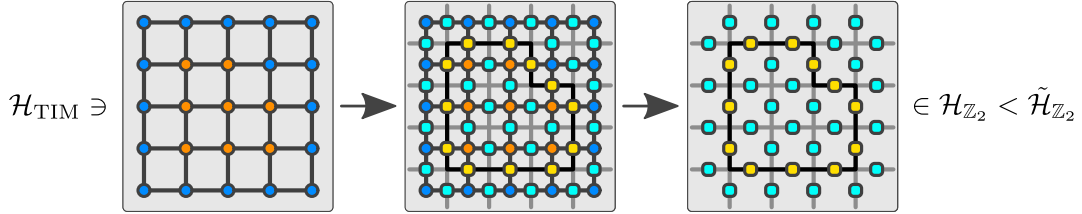
$$H_{TIM} = -J \sum_{\langle i,j \rangle} \sigma_i^z \sigma_j^z - h \sum_i \sigma_i^x = J \left[ - \sum_{\langle i,j \rangle} \sigma_i^z \sigma_j^z - g \sum_i \sigma_i^x \right] \quad (1.145)$$

with the ferromagnetic spin-spin coupling  $J \in \mathbb{R}_0^+$  and the transverse magnetic field  $h \in \mathbb{R}$ . Usually one rescales time and introduces the parameter  $g \equiv \frac{h}{J}$ . We consider a two-dimensional system on a square lattice in the following. Then for  $g \rightarrow 0$  the system is in a symmetry-broken ferromagnetic phase with degenerate ground state space, for  $g \rightarrow \infty$  the symmetric (paramagnetic) phase is restored. There is a quantum phase transition at the critical point  $0 < g_c < \infty$  for  $T = 0$  which survives for  $T > 0$  in two and more spatial dimensions. In the ferromagnetic phase at  $g = 0$  the (gapped) Hamiltonian reads  $H_{TIM} = - \sum_{\langle i,j \rangle} \sigma_i^z \sigma_j^z$  where elementary excitations can be created by a local spin-flip  $\sigma_i^x$  which is encircled by a domain wall on the dual lattice (i.e. the four bonds with its nearest neighbours with negative correlation). Clusters of such excitations yield domains of flipped spins. The interior of the domain itself gets not punished by the Hamiltonian though — only the *boundary* costs energy. That is, the systems configuration (and hence its energy) can be described completely in terms of its domain boundaries on the dual lattice (up to the global  $\mathbb{Z}_2$  symmetry). The family of all domain walls constitutes a set of *closed strings* or *loops* on the dual lattice. Such a loop configuration is static for  $g = 0$  but starts to fluctuate coherently if the magnetic field is switched on as  $g\sigma_i^x$  creates and annihilates elementary excitations. In a certain sense it seems more natural to think of those closed strings as the fundamental entities of the model than its actual constituents, the spins living on the sites. At least this is a completely equivalent way of describing the theory.

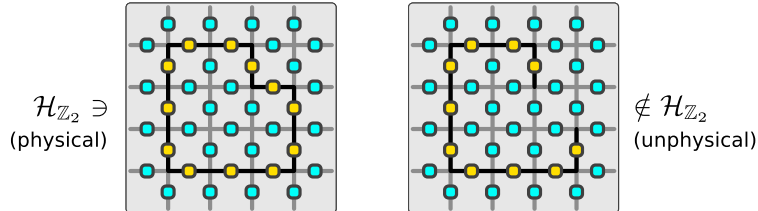
The  $\mathbb{Z}_2$ -Ising gauge theory emerges naturally if we try to reformulate the TIM in terms of domain walls or loops. The basic idea is to switch to the dual lattice and place *new* spins on its

<sup>12</sup>This will become clear in the course of the discussion below. But the crucial point is that the full JORDAN algebra  $\mathcal{O}(\mathcal{H})$  of bounded self-adjoint operators on the system Hilbert space  $\mathcal{H}$  is identified with observables.

boundaries (which coincide with the boundaries of the original lattice) and *encode* the existence of a domain wall in the original theory by a flipped spin in the  $x$ -basis, say  $|-\rangle$ :



In this sense we can map any state of the TIM to its corresponding domain wall configuration encoded in the boundary spins of the dual lattice. No information is lost by this procedure but the global spin orientation! That is, we map all  $2^{(L+1)^2}$  basis states of the TIM onto  $2^{(L+1)^2-1}$  new basis states in some new Hilbert space  $\tilde{\mathcal{H}}_{\mathbb{Z}_2}$ . But there is *too much* information encoded in the new system as the original system comprised  $N = (L+1)^2$  spins if we consider a lattice of  $L \times L$  faces *without* periodic boundary conditions, its Hilbert space therefore reads  $\mathcal{H}_{\text{TIM}} = \otimes_{s \in \mathbb{S}} \mathbb{C}_s^2$  with one spin for each of the  $(L+1)^2$  sites  $s \in \mathbb{S}$ . The new system comprises one spin per *bond* of the dual lattice (which is itself a square lattice of the same dimensions). There are  $2L(L+1) = 2L^2 + 2L$  bonds and the Hilbert space reads  $\tilde{\mathcal{H}}_{\mathbb{Z}_2} = \otimes_{e' \in \mathbb{E}'} \mathbb{C}_{e'}^2$  with one spin for all  $2L^2 + 2L$  dual edges  $e' \in \mathbb{E}'$ . So the “loop state space”  $\tilde{\mathcal{H}}_{\mathbb{Z}_2}$  has more dimensions than the original Hilbert space  $\mathcal{H}_{\text{TIM}}$  and, in this sense, encodes more information. The reason for this growth in encoding capacity is evidently that not every state in  $\tilde{\mathcal{H}}_{\mathbb{Z}_2}$  can be mapped back to or interpreted as a loop configuration of the original TIM:



In other words: If we define a theory, that is a Hamiltonian, on this enlarged Hilbert space which describes the *physics* of the original model, namely the TIM, there are more *mathematical* degrees of freedom available as there are physical degrees to describe. The physical degrees of freedom being the  $(L+1)^2$  original spins which could all be manipulated and set independently *by physical means*. We have to get rid of the  $2L^2 + 2L - [(L+1)^2 - 1] = L^2$  superfluous degrees of freedom which we cannot interpret in terms of physical entities in the original model<sup>13</sup>. The key is that we have to distinguish between *physical* and *unphysical* states in  $\tilde{\mathcal{H}}_{\mathbb{Z}_2}$ : The physical ones are those states that can be interpreted as closed loop- or domain configurations (see figure above). It is easy to see that the global requirement of a closed string net can be enforced locally by demanding that there is an even number of adjacent flipped spins at each site (each vertex of the “flipped-spin-graph” must be of even degree). To formalise this requirement, let us denote

<sup>13</sup>The additional  $-1$  in  $[(L+1)^2 - 1]$  is due to the lost  $\mathbb{Z}_2$  symmetry of the mapping. That is, the loop representation cannot distinguish between a state and its global spin-flipped counterpart. This global symmetry of the TIM is a single degree of freedom which is not present in the Hilbert space of loop states. Consequently we should not subtract it in the above calculation.

the basis of  $\tilde{\mathcal{H}}_{\mathbb{Z}_2}$  by  $|x\rangle$  where  $x \in \{+, -\}^{\mathbb{E}'}$ . We call a dual edge  $e'$  in the state  $|-\rangle_{e'}$  *occupied by a string* and *unoccupied* otherwise. Define the operator

$$A_{s'} := \prod_{e' \in s'} \tau_{e'}^x \quad (1.146)$$

for each vertex  $s' \in \mathbb{S}'$  of the dual lattice which multiplies the occupancies of its adjacent spins. Note that  $\tau_{e'}^{x,y,z}$  denotes the spin- $\frac{1}{2}$  representations of  $SU(2)$  acting on  $\tilde{\mathcal{H}}_{\mathbb{Z}_2}$  whereas  $\sigma_s^{x,y,z}$  denotes the corresponding representation on  $\mathcal{H}_{\text{TIM}}$ . For short: The Pauli matrices  $\tau$  and  $\sigma$  act on dual edges and original sites, respectively. Then the requirement of a basis state  $|x\rangle$  to be physical reads

$$A_{s'} |x\rangle = |x\rangle \quad (1.147)$$

which is called *gauge condition* or GAUSS'S law. It is easily verified that there are exactly  $(L+1)^2 - 1 = L^2 + 2L$  basis states which satisfy this condition which is exactly the number of physical degrees of freedom in the original theory minus the lost  $\mathbb{Z}_2$  symmetry. This is the base-two logarithm of the dimension of the *physical subspace*

$$\mathcal{H}_{\mathbb{Z}_2} := \text{span} \{ |\Psi\rangle \in \tilde{\mathcal{H}}_{\mathbb{Z}_2} \mid \forall s' \in \mathbb{S}' : A_{s'} |\Psi\rangle = |\Psi\rangle \} \subset \tilde{\mathcal{H}}_{\mathbb{Z}_2} \quad (1.148)$$

which can be computed formally by well-known facts about the stabiliser formalism, see [37] for an introduction: First note that  $\mathcal{H}_{\mathbb{Z}_2}$  is a stabiliser subspace  $\mathcal{PS}$  with stabiliser

$$\mathcal{S} = \text{span} \{ A_{s'} \mid s' \in \mathbb{S}' \} . \quad (1.149)$$

Then it can be shown that  $\dim \mathcal{H}_{\mathbb{Z}_2} = 2^{n-k}$  where  $n$  is the total number of spins in the system, here  $n = 2L^2 + 2L$ , and  $k$  denotes the number of independent stabiliser generators, here the number of sites of the dual lattice minus one<sup>14</sup>  $k = L^2 + 1 - 1 = L^2$ . This results in  $n - k = 2L^2 + 2L - L^2 = L^2 + 2L = (L+1)^2 - 1$  which is the number of required physical degrees of freedom.

This discussion demonstrates that the new spins on the dual edges are not physical degrees of freedom on their own. There *are* physical degrees of freedom hidden in the Hilbert space  $\tilde{\mathcal{H}}_{\mathbb{Z}_2}$  but they are not local in the sense that each physical degree of freedom corresponds to a single spin on some dual edge. The new spins are just the mathematical substrate beneath the physical entities — which are closed strings. To put it differently: We did not ask for the spins on the dual edges. But as long as we lack mathematical tools that are more convenient to represent closed strings, we have to put up with them and contrive a method to throw away the additional degrees of freedom that come along; namely the local gauge condition.

So far we found a representation of the original Hilbert space  $\mathcal{H}_{\text{TIM}}$  (modulo a global spin-flip) in the larger Hilbert space  $\tilde{\mathcal{H}}_{\mathbb{Z}_2}$  and called it  $\mathcal{H}_{\mathbb{Z}_2}$ . What are the counterparts of physical operations described by bounded operators in  $\mathcal{B}(\mathcal{H}_{\text{TIM}})$  and observables in  $\mathcal{O}(\mathcal{H}_{\text{TIM}})$ ? As a physical operation maps physical states onto physical states we have to restrict ourselves to bounded operators  $B$  in  $\mathcal{B}(\tilde{\mathcal{H}}_{\mathbb{Z}_2})$  such that  $B\mathcal{H}_{\mathbb{Z}_2} \leq \mathcal{H}_{\mathbb{Z}_2}$  (that is, endomorphisms on  $\mathcal{H}_{\mathbb{Z}_2}$ ). For observables one additionally demands Hermiticity. For any original operator  $B \in \mathcal{B}(\mathcal{H}_{\text{TIM}})$  there is a corresponding operator  $B' \in \mathcal{B}(\tilde{\mathcal{H}}_{\mathbb{Z}_2})$  which preserves physical states. This mapping is not one-to-one due to the trivialisation of the global spin-flip  $X = \prod_s \sigma_s^x$ , that is, the corre-

<sup>14</sup>There are  $L^2$  dual sites “inside” the original lattice and an additional one in the surrounding area. So this gives a total of  $L^2 + 1$  dual sites. Inspection shows that the gauge condition  $A_a$  for the exterior site  $a$  can be expressed by the product of all other gauge conditions. Therefore we find  $L^2 + 1 - 1$  *independent* gauge conditions  $A_s$ .

sponding operator of  $X$  is the identity  $\mathbb{1}$  on  $\tilde{\mathcal{H}}_{\mathbb{Z}_2}$  as a global spin-flip does not change the loop structure of the domain boundaries. Note that to check whether  $B\mathcal{H}_{\mathbb{Z}_2} \leq \mathcal{H}_{\mathbb{Z}_2}$  it is sufficient to show that  $B$  is consistent with the gauge conditions, i.e.  $[B, A_s] = 0$  for all dual sites  $s$ .

The scene is set. But where are the actors? We originally aimed at a translation of the TIM, defined by its Hamiltonian  $H_{\text{TIM}}$ , into the “loop language”. Therefore we have to translate  $H_{\text{TIM}}$  to a new Hamiltonian  $H_{\mathbb{Z}_2}$  on  $\tilde{\mathcal{H}}_{\mathbb{Z}_2}$  which has a physical interpretation. We saw that this is equivalent to claim  $[A_{s'}, H_{\mathbb{Z}_2}] = 0$  for all dual sites  $s' \in S'$ . This condition is automatically satisfied if we carefully translate the summands of  $H_{\text{TIM}}$  to their counterparts of  $H_{\mathbb{Z}_2}$ :

- We identified a domain wall with a spin in state  $|-\rangle$  on the corresponding dual edge. Algebraically this implies the mapping

$$\sigma_i^z \sigma_j^z \mapsto \tau_{e'=(ij)}^x \quad \text{for } i \in N_j \quad (1.150)$$

between subalgebras of  $\mathcal{B}(\mathcal{H}_{\text{TIM}})$  and  $\mathcal{B}(\tilde{\mathcal{H}}_{\mathbb{Z}_2})$ . A domain wall between sites  $i$  and  $j$  is characterised by  $\sigma_i^z \sigma_j^z = -1$  in the original model and by  $\tau_{e'=(ij)}^x = -1$  in the loop model. Note that the gauge condition is built into this mapping as a multiplication of correlations  $\sigma_i^z \sigma_j^z$  along a closed path reveals.

- The magnetic field creates elementary excitations in the original model, that is, flips spins. In the loop model the corresponding elementary excitations are minimal loops of four edges that surround the flipped spin on the original lattice. This suggests the mapping

$$\sigma_i^x \mapsto B_{p'} \equiv \prod_{e' \in p'=i} \tau_{e'}^z \quad (1.151)$$

where  $p' = i$  denotes the face (or plaquette) of the dual lattice that corresponds to site  $i$  on the original lattice. Indeed,  $B_{p'}$  flips the dual spins on the perimeter of the dual face  $p'$ . Note that  $[A_{s'}, B_{p'}] = 0$  for all dual sites  $s'$  and faces  $p'$  which tells us that  $B_{p'}$  is a *physical* operator. This is to be expected as it represents a single spin flip in the original model, which is a physical operation after all.

Note that we did neither define a full algebra homomorphism on  $\mathcal{B}(\mathcal{H}_{\text{TIM}})$  nor is this mapping onto with respect to  $\mathcal{B}(\tilde{\mathcal{H}}_{\mathbb{Z}_2})$  (not all *mathematical* operations on the new Hilbert space have *physical* counterparts in the old theory). Application of this partial mapping yields the new Hamiltonian

$$H_{\mathbb{Z}_2} = - \sum_{e' \in \mathbb{E}'} \tau_{e'}^x - g \sum_{p' \in \mathbb{P}'} \prod_{e' \in p'} \tau_{e'}^z = - \sum_{e' \in \mathbb{E}'} \tau_{e'}^x - g \sum_{p' \in \mathbb{P}'} B_{p'} \quad (1.152)$$

that describes the dynamics of the TIM up to its global  $\mathbb{Z}_2$  symmetry on  $\tilde{\mathcal{H}}_{\mathbb{Z}_2}$ . Since it commutes with all gauge conditions, it is a physical operator according to our interpretation and thus an endomorphism on the physical subspace  $\mathcal{H}_{\mathbb{Z}_2}$ . We may therefore restrict  $H_{\mathbb{Z}_2}$  to  $\mathcal{H}_{\mathbb{Z}_2}$ .

As we are now deep within the “dual world” it is convenient to switch perspective and drop the “dual” altogether, along with the primes for sites, edges and faces. Let us have a look at the symmetries of  $H_{\mathbb{Z}_2}$ . To this end consider an arbitrary binary mapping

$$\eta : S \rightarrow \{-1, 1\}, \quad s \mapsto \eta_s \quad (1.153)$$



on the sites and define the induced algebra isomorphism

$$\hat{\eta} : \mathcal{B}(\tilde{\mathcal{H}}_{\mathbb{Z}_2}) \rightarrow \mathcal{B}(\tilde{\mathcal{H}}_{\mathbb{Z}_2}), \quad \begin{cases} \tau_e^x & \mapsto \tau_e^x \\ \tau_{e=(st)}^z & \mapsto \eta_s \tau_{e=(st)}^z \eta_t \end{cases}. \quad (1.154)$$

It is easy to see that the plaquette operators  $B_p$  are invariant under this mapping since there is always an even number of factors  $-1$  involved in their transformation. As a consequence, the Hamiltonian  $H_{\mathbb{Z}_2}$  remains invariant with respect to any choice  $\eta$ . Note that a representation of  $\hat{\eta}$  can be given in terms of the gauge operators  $A_s$ , namely

$$\hat{\eta} : \mathcal{B}(\tilde{\mathcal{H}}_{\mathbb{Z}_2}) \rightarrow \mathcal{B}(\tilde{\mathcal{H}}_{\mathbb{Z}_2}), \quad B \mapsto \left[ \prod_{s, \eta_s = -1} A_s \right] B \left[ \prod_{s, \eta_s = -1} A_s \right] \quad (1.155)$$

which is easily verified to be equivalent to definition (1.154). From this perspective, the symmetries of the Hamiltonian read  $[A_s, H_{\mathbb{Z}_2}] = 0$  for all sites  $s$ . In contrast to the *global*  $\mathbb{Z}_2$  symmetry of the TIM, these are *local*  $\mathbb{Z}_2$  symmetries of our new theory which we shall henceforth refer to as  *$\mathbb{Z}_2$  Ising gauge theory*.

There is another crucial difference to the former global symmetry. The latter was represented by the global spin flip  $X$  which is a *physical* operation that maps *physically distinct* states onto each other, for instance  $X|\uparrow \dots \uparrow\rangle = |\downarrow \dots \downarrow\rangle$ . As  $\sigma_i^z$  is a physical operator in the original TIM, the two states  $|\uparrow \dots \uparrow\rangle$  and  $|\downarrow \dots \downarrow\rangle$  clearly represent *different states*. If we consider the local symmetries  $A_s$  of the new theory, we have to keep in mind that the *physical states* obey the gauge condition  $A_s|\Psi\rangle = |\Psi\rangle$  and the *physical operators*  $B$  have to be consistent with the latter, that is,  $[B, A_s] = 0$ . We are led to the conclusion, that the symmetries  $A_s$  have *no effect* on any physically relevant quantity and do not modify any *physical state*. In short: These are no physical symmetries of the described theory but emergent symmetries of the underlying mathematical machinery. They are a consequence of our attempt to embed a physical theory into a much larger mathematical Hilbert space. *This is the crucial point of gauge theories.*

Speaking of symmetries is it natural to ask whether they can break spontaneously. For the TIM the answer is clearly *yes* as we know that in the ferromagnetic phase there is a degenerate ground state manifold which includes states that transform under some non-trivial representation of the global symmetry group. For a pure gauge symmetry, in our case  $A_s$  on each site  $s$ , the answer must be *no* since states that break the gauge symmetry are *unphysical* by definition. This subtlety is pointed out very clearly in Ref. [15] which is also a good starting point for the  $\mathbb{Z}_2$  Ising gauge theory. Note that the notion of gauge symmetries can be developed via another route, starting from *classical* gauge theories defined in terms of actions which remain invariant with respect to a local gauge group. In this framework there are no “unphysical states” *a priori*. The statement that local gauge symmetries cannot break spontaneously remains true nonetheless. This, however, requires a non-trivial proof and is known as ELITZUR’s theorem [97]<sup>15</sup>.

It is now interesting to ask in which sense the phase transition of the TIM survived the mapping to the Ising gauge theory. As the local symmetries cannot break and there is no

<sup>15</sup> The reader may be curious how this goes together with the creation of the weak gauge boson’s mass by means of the Higgs mechanism. This is commonly presented as the “spontaneous breaking of the  $SU(2)$  gauge symmetry” which should not be possible according to our understanding of gauge symmetries. There is indeed a lot of confusion even among scientists regarding this point. In contrast to many accounts given in literature, it remains true that *local gauge symmetries cannot be broken spontaneously*. What can break are global residuals of the gauge symmetry after gauge fixing, see e.g. [98]. In contrast to most pedagogical introductions, there are *gauge invariant* treatments of the  $SU(2)$  Higgs model [99]. A nice discussion on this fascinating topic can be found in [100].

remaining non-trivial global symmetry, the phase transition at  $g_c$  cannot be detected by any local order parameter. In particular, there is no physical state with finite  $\tau^z$ -magnetisation since

$$\langle \Psi | \tau_e^z | \Psi \rangle = \langle \Psi | A_s \tau_e^z | \Psi \rangle = - \langle \Psi | \tau_e^z A_s | \Psi \rangle = - \langle \Psi | \tau_e^z | \Psi \rangle \quad (1.156)$$

for  $s \in e$  and  $|\Psi\rangle \in \mathcal{H}_{\mathbb{Z}_2}$ . Thus there cannot be a magnetised phase and  $\tau^z$  is no longer an order parameter. Such phase transitions without spontaneous symmetry breaking that cannot be detected by local order parameters were first introduced by Wegner in [95]. They are closely related to topologically ordered phases as their fundamental physical constituents are string-like objects (or branes in higher dimensions). The characterisation of the two different phases can therefore be given in terms of closed strings and their behaviour. The basic idea is that for  $g = 0$  the Hamiltonian reads

$$H_{\mathbb{Z}_2} = - \sum_{e \in \mathbb{E}} \tau_e^x \quad (1.157)$$

with unique gauge invariant ground state  $|+\rangle^{\otimes N}$ . Elementary (gauge invariant) excitations are created by plaquette operators  $B_p$  and feature a closed loop of flipped spins around a plaquette  $p$ . The gauge invariant eigenstates of this Hamiltonian are therefore nets of closed strings where  $|+\rangle$  denotes vacant edges and  $|-\rangle$  denotes strings. For  $g \rightarrow g_c$  the second term in  $H_{\mathbb{Z}_2}$ , i.e.  $-g \sum_{p \in \mathbb{P}} B_p$ , creates and annihilates closed strings and thus causes the loops to fluctuate. Whereas in the *confined phase* for  $g \rightarrow 0$  stretching of loops is punished by an energy penalty (there is a finite *string tension*), the fluctuations decrease the string tension until it vanishes at the critical value  $g = g_c$ ; this marks the transition to the *deconfined phase*. There the loops traverse the whole system and the loop net *percolates*. This subtle transition is indicated by a change in the decay behaviour of loop correlations  $Z[\mathcal{C}] \equiv \prod_{e \in \mathcal{C}} \tau_e^z$  along closed loops<sup>16</sup>  $\mathcal{C}$  [96]:

$$\langle Z[\mathcal{C}] \rangle \xrightarrow{R[\mathcal{C}] \rightarrow \infty} \begin{cases} e^{-A[\mathcal{C}]} & g < g_c \\ e^{-P[\mathcal{C}]} & g > g_c \end{cases} \quad (1.158)$$

Here  $R[\bullet]$  denotes the characteristic length of the loop  $\mathcal{C}$ , say its diameter,  $A[\bullet]$  denotes its area and  $P[\bullet]$  its perimeter, respectively. Note that for  $g > g_c$  the correlation still vanishes exponentially, so one cannot speak of an “ordered” phase as we did in the case of the TIM for  $g < g_c$ . For  $g < g_c$  the decay of the *Wilson loops*  $\mathcal{C}$  follows an *area law*, for  $g > g_c$  it is governed by a *perimeter law*. For further details the reader is referred to [96] where the 3 + 1-dimensional quantum mechanical  $\mathbb{Z}_2$  Ising gauge theory is derived by means of the well-known quantum-classical correspondence [96, 101] from the classical Ising gauge theory in four spatial dimensions.

<sup>16</sup>Note that unlike open strings of  $\tau_e^z$  operators, *loop operators*  $Z[\mathcal{C}]$  commute with all gauge operators  $A_s$  and therefore describe physical quantities.

### 1.4.2 The $\mathbb{Z}_2$ -Gauge-Higgs model

In the previous paragraph we derived the  $\mathbb{Z}_2$  Ising gauge theory by translating the  $D \geq 2$ -dimensional transverse field Ising model into its natural “loop language”. The new Hilbert space featured more degrees of freedom than the original theory and we had to introduce a local gauge condition to get rid of the superfluous, purely mathematical degrees of freedom. In the end we found a theory of fluctuating *closed strings* or *loops* with a quantum phase transition where the string net percolates.

Here we present a more complicated extension of the pure Ising gauge theory by introducing additional spins on the sites of the lattice which are commonly referred to as *Higgs field*. As we will see, this allows *open strings* (contrary to the pure Ising gauge theory) with *charges* attached to their endpoints. In contrast to most introductions found in the literature, we are going to construct this theory in  $2 + 1$  dimensions by means of the Toric Code Model (TCM) [70]. This approach is motivated by Ref. [74].

#### ■ Derivation

Let us start with a two-dimensional square lattice and spins attached to its edges. This is the structure of the Toric Code and we call its Hilbert space  $\mathcal{H}_{\text{TCM}} = \bigotimes_{e \in \mathbb{E}} \mathbb{C}_e^2$ . The Toric Code Hamiltonian with parallel magnetic field,  $h_y = 0$  and  $h_x, h_z \geq 0$ , reads

$$H_{\text{TCM}} = -h_x \sum_e \tau_e^x - h_z \sum_e \tau_e^z - J_A \sum_s A_s - J_B \sum_p B_p \quad (1.159)$$

where  $A_s$  and  $B_p$  are defined as above and shall be termed *star*- and *plaquette* operators, respectively. We restrict ourselves in the following to the special case  $h_x = 1 = J_A$  and  $h_z \equiv \lambda$ ,  $J_B \equiv \omega$ , that is

$$H_{\text{TCM}} = -\sum_e \tau_e^x - \lambda \sum_e \tau_e^z - \sum_s A_s - \omega \sum_p B_p. \quad (1.160)$$

Now attach one additional spin to each site  $s$  of the lattice and denote the spin- $\frac{1}{2}$  representations by  $\sigma_s^k$ ,  $k = x, y, z$ . The new Hilbert space is  $\tilde{\mathcal{H}}_{\text{GHM}} = \bigotimes_{s \in \mathbb{S}} \mathbb{C}_s^2 \otimes \bigotimes_{e \in \mathbb{E}} \mathbb{C}_e^2$ . On an  $L \times L$  lattice there are  $2L(L+1)$   $\tau$ -degrees of freedom on the edges and now  $(L+1)^2$  additional  $\sigma$ -degrees of freedom on the sites. We can transfer the Toric Code model to the new Hilbert space by setting the additional spins to  $|+\rangle$ . Formally we consider the linear subspace

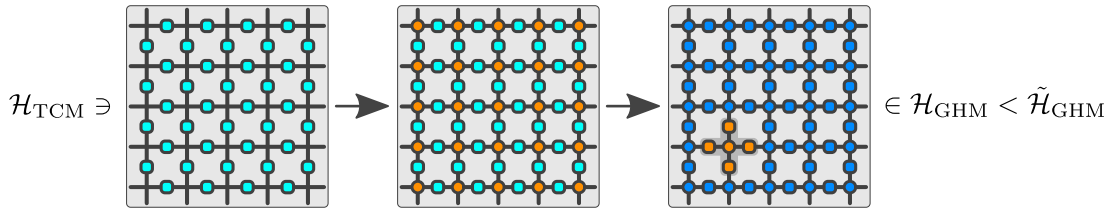
$$\tilde{\mathcal{H}}_{\text{TCM}} = \{|\Psi\rangle \in \tilde{\mathcal{H}}_{\text{GHM}} \mid \forall_{s \in \mathbb{S}} : \sigma_s^x |\Psi\rangle = |\Psi\rangle\} \subset \tilde{\mathcal{H}}_{\text{GHM}} \quad (1.161)$$

and the natural extension

$$\tilde{H}_{\text{TCM}} \equiv H_{\text{TCM}} \otimes \bigotimes_{s \in \mathbb{S}} \mathbb{1}_s. \quad (1.162)$$

If we consider the “dummy spins” on the sites as *unphysical* degrees of freedom — a purely formal extension of the theory — then we should consider only bounded operators  $B \in \mathcal{B}(\tilde{\mathcal{H}}_{\text{GHM}})$  which satisfy  $[B, \sigma_s^x] = 0$  for all sites  $s$  as *physical* operators. It is trivial that the whole “physical theory” of the Toric Code is now embedded in the mathematically larger Hilbert space  $\tilde{\mathcal{H}}_{\text{GHM}}$ . To this end we have to impose restrictions on both, the *physical* Hilbert space and the *physical* operators.

This is basically the same as in the case of the pure Ising gauge theory with the subtle difference that there is a representation of the theory (the current one) where the unphysical degrees of freedom *separate* in the sense that there is a one-to-one correspondence between such degrees of freedom and the spins on the sites. This sounds rather trivial (and up to now, it is). But our theory now lives in a larger Hilbert space and we could use this new freedom to *transform* the theory unitarily. The basic idea is to rotate the physical subspace  $\tilde{\mathcal{H}}_{\text{TCM}}$  unitarily into an isomorphic subspace  $\mathcal{H}_{\text{GHM}}$ . Thereby the Hamiltonian  $\tilde{H}_{\text{TCM}}$ , the gauge condition  $\sigma_s^x$  and the physical observables transform accordingly. In the new subspace the theory *looks different* as the physical entities are different; nevertheless it remains *mathematically* equivalent. Pictorially the complete procedure reads



where the first step illustrates the extension by unphysical degrees of freedom and the second one the unitary rotation which we shall describe now. A basis of  $\tilde{\mathcal{H}}_{\text{TCM}}$  is given by  $\{|x, y\rangle\}$  where  $x \in \{+, -\}^E$  and  $y \in \{+\}^S$ . Note that we can consider each configuration of spins on the edges as a net of open and closed strings (where edges in state  $|-\rangle$  are occupied by a string). Let us now term Higgs spins in state  $|+\rangle$  as *unoccupied* and in state  $|-\rangle$  as *occupied by a charge*. The basis transformation we have in mind attaches a charge to each endpoint of an open string. Formally this reads

$$T := \prod_{e \in E} [\mathbb{1}_e P_e^+ + \tilde{I}_e P_e^-] \quad (1.163)$$

with the projectors  $P_e^\pm = \frac{1}{2}(\mathbb{1}_e \pm \tau_e^x)$  and the operator  $\tilde{I}_{e=(st)} \equiv \sigma_s^z \sigma_t^z$  which creates a pair of charges<sup>17</sup> on adjacent sites. It is straightforward to show that  $T^\dagger = T$  and  $T^\dagger T = \mathbb{1}$  and easy to see that  $T$  acts on the basis  $\{|x, y\rangle\}$  in the described fashion. What remains is the formal transformation of the theory according to  $T$ . The new physical subspace is

$$\mathcal{H}_{\text{GHM}} \equiv T \tilde{\mathcal{H}}_{\text{TCM}} \quad (1.164)$$

with a basis  $\{T|x, y\rangle\}$  of states that can be thought of as nets of open and closed strings living on the *gauge field*  $\tau_e$  and charges attached to the endpoints of open strings living on the *Higgs field*  $\sigma_s$ . To transform the Hamiltonian and the gauge condition it proves useful to transform the four spin representations

$$T \tau_{e=(st)}^z T^\dagger = \sigma_s^z \tau_e^z \sigma_t^z \equiv I_e \quad (1.165a)$$

$$T \tau_e^x T^\dagger = \tau_e^x \quad (1.165b)$$

$$T \sigma_s^z T^\dagger = \sigma_s^z \quad (1.165c)$$

$$T \sigma_s^x T^\dagger = \sigma_s^x A_s \equiv \hat{A}_s \quad (1.165d)$$

<sup>17</sup>Such pairs of charges are sometimes called *mesons* in the literature.

as one checks by a short calculation. Hence the new gauge condition reads

$$T\sigma_s^x T^\dagger |\Psi\rangle = \sigma_s^x A_s |\Psi\rangle = \hat{A}_s |\Psi\rangle = |\Psi\rangle \quad (1.166)$$

which is exactly the defining property of  $\mathcal{H}_{\text{GHM}} = \{|\Psi\rangle \in \tilde{\mathcal{H}}_{\text{GHM}} \mid \forall_{s \in \mathcal{S}} : \hat{A}_s |\Psi\rangle = |\Psi\rangle\}$ . Now it becomes clear that this new theory is an extension of the pure Ising gauge theory as the gauge condition  $A_s$  is now augmented by the Higgs field  $\sigma_s^x$ . Note that the *unphysical* degrees of freedom are now “hidden” in the Hilbert space  $\mathcal{H}_{\text{GHM}}$  and can no longer be identified with a single spin as each local gauge condition  $\hat{A}_s$  acts on multiple (adjacent) spins.

Finally an application of the unitary transformation  $T$  on the Toric Code Hamiltonian yields

$$\begin{aligned} H_{\text{GHM}} \equiv T\tilde{H}_{\text{TCM}}T^\dagger &= -\sum_e T\tau_e^x T^\dagger - \lambda \sum_e T\tau_e^z T^\dagger - \sum_s T A_s T^\dagger - \omega \sum_p T B_p T^\dagger \\ &= -\sum_e \tau_e^x - \lambda \sum_e I_e - \sum_s A_s - \omega \sum_p B_p \\ &= -\sum_e \tau_e^x - \lambda \sum_e I_e - \sum_s \sigma_s^x - \omega \sum_p B_p \end{aligned}$$

where we used that  $\sigma_s^x = A_s$  on  $\mathcal{H}_{\text{GHM}}$  due to the gauge condition and  $T B_p T^\dagger = B_p$  since the operations  $\sigma_s^z$  on the Higgs field cancel.

This Hamiltonian

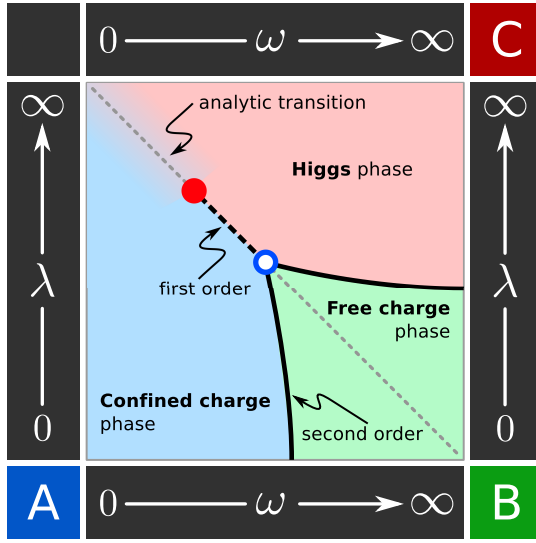
$$H_{\text{GHM}} = -\sum_e \tau_e^x - \sum_s \sigma_s^x - \lambda \sum_e I_e - \omega \sum_p B_p \quad (1.167)$$

is the quantum mechanical  $(2+1)$ -dimensional  $\mathbb{Z}_2$ -Gauge-Higgs model (GHM) introduced by Fradkin and Shenker in [2]. It is now straightforward to generalise  $H_{\text{GHM}}$  to arbitrary spatial dimensions  $D \geq 2$  where  $I_e$  acts on the edges and  $B_p$  on all faces. The gauge condition reads in  $D$  dimensions still  $\sigma_s^x A_s |\Psi\rangle = |\Psi\rangle$  where  $A_s$  denotes the product of all  $2D$  operators  $\tau_e^x$  adjacent to site  $s$ .

### ■ Phase structure

The Toric Code is analytically solvable for vanishing magnetic field but there is — to the best of my knowledge — no known method to derive the exact phase structure if the magnetic field is switched on. Thus we cannot expect analytical solutions for the  $(2+1)$ -dimensional GHM either and this remains true for any other dimension  $D \geq 2$ . Fradkin and Shenker provided a qualitative structure of the phase diagram in the  $\omega$ - $\lambda$ -plane by perturbative arguments on the axes and an analyticity result for an area connecting both axes via small- $\omega$  and large- $\lambda$  regions, see [2]. Other early approaches relied on mean field approximations [102, 103] which can be improved [104] to reproduce most of the essential features of the phase diagram but nevertheless remain qualitatively poor approximations. Another approach is to contrive a continuum field theory in the vicinity of the critical point (see below) [105].

The more recent and most detailed results are based on quantum Monte Carlo (QMC) simulations [106, 107] and verify the perturbative results obtained before. Some of them [74] are motivated by the equivalence to the Toric Code since the existence of a free-charge phase (see below) implies the stability of the topologically ordered TCM phase against small magnetic



■ **Figure 1.14:** The qualitative phase diagram of the  $(2+1)$ -dimensional  $\mathbb{Z}_2$ -Gauge-Higgs model. There are three phases: The confined phase (A) with finite gauge string tension and confined pairs of charges. The deconfined phase (B) of free charges and monopoles which corresponds to the topological phase of the toric code. And the Higgs phase (C) where pairs of monopoles are confined by Higgs excitations. The phases (A) and (C) are connected by an analytic parameter region without phase transition and thus belong formally to the *same* phase. The free charge phase (B) is separated by second order phase transitions from the other phases. These phase boundaries start on the axes and join at a multicritical point (blue circle) where a first order line emerges. The latter ends at a critical point (red disc) where the analytic regime begins. In  $(2+1)$  dimensions the theory is self-dual which becomes manifest by the (grey dotted) self-duality line.

fields. This motivated also other approximate approaches such as large spin analysis and perturbative expansions in [108] which can then be reinterpreted as results for the GHM.

Only recently the rapidly developing field of quantum simulation smoothed the way to efficient realisations of lattice gauge theories in cold atomic setups [109] — at least in theory. This is a promising approach which could outperform any QMC simulation on classical hardware once scalable quantum simulators are available. All these results culminate in the qualitative phase diagram of the GHM in  $(2+1)$  dimensions in Fig. 1.14. Although some of its details cannot be understood in terms of simple arguments, the basic structure can be inferred by a consideration of limiting cases:

**A Confined charge phase:** The phase of confined charges is reached for  $\omega \rightarrow 0$  and  $\lambda \rightarrow 0$ . There the dominant contributions in the Hamiltonian read

$$H_{\text{GHM}} \approx - \sum_e \tau_e^x - \sum_s \sigma_s^x \quad (1.168)$$

and the ground state is the unique  $x$ -polarised state  $|\text{GS}_{\text{conf}}\rangle = |+\rangle^E |+\rangle^S$ . Elementary excitations must be *gauge invariant* and are described by the neglected summands of the Hamiltonian, namely

$$\begin{aligned} I_{e=(st)} &= \sigma_s^z \tau_e^z \sigma_t^z && \text{Mesons} \\ B_p &= \prod_{e \in p} \tau_e^z && \text{Loops} \end{aligned}$$

which commute with all gauge conditions  $A_s$ .  $I_e$  creates two charges on adjacent sites connected by a gauge string, i.e.  $|-\rangle_s |-\rangle_e |-\rangle_t$ . This is commonly called a meson and represents the elementary charge excitation of the theory in the confined charge phase.  $B_p$  creates a closed string on the perimeter of the plaquette  $p$  without any charge. Note that  $I_e |\text{GS}_{\text{conf}}\rangle$  is an excited eigenstate with  $+6$  energy with respect to the ground state and  $B_p |\text{GS}_{\text{conf}}\rangle$  costs total energy  $+8$ . Thus there is a mass gap in the thermodynamic limit and the charges are massive particles. In this limit it is evident why the phase is

characterised by *confined charges*: Particles/Charges occur only in pairs<sup>18</sup> forming mesons and are connected by gauge strings to their partner which is their antiparticle. But strings are penalised by  $-\sum_e \tau_e^x$  which causes an energetically induced *string tension*. This is the same string tension we encountered before in the pure Ising gauge theory. But now this is an open string with particles attached to its ends. The string tension contracts the strings and keeps the particles close, they are *confined*. This is in fact one of the simplest models which exhibits charge confinement in one of its phases; which was the original motivation to study the model in the first place. It is much simpler (and still hard enough) to study the confinement-deconfinement transition in such a toy-model than to scrutinise the complete  $SU(3)$  Yang-Mills theory of quantum chromodynamics (QCD).

**B** **Free charge phase:** The free charge or *Coulomb* phase is found for  $\omega \rightarrow \infty$  and  $\lambda \rightarrow 0$  where the Hamiltonian reads approximately

$$H_{\text{GHM}} = -\sum_s \sigma_s^x - \omega \sum_p B_p. \quad (1.169)$$

This is a frustration-free Hamiltonian and the ground states are  $|\text{GS}_{\text{free}}\rangle = |\text{TCM}, \mathbf{n}\rangle |+\rangle^{\text{S}}$  where  $|\text{TCM}, \mathbf{n}\rangle$  denotes the toric code ground state with the  $\mathbb{Z}_2$  topological quantum numbers  $\mathbf{n} = (n_1, \dots, n_{2g}) \in \{-1, +1\}^{2g}$ . As the dimension of the toric code ground state depends on the *genus*  $g$  of the compact, closed 2-manifold into which the lattice is embedded, there are  $2^{2g}$  linearly independent ground states  $|\text{TCM}, \mathbf{n}\rangle$  each characterised by its set of  $2g$  topological quantum numbers. This translates in  $(2+1)$  dimensions into the  $2^{2g}$ -fold degeneracy of the above limiting Hamiltonian's ground state manifold. Note that the no-charge condition of the toric code, namely  $A_s |\Psi\rangle = |\Psi\rangle$ , is enforced by the gauge constraint which reads  $\hat{A}_s = A_s$  on a completely  $x$ -polarised Higgs field.

As elementary excitations we find mesons  $I_e$  which raise the energy by  $+4$  as the string in between is no longer penalised. *Dual* strings of gauge fields  $\tau_e^x$  do not affect the ground states as they commute with the plaquette operators but open ones do: They create pairs of monopoles  $B_p = -1$  at their endpoints in two dimensions and *strings* of monopoles above and below them in  $D > 2$  dimensions. In any case there are *free (massive) charges* without strings that keep them close, hence the term *deconfined phase*. In  $(2+1)$  dimensions the "dual charges", namely the monopoles, are deconfined as well. This is exactly the gauge theory analogue of the topologically ordered phase that characterises the toric code.

**C** **Higgs phase:** In  $(2+1)$  dimensions the Higgs phase is dual to the phase of confined charges. This duality is based on the self-duality of the model and results in the symmetry of the phase diagram with respect to a reflection about the grey dotted line in Fig. 1.14. The Higgs phase is found around  $\omega \rightarrow \infty$  and  $\lambda \rightarrow \infty$  where the dominant contributions read

$$H_{\text{GHM}} = -\lambda \sum_e I_e - \omega \sum_p B_p. \quad (1.170)$$

As this is a frustration-free Hamiltonian the ground state can be given in terms of the stabiliser  $\mathcal{S} = \text{span} \{I_e, B_p, \hat{A}_s \mid s \in \text{S}, e \in \mathbb{E}, p \in \mathbb{P}\}$ . To see that it is unique return to the toric code formulation by transformation via  $T^\dagger$ . There the Hamiltonian reads  $H_{\text{GHM}} = -\lambda \sum_e \tau_e^z - \omega \sum_p B_p$  with the trivial gauge constraint  $\sigma_s^x |\Psi\rangle = |\Psi\rangle$ . It is now obvious

<sup>18</sup>Single particles cannot be created without violation of the gauge constraint.

that the unique ground state reads  $|\text{GS}_{\text{Higgs}}\rangle' = |\uparrow\rangle^E |+\rangle^S = \frac{1}{\sqrt{2}} (|+\rangle + |-\rangle)^E |+\rangle^S$  which describes the equal-weighted superposition of all possible open and closed string configurations on the gauge field. Transforming back to the GHM Hilbert space yields the unique ground state  $|\text{GS}_{\text{Higgs}}\rangle = T |\text{GS}_{\text{Higgs}}\rangle'$  which is still the equal-weight superposition of all possible string configurations of the confined charge phase (now with charges attached to open strings).

Since it holds  $I_e |\text{GS}_{\text{Higgs}}\rangle$  and  $B_p |\text{GS}_{\text{Higgs}}\rangle$  for all edges and faces, it is clear that the elementary excitations can be created by the gauge invariant operators  $\sigma_s^x$  and  $\tau_e^x$ . The former creates a dual string<sup>19</sup> of *Higgs excitations* surrounding site  $s$ , the latter a *pair of monopoles* on the adjacent dual sites with a Higgs excitation in between. Note that there is a qualitative difference between  $D = 2$  and  $D > 2$  spatial dimensions: In two dimensions an open string of  $\tau_e^x$  operators creates two monopoles at its ends and the string itself suffers no energy penalty. In higher dimensions the same string creates a *closed loop* of monopoles that follows the string on both sides, thus the total energy depends on the string length. For finite  $\omega$  and  $\lambda$  the remaining summands of the Hamiltonian impose a non-trivial dispersion on these excitations and cause them to fluctuate by creation and annihilation processes.

It is evident that the whole description is dual to the one given above for the confined charge phase. The duality refers to the identification

$$\begin{array}{lll} \text{Meson} & \longleftrightarrow & \text{Pair of monopoles connected by Higgs string} \\ \text{Gauge loop} & \longleftrightarrow & \text{Dual Higgs loop} \end{array}$$

which can be formalised by consideration of the dual lattice with gauge fields  $\tau_{e'}$  on dual edges and Higgs fields  $\sigma_{p'}$  on dual sites<sup>20</sup> and an algebra homomorphism defined via

$$\begin{array}{lll} \tau_e^x & \mapsto & I_{e'=(p',q')} = \sigma_{p'}^z \tau_{e'}^z \sigma_{q'}^z \\ I_{e=(s,t)} = \sigma_s^z \tau_e^z \sigma_t^z & \mapsto & \tau_{e'}^x \\ B_p = \prod_{e \in p} \tau_e^z & \mapsto & \sigma_{s'}^x \\ \sigma_s^x & \mapsto & B_{p'} . \end{array}$$

This encodes the statements that the duality transform maps gauge strings  $\tau_e^x$  on edge  $e$  onto Higgs strings  $I_{e'}$  on the dual edge  $e' = e$  and charges  $\sigma_s^x$  on site  $s$  onto monopoles  $B_{p'}$  on the dual face  $p' = s$ . An application of this transformation on  $H_{\text{GHM}}$  yields the dual Hamiltonian

$$H'_{\text{GHM}} = - \sum_{e'} I_{e'} - \sum_{p'} B_{p'} - \lambda \sum_{e'} \tau_{e'}^x - \omega \sum_{s'} \sigma_{s'}^x \quad (1.171)$$

which describes the same theory with modified couplings on the dual lattice. This duality is responsible for the (grey dotted) self-duality line in Fig. 1.14 as it maps the upper right corner ( $\lambda \rightarrow \infty$  and  $\omega \rightarrow \infty$ ) onto the lower left corner ( $\lambda \rightarrow 0$  and  $\omega \rightarrow 0$ ) of the phase diagram.

This works only in two spatial dimensions<sup>21</sup> and is an equivalent way to express the well-known self-duality of the toric code. Dualities of Ising type lattice gauge theories are a

<sup>19</sup>In higher dimensions this becomes a *surface* or *brane* that encloses the corresponding site  $s$ .

<sup>20</sup>That is, the dual Higgs fields live on the faces of the old lattice.

<sup>21</sup>Only there the correspondence  $e = e'$ ,  $s = p'$  and  $p = s'$  holds.



powerful tool to translate systems and the mathematical challenges that come along into one another [95, 110]. If systems are self-dual, this proves often very useful to compute critical points analytically<sup>22</sup>.

The phase transitions that separate the three phases are illustrated in Fig. 1.14. The free charge phase is separated by two second order lines that originate at the boundaries of the (compactified) parameter space and join at a multicritical point (blue circle). In [2] it was shown that the second order transitions of the pure  $\mathbb{Z}_2$  Ising gauge theory for  $\lambda = 0$  and the second order transition of the Ising model for  $\omega = \infty$  are stable against perturbations so that the second order lines enter the interior of the  $\omega$ - $\lambda$ -plane. They proved furthermore that there is a region of analytic behaviour (i.e. without phase transitions) that connects the large- $\omega$  and large- $\lambda$  regime (C) with the small- $\omega$  and small- $\lambda$  regime. Formally speaking, the Higgs- and confinement regimes belong to the same quantum phase. This can be motivated if one considers the toric code: The confined phase corresponds to a toric code with strong magnetic field in  $x$ -direction whereas the Higgs phase describes a toric code with a strong magnetic field in  $z$ -direction. If one starts with a strong  $h_x$  field and therefore with a nearly  $\tau^x$ -polarised state and then *rotates* the magnetic field adiabatically into the  $z$ -direction, one ends up in a nearly  $\tau^z$ -polarised state — which corresponds to the Higgs phase. It is clear that there will be no phase transition as long as the magnetic fields remain dominant along the path from (A) to (B). This is not true if the other contributions are relevant as the existence of a first order line separating phase (A) and (C) shows. On its lower-left side in the confined charge phase there is a high density of fluctuating, weakly confined *charges*. On its upper-right side in the Higgs phase there is a high density of fluctuating, weakly confined *monopoles*. At the first order transition the densities of monopoles and charges exchange rapidly. In contrast, the second order lines are characterised by the continuous vanishing of the gauge string tension and the Higgs string tension which indicates the transition from confinement of charges and monopoles to the free charge phase, respectively.

In Chapter 3 we approximate the phase diagram in Fig. 1.14 by simple mean field techniques for comparison and subsequently construct a purely dissipative analogue of the  $\mathbb{Z}_2$ -Gauge-Higgs model. We show that the basic features of the Hamiltonian mean field phase diagram can be recovered in the purely dissipative setup.

### ■ Relation to Maxwell's theory

Above we used terms such as “(electrical) charges” and “(magnetic) monopoles” without any justification. There is, however, a tight connection to Maxwell's theory of electromagnetism which is a  $U(1)$  gauge theory after all. Actually we are working with a quantum mechanical version of discretised electromagnetism [111]. To this end, consider a two-dimensional square lattice with two discrete binary<sup>23</sup> vector fields  $\{A_e\}$  and  $\{E_e\}$  living on the edges and a discrete binary scalar field  $\{\rho_s\}$  living on the sites. The discrete curl of  $A$  is a one-component field (perpendicular to the lattice) that lives on *faces*  $p$  and is given by the discrete sum

$$[\nabla \times A]_p = \partial_x A_y - \partial_y A_x = (A_{ey} - A_{ey+x}) - (A_{ex} - A_{ex+y}). \quad (1.172)$$

<sup>22</sup>Think of the celebrated self-duality of the two-dimensional classical Ising model employed by Kramers and Wannier to derive the exact critical point.

<sup>23</sup>We call a quantity  $X$  *binary* if  $X \in \{0, 1\}$ .

Here  $ex$  ( $ey$ ) denotes the lower (left) boundary of face  $p$  in  $x$  ( $y$ ) direction.  $ex + y$  ( $ey + x$ ) denotes the next edge parallel to  $ex$  ( $ey$ ) in  $y$ - ( $x$ -) direction. The discrete divergence of  $E$  is a scalar that lives on *vertices*  $s$  and reads

$$[\nabla E]_s = \partial_x E_x + \partial_y E_y = (E_{s+x} - E_{s-x}) - (E_{s+y} - E_{s-y}) \quad (1.173)$$

where  $s \pm x$  ( $s \pm y$ ) denotes the edge adjacent to  $s$  in  $\pm x$ - ( $\pm y$ -) direction.

Let us now make the identifications

$$\tau_e^z \leftrightarrow e^{i\pi A_e} \quad (1.174a)$$

$$\tau_e^x \leftrightarrow e^{i\pi E_e} \quad (1.174b)$$

$$\sigma_s^x \leftrightarrow e^{i\pi \rho_s} \quad (1.174c)$$

and recall that  $A_e, E_e, \rho_s \in \{0, 1\}$ . If we introduce the *magnetic flux density*  $b_p \equiv \nabla \times A$ , we find the additional identification

$$B_p = \prod_{e \in p} \tau_e^z \leftrightarrow \prod_{e \in p} e^{i\pi A_e} = e^{i\pi \sum_{e \in p} A_e} = e^{i\pi [\nabla \times A]_p} = e^{i\pi b_p} \quad (1.175)$$

which justifies the term ‘‘monopole’’ and ‘‘magnetic flux’’ for faces with  $B_p = -1 \Leftrightarrow b_p = 1$ . Note that we used that  $A_e$  is a binary field and therefore  $e^{-i\pi A_e} = e^{i\pi A_e}$ . Analogously we derive

$$A_s = \prod_{e \in s} \tau_e^x \leftrightarrow \prod_{e \in s} e^{i\pi E_e} = e^{i\pi \sum_{e \in s} E_e} = e^{i\pi [\nabla E]_s}. \quad (1.176)$$

In this formulation the *gauge condition* reads

$$\sigma_s^x A_s |\Psi\rangle = |\Psi\rangle \leftrightarrow e^{i\pi \rho_s} e^{i\pi [\nabla E]_s} = 1 \Leftrightarrow e^{i\pi [\nabla E]_s} = e^{i\pi \rho_s} \quad (1.177)$$

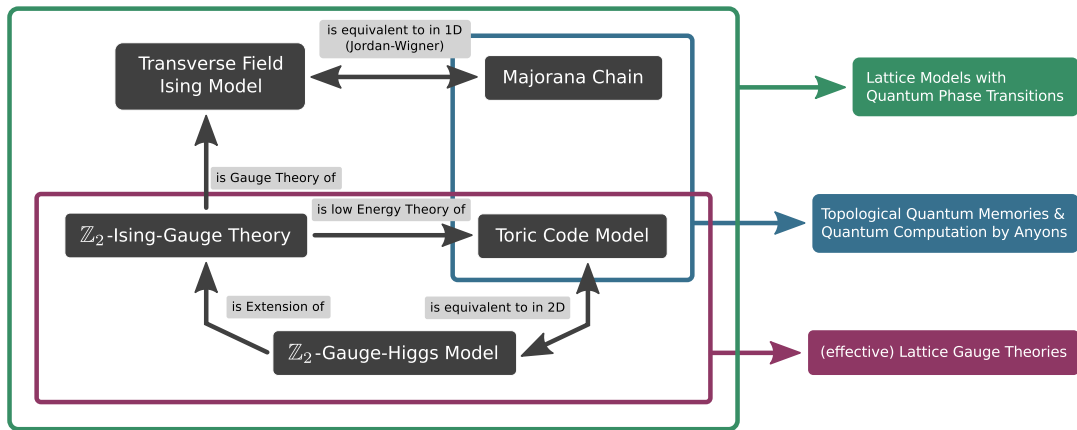
for any *physical state*  $|\Psi\rangle$ . We conclude that

$$\forall_{s \in S} : \quad [\nabla E]_s = \rho_s \quad (1.178)$$

which is just the discrete version of GAUSS’S law  $\nabla E = \rho$  where  $\rho$  denotes the continuous charge density. This explains why the gauge condition is often referred to as GAUSS’S law and why we consider a site  $s$  where  $\sigma_s^x = -1$  as ‘‘occupied by a charge’’. Note that the open (closed) gauge strings in the confined phase are nothing else than open (closed) electrical flux lines attached at (electrical) charges if they are open. In the pure Ising gauge theory there was no Higgs field and consequently there were no charges. Then there are only *closed* electric flux lines which is microscopically enforced by GAUSS’S law  $\nabla E = 0$ . This is the gauge condition  $A_s |\Psi\rangle = |\Psi\rangle$  which we derived by demanding that there is an *even* number of gauge strings adjacent to each site  $s$  which, in turn, is a discrete version of GAUSS’S law.

## 1.5 The overall picture

In the preceding preliminaries we presented several lattice models that feature *quantum phase transitions*. In particular the *toric code model* (TCM) in 1.3.3, the *Majorana chain* (MC) and the *transverse field Ising model* (TIM) in 1.3.4, the  $\mathbb{Z}_2$ -Ising-Gauge theory in 1.4.1, and the  $\mathbb{Z}_2$ -Gauge-Higgs model in 1.4.2. All of these models are more or less obviously connected, some are even mathematically equivalent in particular spatial dimensions. I do not want to give detailed explanations at this point (some of the connections were discussed in the corresponding sections above), but I want the reader to be aware of this network of physical models, their relations and equivalences. As this thesis deals — directly or indirectly — with most of these models, it is of crucial importance to keep the *overall picture* in mind; this overall picture looks as follows:



We saw in 1.3.4 that the Majorana chain with open boundary conditions can be mapped on the transverse field Ising model in one spatial dimension by a Jordan-Wigner transformation (and vice versa). Therefore the two models are mathematically equivalent even though they describe physically different settings. In 1.4.1 we motivated the  $\mathbb{Z}_2$ -Ising-Gauge theory by introduction of unphysical degrees of freedom in a “loop representation” of the transverse field Ising model in two dimensions. Afterwards, in 1.4.2, we introduced the  $\mathbb{Z}_2$ -Gauge-Higgs model via its mathematical equivalence to the toric code model in two dimensions. It became clear by comparison of the gauge conditions and an interpretation in terms of MAXWELL’S theory that the  $\mathbb{Z}_2$ -Gauge-Higgs model is an “extension” of the pure  $\mathbb{Z}_2$ -Ising-Gauge theory which allows additionally for electrical charges due to the Higgs field. It is furthermore easy to see that the low energy sector of the toric code model with strongly suppressed electrical charges and a magnetic field in  $x$ -direction is effectively described by the pure  $\mathbb{Z}_2$ -Ising-Gauge theory. The Majorana chain is a paradigmatic example for a *topological phase* with a topological invariant that characterises its Hamiltonian. In contrast, the toric code is a paradigmatic toy model for systems with *topological order* whose low energy physics is described by a topological quantum field theory and whose ground states exhibit a string-net structure. Both models can be employed as a topological quantum memory and feature anyonic excitations. The Majorana chain can even serve as a building block for a topological quantum computer since its Majorana fermions exhibit *non-abelian* statistics (which is not true for the toric code).

To see where and how we refer to the above models and to conclude the preliminaries, let us give a short outlook on the topics of this thesis:

- In Chapter 2 we introduce a dissipative counterpart of the transverse field Ising model in terms of competing jump operators and described by a Lindblad equation. We analyse its phase structure with and without additional Hamiltonian contributions in detail.
- In Chapter 3 we extend the notion of a *dissipative counterpart* to the  $\mathbb{Z}_2$ -Gauge-Higgs model. We introduce competing jump operators so that particular combinations of the latter drive the system towards each of the three quantum phases of the  $\mathbb{Z}_2$ -Gauge-Higgs model. We give a short mean field analysis of the phase structure of our *dissipative  $\mathbb{Z}_2$ -Gauge-Higgs model*.
- In Chapter 4 we give some critical comments on the dissipative realisation of the Majorana chain as proposed in Ref. [1] by Diehl *et al.*. We argue that their proposed *number conserving* jump operators do not yield steady states with topological properties.
- In Chapter 5 we introduce jump operators that provably cool into the Majorana chain ground state. However, numeric results suggest that such straightforward dissipative implementations do not yield a *self-correcting quantum memory*.
- In Appendix E we get off the subject and discuss some mathematical aspects of (*quasi*) *locality* in physics.

This is on the agenda. Let's get started.

# Spontaneous symmetry breaking by dissipation

*“Symmetry is a vast subject, significant in art and nature. Mathematics lies at its root, and it would be hard to find a better one on which to demonstrate the working of the mathematical intellect.”*

Hermann Weyl

In the preliminaries we discussed the transverse field Ising model (TIM) as it came along with the Majorana chain, see Subsection 1.3.4 and especially paragraph 1.3.4. The transverse field Ising model is known as a paradigmatic example for quantum phase transitions and spontaneous symmetry breaking in the quantum regime as it features a disordered paramagnetic phase and a symmetry-broken ferromagnetic phase with long range order.

In this chapter we take the TIM Hamiltonian and its phases as a model to contrive a competing dissipative process in terms of Lindbladian jump operators that drives the system (1) into the symmetric paramagnetic phase at one end of the parameter space and (2) into the symmetry-broken ferromagnetic phase at the other end. We hope to find a *dissipative phase transition* that separates both phases and includes dissipative *spontaneous symmetry breaking*. We are also interested in the competition of Hamiltonian and dissipative dynamics if one parallels the TIM Hamiltonian with its dissipative counterpart. To scrutinise the proposed model, we employ both a detailed mean field analysis and quantum trajectory Monte Carlo simulations.

This chapter is structured as follows. In Section 2.1 we introduce our dissipative model. In Section 2.2 we present a formal treatment of its strong dissipative symmetries. In Section 2.3 we give a detailed mean field analysis of the phase diagram. The mean field jump operators are derived in Subsection 2.3.1, their static solutions are examined in 2.3.2 with and without competing Hamiltonian contributions and the dynamics of the mean field theory is discussed in 2.3.3. In Section 2.4 we compare the mean field theories of the Hamiltonian theory and our dissipative counterpart. In Section 2.5 we provide an analytical treatment of the minimal instance for the dissipative theory and classify its non-equilibrium steady states. In Section 2.6 we finally present some Monte Carlo simulations for small systems in one and two dimensions. Additional information can be found in Appendix A where we derive some general equations for dissipative mean field theories, in Appendix B where we give an extended derivation of the mean field jump operators, in Appendix C where we describe our QTMC implementation, and in Appendix D where we present a few auxiliary calculations.

## 2.1 The Setting

As stated above, our starting point is the well-known transverse field Ising model in arbitrary spatial dimensions  $d$ . Its Hamiltonian reads

$$H_{\text{TIM}} = -J \sum_{\langle n,m \rangle} \sigma_n^z \sigma_m^z - h \sum_n \sigma_n^x \quad (2.1)$$

where we denote by

$$\sum_{\langle n,m \rangle} \equiv \frac{1}{2} \sum_{n=1}^N \sum_{m \in \mathcal{N}_n} \quad (2.2)$$

the sum over all next-nearest neighbour pairs  $\langle n, m \rangle$ .  $J \geq 0$  denotes a ferromagnetic spin-spin coupling and  $h \in \mathbb{R}$  the transverse magnetic field in  $x$ -direction. As we saw in the course of our discussion of the Majorana chain in Subsection 1.3.4, both models are mathematically equivalent in one spatial dimension and with open boundary conditions via a Jordan-Wigner transformation, see paragraph 1.3.4. We derived by means of a BOGOLIUBOV-DE GENNES transformation the exact spectrum for the Majorana chain and thereby found a quantum phase transition — which led us to the conclusion that the transverse field Ising model features a quantum phase transition as well. The disordered *paramagnetic* phase features the  $\mathbb{Z}_2$ -symmetry of the Hamiltonian and corresponds to a unique ground state:

$$H_{\text{TIM}} \xrightarrow{h \gg J} -h \sum_n \sigma_n^x \Rightarrow |\text{GS}\rangle = |+\rangle^{\otimes N} \quad \text{for } h > 0 \quad (2.3)$$

In the other limit one finds the pure quantum Ising model

$$H_{\text{TIM}} \xrightarrow{h \rightarrow 0} -J \sum_{\langle n,m \rangle} \sigma_n^z \sigma_m^z \Rightarrow |\text{GS}\rangle \in \text{span} \left\{ |\uparrow\rangle^{\otimes N}, |\downarrow\rangle^{\otimes N} \right\} \quad \text{for } J > 0 \quad (2.4)$$

with a degenerate ground state space. The latter comprises states that break the  $\mathbb{Z}_2$  spin-flip symmetry of the system spontaneously. But in contrast to *classical* spontaneous symmetry breaking, where the system itself ends up randomly in one of several states of lower symmetry, the actual ground state for *finite*  $h$  remains *symmetric* as it is close to the superposition

$$|\text{GS}, h \approx 0\rangle = \frac{1}{\sqrt{2}} \left( |\uparrow\rangle^{\otimes N} + |\downarrow\rangle^{\otimes N} \right). \quad (2.5)$$

In this *ferromagnetic* phase the  $\mathbb{Z}_2$ -symmetry is spontaneously broken in the sense that any measurement leads to decoherence and results in a state after projection that violates the  $\mathbb{Z}_2$ -symmetry. In the context of *quantum phases* this implies that the actual ground state features *finite correlations*  $\langle \sigma_m^z \sigma_n^z \rangle$  for  $|m - n| \rightarrow \infty$  and long-range entanglement between states that break the  $\mathbb{Z}_2$ -symmetry (which makes the state susceptible to decoherence). But the system does *not* jump spontaneously in a state with finite  $\sigma^z$ -magnetisation as it is expected from classical spontaneous symmetry breaking.

Nevertheless it is well-known that straightforward mean field approaches yield solutions where the expectation value  $m_z = \langle \sigma_m^z \rangle$  obtains a finite value. These results indeed indicate the quantum phase transition correctly but one has to keep in mind that the pure quantum

formalism (without decoherence) does not predict a finite  $\sigma^z$ -magnetisation. The spontaneous symmetry breaking is “hidden” in that regard but can nevertheless be detected by correlations (which is impossible in mean field theory).

The basic idea that we elaborate in this chapter is the following: Can one come up with a purely *dissipative* process (in terms of Lindblad jump operators) that “mimics” the phase structure of the TIM so that in one parameter regime the system is driven towards a *ferromagnetic* state in span  $\{|\uparrow\rangle^{\otimes N}, |\downarrow\rangle^{\otimes N}\}$  with finite correlations and in the opposite parameter regime the symmetric state  $|+\rangle^{\otimes N}$  is reached? One would then expect a (second order) phase boundary separating these two phases and could drive a *non-equilibrium phase transition* by crossing this boundary. Due to the dissipation we anticipate *mixed states* when driving the system from the symmetric into the symmetry-broken phase. Additional questions arise when we parallel this dissipative analogue with the actual *Hamiltonian* dynamics.

Before we can follow these questions, we have to come up with competing jump operators that meet our expectations. As there are *two* distinct phases, it is reasonable to propose *two* competing baths defined by their jump operators:

► **Definition 2.1: Dissipative Transverse Field Ising Model**

Consider a  $d$ -dimensional square lattice with spins attached to the sites. Then we define the *dissipative transverse field Ising model* by the jump operators

$$d_i := \frac{\sqrt{\kappa_F}}{2} \sigma_i^x \left( \mathbb{1} - \frac{1}{q} \sum_{j \in N_i} \sigma_j^z \sigma_i^z \right) \quad (2.6a)$$

$$c_i := \frac{\sqrt{\kappa_P}}{2} \sigma_i^z (\mathbb{1} - \sigma_i^x) = \sigma_i^{+,x} \quad (2.6b)$$

for each site  $i$ .  $q = 2d$  is the coordination number and  $N_i$  is the set of nearest-neighbours for  $i$ .  $\kappa_F$  denotes the coupling strength for the *ferromagnetic bath*  $\{d_i\}$  and  $\kappa_P$  the coupling strength for the *paramagnetic bath*  $\{c_i\}$ . The dynamics is given by the Lindblad master equation

$$\partial_t \rho = \sum_i \left[ d_i \rho d_i^\dagger - \frac{1}{2} \{d_i^\dagger d_i, \rho\} \right] + \sum_i \left[ c_i \rho c_i^\dagger - \frac{1}{2} \{c_i^\dagger c_i, \rho\} \right] \quad (2.7)$$

and the non-equilibrium steady states (NESS) satisfy  $\partial_t \rho_{\text{NESS}} = 0$ .

The motivation for these jump operators is evident:  $d_i$  “measures” the average correlation of spin  $i$  with its nearest neighbours via  $\frac{1}{q} \sum_{j \in N_i} \sigma_j^z \sigma_i^z$ . For ferromagnetic states in

$$\text{span} \left\{ |\uparrow\rangle^{\otimes N}, |\downarrow\rangle^{\otimes N} \right\}$$

this yields 1 and  $d_i$  annihilates such states; they are *dark states* for the ferromagnetic process  $\{d_i\}$ . States with anticorrelated neighbours are driven towards perfect correlation by the spin flip  $\sigma_i^x$  that occurs when  $\frac{1}{q} \sum_{j \in N_i} \sigma_j^z \sigma_i^z < 1$ . The steady states of the dissipative process  $\{d_i\}$  are exactly the ground states of the TIM for vanishing magnetic field  $h = 0$  (and their incoherent mixtures). In contrast,  $c_i$  is just the raising operator in the  $\sigma^x$ -eigenbasis that acts strictly local on spin  $i$ . The paramagnetic process  $\{c_i\}$  drives the system in the completely  $x$ -polarised state  $|+\rangle^{\otimes N}$  — which is clearly a unique dark state and equals the ground state of the TIM for  $h \rightarrow \infty$  or  $J = 0$ .

The principal question of this chapter is: What happens if we vary the parameters from  $\kappa_F = 0$  and/or  $\kappa_P = \infty$  to  $\kappa_F = \infty$  and/or  $\kappa_P = 0$ ? This question includes both aspects of the Lindblad equation, the non-equilibrium steady states and the relaxation to the latter. To complicate the system, one may include the *Hamiltonian*  $H_{\text{TIM}}$  and examine the effects of competing unitary and dissipative contributions on the dynamics and steady states.

Before we start with the analysis, there is a technical remark in order: It took roughly a year to write this thesis. As a consequence there are passages which were written at early stages of my studies. Therefore the notation is not always consistent; some notations changed over time and reached their evolutionary fixed point at later stages. In the following, the ferromagnetic jump operators are sometimes written in the slightly modified form

$$d_i = \sigma_i^x \left( \frac{1}{q} \sum_{j \in N_i} \sigma_j^z \sigma_i^z - \mathbb{1} \right). \quad (2.8)$$

In these cases the couplings  $\kappa_F$  and  $\kappa_P$  are written explicitly in front of the Lindbladian superoperator  $\mathcal{L}[\bullet]$ . It is obvious that this is equivalent to Def. 2.1 up to a phase factor and a rescaling of  $\kappa_F$ . With this in mind, we can start our discussion of the dissipative transverse field Ising model with some symmetry considerations in the next section.



## 2.2 Symmetry considerations

In this section we rigorously derive the complete group of *strong symmetries* for the dissipative system given in Def. 2.1. To this end we start with some notes on symmetries of Lindblad superoperators in 2.2.1. In Subsec. 2.2.2 follows the detailed derivation for the dissipative TIM.

### 2.2.1 General definitions

Let us start with some definitions concerning symmetries of master equations in Lindblad form. In contrast to symmetries of Hamiltonian systems, there is a bit more freedom regarding symmetries of dissipative processes that are described by a Lindblad master equation. The following definition is motivated by Ref. [112]:

#### ► Definition 2.2: Symmetries of Lindblad operators

Given a master equation in Lindblad form

$$\partial_t \rho = -i [H, \rho] + \sum_{i=1}^M \sum_j \kappa_i \left[ c_{i,j} \rho c_{i,j}^\dagger - \frac{1}{2} \{ c_{i,j}^\dagger c_{i,j}, \rho \} \right] \equiv -i [H, \rho] + \mathcal{L}(\{\kappa_i\}, \{c_{i,j}\})[\rho] \quad (2.9)$$

where  $\kappa_i > 0$  denotes the coupling strength to bath  $i$ . The coupling is described by the jump operators  $c_{i,j}$  where  $i$  is the bath index and  $j$  denotes the lattice site. The unitary dynamics is governed by the Hamiltonian  $H$  and the dissipative dynamics by the Lindblad superoperator  $\mathcal{L}$ .

For brevity define

$$\mathfrak{L}[\rho] \equiv -i [H, \rho] + \mathcal{L}(\{\kappa_i\}, \{c_{i,j}\})[\rho] \quad (2.10)$$

which is the generator of a completely positive and trace preserving (CPTP) map on the convex set of density matrices  $\mathcal{D}(\mathcal{H})$  where  $\mathcal{H}$  is the system Hilbert space.

A *unitary* (*antiunitary*) operator  $U$  ( $UK$ ) that leaves  $\mathfrak{L}$  invariant is called a **weak symmetry**:

$$\mathfrak{L}[U\rho U^\dagger] = U\mathfrak{L}[\rho]U^\dagger \quad (2.11)$$

In case of an antiunitary operator  $UK$ , the additional relation  $\mathfrak{L}[K\rho] = K\mathfrak{L}[\rho]$  must hold. Here  $K$  denotes the (antilinear) complex conjugation.

For a **strong symmetry**  $U$  ( $UK$ ) we require

$$UHU^\dagger = H \quad (2.12a)$$

$$\text{and } \forall_{i,j} U c_{i,j} U^\dagger = e^{i\alpha_{i,j}} c_{i,j} \quad \text{where } \alpha_{i,j} \in \mathbb{R}. \quad (2.12b)$$

That is, each summand in the dissipative part of  $\mathfrak{L}$  remains invariant and  $U$  ( $UK$ ) is a symmetry of the Hamiltonian system.

Is  $U$  a symmetry and a local unitary, that is  $U = \prod_j U_j$  and  $\text{supp}(U_j) = \{j\}$  for all sites  $j$ , we call it a **local symmetry**.

Let us now proceed with an application of this definition to our dissipative TIM.

### 2.2.2 Symmetries of the TIM master equation

In this subsection we derive all possible *strong local symmetries* of the dissipative TIM master equation introduced above. To this end, recall that

$$c_j = \frac{1}{2} (\sigma_j^z - i\sigma_j^y), \quad d_j = -\frac{i}{q} \sum_{m \in N_j} \sigma_m^z \sigma_j^y - \sigma_j^x, \quad \text{and} \quad H = -J \sum_{\langle n,m \rangle} \sigma_n^z \sigma_m^z - h \sum_n \sigma_n^x \quad (2.13)$$

and consequently we are looking for local unitary operators  $U = \prod_j U_j$  such that

$$UHU^\dagger = H \quad (2.14a)$$

$$\forall_j U c_j U^\dagger = e^{i\alpha_j} c_j \quad (2.14b)$$

$$\forall_j U d_j U^\dagger = e^{i\beta_j} d_j. \quad (2.14c)$$

Let us proceed systematically:

Antiunitary symmetries

First, let us consider an *antiunitary* operator  $UK$ . We demand  $\mathcal{L}[K\rho] = K\mathcal{L}[\rho]$ , so

$$K(-i[H, \rho] + \mathcal{L}[\rho]) = i[H, K\rho] + \mathcal{L}[K\rho] \stackrel{!}{=} -i[H, K\rho] + \mathcal{L}[K\rho]. \quad (2.15)$$

Here we used the fact that  $H$ ,  $c_j$  and  $d_j$  are real operators. We conclude that

$$\forall_\rho [H, \rho] = 0 \quad \Rightarrow \quad H = \lambda \mathbf{1}, \quad \lambda \in \mathbb{R}. \quad (2.16)$$

Since this conditions are not met by the Hamiltonian at hand, the system cannot feature any antiunitary strong local symmetries.

Especially the reflection at the  $\sigma_x$ - $\sigma_z$ -plane is not a symmetry as long as the Hamiltonian dynamics is present. This can be seen easily as follows: The aforementioned reflection demands

$$\begin{aligned} \sigma_x &\rightarrow \sigma_x \\ \sigma_y &\rightarrow -\sigma_y \\ \sigma_z &\rightarrow \sigma_z \end{aligned}$$

and we immediately identify  $\mathbb{1}K$  as the appropriate *antiunitary* operator. If we set  $H = 0$ , and thus consider a pure dissipatively driven system, this becomes a symmetry and we expect the ferromagnetic solutions to stick to the  $\sigma_x$ - $\sigma_z$ -plane. We will see that this is indeed the case, see paragraph 2.3.2 for instance. ■

## Unitary symmetries

Let us now strive towards possible unitary strong local symmetries. Therefore equations (2.14) must be fulfilled by some *local* unitary  $U = \prod_i U_i$ . For reasons which become clear later on, we start with Eq. (2.14c).

■ On  $Ud_jU^\dagger = e^{i\beta_j}d_j$

First expand the left and right hand side. One finds

$$Ud_jU^\dagger = -\frac{i}{q} \sum_{m \in N_j} (U_m \sigma_m^z U_m^\dagger) (U_j \sigma_j^y U_j^\dagger) - U_j \sigma_j^x U_j^\dagger \quad (2.17a)$$

$$e^{i\beta_j}d_j = -\frac{i}{q} \sum_{m \in N_j} e^{i\beta_j} \sigma_m^z \sigma_j^y - e^{i\beta_j} \sigma_j^x \quad (2.17b)$$

and by subtraction the equations read

$$-\frac{i}{q} \sum_{m \in N_j} [(U_m \sigma_m^z U_m^\dagger) (U_j \sigma_j^y U_j^\dagger) - e^{i\beta_j} \sigma_m^z \sigma_j^y] - [U_j \sigma_j^x U_j^\dagger - e^{i\beta_j} \sigma_j^x] = 0. \quad (2.18)$$

Apply  $\text{Tr}_j [\cdot]$  on both sides of the equation and note that  $\text{Tr}_j [U_m \sigma_m^z U_m^\dagger] = \text{Tr}_j [\sigma_m^z] = 0$ , given  $m \neq j$ . Thus we arrive at

$$U_j \sigma_j^x U_j^\dagger - e^{i\beta_j} \sigma_j^x = 0 \Leftrightarrow U_j \sigma_j^x U_j^\dagger = e^{i\beta_j} \sigma_j^x \quad (2.19)$$

and consequently

$$-\frac{i}{q} \sum_{m \in N_j} [(U_m \sigma_m^z U_m^\dagger) (U_j \sigma_j^y U_j^\dagger) - e^{i\beta_j} \sigma_m^z \sigma_j^y] = 0. \quad (2.20)$$

A second application of  $\text{Tr}_{\{i,j\}} [\cdot]$  ( $i \in N_j$ ) yields

$$(U_i \sigma_i^z U_i^\dagger) (U_j \sigma_j^y U_j^\dagger) - e^{i\beta_j} \sigma_i^z \sigma_j^y = 0 \Leftrightarrow (U_i \sigma_i^z U_i^\dagger) (U_j \sigma_j^y U_j^\dagger) = e^{i\beta_j} \sigma_i^z \sigma_j^y. \quad (2.21)$$

It is now clear that

$$\forall_{i \in N_j} U_i \sigma_i^z U_i^\dagger = e^{i\beta_{j,2}} \sigma_i^z \quad (2.22a)$$

$$U_j \sigma_j^y U_j^\dagger = e^{i\beta_{j,1}} \sigma_j^y \quad (2.22b)$$

where  $\beta_{j,1} + \beta_{j,2} = \beta_j$  since  $i$ - and  $j$ -operators act on distinct Hilbert spaces. To get rid of the  $j$ -indices, apply Eq. (2.19) to Eq. (2.21):

$$(U_i \sigma_i^z U_i^\dagger) (U_j \sigma_j^z U_j^\dagger) = e^{2i\beta_j} \sigma_i^z \sigma_j^z \quad (2.23)$$

A permutation of  $i$  and  $j$  yields

$$(U_i \sigma_i^z U_i^\dagger) (U_j \sigma_j^z U_j^\dagger) = e^{2i\beta_i} \sigma_i^z \sigma_j^z \quad (2.24)$$

and consequently  $\beta_i = \beta_j$  whenever  $i \in N_j$ . Therefore, on each connected component of the lattice, we find  $\beta_j \equiv \beta$  being independent of  $j$ . To sum up, Eq. (2.14c) implies:

► Remark 2.1: Requirements for strong local Symmetries I

$$U_j \sigma_j^x U_j^\dagger = e^{i\beta} \sigma_j^x \quad (2.25a)$$

$$U_j \sigma_j^y U_j^\dagger = e^{i\beta_1} \sigma_j^y \quad (2.25b)$$

$$U_j \sigma_j^z U_j^\dagger = e^{i\beta_2} \sigma_j^z \quad \text{where } \beta_1 + \beta_2 = \beta \quad (2.25c)$$

These results are crucial and prove useful as we proceed with Eq. (2.14c).

■ On  $UHU^\dagger = H$

Expand the left hand side and apply the relations we just found:

$$\begin{aligned} UHU^\dagger &= -J \sum_{\langle n,m \rangle} (U_n \sigma_n^z U_n^\dagger) (U_m \sigma_m^z U_m^\dagger) - h \sum_n U_n \sigma_n^x U_n^\dagger \\ &= -J \sum_{\langle n,m \rangle} e^{2i\beta_2} \sigma_n^z \sigma_m^z - h \sum_n e^{i\beta} \sigma_n^x \\ &\stackrel{!}{=} -J \sum_{\langle n,m \rangle} \sigma_n^z \sigma_m^z - h \sum_n \sigma_n^x \end{aligned}$$

Tracing out via  $\text{Tr}_j[\cdot]$  yields  $e^{i\beta} \sigma_j^x = \sigma_j^x$ , that is  $\beta = 2\pi k$  ( $k \in \mathbb{Z}$ ). Since it follows

$$\sum_{\langle n,m \rangle} e^{2i\beta_2} \sigma_n^z \sigma_m^z = \sum_{\langle n,m \rangle} \sigma_n^z \sigma_m^z \quad (2.26)$$

we arrive at  $e^{2i\beta_2} \sigma_i^z \sigma_j^z = \sigma_i^z \sigma_j^z \Rightarrow \beta_2 = \pi l$  ( $l \in \mathbb{Z}$ ) via  $\text{Tr}_{\{i,j\}}[\cdot]$  ( $i \in N_j$ ). By  $\beta_1 + \beta_2 = \beta$  we find  $\beta_2 = \pi(2k - l)$ , that is  $e^{i\beta_1} = e^{i\beta_2} = \pm 1$ . Let us summarise what we found so far:

► Remark 2.2: Requirements for strong local Symmetries II

$$U_j \sigma_j^x U_j^\dagger = \sigma_j^x \quad (2.27a)$$

$$U_j \sigma_j^y U_j^\dagger = \pm \sigma_j^y \quad (2.27b)$$

$$U_j \sigma_j^z U_j^\dagger = \pm \sigma_j^z \quad (2.27c)$$

Note that only two of these equations are independent as any combination of two equations yields the third.

■ On  $Uc_jU^\dagger = e^{i\alpha_j}c_j$

By application of the latest results one finds

$$Uc_jU^\dagger = \frac{1}{2} \left( U_j\sigma_j^zU_j^\dagger - iU\sigma_j^yU_j^\dagger \right) = \pm \frac{1}{2} \left( \sigma_j^z - i\sigma_j^y \right) \stackrel{!}{=} e^{i\alpha_j}c_j \quad (2.28)$$

and therefore  $\alpha_j = \beta_1 = \beta_2 \equiv \alpha$ . So there are no additional constraints due to the relation  $Uc_jU^\dagger = e^{i\alpha_j}c_j$ . ■

In order to solve the system of equations (2.27), we employ the following parametrisation of the 4-parameter Lie group  $U(2)$  [113]<sup>24</sup>. For all  $U \in U(2)$  exist  $(\alpha_1, \alpha_2, \tau, \theta) \in [0, 2\pi]^3 \times [0, \frac{\pi}{2}]$  such that

$$U = VAV^\dagger \quad \text{where} \quad A = \begin{bmatrix} e^{i\alpha_1} & 0 \\ 0 & e^{i\alpha_2} \end{bmatrix} \quad \text{and} \quad V = \begin{bmatrix} e^{i\tau} \cos \theta & -\sin \theta \\ \sin \theta & e^{-i\tau} \cos \theta \end{bmatrix}. \quad (2.29)$$

Inserting this parametrisation in two of the equations (2.27) yields after some straightforward calculations the following solutions

$$(+) : U_j = e^{i\varphi} \mathbb{1}_j \quad \text{and} \quad (-) : U_j = e^{i\varphi} \sigma_j^x \quad \text{where} \quad \varphi \in \mathbb{R}, \quad (2.30)$$

as expected. Therefore the strong local symmetry group is (up to a global phase)  $\{\mathbb{1}, X\} \cong \mathbb{Z}_2$  which is represented by a *global*  $\pi$ -rotation about the  $\sigma^x$ -axis, that is,  $X = \prod_i \sigma_i^x$ . Thus we expect the (ferromagnetic) solutions to transform with respect to this symmetry group.

► **Result 2.1: Strong symmetries of the dissipative TIM**

The group of *strong local symmetries* for the dissipative transverse field Ising model is

$$\{\mathbb{1}, X\} \cong \mathbb{Z}_2 \quad \text{where} \quad X = \prod_i \sigma_i^x \quad (2.31)$$

denotes a global spin-flip or  $\pi$ -rotation about the  $\sigma^x$ -axis.

Please note that this global symmetry group  $\{\mathbb{1}, X\} \cong \mathbb{Z}_2$  is exactly the global spin-flip symmetry that characterises the transverse field Ising model.

<sup>24</sup>At this point the solutions are easy to see. However, we proceed rigorously by solving the equation systems.

## 2.3 A mean field approach

The original motivation for the dissipative TIM was the presumed non-equilibrium phase transition that separates the ferromagnetic and the paramagnetic phase. Our top priority is therefore to learn as much as possible about its phase diagram. Whereas the paramagnetic jump operators act locally on single spins and do not interact with other sites, the ferromagnetic jump operators *do* interact with the nearest-neighbours. In fact, this is inevitable as the ferromagnetic steady states are characterised by their non-trivial transformation with respect to the strong symmetry group  $\mathbb{Z}_2$ . To achieve this, the jumps have to establish *correlations* and not *polarisation* which requires interactions between adjacent spins. Unfortunately this renders the dissipative TIM analytically challenging if not intractable.

As we cannot count on analytical solutions, we have to put up with approximate ones. Here we focus on a mean field solution of the dissipative TIM — motivated by the qualitative success of mean field approaches for its *Hamiltonian* counterpart.

This is the main part of the current chapter and we proceed as follows. In the next subsection 2.3.1 we present a brief derivation of the effective mean field jump operators. The stationary mean field solutions are examined in Subsec. 2.3.2 in detail; both with and without competing Hamiltonian contributions. We also discuss the limit of the theory for infinite dimensions. In Subsec. 2.3.3 we investigate the *dynamical* behaviour of the theory with focus on its behaviour near the phase transition. In addition we derive a continuous version of the mean field theory.

### 2.3.1 Derivation of the mean field Lindblad superoperator

For the sake of clarity, we give at this point a condensed derivation of the mean field jump operators. A detailed version of the following steps can be found in Appendix B.

Preliminary remarks

In order to derive a mean field version of the dissipative theory given in Def. 2.1, recall that the jump operators read

$$c_j = \frac{1}{2} (\sigma_j^z - i\sigma_j^y) \quad \text{and} \quad d_j = \sigma_j^x \left[ \frac{1}{q} \sum_{m \in N_j} \sigma_m^z \sigma_j^z - 1 \right] \quad (2.32)$$

and the (combined) dynamics of Hamiltonian and dissipative contributions is given by the Lindblad master equation

$$\partial_t \rho = -i[H, \rho] + \kappa_P \sum_j \left[ c_j \rho c_j^\dagger - \frac{1}{2} \{c_j^\dagger c_j, \rho\} \right] + \kappa_F \sum_j \left[ d_j \rho d_j^\dagger - \frac{1}{2} \{d_j^\dagger d_j, \rho\} \right] \quad (2.33a)$$

$$\equiv -i[H, \rho] + \mathcal{L}[\rho] \quad (2.33b)$$

where  $\kappa_P, \kappa_F \geq 0$  describe the strength of the coupling to the external baths and  $\mathcal{L}$  denotes the Lindblad superoperator; the generator of a completely positive and trace preserving (CPTP) map on the space of density matrices that encodes the dissipatively induced ensemble evolution of the system.

Each spin is described by its two-dimensional Hilbert space  $\mathcal{H}_i = \mathbb{C}_i^2$ ; therefore the systems Hilbert space is  $\mathcal{H} = \otimes_j \mathcal{H}_j$ . In the following we write  $\overline{\mathcal{H}}_i = \otimes_{j,j \neq i} \mathcal{H}_j$  and  $\text{Tr}_i [X] \equiv \text{Tr}_{\overline{\mathcal{H}}_i} [X]$  for tracing out the whole system *except* the  $i$ th spin.

Derivation of the mean field jump operators

In self-consistent field theory (or mean field theory) the nearest neighbour couplings are replaced by the interaction with an *effective mean field* arising from the spin environment. To this end, the product ansatz

$$\rho = \prod_{l=1}^N \rho_l \quad (2.34)$$

is inserted into the master equation; here  $\rho_l$  operates *nontrivially* only on  $\mathcal{H}_l$ . We note that  $\text{Tr}_i [\rho] = \rho_i$ . Due to the product ansatz above, the master equation decouples into  $N$  independent differential equations for  $\{\rho_i\}_{1 \leq i \leq N}$ . That is

$$\underbrace{\text{Tr}_i [\partial_t \rho]}_{\text{Derivative}} = -i \underbrace{\text{Tr}_i [[H, \rho]]}_{\text{Unitary term}} + \underbrace{\kappa_P \sum_j \text{Tr}_i \left[ c_j \rho c_j^\dagger - \frac{1}{2} \{c_j^\dagger c_j, \rho\} \right]}_{\text{Paramagnetic term}} + \underbrace{\kappa_F \sum_j \text{Tr}_i \left[ d_j \rho d_j^\dagger - \frac{1}{2} \{d_j^\dagger d_j, \rho\} \right]}_{\text{Ferromagnetic term}}$$

is expected to be of the form

$$\partial_t \rho_i = -i [H_i^{\text{mf}}, \rho_i] + \mathcal{L}_i^{\text{mf}}[\rho_i] \quad (2.35)$$

where  $H_i^{\text{mf}}$  and  $\mathcal{L}_i^{\text{mf}}$  denote the local mean field versions of the Hamiltonian and the Lindbladian, respectively. In the next paragraphs the exact form of  $H_i^{\text{mf}}$  and  $\mathcal{L}_i^{\text{mf}}$  is derived. The left-hand side is easily evaluated to

$$\text{Tr}_i [\partial_t \rho] = \partial_t \text{Tr}_i \left[ \prod_{l=1}^N \rho_l \right] = \partial_t \rho_i \quad (2.36)$$

so that we can proceed with the unitary term:

#### ■ Unitary term

This term yields the well-known mean field theory for the transverse field Ising model and reads

$$-i \text{Tr}_i [[H, \rho]] = \dots = -i [-Jq m_z \sigma_i^z - h \sigma_i^x, \rho_i]. \quad (2.37)$$

For this calculation we used the fact that  $\text{Tr}_i [[X, \rho]] = \text{Tr}_i [X\rho] - \text{Tr}_i [\rho X] = \rho_i (\langle X \rangle - \langle X \rangle) = 0$  if  $X$  acts nontrivially on  $\overline{\mathcal{H}}_i$  only and assumed a *homogeneous system*; that is,  $m_z \equiv \langle \sigma_n^z \rangle = \text{Tr}_i [\sigma_n^z \rho_n]$  is independent of  $n (\neq i)$ . Therefore the mean field Hamiltonian reads

$$H_i^{\text{mf}} = -Jq m_z \sigma_i^z - h \sigma_i^x = -\mathbf{h}_{\text{mf}} \sigma_i \quad (2.38)$$

where  $\sigma_i = [\sigma_i^x, \sigma_i^y, \sigma_i^z]^T$  and  $\mathbf{h}_{\text{mf}} = [h, 0, Jq m_z]^T$  denotes the *mean field*.

### ■ Paramagnetic term

Let us continue with the paramagnetic term. Since

$$c_j = \frac{1}{2} (\sigma_j^z - i\sigma_j^y) = \sigma_j^{x,+} \quad (2.39)$$

acts non-trivially on  $\mathcal{H}_i$  only, we find immediately

$$\text{Tr}_i [c_j \rho c_j^\dagger] = c_j \rho_i c_j^\dagger, \quad \text{Tr}_i [c_j^\dagger c_j \rho] = c_j^\dagger c_j \rho_i, \quad \text{Tr}_i [\rho c_j^\dagger c_j] = \rho_i c_j^\dagger c_j \quad (2.40)$$

and for  $j \neq i$

$$\text{Tr}_i [c_j \rho c_j^\dagger] = \text{Tr}_i [c_j^\dagger c_j \rho] = \text{Tr}_i [\rho c_j^\dagger c_j] = \rho_i \langle c_j^\dagger c_j \rangle. \quad (2.41)$$

If we use these results, it is straightforward to show

$$\kappa_P \sum_j \text{Tr}_i \left[ c_j \rho c_j^\dagger - \frac{1}{2} \{c_j^\dagger c_j, \rho\} \right] = \kappa_P \left( c_i \rho_i c_i^\dagger - \frac{1}{2} \{c_i^\dagger c_i, \rho_i\} \right) = \kappa_P \mathcal{L}(c_i) [\rho_i] \quad (2.42)$$

which was expected since the paramagnetic jump operators  $c_j$  act locally and independent of the neighbours  $N_j$ . Consequently they remain unaffected by the mean field approximation.

### ■ Ferromagnetic term

The ferromagnetic term is the most complicated one since the jump operator  $d_j$  acts on spin  $j$  and its neighbours  $N_j$ . First we note that for  $j \notin N_i \cup \{i\}$

$$\text{Tr}_i [d_j \rho d_j^\dagger] = \text{Tr}_i [d_j^\dagger d_j \rho] = \text{Tr}_i [\rho d_j^\dagger d_j] = \rho_i \langle d_j^\dagger d_j \rangle \quad (2.43)$$

and therefore

$$\sum_{j \notin N_i \cup \{i\}} \text{Tr}_i \left[ d_j \rho d_j^\dagger - \frac{1}{2} \{d_j^\dagger d_j, \rho\} \right] = \sum_{j \notin N_i \cup \{i\}} \left\{ \text{Tr}_i [d_j \rho d_j^\dagger] - \frac{1}{2} \text{Tr}_i [\{d_j^\dagger d_j, \rho\}] \right\} = 0 \quad (2.44)$$

vanishes. This reduces the sum that remains to be evaluated to

$$\kappa_F \sum_j \text{Tr}_i \left[ d_j \rho d_j^\dagger - \frac{1}{2} \{d_j^\dagger d_j, \rho\} \right] = \underbrace{\kappa_F \sum_{j \in N_i} \left\{ \text{Tr}_i [d_j \rho d_j^\dagger] - \frac{1}{2} \text{Tr}_i [\{d_j^\dagger d_j, \rho\}] \right\}}_{\text{Nearest neighbours (NN)}} \quad (2.45a)$$

$$+ \underbrace{\kappa_F \left( \text{Tr}_i [d_i \rho d_i^\dagger] - \frac{1}{2} \text{Tr}_i [\{d_i^\dagger d_i, \rho\}] \right)}_{\text{Spin } i \text{ (Si)}}. \quad (2.45b)$$

which comprises  $q + 1 = 2d + 1$  terms in total for a  $d$ -dimensional lattice. We have to calculate the partial traces for the nearest neighbours (NN) and the spin itself (Si) separately:



► **Nearest neighbours (NN)**

Let us first consider the case where  $j \in N_i \Leftrightarrow i \in N_j (\Rightarrow i \neq j)$ . Straightforward but cumbersome calculations yield the three summands

$$\begin{aligned}\mathrm{Tr}_i \left[ d_j \rho d_j^\dagger \right] &= \frac{1}{q^2} [C(q, m_z) \rho_i + (q-1) m_z \{ \sigma_i^z, \rho_i \} + \sigma_i^z \rho_i \sigma_i^z] - \frac{m_z}{q} [(q-1) 2 m_z \rho_i + \{ \sigma_i^z, \rho_i \}] + \rho_i \\ \mathrm{Tr}_i \left[ d_j^\dagger d_j \rho \right] &= \frac{1}{q^2} [C(q, m_z) \rho_i + 2(q-1) m_z \sigma_i^z \rho_i + \sigma_i^z \sigma_i^z \rho_i] - \frac{2 m_z}{q} [(q-1) m_z \rho_i + \sigma_i^z \rho_i] + \rho_i \\ \mathrm{Tr}_i \left[ \rho d_j^\dagger d_j \right] &= \frac{1}{q^2} [C(q, m_z) \rho_i + 2(q-1) m_z \rho_i \sigma_i^z + \rho_i \sigma_i^z \sigma_i^z] - \frac{2 m_z}{q} [(q-1) m_z \rho_i + \rho_i \sigma_i^z] + \rho_i.\end{aligned}$$

The last equation can of course be deduced by symmetry arguments and has not to be computed by hand. The constant term  $C(q, m_z)$  is not important as it cancels in the next step. The combination of these three terms yields

$$\sum_{j,j \in N_i} \left\{ \mathrm{Tr}_i \left[ d_j \rho d_j^\dagger \right] - \frac{1}{2} \mathrm{Tr}_i \left[ \left\{ d_j^\dagger d_j, \rho \right\} \right] \right\} = \frac{1}{q} \left( \sigma_i^z \rho_i \sigma_i^z - \frac{1}{2} \{ \sigma_i^z \sigma_i^z, \rho_i \} \right) \quad (2.47)$$

and we found as additional mean field jump operator the  $\sigma^z$ -dephasing

$$\bar{v}_j := \frac{1}{\sqrt{q}} \sigma_j^z. \quad (2.48)$$

the coupling strength of which is rescaled by the dimension  $q = 2d$ .

► **Spin  $i$  (Si)**

Finally the special case  $j = i$  is left and we find by straightforward calculations

$$\mathrm{Tr}_i \left[ d_i \rho d_i^\dagger \right] = \bar{b}_i \rho_i \bar{b}_i^\dagger + \bar{d}_i \rho_i \bar{d}_i^\dagger \quad \text{and} \quad \mathrm{Tr}_i \left[ d_i^\dagger d_i \rho \right] = \bar{b}_i^\dagger \bar{b}_i \rho_i + \bar{d}_i^\dagger \bar{d}_i \rho_i$$

and subsequently

$$\mathrm{Tr}_i \left[ \left\{ d_i^\dagger d_i, \rho \right\} \right] = \left\{ \bar{b}_i^\dagger \bar{b}_i, \rho_i \right\} + \left\{ \bar{d}_i^\dagger \bar{d}_i, \rho_i \right\}. \quad (2.49)$$

Here we introduced the mean field jump operators

$$\bar{d}_j := \sigma_j^x (m_z \sigma_j^z - \mathbf{1}) \quad (2.50a)$$

$$\bar{b}_j := \frac{1}{\sqrt{q}} \sqrt{1 - m_z^2} \sigma_j^y. \quad (2.50b)$$

We arrive at

$$\mathrm{Tr}_i \left[ d_i \rho d_i^\dagger \right] - \frac{1}{2} \mathrm{Tr}_i \left[ \left\{ d_i^\dagger d_i, \rho \right\} \right] = \bar{d}_i \rho_i \bar{d}_i^\dagger - \frac{1}{2} \left\{ \bar{d}_i^\dagger \bar{d}_i, \rho_i \right\} + \bar{b}_i \rho_i \bar{b}_i^\dagger - \frac{1}{2} \left\{ \bar{b}_i^\dagger \bar{b}_i, \rho_i \right\} \quad (2.51)$$

with the new mean field jump operators  $\bar{b}_j$  and  $\bar{d}_j$ . ◀

Therefore the *total* contributions of the ferromagnetic jump operators  $d_j$  are

$$\sum_j \text{Tr}_i \left[ d_j \rho d_j^\dagger - \frac{1}{2} \{d_j^\dagger d_j, \rho\} \right] = \mathcal{L}(\bar{d}_i) [\rho_i] + \mathcal{L}(\bar{b}_i) [\rho_i] + \mathcal{L}(\bar{o}_i) [\rho_i] \quad (2.52)$$

with the three superoperators

$$\mathcal{L}(\bar{d}_i) [\rho_i] = \bar{d}_i \rho_i \bar{d}_i^\dagger - \frac{1}{2} \{ \bar{d}_i^\dagger \bar{d}_i, \rho_i \} \quad (2.53a)$$

$$\mathcal{L}(\bar{b}_i) [\rho_i] = \bar{b}_i \rho_i \bar{b}_i^\dagger - \frac{1}{2} \{ \bar{b}_i^\dagger \bar{b}_i, \rho_i \} \quad (2.53b)$$

$$\mathcal{L}(\bar{o}_i) [\rho_i] = \bar{o}_i \rho_i \bar{o}_i^\dagger - \frac{1}{2} \{ \bar{o}_i^\dagger \bar{o}_i, \rho_i \} \quad (2.53c)$$

and the effective jump operators  $\bar{d}_i$ ,  $\bar{b}_i$  and  $\bar{o}_i^z$  defined above. ■

By combining all results derived above, we finally arrive at the mean field version of the Lindblad master equation:

► **Result 2.2: Mean field Lindblad equation for dissipative TIM**

The mean field version of the Lindblad master equation for the dissipative TIM reads

$$\partial_t \rho_i = -i [H_i^{\text{mf}}, \rho_i] + \kappa_P \mathcal{L}(c_i) [\rho_i] + \kappa_F \mathcal{L}(\bar{d}_i) [\rho_i] + \kappa_F \mathcal{L}(\bar{b}_i) [\rho_i] + \kappa_F \mathcal{L}(\bar{o}_i) [\rho_i]$$

with the four effective jump operators

$$\bar{d}_j = \sigma_j^x (m_z \sigma_j^z - \mathbb{1}) \quad (2.54a)$$

$$\bar{b}_j = \frac{1}{\sqrt{q}} \sqrt{1 - m_z^2} \sigma_j^y \quad (2.54b)$$

$$\bar{o}_j = \frac{1}{\sqrt{q}} \sigma_j^z \quad (2.54c)$$

$$c_j = \frac{1}{2} (\sigma_j^z - i \sigma_j^y) \quad (2.54d)$$

and the mean field Hamiltonian

$$H_i^{\text{mf}} = -Jq m_z \sigma_i^z - h \sigma_i^x = -\mathbf{h}_{\text{mf}} \sigma_i. \quad (2.54e)$$

for the unitary evolution of the transverse field Ising model.

We are now prepared for the detailed mean field analysis of the dissipative TIM in the next two subsections. There we employ the results derived in Appendix A to find the self-consistent steady states and their dynamics for the dissipative process derived in this subsection.

### 2.3.2 Static solutions

In this section we examine the non-equilibrium steady states of the dissipatively driven transverse field Ising model by means of the previously derived mean field jump operators. To this end we employ the equations derived in Appendix A for general mean field theories of dissipative processes governed by Lindblad master equations.

A first overview

Let us first derive the specific mean field equations of the theory and subsequently compute the steady states numerically for various parameters to get an overview of the phase structure. In the following paragraphs the different parameter regimes are then examined more carefully.

To apply the mean field equation Eq.(A.26) which determines the steady states, we first have to compute the system matrix  $(L_{i,j})$  defined in Eq. (A.8). Note that we deal with a single mean field  $\mathbf{m}$  and therefore  $\alpha \equiv 1$  in all equations of Appendix A. Recall the four mean field jump operators (we omit the overlines in the following)

$$d \equiv \sqrt{\kappa_F} \sigma^x (\mathbb{1} - m_z \sigma^z), \quad b \equiv \sqrt{\frac{\kappa_F}{q}} \sqrt{1 - m_z^2} \sigma^y, \quad o \equiv \sqrt{\frac{\kappa_F}{q}} \sigma^z, \quad c \equiv \frac{\sqrt{\kappa_P}}{2} (\sigma^z - i\sigma^y) \quad (2.55)$$

and the mean field unitary dynamics defined by

$$H_{\text{TIM}}^{\text{mf}} = -Jqm_z \sigma^z - h\sigma^x \equiv \mathbf{h}^{\text{mf}} \boldsymbol{\sigma} \quad \text{with} \quad \mathbf{h}^{\text{mf}} = \begin{bmatrix} -h & 0 & -Jqm_z \end{bmatrix}^T. \quad (2.56)$$

The coordinate representation  $l_{\mu,\lambda}$  (where  $\mu = 1, 2, 3, 4$  or  $d, b, o, c$  and  $\lambda = 1, 2, 3$  or  $x, y, z$ ) of the four jump operators can be computed via

$$l_{\mu,\lambda} = \frac{1}{2} \text{Tr} [\sigma^\lambda L_\mu] \quad \text{where} \quad L_\mu \in \{d, b, o, c\} \quad (2.57)$$

and we find

$$l_d = \sqrt{\kappa_F} \begin{bmatrix} 1 & im_z & 0 \end{bmatrix}^T \quad (2.58a)$$

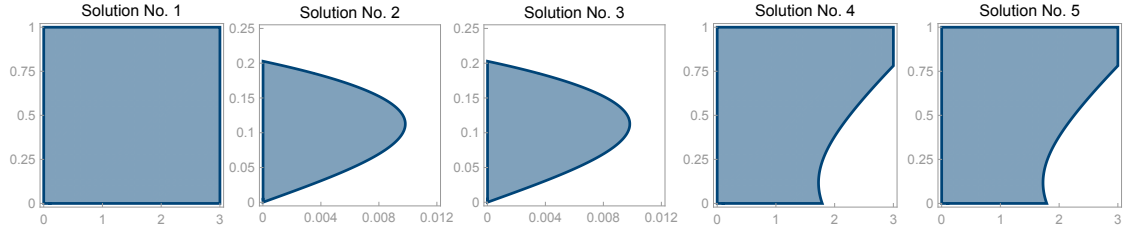
$$l_b = \sqrt{\frac{\kappa_F}{q}} \begin{bmatrix} 0 & \sqrt{1 - m_z^2} & 0 \end{bmatrix}^T \quad (2.58b)$$

$$l_o = \sqrt{\frac{\kappa_F}{q}} \begin{bmatrix} 0 & 0 & 1 \end{bmatrix}^T \quad (2.58c)$$

$$l_c = \frac{\sqrt{\kappa_P}}{2} \begin{bmatrix} 0 & -i & 1 \end{bmatrix}^T \quad (2.58d)$$

which then yields according to Eq. (A.8) the system matrix

$$(L_{i,j}) = \begin{bmatrix} \kappa_F & im_z \kappa_F & 0 \\ -im_z \kappa_F & \frac{\kappa_F}{q} [(q-1)m_z^2 + 1] + \frac{\kappa_P}{4} & \frac{i\kappa_P}{4} \\ 0 & -\frac{i\kappa_P}{4} & \frac{\kappa_F}{q} + \frac{\kappa_P}{4} \end{bmatrix} \quad (2.59)$$



■ **Figure 2.1:** Classification of the mean field solutions. There are five *algebraic* solutions to the mean field equations. They are *physical*, in the sense that  $\mathbf{a} \in \mathbb{R}^3$  and  $\|\mathbf{a}\| \leq 1$ , in the blue regions. On the horizontal axis  $\kappa_P$  and on the vertical axis  $\kappa_F$  is varied. The unitary parameters are fixed at  $J = 0.2 = h$  and the coordination number is  $q = 6$ . Note the change of scales in the plots of solutions No. 2 and 3.

and hence the real  $R_{i,j}$  and imaginary part  $I_{i,j}$  read

$$\left( R_{i,j} \right) = \begin{bmatrix} \kappa_F & 0 & 0 \\ 0 & \frac{\kappa_F}{q} [(q-1)m_z^2 + 1] + \frac{\kappa_P}{4} & 0 \\ 0 & 0 & \frac{\kappa_F}{q} + \frac{\kappa_P}{4} \end{bmatrix}, \quad \left( I_{i,j} \right) = \begin{bmatrix} 0 & m_z \kappa_F & 0 \\ -m_z \kappa_F & 0 & \frac{\kappa_P}{4} \\ 0 & -\frac{\kappa_P}{4} & 0 \end{bmatrix}. \quad (2.60)$$

To apply Eq. (A.34) the trace  $R = L_{i,i} = R_{i,i}$  is required; it reads

$$R = \frac{\kappa_F}{q} [2 + q + (q-1)m_z^2] + \frac{\kappa_P}{q}. \quad (2.61)$$

We are now ready to insert our results for  $R_{i,j}$ ,  $I_{i,j}$ ,  $R$ , and  $h^{mf,i}$  in

$$Rm^n = \epsilon^{ijn} [I_{i,j} + h^{mf,i} m^j] + m^i R_{n,i} \quad \text{for } n = x, y, z \quad (2.62)$$

which yields the non-linear system of equations

$$q (2Jqa_y a_z + \kappa_P) = a_x [2\kappa_F ((q-1)a_z^2 + 2) + q\kappa_P] \quad (2.63a)$$

$$a_z (h - Jqa_x) = a_y \left[ \left(1 + \frac{1}{q}\right) \kappa_F + \frac{\kappa_P}{4} \right] \quad (2.63b)$$

$$\left(1 - \frac{1}{q}\right) a_z (1 - a_z^2) \kappa_F = ha_y + a_z \frac{\kappa_P}{4} \quad (2.63c)$$

Remember that the self-consistency demands  $m_i = \text{Tr}[\sigma^i \rho] = a_i$ . So we just applied the replacement rule  $m_i \mapsto a_i$  for  $i = x, y, z$  to all three equations. The equations (2.63) determine all non-equilibrium steady states of the mean field theory and can be solved analytically for arbitrary parameters  $J, h, \kappa_F, \kappa_P \in \mathbb{R}_0^+$  and  $q \geq 2$ . However, the solutions are quite lengthy for this generic case and we do not present them here for the gain of insight would be negligible. The analytical treatment gives 5 *distinct solutions* where four of them can be grouped to two pairs such that the partners differ by a sign. Not all *mathematical* solutions can be interpreted as *physical solutions* since only real vectors  $\mathbf{a} \in \mathbb{R}^3$  inside the unit ball,  $|\mathbf{a}| \leq 1$ , can be used to form valid density matrices  $\rho = \frac{1}{2} (\mathbb{1} + \mathbf{a}\sigma)$ .

In Fig. 2.1 we show the regions (blue) in dependence of  $\kappa_P$  (horizontal axis) and  $\kappa_F$  (vertical axis) for fixed unitary parameters  $J = 0.2 = h$ , where the solutions obey these conditions. Solution No. 1 is physical throughout the whole parameter range whereas the other four solutions

(the two pairs mentioned above) feature physical and unphysical regions. Notably, the “region of physicality” for Solutions No. 2 and 3 is extremely limited in  $\kappa_P$ -direction and bounded in the  $\kappa_F$ -direction as well. In contrast, the region of physicality for Solutions No. 4 and 5 seems (and indeed is) unbounded for  $\kappa_F \rightarrow \infty$ . Obviously we can expect a phase transitions (at least in mean field approximation) where the different solutions become (un)physical.

But this is not the end of the story since we are only interested in static solutions of the dynamical system (see Eq.(A.39))

$$\partial_t \mathbf{a} = \mathbf{F}(a_x, a_y, a_z) \quad (2.64)$$

that are *stable* against small perturbations of  $\mathbf{a}$ . A realistic system will not linger in an unstable fixed point as small perturbations are ubiquitous. We already derived the flow  $\mathbf{F}$  in Eq. (A.38),

$$[\mathbf{F}(a_x, a_y, a_z)]_n = 2\epsilon^{ijn} [I_{i,j} + h^{\text{mf},j} a_j] + 2(R_{n,i} - R\delta_{ni}) a_i \quad (2.65)$$

which in our case reads

$$\mathbf{F}(a_x, a_y, a_z) = \begin{bmatrix} -a_x \left[ 2\kappa_F \left( \left(1 - \frac{1}{q}\right) a_z^2 + \frac{2}{q} \right) + \kappa_P \right] + 2Jq a_y a_z + \kappa_P \\ 2a_z (h - Jq a_x) - a_y \left[ 2\left(1 + \frac{1}{q}\right) \kappa_F + \frac{\kappa_P}{2} \right] \\ 2\left(1 - \frac{1}{q}\right) a_z (1 - a_z^2) \kappa_F - 2h a_y - a_z \frac{\kappa_P}{2} \end{bmatrix} \quad (2.66)$$

The steady states (or fixed points) are given by the condition  $\mathbf{F} \stackrel{!}{=} 0$  as computed above. The stability of these fixed points can be inferred from the spectrum of the *Fréchet* derivative

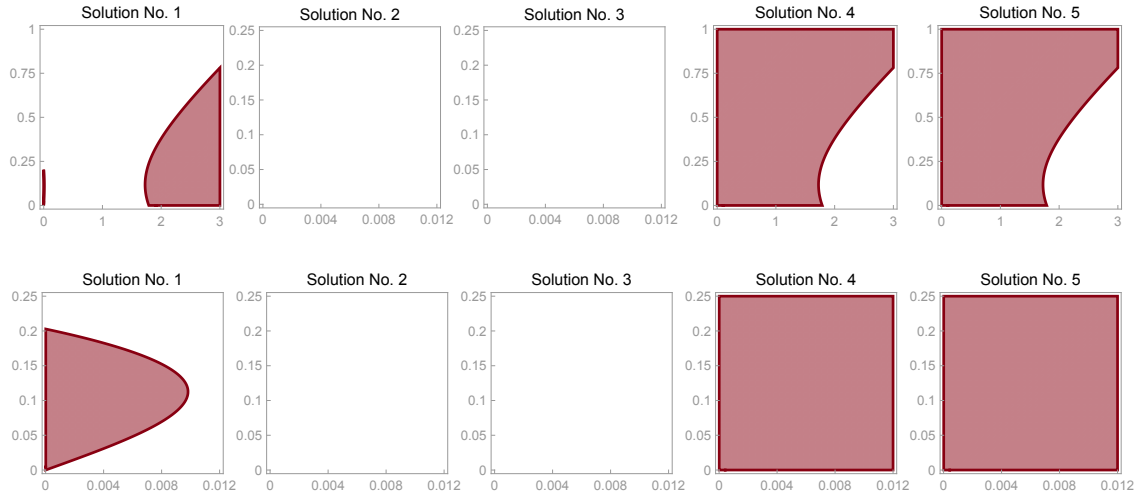
$$\mathbf{DF} = J_{\mathbf{F}} \equiv \left[ \frac{\partial F_i}{\partial a_j} \right]_{ij} \quad (2.67)$$

which is given in coordinate representation by the Jacobian matrix  $J_{\mathbf{F}}$ . The matrix is easily computed and reads in our case

$$[\mathbf{DF}](\mathbf{a}) = \begin{bmatrix} -2 \left[ \left(1 - \frac{1}{q}\right) a_z^2 + \frac{2}{q} \right] \kappa_F - \kappa_P & 2Jq a_z & 2Jq a_y - 4\left(1 - \frac{1}{q}\right) a_x a_z \kappa_F \\ -2Jq a_z & -2\left(1 + \frac{1}{q}\right) \kappa_F - \frac{\kappa_P}{2} & 2(h - Jq a_x) \\ 0 & -2h & -2\left(1 - \frac{1}{q}\right) (3a_z^2 - 1) \kappa_F - \frac{\kappa_P}{2} \end{bmatrix}. \quad (2.68)$$

It is a well-known fact that a stationary solution  $\tilde{\mathbf{a}}$ , i.e.  $\mathbf{F}(\tilde{\mathbf{a}}) = 0$ , is stable if and only if the real part of the spectrum  $\sigma[\mathbf{DF}](\tilde{\mathbf{a}})$  is completely negative, namely  $\max \text{Re} [\sigma[\mathbf{DF}](\tilde{\mathbf{a}})] < 0$ . If there are zero (positive) eigenvalues, the stationary state becomes metastable (unstable). The eigenvalues of  $\mathbf{DF}$  can be computed analytically – though they are quite lengthy and we do not present them explicitly.

In Fig. 2.2 we show the regions (red) in the  $\kappa_P$ - $\kappa_F$ -plane where the solutions are physical *and* stable. In the upper row of Fig. 2.2 the scale for each solution equals the scale in Fig. 2.1; the lower row shows the (small) region corresponding to solutions No. 2 and 3 for all five solutions in detail. We realise that solution No. 1 becomes stable in the region where the solutions No. 4 and 5 are unstable (and unphysical). The additional solutions No. 2 and 3 are unstable throughout the  $\kappa_P$ - $\kappa_F$ -plane. Although irrelevant, they seem to cause the first solution to become stable in their region of existence once more. That is, there is a (small) regime for  $0 < \kappa_P \lesssim 0.01$  and  $0 < \kappa_F \lesssim 0.2$  where both, the (paramagnetic, see below) solution No. 1 and



■ **Figure 2.2:** Not all *physical* solutions in Fig. 2.1 are stable and thus *physically relevant*. Here the *stable* parameter regions ( $\kappa_P$  and  $\kappa_F$ , as in Fig. 2.1) are marked red. In the first row the parameter ranges are the same as in Fig. 2.1 whereas in the second row the (small) section of the additional solutions No. 2 and 3 is shown in detail for all five solutions. Note that the solutions No. 2 and 3 are completely unstable but cause solution No. 1 to become (meta-) stable in the corresponding region. At the second-order phase transition, the stability of the ferromagnetic solutions No. 4 and 5 is passed on to the paramagnetic solution No. 1.

the (ferromagnetic) solutions No. 4 and 5 are stable. We will examine this region in detail in one of the following subsections.

Let us shortly summarise what we found so far: There are *three* relevant solutions to the mean field equations. Two of which (No. 4 and 5) presumably are linked via the  $\mathbb{Z}_2$  symmetry of the theory. They represent the *symmetry broken phase* of the theory. The first solution (No. 1) becomes stable when the  $\mathbb{Z}_2$ -broken solutions become unphysical and represents the disordered (paramagnetic) phase where the  $\mathbb{Z}_2$  symmetry is restored. Furthermore there is a small parameter regime with ferromagnetic *and* paramagnetic solutions which may indicate a region of metastability.

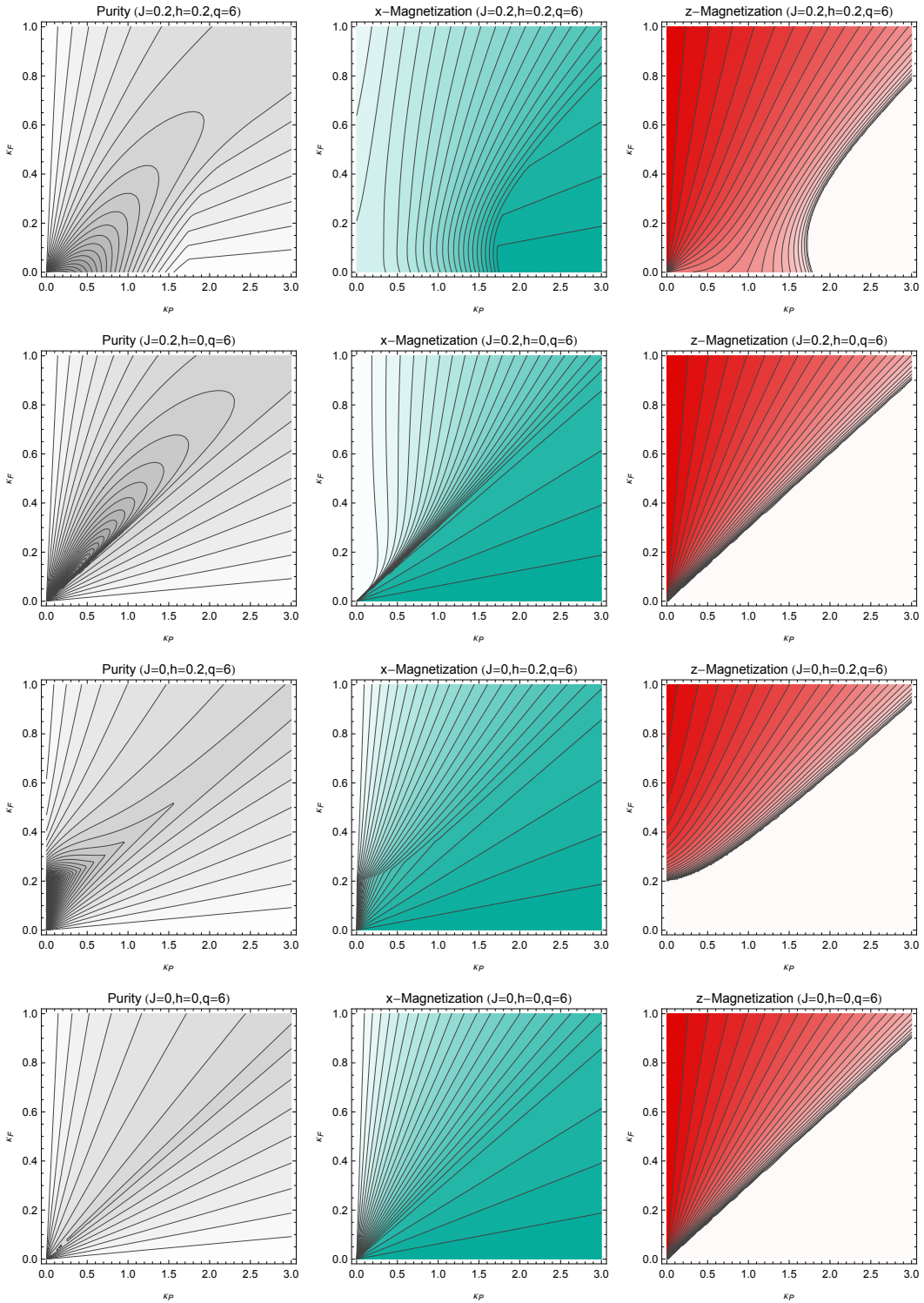
To underpin our claims and to provide a first overview of the phase diagram, we produced colour-coded plots of the purity  $\gamma$ , the  $x$ -magnetisation  $\langle \sigma^x \rangle = a_x$  and the  $z$ -magnetisation  $\langle \sigma^z \rangle = a_z$  in the  $\kappa_P$ - $\kappa_F$ -plane, see Fig. 2.3. Each row corresponds to one of the four generic parameter regimes (top down):  $J \neq 0 \neq h$ ,  $J \neq 0 = h$ ,  $J = 0 \neq h$ , and  $J = 0 = h$ . All plots show the data for the stable solution with the maximum  $z$ -magnetisation (which is solution No. 1 in the paramagnetic and No. 5 in the ferromagnetic regime; solution No. 4 has the same  $z$ -magnetisation as No. 5 but with opposite sign). Let us point out our first findings:

- In the first row a finite magnetic field and nearest-neighbour spin-spin coupling are present,  $J \neq 0 \neq h$ . Clearly there is a second-order phase transition with  $\langle \sigma^z \rangle$  as order parameter. For  $\kappa_P \gg \kappa_F$  the system is driven towards a paramagnetic phase with vanishing  $z$ -magnetisation while for  $\kappa_F \gg \kappa_P$  a finite  $z$ -magnetisation indicates the spontaneous breaking of the  $\mathbb{Z}_2$ -symmetry. The ferromagnetic phase is stabilised against the paramagnetic  $\kappa_P$ -jumps up to  $\kappa_P \sim 1.7$  due to the unitary dynamics of the system. To this end, recall that the mean field phase transition of  $H_{\text{TIM}}^{\text{mf}}$  for  $T = 0$  occurs at  $h = qJ$ . For the plots we set  $q = 6$  and thus  $h = 0.2 < 6 \cdot 0.2 = qJ$ , i.e. the *Hamiltonian system* is in the ferromagnetic (quantum) phase. We conclude that this phase is (to a certain extent)

resilient with respect to the incompatible jumps  $c_j$ . Notice that, due to the finite magnetic field  $h > 0$ , there is finite  $x$ -magnetisation remaining on the  $\kappa_F$ -axis (i.e. for  $\kappa_P \rightarrow 0$ ). The leftmost plot shows that in the limiting cases  $\kappa_F \rightarrow \infty$  and  $\kappa_P \rightarrow \infty$  the system is driven towards pure steady states since a single bath dominates the dissipative and Hamiltonian dynamics at such extreme points of the parameter space.

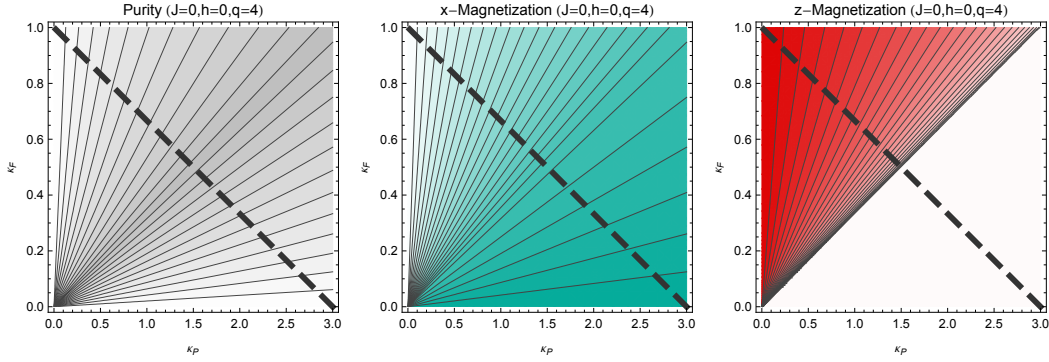
- In the second row the nearest-neighbour spin-spin coupling is present,  $J \neq 0$ , but the magnetic field is switched off,  $h = 0$ . The phase transition remains qualitatively the same – however, the stability of the quantum phase against paramagnetic driving is apparently lost. This might puzzle the reader at first sight since the system is now even “deeper” in the ferromagnetic phase as before ( $h = 0 < 6 \cdot 0.2 = qJ$ ) and we will give more details on this account in subsequent sections. Note that due to the missing magnetic field, the  $x$ -magnetisation vanishes completely for  $\kappa_P \rightarrow 0$  as it is created solely by the paramagnetic bath. We furthermore realise that the rate of change of the  $x$ -magnetisation at the phase border for small couplings  $\kappa_P$  and  $\kappa_F$  becomes larger. So it seems reasonable that the second order line becomes a first order phase transition for specific unitary regimes. We give more details on this account in the following subsections.
- In the third row the spin-spin coupling is switched off,  $J = 0$ , and the magnetic field remains finite,  $h \neq 0$ . Now the Hamiltonian system is in the paramagnetic regime since  $h = 0.2 > 6 \cdot 0 = qJ$ . Again, this quantum phase proves resilient against small ferromagnetic driving  $\kappa_F \lesssim 0.2$  and the symmetry broken phase is shifted towards larger  $\kappa_F$  due to the Hamiltonian contributions. However, we stress that the details are clearly *not* analogous to the first case with  $J \neq 0 \neq h$  – as can be seen from the peculiar structure of the purity plot, for instance. We point out that at this stage it is far from clear how the transition between the diagrams in the first and the third row looks like – especially in the context of the second row diagrams. More on that later.
- In the fourth row all Hamiltonian contributions vanish,  $J = 0 = h$ , and the system is purely dissipative. All diagrams feature a “ray-like” structure since there is just one free parameter left, namely the relative coupling  $\kappa = \frac{\kappa_P}{\kappa_F}$ . Note that all extended stability regions (see above) vanish and the system is governed by the competition of the two baths. Remarkably, the second order phase transition is present even if all Hamiltonian contributions are switched off. Actually this is one of the most interesting points and one of the key messages of this thesis: In a certain way, the two competing baths *mimic* the well-known phase transition of the transverse field Ising model. This observation tells us in addition that the phase transitions in the previous cases (with some unitary dynamics) are *not* mere residual effects of the formerly known quantum phase transition induced by  $H_{\text{TIM}}^{\text{mf}}$ .

In the following subsections the above mentioned phenomena are examined in detail. Nevertheless, our focus is on the novel *purely dissipative phase transition* for vanishing Hamiltonian contributions. Therefore we start in the next paragraph with this special case. In the subsequent paragraphs we consider the effects of the Hamiltonian dynamics and analyse the mean field theory’s behaviour in the high-dimensional limit  $q \rightarrow \infty$ , where it is expected to become exact.



■ **Figure 2.3:** Stable steady states of dissipative TIM in mean field approximation with maximum  $z$ -magnetisation in dependence of the bath couplings  $\kappa_P$  and  $\kappa_F$  for different unitary contributions  $J$  and  $h$ . All results refer to a 3-dimensional ( $q = 6$ ) system. The first column shows the purity (white denotes pure states), the second column the  $x$ -magnetisation (dark green is fully polarised), and the third column the  $z$ -magnetisation (dark red is fully polarised). The  $z$ -magnetisation is an order parameter and indicates a second-order phase transition. More comments are given in the text.





■ **Figure 2.4:** Stable steady states of *purely* dissipative TIM in mean field approximation with maximum  $z$ -magnetisation in dependence of the bath couplings  $\kappa_P$  and  $\kappa_F$ . All results refer to a 2-dimensional ( $q = 4$ ) system. As in Fig. 2.3 we show (from left to right) the purity, the  $x$ -magnetisation, and the  $z$ -magnetisation. The second-order phase transition is indicated in the rightmost plot by the transition from  $a_z = 0$  to  $a_z > 0$ . Note that the state depends only on the relative coupling strength  $\kappa = \kappa_P/\kappa_F$  since we set  $J = 0 = h$ . So we may restrict ourselves to plots along some diagonal as indicated by the bold lines.

#### No unitary dynamics

Let us consider the purely dissipative system, i.e. set  $J = 0 = h$  in the mean field equations (2.63). Its phase diagram is shown in Fig. 2.4. We are interested in the *competition* of the two baths. It is therefore reasonable to assume  $\kappa_F > 0$  and  $\kappa_P > 0$  and introduce the relative coupling  $\kappa = \frac{\kappa_P}{\kappa_F}$  (see Fig. 2.4) which allows further simplifications. This yields the mean field equations

$$\kappa q = a_x \left( 2a_z^2(q-1) + \kappa q + 4 \right) \quad (2.69a)$$

$$0 = a_y \quad (2.69b)$$

$$0 = 4a_z \left( a_z^2 - 1 \right) (q-1) + a_z \kappa q \quad (2.69c)$$

for the purely dissipative setting. The flow in the Bloch ball is given by

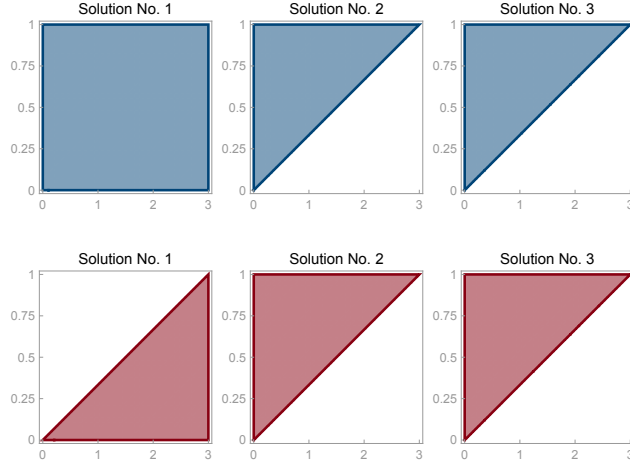
$$\mathbf{F}(a_x, a_y, a_z)|_{J=0=h} = \begin{bmatrix} -a_x \left[ 2\kappa_F \left( \left(1 - \frac{1}{q}\right)a_z^2 + \frac{2}{q} \right) + \kappa_P \right] + \kappa_P \\ -a_y \left[ 2\left(1 + \frac{1}{q}\right)\kappa_F + \frac{\kappa_P}{2} \right] \\ 2\left(1 - \frac{1}{q}\right)a_z \left(1 - a_z^2\right) \kappa_F - a_z \frac{\kappa_P}{2} \end{bmatrix} \quad (2.70)$$

with the triangular Jacobian matrix

$$[\mathbf{DF}](\mathbf{a})|_{J=0=h} = \begin{bmatrix} -2 \left[ \left(1 - \frac{1}{q}\right)a_z^2 + \frac{2}{q} \right] \kappa_F - \kappa_P & 0 & -4a_x a_z \kappa_F \left(1 - \frac{1}{q}\right) \\ 0 & -2\left(1 + \frac{1}{q}\right)\kappa_F - \frac{\kappa_P}{2} & 0 \\ 0 & 0 & -2\left(1 - \frac{1}{q}\right) (3a_z^2 - 1) \kappa_F - \frac{\kappa_P}{2} \end{bmatrix},$$

the spectrum of which can be read off.

If one computes the solutions of the mean field equations (2.69) one finds *three* of them. The additional solutions No. 2 and 3, which were responsible for the small region with three steady states, are no longer present. If we compute the parameter ranges where the three remaining



■ **Figure 2.5:** Classification of the mean field solutions for the purely dissipative system. Only three of the five algebraic solutions are left if  $J = 0 = h$ . In the upper row we show the regions (blue) in the  $\kappa_P$ - $\kappa_F$ -plane where the solutions become physical (see also Fig. 2.1 and 2.2). In the lower row the regions where these solutions are physical *and* stable is highlighted red. The two ferromagnetic solutions No. 2 and 3 are stable for  $\kappa_P < 3\kappa_F$  whereas for  $\kappa_P \geq 3\kappa_F$  the paramagnetic solution No. 1 describes the system.

solutions are *physical* and *stable* the simplified scheme in Fig. 2.5 is obtained. This result is clearly consistent with our findings in Fig. 2.3: The paramagnetic solution is stable for  $\kappa_P \geq 3\kappa_F$  (where the '3' is a consequence of  $q = 4$ ) and becomes unstable when the two ferromagnetic solutions become physical.

As a consequence of the simplicity of the mean field equations, the three solutions can be expressed in a compact form:

$$\mathbf{a}_P = \left[ \frac{\kappa q}{\kappa q + 4} \quad 0 \quad 0 \right]^T \quad (2.71a)$$

$$\mathbf{a}_{F1} = \left[ \frac{2\kappa q}{(\kappa + 4)q + 4} \quad 0 \quad -\frac{1}{2} \sqrt{4 - \frac{\kappa q}{q-1}} \right]^T \quad (2.71b)$$

$$\mathbf{a}_{F2} = \left[ \frac{2\kappa q}{(\kappa + 4)q + 4} \quad 0 \quad +\frac{1}{2} \sqrt{4 - \frac{\kappa q}{q-1}} \right]^T \quad (2.71c)$$

Clearly, the ferromagnetic solutions become physical iff

$$4 - \frac{\kappa q}{q-1} \geq 0 \quad \Leftrightarrow \quad \kappa \leq \kappa_c \equiv 4 \left( 1 - \frac{1}{q} \right) \quad (2.72)$$

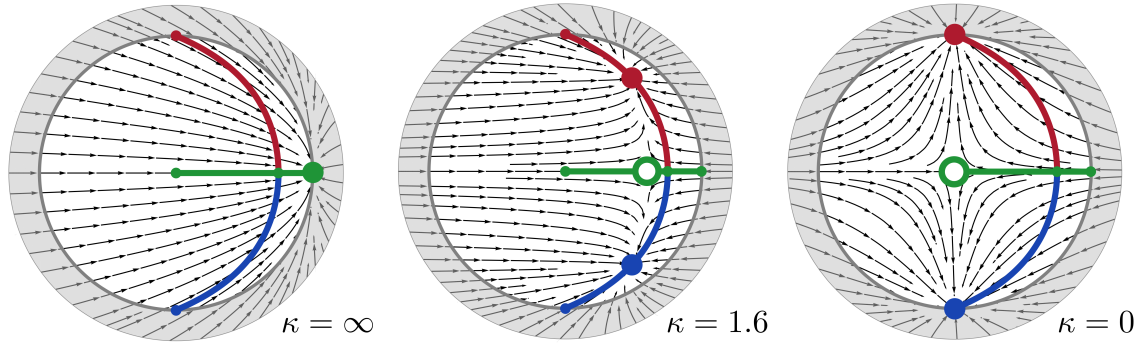
which we call the *critical coupling*  $\kappa_c$  henceforth. However, from these equations we *cannot* deduce the instability of the paramagnetic solution for  $\kappa < \kappa_c$ . We have to insert the latter into the three eigenvalues of  $[\mathbf{DF}](\mathbf{a})|_{J=0=h}$ . This yields

$$\lambda_1^P = 2 - \frac{1}{2} \left( \kappa + \frac{4}{q} \right) \leq 0, \quad \lambda_2^P = -\frac{\kappa q + 4}{q} < 0, \quad \lambda_3^P = -\frac{\kappa}{2} - \frac{2}{q} - 2 < 0 \quad (2.73)$$

and we see that the paramagnetic solution becomes unstable for  $\kappa < \kappa_c = 4 \left( 1 - \frac{1}{q} \right)$  where  $\lambda_1^P > 0$ . The same procedure for the ferromagnetic states yields

$$\lambda_1^F = \kappa - 4 \left( 1 - \frac{1}{q} \right) \leq 0, \quad \lambda_2^F = -\frac{\kappa}{2} - \frac{2}{q} - 2 < 0, \quad \lambda_3^F = -\frac{\kappa}{2} - \frac{2}{q} - 2 < 0 \quad (2.74)$$

which leads us to the conclusion that they indeed become stable the moment they become physical (i.e. real-valued), namely for  $\kappa < \kappa_c = 4 \left( 1 - \frac{1}{q} \right)$  when  $\lambda_1^F$  becomes negative.



■ **Figure 2.6:** Illustration of the mean field dynamics for a purely dissipative ( $J = 0 = h$ ) system as flow in a cross section ( $a_y = 0$ ) of the Bloch ball.  $a_x$  varies on the horizontal,  $a_z$  on the vertical axis. The vector field describes  $\hat{a}_x$  and  $\hat{a}_z$  and colour-codes the  $y$ -component, i.e.  $\hat{a}_y$  (black arrows imply  $\hat{a}_y = 0$ ). The Bloch ball's surface (the Bloch *sphere*) is denoted as thick grey line. The shaded region does not describe any physical states ( $\|\mathbf{a}\| > 1$ ). The relative bath strength  $\kappa = \kappa_P/\kappa_F$  varies from left to right, where the leftmost plot describes a purely paramagnetic and the rightmost plot a purely ferromagnetic system. During variation of  $\kappa$  from  $\infty$  to 0 the steady states run along the bold lines. For  $\kappa > \kappa_c$  the symmetry is spontaneously broken and the paramagnetic (green) steady state becomes unstable (circle). Note that the symmetry breaking appears inside the Bloch ball and therefore at a mixed state.

These calculations are as correct as they are simple; but they lack presentiveness as the connection between the emergence of the *ferromagnetic* solutions on the one side and the decay of the *paramagnetic* solution on the other side remains elusive. This connection becomes clear instantaneously if we plot the *dynamical field*  $F(\mathbf{a})$  as a vector field in the Bloch ball. As we already derived that all steady states have  $a_y = 0$ , it seems reasonable to plot the flux in a cross-section of the Bloch ball, namely the  $a_x$ - $a_z$ -plane. This is shown in Fig. 2.6 for the three showcases  $\kappa = \infty$  (paramagnetic phase),  $\kappa = 1.6$  (close to phase transition) and  $\kappa = 0$  (ferromagnetic phase).

There we see:

- In the paramagnetic regime,  $\kappa = \infty$ , there is a single steady state *within* the Bloch ball (more precisely: on its boundary). Since it is located at the  $a_x = 1$  and  $a_z = 0$  pole of the sphere, we identify this fixed point with a *pure paramagnetic steady state*. Clearly this is solution No. 1 as no other physical solution exists in this parameter regime. Note that the orthogonal components of the flux lines towards the surface of the Bloch ball (bold grey circle) point *into* the ball without exception. This is a consequence of the fact that  $\exp(\mathcal{L}t)$  is a CPTP map for all times  $t$ ; therefore it is impossible for a Bloch vector  $\mathbf{a}$  to leave the Bloch ball and become “unphysical” if its dynamics is governed by the equations of motion, namely the Lindblad master equation.
- Lowering  $\kappa$  drives the steady state along the green line *into* the Bloch ball, thus rendering the steady state mixed. At the point where the red and blue lines emerge the symmetry breaking occurs. For the plots in Fig. 2.6 we set  $q = 4$  and therefore one finds  $\kappa_c = 3$ . Hence the symmetry breaking already occurred in the second plot as  $\kappa = 1.6 < 3 = \kappa_c$ : The paramagnetic solution remains physical (meaning: in the Bloch ball) but becomes unstable (green circle). This instability manifests itself by the saddle point structure of the flux lines. In contrast, the ferromagnetic solutions are both physical *and* stable and move along the red and blue arcs towards the full  $z$ -magnetised poles of the Bloch ball. Since the ferromagnetic solutions become physical by becoming real-valued, they do not enter

the Bloch ball through the drawn surface but rather from “another dimension”, namely the complex environment of the Bloch ball as subset of  $\mathbb{C}^3$ .

- In the purely ferromagnetic regime,  $\kappa = 0$ , the fixed points are located at the z-poles of the Bloch ball. Since they once more reached its surface, they are *pure* states.

From this perspective all the previous abstract computations fit together quite nicely. Note that the important part of the dynamics, as encoded by the flux  $F$ , is located in the shown  $a_x$ - $a_z$ -plane. The rest of the Bloch ball (i.e. points with  $a_y \neq 0$ ) is driven towards this plane, independently of the  $a_x$ - $a_z$  projection, as can be seen from the second component in Eq. (2.70).

### ■ Phase diagram, critical exponents and entropy

To conclude this subsection on the steady states of the purely dissipative system, let us give explicit formulas for magnetisation and entropy. Actually, we just need to read off the expressions from the solutions given above. The magnetisation reads

$$m_x = \begin{cases} \frac{\kappa q}{\kappa q + 4} & \text{for } \kappa > \kappa_c \\ \frac{2\kappa q}{(\kappa + 4)q + 4} & \text{for } \kappa \leq \kappa_c \end{cases} \quad (2.75a)$$

$$m_y = 0 \quad (2.75b)$$

$$m_z = \begin{cases} 0 & \text{for } \kappa > \kappa_c \\ \pm \frac{1}{2} \sqrt{4 - \frac{\kappa q}{q-1}} & \text{for } \kappa \leq \kappa_c \end{cases} \quad (2.75c)$$

This function is shown for  $q = 4$  in Fig. 2.7. Note that  $\kappa_c = 4 \left(1 - \frac{1}{4}\right) = 3$ . At this point it is easy to derive the mean field critical exponent  $\beta$  for the ordered phase ( $\kappa \leq \kappa_c$ ) that is defined via

$$\beta := \lim_{\tau \rightarrow 0} \frac{\ln |m_z(\tau)|}{\ln |\tau|} \quad \text{with } \tau \equiv \frac{\kappa - \kappa_c}{\kappa_c} \quad (2.76)$$

and describes the power-law behaviour of the order parameter  $m_z$  with respect to the control parameter  $\kappa$  near (and below) the critical coupling  $\kappa_c$ , i.e.

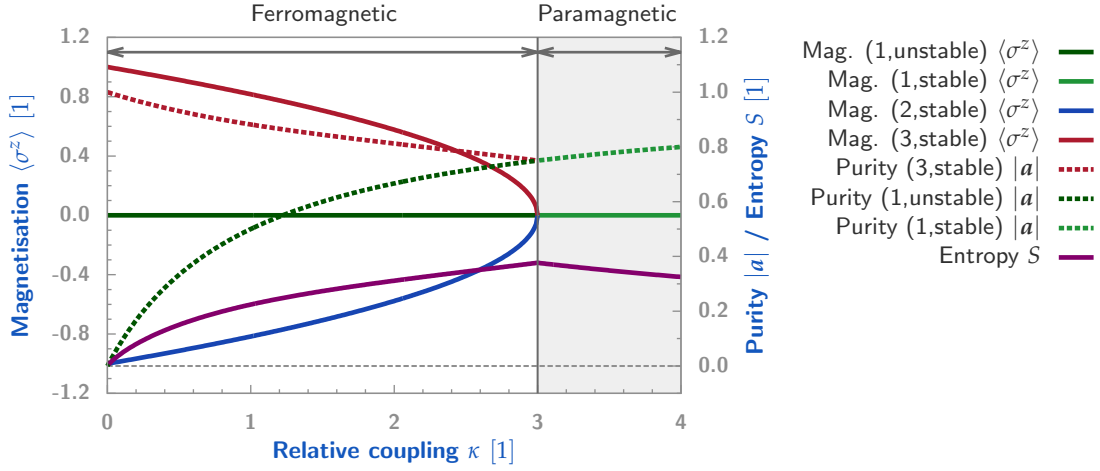
$$m_z(\tau) = (-\tau)^\beta = \left(\frac{\kappa_c - \kappa}{\kappa_c}\right)^\beta. \quad (2.77)$$

If we recast the magnetisation in terms of  $\kappa_c$  (instead of  $q$ ) we find  $m_z = \sqrt{\frac{\kappa_c - \kappa}{\kappa_c}}$  for  $\kappa \leq \kappa_c$ . Then it is trivial to see that  $\beta = 0.5$  which, after all, is not surprising in a mean field context. As usual in mean field theories, the dependence of the lattice dimension  $D$  (or coordination number  $q$ ) is completely lost – the critical exponent is *superuniversal*.

In Fig. 2.7 we furthermore show the norm of the Bloch vector  $|\mathbf{a}|$  as a measure of purity (dashed lines). Note that the connection between purity  $\gamma$  and  $|\mathbf{a}|$  is given via

$$\gamma = \text{Tr} [\rho^2] = \frac{1}{2} (1 + |\mathbf{a}|^2) \quad (2.78)$$

So they are actually the same; the only difference being  $\gamma \in [0.5, 1]$  (for *one* qubit!) and  $|\mathbf{a}| \in [0, 1]$ . Thus we denote both  $\gamma$  and  $|\mathbf{a}|$  as “purity” in the mean field context. In Fig. 2.7 it becomes



■ **Figure 2.7:** Phase diagram of purely dissipative TIM in mean field approximation. The  $z$ -magnetisation  $\langle \sigma^z \rangle$  is shown for all three solutions of the mean field equations in dependence of the relative coupling  $\kappa$ . Note that the paramagnetic solution No. 1 becomes unstable in the ferromagnetic regime (dark green). The purity  $\gamma$  is shown for the paramagnetic and, exemplarily, one of the two ferromagnetic solutions. It reaches 1 (indicating a pure state) for  $\kappa \rightarrow 0$  and the ferromagnetic solution as well as for  $\kappa \rightarrow \infty$  and the paramagnetic solution (to be read off at the *second*  $y$ -axis). The entropy  $S$  was calculated for stable states, i.e. for one of the ferromagnetic states if  $\kappa \leq 3$  and for the paramagnetic state if  $\kappa > 3$ . Note the cusp feature of  $S$  at the critical coupling  $\kappa_c = 3$ .

clear that the purity drops to its minimum at the phase transition. This however is not true in general as we will see in the next paragraph.

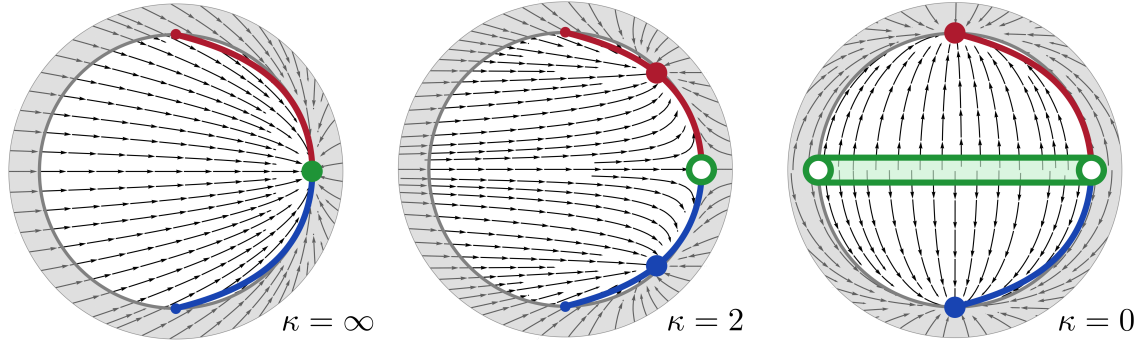
Another interesting quantity in an open system setup is the VON NEUMANN entropy  $S$  which, for a single spin, is a function of the Bloch vector

$$S[\rho_a] = -\frac{1}{2} \log \left[ \frac{1-a^2}{4} \cdot \left( \frac{1+a}{1-a} \right)^a \right], \quad (2.79)$$

see Eq. (D.7) in Appendix D. In Fig. 2.7 the entropy is denoted as solid purple line. In accordance with the purity it reaches its maximum at the phase transition. We want to draw the readers attention to the *cusp feature* at the critical point, i.e. there is a discontinuity of  $\frac{\partial S}{\partial \kappa}$  at  $\kappa_c$  which is consistent with our notion of a second order phase transition.

#### High-dimensional limit without unitary dynamics

It is widely accepted that mean field approximations become more reliable for high-dimensional systems as the number of nearest-neighbour interaction becomes larger. Clearly, interactions with many (nearest) neighbours are more faithfully represented by a homogeneous mean field. There are two ways to achieve this: First, the interaction *range* may be extended and thereby the number of interacting neighbours. Second, the (spatial) *dimension* of the underlying lattice directly determines the number of next-nearest neighbours (coordination number  $q$ ). Increasing the dimension therefore improves the accuracy of mean field predictions. As a consequence, it is important and enlightening to analyse the mean field theory in the limit  $q \rightarrow \infty$ .



■ **Figure 2.8:** Illustration of the mean field dynamics for a purely dissipative ( $J = 0 = h$ ) system as flow in a cross section ( $a_y = 0$ ) of the Bloch ball in the high-dimensional ( $q = \infty$ ) limit. See Fig. 2.6 for further explanations. A comparison with the finite- $q$  systems shows that the phase transition now occurs *on the Bloch sphere*, i.e. in a *pure* paramagnetic phase. As before, the ferromagnetic states move along the red and blue arcs to their corresponding pole. Note that, although pure for  $k \geq \kappa_c$ , in the ordered phase (for  $k < \kappa_c$ ) the states “dive” into the Bloch ball and become mixed until they “resurface” for  $\kappa \rightarrow 0$  and become pure once more.

The mean field equations of the purely dissipative system now read

$$\kappa = a_x (2a_z^2 + \kappa) \quad (2.80a)$$

$$0 = a_y \quad (2.80b)$$

$$0 = 4a_z (a_z^2 - 1) + a_z \kappa \quad (2.80c)$$

as can be seen easily from Eq. (2.69). The flow in the Bloch ball reads

$$\mathbf{F}(a_x, a_y, a_z)|_{J=0=h,q=\infty} = \begin{bmatrix} -a_x [2\kappa_F a_z^2 + \kappa_P] + \kappa_P \\ -a_y [2\kappa_F + \frac{\kappa_P}{2}] \\ 2a_z (1 - a_z^2) \kappa_F - a_z \frac{\kappa_P}{2} \end{bmatrix} \quad (2.81)$$

which follows straightforwardly from Eq. (2.70). To obtain the solutions of the new mean field equations we may solve them directly or perform the limit  $q \rightarrow \infty$  on the finite- $q$  solutions. Both procedures yield the simple fixed points

$$\mathbf{a}_P^\infty = [1 \ 0 \ 0]^T \quad (2.82a)$$

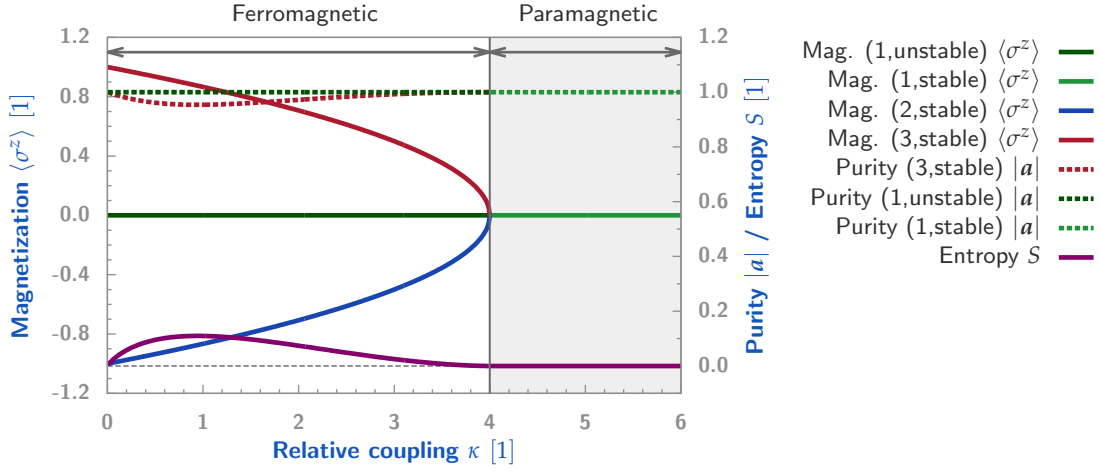
$$\mathbf{a}_{F1}^\infty = \left[ \frac{2\kappa}{\kappa+4} \ 0 \ -\frac{1}{2}\sqrt{4-\kappa} \right]^T \quad (2.82b)$$

$$\mathbf{a}_{F2}^\infty = \left[ \frac{2\kappa q}{\kappa+4} \ 0 \ +\frac{1}{2}\sqrt{4-\kappa} \right]^T \quad (2.82c)$$

and the critical coupling becomes

$$\kappa_c^\infty = \lim_{q \rightarrow \infty} 4 \left( 1 - \frac{1}{q} \right) = 4. \quad (2.83)$$

This is an important result: The critical coupling remains *finite* and therefore a non-trivial phase transition survives in the high-dimensional limit. However, there is a peculiarity which can be



■ **Figure 2.9:** Phase diagram of purely dissipative TIM in mean field approximation and in the high-dimensional ( $q = \infty$ ) limit. See Fig. 2.7 for further explanations. In the case at hand the phase transition occurs at  $\kappa_c = 4$  where the ferromagnetic solutions become physical *and mixed*. Note that in contrast to the finite- $q$  case (cf. 2.7), here the purity in the paramagnetic phase is *constant* and equal to one. As a consequence the entropy vanishes in the paramagnetic phase, becomes finite for  $0 < \kappa < 4$ , and vanishes again for  $\kappa = 0$ . We stress that the maximum entropy is reached somewhere in the ferromagnetic phase and not at the phase transition.

seen in Fig. 2.8 (cf. Fig. 2.6) and Fig. 2.9 (cf. Fig. 2.7). Since  $\mathbf{a}_p^\infty$  is obviously independent of  $\kappa$ , the state remains *fixed* at the pure and completely  $x$ -polarised state throughout the paramagnetic phase  $4 \leq \kappa \leq \infty$ . However, when  $\kappa$  crosses  $\kappa_c$  from above, the stationary paramagnetic solution becomes unstable and, as before, the two stable ferromagnetic solutions start their trip towards  $z$ -polarised poles. See the cross-sections in Fig. 2.8 for an illustration in terms of the dynamical flux  $F$ . If we consider the  $z$ -magnetisation, purity  $|a|$  and the entropy  $S$  in dependence of  $\kappa$  we find the phase diagram in Fig. 2.9. Here it becomes obvious what can be seen in Fig. 2.8 with difficulty: The ferromagnetic solutions “dive” into the Bloch ball and the states for  $0 < \kappa < 4$  become (slightly) mixed. Here the minimal purity (and maximal entropy) is reached somewhere in the ferromagnetic phase and *not* at the phase transition, cf. Fig. 2.7. We will see later that this happens also for finite  $q$ , if they are large enough.

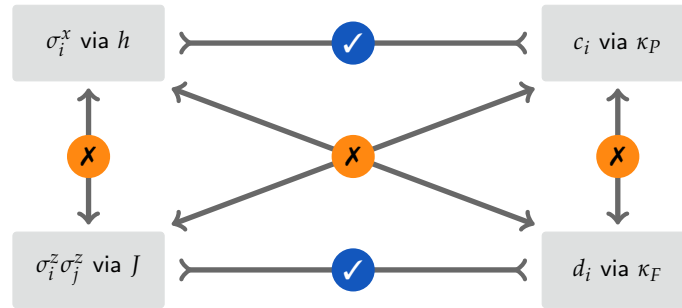
There is another point worth mentioning: For  $\kappa = 0$  there appear further stationary states. This can be easily seen since the mean field equations for this boundary case read

$$\begin{aligned} 0 &= 2a_x a_z^2 \\ 0 &= a_y \\ 0 &= 4a_z (a_z^2 - 1) \end{aligned}$$

which are not only solved by our previously derived stationary states but additionally by all Bloch vectors with vanishing  $a_z$ -component. That is, the equatorial plane becomes stationary as indicated by the green bar in Fig. 2.8. However, the additional stationary states are unstable as an inspection of the spectrum  $\sigma[DF](a_z = 0)$  shows (it is also clear from the flow in the cross-sections). So we are left with a non-trivial phase transition in the high-dimensional limit with a constant and pure paramagnetic phase and an unstable stationary equatorial  $a_x$ - $a_y$ -plane for vanishing paramagnetic driving  $\kappa_P$ .

## Competing unitary and dissipative dynamics

How changes the purely dissipative phase diagram if additional unitary contributions are switched on? This setting can be described as generic transverse field Ising model with additional dissipative driving where one dissipative process favours the paramagnetic ground state of the *Hamiltonian* system and the other bath drives the spins towards the (degenerate) ferromagnetic ground state space. In this sense we augmented the Hamiltonian dynamics by a “mimicked” or “replicated” dissipative one. As a consequence, there arise various competitions among unitary and dissipative terms:

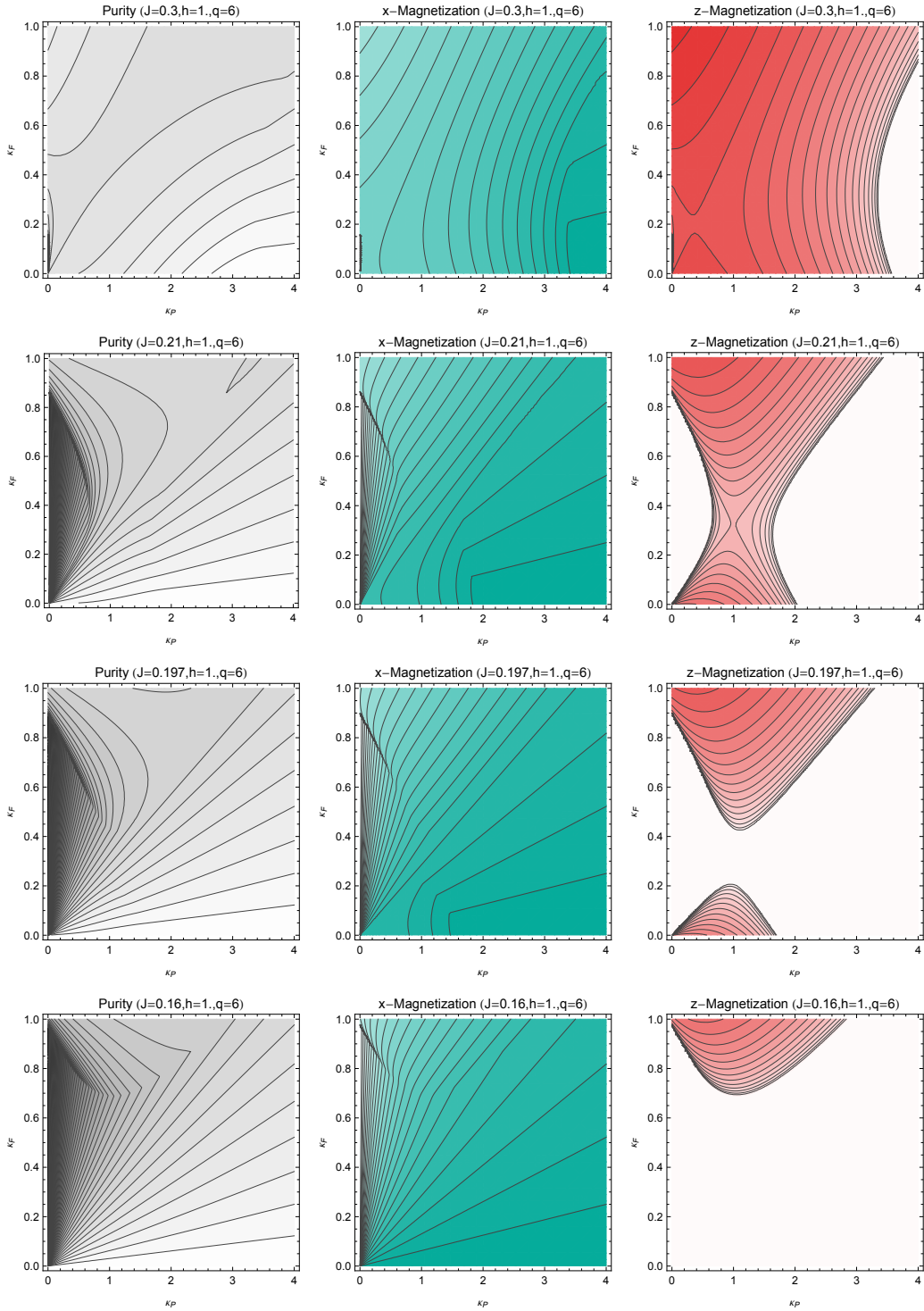


We already caught a glimpse of the consequences in the preliminary paragraph 2.3.2 where Fig. 2.3 provides a brief overview of the phase structure with unitary contributions. In the following we give a detailed (numerical) description of peculiarities in this regime. Since the mean field equations (2.63) for the most generic case are rather lengthy, there exist no compact or informative analytic expressions. Therefore we restrict ourselves to numerical solutions of Eq. (2.63) and intuitively accessible illustrations of the mean field flux (2.66) in the Bloch ball.

It became clear by inspection of the purely dissipative system that there is a non-trivial phase transition analogue to the (quantum) phase transition of the TIM. Consequently one could expect that the dissipative phase transition is modified by the unitary contributions such that the ferromagnetic phase becomes (to some extent) stable against paramagnetic driving due to a large spin-spin coupling  $J$ . Respectively a strong magnetic field  $h$  might stabilise the dissipatively induced paramagnetic phase against ferromagnetic driving. Such phenomena were indeed observed in the preliminary paragraph 2.3.2, see Fig. 2.3. The effect, however, was *not symmetric* and by means of Fig. 2.3 alone it was impossible to derive the transition between the parameter range where the ferromagnetic phase is stabilised against paramagnetic driving and the analogous range where the paramagnetic phase is resilient to the ferromagnetic bath. This question is answered by Fig. 2.10 where we show the phase diagram for fixed magnetic field  $h = 1$  and decreasing spin-spin coupling  $J$  (top to down):

- If the spin-spin coupling dominates the magnetic field (first row), the ferromagnetic phase extends to the  $\kappa_P$ -axis and becomes stable against paramagnetic driving; up to  $\kappa_P \sim 3.5$  for the shown parameters. This is not surprising since the Hamiltonian system is in the ferromagnetic (mean field) phase, i.e.  $h = 1 < 6 \cdot 0.3 = qJ$ .
- For slightly decreased spin-spin coupling (second row) a *paramagnetic island* at the  $\kappa_F$ -axis emerges. Note that the Hamiltonian system is still in the ferromagnetic phase,  $h = 1 < 6 \cdot 0.21 = qJ$ , but approaches the mean field phase transition at  $J = 0.1\bar{6}$ . Interestingly, the  $z$ -magnetisation reaches its (finite) minimum at the saddle point and *increases* again for  $\kappa_F \rightarrow 0$ . This is a cooperative effect where the presence of *two competing baths* (on the





■ **Figure 2.10:** Steady states of dissipative TIM with unitary dynamics for varying  $J$ . We show for each parameter  $J = 0.3, 0.21, 0.197,$  and  $0.16$  the purity,  $x$ -magnetisation and  $z$ -magnetisation of the steady state which maximises the latter. The four steps explain how the phase diagrams in Fig. 2.3 transform into each other: For specific parameter regimes there are separated ferromagnetic and paramagnetic islands, respectively. Additionally, there is evidence in the 2nd, 3rd and 4th row for a first order line originating on the  $\kappa_F$ -axis at  $\kappa_F \approx 0.9$  which becomes a second order phase transition at some point in the  $\kappa_P$ - $\kappa_F$ -plane. More details are given in the text.

saddle point) disturbs the Hamiltonian phase and weakens its z-magnetisation more than a *single paramagnetic bath* which, nevertheless, is in conflict with the Hamiltonian phase.

- There is a second interesting phenomenon: The infinite phase boundary separating the ferromagnetic and the *outer* paramagnetic phase is clearly of second order. The phase boundary of the paramagnetic *island* is of second order for small ferromagnetic coupling  $\kappa_F$  but becomes a *first order transition* for  $\kappa_F \gtrsim 0.6$  as indicated by the purity and  $x$ -magnetisation plots. Note that this first order transition is accompanied by a considerable drop in purity. From this point of view it seems more appropriate to speak of a “mixed island” instead of a “paramagnetic island”. We will investigate the first order transition in the course of this paragraph, see Fig. 2.12.
- When the spin-spin coupling decreases further (third row), the ferromagnetic bridge splits at the saddle and converts the phase diagram, at least qualitatively, to its dual: Instead of a paramagnetic island close to the  $\kappa_F$  axis there is now a *ferromagnetic island* close to the  $\kappa_P$ -axis. The Hamiltonian system is still in the ferromagnetic phase,  $h = 1 < 6 \cdot 0.197$ , and stabilises the ferromagnetic phase against a *dominant* paramagnetic bath. As before, there is a regime where the *competition* between ferromagnetic and paramagnetic jump operators causes the Hamiltonian phase to become symmetric once more, namely the (horizontal) paramagnetic bridge.
- The ferromagnetic island shrinks as the Hamiltonian contributions approach their critical point and vanishes completely at the critical point for  $h = 1 \geq 6 \cdot 1.6 = qJ$  (fourth row). In this regime the strong magnetic field  $h$  stabilises the paramagnetic phase against ferromagnetic jumps up to  $\kappa_F \sim 1$  for  $\kappa_P \rightarrow 0$ . This is, to some extent, the dual of the phase diagram in the first row as they can be mapped onto each other by a reflection about the angle bisector and a subsequent exchange of paramagnetic and ferromagnetic phases.
- This duality is not perfect since the first order transition survives (and there is no such transition visible in the first row): The phase boundary starts at the  $\kappa_F$ -axis as a *first order transition* (this can be seen most clearly in the  $x$ -magnetisation plot) and becomes a *second order transition* as one follows the phase boundary.

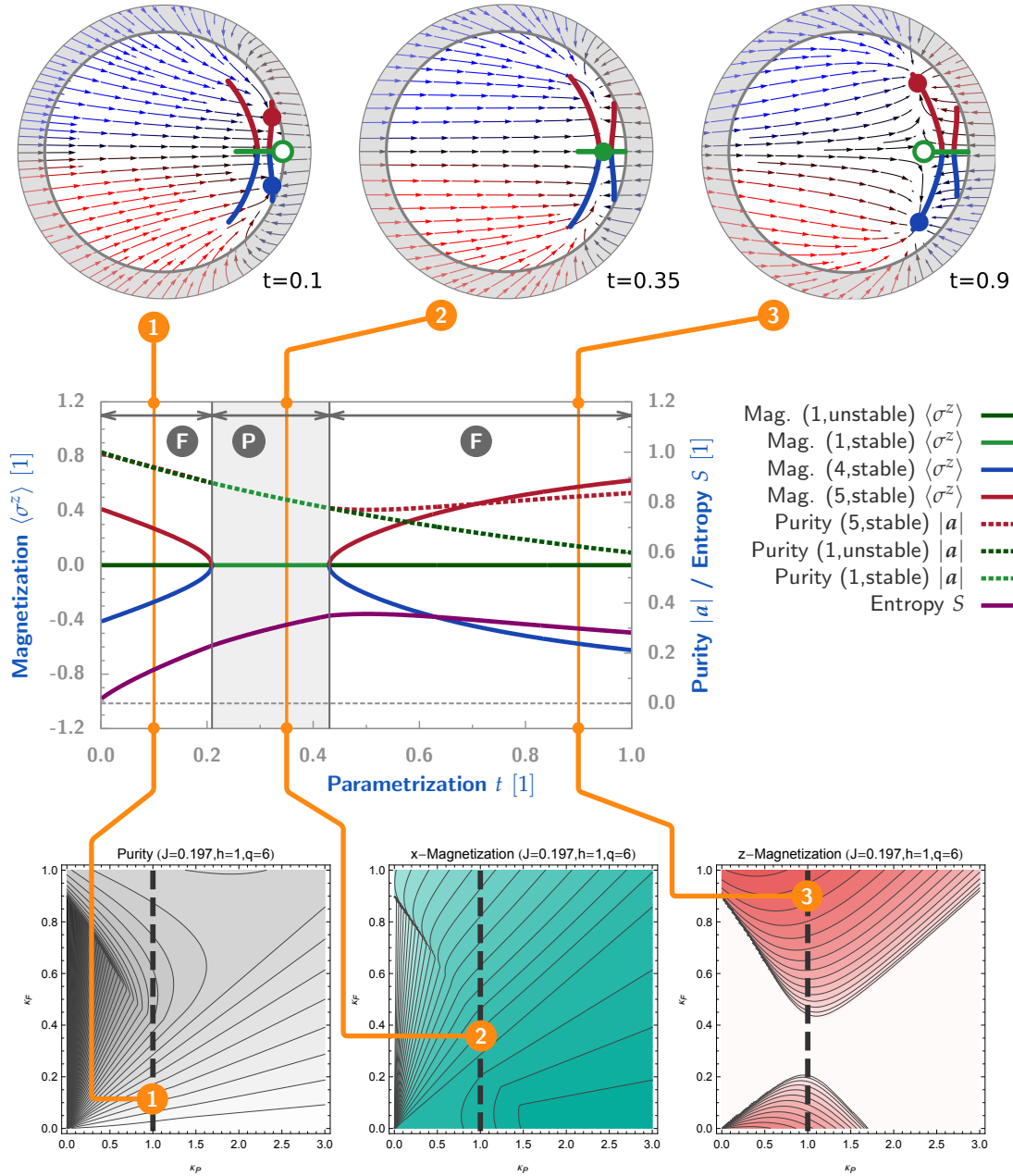
This analysis illuminates the unclear points raised during the discussion of Fig. 2.3 and prompts new questions at once:

1. What does the ferromagnetic island look like in terms of purity, entropy etc.? Is there a difference to the other connected component of the ferromagnetic phase?
2. How does the first order transition emerge in the mean field framework? How is it characterised by the dynamical flow in the Bloch ball?

To shed light on these questions we examined the theory on straight lines in the parameter space that traverse the critical regions in the phase diagram. The results are shown in Fig. 2.11 which examines the ferromagnetic island, and Fig. 2.12 which explains the emergence of the first order phase transition.

Let us first deal with the ferromagnetic island and Fig. 2.11:

- In the lower row we show the phase space in the  $\kappa_P$ - $\kappa_F$ -plane for  $J = 0.197$  and  $h = 1$ , which is a slice of the parameter space where the ferromagnetic bridge is split and the island is completely separated. In the following we examine the steady states on the



■ **Figure 2.11:** Details of the phase diagram of the dissipative TIM with unitary dynamics and a ferromagnetic island at the  $\kappa_p$ -axis. In the lower row we show the purity,  $x$ -magnetisation and  $z$ -magnetisation in the  $\kappa_p$ - $\kappa_F$ -planes for  $J = 0.197$  and  $h = 1$  (see 3rd row of Fig. 2.10). In the middle we plot the  $z$ -magnetisation and purity for all physical solutions (No. 1, 4 and 5) and the entropy for the solution with maximal  $z$ -magnetisation along the bold dashed line shown in the 2D-plots below. We denote the ferromagnetic (paramagnetic) phases by F (P). The paramagnetic solution (green) becomes unstable (dark green) in the ranges where ferromagnetic solutions exist. The latter are stable throughout their range of existence. In the upper row we plot the dynamical flow  $F$  on a cross-section of the Bloch ball for three distinguished parameter sets labelled by 1, 2 and 3 in the 2D-plots and by vertical orange lines in the plot below. As before, open circles denote unstable fixed points while filled discs mark the stable ones. The paths of these fixed points along the dashed parameter path are drawn with bold coloured lines. Note that due to the unitary dynamics the ferromagnetic fixed points are no longer located on the  $a_x$ - $a_z$ -plane with  $a_y = 0$ ! The shown cross sections with *three* fixed points are defined by the plane spanned by these three points. The cross section with a single (paramagnetic) fixed point lies in the  $a_x$ - $a_z$ -plane. The colour of the arrows encodes their component orthogonal to the shown plane. Further details are given in the text.

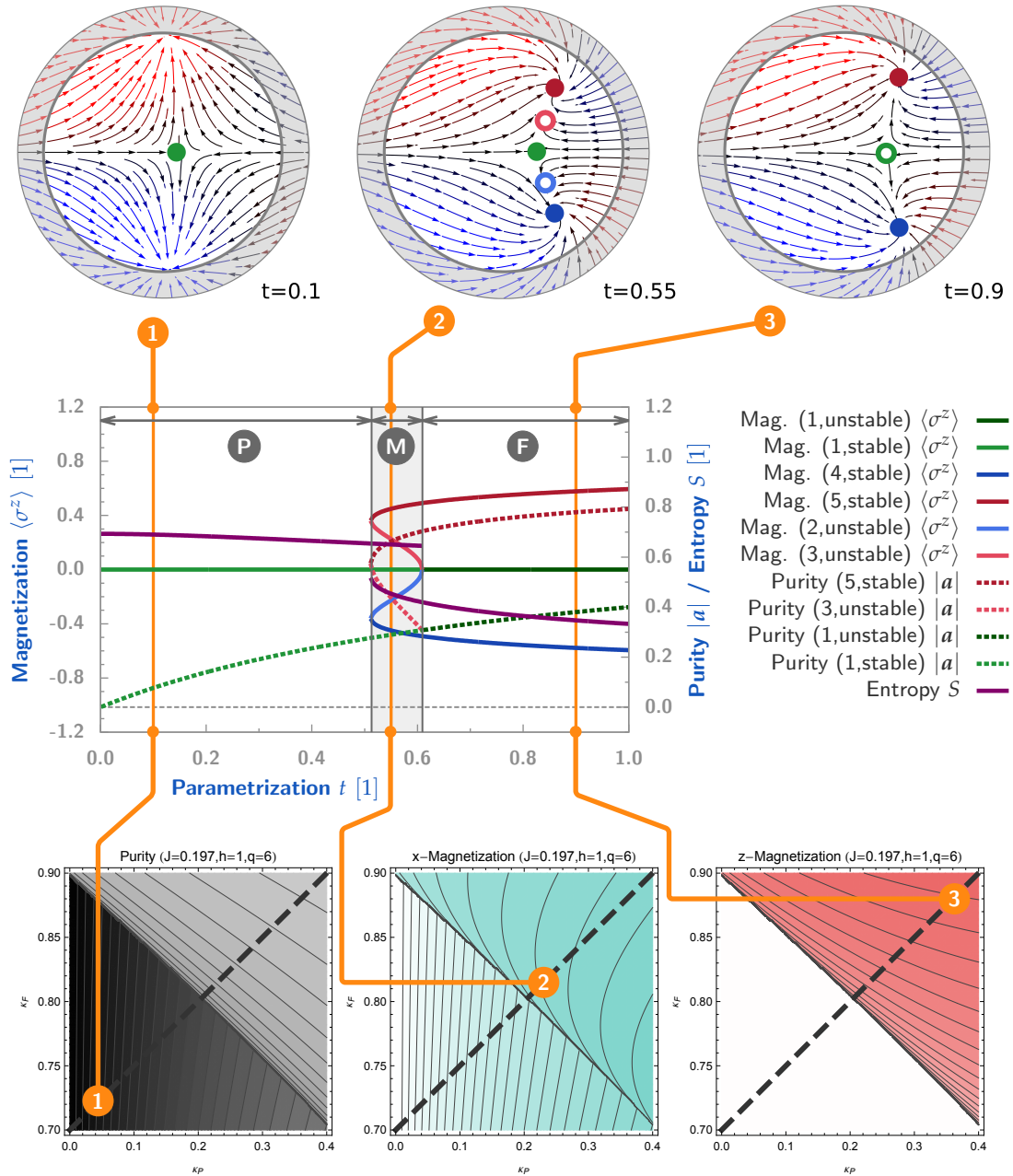
bold dashed line in detail. Note that this line crosses a phase boundary twice but misses the suspected first order transition when it enters the ferromagnetic bulk region (see the  $x$ -magnetisation plot).

- In the middle row we plot the  $z$ -magnetisation, purity and entropy for the paramagnetic and ferromagnetic solutions along the mentioned line. First, both phase transitions are clearly of second order; so the first order line terminates in fact at some multicritical point on the phase boundary. Second, in the ferromagnetic island (1) the steady states become *pure* for  $\kappa_F \rightarrow 0$  and finite  $\kappa_P$  though they do *not* become completely  $z$ -polarised — contrary to the limit  $\kappa_F \rightarrow \infty$  (3) where the system reaches pure and completely  $z$ -polarised steady states (as in the purely dissipative setup). In addition, the two depicted phase transitions are qualitatively *different* since the entropy reaches its maximum at the second one and traverses the first one without any indication of a phase transition.
- In the upper row we show the dynamical flux  $F$  at three distinct points (1), (2), and (3) in the parameter space. The depicted cross-section is defined by the plane spanned by the three steady states to provide insight into the non-trivial three-dimensional flow. If only a single steady state is present, the cross section is chosen parallel to the  $a_x$ - $a_z$ -plane. The color of the arrows encodes the component of  $F$  perpendicular to the cross-section. We denote stable (unstable) solutions by disks (circles). The first plot at  $t = 0.1$  illustrates the fact that the symmetry-broken steady states become pure for  $\kappa_F \rightarrow 0$  on the ferromagnetic island though they do not reach the poles of the Bloch sphere. When we reach the paramagnetic bridge ( $t = 0.35$ ) the ferromagnetic solutions vanish and any initial state is driven towards the same steady state. For larger  $\kappa_F$  ( $t = 0.9$ ) the ferromagnetic solutions re-emerge and tend towards the poles whereas the (now unstable) paramagnetic solution reaches the completely mixed state in the limit  $\kappa_F \rightarrow \infty$ . Note that the qualitative structure of the flow  $F$  in the vicinity of and beyond the second phase transition is closely related to the purely dissipative transition, see e.g. Fig 2.6.

We conclude that there are qualitative differences between the symmetry-broken phases on the ferromagnetic island on the one hand and in the bulk region on the other hand. In addition, we found the remarkable result that the symmetry-broken steady states on the ferromagnetic island become pure for finite unitary dynamics *and* paramagnetic driving given the ferromagnetic bath decouples.

Now let us turn towards the first order transition and Fig. 2.12:

- In the lower 2D plots we show a small section adjacent to the  $\kappa_F$ -axis which includes the suspected line of first order transition. The following inspection is based on the path along the angle bisector which traverses the phase transition almost perpendicularly.
- The middle plot along the mentioned path, first, confirms beyond doubt that the transition is of first order, and second, reveals the (mathematical) mechanism that is responsible for this phenomenon: In the grey region denoted by (M) the peculiar additional solutions No. 2 and 3 (see e.g. Fig. 2.1) become physical but remain unstable. In this intermediate, metastable parameter range the paramagnetic *and* the ferromagnetic solutions become stable and the shown behaviour of the  $z$ -magnetisation reminds of a hysteresis: Coming from the ferromagnetic regime the system lowers the  $z$ -magnetisation but *remains* in the ferromagnetic phase when it enters the metastable region. When it leaves the latter and enters the paramagnetic phase, the current (ferromagnetic) state becomes suddenly unphysical



■ **Figure 2.12:** Details of the phase diagram of the dissipative TIM with unitary dynamics near the  $\kappa_F$ -axis in the region with *three* stable solutions. For details on the structure of the illustration we refer the reader to the caption of Fig. 2.11. The shown transition from the symmetric (1) to the symmetry-broken phase (3) is of first order with an intermediate region (2) where both, the paramagnetic and ferromagnetic solutions are stable. Note that in the 2D plots the solution with maximum  $z$ -magnetisation is shown, which prevents the intermediate region to become visible. In this region the additional solutions No. 2 and 3 become physical (but remain unstable) and connect the ferromagnetic solutions with the paramagnetic one. In the Bloch ball cross-sections the unstable solutions are marked with circles of the corresponding colour. Note that due to the non-trivial flow perpendicular to the shown planes, the (in-)stability of the fixed points *cannot* be inferred from the shown flux lines. For instance, at  $t = 0.1$  (first Bloch ball from the left) the (green) paramagnetic solution seems to be unstable according to the shown flux lines. This, however, is not true as a thorough analysis reveals. More details are given in the text.

and the new stable (paramagnetic) solution emerges *separated* from the current state. The reversed process occurs if the system enters the metastable region from the paramagnetic and proceeds to the ferromagnetic phase. Due to this mechanism it is impossible to traverse this line<sup>25</sup> *adiabatically*.

- The metastable region is comparatively thin and may be considered as a single *transition line*. Consistently with our findings the entropy is discontinuous at this line (since the purity is) — a typical feature of a first order phase transition.
- The dynamical flow  $F$  in the upper row looks peculiar and is highly misleading without further comments: In contrast to the purely dissipative setting where the interesting dynamics takes place *in* the  $a_x$ - $a_z$ -plane at  $a_y = 0$ , this is not true when unitary components are present. The latter *rotates* the ferromagnetic steady states (slightly) about the  $a_x$ -axis out of the aforementioned plane. The flow features additional vortex-like structures due to the unitary evolution which, for instance, are responsible for the “dummy steady-states” in the  $t = 0.1$  cross-section where the flux flows *out of* and *into* the plane. Another effect of this complicated dynamics is the *apparent* instability of the paramagnetic steady state at  $t = 0.55$  which cannot be verified by inspection of the Jacobian matrix<sup>26</sup>. Since the unstable additional solutions (light red and blue circles) lie *not* within the shown plane, one *cannot* infer any useful information from the plotted projection of the flux.
- When the system is deep inside the ferromagnetic phase for  $\kappa_F \rightarrow \infty$  ( $t = 0.9$ ), the flux resembles qualitatively the purely dissipative one (up to the out-of-plane components), cf. Fig 2.6.

The discussion of Fig. 2.12 provided two crucial and closely related insights: First, we understood how a first order phase transition emerges in mean field theory as a manifestation of a thin metastable region with *three* stable solutions. And second, the additional solutions (which first appeared as mere mathematical artefacts) are now closely linked to the mechanism that is responsible for the first order phase transition and the emergence of a metastable parameter regime.

In the next paragraph we have a look at the high-dimensional limit of the generic case to estimate which of the phenomena that were treated above might be mean-field artefacts.

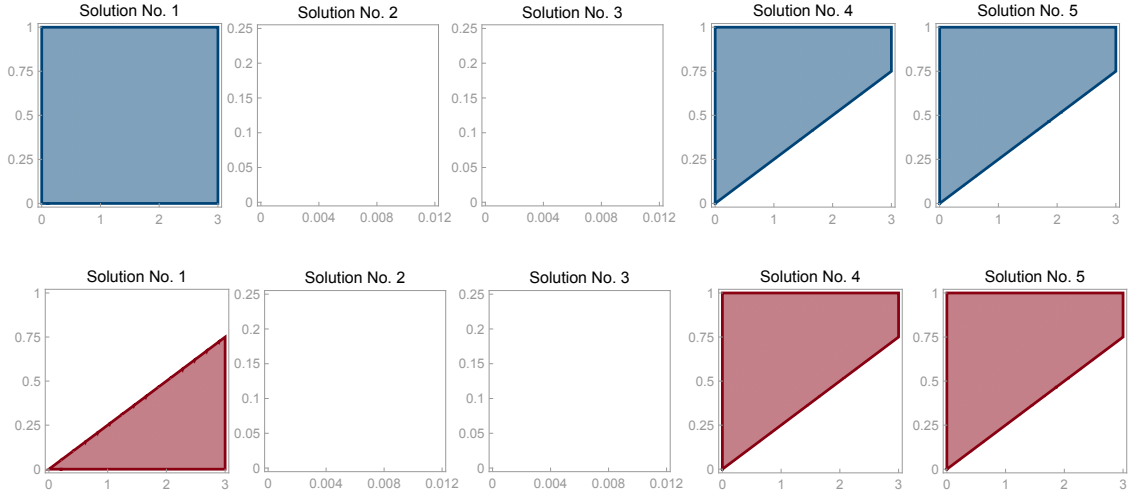
#### High-dimensional limit with unitary dynamics

Here we examine the high-dimensional limit  $q \rightarrow \infty$  of the mean field theory with non-vanishing unitary contributions. The procedure is the same as in the previous paragraph 2.3.2: We start from the finite- $q$  mean field equations (2.63) with unitary dynamics and perform the limit  $q \rightarrow \infty$ . We immediately realise that this limit is not well-defined if we consider the spin-spin coupling  $J$  to be constant. This comes as no surprise since in the high-dimensional limit the number of neighbours diverges and with it the nearest-neighbour interaction energy per spin. Thus we have to renormalise the spin-spin coupling according to

$$J \mapsto J' \equiv \frac{J}{q}. \quad (2.84)$$

<sup>25</sup>Actually it is some sort of hyperplane in the parameter space spanned by  $J$ ,  $h$ ,  $\kappa_F$ , and  $\kappa_P$ .

<sup>26</sup>This is an artefact of the projection used for these illustrations and occurs whenever a vortex is cut lengthways.



■ **Figure 2.13:** Regions in the  $\kappa_P$ - $\kappa_F$ -plane where the five algebraic solutions are *physical* (upper row, blue regions) and *stable* (lower row, red regions), respectively. There are two striking differences: First, the additional solutions No. 2 and 3 are no longer physical at any point in the parameter space<sup>28</sup>. Second, the phase boundary is shifted towards  $\kappa_P = 0$ , i.e. the relative contribution of ferromagnetic ( $\kappa_F$ ) and paramagnetic ( $\kappa_P$ ) jump operators is modified. Compare with the finite- $q$  results of Fig. 2.1 (physical solutions) and Fig. 2.2 (stable solutions).

So we reduce the spin-spin coupling  $J$  for increasing  $q$  to compensate for the diverging number of nearest neighbours<sup>27</sup>. With this substitution, we finally obtain the mean field equations:

$$2Ja_y a_z + \kappa_P = a_x (2\kappa_F a_z^2 + \kappa_P) \quad (2.85a)$$

$$a_z (h - Ja_x) = a_y \left( \kappa_F + \frac{\kappa_P}{4} \right) \quad (2.85b)$$

$$a_z (1 - a_z^2) \kappa_F = ha_y + a_z \frac{\kappa_P}{4} \quad (2.85c)$$

The flow in the Bloch ball follows from Eq. (2.66) and reads

$$F(a_x, a_y, a_z) \Big|_{q=\infty} = \begin{bmatrix} -a_x (2\kappa_F a_z^2 + \kappa_P) + 2J a_y a_z + \kappa_P \\ 2a_z (h - Ja_x) - a_y (2\kappa_F + \frac{\kappa_P}{2}) \\ 2a_z (1 - a_z^2) \kappa_F - 2ha_y - a_z \frac{\kappa_P}{2} \end{bmatrix}. \quad (2.86)$$

One can solve Eq. (2.85) for stationary solutions analytically and obtains five distinct solutions, as in the case of finite  $q$  above. They are still lengthy, so we do not present them here in detail. Their classification in the  $\kappa_P$ - $\kappa_F$ -plane is illustrated in Fig. 2.13. Compare these results with the plots in Fig. 2.1 and Fig. 2.2 (same parameters, same scaling, finite  $q$ ). There are two striking differences:

1. The additional solutions No. 2 and 3 are no longer physical at any point in the parameter space. Therefore the first order phase transition and the region of three stable solutions

<sup>27</sup>The reader may ask why this was not necessary in the purely dissipative setting before. The reason is that  $\kappa_F$  (the dissipative analogue of  $J$ ) is already renormalised for  $q \rightarrow \infty$  due to the coefficient  $q^{-1}$  in the definition of the jump operators  $d_j$ .

(see previous paragraph 2.3.2) do *not* survive in the high-dimensional limit. It is therefore questionable whether these phenomena are genuine effects or mere mean field artefacts.

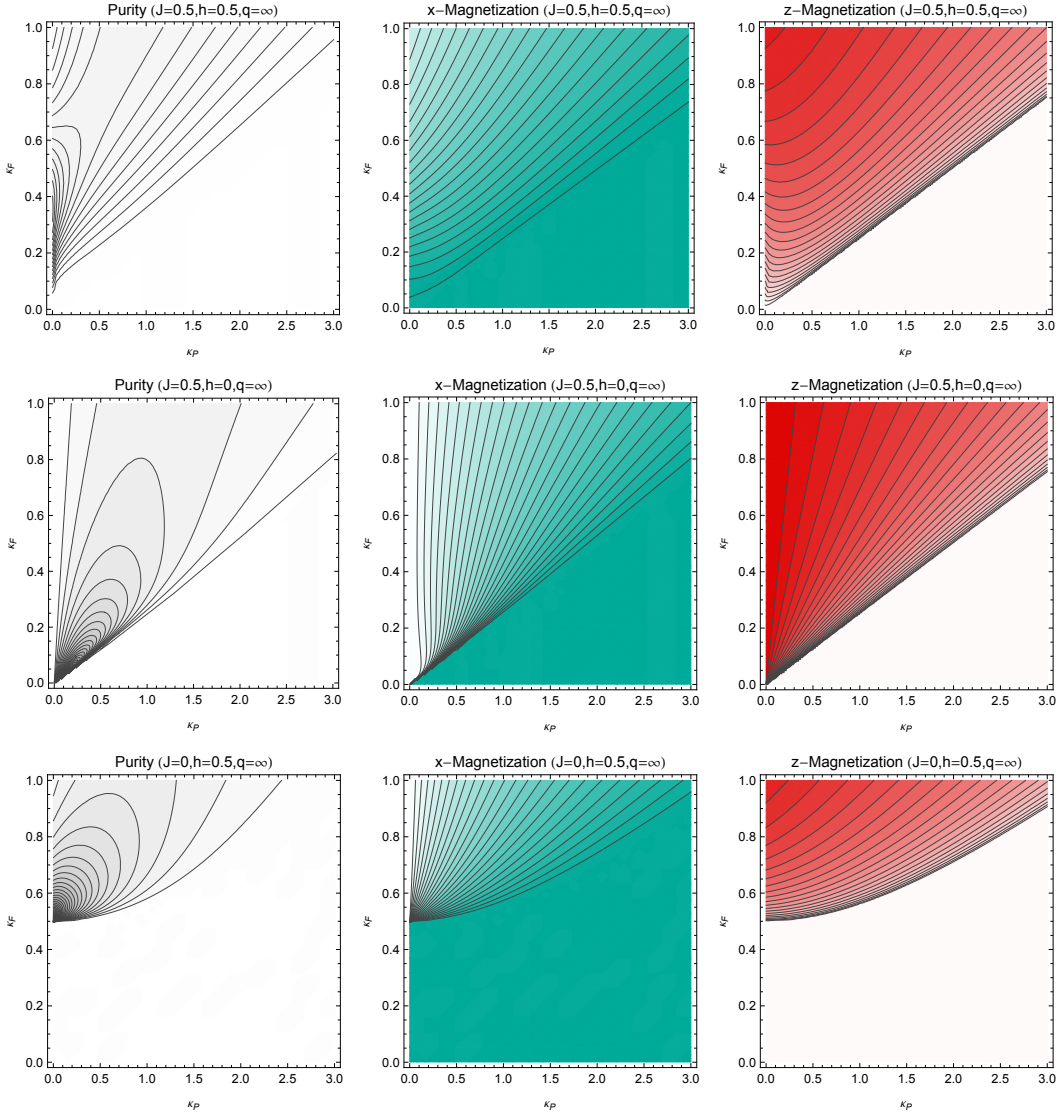
2. The phase boundary is shifted towards  $\kappa_P = 0$ , i.e. the relative contributions of the competing baths are modified. This is not unexpected as the baths are not symmetric: The ferromagnetic jump operators  $d_i$  interact with the nearest-neighbours and for this reason are sensitive to the lattice dimension. In contrast, the paramagnetic jump operators  $c_i$  act on single sites only and therefore remain unaffected in the high-dimensional limit.

The qualitative structure of the phase diagram is unaffected by the limit  $q \rightarrow \infty$ , as can be seen in Fig. 2.14 where we show the three generic cases  $J = 0.5 = h$ ,  $J = 0.5$  and  $h = 0$ ,  $J = 0$  and  $h = 0.5$  (the purely dissipative setting,  $J = 0 = h$ , was outlined in the previous paragraph). Compare these results with the plots of the first three rows in Fig. 2.3 (finite- $q$  setting). The phase boundary in the first row is shifted towards  $\kappa_P = 0$  as already mentioned. However, for larger spin-spin couplings  $J > h > 0$  the first row of Fig. 2.3 can be reproduced. The second and third rows are quite similar with respect to the  $x$ - and  $z$ -magnetisation. But there is an obvious difference between the purity structures in the third rows of Fig. 2.3 and Fig. 2.14. Note that this is the parameter regime where we found the first order transition. The kink structure in the purity graph in Fig. 2.3 for  $h > J = 0$  is a consequence of this phenomenon. As we already mentioned, we do not expect this first order transition to survive in the present case. Consequently, the purity structure in the corresponding plot of Fig. 2.14 looks differently. Nevertheless, a residue of the first order anomaly seems to be present near the  $\kappa_F$ -axis, as can be seen e.g. in the purity plot of the first row of Fig. 2.14. There is, however, no phase transition (neither first nor second order) in this region, as a detailed inspection reveals.

We do not discuss all details of the phase diagram for arbitrary parameters  $J$ ,  $h$ ,  $\kappa_P$  and  $\kappa_F$  here since the main message is not *how* it looks like but *that* the qualitative phase structure survives in the high-dimensional limit (up to the first-order anomaly etc.). However, there is one peculiarity which we examine in the following that occurred already in the finite- $q$  setting: For vanishing magnetic field ( $J = 0.5$  and  $h = 0$  in the high-dimensional setup and  $J = 0.2$  and  $h = 0$  in the finite dimensional setup) the phase boundary becomes a straight line where the  $z$ -magnetisation features a ray-like structure but the  $x$ -magnetisation does not. If one considers the second rows of Fig. 2.3 and Fig. 2.14, the question arises whether the phase transition remains of second order near the origin since there the  $x$ -magnetisation drops quite rapidly when the phase boundary is crossed and the system enters the ferromagnetic phase. We therefore scrutinise this transition for small  $\kappa_P$  and  $\kappa_F$  along a straight line in the  $\kappa_P$ - $\kappa_F$ -plane; the results are shown in Fig. 2.15. The structure of the illustration has already been introduced before (see paragraph 2.3.2 for instance). Here some comments on the results:

- The 2D plots confirm what we already found in the purely dissipative high-dimensional limit: The paramagnetic phase is the pure, completely  $x$ -polarised state and is independent of the bath couplings *as long as they remain in the paramagnetic phase*. When the phase boundary is crossed, the symmetry broken states depend on the parameters and become mixed unless  $\kappa_P = 0$ .
- The 2D purity plot reveals a dent of reduced purity near the origin which separates the pure paramagnetic phase and the pure ferromagnetic phase for  $\kappa_P \rightarrow 0$ . Note that the overall purity is comparatively high (for this example, the minimum length  $|a|$  of the Bloch vector is  $\sim 0.6$ ).





■ **Figure 2.14:** Stable steady states of dissipative TIM in mean field approximation with maximum  $z$ -magnetisation in dependence of the bath couplings  $\kappa_P$  and  $\kappa_F$  for different unitary contributions  $J$  and  $h$  and in the high-dimensional limit  $q \rightarrow \infty$ . The first column shows the purity (white denotes pure states), the second column the  $x$ -magnetisation (dark green is fully polarised), and the third column the  $z$ -magnetisation (dark red is fully polarised). Compare these results to the finite- $q$  plots in Fig. 2.3 and note the missing structure in the paramagnetic phase. As in the purely dissipative setting the paramagnetic phase is pure and independent of the bath couplings  $\kappa_P$  and  $\kappa_F$ . More comments are given in the text.

- The 2D  $z$ -magnetisation plot shows that the structure is not exactly linear near the origin. This contrasts the  $z$ -magnetisation in the purely dissipative setting where the ray-structure is perfect as there is only one relevant parameter left, namely the relative coupling  $\kappa$ .
- The plot in the second row shows the usual quantities along the dashed line crossing the phase boundary from top left to down right. Now it becomes clear that the phase transition is of second order although the shape of the  $z$ -magnetisation is slightly deformed compared to the purely dissipative setting (which was described by a simple square root). It seem reasonable (and can be checked easily) that the initial slope of the order parameter increases the closer the crossing is probed to the origin.
- The previously mentioned dent of purity in the symmetry-broken phase is easily identified in the plot. Hence the entropy reaches its maximum *not at* but *near* the phase transition.
- The differences to the purely dissipative setting manifest not only in the quantitative behaviour of the magnetisation and purity but also in the structure of the flux lines shown in the cross sections of the Bloch balls in the upper row. Note that in the case of three fixed points the cross-sections are defined by the plane spanned by these three points; in the case of a single fixed point the plane is chosen parallel to the  $a_x$ - $a_z$ -plane. Due to the unitary dynamics, the ferromagnetic stationary states gain non-vanishing  $a_y$ -components of opposite sign. As a consequence, the shown cross-sections ( $t = 0.1$  and  $t = 0.5$ ) are tilted towards the  $a_x$ - $a_z$ -plane. The paths of the ferromagnetic stationary states for  $0 \leq t \leq 1$  are drawn with bold lines in the corresponding colours and projected onto the cross-section. As the perspective changes from  $t = 0.1$  to  $t = 0.5$ , the endpoints appear to be *inside* the Bloch ball for  $t = 0.5$  whereas they clearly are attached to the surface as can be seen at  $t = 0.1$ .

There are two features that are noteworthy: First, near the purity dent the flux features a remarkable vortex structure near the stationary states. Such vortices result from the combination of unitary and dissipative dynamics and do not occur in the purely dissipative setting. Second, the shape of the paths projected onto the  $a_x$ - $a_z$ -plane ( $t = 0.9$ ) is slightly distorted as compared with the purely dissipative setting in Fig. 2.6. This is another manifestation of the already mentioned deformed shape of the order parameter function  $m_z = m_z(t)$ .

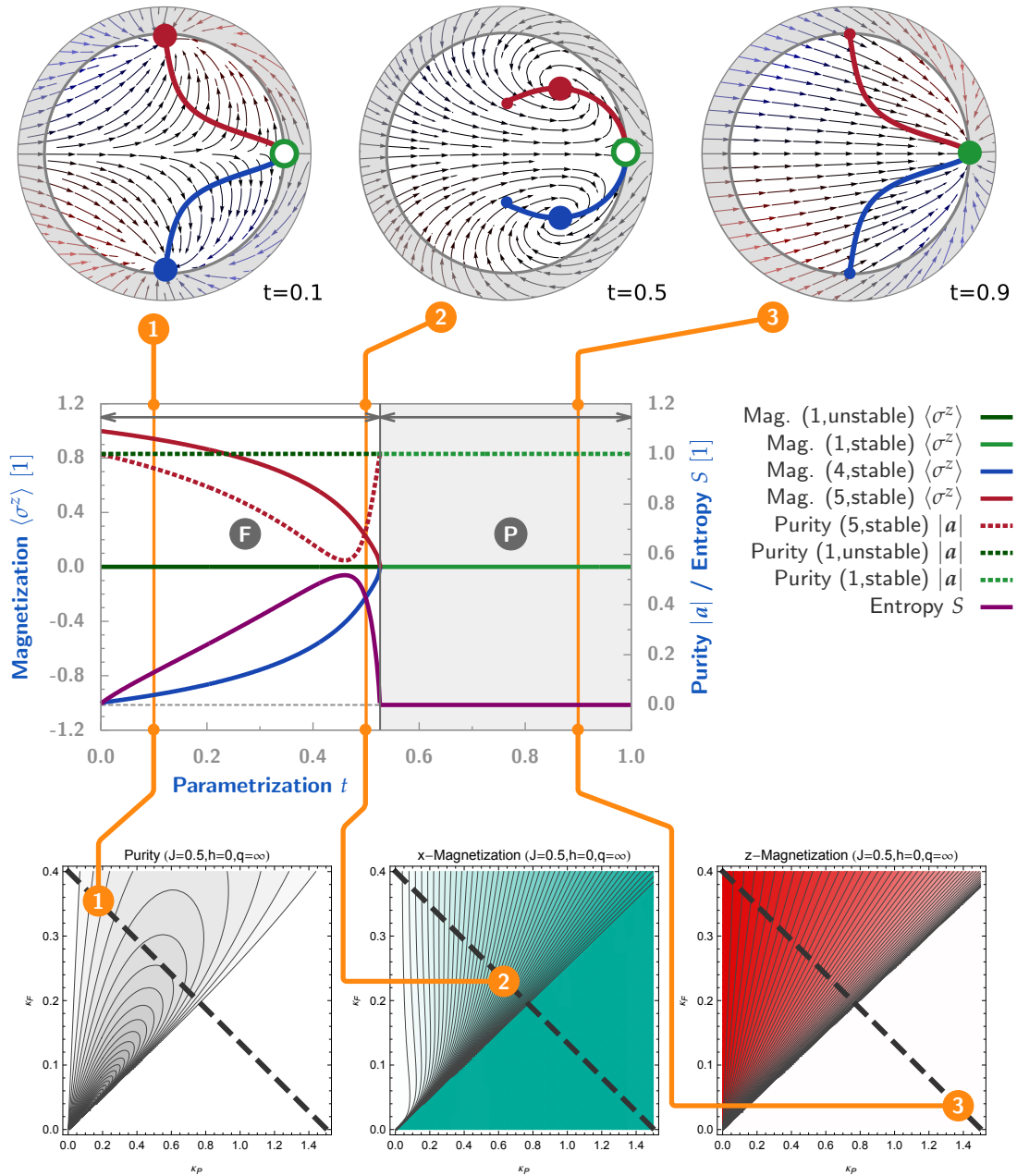
Thereby we conclude the analysis of the mean field steady states and proceed in the next subsections with some properties regarding the *dynamics* of the mean field theory.

### 2.3.3 Dynamic evolution

So far we were only concerned with the *steady state properties* of our dissipatively driven transverse field Ising model. But how does the system approach this (or these) steady state(s)? We already saw that in mean field approximation the time evolution is determined by the dynamical system

$$\partial_t \mathbf{a} = F(\mathbf{a}) \quad (2.87)$$

where  $\mathbf{a}$  is the Bloch vector (that lives in the closed unit ball  $\overline{B}_1(0)$ ) and  $F$  is a vector field or *flow* on  $\overline{B}_1(0) \subseteq \mathbb{R}^3$  determined by the (mean field) jump operators. See Eq. (A.37) f. in that regard. In the previous section we investigated the steady states for both, purely dissipative *and* unitary dynamics. In the following we omit the unitary contributions completely and focus on purely



■ **Figure 2.15:** Details of the phase diagram of the dissipative TIM with unitary dynamics,  $J = 0.5$  and  $h = 0$ , in the high-dimensional limit. For details on the structure of the illustration we refer the reader to the caption of Fig. 2.11. The 2D plots alone leave open the question whether the phase transition is of first or second order, especially close to the origin. We probe this transition on the dashed line and find clearly a second order phase transition which, however, shows a different behaviour in the ferromagnetic phase as compared to the purely dissipative setting. Note the distinctive fall of the purity (and hence rise of the entropy) shortly after the symmetry breaking occurs. In this parameter region the flux lines in the Bloch ball cross-sections exhibit a remarkable vortex structure. Recall that the cross-sections with three steady states are tilted towards the  $a_x$ - $a_z$ -plane. As a consequence, the projected paths of the steady states appear distorted in the second Bloch ball. More details are given in the text.

dissipatively driven system, i.e.  $J = 0 = h$  from now on. This is justified as our primary goal is the analysis of purely dissipative driven phase transitions. Therefore the flux – see Eq. (2.70) – reads:

$$F(a_x, a_y, a_z)|_{J=0=h} = \begin{bmatrix} -a_x \left[ 2\kappa_F \left( (1 - \frac{1}{q})a_z^2 + \frac{2}{q} \right) + \kappa_P \right] + \kappa_P \\ -a_y \left[ 2(1 + \frac{1}{q})\kappa_F + \frac{\kappa_P}{2} \right] \\ 2(1 - \frac{1}{q})a_z (1 - a_z^2) \kappa_F - a_z \frac{\kappa_P}{2} \end{bmatrix} \quad (2.88)$$

Clearly, by rescaling time  $t \mapsto \kappa_F t$  in the dynamical system (2.87) we get rid of one parameter and find

$$F(\mathbf{a}) \equiv \kappa_F^{-1} F(a_x, a_y, a_z)|_{J=0=h} = \begin{bmatrix} -a_x \left[ 2(1 - \frac{1}{q})a_z^2 + \frac{4}{q} + \kappa \right] + \kappa \\ -a_y \left[ 2(1 + \frac{1}{q}) + \frac{\kappa}{2} \right] \\ -a_z \left[ \frac{\kappa}{2} - 2(1 - \frac{1}{q})(1 - a_z^2) \right] \end{bmatrix} \quad (2.89)$$

with the relative coupling  $\kappa = \frac{\kappa_P}{\kappa_F}$ . We already know that the non-linear dynamical system (2.87) has a *unique* stable fixed point for  $\kappa \geq \kappa_c = 4(1 - q^{-1})$  and *two* stable fixed points otherwise. Which fixed point is reached depends crucially on the initial conditions, as can be seen from Fig. 2.6 where we showed the flux  $F(\mathbf{a})$  for the purely dissipative TIM in a cross section of the Bloch ball. The evolution follows the flux lines, which is a manifestation of Eq. (2.87), until it reaches one of the stable points<sup>29</sup>. The relaxation process features an exponential approach to the stationary states. We consider this point more thoroughly in the next paragraph.

#### Relaxation for late times

The full dynamical system is non-linear and coupled, thus the exact solutions are complicated and provide no insight whatsoever. But it might be enlightening to examine the relaxation for *late times*, or – equivalently – close to the steady state. To this end, assume that  $\lim_{t \rightarrow \infty} \mathbf{a}(t) = \mathbf{a}_{\text{NESS}}$  is the (not necessarily unique) steady state for initial conditions  $\mathbf{a}(0) = \mathbf{a}_0$ . We can then write  $\mathbf{a}(t) = \mathbf{a}_{\text{NESS}} + \delta \mathbf{a}(t)$  with the deviation  $\delta \mathbf{a}(t)$ . For late times or close to the steady state we can assume that the deviations are small, i.e.  $|\delta \mathbf{a}| \ll 1$ , and linearise  $F(\mathbf{a})$  at  $\mathbf{a}_{\text{NESS}}$  in  $\delta \mathbf{a}$ . More formally

$$\partial_t \delta \mathbf{a} = \partial_t \mathbf{a} = F(\mathbf{a}_{\text{NESS}} + \delta \mathbf{a}) = F(\mathbf{a}_{\text{NESS}}) + DF(\mathbf{a}_{\text{NESS}}) \delta \mathbf{a} + \mathcal{O}(\delta \mathbf{a}) \quad (2.90)$$

which is just a multidimensional Taylor series. Note that  $\partial_t \mathbf{a}(t) = \partial_t \delta \mathbf{a}(t)$  and  $F(\mathbf{a}_{\text{NESS}}) = 0$  by definition. Therefore we find

$$\partial_t \delta \mathbf{a} = DF(\mathbf{a}_{\text{NESS}}) \delta \mathbf{a} \quad \text{for } |\delta \mathbf{a}| \ll 1 \quad (2.91)$$

as an approximate dynamics close to the steady state. Recall that we already computed the derivative  $DF$  in (2.3.2) for the stability analysis. There we found the triangular matrix

$$DF(\mathbf{a}) = \begin{bmatrix} -2 \left[ (1 - \frac{1}{q})a_z^2 + \frac{2}{q} \right] - \kappa & 0 & -4a_x a_z (1 - \frac{1}{q}) \\ 0 & -2(1 + \frac{1}{q}) - \frac{\kappa}{2} & 0 \\ 0 & 0 & -2(1 - \frac{1}{q})(3a_z^2 - 1) - \frac{\kappa}{2} \end{bmatrix}, \quad (2.92)$$

<sup>29</sup>It actually never reaches the fixed points for finite times, only asymptotically for  $t \rightarrow \infty$ .

with the eigenvalues on the diagonal. At the paramagnetic fixed point ( $\kappa \geq \kappa_c$ ) it reads

$$DF(\mathbf{a}_p) = \begin{bmatrix} -\kappa + \kappa_c - 4 & 0 & 0 \\ 0 & \frac{1}{2}(-\kappa + \kappa_c - 8) & 0 \\ 0 & 0 & \frac{1}{2}(\kappa_c - \kappa) \end{bmatrix} \quad (2.93)$$

and at one of the ferromagnetic fixed points ( $\kappa \leq \kappa_c$ ) one finds

$$DF(\mathbf{a}_{F1}) = \begin{bmatrix} \frac{1}{2}(-\kappa + \kappa_c - 8) & 0 & \frac{2\kappa\kappa_c}{\kappa - \kappa_c + 8} \sqrt{1 - \frac{\kappa}{\kappa_c}} \\ 0 & \frac{1}{2}(-\kappa + \kappa_c - 8) & 0 \\ 0 & 0 & \kappa - \kappa_c \end{bmatrix}. \quad (2.94)$$

Here we substituted the coordination number  $q$  by the critical coupling  $\kappa_c$ , i.e.  $q = 4(4 - \kappa_c)^{-1}$ . Let us now solve the linear system of differential equations (2.91) for paramagnetic and ferromagnetic fixed points separately.

#### ■ Paramagnetic fixed point

At the paramagnetic fixed point the system is already decoupled since  $DF(\mathbf{a}_p)$  is diagonal. Thus the solutions of the three independent differential equations can be read off and one finds

$$\delta a_x(t) = \delta a_x(0) e^{-(\kappa - \kappa_c + 4)t} \quad (2.95a)$$

$$\delta a_y(t) = \delta a_y(0) e^{-\frac{1}{2}(\kappa - \kappa_c + 8)t} \quad (2.95b)$$

$$\delta a_z(t) = \delta a_z(0) e^{-\frac{1}{2}(\kappa - \kappa_c)t}. \quad (2.95c)$$

Note that all three exponents are negative for  $t > 0$  since  $\kappa > \kappa_c$  in the paramagnetic phase (i.e. when the fixed point  $\mathbf{a}_p$  is stable<sup>30</sup>). Even when  $\kappa$  approaches the critical value  $\kappa_c$  from above, the relaxation of  $\delta a_x$  and  $\delta a_y$  remains exponential. This is obviously not true for the relaxation in  $a_z$ -direction:  $\delta a_z(t)$  becomes constant as  $\kappa \searrow \kappa_c$ . That is, the paramagnetic solution becomes metastable in the  $a_z$ -direction at the critical point. This is not really surprising since we found previously that the two ferromagnetic solutions emerge in this direction from the unique paramagnetic fixed point, see for instance the flux in Fig. 2.6. ■

#### ■ Ferromagnetic fixed point

At the ferromagnetic fixed points  $DF(\mathbf{a}_{Fi})$ ,  $i = 1, 2$ , is a triangular matrix and the system of differential equations couples  $\delta a_x$  and  $\delta a_z$ . To decouple the equations we have to diagonalise  $DF(\mathbf{a}_{F1})$  which is straightforward and yields the three decoupled differential equations

$$\partial_t \delta \tilde{a}_x = -(\kappa_c - \kappa) \delta \tilde{a}_x \quad (2.96a)$$

$$\partial_t \delta \tilde{a}_y = -\frac{1}{2}(8 + \kappa - \kappa_c) \delta \tilde{a}_y \quad (2.96b)$$

$$\partial_t \delta \tilde{a}_z = -\frac{1}{2}(8 + \kappa - \kappa_c) \delta \tilde{a}_z \quad (2.96c)$$

<sup>30</sup>Actually, the point is that *because* all three exponents are negative, the solution  $\mathbf{a}_p$  is stable in the paramagnetic regime.

For the sake of brevity, we introduce the coefficient

$$C_\kappa = \frac{4\kappa\kappa_c}{(8+3\kappa-3\kappa_c)(8+\kappa-\kappa_c)} \sqrt{1-\frac{\kappa}{\kappa_c}} \quad \text{for } 0 \leq \kappa \leq \kappa_c. \quad (2.97)$$

Then the eigenmodes

$$\begin{aligned} \delta\tilde{a}_x(t) &= \delta a_x(t) \\ \delta\tilde{a}_y(t) &= \delta a_y(t) \\ \delta\tilde{a}_z(t) &= \delta a_x(t) - C_\kappa \delta a_z(t). \end{aligned}$$

can be determined by the eigenvectors of  $DF(\mathbf{a}_{F1})$ . The solution of the differential equations in terms of eigenmodes is trivial and yields

$$\begin{aligned} \delta\tilde{a}_x(t) &= \delta\tilde{a}_x(0) e^{-(\kappa_c-\kappa)t} \\ \delta\tilde{a}_y(t) &= \delta\tilde{a}_y(0) e^{-\frac{1}{2}(8+\kappa-\kappa_c)t} \\ \delta\tilde{a}_z(t) &= \delta\tilde{a}_z(0) e^{-\frac{1}{2}(8+\kappa-\kappa_c)t} \end{aligned}$$

which can be recast in the original degrees of freedom, that is

$$\delta a_x(t) = [\delta a_x(0) - C_\kappa \delta a_z(0)] e^{-\frac{1}{2}(8+\kappa-\kappa_c)t} + C_\kappa \delta a_z(0) e^{-(\kappa_c-\kappa)t} \quad (2.100a)$$

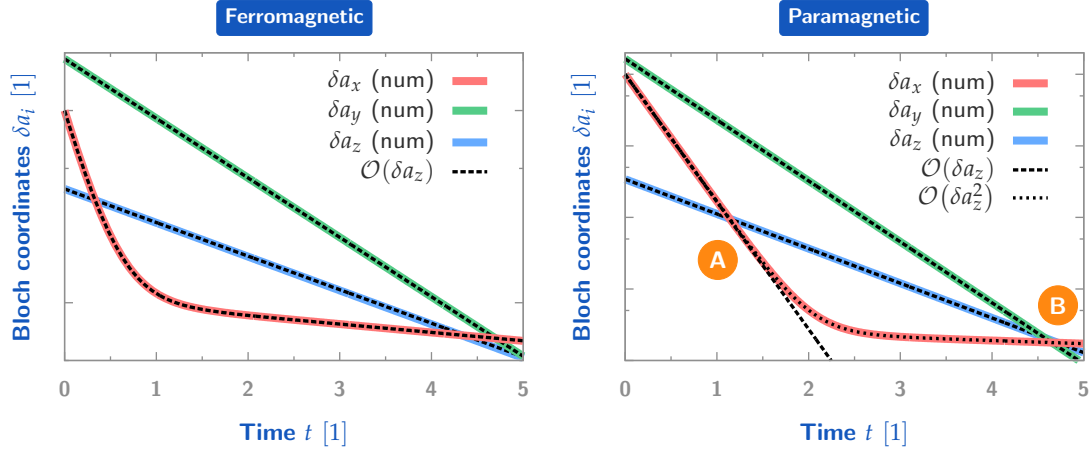
$$\delta a_y(t) = \delta a_y(0) e^{-\frac{1}{2}(\kappa-\kappa_c+8)t} \quad (2.100b)$$

$$\delta a_z(t) = \delta a_z(0) e^{-(\kappa_c-\kappa)t}. \quad (2.100c)$$

As before, the relaxation in  $a_y$ -direction remains exponential<sup>31</sup> even in the vicinity of  $\kappa_c$ . The relaxation of  $a_z$  is exponential and becomes stationary for  $\kappa \nearrow \kappa_c$ . We note that the exponential decay of  $\delta a_z$  is faster in the ferromagnetic than in the paramagnetic regime due to the doubled decay rate. The relaxation of  $a_x$  is most complicated due to the coupling in the original equations and depends not only on the initial value  $\delta a_x(0)$  but also on the position in  $a_z$  direction, namely  $\delta a_z(0)$ . The contribution of this  $a_z$  dependency however vanishes for  $\kappa \nearrow \kappa_c$  as  $C_\kappa \rightarrow 0$  in this limit. Due to the two exponential components in  $\delta a_x(t)$  there are two regimes of decay: Close to the critical point,  $\kappa \approx \kappa_c$ , it holds  $\frac{1}{2}(\kappa - \kappa_c + 8) \gg \kappa_c - \kappa$ . At the beginning ( $t$  small) the first summand in Eq. (2.100a) dominates the relaxation. Later ( $t$  large) the first part is already small and the (slower) relaxation is dominated by the second summand proportional to  $C_\kappa$ . ■

We illustrate both relaxation processes near the fixed points for paramagnetic and ferromagnetic systems in Fig. 2.16 (logarithmic  $\delta a_i$ -axis vs. linear time axis) by numerical integration of the complete dynamical system and compare these results with our analytically derived solutions for late times. In accordance with our assumptions, the exact solutions fit perfectly — up to one exception — with our analytic solutions since the initial deviations  $|\delta a_i(0)| = 0.001$  were chosen small enough. The exception being the evolution of  $\delta a_x$  in the paramagnetic regime with an interval of slower exponential decay for late times which is not captured by our analytical solution. The two exponential regimes for the relaxation in  $a_x$ -direction *in the ferromagnetic system* become clearly visible. However, the same structure occurs on the paramagnetic side where we did *not* expect it. There is only one possible solution: The second regime of slower decay in the *ferromagnetic* system is a feature of *first order* in  $\delta a$ . As we linearised the theory,

<sup>31</sup>Remember that  $\kappa_c = 4(1 - q^{-1}) \leq 4$  so that  $\kappa - \kappa_c + 8 > 0$  for all admissible  $\kappa$ .



■ **Figure 2.16:** Dynamics of the purely dissipative TIM in mean field approximation with initial states close to the ferromagnetic (left plot) and paramagnetic (right plot) steady states. Equivalently this describes the dynamics of any evolution at late times – at least qualitatively. The initial offset for all coordinates is  $|\delta a_i(0)| = 0.001$ . Furthermore we set  $q = 4$  (i.e.  $\kappa_c = 3$ ) and  $\kappa = 0.29$  ( $\kappa = 0.31$ ) in the ferromagnetic (paramagnetic) plot. The coloured lines represent results of numerical integrations of the complete dynamical system and therefore serve as reference solutions. The results for late times calculated exactly in the text are drawn with dashed black lines. Note that the scaling of the vertical axis is logarithmic but *different* for each solution  $\delta a_i$ , so one *cannot* compare absolute values and slopes in one plot. However, one *can* compare the numerical results with the analytical derived results. Obviously they fit perfectly in the ferromagnetic regime (so  $|\delta a_i(0)| = 0.001$  is “small enough”). However, the evolution of  $\delta a_x$  in the paramagnetic regime deviates from the analytical solution obtained by linearising the dynamical system *at late times* (B) whereas it fits well if  $\delta a_x$  is still larger (A). This can be fixed by including quadratic orders of  $\delta a_z$  in the calculation (dotted line). More details are given in the text.

the analogue regime in the *paramagnetic* system must be a feature of *second order* in  $\delta a$ ! This is consistent with the fact that  $\delta a_x$  relaxes faster than  $\delta a_z$ . During the evolution of the system a point is reached (close to the steady state) where  $\delta a_x \ll \delta a_z$  holds. Then the dynamics of  $\delta a_x$  is no longer determined by the first order contribution  $\delta a_x$  but by the second order contribution  $\delta a_z^2$ .

#### ■ Higher-order contributions

Let us have a look at the details. To this end (and since we need it in the next paragraph anyway) we write the *complete* dynamical system  $\partial_t \delta \mathbf{a} = \mathbf{F}(\mathbf{a}_{\text{NESS}} + \delta \mathbf{a})$  in terms of  $\delta a_i$  (without linearising it). Straightforward but cumbersome calculations yield for the *paramagnetic* fixed point  $\mathbf{a}_P$

$$\partial_t \delta a_x = \kappa_4 \delta a_x + \frac{\kappa \kappa_c}{2 \kappa_4} \delta a_z^2 - \frac{\kappa_c}{2} \delta a_x \delta a_z^2 \quad (2.101a)$$

$$\partial_t \delta a_y = \frac{1}{2} \kappa_8 \delta a_y \quad (2.101b)$$

$$\partial_t \delta a_z = \frac{1}{2} (\kappa_c - \kappa) \delta a_z - \frac{\kappa_c}{2} \delta a_z^3 \quad (2.101c)$$

and for the *ferromagnetic* fixed point  $a_{F1}$

$$\partial_t \delta a_x = \frac{1}{2} \kappa_8 \delta a_x - \frac{2\kappa \tilde{\kappa} \kappa_c}{\kappa_8} \delta a_z + \frac{\kappa \kappa_c}{\kappa_8} \delta a_z^2 + \tilde{\kappa} \kappa_c \delta a_x \delta a_z - \frac{\kappa_c}{2} \delta a_x \delta a_z^2 \quad (2.102a)$$

$$\partial_t \delta a_y = \frac{1}{2} \kappa_8 \delta a_y \quad (2.102b)$$

$$\partial_t \delta a_z = (\kappa - \kappa_c) \delta a_z + \frac{3}{2} \tilde{\kappa} \kappa_c \delta a_z^2 - \frac{1}{2} \kappa_c \delta a_z^3 \quad (2.102c)$$

where we introduced  $\tilde{\kappa} \equiv \sqrt{1 - \frac{\kappa}{\kappa_c}}$ ,  $\kappa_4 \equiv \kappa_c - \kappa - 4$  and  $\kappa_8 \equiv \kappa_c - \kappa - 8$  to shorten the expressions. The answer to the unexpected second relaxation regime for  $\delta a_x$  in the paramagnetic case is apparent if we compare the right-hand sides of the equations which determine the time evolution of  $\delta a_x$ , namely Eq. (2.101a) and Eq. (2.102a): Whereas near a *ferromagnetic* fixed point the leading order in  $\delta a_z$  is *linear*<sup>32</sup> (blue summand), there is only a *second* order contribution (blue summand) near a *paramagnetic* fixed point. This second order contribution becomes relevant at late times when due to the fast  $\delta a_x$ -relaxation it holds  $\delta a_x \ll \delta a_z$ . And this very contribution was lost due to our linearisation!

To fix the problem we have to include this second order contribution and solve the new (partially linearised) dynamical system near a paramagnetic fixed point

$$\partial_t \delta a_x = \kappa_4 \delta a_x + \frac{\kappa \kappa_c}{2\kappa_4} \delta a_z^2 \quad (2.103a)$$

$$\partial_t \delta a_y = \frac{1}{2} \kappa_8 \delta a_y \quad (2.103b)$$

$$\partial_t \delta a_z = \frac{1}{2} (\kappa_c - \kappa) \delta a_z \quad (2.103c)$$

which describes the dynamics for  $|\delta a| \ll 1$ . The solutions for  $\delta a_y$  and  $\delta a_z$  are easily derived and read

$$\delta a_y(t) = \delta a_y(0) e^{\frac{1}{2} \kappa_8 t} \quad (2.104a)$$

$$\delta a_z(t) = \delta a_z(0) e^{\frac{1}{2} (\kappa_c - \kappa) t} \quad (2.104b)$$

which we found already to be a correct description in Fig. 2.16. Now insert the solution for  $\delta a_z$  into Eq. (2.103a) and solve the inhomogeneous differential equation. The solution can be derived by standard methods and reads

$$\delta a_x(t) = \left[ \delta a_x(0) - \frac{\kappa \kappa_c}{8\kappa_4} \delta a_z(0)^2 \right] e^{\kappa_4 t} + \frac{\kappa \kappa_c}{8\kappa_4} \delta a_z(0)^2 e^{-(\kappa - \kappa_c) t} \quad (2.105)$$

where we highlighted the additional term as a result of the quadratic contribution. In Fig. 2.16 we plot this solution as dotted black line — this verifies our new result. ■

### Critical Slowing-down

So far we were concerned with the limit for late times or systems close to the steady state. Let us now consider systems far in the ferromagnetic ( $\kappa \rightarrow 0$ ) and paramagnetic ( $\kappa \rightarrow \infty$ ) regime as

<sup>32</sup>Note that due to  $\delta a_z \ll 1$  it is still true that  $\delta a_z^2 \ll \delta a_z$ , so the linear order dominates the quadratic order of the *same* variable.



well as critical systems with  $\kappa = \kappa_c$ . We do *not* assume that the systems are close to the steady state whatsoever. In what follows our focus is on the transition from one phase to the other and its impact on the relaxation of the system. So let us proceed systematically:

#### ■ Paramagnetic system ( $\kappa \gg \kappa_c$ )

Here we assume that  $\kappa \gg \kappa_c$  is large (but finite). If we take this into account, the dynamical system (2.101) can be simplified to

$$\partial_t \delta a_x = -\kappa \delta a_x + \frac{\kappa_c}{2} \delta a_z^2 \quad (2.106a)$$

$$\partial_t \delta a_y = -\frac{\kappa}{2} \delta a_y \quad (2.106b)$$

$$\partial_t \delta a_z = -\frac{\kappa}{2} \delta a_z \quad (2.106c)$$

if we recall that  $|\delta a| \leq 2$  is bounded by the diameter of the Bloch ball and thus *bounded*. Note that we keep in Eq. (2.106a) the quadratic component although its coefficient is much smaller than  $\kappa$ . This is motivated by our previous findings: If  $\kappa$  is finite and  $\delta a_x$  relaxes faster than  $\delta a_z$  there will be a regime for late times where  $|\kappa \delta a_x| \ll \delta a_z^2$ . Then this quadratic contribution becomes relevant once more.

The solutions can be easily derived by standard techniques and read

$$\delta a_x = \left[ \delta a_x(0) - \frac{\kappa_c}{2} \delta a_z(0)^2 t \right] e^{-\kappa t} \quad (2.107a)$$

$$\delta a_y = \delta a_y(0) e^{-\frac{\kappa}{2} t} \quad (2.107b)$$

$$\delta a_z = \delta a_z(0) e^{-\frac{\kappa}{2} t} \quad (2.107c)$$

where  $\delta a_x$  gets modified by a contribution proportional to  $\delta a_z(0)^2$  as before, see Eq. (2.107a). Note that the solution for  $\delta a_x$  hints at a conversion as  $t$  runs from zero to infinity if  $\delta a_x(0) > 0$  and  $\delta a_z(0) \neq 0$ . The bottom line is that deep in the paramagnetic phase, away from the critical point, the relaxation is exponentially fast in all degrees of freedom. A numerical inspection similar to that in Fig. 2.16 confirms the correctness of these results. Since this is neither an interesting nor enlightening task, we omit this plot.

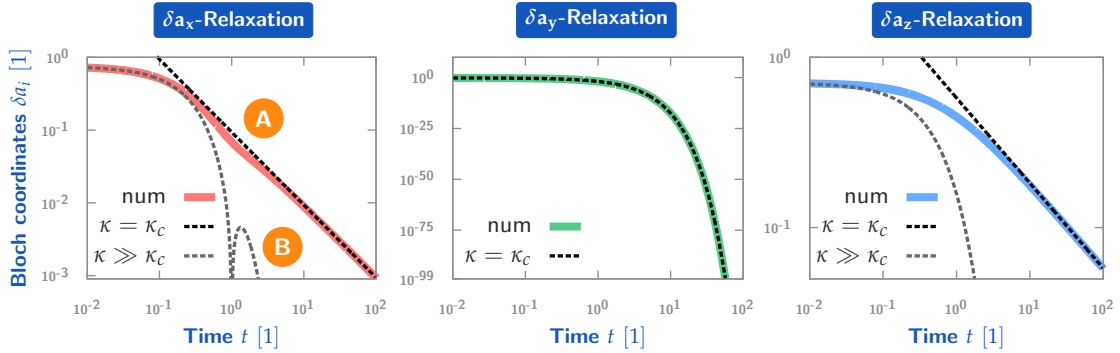
#### ■ Critical system ( $\kappa = \kappa_c$ )

Let us now turn towards the most interesting case, namely that of a critical system for  $\kappa = \kappa_c$ . We already saw that *close to the steady state* the  $\delta a_z$ -relaxation vanishes at the critical point due to the emergence of two stable solutions in  $a_z$ -direction. The relaxation in  $a_x$ - and  $a_y$ -direction however remained exponential. We are now interested in the analogous dynamics *away from the steady state*. If we set  $\kappa = \kappa_c$  we are free to choose between the dynamical system in Eq. (2.101) and the one in Eq. (2.102). In both cases the result reads

$$\partial_t \delta a_x = -4 \delta a_x - \frac{\kappa_c^2}{8} \delta a_z^2 - \frac{\kappa_c}{2} \delta a_x \delta a_z^2 \quad (2.108a)$$

$$\partial_t \delta a_y = -4 \delta a_y \quad (2.108b)$$

$$\partial_t \delta a_z = -\frac{\kappa_c}{2} \delta a_z^3 \quad (2.108c)$$



■ **Figure 2.17:** Dynamics of the purely dissipative TIM in mean field approximation at the critical coupling  $\kappa_c$ . The initial state is far away from the stationary point and we set  $q = 4$ . All three plots are full-logarithmic. The numerical solutions of the full dynamical system are shown as coloured lines whereas the analytical solutions for  $t \rightarrow \infty$  are shown as dashed black lines. For comparison we plot the analytical solutions for strongly paramagnetic systems ( $\kappa \gg \kappa_c$ ) as dashed grey lines. As shown in the text, the  $\delta a_y$ -relaxation remains exponential irrespective of the coupling  $\kappa$  (centred plot). In contrast, the  $\delta a_x$ - and  $\delta a_z$ -relaxation become algebraic for late times and the analytic results join with the numerical ones perfectly. However, the relaxation *in the beginning* is dominated by exponential contributions as can be seen from the comparison with the (exponentially decaying) paramagnetic solutions. Note that there is a dent at (A) in the exact (numerical) evolution of  $\delta a_x$  which is a consequence of the complex differential equation which governs this relaxation process (and which was responsible for the approximations we had to apply, see e.g. Eq. (2.108a)). The feature in (B) follows from the conversion of  $\delta a_x$  as mentioned in the text and described by Eq. (2.107a) for appropriate initial conditions.

and we immediately find the solution for  $\delta a_y$

$$\delta a_y(t) = \delta a_y(0) e^{-4t} \quad (2.109)$$

and the solution for  $\delta a_z$  is

$$\delta a_z(t) = \frac{\delta a_z(0)}{\sqrt{\delta a_z(0)^2 \kappa_c \cdot t + 1}} \xrightarrow{t \rightarrow \infty} \frac{t^{-\frac{1}{2}}}{\sqrt{\kappa_c}} \quad (2.110)$$

which can be found by a separation of variables. So even away from the steady state the relaxation in  $a_z$ -direction is no longer exponential. As we are not infinitesimally close to the steady state, the relaxation does not cease but becomes *algebraic* with critical (mean field) exponent  $\eta_z = -\frac{1}{2}$ . This is some sort of *critical slowing down* in the dynamics of the dissipative system which is intimately connected with the suspected vanishing of the dissipative gap in the (real part of the) spectrum of the Lindbladian superoperator  $\mathcal{L}$ .

The solution of Eq. (2.108a) is not that simple. For the sake of simplicity let us consider solutions for late times, i.e.  $t \rightarrow \infty$ . To this end insert the late-time solution for  $\delta a_z$ ; then the differential equation reads

$$\partial_t \delta a_x = -4 \delta a_x - \frac{\kappa_c}{8t} - \frac{1}{2t} \delta a_x \quad (2.111)$$

a formal solutions of which can be given in terms of the *imaginary error function*

$$\operatorname{erfi}(x) := -i \operatorname{erf}(ix) \quad \text{where} \quad \operatorname{erf}(x) := \frac{2}{\sqrt{\pi}} \int_0^x e^{-t^2} dt \quad (2.112)$$

denotes the (GAUSS) error function. It reads

$$\delta a_x(t) = C \frac{e^{-4t}}{\sqrt{t}} - \frac{\sqrt{\pi}\kappa_c}{16\sqrt{t}} e^{-4t} \operatorname{erfi}(2\sqrt{t}) \quad (2.113)$$

with the integration constant  $C$ . This is a downright useless expression as it tells us nothing about the behaviour of the solution for late times. Thus we should try to approximate  $\operatorname{erfi}(2\sqrt{t})$  for  $t \rightarrow \infty$ . We note that there is the following connection

$$\operatorname{erfi}(x) = -i(1 - \operatorname{erfc}(ix)) \quad (2.114)$$

with the *complementary error function*

$$\operatorname{erfc}(x) := 1 - \operatorname{erf}(x) = \frac{2}{\sqrt{\pi}} \int_x^\infty e^{-t^2} dt \quad (2.115)$$

which in turn has an asymptotic expansion for  $x \rightarrow \infty$  reading

$$\operatorname{erfc}(x) = \frac{e^{-x^2}}{x\sqrt{\pi}} \sum_{n=0}^{N-1} (-1)^n \frac{(2n-1)!!}{(2x^2)^n} + R_N(x) \quad (2.116)$$

with a remainder  $R_N(x) \in \mathcal{O}(x^{-2N+1}e^{-x^2})$ . For our solution we find

$$\operatorname{erfi}(2\sqrt{t}) = \frac{e^{4t}}{2\sqrt{\pi}\sqrt{t}} \sum_{n=0}^{N-1} \frac{(2n-1)!!}{(8t)^n} - i + R'_N(2i\sqrt{t}) \quad (2.117)$$

and consequently

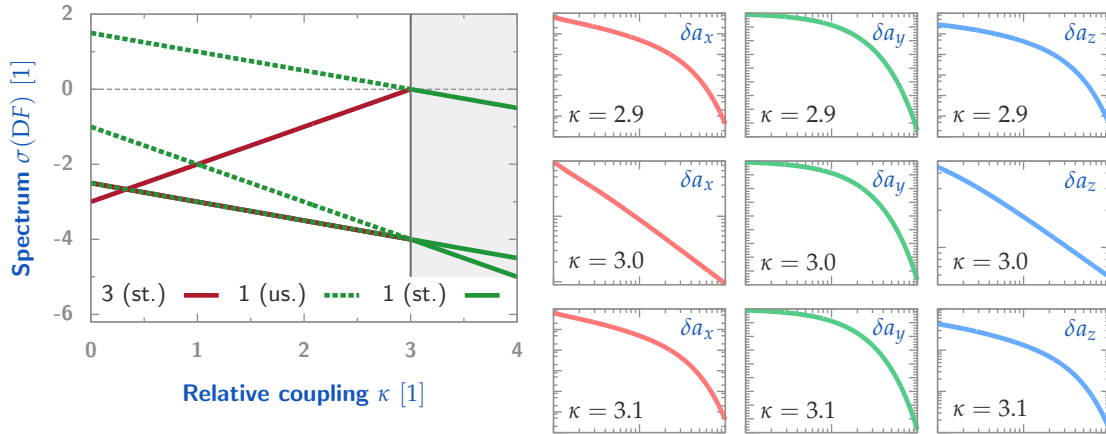
$$\delta a_x(t) = C \frac{e^{-4t}}{\sqrt{t}} - \frac{\kappa_c}{32t} \sum_{n=0}^{N-1} \frac{(2n-1)!!}{(8t)^n} + \frac{i\sqrt{\pi}\kappa_c}{16\sqrt{t}} e^{-4t} + R''_N(2i\sqrt{t}). \quad (2.118)$$

The exponential and algebraic parts are now separated and the slowest decaying summand determines the behaviour for  $t \rightarrow \infty$  when the exponential contributions already vanish. The dominant algebraic contribution is given by the first summand of the series (i.e.  $n = 0$ ) and reads

$$\delta a_x(t) \xrightarrow{t \rightarrow \infty} -\frac{\kappa_c}{32} t^{-1} \quad (2.119)$$

which is the approximate result for the long-term behaviour of the  $a_x$ -deviation from the steady state at the critical point.

In Fig. 2.17 we compare our analytical and the results obtained by numerical integration of the full dynamical system. There are two points worth mentioning: First, we succeeded in deriving analytical results for late times as they obviously describe the exact behaviour perfectly once the exponential contributions vanish. Second, the term “critical slowing down” is justified as a comparison of the *timescales* of the (algebraic)  $\delta a_x/\delta a_z$ -relaxation and the (still exponential)  $\delta a_y$ -relaxation shows. For comparison we plot the previously derived solutions for  $\kappa \gg \kappa_c$ , see Eq.(2.107), as well. Thereby it becomes clear that the initial relaxation remains exponential as in



■ **Figure 2.18:** Critical slowing down at the phase transition. On the left-hand side we show the spectrum  $\sigma(DF)$  of the Jacobian matrix  $DF$  of the flow  $F(a_x, a_y, a_z)$  at a ferromagnetic (paramagnetic) steady state for  $\kappa \leq 3 = \kappa_c$  ( $\kappa > 3$ ). The ferromagnetic solution (No. 3, red line) is stable in the range where it is physical which can be seen from the fact that  $DF$  clearly is negative (semidefinite). The paramagnetic solution (No. 1, green line) is stable for  $\kappa > \kappa_c$  but becomes unstable for  $\kappa \leq \kappa_c$  since in this range an eigenvalue becomes positive. At the phase transition the spectral gap of  $DF$  closes which leads to an algebraic relaxation rate in  $a_z$ -direction even close to the stationary state. On the right-hand side we show the time evolutions of the distances  $\delta a_i(t) = |a_i(t) - \lim_{t \rightarrow \infty} a_i(t)|$  (see text) for couplings  $\kappa$  below, at, and above the critical value  $\kappa_c = 3$ . Since the plots are in a full-logarithmic reference frame, we conclude that the  $a_x$ - and  $a_z$ -relaxation become algebraic close to the phase transition and for long times. The  $a_y$ -relaxation remains exponential for all times and couplings. The reason that *two* directions decay algebraically even though just *one* eigenvalue in  $\sigma(DF)$  vanishes is explained in the text by solving suitable limiting cases of the dynamical system analytically.

the paramagnetic regime and becomes algebraic at late times when the fast decaying exponential contributions vanish.

Interestingly the critical exponent  $\eta_x = -1$  (see Eq. (2.119)) differs from the one for relaxation in  $a_z$ -direction, namely  $\eta_z = -\frac{1}{2}$ . We furthermore point out that the algebraic decay in  $a_x$ -direction will eventually proceed to an *exponential* decay close to the steady state. In contrast to the  $\delta a_z$ -relaxation, where we found a vanishing eigenvalue of the derivative  $DF$  at the critical point and therefore an algebraic approach even close to the steady state, there is no such infinitesimal property in  $a_x$ -direction. This is pointed out in Fig. 2.18 where we show on the left-hand side the spectrum of  $DF$  at a stable fixed point for varying  $\kappa$  and on the right-hand side the relaxation in  $a_x$ -,  $a_y$  and  $a_z$ -direction below, at and above the critical coupling  $\kappa_c = 3$  for an initial state far from the fixed point. It can clearly be seen that the  $\delta a_y$ -relaxation remains exponential at the phase transition whereas the  $\delta a_x$ - and  $\delta a_z$ -relaxation are exponential away from the critical point but become algebraic at  $\kappa_c = 3$  (these are full-logarithmic plots). The spectrum reveals that only *one* of the three eigenvalues vanishes at the critical coupling<sup>33</sup> whilst the relaxation becomes algebraic in *two* directions *away from the fixed point*.

<sup>33</sup>That was already derived in the course of the stability analysis in 2.3.2.

### ■ Ferromagnetic system ( $\kappa \rightarrow 0$ )

In a purely ferromagnetic system ( $\kappa = 0$ ) the dynamical equations (2.102) read

$$\partial_t \delta a_x = \frac{1}{2}(\kappa_c - 8) \delta a_x + \kappa_c \delta a_x \delta a_z - \frac{\kappa_c}{2} \delta a_x \delta a_z^2 \quad (2.120a)$$

$$\partial_t \delta a_y = \frac{1}{2}(\kappa_c - 8) \delta a_y \quad (2.120b)$$

$$\partial_t \delta a_z = -\kappa_c \delta a_z + \frac{3}{2}\kappa_c \delta a_z^2 - \frac{1}{2}\kappa_c \delta a_z^3 \quad (2.120c)$$

which is still much more complicated than in the paramagnetic phase or at the phase transition. We will not derive analytical solutions in this case as we cannot expect to gain much insight. The paramagnetic system served as a paradigmatic case and provided us via straightforward calculations with simple solutions that showed the exponential decay towards the paramagnetic steady state. Numerical integrations of the system (2.120) show that the exponential decay in all three directions dominates the dynamics away from the steady state<sup>34</sup> like in the paramagnetic regime which was examined above. An example is given in the first row of Fig. 2.18 (right-hand side) which is almost indistinguishable from the paramagnetic evolution.

Note that there is a subtle but crucial difference between the ferromagnetic system (2.102) and the paramagnetic analogue (2.101). The latter features a *unique* fixed point and any (physical) initial state ends up in this steady state. The ferromagnetic dynamical system in terms of  $\delta \mathbf{a}$  describes the distance to one of the *two* (stable) fixed points. So if the initial state is chosen in the “wrong” hemisphere of the Bloch ball,  $\delta \mathbf{a}$  is driven towards a fixed point but does *not vanish* for  $t \rightarrow \infty$  (for instance,  $\kappa = 0$  leads to  $\lim_{t \rightarrow \infty} |\delta \mathbf{a}(t)| = 2$ ). Furthermore there is the unstable (paramagnetic) fixed point close to the origin. Whereas the attraction domain of the ferromagnetic fixed points are the northern and southern hemisphere minus the equatorial plane (which are of positive measure), the attraction domain of the unstable paramagnetic fixed point is precisely this plane which is of measure zero. This more delicate structure of attractors and attraction domains is linked to the complexity of the dynamical system (in contrast to the paramagnetic case).

The multiple fixed points can be most easily illustrated by Eq. (2.120c) where the roots and signs of the polynomial

$$-\delta a_z + \frac{3}{2}\delta a_z^2 - \frac{1}{2}\delta a_z^3 = \frac{1}{2}(2 - \delta a_z)(\delta a_z - 1)\delta a_z \quad (2.121)$$

determine the evolution of  $\delta a_z$ . The root  $\delta a_z = 1$  corresponds to the unstable paramagnetic fixed point whereas the roots  $\delta a_z = 0$  and  $\delta a_z = 2$  describe the stable ferromagnetic fixed points. Note that the expression becomes negative for  $\delta a_z \in (0, 1)$  which describes the relaxation to  $\delta a_z = 0$ . For  $\delta a_z \in (1, 2)$  it becomes positive and describes the repulsion to the second ferromagnetic fixed point  $a_{F2}$ . ■

### Inhomogeneous mean field theory

The mean field theory we used so far was raised on the assumption of a *homogeneous* system. This simplification was incorporated in the derivation of the ferromagnetic mean field jump operators, namely in Eq. (2.43) f. and the same assumption led to the well-known mean field

<sup>34</sup>Close to the steady state we already know this fact since  $\sigma(DF)$  is negative.

Hamiltonian of the TIM in Eq. (2.38). We already pointed out in the course of our general treatment on mean field theories of dissipative processes (see Appendix A) that there is no *a priori* requirement for a homogeneous system and a *single* mean field whatsoever. Basically, inhomogeneities can be taken into account by the introduction of one mean field *per site* or  $3N$  mean field degrees of freedom for  $N$  spins. The system in such a theory is still described by a density matrix in product form,  $\rho(t) = \prod_i \rho_i(t)$ , but the state  $\rho_i(t)$  is site-dependent and couples dynamically to the neighbouring states  $\rho_j(t)$ ,  $j \in N_i$ .

In the following, we perform these computations for the dissipative TIM and derive the inhomogeneous mean field equations. This includes a modification of the derivation of the ferromagnetic mean field jump operators. In the last paragraph the resulting dynamical systems are solved numerically for systems of several spins and we identify the two regimes of *homogenising* and *relaxation*.

### ■ Inhomogeneous dissipative dynamics

Let us proceed with a more general derivation of the ferromagnetic mean field jump operators (see paragraph 2.3.1 for the homogeneous case). We denote by  $m_i^z \equiv \text{Tr} [\rho_i \sigma_i^z]$  the site-dependent polarisation in z-direction. The computation runs along the same lines as in 2.3.1. We calculate the relevant partial traces:

#### ► First case: $i \in N_j$

First, introduce  $M_j^i \equiv \sum_{l \in N_j, l \neq i} m_l^z$  to shorten the following expressions. Then the jump contribution yields

$$\begin{aligned} \text{Tr}_i [d_j \rho d_j^\dagger] &= \frac{1}{q^2} \sum_{m,n \in N_j} \text{Tr}_i [\sigma_m^z \bar{\rho}_j \sigma_n^z] - \frac{m_j^z}{q} \sum_{m \in N_j} \text{Tr}_i [\{\sigma_m^z, \bar{\rho}_j\}] + \rho_i \\ &= \frac{1}{q^2} [C_{ij}(q, \{m_l^z\}) \rho_i + M_j^i \{\sigma_i^z, \rho_i\} + \sigma_i^z \rho_i \sigma_i^z] - \frac{m_j^z}{q} [2M_j^i \rho_i + \{\sigma_i^z, \rho_i\}] + \rho_i \end{aligned}$$

and the effective Hamiltonian results in

$$\begin{aligned} \text{Tr}_i [d_j^\dagger d_j \rho] &= \frac{1}{q^2} \sum_{m,n \in N_j} \text{Tr}_i [\sigma_m^z \sigma_n^z \bar{\rho}_j] - \frac{2m_j^z}{q} \sum_{m \in N_j} \text{Tr}_i [\sigma_m^z \bar{\rho}_j] + \rho_i \\ &= \frac{1}{q^2} [C_{ij}(q, \{m_l^z\}) \rho_i + 2M_j^i \sigma_i^z \rho_i + \sigma_i^z \sigma_i^z \rho_i] - \frac{2m_j^z}{q} [M_j^i \rho_i + \sigma_i^z \rho_i] + \rho_i \end{aligned}$$

which combines, after some straightforward calculations, to

$$\kappa_F \sum_{j \in N_i} \left[ \text{Tr}_i [d_j \rho d_j^\dagger] - \frac{1}{2} \text{Tr}_i [\{d_j^\dagger d_j, \rho\}] \right] = \frac{\kappa_F}{q} \left[ \sigma_i^z \rho_i \sigma_i^z - \frac{1}{2} \{\sigma_i^z \sigma_i^z, \rho_i\} \right]. \quad (2.122)$$

This is the well known z-dephasing induced by the correlation part in  $d_i = \sigma_i^x \left( \mathbb{1} - \sum_{j \in N_i} \sigma_i^z \sigma_j^z \right)$ .

► **Second case:**  $i = j$

First, introduce the quantities

$$\bar{M}_i^z \equiv \sqrt{\frac{1}{q} \sum_{j \in N_i} (m_j^z)^2} \quad \text{and} \quad M_i^z \equiv \frac{1}{q} \sum_{j \in N_i} m_j^z. \quad (2.123)$$

Tracing out all but the central spin  $i$  yields for the jumps

$$\text{Tr}_i [d_i \rho d_i^\dagger] = \frac{1}{q^2} \sum_{m,n \in N_i} \text{Tr}_i [\sigma_m^z \bar{\rho}_i \sigma_n^z] \sigma_i^y \rho_i \sigma_i^y + \frac{i}{q} \sum_{m \in N_i} m_m^z \sigma_i^y \rho_i \sigma_i^x - \frac{i}{q} \sum_{m \in N_i} m_m^z \sigma_i^x \rho_i \sigma_i^y + \sigma_i^x \rho_i \sigma_i^x.$$

We calculate further

$$\sum_{m,n \in N_i} \text{Tr}_i [\sigma_m^z \bar{\rho}_i \sigma_n^z] = \sum_{m,n \in N_i} \langle \sigma_m^z \sigma_n^z \rangle = \sum_{m,n \in N_i \wedge m \neq n} m_m^z m_n^z + q \equiv \tilde{M}_i^z + q. \quad (2.124)$$

This yields

$$\text{Tr}_i [d_i \rho d_i^\dagger] = \frac{1}{q^2} \tilde{M}_i^z \sigma_i^y \rho_i \sigma_i^y + \frac{1}{q} \sigma_i^y \rho_i \sigma_i^y + i M_i^z (\sigma_i^y \rho_i \sigma_i^x - \sigma_i^x \rho_i \sigma_i^y) + \sigma_i^x \rho_i \sigma_i^x.$$

If we use

$$(M_i^z)^2 = \frac{1}{q^2} \sum_{m \in N_i, n \in N_i} m_m^z m_n^z = \frac{1}{q^2} \tilde{M}_i^z + \frac{1}{q^2} \sum_{n \in N_i} (m_n^z)^2 = \frac{1}{q^2} \tilde{M}_i^z + \frac{1}{q} (\bar{M}_i^z)^2 \quad (2.125)$$

it follows

$$\text{Tr}_i [d_i \rho d_i^\dagger] = \left[ (M_i^z)^2 - \frac{1}{q} (\bar{M}_i^z)^2 \right] \sigma_i^y \rho_i \sigma_i^y + \frac{1}{q} \sigma_i^y \rho_i \sigma_i^y + i M_i^z (\sigma_i^y \rho_i \sigma_i^x - \sigma_i^x \rho_i \sigma_i^y) + \sigma_i^x \rho_i \sigma_i^x.$$

One could now proceed with the calculation of  $\text{Tr}_i [d_i^\dagger d_i \rho]$  although it is already easy to infer the effective jump operators without any further calculations. We prefer the latter: It is now not difficult to see that

$$\text{Tr}_i [d_i \rho d_i^\dagger] = [\sigma_i^x (\mathbb{1} - M_i^z \sigma_i^z)] \rho_i [\sigma_i^x (\mathbb{1} - M_i^z \sigma_i^z)]^\dagger \quad (2.126a)$$

$$+ \left[ \frac{1}{\sqrt{q}} \sqrt{1 - (\bar{M}_i^z)^2} \sigma_i^y \right] \rho_i \left[ \frac{1}{\sqrt{q}} \sqrt{1 - (\bar{M}_i^z)^2} \sigma_i^y \right]^\dagger \quad (2.126b)$$

and we conclude that the remaining (ferromagnetic) mean field jump operators read

$$\bar{d}_i = \sqrt{\kappa_F} \sigma_i^x (\mathbb{1} - M_i^z \sigma_i^z) \quad \text{and} \quad \bar{b}_i = \sqrt{\frac{\kappa_F}{q}} \sqrt{1 - (\bar{M}_i^z)^2} \sigma_i^y \quad (2.127)$$

Note that in the homogeneous limit,  $m_i^z \equiv m_z$  for all sites  $i$ , it holds  $M_i^z = m_z$  and  $\bar{M}_i^z = |m_z|$  and the above operators reduce to the homogeneous jump operators we used up to now. These results are not surprising and meet our expectations as the inhomogeneity demands the substitutions

$$m_z \mapsto M_i^z = \frac{1}{q} \sum_{j \in N_i} m_j^z \quad \text{and} \quad m_z^2 \mapsto (\bar{M}_i^z)^2 = \frac{1}{q} \sum_{j \in N_i} (m_j^z)^2 \quad (2.128)$$

which take the magnetisation of the nearest neighbours into account.

Let us sum up what we found so far:

► **Result 2.3: Inhomogeneous Mean Field Lindblad Equation**

The *inhomogeneous* mean field version of the Lindblad master equation describing the purely dissipative transverse field Ising model reads for each site  $i$

$$\partial_t \rho_i = \underbrace{\mathcal{L}(c_i)}_{\text{paramagnetic}} [\rho_i] + \underbrace{\mathcal{L}(\bar{d}_i) [\rho_i] + \mathcal{L}(\bar{b}_i) [\rho_i] + \mathcal{L}(\bar{o}_i) [\rho_i]}_{\text{ferromagnetic}}$$

with the three ferromagnetic mean field jump operators

$$\bar{d}_i = \sqrt{\kappa_F} \sigma_i^x (\mathbb{1} - M_i^z \sigma_i^z) \quad (2.129a)$$

$$\bar{b}_i = \sqrt{\frac{\kappa_F}{q}} \sqrt{1 - (\bar{M}_i^z)^2} \sigma_i^y \quad (2.129b)$$

$$\bar{o}_i = \sqrt{\frac{\kappa_F}{q}} \sigma_i^z \quad (2.129c)$$

and the paramagnetic jump operator

$$c_j = \frac{\sqrt{\kappa_P}}{2} (\sigma_j^z - i\sigma_j^y) \quad (2.129d)$$

which remains unaffected by the mean field approximation.

There are  $3N$  mean field degrees of freedom  $m_i^x$ ,  $m_i^y$ , and  $m_i^z$  in a system with  $N$  spins. Their dynamical relevant combinations read

$$M_i^z = \frac{1}{q} \sum_{j \in N_i} m_j^z \quad \text{and} \quad \bar{M}_i^z = \sqrt{\frac{1}{q} \sum_{j \in N_i} (m_j^z)^2} \quad (2.130)$$

for each site  $i$  and the coordination number  $q$ .

Let us now turn towards the mean field equations of this theory.

■ **Inhomogeneous mean field equations**

The dynamical equations for multiple mean fields were derived in Appendix A for general dissipative systems. The dynamical system (A.37) reads for vanishing unitary dynamics  $h^{\text{mf}} = 0$  and one mean field per site (i.e.  $\alpha = i = 1, \dots, N$ )

$$\partial_t m_\alpha^n = 2\epsilon^{ijn} I_{i,j}^\alpha + 2(R_{n,i}^\alpha - R^\alpha \delta_{ni}) m_\alpha^i \quad (2.131)$$

where  $I_{i,j}^\alpha$  and  $R_{i,j}^\alpha$  are defined in (A.8).



The mean field jump operators read in the Pauli basis

$$\mathbf{l}_d^\alpha = \sqrt{\kappa_F} \begin{bmatrix} 1 & iM_\alpha^z & 0 \end{bmatrix}^T \quad (2.132a)$$

$$\mathbf{l}_b^\alpha = \sqrt{\frac{\kappa_F}{q}} \begin{bmatrix} 0 & \sqrt{1 - (\overline{M}_\alpha^z)^2} & 0 \end{bmatrix}^T \quad (2.132b)$$

$$\mathbf{l}_o^\alpha = \sqrt{\frac{\kappa_F}{q}} \begin{bmatrix} 0 & 0 & 1 \end{bmatrix}^T \quad (2.132c)$$

$$\mathbf{l}_c^\alpha = \frac{\sqrt{\kappa_P}}{2} \begin{bmatrix} 0 & -i & 1 \end{bmatrix}^T. \quad (2.132d)$$

If we insert these in the definition of the real matrices  $\mathbf{I}^\alpha$  and  $\mathbf{R}^\alpha$ , Eq. (2.131) reads

$$\partial_t a_i^x = \kappa + \frac{a_i^x}{q} \left[ 2\Delta_i^2 - (4 + q\kappa) \right] \quad (2.133a)$$

$$\partial_t a_i^y = -\frac{a_i^y}{2q} [(4 + q\kappa) + 4q] = -\lambda a_i^y \quad (2.133b)$$

$$\partial_t a_i^z = 4M_i^z + \frac{a_i^z}{2q} \left[ 4\Delta_i^2 - \{(4 + q\kappa) + 4q\} \right] \quad (2.133c)$$

where we introduced the shortcuts  $\Delta_i^2 \equiv (\overline{M}_i^z)^2 - q(M_i^z)^2$  and  $\lambda \equiv (2q)^{-1} [(4 + q\kappa) + 4q]$ , replaced  $\alpha$  by the site index  $i$ , used the self-consistency condition  $m_\alpha^k = a_\alpha^k$  and rescaled time to introduce the relative coupling  $\kappa = \frac{\kappa_P}{\kappa_F}$ . Here  $\mathbf{a}_\alpha = \mathbf{a}_i$  denotes the Bloch vector on site  $i$ , i.e.  $\rho_i = \frac{1}{2} (\mathbb{1} + \mathbf{a}_i \cdot \boldsymbol{\sigma}_i)$ .

The relaxation in  $a_i^y$ -direction is free, i.e. decoupled from the dynamics in  $a_i^x$ - and  $a_i^z$ -direction. As in the homogeneous case, it is exponential for all couplings  $\kappa$  and reads

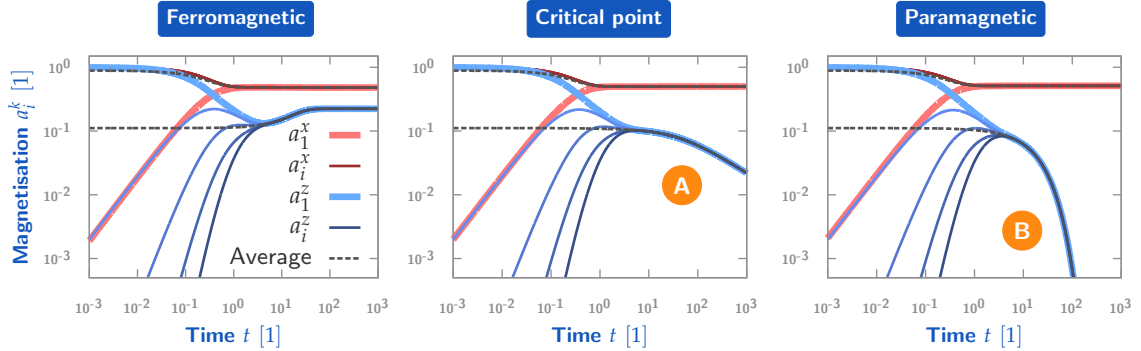
$$a_i^y(t) = a_i^y(0) e^{-\lambda t}. \quad (2.134)$$

So this component of the mean fields is not interesting and we omit it completely in the following treatment of the mean field dynamics. If we rewrite the remaining differential equations in terms of  $\lambda$  we end up with

$$\partial_t a_i^x = \kappa + \left[ \frac{2}{q} \Delta_i^2 - 2(\lambda - 2) \right] a_i^x \quad (2.135a)$$

$$\partial_t a_i^z = 4M_i^z + \left[ \frac{2}{q} \Delta_i^2 - \lambda \right] a_i^z \quad (2.135b)$$

for each site  $i$ . Note that the neighbouring fields are hidden in  $\Delta_i^2$  and we have to solve a system of  $2N$  non-linear differential equations in  $a_i^x$  and  $a_i^z$ . There is no sense in solving this system analytically, so we restrict ourselves to numerical integrations in the following paragraph to gain insight into the dynamics of several coupled spins.



■ **Figure 2.19:** Mean field dynamics of the inhomogeneous purely dissipative TIM in one dimension for  $L = 9$  spins and with PBC. We show the dynamics of  $a_i^x$  and  $a_i^z$  for  $i = 1, \dots, 9$  in (left to right) the ferromagnetic ( $\kappa = 1.9$ ), critical ( $\kappa = 2.0 = \kappa_c$  for  $q = 2$ ) and paramagnetic ( $\kappa = 2.1$ ) regime. Note that due to the cyclic symmetry of the system there are only *five* different magnetisations visible. The dashed grey lines denote the average magnetisation  $L^{-1} \sum_i a_i^k$  for  $k = x, z$ . The system was initialised with spin 1 polarised in  $z$ -direction,  $|\Psi_0\rangle_1 = |\uparrow\rangle$ , and the rest of the spins polarised in  $x$ -direction,  $|\Psi_0\rangle_i = |+\rangle$  for  $i = 2, \dots, 9$ . Note that there are two distinct regimes in the relaxation process: Up to  $t \approx 5$  the system homogenises, subsequently the now *homogeneous* system is driven towards the NESS. Whereas there is no obvious impact of the coupling on the *homogenisation*, the homogeneous *relaxation process* becomes algebraic at the critical point (A) for late times and remains exponential (B) in the paramagnetic & ferromagnetic regime. Note that the initial polarisation of spin 1 breaks the  $\mathbb{Z}_2$  symmetry of the dissipative process explicitly and is thus responsible for the reached steady state in the ferromagnetic regime. Further comments are given in the text.

### ■ Results: Homogenising and relaxation

Here we solve the dynamical equations (2.135) in small one- and two-dimensional systems numerically and visualise the relaxation of initially inhomogeneous systems to their non-equilibrium steady state.

#### ► One-dimensional system

In Fig. 2.19 we show the results of a numerical integration of (2.135) for a  $L = 9$  spin chain with PBC. To illustrate the response of the system on a localised perturbation, the first spin was initialised in the completely  $z$ -polarised state  $|\uparrow\rangle$  whereas the rest of the system was initialised completely  $x$ -polarised, namely in  $|+\rangle$ . We plot  $a_i^x$  and  $a_i^z$  logarithmically vs. a logarithmic timescale for  $0.001 \leq t \leq 1000$  and compute furthermore the average magnetisation  $L^{-1} \sum_i a_i^k$  ( $k = x, z$ ) for each quantity. The perturbed spin is denoted by bold lines whereas the other spins are drawn with thin ones. We computed the time evolution for comparison in the ferromagnetic ( $\kappa = 1.9$ ), critical ( $\kappa = 2 = \kappa_c$ ) and paramagnetic ( $\kappa = 2.1$ ) regime. Let us analyse the results in detail:

- There are two distinct regimes: First *homogenisation*, then *relaxation*. Up to  $t \lesssim 5$  the system reduces the inhomogeneity quickly until it ends up in a homogeneous non-stationary state. Subsequently the *homogeneous* system is driven towards the  $\kappa$ -dependent fixed point. Note that the time interval in which the homogenisation takes place seems to be rather independent of the relative coupling  $\kappa$  and therefore the system's phase.
- During the homogenisation the initially  $z$ -polarised spin “shares”  $z$ -magnetisation with the other spins (the more the closer the interacting spin). However, on an absolute scale

its own local relaxation dominates the dynamics since  $a_1^z$  first drops from 1 to  $\sim 0.2$  until it is of the same order as the remaining  $a_i^z$  (logarithmic scale!).

- In the ferromagnetic phase the  $\mathbb{Z}_2$  symmetry of the dissipative process is explicitly broken by the chosen initial condition, namely the z-polarised spin (the other spins are perfectly symmetric with respect to the global spin-flip  $\prod_i \sigma_i^x$ ). As we chose the first spin to point in positive  $a_z$ -direction, the reached ferromagnetic steady state is the one with the same sign.
- At the critical point and in the paramagnetic phase the reached steady state is obviously independent of the initial state as it is unique. However, the relaxation of the system towards its steady state depends crucially on  $\kappa$ : At the critical point,  $\kappa = \kappa_c = 2$ , the relaxation becomes algebraic for late times (A) whereas it remains exponential for all times in the paramagnetic regime,  $\kappa > \kappa_c = 2$ , as can be seen at (B). This was to be expected since the homogeneous system is described by our previous results based on the homogeneous mean field equations.
- Note that due to the periodic boundary conditions the evolution of  $a_2^z$  and  $a_9^z$  (and corresponding pairs) coincides. Consequently there are only *five* distinct time evolutions visible in the plots.

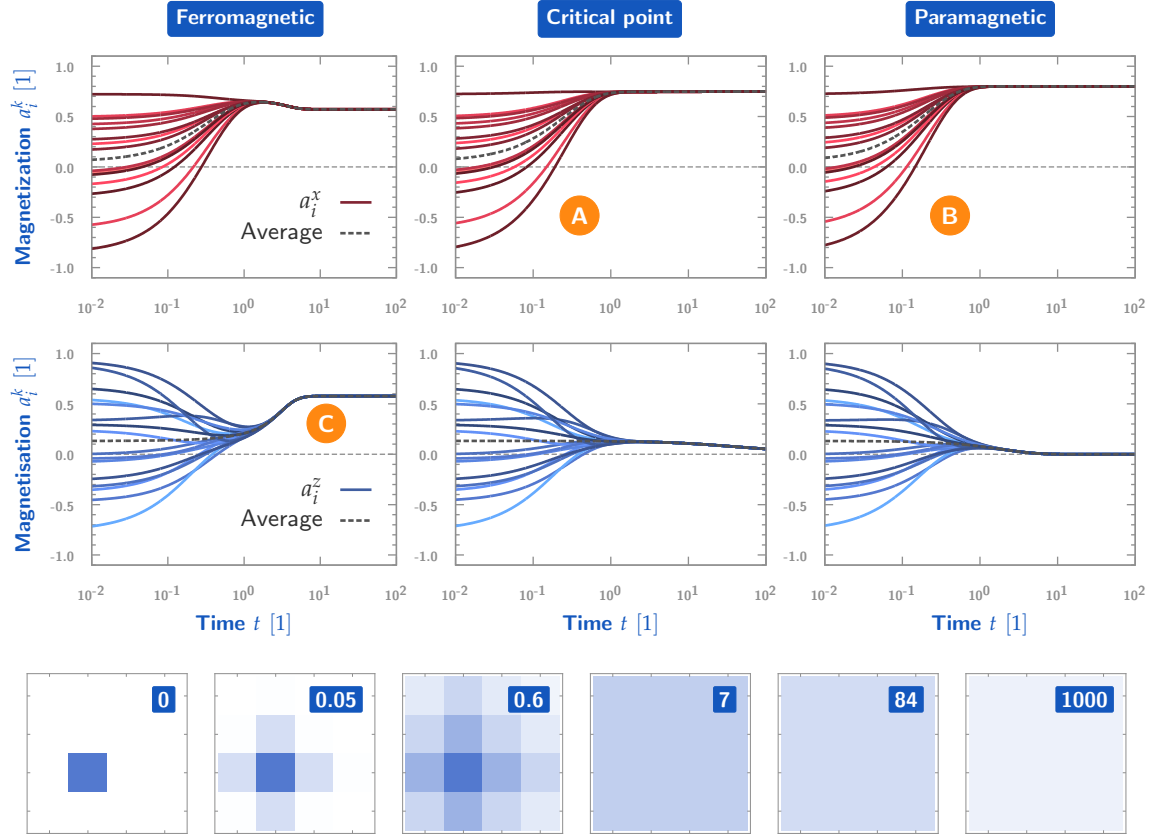
Besides all details, the crucial result of this inspection is the following: Inhomogeneous systems homogenise rapidly — in all phases (even at the critical point) and independently of  $\kappa$ . Therefore, subsequent to a short initial time interval, they are well described by the homogeneous mean field equations which we employed for all our previous inspections. The *homogeneity assumption* in the derivation of the mean field theory is thus legit, at least from this more general mean field point of view and in the purely dissipative setup. We will see below that this holds also in two dimensions and there is *no evidence* of dynamical instabilities or other phenomena caused by multiple, coupled spins.

#### ► Two-dimensional system

In the upper two rows of Fig. 2.20 we show the results of a numerical integration of (2.135) for a  $L = 4 \times 4$  spin plaquette with PBC. To illustrate the evolution towards homogeneity, we initialised the 16 spins randomly in pure states with  $a_i^y = 0$  and  $a_i^x = \cos \theta_i$ ,  $a_i^z = \sin \theta_i$  where  $\Theta_i \in \mathcal{U}(0, 2\pi)$  is uniformly distributed. Here we plot  $a_i^x$  and  $a_i^z$  *linearly*<sup>35</sup> vs. a logarithmic timescale for  $0.01 \leq t \leq 100$  and compute the average magnetisation  $L^{-1} \sum_i a_i^k$  ( $k = x, z$ ) for each quantity. We computed the time evolution for comparison in the ferromagnetic ( $\kappa = 2$ ), critical ( $\kappa = 3 = \kappa_c$ ) and paramagnetic ( $\kappa = 4$ ) regime. Here some remarks:

- The qualitative structure of the time evolution is confirmed: The system homogenises rapidly and subsequently evolves homogeneously to the steady state. This can be observed in both phases, at the critical point and for both,  $a_i^x$  and  $a_i^z$ . The partitioning of the time evolution into homogenisation and relaxation can be most clearly seen in the centred plot of  $a_i^z$  for a critical system. There the homogenisation for  $0 \leq t \lesssim 1$  is followed by a nearly algebraic approach to the critical steady state. This approach becomes exponential in the paramagnetic regime.
- Comparison of (A) and (B) verifies the statement from above that the homogenisation process remains (qualitatively) unaffected by changes of  $\kappa$ . Especially, there is *no slowing down* at the critical point during the homogenisation (A).

<sup>35</sup>This is more convenient since there are zeros in the plots.



■ **Figure 2.20:** Mean field dynamics of the inhomogeneous purely dissipative TIM in two dimensions for  $L = 4 \times 4$  spins and with PBC. We show the dynamics of  $a_i^x$  (upper row) and  $a_i^z$  (middle row) for  $i = 1, \dots, 16$  in (left to right) the ferromagnetic ( $\kappa = 2$ ), critical ( $\kappa = 3 = \kappa_c$  for  $q = 4$ ) and paramagnetic ( $\kappa = 4$ ) regime. The dashed grey lines denote the average magnetisation  $L^{-1} \sum_i a_i^k$  for  $k = x, z$ . For the plots in the upper two rows the system was initialised in a random configuration of spins in pure states with  $a_i^y = 0$  and  $a_i^x = \cos \theta_i$ ,  $a_i^z = \sin \theta_i$  where  $\theta_i \in \mathcal{U}(0, 2\pi)$  is uniformly distributed. Here the two regimes (homogenisation and relaxation) are clearly visible. Note that the coupling  $\kappa$  has hardly any effect on the structure and duration of the homogenisation process, see (A) and (B), whereas the relaxation crucially depends on  $\kappa$ . The average initial  $z$ -magnetisation breaks the  $\mathbb{Z}_2$  symmetry and determines the final steady state in the ferromagnetic phase, see (C). In the lower row we show the time evolution of  $a_i^z$  for a critical system  $\kappa = \kappa_c$  with a single  $z$ -polarized spin (blue square in the leftmost plot) for  $t = 0$ ; the other spins were initialised in the (paramagnetic) steady state of the critical system. The numbers denote the shown time slice on a logarithmic time scale. For  $0 \leq t \lesssim 1$  the system is homogenising, subsequently the homogeneous system is driven towards the steady state with vanishing  $z$ -magnetisation.

► In the ferromagnetic regime, the (sign of the) final steady state depends on the initial average  $z$ -magnetisation which breaks the  $\mathbb{Z}_2$  symmetry, see (C) and the dashed line for  $t \rightarrow 0$  in the same plot.

The lower row of Fig. 2.20 shows a spatially resolved time evolution of the discrete field  $a_i^z$  in the  $L = 4 \times 4$  critical ( $\kappa = \kappa_c$ ) system for distinguished time slices on a logarithmic time scale. The system was initialised with a single completely  $z$ -polarised spin (blue square in leftmost plot) and all other spins in the homogeneous steady state. The first three slices for  $0 \leq t \lesssim 1$  show the *homogenisation* and the last three the *relaxation* to the critical steady state with vanishing  $z$ -magnetisation. The slices at  $t = 0.05$  and  $t = 0.6$  illustrate the influences of the

localised perturbation on its neighbouring spins and the dispersion of  $z$ -magnetisation through the system.

The numerical results in this and the previous paragraph suggest a qualitatively different relaxation of inhomogeneities as compared to the relaxation of the homogeneous system. We tackle this phenomenon in the next subsection by means of a continuum theory.

Continuous mean field theory for dissipative dynamics

If one considers *large* lattices of spins and perturbations with characteristic length scales much larger than the lattice constant, it is convenient to switch to a continuum description,

$$a_i^k \mapsto a^k(x) \quad \text{with } x \in \mathbb{R}^D \quad \text{and } k = x, z. \quad (2.136)$$

As a consequence, the set of  $2N$  differential equations in (2.135) has to be replaced by a field equation. Before we derive such a continuum description, it is convenient to change the dynamical degrees of freedom

$$a_i^x = a_x + \delta a_i^x \quad \text{and} \quad a_i^z = a_z + \delta a_i^z \quad (2.137)$$

since we are interested in the relaxation of inhomogeneities  $\delta a_i^k$  towards a *homogeneous* steady state  $a_k$ . In the following we express the differential equations (2.135) in terms of  $\delta a_i^k$  and linearise them to obtain a solvable theory for spatial perturbations with long wavelengths and small amplitudes.

Let us start with  $\Delta_i^2 = \left(\overline{M}_i^z\right)^2 - q \left(M_i^z\right)^2$ . It is straightforward to show

$$\begin{aligned} \Delta_i^2 &= \frac{1}{q} \sum_{j \in N_i} (a_z + \delta a_j^z)^2 - \frac{1}{q} \left[ \sum_{j \in N_i} (a_z + \delta a_j^z) \right]^2 \\ &= (1-q)a_z^2 + \frac{2a_z}{q}(1-q) \sum_{j \in N_i} \delta a_j^z + \mathcal{O}(\delta a_j^z{}^2) \end{aligned}$$

and the average  $z$ -magnetisation at site  $i$  reads

$$M_i^z = \frac{1}{q} \sum_{j \in N_i} (a_z + \delta a_j^z) = a_z + \frac{1}{q} \sum_{j \in N_i} \delta a_j^z.$$

Hence we find for the first equation (2.135a)

$$\begin{aligned} \partial_t \delta a_i^x &= \kappa + \left[ \frac{2}{q} \Delta_i^2 - 2(\lambda - 2) \right] a_i^x \\ &= \kappa + \left[ \frac{2}{q} (1-q)a_z^2 + \frac{4a_z}{q^2} (1-q) \sum_{j \in N_i} \delta a_j^z - 2(\lambda - 2) \right] (a_x + \delta a_i^x) + \mathcal{O}(\delta a_j^z{}^2) \\ &\approx \left[ \kappa - \frac{\kappa_c}{2} a_x a_z^2 - 2a_x (\lambda - 2) \right] + \left[ -\frac{\kappa_c}{2} a_z^2 - 2(\lambda - 2) \right] \delta a_i^x - \frac{\kappa_c a_x a_z}{q} \sum_{j \in N_i} \delta a_j^z \end{aligned}$$

and for the second one (2.135b)

$$\begin{aligned}
\partial_t a_i^z &= 4M_i^z + \left[ \frac{2}{q} \Delta_i^2 - \lambda \right] a_i^z \\
&= 4a_z + \frac{4}{q} \sum_{j \in N_i} \delta a_j^z + \left[ \frac{2}{q} (1-q) a_z^2 + \frac{4a_z}{q^2} (1-q) \sum_{j \in N_i} \delta a_j^z - \lambda \right] (a_z + \delta a_i^z) + \mathcal{O}(\delta a_j^z{}^2) \\
&\approx \left[ 4a_z - \frac{\kappa_c}{2} a_z^3 - \lambda a_z \right] + \left[ -\frac{\kappa_c}{2} a_z^2 - \lambda \right] \delta a_i^z + \left[ \frac{4}{q} - \frac{\kappa_c a_z^2}{q} \right] \sum_{j \in N_i} \delta a_j^z.
\end{aligned}$$

Let us now abandon the discrete lattice with sites  $i$  and write the linearised equations in terms of fields  $a^k(\mathbf{x})$  with continuous coordinates  $\mathbf{x} \in \mathbb{R}^D$ . We identify site  $i$  with the point  $\mathbf{x}_i$  and denote by  $\mathbf{e}_\mu$  the basis vector of  $\mathbb{R}^D$  in  $\mu$ -direction. Let  $d$  be the distance of nearest neighbours in the lattice  $\{\mathbf{x}_i\}$ , i.e. the lattice constant. Recall that for any function  $f \in C^2(\mathbb{R}^D, \mathbb{R})$  the second derivative in  $\mu$ -direction can be written in terms of finite differences

$$\partial_\mu^2 f(\mathbf{x}) = \frac{f(\mathbf{x} + d\mathbf{e}_\mu) - 2f(\mathbf{x}) + f(\mathbf{x} - d\mathbf{e}_\mu)}{d^2} + \mathcal{O}(d^2). \quad (2.138)$$

With that said we find

$$a_{i+\mu}^z + a_{i-\mu}^z \equiv a^z(\mathbf{x}_i + d\mathbf{e}_\mu) + a^z(\mathbf{x}_i - d\mathbf{e}_\mu) = 2a^z(\mathbf{x}_i) + d^2 \partial_\mu^2 a^z(\mathbf{x}_i) + \mathcal{O}(d^4) \quad (2.139)$$

and consequently

$$\begin{aligned}
\frac{1}{q} \sum_{j \in N_i} a_j^z &= \frac{1}{q} \sum_\mu (a^z(\mathbf{x}_i + \mathbf{e}_\mu) + a^z(\mathbf{x}_i - \mathbf{e}_\mu)) = a^z(\mathbf{x}_i) + \frac{d^2}{q} \sum_\mu \partial_\mu^2 a^z(\mathbf{x}_i) + \mathcal{O}(d^4) \\
&= a^z(\mathbf{x}_i) + \frac{d^2}{q} \Delta a^z(\mathbf{x}_i) + \mathcal{O}(d^4)
\end{aligned}$$

which finally yields

$$\frac{1}{q} \sum_{j \in N_i} \delta a_j^z = \delta a^z(\mathbf{x}_i) + \frac{d^2}{q} \Delta \delta a^z(\mathbf{x}_i) + \mathcal{O}(d^4) \quad (2.140)$$

where we used  $a_i^z = a_z + \delta a_i^z$  and the fact that  $a_z$  is homogeneous.

If we consider a lattice  $\{\mathbf{x}_i\}$  embedded in  $\mathbb{R}^D$  with  $d \ll 1$ , the following substitutions yield a continuous theory that approximates the discrete mean field theory on the lattice sites  $\mathbf{x}_i$ :

$$a_i^k \mapsto a^k(\mathbf{x}) \quad \text{with } \mathbf{x} \in \mathbb{R}^D \quad \text{and } k = x, z \quad (2.141a)$$

$$\frac{1}{q} \sum_{j \in N_i} \delta a_j^z \mapsto \delta a^z(\mathbf{x}) + \frac{d^2}{q} \Delta \delta a^z(\mathbf{x}) \quad (2.141b)$$

One easily derives the dynamical field equations

$$\delta \dot{a}^x = \left[ \kappa - \frac{\kappa_c}{2} a_x a_z^2 + \kappa_4 a_x \right] + \left[ -\frac{\kappa_c}{2} a_z^2 + \kappa_4 \right] \delta a^x - \kappa_c a_x a_z \delta a^z - \kappa_c a_x a_z \frac{d^2}{q} \Delta \delta a^z \quad (2.142a)$$

$$\delta \dot{a}^z = \left[ -\frac{\kappa_c}{2} a_z^3 - \frac{\kappa - \kappa_c}{2} a_z \right] + \left[ -\frac{3\kappa_c}{2} a_z^2 - \frac{\kappa - \kappa_c}{2} \right] \delta a^z + \left[ 4 - \kappa_c a_z^2 \right] \frac{d^2}{q} \Delta \delta a^z \quad (2.142b)$$

where we substituted  $\lambda = 4 + \frac{1}{2}(\kappa - \kappa_c)$ . Or for short

$$\delta \hat{a}^x = A_x + B_x \delta a^x + C_x \delta a^z + D_x \Delta \delta a^z \quad (2.143a)$$

$$\delta \hat{a}^z = A_z + B_z \delta a^x + C_z \delta a^z + D_z \Delta \delta a^z \quad (2.143b)$$

with the parameters  $A_k$ ,  $B_k$ ,  $C_k$ , and  $D_k$  defined via identification with Eq. (2.142). A Fourier transform of Eq. (2.143) with respect to the spatial coordinates yields

$$\delta \hat{a}^x = A_x \delta(\mathbf{\kappa}) + B_x \delta \hat{a}^x + C_x \delta \hat{a}^z - D_x k^2 \delta \hat{a}^z \quad (2.144a)$$

$$\delta \hat{a}^z = A_z \delta(\mathbf{\kappa}) + B_z \delta \hat{a}^x + C_z \delta \hat{a}^z - D_z k^2 \delta \hat{a}^z \quad (2.144b)$$

where we employed the rule  $\mathcal{F}[\partial_\mu^2 f](\mathbf{k}) = -k^2 \mathcal{F}[f](\mathbf{k})$  and the shorthand notation  $\hat{f} \equiv \mathcal{F}[f]$ . We can rewrite Eq. (2.144) in matrix form

$$\frac{d}{dt} \begin{bmatrix} \delta \hat{a}^x(t, \mathbf{k}) \\ \delta \hat{a}^z(t, \mathbf{k}) \end{bmatrix} = \begin{bmatrix} A_x \\ A_z \end{bmatrix} \delta(\mathbf{k}) + \underbrace{\begin{bmatrix} B_x & C_x - k^2 D_x \\ B_z & C_z - k^2 D_z \end{bmatrix}}_{\equiv \mathcal{M}(k)} \cdot \begin{bmatrix} \delta \hat{a}^x(t, \mathbf{k}) \\ \delta \hat{a}^z(t, \mathbf{k}) \end{bmatrix} \quad (2.145)$$

with  $B_z = 0$ . As we are interested in *spatial perturbations* of the homogeneous steady state, it is reasonable to restrict ourselves to solutions with non-vanishing wave number  $k \neq 0$ , thus the interesting differential equations read

$$\frac{d}{dt} \begin{bmatrix} \delta \hat{a}^x(t, \mathbf{k}) \\ \delta \hat{a}^z(t, \mathbf{k}) \end{bmatrix} = \underbrace{\begin{bmatrix} B_x & C_x - k^2 D_x \\ 0 & C_z - k^2 D_z \end{bmatrix}}_{\equiv \mathcal{M}(k)} \cdot \begin{bmatrix} \delta \hat{a}^x(t, \mathbf{k}) \\ \delta \hat{a}^z(t, \mathbf{k}) \end{bmatrix}. \quad (2.146)$$

The spectrum  $\sigma(\mathcal{M})$  can be read off and we find the eigenvalues

$$\Gamma_1(k) = B_x = -\frac{\kappa_c}{2} a_z^2 + \kappa_4 \quad (2.147a)$$

$$\Gamma_2(k) = C_z - k^2 D_z = -\frac{3\kappa_c}{2} a_z^2 - \frac{\kappa - \kappa_c}{2} - \frac{(kd)^2}{q} \left[ 4 - \kappa_c a_z^2 \right]. \quad (2.147b)$$

We see that  $d$  is just a scaling parameter for the spatial dimensions (and the reciprocal space) and we are free to set it to one, so  $d = 1$  from now on. The damping spectrum depends on the homogeneous steady state  $(a_x, a_z)$  which, in turn, depends on  $\kappa$ . The expressions for the paramagnetic ( $\kappa \geq \kappa_c$ ) and ferromagnetic ( $\kappa < \kappa_c$ ) steady states are already known since the homogeneous steady states of the inhomogeneous theory are the steady states of the homogeneous theory. Let us write the results in Eq. (2.71) one more time:

$$\mathbf{a}_p = \left[ -\frac{\kappa}{\kappa_4} \quad 0 \quad 0 \right]^T \quad \text{and} \quad \mathbf{a}_{F1,2} = \left[ -\frac{2\kappa}{\kappa_8} \quad 0 \quad \mp \sqrt{1 - \frac{\kappa}{\kappa_c}} \right]^T \quad (2.148)$$

Here  $\mathbf{a}_p$  is the (homogeneous) paramagnetic steady state and  $\mathbf{a}_{F1,2}$  are the (homogeneous) ferromagnetic steady states. The damping spectrum simplifies considerably if we insert these results for  $a_z$ .

Straightforward calculations yield

$$\Gamma_1(k) = \begin{cases} \kappa_4 = -4 - (\kappa - \kappa_c) & \text{for } \kappa > \kappa_c \\ \frac{\kappa_8}{2} = -4 + \frac{\kappa_c - \kappa}{2} & \text{for } \kappa \leq \kappa_c \end{cases} \quad (2.149a)$$

$$\Gamma_2(k) = \begin{cases} -\frac{\kappa - \kappa_c}{2} - (4 - \kappa_c) k^2 & \text{for } \kappa > \kappa_c \\ -(\kappa_c - \kappa) - \frac{4 + (\kappa - \kappa_c)}{4} (4 - \kappa_c) k^2 & \text{for } \kappa \leq \kappa_c \end{cases}. \quad (2.149b)$$

To compare these results with the homogeneous ones of paragraph 2.3.3, one has to solve the differential equation (2.146). As before, the solutions depend on the phase and we have to treat the cases  $\kappa > \kappa_c$  and  $\kappa \leq \kappa_c$  separately:

#### ► Paramagnetic phase

For  $\kappa > \kappa_c$  we have  $a_z = 0$  and thus  $C_x = 0 = D_x$  which makes  $\mathcal{M}(k)$  diagonal for all wave numbers  $k$ . As a result, the solutions are trivially derived and read

$$\delta \hat{a}^x(t, \mathbf{k}) = \delta \hat{a}^x(0, \mathbf{k}) e^{\Gamma_1(k)t} = \delta \hat{a}^x(0, \mathbf{k}) e^{-(4 + \kappa - \kappa_c)t} \quad (2.150a)$$

$$\delta \hat{a}^z(t, \mathbf{k}) = \delta \hat{a}^z(0, \mathbf{k}) e^{\Gamma_2(k)t} = \delta \hat{a}^z(0, \mathbf{k}) e^{-\frac{\kappa - \kappa_c}{2}t - (4 - \kappa_c)k^2t} \quad (2.150b)$$

where the relaxation rate of  $\delta \hat{a}^z$  depends explicitly on the wave number  $k$ . As a consistency check, consider the limiting case  $k \rightarrow 0$  of (nearly) homogeneous modes. Then the solutions read  $\delta \hat{a}^x(t, \mathbf{k}) = \delta \hat{a}^x(0, \mathbf{k}) e^{-(\kappa - \kappa_c + 4)t}$  and  $\delta \hat{a}^z(t, \mathbf{k}) = \delta \hat{a}^z(0, \mathbf{k}) e^{-\frac{1}{2}(\kappa - \kappa_c)t}$  for  $k \ll 1$ . These are exactly the homogeneous results we found in 2.3.3, see Eq. (2.95).

#### ► Ferromagnetic phase

For  $\kappa \leq \kappa_c$  we have  $a_z \neq 0$  and thus  $C_x \neq 0 \neq D_x$  which makes  $\mathcal{M}(k)$  a triangular matrix that has to be diagonalised. This is a standard procedure and left as an exercise to the reader. One finds

$$\begin{aligned} \delta \hat{a}^x(t, \mathbf{k}) &= [\delta \hat{a}^x(0, \mathbf{k}) - \hat{C}_\kappa(k) \delta \hat{a}^z(0, \mathbf{k})] e^{\Gamma_1(k)t} + \hat{C}_\kappa(k) \delta \hat{a}^z(0, \mathbf{k}) e^{\Gamma_2(k)t} \\ &= [\delta \hat{a}^x(0, \mathbf{k}) - \hat{C}_\kappa(k) \delta \hat{a}^z(0, \mathbf{k})] e^{-\frac{1}{2}(8 + \kappa - \kappa_c)t} \\ &\quad + \hat{C}_\kappa(k) \delta \hat{a}^z(0, \mathbf{k}) e^{-(\kappa_c - \kappa)t + \frac{\kappa_4}{4}(4 - \kappa_c)k^2t} \end{aligned} \quad (2.151a)$$

and

$$\begin{aligned} \delta \hat{a}^z(t, \mathbf{k}) &= \delta \hat{a}^z(0, \mathbf{k}) e^{\Gamma_2(k)t} \\ &= \delta \hat{a}^z(0, \mathbf{k}) e^{-(\kappa_c - \kappa)t + \frac{\kappa_4}{4}(4 - \kappa_c)k^2t} \end{aligned} \quad (2.151b)$$

which are of the same structure as found in 2.3.3, see Eq. (2.100). The coupling of the  $\delta \hat{a}^x$ - to the  $\delta \hat{a}^z$ -relaxation is described by the  $k$ -dependent coefficient

$$\hat{C}_\kappa(k) \equiv \frac{k^2 D_x - C_x}{B_x - C_z + k^2 D_z} = \frac{4\kappa\kappa_c (q^{-1}k^2 - 1)}{(8 + 3\kappa - 3\kappa_c + \frac{2\kappa_4}{q}k^2)(8 + \kappa - \kappa_c)} \sqrt{1 - \frac{\kappa}{\kappa_c}} \quad (2.152)$$



for  $0 \leq \kappa \leq \kappa_c$ . Note that  $\hat{C}_\kappa(0) = C_\kappa$  (the definition of  $C_\kappa$  can be found in Eq. (2.97)). Therefore the above solutions coincide with the homogeneous solutions (2.100) in the limit of small wave numbers  $k \rightarrow 0$ . ◀

Recall that we found afterwards in paragraph 2.3.3 that in the *paramagnetic phase* there is a second regime of exponential decay for late times which is a second order effect and thus gets lost in the linearised theory. As there were no second order contributions taken into account in the above derivations, we cannot expect the paramagnetic result for  $\delta\hat{a}^x$  to describe this second regime properly. We could take remedial action by inclusion of the relevant second order contributions. As we cannot expect to benefit from this much more cumbersome calculations, we put up with the simpler solutions derived above.

These solutions reveal how the relaxation depends on the eigenvalues  $\Gamma_1$  and  $\Gamma_2$ . Let us shortly point out important facts: First,  $\Gamma_1$  remains negative for all couplings  $\kappa$  and wave numbers  $k$  since  $\Gamma_1 < -2$  for any finite  $q$ . This corresponds to the previous result that in the homogeneous system  $\delta a_x$  vanishes exponentially for late times — even at the critical point. Second,  $\Gamma_2$  remains negative for all couplings  $\kappa$  and all *finite* wave numbers  $k > 0$ , particularly

$$\Gamma_2(k) \stackrel{\kappa=\kappa_c}{=} -(4 - \kappa_c) k^2 < 0 \quad \text{for } k > 0. \quad (2.153)$$

To sum it up: The damping spectrum of  $\mathcal{M}(k)$  is negative and gapped away from the critical point,  $\kappa \neq \kappa_c$ . This implies an exponential relaxation of *all* modes close to the homogeneous steady state. The gap closes at the critical point,  $\kappa = \kappa_c$  since then  $\Gamma_2(0) = 0$ . This corresponds to the previously derived critical slowing down in  $a_z$ -direction. The important point is that both,  $\Gamma_1(k)$  and  $\Gamma_2(k)$  remain negative even at the critical point for finite  $k > 0$ , i.e. inhomogeneous perturbations. This substantiates our former finding that the *homogenisation* of  $\delta a^x$  and especially  $\delta a^z$  remains fast, that is exponential, for all couplings  $\kappa$  — even at the critical point where the *homogeneous* system experiences a critical slowing down.

This concludes our investigation of the dynamical properties of the mean field theory for the purely dissipative transverse field Ising model. In the next section we look closely at the relation of the purely *dissipative* transition from a symmetric paramagnetic phase to a symmetry-broken ferromagnetic one and the *thermal* analogue, namely the paradigmatic phase transition of the TIM in  $D \geq 2$  dimensions at finite temperature.

## 2.4 Comparing the mean field theories of $\mathcal{L}^{\text{mf}}$ , $H^{\text{mf}}$ and $H_p^{\text{mf}}$

At the outset of this chapter we motivated the introduction of the *dissipative* transverse field Ising model by its *Hamiltonian* prototype and its two distinct *quantum* phases. Quantum phase transitions occur by definition at zero temperature where the critical fluctuations that are responsible for the non-analyticities are of purely quantum mechanical origin. For the transverse field Ising model in two and higher dimensions this quantum phase transition passes into a *classical* phase transition with additional contributions by quantum fluctuations for finite but small temperatures. The higher the temperature at which the critical behaviour can be observed the more diminish the contributions due to quantum fluctuations.

The previous discussions showed that the purely dissipative TIM can be driven into a non-equilibrium phase transition by variation of the relative coupling  $\kappa$ . At the critical point the state is *mixed* and the entropy reaches its maximum at a cusp. In this sense we cannot claim to drive a *quantum* phase transition. We do not, however, drive a *thermal* phase transition either since the (mixed) steady states are not in thermal equilibrium. It is therefore interesting to ask whether there are non-trivial relations between the *thermal* states of either the original TIM or the parent Hamiltonian of the dissipative process and the non-equilibrium phase transition; for instance if we compare them by means of entropy as a common parameter<sup>36</sup>.

For these reasons we aim at a comparison of the phases and symmetry breaking described by the mean-field theories of

1. the *Hamiltonian* transverse field Ising model  $H^{\text{mf}}$ ,
2. the *dissipative* transverse field Ising model  $\mathcal{L}^{\text{mf}}$  and
3. the *parent Hamiltonian* of the dissipative transverse field Ising model  $H_p^{\text{mf}}$ .

This is the to-do list for this section.

### 2.4.1 Mean field results & Short summary

Before we compare the three theories, let us first collect what we found so far and derive some missing facts that are needed for the intended comparison.

Mean field theory of the transverse field Ising model  $H^{\text{mf}}$

The exact transverse Ising model Hamiltonian reads

$$H = -J \sum_{\langle n,m \rangle} \sigma_n^z \sigma_m^z - h \sum_n \sigma_n^x \quad (2.154)$$

and in mean field approximation the former simplifies to

$$H^{\text{mf}} = -Jqm_z \sigma^z - h \sigma^x = -\mathbf{h}_{\text{mf}} \sigma \quad (2.155)$$

<sup>36</sup>As stated above, there is no *temperature* for the dissipative setting. Nevertheless we can compute the *entropy* for both the dissipative non-equilibrium and the thermal states to compare them on an equal footing.

as we derived at the beginning of paragraph 2.3.1 in Section 2.3. The self-consistency condition reads

$$m_z = \text{Tr}[\rho\sigma^z] = a_z \quad \text{with} \quad \rho = \frac{1}{2}(\mathbb{1} + \mathbf{a}\sigma) \quad (2.156)$$

and the Bloch vector  $\mathbf{a}$  that parametrises the (mixed) state  $\rho$ . For a thermal state at inverse temperature  $\beta$  it holds

$$\rho = \frac{e^{-\beta H^{\text{mf}}}}{\text{Tr}[e^{-\beta H^{\text{mf}}}]}. \quad (2.157)$$

One easily finds

$$e^{-\beta H^{\text{mf}}} = e^{\beta h_{\text{mf}}\sigma} = e^{\beta h_{\text{mf}}\hat{h}_{\text{mf}}\sigma} = \mathbb{1} \cosh(\beta h_{\text{mf}}) + \hat{h}_{\text{mf}}\sigma \sinh(\beta h_{\text{mf}})$$

with the normalised mean field  $\hat{h}_{\text{mf}}$ ; it follows immediately  $\text{Tr}[e^{-\beta H^{\text{mf}}}] = 2 \cosh(\beta h_{\text{mf}})$ .

Then it can be seen that

$$\rho = \frac{\mathbb{1} \cosh(\beta h_{\text{mf}}) + \hat{h}_{\text{mf}}\sigma \sinh(\beta h_{\text{mf}})}{2 \cosh(\beta h_{\text{mf}})} = \frac{1}{2} \left( \mathbb{1} + \tanh(\beta h_{\text{mf}}) \hat{h}_{\text{mf}}\sigma \right) \quad (2.158)$$

and we conclude that  $\mathbf{a} = \tanh(\beta h_{\text{mf}}) \hat{h}_{\text{mf}}$  which spells for the self-consistency

$$m_z = \tanh(\beta h_{\text{mf}}) \hat{h}_{\text{mf}}^z. \quad (2.159)$$

Note that  $\hat{h}_{\text{mf}} = (h^2 + (Jqm_z)^2)^{-1/2} [h, 0, Jqm_z]^T$ , so we find the implicit equation

$$\sqrt{h^2 + (Jqm_z)^2} m_z = Jqm_z \tanh(\beta h_{\text{mf}}) \quad (2.160)$$

for the magnetisation  $m_z$ . If we introduce the scaled coupling  $g = \frac{h}{Jq}$  we end up with

$$\sqrt{g^2 + m_z^2} = \tanh\left(\tilde{\beta}\sqrt{g^2 + m_z^2}\right) \quad \text{or} \quad m_z = 0 \quad (2.161)$$

as possible mean field magnetisations. Here we introduced the inverse temperature  $\tilde{\beta} = \frac{Jq}{k_B T}$  in units of  $Jq$ . Any solution  $m_z = m_z(g, \tilde{\beta})$  of these equations provides us with a state

$$\mathbf{a}(g, \tilde{\beta}) = \mathbf{a}(g, m_z(g, \tilde{\beta})) = \frac{\tanh\left(\tilde{\beta}\sqrt{g^2 + m_z^2}\right)}{\sqrt{g^2 + m_z^2}} \begin{bmatrix} g \\ 0 \\ m_z \end{bmatrix} = \begin{bmatrix} g \\ 0 \\ m_z \end{bmatrix}. \quad (2.162)$$

A necessary condition for non-zero magnetisation is obviously

$$\tilde{\beta} > 1 \quad \Leftrightarrow \quad Jq > k_B T. \quad (2.163)$$

At zero temperature one finds  $\sqrt{g^2 + m_z^2} = 1$  if  $J \neq 0$ , that is  $m_z(g, T = 0) = \sqrt{1 - g^2}$ . So on the  $T = 0$ -axis the critical field is  $g_c = \frac{h_c}{Jq} = 1$ .

The entropy of the system is given by the expression

$$S[\rho] = -\frac{1}{2} \log \left[ \frac{1-a^2}{4} \cdot \left( \frac{1+a}{1-a} \right)^a \right] \quad \text{where} \quad a = \tanh \left( \tilde{\beta} \sqrt{g^2 + m_z^2} \right) \quad (2.164)$$

A derivation can be found in Appendix D.

Mean field theory of the dissipative process  $\mathcal{L}^{\text{mf}}$

Let us outline what we found so far for the dissipative mean field theory: The *exact* dissipative process is described by the Lindblad equation

$$\partial_t \rho = \kappa_P \sum_j \left[ c_j \rho c_j^\dagger - \frac{1}{2} \{c_j^\dagger c_j, \rho\} \right] + \kappa_F \sum_j \left[ d_j \rho d_j^\dagger - \frac{1}{2} \{d_j^\dagger d_j, \rho\} \right] \quad (2.165)$$

with the jump operators

$$c_j = \frac{1}{2} \sigma_j^z (\mathbb{1} - \sigma_j^x) \quad \text{and} \quad d_j = \sigma_j^x \left( \frac{1}{q} \sum_{m \in N_j} \sigma_m^z \sigma_j^y - \mathbb{1} \right). \quad (2.166)$$

We derived in paragraph 2.3.1 (Section 2.3) the *mean field approximation* of this theory. The dynamics is then described by

$$\partial_t \rho = \kappa_P \mathcal{L}(c) [\rho] + \kappa_F \mathcal{L}(\bar{d}) [\rho] + \kappa_F \mathcal{L}(\bar{b}) [\rho] + \kappa_F \mathcal{L}(\bar{o}) [\rho] \quad (2.167)$$

with the four effective jump operators

$$\bar{d} = \sigma^x (m_z \sigma^z - \mathbb{1}), \quad \bar{b} = \frac{1}{\sqrt{q}} \sqrt{1 - m_z^2} \sigma^y, \quad \bar{o} = \frac{1}{\sqrt{q}} \sigma^z, \quad \text{and} \quad c = \frac{1}{2} \sigma^z (\mathbb{1} - \sigma^x).$$

The self-consistency equation reads once again

$$m_z = \text{Tr} [\rho \sigma^z] = a_z \quad \text{with} \quad \rho = \frac{1}{2} (\mathbb{1} + \mathbf{a} \sigma) \quad \text{and the Bloch vector } \mathbf{a}. \quad (2.168)$$

We will be concerned with the stationary states  $\dot{\rho}_s = 0 \Leftrightarrow \dot{\mathbf{a}}_s = 0$ . If we substitute  $m_z \rightarrow a_z$  (according to the self-consistency condition) on the right-hand side of Eq. (2.167), set the left-hand side to zero and solve for  $\mathbf{a}$ , we find the following three solutions

$$\text{Paramagnetic solution} : \quad \mathbf{a}_P = \left[ \frac{q\kappa}{4+q\kappa} \quad 0 \quad 0 \right]^T \quad (2.169a)$$

$$\text{Ferromagnetic solution } (-) : \quad \mathbf{a}_F^- = \left[ \frac{2q\kappa}{4(1+q)+q\kappa} \quad 0 \quad -\sqrt{1 - \frac{q\kappa}{4(q-1)}} \right]^T \quad (2.169b)$$

$$\text{Ferromagnetic solution } (+) : \quad \mathbf{a}_F^+ = \left[ \frac{2q\kappa}{4(1+q)+q\kappa} \quad 0 \quad \sqrt{1 - \frac{q\kappa}{4(q-1)}} \right]^T \quad (2.169c)$$

with the coupling ratio  $\kappa = \frac{\kappa_P}{\kappa_F}$ . This was shown in paragraph 2.3.2 of the previous section 2.3.2.

The symmetry breaking is characterised by the transition from imaginary  $z$ -components of the ferromagnetic solutions to real ones (i.e. physical states). Thus the critical coupling ratio is

$$\kappa_c = 4 \left(1 - \frac{1}{q}\right) \quad (2.170)$$

and the magnetisation is given by the function

$$m_z = (\mathbf{a}_F^\pm)_z = \pm \sqrt{1 - \frac{q\kappa}{4(q-1)}} \quad \text{or} \quad m_z = (\mathbf{a}_P)_z = 0 \quad (2.171)$$

where the paramagnetic solution ( $m_z = 0$ ) becomes unstable at the phase transition. Please note that the critical coupling remains finite for  $q \rightarrow \infty$ , i.e.  $\lim_{q \rightarrow \infty} \kappa_c = 4$ . Since the mean-field theory is believed to yield reliable results in high dimensions, this supports the claim of a non-trivial, dissipatively driven phase transition above its critical dimension  $d_c$ .

The entropy of the system is given by (see Appendix D):

$$S[\rho] = -\frac{1}{2} \log \left[ \frac{1-a^2}{4} \left( \frac{1+a}{1-a} \right)^a \right] \quad \text{with} \quad a = \begin{cases} \frac{q\kappa}{4+q\kappa} & \text{if } \kappa \geq \kappa_c \\ \left[ \left( \frac{2q\kappa}{4(1+q)+q\kappa} \right)^2 - \frac{q\kappa}{4(q-1)} + 1 \right]^{1/2} & \text{if } \kappa < \kappa_c \end{cases}$$

Clearly, for  $\kappa \rightarrow 0$  (meaning  $\kappa_P \rightarrow 0$  and/or  $\kappa_F \rightarrow \infty$ ) it follows  $S[\rho] \rightarrow 0$ . Analogously we find  $S[\rho] \rightarrow 0$  for  $\kappa \rightarrow \infty$  (meaning  $\kappa_P \rightarrow \infty$  and/or  $\kappa_F \rightarrow 0$ ). This behaviour characterises the pure steady states for non-competing bath couplings.

Mean field theory of the parent Hamiltonian  $H_P^{\text{mf}}$

So far we considered only the prototypical Hamiltonian of the transverse field Ising model. However, for the dissipative process the *parent Hamiltonian* is clearly more important than some abstract prototype (which was merely used to motivate the jump operators) as the former governs the non-Hermitian damping (decoherence) of states in periods where no jump occurs. It is therefore more probable that the dissipative steady states are related to the thermal states of the parent Hamiltonian than to the analogue states of the original TIM.

If we consider the mean field theory of the parent Hamiltonian, there are two *inequivalent* approaches that yield similar results which, however, differ by some prefactors: We could (1) start with the exact parent Hamiltonian and perform a mean field approximation or (2) construct the parent Hamiltonian directly from the *mean field* jump operators. In the next paragraph we show the first approach (1), followed by the alternative derivation (2) in the subsequent paragraph.

■ **First approach: Mean field theory for the parent Hamiltonian**

The exact parent Hamiltonian for the dissipative dynamics is defined via

$$H_P = \kappa_P \sum_j c_j^\dagger c_j + \kappa_F \sum_j d_j^\dagger d_j \quad (2.172)$$

with the exact jump operators  $c_j$  (paramagnetic bath) and  $d_j$  (ferromagnetic bath).

One computes easily

$$c_j^\dagger c_j = \frac{1}{2} (\mathbb{1} - \sigma_j^x) \quad \text{and} \quad d_j^\dagger d_j = \frac{1}{q^2} \sum_{m,n \in N_j} \sigma_m^z \sigma_n^z - \frac{2}{q} \sum_{m \in N_j} \sigma_m^z \sigma_j^z + \mathbb{1} \quad (2.173)$$

and we finally obtain the parent Hamiltonian

$$H_P = \left( \frac{\kappa_P}{2} + \kappa_F \right) N - \underbrace{\frac{\kappa_P}{2} \sum_j \sigma_j^x}_{\text{Magnetic field}} - \underbrace{\frac{4\kappa_F}{q} \sum_{\langle m,n \rangle} \sigma_m^z \sigma_n^z}_{\text{NN Ferromagnetic}} + \underbrace{\frac{\kappa_F}{q^2} \sum_j \sum_{m,n \in N_j} \sigma_m^z \sigma_n^z}_{\text{NNN Antiferromagnetic}} \quad (2.174)$$

where  $N$  denotes the number of sites. In one dimension this Hamiltonian is known as the ANNNI model in transverse magnetic field [114]. The mean field theory follows from the product ansatz  $\rho = \prod_j \rho_j$  and the VON NEUMANN equation  $\partial_t \rho = -i [H_P, \rho]$  via the partial trace

$$\partial_t \rho_i = \text{Tr}_{\neq i} [\partial_t \rho] = -i \text{Tr}_{\neq i} [[H_P, \rho]] = -i \sum_j \left\{ \kappa_P \text{Tr}_{\neq i} [[c_j^\dagger c_j, \rho]] + \kappa_F \text{Tr}_{\neq i} [[d_j^\dagger d_j, \rho]] \right\}.$$

We already computed

$$\begin{aligned} \text{Tr}_{\neq i} [d_j^\dagger d_j \rho] &= \frac{1}{q^2} [C(q, m_z) \rho_i + 2(q-1) m_z \sigma_i^z \rho_i + \rho_i] - \frac{2m_z}{q} [(q-1) m_z \rho_i + \sigma_i^z \rho_i] + \rho_i \\ \text{Tr}_{\neq i} [\rho d_j^\dagger d_j] &= \frac{1}{q^2} [C(q, m_z) \rho_i + 2(q-1) m_z \rho_i \sigma_i^z + \rho_i] - \frac{2m_z}{q} [(q-1) m_z \rho_i + \rho_i \sigma_i^z] + \rho_i \end{aligned}$$

for  $j \in N_i$  as well as

$$\text{Tr}_{\neq i} [d_j^\dagger d_j \rho] = \bar{b}_i^\dagger \bar{b}_i \rho_i + \bar{d}_i^\dagger \bar{d}_i \rho_i \quad \text{and} \quad \text{Tr}_{\neq i} [\rho d_j^\dagger d_j] = \rho_i \bar{b}_i^\dagger \bar{b}_i + \rho_i \bar{d}_i^\dagger \bar{d}_i$$

for  $j = i$  with the mean field jump operators

$$\bar{d}_j = \sigma_j^x (m_z \sigma_j^z - \mathbb{1}) \quad \text{and} \quad \bar{b}_j = \frac{1}{\sqrt{q}} \sqrt{1 - m_z^2} \sigma_j^y.$$

See paragraph 2.3.2 of the previous section 2.3.2 for the derivation or Appendix B for details.

Note that  $\text{Tr}_{\neq i} [[c_j^\dagger c_j, \rho]] = 0$  if  $i \neq j$  and  $\text{Tr}_{\neq i} [[d_j^\dagger d_j, \rho]] = 0$  if  $i \notin N_j \cup \{j\}$ , so we find

$$i \partial_t \rho_i = \kappa_P \text{Tr}_{\neq i} [[c_i^\dagger c_i, \rho]] + \kappa_F \text{Tr}_{\neq i} [[d_i^\dagger d_i, \rho]] + \kappa_F \sum_{j \in N_i} \text{Tr}_{\neq i} [[d_j^\dagger d_j, \rho]]. \quad (2.175)$$

Invoking the former results yields

$$\begin{aligned}\text{Tr}_{\neq i} \left[ [c_i^\dagger c_i, \rho] \right] &= [c_i^\dagger c_i, \rho_i] = \frac{1}{2} [\mathbb{1} - \sigma_i^x, \rho_i] = \left[ -\frac{\sigma_i^x}{2}, \rho_i \right] \\ \text{Tr}_{\neq i} \left[ [d_i^\dagger d_i, \rho] \right] &= \frac{1}{q} [\bar{b}_i^\dagger \bar{b}_i, \rho_i] + [\bar{d}_i^\dagger \bar{d}_i, \rho_i] = [\bar{d}_i^\dagger \bar{d}_i, \rho_i] = [-2m_z \sigma_i^z, \rho_i] \\ \sum_{j \in N_i} \text{Tr}_{\neq i} \left[ [d_j^\dagger d_j, \rho] \right] &= q \left[ \frac{2(q-1)}{q^2} m_z [\sigma_i^z, \rho_i] - \frac{2m_z}{q} [\sigma_i^z, \rho_i] \right] = \left[ -\frac{m_z}{q} \sigma_i^z, \rho_i \right]\end{aligned}$$

so that

$$\partial_t \rho_i = -i \left[ -\frac{\kappa_P}{2} \sigma_i^x - 2\kappa_F m_z \sigma_i^z - \frac{\kappa_F m_z}{q} \sigma_i^z, \rho_i \right] \equiv -i [H_P^{\text{mf}}, \rho_i]. \quad (2.176)$$

That is, the mean field parent Hamiltonian reads

$$H_P^{\text{mf}} = -\frac{\kappa_P}{2} \sigma_i^x - \kappa_F m_z (2 + q^{-1}) \sigma_i^z = -\mathbf{h}_P^{\text{mf}} \boldsymbol{\sigma} \quad (2.177)$$

with the mean field  $\mathbf{h}_P^{\text{mf}} = \left[ \frac{\kappa_P}{2} \quad 0 \quad \kappa_F m_z (2 + q^{-1}) \right]^T$ . The self-consistency equation is the same as before and we find the transcendent mean field equation

$$m_z = \tanh \left( \beta \mathbf{h}_P^{\text{mf}} \right) \hat{\mathbf{h}}_P^{\text{mf}, z} \quad (2.178)$$

for a thermal state  $\rho = \rho(\beta)$ . With the normalised mean field  $\hat{\mathbf{h}}_P^{\text{mf}}$  we arrive at the implicit equation

$$\sqrt{\frac{\kappa_P^2}{4} + \kappa_F^2 m_z^2 (2 + q^{-1})^2} m_z = \kappa_F m_z (2 + q^{-1}) \tanh \left( \beta \mathbf{h}_P^{\text{mf}} \right) \quad (2.179)$$

for the magnetisation  $m_z$ . If we introduce the scaled coupling  $g_P = \frac{\kappa_P}{2\kappa_F(2+q^{-1})} = \frac{\kappa}{2(2+q^{-1})}$  we end up with the same equations as before

$$\sqrt{g_P^2 + m_z^2} = \tanh \left( \tilde{\beta}_P \sqrt{g_P^2 + m_z^2} \right) \quad \text{or} \quad m_z = 0 \quad (2.180)$$

as possible mean field magnetisations. Here we introduced the inverse temperature  $\tilde{\beta}_P = \frac{\kappa_F(2+q^{-1})}{k_B T}$  in units of  $\kappa_F(2+q^{-1})$ . Any solution  $m_z = m_z(g_P, \tilde{\beta}_P)$  of these equations provides a thermal state

$$\mathbf{a}(g_P, \tilde{\beta}_P) = \mathbf{a}(g_P, m_z(g_P, \tilde{\beta}_P)) = [g_P \quad 0 \quad m_z]^T. \quad (2.181)$$

The necessary condition for non-zero magnetisations is

$$\tilde{\beta}_P > 1 \quad \Leftrightarrow \quad \kappa_F(2+q^{-1}) > k_B T. \quad (2.182)$$

At zero temperature this reads  $\sqrt{g_P^2 + m_z^2} = 1$  if  $\kappa_F \neq 0$ , that is  $m_z(g_P, T=0) = \sqrt{1 - g_P^2}$ . So on the  $T=0$ -axis the critical coupling is  $g_{P,c} = \frac{\kappa_c}{2(2+q^{-1})} = 1$ . For the sake of completeness, the entropy of the system can be computed via

$$S[\rho] = -\frac{1}{2} \log \left[ \frac{1-a^2}{4} \left( \frac{1+a}{1-a} \right)^a \right] \quad \text{where} \quad a = \tanh \left( \tilde{\beta}_P \sqrt{g_P^2 + m_z^2} \right). \quad (2.183)$$

### ■ Second approach: Parent Hamiltonian for the mean-field dynamics

Let us now follow the alternative approach and derive the parent Hamiltonian for the mean field jump operators. As before, the parent Hamiltonian can be written as

$$\bar{H}_P^{\text{mf}} = \kappa_P \sum_j \bar{c}_j^\dagger \bar{c}_j + \kappa_F \sum_j \bar{d}_j^\dagger \bar{d}_j + \kappa_F \sum_j \bar{b}_j^\dagger \bar{b}_j + \kappa_F \sum_j \bar{o}_j^\dagger \bar{o}_j \quad (2.184)$$

with the mean field jump operators

$$\bar{d}_j = \sigma_j^x (m_z \sigma_j^z - \mathbb{1}), \quad \bar{b}_j = \frac{1}{\sqrt{q}} \sqrt{1 - m_z^2} \sigma_j^y, \quad \bar{o}_j = \frac{1}{\sqrt{q}} \sigma_j^z, \quad \text{and} \quad c_j = \frac{1}{2} \sigma_j^z (\mathbb{1} - \sigma_j^x).$$

For a single site the Hamiltonian reads

$$\begin{aligned} \bar{h}_P^{\text{mf}} &= \kappa_P \bar{c}^\dagger \bar{c} + \kappa_F \bar{d}^\dagger \bar{d} + \kappa_F \bar{b}^\dagger \bar{b} + \kappa_F \bar{o}^\dagger \bar{o} \\ &= \frac{\kappa_P}{2} (\mathbb{1} - \sigma^x) + \kappa_F (m_z \sigma^z - \mathbb{1}) (m_z \sigma^z - \mathbb{1}) + \frac{\kappa_F}{q} (1 - m_z^2) \mathbb{1} + \frac{\kappa_F}{q} \mathbb{1}. \end{aligned}$$

Dropping terms that are proportional to the identity yields

$$\bar{h}_P^{\text{mf}} = -\frac{\kappa_P}{2} \sigma^x - 2\kappa_F m_z \sigma^z \equiv -\bar{h}_P^{\text{mf}} \sigma \quad (2.185)$$

with the mean-field  $\bar{h}_P^{\text{mf}} = \left[ \kappa_P/2 \quad 0 \quad 2\kappa_F m_z \right]^T$ . Obviously this is the theory according to the first approach in the high-dimensional limit  $q \rightarrow \infty$ . That is, we immediately end up with the self-consistency equation

$$\sqrt{\bar{g}_P^2 + m_z^2} = \tanh \left( \bar{\beta}_P \sqrt{\bar{g}_P^2 + m_z^2} \right) \quad \text{or} \quad m_z = 0 \quad (2.186)$$

where  $\bar{g}_P = \frac{\kappa_P}{4\kappa_F} = \frac{\kappa}{4}$  and  $\bar{\beta}_P = \frac{2\kappa_F}{k_B T}$  in units of  $2\kappa_F$ . The necessary condition for non-zero magnetisations is

$$\bar{\beta}_P > 1 \quad \Leftrightarrow \quad \kappa_F > \frac{k_B T}{2}. \quad (2.187)$$

At zero temperature one finds  $\sqrt{\bar{g}_P^2 + m_z^2} = 1$  if  $\kappa_F \neq 0$ , that is  $m_z(\bar{g}_P, T=0) = \sqrt{1 - \bar{g}_P^2}$ . In this case the critical coupling on the  $T=0$ -axis is  $\bar{g}_{P,c} = \frac{\kappa_c}{4} = 1$ . The entropy can be computed via Eq. (2.183) if one sets

$$a = \tanh \left( \bar{\beta}_P \sqrt{\bar{g}_P^2 + m_z^2} \right). \quad (2.188)$$

We are now prepared to compare the mean field theories that we outlined above.



### 2.4.2 Comparison of phase transitions

As a measure of purity in a one-qubit system we may employ the VON NEUMANN entropy  $S$ , the purity  $\gamma$  or the length  $a$  of the Bloch vector. Since all of these quantities are connected by monotone relations, it is actually irrelevant which measure we use to quantify the “purity” of a state. For the sake of simplicity we will use the length  $a$  to determine the critical line in the phase diagrams for each mean-field theory. To call on purity as *parameter* provides a link between dissipatively driven phase transitions and “classical” thermal phase transitions.

The critical purity in the *dissipative* setting surely is

$$a_D^{\text{crit}} = |a_P(\kappa = \kappa_c)| = \frac{q\kappa_c}{4 + q\kappa_c} = \frac{4(q-1)}{4 + 4(q-1)} = 1 - \frac{1}{q} = \frac{\kappa_c}{4}. \quad (2.189)$$

In the *Hamiltonian* mean field theories the critical purity is given by

$$a^{\text{crit}} = \tanh\left(\tilde{\beta}_{P,c} \sqrt{g_{P,c}^2 + m_z^2}\right) = \sqrt{g_{P,c}^2 + m_z^2} \stackrel{m_z=0}{=} g_{P,c}$$

since the magnetisation vanishes at the phase transition (which is of 2nd order). For the first approach (mean field theory of the exact parent Hamiltonian) we end up with

$$a_1^{\text{crit}} = g_{P,c} = \frac{\kappa_c}{2(2 + q^{-1})} \quad (2.190)$$

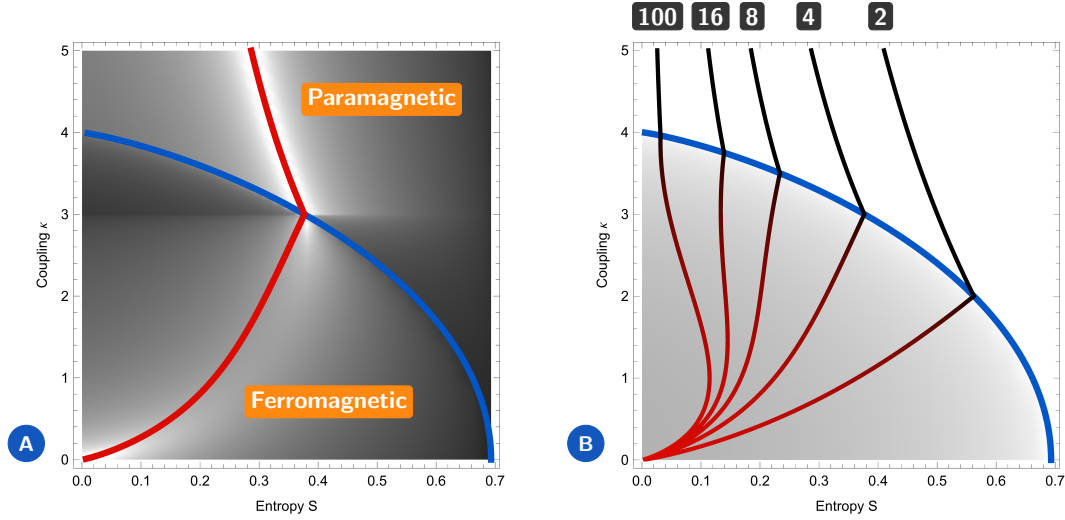
whereas the second approach (parent Hamiltonian of the mean field jump operators) yields

$$a_2^{\text{crit}} = \bar{g}_{P,c} = \frac{\kappa_c}{4}. \quad (2.191)$$

Note that there is actually *no* sensible way to compare the mean field theory of the *original* TIM with the dissipative results since there is no *a priori* relation between the Hamiltonian parameters  $J$  and  $h$  ( $g$ ) on the one hand, and the dissipative couplings  $\kappa_F$  and  $\kappa_P$  ( $\kappa$ ) on the other hand. The original theory was just the *prototype* for our dissipative model after all — there is no rigorous mathematical relation involved.

We are led to the conclusion that, at least in mean-field approximation, the purity (and thereby the *entropy*) provides a useful parameter to compare formerly “incomparable” systems (namely, the dissipative setting with the thermal Hamiltonian setting) and additionally infer a relation between both phase transitions: The dissipative and the thermal phase transition (according to the second approach) occur at the *same* purity, compare Eq. (2.189) and (2.191). In that regard, the dissipative phase transition simulates the thermal phase transition of the underlying parent Hamiltonian.

Please note that the transition according to the first approach, see Eq. (2.190), deviates from the dissipative transition, cf. Eq. (2.189). This is due to additional contributions proportional to  $q^{-1}$ . In the high-dimensional limit  $q \rightarrow \infty$  both approaches lead to the same mean field results. We should stress that this result is the most consistent one: The *dissipative* phase transition of the mean field theory is related via purity/entropy to the *thermal* phase transition of its very own parent Hamiltonian.



■ **Figure 2.21:** Comparison of the *dissipative* and the *thermal* TIM in mean field approximation. Both plots show properties of the *stationary* and *thermal* states in dependence of the entropy  $S$  (horizontal axis) and the relative coupling  $\kappa$  (vertical axis). In (A) we show the trace distance of the stationary state for a given  $\kappa$  and the thermal states for this parameter and varying temperature (converted to entropy). The lighter the color, the closer is the thermal state at this point to the stationary state of the dissipative system. The blue line marks the thermal phase transition where the lower area represents the ferromagnetic phase. The red line marks the entropy of the dissipative stationary state in dependence of  $\kappa$ . Note that the cusp feature – which indicates the *dissipative* phase transition – coincides with the phase boundary of the *thermal* system. In (B) we show these lines for different coordination numbers  $q = 2, 4, 8, 16, 100$  with color-coded  $z$ -magnetisation (black:  $m_z = 0$ , red:  $m_z > 0$ ). The background color encodes the  $z$ -magnetisation of the *thermal* state (white:  $m_z = 0$ , grey:  $m_z > 0$ ).

In Fig. 2.21 we illustrate these findings. To this end we translated the Bloch vector length  $a$  (or *purity*) into the VON NEUMANN entropy  $S = S(a)$  as this is the more natural quantity. There are some comments in order:

- In (A) we show as a 2D colour plot the trace distance between the *thermal state* of the parent Hamiltonian and the *dissipative steady state*. The lighter the color the closer are both states. The thermal phase transition is marked by a blue curve that separates the paramagnetic and the ferromagnetic region in the shown  $S$ - $\kappa$ -plane<sup>37</sup>. The entropy  $S_D$  of the *dissipative* steady state is shown as a function of the coupling  $\kappa$  (red line). According to our previous result, the cusp feature (which marks the dissipative phase transition) coincides with the thermal phase transition at a particular point  $(S_c, \kappa_c)$  in the thermal phase diagram. The trace distance reveals that the dissipative fixed point equals thermal states in the paramagnetic phase, with a temperature  $\beta$  specified via  $S_D(\kappa) \stackrel{!}{=} S(\beta)$ . This is not true in the ferromagnetic phase unless  $\kappa \rightarrow 0$  and  $S \rightarrow 0$  where both states meet again at the poles of the Bloch ball. The result in the paramagnetic phase is to some extent unavoidable: There both the thermal and the stationary state are restricted to the positive  $\sigma^x$ -axis and start at the completely  $x$ -polarised state on the Bloch sphere. Consequently there has to be a temperature  $\beta = \beta(\kappa)$  for all couplings  $\kappa$  such that the thermal state “overtakes” the stationary state on this axis. This is no longer true in the ferromagnetic phase since there both states are restricted to the  $\sigma^x$ - $\sigma^z$ -plane and therefore can “avoid” each other until their reunion at the poles.

<sup>37</sup>For the thermal states one can think of the entropy axis as a (deformed) temperature axis.

- ▀ In (B) we show the same plane where the blue curve once again marks the thermal phase boundary. The coloured background encodes the  $z$ -magnetisation for the *thermal* states (white:  $m_z = 0$ , grey:  $m_z = 1$ ), the colour of the curves indicates the  $z$ -magnetisation of the *dissipative* steady states (black:  $m_z = 0$ , red:  $m_z = 1$ ). The family of curves illustrates dissipative steady states for varying coordination numbers (or dimensions)  $q = 2, 4, 8, 16, 100$ . To this end keep in mind that the parent Hamiltonian  $\bar{h}_P^{\text{mf}}$  is *independent* of  $q$  and consequently the phase boundary (blue curve) remains the same for all dimensions. The plot illustrates that the dissipative phase transition coincides with the thermal phase boundary in any case but at different points  $(S_c, \kappa_c)$  in the  $S$ - $\kappa$ -plane. In the high-dimensional limit the dissipative phase transition occurs at  $\lim_{q \rightarrow \infty} \kappa_c = 4$  in a pure paramagnetic state. This corresponds to our findings in paragraph 2.3.2 (Section 2.3). From this perspective, the *dissipative* phase transition in *infinite* dimensions equals the *quantum* phase transition at  $T = 0$  of the parent Hamiltonian.

This concludes the comparison of dissipative and thermal mean field phase transitions for the transverse field Ising model. In the next section we continue with the analytical solution of a minimal 2-spin instance with and without Hamiltonian contributions.

## 2.5 Exact solutions of a minimal instance

Here we investigate the smallest instance of the dissipatively driven transverse field Ising model by exact calculations. We give an analysis of both the steady states and the dynamics of the system in the formerly introduced superoperator formalism. Since the system is finite and small, we cannot expect features of non-trivial, *spontaneous* symmetry breaking to occur (as predicted by the mean-field theory). However, we aim at a deeper understanding of this paradigmatic example for two competing baths, one of which features a non-trivial dark state subspace due to global symmetries.

### 2.5.1 The system in superoperator language

Let us assume our system comprises two spins described by pure states in  $\mathcal{H}_2 = \mathbb{C}^2 \otimes \mathbb{C}^2$ . General states are described by density matrices  $\rho \in \mathcal{S} \equiv \mathcal{S}(\mathcal{H}_2) \subseteq \mathcal{B}(\mathcal{H}_2) \equiv \mathcal{B}$  where  $\mathcal{S}(\mathcal{H}_2)$  denotes the convex *set* of positive-semidefinite, Hermitian operators of trace one and  $\mathcal{B}(\mathcal{H}_2)$  is the vector space of bounded linear operators on the Hilbert space. Here these operators can be identified with complex  $4 \times 4$  matrices if we choose the computational basis  $\{|\uparrow\uparrow\rangle, |\uparrow\downarrow\rangle, |\downarrow\uparrow\rangle, |\downarrow\downarrow\rangle\}$ .

The unitary dynamics is given by the TIM Hamiltonian which reads for two spins

$$H = -J \sigma_1^z \sigma_2^z - h (\sigma_1^x + \sigma_2^x) \quad (2.192)$$

with exchange interaction  $J$  and magnetic field  $h$ . The dissipative dynamics is governed by two competing baths described by jump operators

$$c_j = \frac{\sqrt{\kappa_P}}{2} (\sigma_j^z - i\sigma_j^y) \quad \text{and} \quad d_j = \frac{\sqrt{\kappa_F}}{2} \sigma_j^x (\mathbb{1} - \sigma_{j+1}^z \sigma_j^z) \quad (2.193)$$

where  $j = 1, 2$  and all indices are numbers modulo 2.  $\kappa_P$  and  $\kappa_F$  determine the strengths of the “paramagnetic” and “ferromagnetic” baths, respectively.

It is now straightforward to calculate the parent Hamiltonian  $H_P = \sum_j (d_j^\dagger d_j + c_j^\dagger c_j)$  and the quantum jump superoperator  $\mathbf{L} = \sum_j (\bar{d}_j \otimes d_j + \bar{c}_j \otimes c_j)$ . The effective Hamiltonian (including non-Hermitian damping contributions) follows directly via  $H_{\text{eff}} \equiv H - \frac{i}{2} H_P$ . This operator has to be “lifted” in the superoperator representation  $\mathbf{H}_{\text{eff}} = -i [\mathbb{1} \otimes H_{\text{eff}} - \bar{H}_{\text{eff}} \otimes \mathbb{1}]$ . Finally this yields the Lindbladian superoperator  $\mathcal{L} = \mathbf{H}_{\text{eff}} + \mathbf{L}$  (a complex  $16 \times 16$  matrix) which describes the dynamics and stationary states of the system completely via  $\exp(\mathcal{L}t)$  and  $\text{Ker}[\mathcal{L}] \leq |\mathcal{B}\rangle\rangle$ . Here  $|\mathcal{B}\rangle\rangle$  denotes the *vectorised* operator space and  $\leq$  reads “linear subspace of”.

What complicates the analysis of the steady states (a bit) is due to the observation that  $\text{Ker}[\mathcal{L}] \neq |\mathcal{D}\rangle\rangle$  in general, where  $|\mathcal{D}\rangle\rangle \subseteq |\mathcal{B}\rangle\rangle$  denotes the *set* of (physical) steady states. In other words: The operators in the kernel of the Lindbladian are not necessarily *density matrices*. In the next paragraphs we will deal with this hitch.

## 2.5.2 Solutions for steady states

Let us now have a look at the steady states of this simple system. It proves advantageous to split the analysis into three parameter regimes, namely:

$$\begin{aligned} \kappa_P \neq 0 \text{ and } J, h, \kappa_F \text{ arbitrary} &\Rightarrow \text{unique, mixed steady state} \\ \kappa_P = 0, h \neq 0 \text{ and } J, \kappa_F \text{ arbitrary} &\Rightarrow \text{convex line of mixed steady states} \\ \kappa_P = 0, h = 0 \text{ and } J, \kappa_F \text{ arbitrary} &\Rightarrow \text{full Bloch sphere of steady states} \end{aligned}$$

Here  $\kappa_P, \kappa_F$  and  $J$  are always non-negative real numbers.

### ■ $\kappa_P \neq 0$ and $J, h, \kappa_F$ arbitrary

For this generic parameter regime there is no simple representation of  $\text{Ker}[\mathcal{L}]$ . However, numerical solutions are easily calculated and one finds  $\dim \text{Ker}[\mathcal{L}] = 1$ . This is good news since it is known that every Lindblad operator  $\mathcal{L}$  has at least one steady state. Let  $|S\rangle\rangle$  be an arbitrary vector such that  $\text{span}\{|S\rangle\rangle\} = \text{Ker}[\mathcal{L}]$ . We can then choose a phase  $e^{i\varphi}$  so that  $e^{i\varphi}S$  (which is a  $4 \times 4$  matrix) is Hermitian. According to the previous statement, this is always possible. Here  $\varphi$  can be calculated via  $\varphi = -\frac{1}{2}(\varphi_{1,4} + \varphi_{4,1})$  where  $\varphi_{i,j} = \arg S_{i,j}$ . Finally, the normalisation  $\rho_{\text{NESS}} = \frac{e^{i\varphi}S}{\text{Tr}[e^{i\varphi}S]}$  yields the unique steady state. Its positive-semidefiniteness follows from the existence of at least one steady state and the fact that  $\frac{e^{i\varphi}S}{\text{Tr}[e^{i\varphi}S]}$  is the only Hermitian operator with trace one in the kernel of the Lindbladian.

Since there is no simple visualisation of a generic two-spin mixed state<sup>38</sup> it is useful to consider a set of quantities which yield a quite detailed description of the steady state. Clearly, one should consider the (averaged) magnetisations  $\Sigma^i \equiv \frac{1}{2}(\sigma_1^i + \sigma_2^i)$  for  $i = x, y, z$ . First, since our systems features the permutation symmetry  $1 \leftrightarrow 2$  with respect to spin 1 and 2, one can simply measure the one-site magnetisation  $\sigma_1^i$ . Second, it turns out that  $\langle \sigma_1^z \rangle_{\text{NESS}} = 0 = \langle \sigma_1^y \rangle_{\text{NESS}}$  for all NESS (as long as  $\kappa_P \neq 0$ ); so we just compute  $\langle \sigma_1^x \rangle_{\text{NESS}}$ . Furthermore, as we explicitly deal with non-unitary evolutions of quantum states, the purity  $\gamma = \text{Tr}[\rho_{\text{NESS}}^2]$  is mandatory.

Additionally we may ask whether the two spins (or qubits) are entangled – and if so, to which extent? To quantify entanglement a variety of *entanglement measures* has been contrived in the quantum information community (see Ref. [115] for a nice review) and lots of them were adopted by other communities such as condensed matter physicists to learn a great deal about the “quantumness” of their many body systems and phases [116]. A well-known entanglement measure whose convex roof extension<sup>39</sup> can be evaluated analytically for arbitrary mixed two-qubit states is the *concurrence* [117]. For an arbitrary mixed state  $\rho$  of two qubits the concurrence can be calculated via

$$\mathcal{C}[\rho] = \max\{\lambda_1 - \lambda_2 - \lambda_3 - \lambda_4, 0\} \quad (2.194)$$

<sup>38</sup>At least not in the three spatial dimensions I have at my disposal.

<sup>39</sup>Usually entanglement measures are defined as functionals on pure state vectors in  $\mathcal{H}$  which satisfy certain properties such as monotony under LOCC operations etc. (for a complete characterisation see Ref. [115]). There is a general procedure to extend such a pure state entanglement measure to mixed states in  $\mathcal{S}(\mathcal{H})$  via a *convex roof extension* which is based on minimising over all possible realisations of a mixed state  $\rho$ . Although mathematically well defined, it proves hard or even impossible to calculate such quantities analytically for large systems. However, for two qubits and the concurrence as pure state entanglement measure, the convex roof can be evaluated analytically.

where  $\lambda_1^2 \geq \lambda_2^2 \geq \lambda_3^2 \geq \lambda_4^2$  is the ordered non-negative spectrum of the positive-semidefinite Hermitian matrix

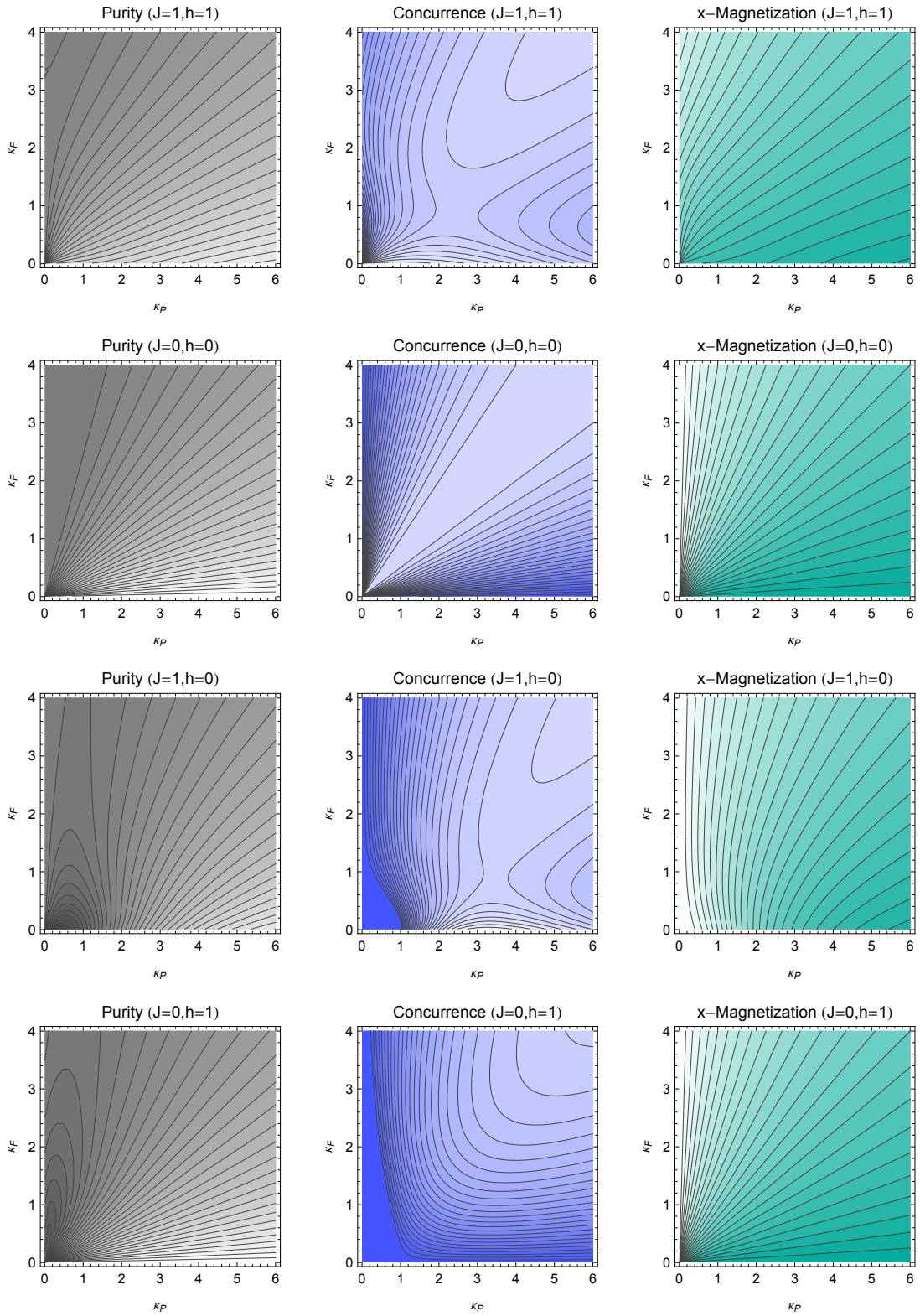
$$R \equiv \sqrt{\bar{\rho}} \bar{\rho} \sqrt{\bar{\rho}} = \sqrt{\bar{\rho}} \sigma_1^y \sigma_2^y \bar{\rho} \sigma_1^y \sigma_2^y \sqrt{\bar{\rho}}. \quad (2.195)$$

$\mathcal{C}[\rho] = 0$  corresponds to unentangled and  $\mathcal{C}[\rho] = 1$  to maximally entangled states. For more details see e.g. Ref. [116].

### ► Evaluation

In Fig. 2.22 we show these three quantities for the four parameter sets  $(J, h) = (1, 1), (0, 0), (1, 0), (0, 1)$  and varying  $\kappa_P$  (horizontal axis) and  $\kappa_F$  (vertical axis). Note that  $J$  and  $h$  determine the *unitary dynamics* whereas  $\kappa_P$  and  $\kappa_F$  determine the *dissipative dynamics* of the system. Some comments on the findings in Fig. 2.22 are in order:

- The purity is highest (light regions) in the high  $\kappa_P$  and low  $\kappa_F$  regions. It drops (grey regions) for lower  $\kappa_P$  and higher  $\kappa_F$  since the two baths do not agree about their favoured dark states. If the unitary dynamics is deactivated (second row) there is one effective parameter ( $\kappa = \frac{\kappa_P}{\kappa_F}$ ) left and the diagram becomes ray-shaped. Interestingly the purity does *not* increase in the high  $\kappa_F$  and low  $\kappa_P$  regime which hints at a discontinuity for  $\kappa_P = 0$  and  $\kappa_F \neq 0$  regarding the steady state set structure (see the next case where  $\kappa_P = 0$  is considered). Unitary dynamics leads to a distortion of the symmetric, purely dissipative case. If the spin-spin interaction  $J$  is present there are no longer pure steady states for  $\kappa_F = 0$  and  $\kappa_P \neq 0$  since the eigenstates of  $H$  and the dark states of  $c_i$  do not match. This is not true for a magnetic field in  $x$ -direction ( $h \neq 0$ ) where the steady states remain pure. Note that the unitary components give rise to an “island of mixed states” close to the completely unitary system, i.e. for  $\kappa_P$  and  $\kappa_F$  small. Clearly, this is justified by the predominance of the baths for  $\kappa_P \rightarrow \infty$  or  $\kappa_F \rightarrow \infty$  which drive the system either to a unique pure steady state ( $c_i$ ) or, at least, to a mixed steady state with enforced non-trivial correlations ( $d_i$ ).
- The concurrence is lowest (highest) in blue (white) regions, i.e. blue regions correspond to unentangled states whereas in lighter regions entanglement is present. In the limit  $\kappa_P \rightarrow \infty$  and  $\kappa_F$  small (or just  $\kappa_F$  small for the purely dissipative setting in the second row) the entanglement drops to zero. If we remember that the steady states becomes pure in this limit we can conclude that the latter features a product structure. Indeed, the exact dark state of the paramagnetic bath is the completely  $x$ -polarised state  $|+\rangle\rangle$  which certainly is a product state. The dark states of the ferromagnetic bath are degenerate and completely  $z$ -polarised, namely  $|\uparrow\rangle\rangle$  and  $|\downarrow\rangle\rangle$ . These are product states, however their coherent superpositions (which are dark states as well) include the maximally entangled bell states  $|\Phi^\pm\rangle\rangle$ . The drop in entanglement can therefore not be explained in the same way as in the paramagnetic case. One has to recall that the disturbance due to the paramagnetic bath lowers the purity significantly – and strongly mixed states exhibit notoriously low entanglement. An interesting feature of the interplay between unitary dynamics ( $J \neq 0$ ) and dissipative dynamics is the emergent saddle-shaped structure where an “isle” of entanglement shows up for low  $\kappa_F$  and a certain range of  $\kappa_P$ . However, the absolute entanglement there,  $\mathcal{C}[\rho_{\text{NESS}}] \approx 0.3$ , is comparatively low.
- The  $x$ -magnetisation is highest (lowest) in green (white) regions. In the context of our previous findings there is nothing unexpected about the plots. The magnetisation becomes



■ **Figure 2.22:** Here we show the purity  $\gamma$ , the concurrence  $\mathcal{C}$  and the  $x$ -magnetisation  $\langle \sigma^x \rangle$  for the four parameter sets  $(J, h) = (1, 1), (0, 0), (1, 0), (0, 1)$  and varying  $\kappa_P$  (horizontal axis) and  $\kappa_F$  (vertical axis). Note that  $J$  and  $h$  determine the *unitary dynamics* whereas  $\kappa_P$  and  $\kappa_F$  determine the *dissipative dynamics* of the system. A discussion of the results is given in the text.

highest in the (nearly) pure steady state for  $\kappa_P \rightarrow \infty$  and  $\kappa_F$  small. If no competing unitary dynamics is present ( $J = 0$ ) it becomes even unity for  $\kappa_F = 0$ .  $\langle \sigma^x \rangle_{\text{NESS}}$  vanishes for  $\kappa_P \rightarrow 0$  and finite  $\kappa_F$  since the set of steady states there is well approximated by the coherent superpositions of  $|\uparrow\rangle\rangle$  and  $|\downarrow\rangle\rangle$  and the convex combinations thereof – all of which are characterised by vanishing  $x$ -magnetisation. This, however, is not true if the magnetic field is switched on in which case a residual  $x$ -magnetisation prevails (see topmost row).

All of these remarks are valid for a non-trivial coupling of the paramagnetic bath  $c_i$ . What happens if we set  $\kappa_P = 0$ ? ◀

■  $\kappa_P = 0, h \neq 0$  and  $J, \kappa_F$  arbitrary

Since we do not expect the steady states to vary qualitatively with the spin-spin coupling, let us just divide all parameters by  $J$  or, equivalently, set  $J = 1$ . Then two free parameters remain, namely  $h$  and  $\kappa_F$ . If one computes the kernel  $\text{Ker}[\mathcal{L}]$  analytically it turns out to be two dimensional with the possible basis

$$S_1 = \begin{bmatrix} 1 & 0 & 0 & -1 \\ 0 & 0 & 0 & 0 \\ 0 & 0 & 0 & 0 \\ -1 & 0 & 0 & 1 \end{bmatrix} \quad \text{and} \quad S_2 = \begin{bmatrix} 0 & \frac{2i+\kappa_F}{2i-\kappa_F} & \frac{2i+\kappa_F}{2i-\kappa_F} & -\frac{i(4h^2+\kappa_F^2+4)}{h(-2i+\kappa_F)} \\ 1 & -\frac{2ih}{-2i+\kappa_F} & -\frac{2ih}{-2i+\kappa_F} & 1 \\ 1 & -\frac{2ih}{-2i+\kappa_F} & -\frac{2ih}{-2i+\kappa_F} & 1 \\ -\frac{i(4h^2+\kappa_F^2+4)}{h(-2i+\kappa_F)} & \frac{2i+\kappa_F}{2i-\kappa_F} & \frac{2i+\kappa_F}{2i-\kappa_F} & 0 \end{bmatrix}.$$

$S_1$  is obviously a density matrix (up to a factor of  $1/2$ ), namely  $|\Phi^-\rangle\rangle\langle\langle\Phi^-|$ .  $S_2$  is not yet Hermitian and of trace one – this can be fixed by multiplication with  $-\frac{2i+\kappa_F}{4ih}$  which yields

$$S_1 = \begin{bmatrix} \frac{1}{2} & 0 & 0 & -\frac{1}{2} \\ 0 & 0 & 0 & 0 \\ 0 & 0 & 0 & 0 \\ -\frac{1}{2} & 0 & 0 & \frac{1}{2} \end{bmatrix} \quad \text{and} \quad S_2 = \begin{bmatrix} 0 & \frac{2-i\kappa_F}{4h} & \frac{2-i\kappa_F}{4h} & \frac{\kappa_F^2+4}{4h^2} + 1 \\ \frac{i\kappa_F+2}{4h} & \frac{1}{2} & \frac{1}{2} & \frac{i\kappa_F+2}{4h} \\ \frac{i\kappa_F+2}{4h} & \frac{1}{2} & \frac{1}{2} & \frac{i\kappa_F+2}{4h} \\ \frac{\kappa_F^2+4}{4h^2} + 1 & \frac{2-i\kappa_F}{4h} & \frac{2-i\kappa_F}{4h} & 0 \end{bmatrix}.$$

Now both basis operators are Hermitian and have trace one. An arbitrary linear combination remains in the kernel but only *real* linear combinations remain *Hermitian*. That would yield a real linear subspace – but only *convex combinations* preserve the *trace*! So we are left with a single real parameter  $\lambda$  and the *potential* set of density matrices

$$S(\lambda) = \lambda \cdot S_1 + (1 - \lambda) \cdot S_2 \quad \text{with} \quad \lambda \in \mathbb{R}. \quad (2.196)$$

It can be easily shown that  $\min \sigma(S_2) < 0$  for all parameters  $h$  and  $\kappa_F$  ( $\sigma(\bullet)$  denotes the spectrum of an operator), i.e.  $S_2$  is *not* a density matrix. This, however, is not true for  $\sigma(S(\lambda))$  – at least not for all  $\lambda \in \mathbb{R}$ . We end up with a convex set of density operators defined via

$$\mathcal{D} = \{S(\lambda) \in \mathcal{B} \mid \lambda \in [a, b]\} \quad \text{where} \quad [a, b] = \{\lambda \in \mathbb{R} \mid \min \sigma(S(\lambda)) \geq 0\} \quad (2.197)$$

which are exactly the steady states of our theory. This convex set (a “line” in  $\mathcal{B}$ ) can formally be written as  $|\mathcal{D}\rangle\rangle = \text{Ker}[\mathcal{L}] \cap |\mathcal{S}\rangle\rangle$  and is the convex envelope of  $S(a)$  and  $S(b)$ . As we shall see it is  $a < b = 1$  where  $S(a)$  is some mixed state but  $S(b) = |\Phi^-\rangle\rangle\langle\langle\Phi^-|$  is a pure Bell state. So our “steady state line” is attached with one end at an extreme point of the convex set  $\mathcal{S}$  of density matrices and ends at some mixed state on its surface. The CPTP map  $\exp(\mathcal{L}t)$  defines then a flow on  $\mathcal{S}$  towards this line.



### ► Evaluation

In Fig. 2.23 we show the purity and  $x$ -magnetisation in the second and third row for  $h = 0.5$ ,  $h = 1$ ,  $h = 1.5$  and varying  $\kappa_F$  ( $y$ -axis). On the horizontal axis the parameter  $\lambda$  is varied, i.e. the vertical lines can be seen as the line  $\mathcal{D}$  in the space of density matrices. In the light grey region the matrix  $S(\lambda)$  is not positive-semidefinite anymore and  $S(\lambda)$  leaves<sup>40</sup> the convex set  $\mathcal{S}$ .

Instead of the concurrence we show in the upper row of Fig. 2.23 the trace distance to the three pure states

$$|\Phi^-\rangle\rangle = ||\Phi^-\rangle\langle\Phi^-|\rangle\rangle, \quad |\uparrow\rangle\rangle = ||\uparrow\rangle\langle\uparrow|\rangle\rangle \quad \text{and} \quad |+\rangle\rangle = ||+\rangle\langle+\rangle\rangle \quad (2.198)$$

where  $|\Phi^-\rangle = \frac{1}{\sqrt{2}}(|\uparrow\uparrow\rangle - |\downarrow\downarrow\rangle)$  is a Bell state. The trace distance is defined by

$$\text{TD}[\rho, \pi] := \frac{1}{2} \text{Tr} \left[ \sqrt{(\rho - \pi)^2} \right] \quad (2.199)$$

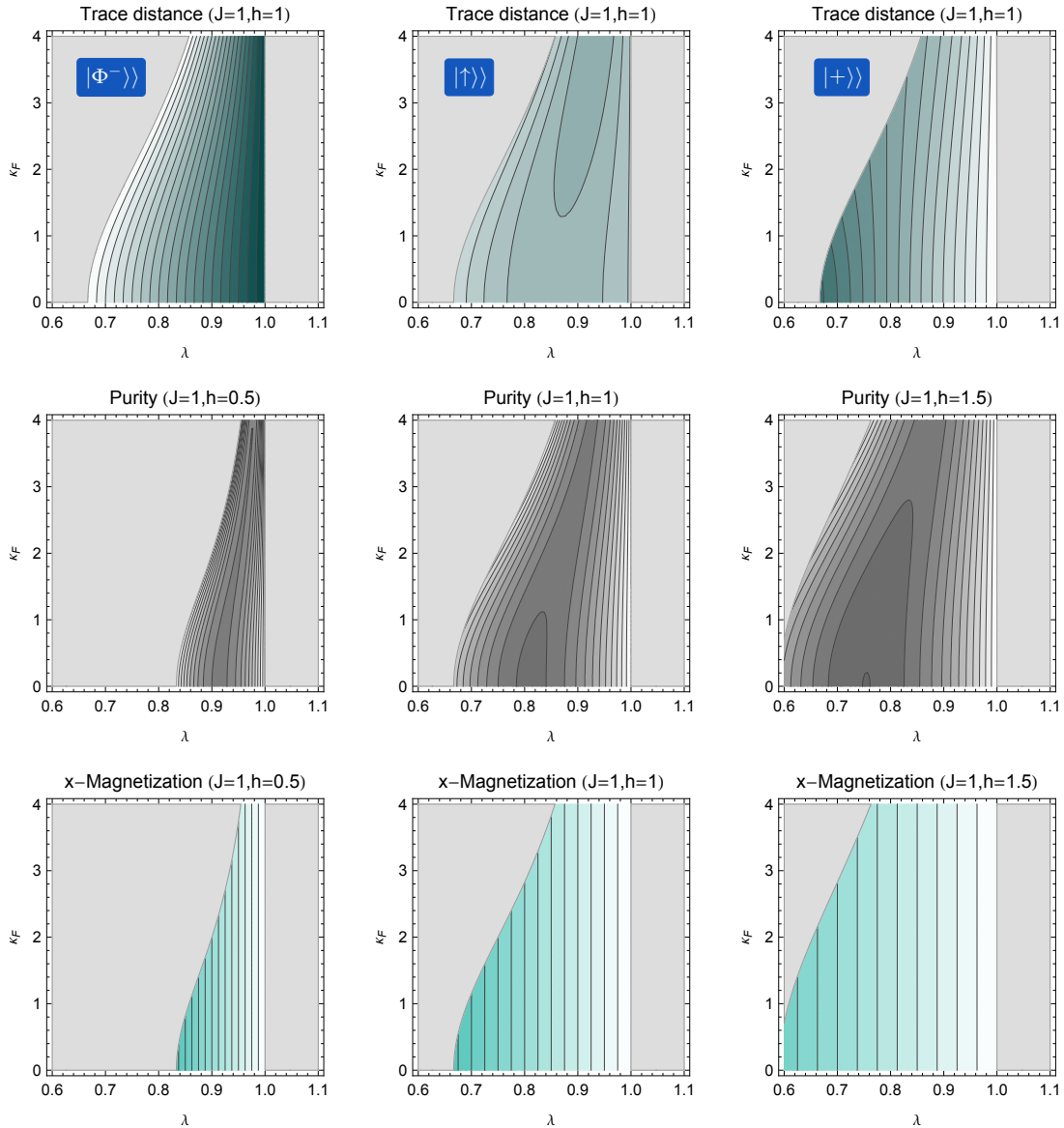
and constitutes a metric on the set of density matrices  $\mathcal{S}$ . It can be computed easily via  $\text{TD}[\rho, \pi] = \frac{1}{2} \sum_i |\lambda_i|$  where  $\{\lambda_i\} \subset \mathbb{R}$  are the real eigenvalues of the Hermitian matrix  $\rho - \pi$ . We use the trace distance to locate the steady state with respect to the three reference states given above.

Let us make some comments on the findings in Fig. 2.23:

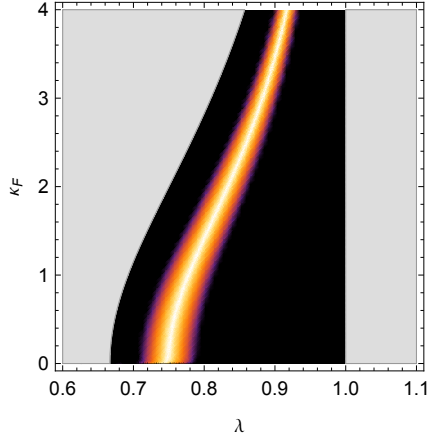
- In the first row the trace distance between the steady state  $S(\lambda)$  and one of the three reference states is color-coded for varying  $\kappa_F$ . In dark-green regions the steady state is close to the reference state; in white regions they are far apart. First, we realise that the  $z$ -polarised state  $|\uparrow\rangle\rangle$  is not near any steady state in  $\mathcal{D}$  and its distance from  $S(\lambda)$  is nearly constant. The  $x$ -polarised state  $|+\rangle\rangle$  and the pure end of  $\mathcal{D}$  ( $\lambda = 1$ ) are far apart (rightmost plot) whereas the mixed extreme point ( $S(a)$ ) approaches  $|+\rangle\rangle$  for decreasing  $\kappa_F$  (it does never reach any pure state, though). However, the leftmost plot shows that the  $\kappa_F$ -independent extreme point  $S(1)$  equals the pure Bell state  $|\Phi^-\rangle\rangle$ . It is noteworthy that  $|\Phi^-\rangle\rangle$  seems to be a special state since the distance function of  $\text{TD}[|\Phi^-\rangle\langle\Phi^-|, S(\lambda)]$  is just rescaled for varying  $\kappa_F$ . Obviously this is not true for the other two reference states where this function changes fundamentally with  $\kappa_F$ .
- In the second row the purity of  $S(\lambda)$  is illustrated for the magnetic fields  $h = 0.5$ ,  $1$  and  $1.5$ . As previously, pure states are characterised by white points and the purity decreases towards black. Clearly, the varying magnetic field does not change  $\mathcal{D}$  qualitatively (other than rescaling the parametrisation  $\lambda$ ). In the rightmost plot for  $h = 1.5$  one can easily see that the extreme point  $S(1)$  indeed is a pure state. Then  $\mathcal{D}$  “dives” into the mixed interior of  $\mathcal{S}$  turning towards more pure states as  $\lambda$  approaches  $a$ . However,  $S(a)$  remains mixed as suggested above – although it becomes more pure with increasing  $\kappa_F$ .
- In the last row the  $x$ -magnetisation is shown for the three magnetic fields. Obviously the magnetisation depends only on the position  $\lambda$  in  $\mathcal{D}$  and not on the bath coupling  $\kappa_F$ . Nevertheless, the magnetisations that can be reached in  $\mathcal{D}$  become more and more restricted to lower values for increasing  $\kappa_F$ . Note that the maximum magnetisation for

<sup>40</sup>Note that “leaving” the convex set of density matrices does not necessarily mean “leaving via pure states on the extreme points of the convex envelope”. One can “leave” in other directions, e.g. by destroying the Hermiticity or positivity (as in our case).

$S(a)$  and  $\kappa_F \rightarrow 0$  is about  $\text{Tr}[\Sigma^x S(a)] \approx 0.7$  which corresponds to the findings for the purity and the distance to  $|+\rangle$ .



■ **Figure 2.23:** Steady states of the 2-spin dissipative TIM with unitary dynamics for  $\kappa_P = 0$  and  $h \neq 0$ . In the first row we show the trace distance between the steady state  $S(\lambda)$  and one of the three reference states (dark green [white]  $\rightarrow$  close to [far from] the reference state). In the second row the purity of  $S(\lambda)$  is illustrated for the magnetic fields  $h = 0.5, 1$  and  $1.5$ . Pure states are characterised by white points and the purity decreases towards black. The last row illustrates the  $x$ -magnetisation for the three magnetic fields (white [green]  $\rightarrow$   $\langle \sigma^x \rangle = 0$  [ $\langle \sigma^x \rangle = 1$ ]).



■ **Figure 2.24:** The plot illustrates the trace distance  $\text{TD}[\rho_{\text{NESS}}^\varepsilon, S(\lambda)]$  between  $S(\lambda)$  and the unique steady state  $\rho_{\text{NESS}}^\varepsilon = \rho_{\text{NESS}}(\kappa_P = 0 + \varepsilon)$  for  $0 < \varepsilon \ll 1$ , that is, finite paramagnetic driving  $\kappa_P > 0$ , close to the parameter regime where the uniqueness is lost. In the grey region  $S(\lambda)$  is unphysical. The warmer the colour the closer is the unique state  $\rho_{\text{NESS}}^\varepsilon$  to  $S(\lambda)$ . The yellow line highlights the point  $\lambda(\kappa_F)$  where the unique NESS joins the convex set of stationary solutions for  $\kappa_P \rightarrow 0$ .

A question that arises now inevitably is the following: How does the transition between  $\kappa_P \neq 0$  (where we found a unique mixed steady state) and the case at hand, i.e.  $\kappa_P = 0$ , look like? In other words: When  $\kappa_P$  approaches adiabatically 0 so that the system remains in its current steady state for all times, where does  $\rho_{\text{NESS}}$  show up in the convex set  $\mathcal{D}$  which we parametrised by  $\lambda$ ? To answer this question it is helpful to plot the trace distance  $\text{TD}[\rho_{\text{NESS}}^\varepsilon, S(\lambda)]$  where  $\rho_{\text{NESS}}^\varepsilon = \rho_{\text{NESS}}(\kappa_P = 0 + \varepsilon)$  for  $0 < \varepsilon \ll 1$  is a unique steady state close to the parameter regime where the uniqueness is lost.

In Fig. 2.24 we calculated this quantity for  $h = 1$ . As above the grey region marks the unphysical matrices  $S(\lambda)$  for  $\lambda \notin [a, b]$ . The trace distance is larger for darker colours. Thus the point in  $\mathcal{D}$  where  $\rho_{\text{NESS}}^\varepsilon$  enters is centred in the bright line where the trace distance vanishes (it vanishes not exactly since  $\varepsilon$  does not). So we come to the conclusion that  $\rho_{\text{NESS}}^\varepsilon$  does not enter  $\mathcal{D}$  at the extreme points (as one might expect) but somewhere in the interior, quite distant from the pure steady state  $|\Phi^-\rangle$ . ◀

■  $\kappa_P = 0, h = 0$  and  $J, \kappa_F$  arbitrary

If we switch off the magnetic field,  $h = 0$ , we expect the set of steady states  $\mathcal{D}$  to grow even further since the ground states of the Hamiltonian now coincide with the dark states of the dissipative process. But let us proceed as above and calculate the kernel of the Lindbladian superoperator. We find  $\dim \text{Ker} [\mathcal{L}] = 4$  and the following basis operators:

$$S_1 = \begin{bmatrix} 1 & 0 & 0 & 0 \\ 0 & 0 & 0 & 0 \\ 0 & 0 & 0 & 0 \\ 0 & 0 & 0 & 0 \end{bmatrix}, \quad S_2 = \begin{bmatrix} 0 & 0 & 0 & 0 \\ 0 & 0 & 0 & 0 \\ 0 & 0 & 0 & 0 \\ 0 & 0 & 0 & 1 \end{bmatrix}, \quad S_3 = \begin{bmatrix} 0 & 0 & 0 & 1 \\ 0 & 0 & 0 & 0 \\ 0 & 0 & 0 & 0 \\ 0 & 0 & 0 & 0 \end{bmatrix}, \quad S_4 = \begin{bmatrix} 0 & 0 & 0 & 0 \\ 0 & 0 & 0 & 0 \\ 0 & 0 & 0 & 0 \\ 1 & 0 & 0 & 0 \end{bmatrix}$$

$S_1$  and  $S_2$  are density matrices, namely  $|\downarrow\rangle\langle\downarrow|$  and  $|\uparrow\rangle\langle\uparrow|$ . This is not surprising since both of them are clearly dark states of  $d_i$  and eigenstates<sup>41</sup> of  $H$ . Since they are eigenstates to the same eigenvalue, each linear combination of  $|\uparrow\uparrow\rangle$  and  $|\downarrow\downarrow\rangle$  remains a dark state of the system (this would be not true if their eigenvalues differed!). But we cannot create *coherent superpositions* by linear combinations in  $\mathcal{S}$  as we could in  $\mathcal{H}$ . This is where  $S_3$  and  $S_4$  enter the stage. Note that those are *no density matrices*, i.e.  $S_3, S_4 \notin \mathcal{S}$ , and there is no possibility transforming them into

<sup>41</sup>They are even ground states; but that does not matter if we are interested in the steady states.

such. They are not even Hermitian, but if we combine  $S_3$  and  $S_4$  in a certain way, we may create *coherences* between  $|\uparrow\uparrow\rangle$  and  $|\downarrow\downarrow\rangle$ .

So we can do *convex combinations* of  $S_1$  and  $S_2$  in order to create *mixtures* and add *complex linear combinations* of  $S_3$  and  $S_4$  in order to create coherences. It is easy to see that all *potential* steady states can thus be written as

$$S(t, u, \varphi) = t \cdot S_1 + (1 - t) \cdot S_2 + ue^{-i\varphi} \cdot S_3 + ue^{i\varphi} \cdot S_4 \quad (2.200)$$

since  $\text{Tr}[S] = 1$  and  $S^\dagger = S$  for all parameters  $t \in \mathbb{R}$ ,  $u \in [0, \infty]$  and  $\varphi \in [0, 2\pi]$ . The non-zero eigenvalues of  $S$  read

$$\lambda_{\pm} = \frac{1}{2} \left( 1 \pm \sqrt{(1 - 2t)^2 + 4u^2} \right) \quad (2.201)$$

and thus we find the necessary and sufficient condition  $\sqrt{(1 - 2t)^2 + 4u^2} \leq 1$  for  $S$  to be positive-semidefinite, ergo a density matrix. It is useful to reparametrise  $S$  via  $t := \frac{1}{2}(r \cos \theta + 1)$  and  $u := \frac{r}{2} \sin \theta$ , where  $r \in [0, 1]$  and  $\theta \in [0, 2\pi]$  make sure that the positivity condition is satisfied. So we have

$$S(r, \theta, \varphi) = \begin{bmatrix} \frac{1}{2}(1 + r \cos \theta) & 0 & 0 & \frac{r}{2}e^{-i\varphi} \sin \theta \\ 0 & 0 & 0 & 0 \\ 0 & 0 & 0 & 0 \\ \frac{r}{2}e^{i\varphi} \sin \theta & 0 & 0 & \frac{1}{2}(1 - r \cos \theta) \end{bmatrix} \quad (2.202)$$

Define now the following four dimensional representation of the Pauli spin algebra

$$\begin{aligned} \tau^x &\equiv |\downarrow\downarrow\rangle \langle \uparrow\uparrow| + |\uparrow\uparrow\rangle \langle \downarrow\downarrow| \\ \tau^y &\equiv i |\uparrow\uparrow\rangle \langle \downarrow\downarrow| - i |\downarrow\downarrow\rangle \langle \uparrow\uparrow| \\ \tau^z &\equiv |\downarrow\downarrow\rangle \langle \downarrow\downarrow| - |\uparrow\uparrow\rangle \langle \uparrow\uparrow| \end{aligned}$$

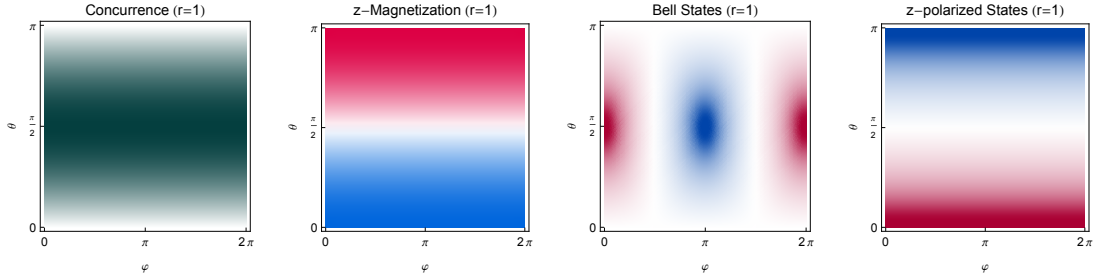
where one easily checks that  $[\tau^i, \tau^j] = 2i\varepsilon_{ijk}\tau^k$  and  $\{\tau^i, \tau^j\} = 2\delta_{ij}\mathbb{1}$ . It is now straightforward to show that the steady states can be parametrised as

$$S(\mathbf{r}) = \frac{1}{2}(\mathbb{1} + \mathbf{r}\boldsymbol{\tau}) \quad \text{where} \quad \mathbf{r} = \begin{bmatrix} r \cos \varphi \sin \theta \\ r \sin \varphi \sin \theta \\ r \cos \theta \end{bmatrix} \quad (2.203)$$

where  $\boldsymbol{\tau}$  is the column vector of the  $\tau^i$ . But  $\mathbf{r}$  is just a usual Bloch vector! So the actual parameters read  $r \in [0, 1]$ ,  $\theta \in [0, \pi]$  and  $\varphi \in [0, 2\pi]$  (the range of  $\theta$  has to be constrained to  $[0, \pi]$  in order to obtain a unique<sup>42</sup> description of steady states). That is, all steady states can be viewed as the states (mixed or pure) of a new spin, namely  $|\downarrow\rangle \equiv |\downarrow\downarrow\rangle$  and  $|\uparrow\rangle \equiv |\uparrow\uparrow\rangle$ . Therefore it is not surprising that the purity reads  $\gamma = \text{Tr}[S^2] = \frac{1}{2}(1 + r^2)$ , which is a well-known expression for a single spin. In a nutshell: For the parameters  $\kappa_P = 0 = h$  the system reduces effectively to a *free* one-spin system.

To illustrate our findings see Fig. 2.25. There we show the concurrence, the z-magnetisation and the trace distance to the reference states  $|\oplus\rangle \equiv |\Phi^+\rangle = \frac{1}{\sqrt{2}}(|\downarrow\rangle + |\uparrow\rangle)$ ,  $|\ominus\rangle \equiv |\Phi^-\rangle = \frac{1}{\sqrt{2}}(|\downarrow\rangle - |\uparrow\rangle)$ ,  $|\downarrow\rangle$  and  $|\uparrow\rangle$  for  $r = 1$ , i.e. the pure shell of the Bloch sphere. The concurrence vanishes at the poles since  $|\downarrow\rangle$  and  $|\uparrow\rangle$  are product states and becomes one on the equator since

<sup>42</sup>Unique up to the usual singularity at  $\theta = 0, \pi$  and  $r = 0$  known from spherical coordinates.



■ **Figure 2.25:** Here we show the concurrence  $\mathcal{C}$  (white  $\rightarrow$   $\mathcal{C}$  small), the z-magnetisation  $\langle \sigma^z \rangle$  and the trace distance to the reference states  $|\oplus\rangle \equiv |\Phi^+\rangle$  (Bell state, red),  $|\ominus\rangle \equiv |\Phi^-\rangle$  (Bell state, blue) and  $|\uparrow\rangle$  (z-polarised, red),  $|\downarrow\rangle$  (z-polarised, blue) for  $r = 1$ , i.e. the pure shell of the Bloch sphere. The darker the color the closer is  $S(\mathbf{r}) = S(\varphi, \theta)$  to the corresponding reference state. Further comments are given in the text.

there the maximally entangled Bell states  $|\Phi^\pm\rangle$  can be found. Note that the latter take in our effective one-spin system the role of  $|+\rangle$  and  $|-\rangle$  for a single qubit, hence the notation  $|\oplus\rangle$  and  $|\ominus\rangle$ . In the effective one-spin picture the entanglement of the underlying physical spins degenerates to a *degree of superposition* of the two basis states  $|\downarrow\rangle$  and  $|\uparrow\rangle$ . The z-magnetisation becomes  $\pm 1$  at the poles and vanishes at the equator, as expected. Note that there can be no x-magnetisation with respect to the physical spins, i.e.  $\langle \Sigma^x \rangle_{\text{NESS}} = 0$  for all steady states  $\rho_{\text{NESS}} = S(\mathbf{r})$ . The trace distance plots show that the states  $|\oplus\rangle$  (red) and  $|\ominus\rangle$  (blue) are located at  $(\theta, \varphi) = (\pi/2, 0)$  and  $(\theta, \varphi) = (\pi/2, \pi)$ , respectively. Analogously one finds the states  $|\uparrow\rangle$  (red) and  $|\downarrow\rangle$  (blue) at the poles of the Bloch sphere. ■

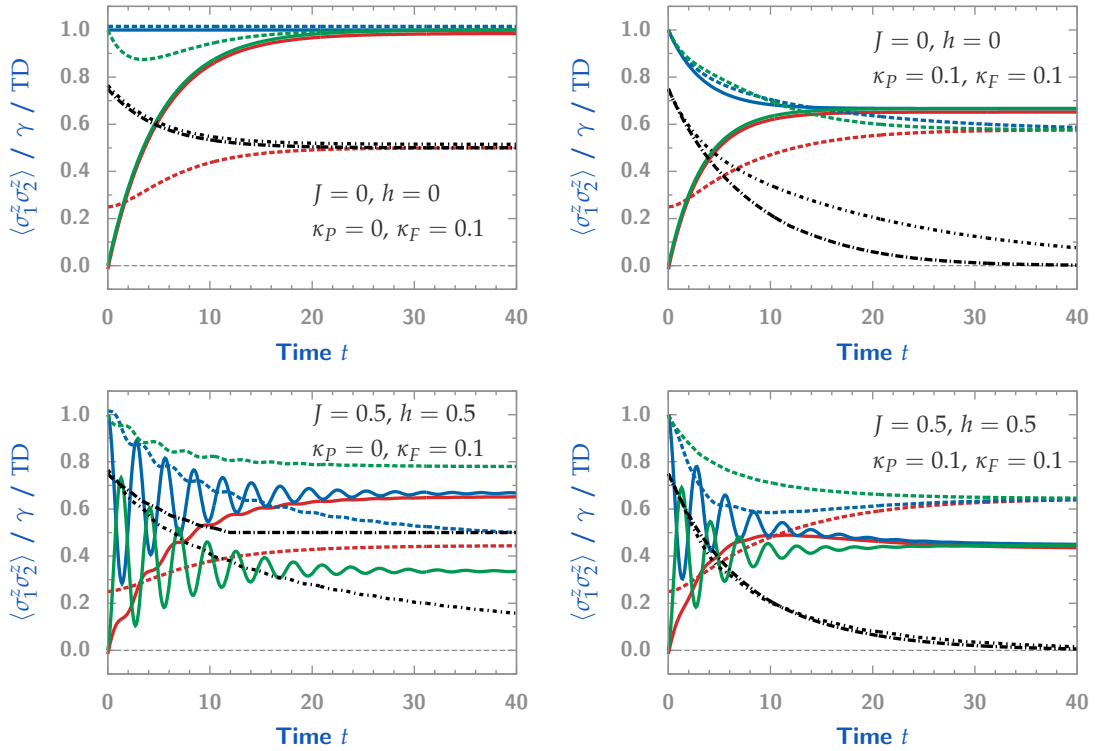
### 2.5.3 Relaxation to steady states

So far we were concerned with the stationary states, i.e. with the properties at  $t \rightarrow \infty$ . Let us now have a look at the dynamic properties of the 2-spin system, that is, its *approach* to a steady state. Since  $|\mathcal{B}\rangle\rangle$  is a sixteen-dimensional complex vector space and  $\mathcal{L}$  is a matrix of corresponding dimension, it is no challenge to compute the time evolution channel

$$U(t) = \exp(\mathcal{L}t) \quad \text{and} \quad |\rho(t)\rangle\rangle = U(t) |\rho_0\rangle\rangle \quad (2.204)$$

analytically for given parameters by means of a CAS. We did this for a representative selection of parameters and found the evolutions depicted in Fig. 2.26. Let us make some short remarks:

- The upper left plot in Fig. 2.26 shows the evolution of the initial states  $|\uparrow\rangle\rangle$  (z-polarised),  $|+\rangle\rangle$  (x-polarised) and  $|\mathbb{1}\rangle\rangle$  (completely mixed) for the parameters  $J = 0 = h$ ,  $\kappa_P = 0$  and  $\kappa_F = 0.1$ . We show for each initial state the correlation  $\langle \sigma_1^z \sigma_2^z \rangle$  and the purity  $\gamma = \text{Tr}[\rho(t)^2]$ . To clarify the relations of the steady states for different initial conditions, the trace distances between  $|\rho_+(t)\rangle\rangle = U(t) |+\rangle\rangle$ ,  $|\rho_\uparrow(t)\rangle\rangle = U(t) |\uparrow\rangle\rangle$  and the completely mixed evolution  $|\rho_\mathbb{1}(t)\rangle\rangle = U(t) |\mathbb{1}\rangle\rangle$  is shown with dashed black lines. The set of steady states for vanishing paramagnetic driving ( $\kappa_P = 0$ ) was derived in the previous subsection and we found a Bloch ball for the completely z-polarised states  $|\uparrow\rangle$  and  $|\downarrow\rangle$ . So we cannot expect a unique steady state, and indeed, the trace distance between  $|\rho_\uparrow(t)\rangle\rangle$ ,  $|\rho_+(t)\rangle\rangle$  and  $|\rho_\mathbb{1}(t)\rangle\rangle$  remains finite for all times. Note that the purity for both,  $|\rho_\uparrow(t)\rangle\rangle$  and  $|\rho_+(t)\rangle\rangle$ , approaches one. However, although both pure, their steady states do not co-



■ **Figure 2.26:** Examples of the exact time evolution of the 2-spin dissipative TIM. Each plot shows the evolution  $|\rho_X(t)\rangle = U(t)|X\rangle$  for the three initial states  $X = \uparrow$  (z-polarized),  $+$  (x-polarized) and  $\mathbb{1}$  (completely mixed). To this end we calculated the spin-spin correlation  $\langle \sigma_1^z \sigma_2^z \rangle$ , the purity  $\gamma = \text{Tr}[\rho(t)]$  and the trace distances  $\text{TD}[\bullet, \bullet]$  for the two pairs  $|\rho_{\mathbb{1}}(t)\rangle, |\rho_{\uparrow}(t)\rangle$  and  $|\rho_{\mathbb{1}}(t)\rangle, |\rho_{+}(t)\rangle$  as functions of time. The four plots correspond to four generic sets of parameters  $J, h, \kappa_P$  and  $\kappa_F$ . A detailed description is given in the text.

$\langle \sigma_1^z \sigma_2^z \rangle$  for  $|\rho_0\rangle = |\mathbb{1}\rangle$  — solid red line  
 $\gamma$  for  $|\rho_0\rangle = |\mathbb{1}\rangle$  — dashed red line  
 $\langle \sigma_1^z \sigma_2^z \rangle$  for  $|\rho_0\rangle = |\uparrow\rangle$  — solid blue line  
 $\gamma$  for  $|\rho_0\rangle = |\uparrow\rangle$  — dashed blue line  
 $\langle \sigma_1^z \sigma_2^z \rangle$  for  $|\rho_0\rangle = |+\rangle$  — solid green line  
 $\gamma$  for  $|\rho_0\rangle = |+\rangle$  — dashed green line  
 $\text{TD}[\rho, \pi]$  for  $|\rho_0, \pi_0\rangle = |\mathbb{1}, +\rangle$  — dashed black line  
 $\text{TD}[\rho, \pi]$  for  $|\rho_0, \pi_0\rangle = |\mathbb{1}, \uparrow\rangle$  — dotted black line

incide<sup>43</sup>. Clearly,  $|\uparrow\rangle$  is already a steady state and therefore undergoes a trivial time evolution. The completely mixed initial state  $|\mathbb{1}\rangle$  does not become pure due to the degenerate dark state space – nevertheless it becomes *purer* since all contributions of states which violate the correlation condition  $\langle \sigma_1^z \sigma_2^z \rangle = 1$  are eliminated. Note that, though mixed, the steady state exhibits perfect spin-spin correlations  $\langle \sigma_1^z \sigma_2^z \rangle = 1$ .

- The upper right plot in Fig. 2.26 shows the same quantities and the same evolutions as above with the only difference that the paramagnetic bath couples with  $\kappa_P = 0.1$  and thus a *unique* (mixed) steady state emerges. The most obvious indication of this new uniqueness is the vanishing of both trace distances – so all three initial states end up in the same steady state. The latter is mixed and exhibits a strong but not perfect positive correlation  $\langle \sigma_1^z \sigma_2^z \rangle$  between the two spins.

<sup>43</sup>The derivation of this statement is left as an exercise to the reader.

- The lower left plot in Fig. 2.26 shows the same evolutions as the upper left plot with an additional unitary dynamics imposed by  $H$  and the parameters  $J = 0.5 = h$ . This additional unitary evolutions changes the long term behaviour of the three initial states qualitatively: Clearly, the oscillations are due to the unitary evolution and superimpose the previously smooth damping caused by the dissipative processes. Whereas in the purely dissipative setting all three initial states ended up in *different* steady states, in the current setting the initial states  $|\mathbb{1}\rangle\rangle$  and  $|\uparrow\rangle\rangle$  tend towards *the same* steady state and only  $|+\rangle\rangle$  ends up elsewhere. This can be easily seen since the trace distance between the first two evolutions vanishes whereas the trace distance between  $|\rho_+(t)\rangle\rangle$  and  $|\rho_{\mathbb{1}}(t)\rangle\rangle$  does not. The different steady states also lead to differing spin-spin correlations as  $t \rightarrow \infty$ . We already understood these phenomena in the previous subsections where we found that the magnetic field  $h \neq 0$  leads to a convex “line”  $\mathcal{D}$  of steady states with two extremal points, one of which is a pure state. In the case at hand  $|\mathbb{1}\rangle\rangle$  and  $|\uparrow\rangle\rangle$  flow towards the same point on this line whereas  $|+\rangle\rangle$  meets it elsewhere.
- The lower right plot in Fig. 2.26 shows the same setting with additional coupling to the paramagnetic bath,  $\kappa_P = 0.1$ . As we saw earlier this leads to a unique steady state. The long-term behaviour is more or less the same as in the purely dissipative setting shown in the upper right plot. At the beginning, the unitary dynamics dominates the evolution and superimposes oscillations on the dissipative damping.

We utilise this system and the analytical results discussed above in Subsection 2.6.2 as a consistency check for a quantum trajectory Monte Carlo simulation of dissipative evolution channels  $U(t)$ . There we will meet the time evolutions again and interpret them as ensembles of quantum trajectories for given ensembles of initial states.

## 2.6 Quantum trajectory Monte Carlo simulation

Here we apply the technique of Quantum Trajectory Monte Carlo (QTMC) simulations to our dissipative transverse field Ising model. We shall use this unravelling of the Lindblad master equation furthermore in the context of dissipative quantum error correction in the subsequent chapters.

### 2.6.1 Technical remarks

We already saw in Subsection 1.1.3 that the time evolution encoded in a Lindblad master equation can be expressed in terms of quantum trajectories via

$$|\rho(t)\rangle\rangle = \exp(\mathcal{L}t) |\rho_0\rangle\rangle = \int_{[0,t],\{\mathbf{L}_j\}} \mathcal{D}[\mathbf{L}] P[\mathbf{L};t] |\rho_c[\mathbf{L};t]\rangle\rangle .$$

where the conditioned density matrix

$$|\rho_c[\mathbf{L};t]\rangle\rangle \equiv (P[\mathbf{L};t])^{-1} \mathcal{T} \left[ \exp(\mathbf{H}_{\text{eff}}t) \prod_{l \in \mathbf{L}} l \right] |\rho_0\rangle\rangle$$

describes a system which experienced a particular sequence  $\mathbf{L}$  of quantum jumps  $L_{j_i}$  at times  $t_i$ . This particular trajectory occurs with probability

$$P[\mathbf{L};t] = \langle\langle \mathbb{1} | e^{\mathbf{H}_{\text{eff}}(t-t_m)} L_{j_m} e^{\mathbf{H}_{\text{eff}}(t_m-t_{m-1})} L_{j_{m-1}} \dots L_{j_1} e^{\mathbf{H}_{\text{eff}}(t_1-0)} |\rho_0\rangle\rangle .$$

Hence it seems reasonable to obtain an approximation of  $\rho(t)$  by a Monte Carlo algorithm which samples over all possible jump trajectories  $\mathbf{L}$  with distribution  $P[\mathbf{L};t]$ . Originally such an unravelling of the master equation in terms of quantum jump trajectories was contrived in [118] and applied for simulation in [119]. However, our straightforward simulation goes along the lines of Ref. [120] which is also a nice review for the trajectory approach in the context of Markovian master equations.

In the following we describe the algorithm without giving a formal proof of its correctness, see [120] for further details. Assuming the initial state is given by a convex combination of pure states  $|\Phi_i\rangle$  via  $\rho_0 = \sum_i p_i |\Phi_i\rangle \langle \Phi_i|$  with the (classical) probability distribution  $\{p_i\}$  and we wish to find the evolution for  $0 \leq t \leq T$ , the procedure for a QTMC simulation reads as follows: Discretise time via  $t_j = j \cdot \Delta t$ ,  $j = 0, 1, 2, \dots, N_T$ , so that  $t_0 = 0$  and  $t_{N_T} = T$ .  $\Delta t$  must be chosen much smaller than the physical timescales of the system under consideration, determined by the excitation energies of the Hamiltonian and the decay rates given by the bath coupling strengths. Now generate a quantum trajectory by choosing an initial state  $|\Psi(t_0)\rangle = |\Phi_i\rangle$  randomly according to the probability distribution  $\{p_i\}$  and proceed as follows:

- (1) Assume we reached time  $t_j$ . Measure your selected observables  $\langle X \rangle(t_j) = \langle \Psi(t_j) | X | \Psi(t_j) \rangle$  and store the results (see below for an explanation).
- (2) Draw a random number  $r \in [0, 1)$ .
- (3) Define  $\Delta P_\mu(t_j) \equiv \Delta t \langle \Psi(t_j) | L_\mu^\dagger L_\mu | \Psi(t_j) \rangle$  for the jump operator  $L_\mu$ . Now calculate  $P_\nu(t_j) \equiv \sum_{\mu=1}^{\nu} \Delta P_\mu(t_j)$  for  $\mu = 1, 2, \dots$  until  $r \leq P_{\nu^*}(t_j)$  for some index  $\nu^*$  for the first time *or* all jump



operators have been added and it is still  $r > P_{N_j}(t_j)$  (where  $N_j$  denotes the number of jump operators). If the first case applies proceed with (a), otherwise with (b).

(a) If  $r \leq P_{v^*}(t_j)$  a jump occurs. The next (renormalised) state is given by

$$|\Psi(t_{j+1})\rangle \equiv \frac{L_{v^*} |\Psi(t_j)\rangle}{\sqrt{\langle \Psi(t_j) | L_{v^*}^\dagger L_{v^*} | \Psi(t_j) \rangle}} \quad (2.205)$$

where one can re-use  $L_{v^*} |\Psi(t_j)\rangle$  which has already been calculated for  $P_{v^*}(t_j)$ .

(b) If  $r > P_{N_j}(t_j)$  no jump occurs and the system evolves according to the effective Hamiltonian  $H_{\text{eff}} = H - \frac{i}{2}H_P$  where  $H$  determines the unitary evolution and the positive Hamiltonian  $H_P$  is responsible for the damping & decoherence. So compute<sup>44</sup>

$$|\Psi(t_{j+1})\rangle = \mathcal{N}^{-1/2} \exp(-iH_{\text{eff}}\Delta t) \approx \mathcal{N}^{-1/2} [\mathbb{1} - iH_{\text{eff}}\Delta t] |\Psi(t_j)\rangle \quad (2.206)$$

where the normalisation

$$\mathcal{N} = \langle \Psi(t_j) | [\mathbb{1} + iH_{\text{eff}}^\dagger\Delta t][\mathbb{1} - iH_{\text{eff}}\Delta t] | \Psi(t_j) \rangle \quad (2.207)$$

is necessary since  $H_{\text{eff}}$  is not Hermitian (due to  $H_P$ ) and thus the time evolution is not unitary.

(4) Start over with (1) until you reach  $t_{N_T} = T$ .

This sequence yields a *single* quantum trajectory  $n$  described by the state  $|\Psi_n(t)\rangle$  (which varies not smooth with  $t$  due to the quantum jumps – even if we take  $t$  as continuous variable). The time evolution starting from  $\rho_0$  is now given by

$$\rho(t) = e^{\mathcal{L}t}\rho_0 = \lim_{N \rightarrow \infty} \frac{1}{N} \sum_{n=1}^N |\Psi_n(t)\rangle \langle \Psi_n(t)| \stackrel{M \gg 1}{\approx} \frac{1}{M} \sum_{n=1}^M |\Psi_n(t)\rangle \langle \Psi_n(t)|. \quad (2.208)$$

That is, we have to perform lots of quantum jump trajectories with initial states distributed according to  $\rho_0$ . For larger systems ( $\sim 10$  spins and more) it is inconvenient to keep the actual (averaged) state  $\rho_M(t) \equiv M^{-1} \sum_{n=1}^M |\Psi_n(t)\rangle \langle \Psi_n(t)|$  in memory during the simulation<sup>45</sup>. Therefore one restricts oneself to store only the averages of *previously chosen observables*; i.e. if  $X$  is a Hermitian (bounded) operator, then

$$\langle X \rangle(t) = \text{Tr} [X e^{\mathcal{L}t} \rho_0] = \lim_{N \rightarrow \infty} \frac{1}{N} \sum_{n=1}^N \langle \Psi_n(t) | X | \Psi_n(t) \rangle \stackrel{M \gg 1}{\approx} \frac{1}{M} \sum_{n=1}^M \langle \Psi_n(t) | X | \Psi_n(t) \rangle \quad (2.209)$$

where each observable requires just a sequence of real numbers instead of a sequence of large complex matrices to be stored. We should mention that this is the most straightforward and lowest order unravelling of the Lindblad equation. One can employ, for instance, higher order

<sup>44</sup>Let us give a quick-and-dirty upper bound for  $\Delta t$  which is necessary to justify the linearisation of the time evolution operator. One certainly demands  $\| -iH_{\text{eff}}\Delta t \| \ll 1$ , so  $\Delta t \ll \| H - i/2H_P \|^{-1}$ . Since  $\| H - i/2H_P \|^{-1} \geq (\| H \| + \| H_P \|)^{-1} \geq (\rho(H) + \rho(H_P))^{-1}$  we are on the safe side for  $\Delta t \ll (\rho(H) + \rho(H_P))^{-1}$  (here  $\rho(\bullet)$  denotes the spectral radius). If we define  $\lambda_{\text{max}} := \max\{|\lambda| \mid \lambda \in \sigma(H) \cup \sigma(H_P)\}$  to be the eigenvalue of  $H$  and  $H_P$  with the largest absolute value, we finally obtain the sufficient condition  $\Delta t \ll \lambda_{\text{max}}^{-1}$  which formalises the statement that  $\Delta t$  must be much smaller than the energy scale of the unitary dynamics and the damping scale of the dissipative dynamics.

<sup>45</sup>Recall that for each discrete time  $t_j$  the state  $\rho_M(t_j)$  is given by a  $4^Q$ -dimensional complex matrix. For  $Q = 10$  spins this is already a  $1048576 \times 1048576$  matrix with complex entries – for each time step  $t_j$ !

Runge-Kutta integrators to obtain continuous-time unravellings which provide higher accuracy than this simple algorithm, see [120] for details.

Our implementation of this algorithm is written in C++ and runs parallelized on a Core i7-2600K workstation. We utilise several open source libraries, namely

- Boost for managing threads and parsing system configurations via regular expressions.
- OpenBLAS as BLAS implementation (mostly BLAS Level 2 operations, namely matrix-vector multiplications).
- Armadillo as wrapper for BLAS functions.

OpenBLAS was compiled manually to take full advantage of its optimisation for the Intel Sandy-Bridge architecture. For a detailed description of our implementation see Appendix C.

## 2.6.2 Comparison with exact evolution: A consistency check

To check whether our QTMC algorithm performs correctly (and to complete the 2-spin example introduced in Sec. 2.5), we simulate the 2-spin TIM and compare the results to the previously derived analytical ones. The simulations for this system took up to several seconds (depending on the number of samples) since the system is small (2 spins  $\rightarrow$  4-dimensional matrix-vector multiplications in the QTMC simulation). This is comparable to the time needed to calculate  $|\rho(t)\rangle\rangle = U(t) |\rho_0\rangle\rangle$  by numerical means<sup>46</sup> – which yields the exact result without any statistical fluctuations. Thus there is no actual benefit due to the QTMC simulation. The latter becomes useful for three spins and more where a numerical computation of  $\exp(\mathcal{L}t)$  becomes time-consuming or even practically impossible.

Dynamics with unique steady state

Let us first investigate the case of a unique steady state with different (pure and mixed) initial states. To this end we simulated the system for unitary parameters  $J = 0.5 = h$  and dissipative couplings  $\kappa_P = 0.1 = \kappa_F$ ; here we can expect a unique steady state and the exact dynamics is already known, see Fig. 2.26 and the related explanations in the text.

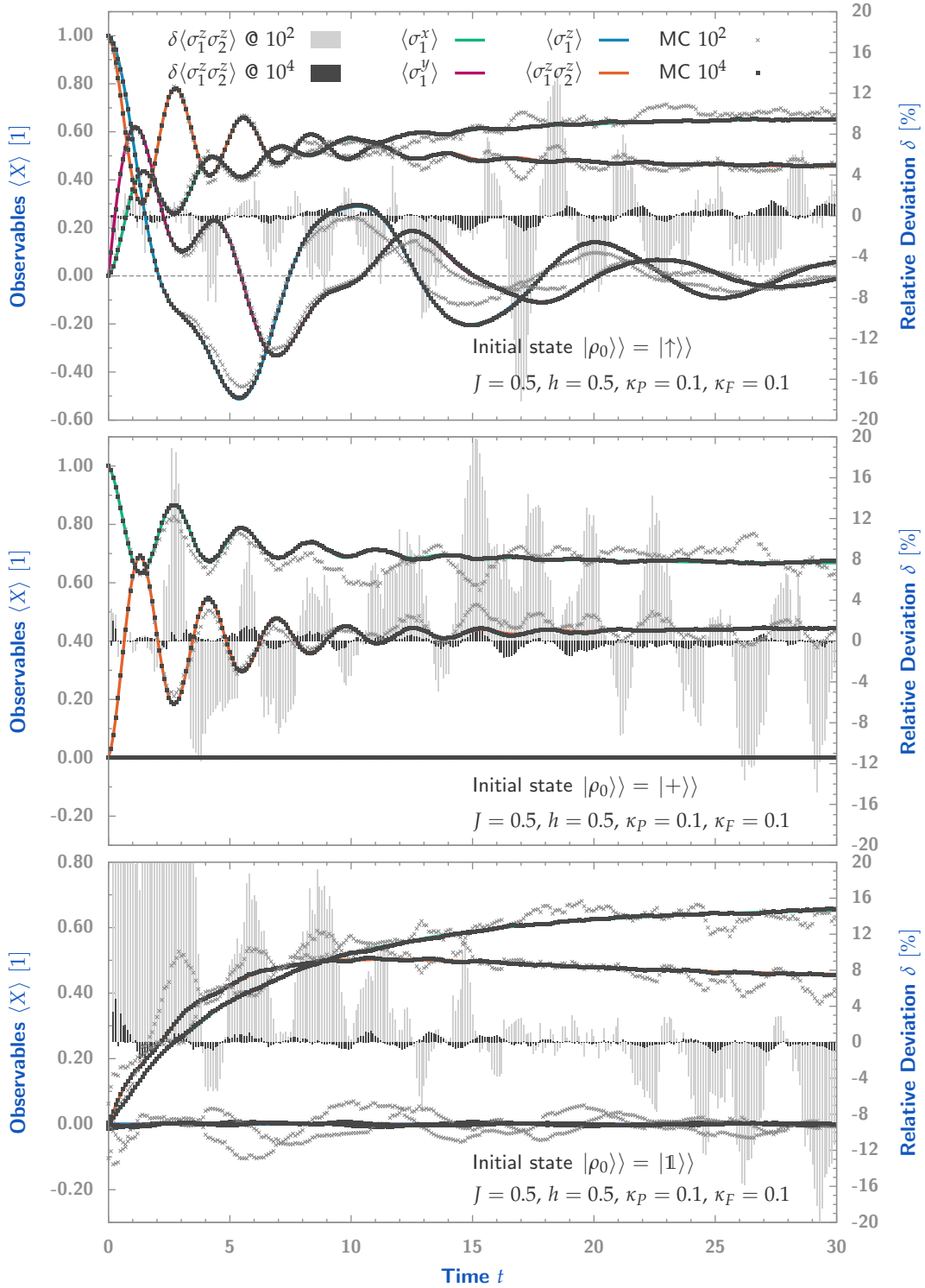
In Fig. 2.27 we compare the QTMC results (points) with the exact time evolution (lines). The three plots correspond to the three initial states (top-down)  $|\rho_0\rangle\rangle = |\uparrow\rangle\rangle$ ,  $|+\rangle\rangle$  and  $|\mathbb{1}\rangle\rangle$ . For all evolutions the four observables  $\sigma_1^x$ ,  $\sigma_1^y$ ,  $\sigma_1^z$  and  $\sigma_1^z \sigma_2^z$  were measured during two simulations, one with 100 samples and another with 10000 samples. The discretisation parameter was set to  $\Delta t = 0.001$  and the total time to  $T = 30$  which led to 30000 steps *per trajectory*. The simulation times ranged from fractions of a second (100 samples) to few seconds (10000 samples).

Besides the observables mentioned above, the relative deviation

$$\delta\langle X \rangle(t) = \frac{\langle X \rangle_{\text{QTMC}}(t) - \langle X \rangle_{\text{A}}(t)}{\langle X \rangle_{\text{A}}(t)} \quad (2.210)$$

of the QTMC result  $\langle X \rangle_{\text{QTMC}}$  and the analytical result  $\langle X \rangle_{\text{A}}$  for the correlation  $X = \sigma_1^z \sigma_2^z$  is shown by a bar graph in the background. The light-grey (dark-grey) bars refer to the simulation with 100 (10000) samples.

<sup>46</sup>This usually requires the Jordan canonical form of  $\mathcal{L}$  to compute  $\exp(\mathcal{L}t)$ .



■ **Figure 2.27:** QMTC simulation of 2-spin TIM with unitary parameters  $J = 0.5 = h$  and bath couplings  $\kappa_P = 0.1 = \kappa_F$  for different initial states. The lines denote the analytical evolution of the observables  $\sigma_1^x$ ,  $\sigma_2^y$ ,  $\sigma_3^z$  and  $\sigma_1^z \sigma_2^z$ , the points denote the corresponding QMTC simulation results for 100 and 10000 samples, respectively. The bar graphs illustrate the relative deviations  $\delta \langle \sigma_1^z \sigma_2^z \rangle$  of the QMTC and analytical results for the spin-spin correlation. Light-grey (dark-grey) bars correspond to the simulations with 100 (10000) samples. Further details are given in the text.

First, we notice that the simulations with 10000 samples clearly reproduce the analytical evolution and our QTMC algorithm seems to perform as expected. The relative deviations are in the order of  $\sim 1\%$  and exhibit a (statistically distorted) periodic behaviour due to the underlying unitary dynamics. Second, the simulations with just 100 samples are much worse (as expected) and follow only roughly the exact evolution. Interestingly, their deviations are quite low in the beginning (for, say,  $0 \leq t \leq 10$ ) if the initial state is pure, whereas for the completely mixed initial state the statistical fluctuations dominate the entire evolution. The answer to this phenomenon is connected with the relative weakness of the baths ( $\kappa_P = \kappa_F = 0.1 < 0.5 = J = h$ ). The statistical component of the QTMC simulation is directly linked to the occurrence of quantum jumps. For  $0 \leq t \leq 10$  the probability of a jump occurring is low and therefore the dynamics is determined by the (non-stochastic) time evolution via  $\exp(-iH_{\text{eff}})$ . Only at late times there is a considerable probability that several jumps occurred and *then* statistics becomes relevant. But this is only true for a pure initial state. If, in contrast, the initial state is (completely) mixed, there are statistical fluctuations from the beginning due to the randomly chosen (pure) initial states. This can be clearly seen in the lower plot of Fig. 2.27.

#### Dynamics with non-unique steady states

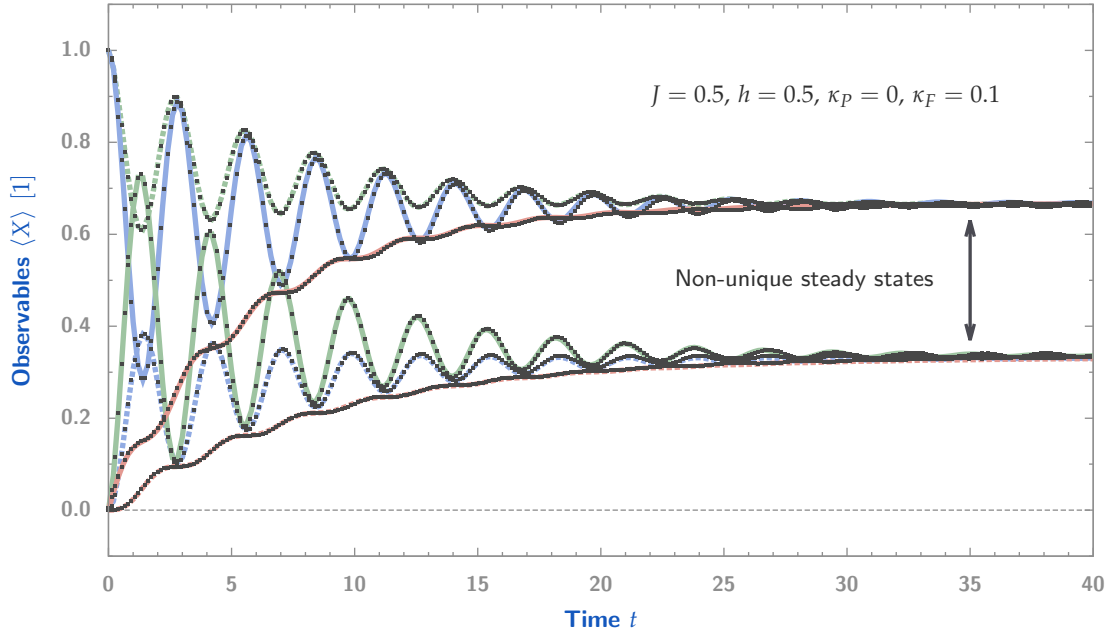
To check whether the QTMC simulation also performs correctly on systems with non-unique steady states, we employ the previously examined parameter set  $J = 0.5 = h$ ,  $\kappa_P = 0$  and  $\kappa_F = 0.1$  with a convex line  $\mathcal{D}$  of steady states. As before, we start with the three different initial states  $|\mathbb{1}\rangle\rangle$ ,  $|\uparrow\rangle\rangle$  and  $|+\rangle\rangle$  and measure the observables  $\sigma_1^x$  and  $\sigma_1^z \sigma_2^z$  for times  $t \in [0, 40]$  (discretisation  $\Delta t = 0.001$ ). To obtain good results even for late times, the QTMC simulations sampled over 50000 trajectories for each initial state.

The results are shown in Fig. 2.28 where dashed lines (solid lines) denote the analytical results for  $\langle \sigma_1^x \rangle(t)$  ( $\langle \sigma_1^z \sigma_2^z \rangle(t)$ ) and the points mark the QTMC results. Obviously the QTMC simulation fits the exact results almost perfectly and therefore reproduces the known fact (see Fig. 2.26 and the related descriptions) that the initial states  $|\mathbb{1}\rangle\rangle$  and  $|\uparrow\rangle\rangle$  evolve towards the same steady state whereas  $|+\rangle\rangle$  is driven to another one.

#### Quantum jump trajectories

We mentioned above that there is no actual benefit from the QTMC simulation regarding the time evolution of observables since the (numerical) exact solution can be calculated in the same time (or even faster) with less errors. However, even for our simple example there *is* an advantage if we want to understand and illustrate the action of the baths since the QTMC simulation enables us to generate *single quantum jump trajectories*.

Figure 2.29 shows four representative trajectories for different parameters and initial states over different periods of time. In the upper part of each plot we show the time evolution of the three observables  $\sigma_1^x$ ,  $\sigma_1^z \sigma_2^z$  and the average z-magnetisation  $\Sigma^z$ . Recall that these values now are *pure quantum mechanical* expectation values computed with respect to some pure state  $|\Psi(t_j)\rangle\rangle$ . In contrast, the time evolutions we considered so far described *classical (ensemble) averages* of quantum mechanical expectation values. The lower part of each plot encodes the occurrence of jumps over time: Each jump is marked by an impulse; red impulses for (one of the two) ferromagnetic ( $d_i$ ) jumps and blue ones for the paramagnetic ( $c_i$ ) jumps. If one performed an



■ **Figure 2.28:** QTM simulation of 2-spin TIM with unitary parameters  $J = 0.5 = h$  and bath couplings  $\kappa_P = 0$  and  $\kappa_F = 0.1$  for three different initial states, namely  $|\uparrow\rangle$ ,  $|+\rangle$  and  $|\mathbb{1}\rangle$ . We show for each evolution the analytic solutions for the two observables  $\sigma_1^x$  (dashed lines) and  $\sigma_1^z \sigma_2^z$  (solid lines) in comparison with the QTM results (points). Depending on the initial states, the evolutions reach different steady states which can be seen from the differing observables for e.g.  $|\rho_{\uparrow}(t)\rangle$  and  $|\rho_{+}(t)\rangle$ . A detailed explanation is given in the text.

$\langle \sigma_1^x \rangle$  for  $|\rho_0\rangle = |\uparrow\rangle$     blue dotted  
 $\langle \sigma_1^x \rangle$  for  $|\rho_0\rangle = |+\rangle$     green dotted  
 $\langle \sigma_1^x \rangle$  for  $|\rho_0\rangle = |\mathbb{1}\rangle$     red dotted  
 $\langle \sigma_1^z \sigma_2^z \rangle$  for  $|\rho_0\rangle = |\uparrow\rangle$     blue solid  
 $\langle \sigma_1^z \sigma_2^z \rangle$  for  $|\rho_0\rangle = |+\rangle$     green solid  
 $\langle \sigma_1^z \sigma_2^z \rangle$  for  $|\rho_0\rangle = |\mathbb{1}\rangle$     red solid  
 QTM C @  $5 \cdot 10^4$     .

experiment where the action of the bath on the system is under observation, these sequences of jumps constitute possible measurement outcomes.

Let us now examine the four trajectories in detail. There are some remarks in order:

- The upper left plot describes a possible evolution of a system which is initially in the state  $|\downarrow\uparrow\rangle$  and couples to the ferromagnetic bath  $d_i$  with  $\kappa_F = 0.1$ . The system will therefore evolve towards a (pure) dark state in the subspace  $\text{span}\{|\downarrow\downarrow\rangle, |\uparrow\uparrow\rangle\}$ . But the initial state has no overlap with any of the dark states. In such a case the *only* possibility to reach a steady state is a jump which creates the missing overlap instantaneously. This jump occurs at  $t \approx 3.4$  and flips the state to  $|\uparrow\uparrow\rangle$  which follows from  $\langle \Sigma^z \rangle = 1$ . We therefore conclude that the jump occurred on the first spin, namely  $d_1$ . It could have occurred with the same probability on the second spin ( $d_2$ ) – then the final state would have been  $|\downarrow\downarrow\rangle$ . This explains why the initial state  $|\uparrow\downarrow\rangle \langle\uparrow\downarrow|$  ends up in a *mixture* of  $|\uparrow\uparrow\rangle$  and  $|\downarrow\downarrow\rangle$ . The reader may ask why, before and after the jump, the system seems to be stationary; the reasons for that are twofold: Before the jump the system is in an eigenstate of  $H_P$  with *finite* energy. In each step the state is therefore *damped* by  $H_{\text{eff}}$ . However, unless the jump happens the system cannot leave its current state and therefore the normalisation after each step restores the state  $|\downarrow\uparrow\rangle$ . Note that the finite energy of this state with respect to  $H_P$  is responsible for  $d_1$  to occur anyway. The longer the system remains in this “excited”

state, the smaller the probability for such a trajectory to occur as part of  $\exp(\mathcal{L}t)$ . After the jump the system is in a dark state which has zero energy with respect to  $H_p$ . There no damping occurs anymore and normalisation is therefore not necessary since  $\exp(-iH_{\text{eff}})$  acts just trivially on  $|\uparrow\uparrow\rangle$ .

- The upper right plot shows a possible evolution of the same system started in

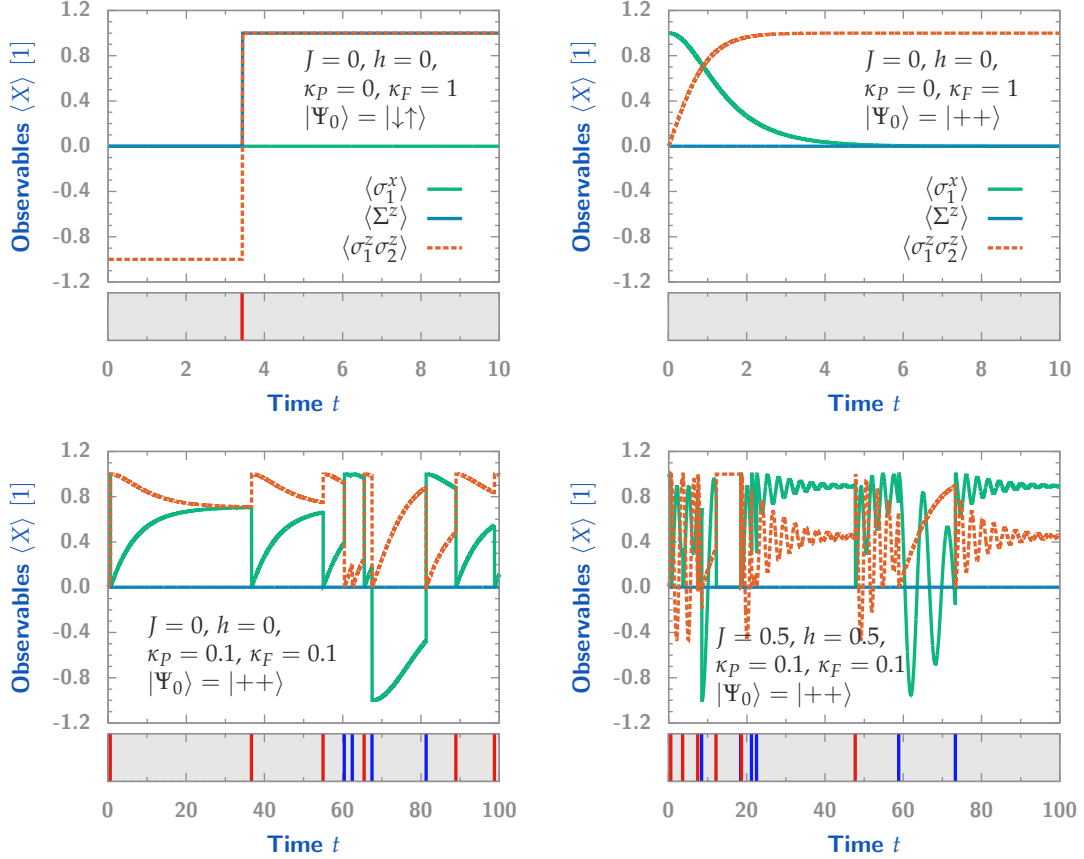
$$|++\rangle = \frac{1}{2} (|\downarrow\downarrow\rangle + |\downarrow\uparrow\rangle + |\uparrow\downarrow\rangle + |\uparrow\uparrow\rangle) \quad (2.211)$$

which obviously has an overlap with dark states in span  $\{|\downarrow\downarrow\rangle, |\uparrow\uparrow\rangle\}$ . This overlap diminishes the probability of a jump  $d_i$  to occur. If the overlap is large (as in this case) the probability that no jump occurs at all becomes large, too. The trajectory at hand is such a history without any jump. But a jump indeed it not necessary since the damping (and subsequent normalisation) via  $\exp(-iH_{\text{eff}})$  gets rid of the non-dark components  $|\downarrow\uparrow\rangle$  and  $|\uparrow\downarrow\rangle$  successively while it preserves the dark states  $|\downarrow\downarrow\rangle$  and  $|\uparrow\uparrow\rangle$ . Hence the system ends up in the Bell state  $|\oplus\rangle = \frac{1}{\sqrt{2}} (|\downarrow\downarrow\rangle + |\uparrow\uparrow\rangle)$  for  $t \rightarrow \infty$  which is consistent with  $\langle \Sigma^z \rangle$  remaining zero and  $\langle \sigma_1^z \sigma_2^z \rangle$  going to one, as depicted in the plot. Note that the other possibility to reach a dark state would have been a jump  $d_i$  with  $d_i |++\rangle = \frac{1}{2} (|\downarrow\downarrow\rangle + |\uparrow\uparrow\rangle)$ . However, the probability for such a trajectory is lower since the energy of  $|++\rangle$  with respect to  $H_p$  is lower than the energy of  $|\downarrow\uparrow\rangle$ .

- In the lower left plot the system is coupled to the two competing baths via  $\kappa_p = 0.1 = \kappa_F$  without unitary dynamics and starts in the completely  $x$ -polarised state as above. Since the unique steady state of this system is mixed, we expect a finite jump density for all times of both  $d_i$  and  $c_i$ , which indeed can be observed in the representative trajectory under consideration. So the single trajectory *cannot* become stationary but rather explores the *ensemble* given by the unique stationary state  $\lim_{t \rightarrow \infty} \rho_+(t)$ . Let us have a closer look at the observables. As expected, each ferromagnetic jump increases the spin-spin correlation  $\langle \sigma_1^z \sigma_2^z \rangle$ . However, since span  $\{|\downarrow\downarrow\rangle, |\uparrow\uparrow\rangle\}$  is not a dark state space of this system, the target states of  $d_i$  decohere due to the damping of  $H_{\text{eff}}$  after each jump. The paramagnetic jumps  $c_i$  increase the  $x$ -magnetisation  $\langle \sigma_1^x \rangle$  up to one exception at  $t \approx 68$ . But be careful: We measure the *first* spins  $x$ -magnetisation and  $c_1$  certainly will increase this quantity. However, imagine the system ended up in the state  $1/\sqrt{2} (|++\rangle + |--\rangle)$  for instance. Then we get  $\langle \sigma_1^x \rangle = 0$ . Now apply  $c_2$  on the *second* spin which yields  $|-\rangle$  after normalisation. But now we clearly find  $\langle \sigma_1^x \rangle = -1$ . We conclude that the *local*  $x$ -magnetisation may be diminished or even flipped by other jump operators. This is what happened at  $t \approx 68$  and we therefore conclude that  $c_2$  occurred at this point in the jump history.
- In the lower right plot the same system with an additional unitary dynamics  $J = 0.5 = h$  gave rise to the jump trajectory. The steady state remains unique and mixed and the jump record does not change qualitatively. The imprint of the unitary dynamics is the (damped) oscillatory behaviour between subsequent jumps. Note that the frequency of these oscillations depends on the energy of the current state with respect to  $H_p$ . If, by chance, the state jumps into an energy eigenstate<sup>47</sup> of  $H_p$  it remains there until another jump occurs. This happens at  $t \approx 12$  perfectly and *almost* perfectly at  $t \approx 59$  where the period of the oscillation is comparatively large.

<sup>47</sup>Since there is no dark state for this system, the parent Hamiltonian becomes a positive operator with finite ground state energy. As a consequence, the probability of a trajectory where the system remains in an eigenstate of  $H_p$  becomes zero for  $t \rightarrow \infty$ . I.e. the state can become stationary for *some time*, but eventually a jump will occur.

Although we cannot gain insight into the *ensemble evolution* (described by the Lindblad master equation) by inspection of single jump trajectories, we learned several new things about the specific processes which give rise to this evolution. Moreover, this examination of specific examples completes the rather abstract treatment of the quantum trajectory interpretation given in the introductory subsection 1.1.3.



■ **Figure 2.29:** Four single realizations of quantum jump trajectories for the 2-spin TIM. We show the three observables  $\sigma_1^x$ ,  $\sigma_1^z \sigma_2^z$  and the mean z-magnetisation  $\Sigma^z$  in the upper part of each plot. In the lower part each impulse marks a quantum jump at a specific time. Red (blue) impulses denote a ferromagnetic jump  $d_i$  (paramagnetic jump  $c_i$ ). In the upper row the parameters  $J = 0 = h$ ,  $\kappa_P = 0$  and  $\kappa_F = 0.1$  were used to simulate the purely dissipative ferromagnetic bath. For the initial state  $|\downarrow\uparrow\rangle$  (upper left plot) there is no overlap with the dark state space and the only possibility to reach a dark state is a discontinuous quantum jump  $d_i$  (red impulse). The resulting dark state is  $|\uparrow\uparrow\rangle$ . For the initial state  $|++\rangle$  (upper right plot) there is a huge overlap with dark states so that the probability of a jump is diminished. The non-unitary evolution by  $H_{\text{eff}}$  eliminates the non-dark components of the initial state and the system ends up in the dark state  $|\uparrow\uparrow\rangle + |\downarrow\downarrow\rangle$  (note that  $\Sigma^z$  vanishes!). In the lower part of the plot, longer time intervals are shown for competing baths  $\kappa_P = 0.1 = \kappa_F$  without ( $J = 0 = h$ ) and with ( $J = 0.5 = h$ ) unitary dynamics. Since the steady states are mixed, there is a non-vanishing jump density for all times. Note that  $d_i$ -jumps (red impulses) increase the correlation  $\sigma_1^z \sigma_2^z$  whereas  $c_i$ -jumps (blue impulses) increase the x-polarisation  $\sigma_x^1$  if they occur on site 1. If the unitary dynamics is switched on, the periods which separate subsequent jumps are characterized by a damped, oscillatory behaviour. Further remarks can be found in the text.

### 2.6.3 Dissipative transverse field Ising model in one and two dimension(s)

In the previous section the simplest instance of the dissipative transverse field Ising model, namely 2 coupled spins, was examined by means of a quantum trajectory Monte Carlo simulation. There were three reasons to do this: First, the simulation complemented the *analytical* treatment of this system which was introduced for didactical purposes<sup>48</sup> in section 2.5. Second, we verified the correctness of the QTMC algorithm in general and the authors implementation of the latter in particular. And thirdly, we got a feel for actual quantum trajectories of the dissipative TIM, that is, the action of the ferromagnetic and paramagnetic jump operators.

Nevertheless the real purpose of QTMC simulations is the investigation of many-body systems that are notoriously hard to treat analytically. Recall that the basic concept is to pay for tractable mathematical representations and operations (meaning: smaller vectors & matrices) by statistical uncertainties that come along with the sampling approach. In our case this bargain reads as follows: To treat a dissipative system with, say, 10 spins in a numerically exact fashion one had to compute the matrix exponential of a  $4^{10} \times 4^{10} = 1.048.576 \times 1.048.576$  complex valued, in general non-Hermitian matrix<sup>49</sup> (the Lindbladian superoperator) for each time  $t$ . This usually involves a diagonalisation or, in the non-Hermitian case, block diagonalisation in terms of (generalised) eigenvectors. This is intractable on a modern workstation PC — at least in a reasonable amount of time. In contrast, the QTMC simulation requires just the *multiplication* of a complex *vector* of size  $2^{10} = 1024$  with a fixed matrix of corresponding dimension<sup>50</sup>. This is tractable but the drawback is sampling: The simple matrix-vector multiplications has to be performed countless times to yield adequate results with small statistical fluctuations. Nevertheless it is still preferable to have (more or less) noisy results than to have no results *at all*.

In the subsequent paragraphs we follow this idea and discuss the results of QTMC simulations for small instances of the purely dissipative TIM in one and two dimensions.

#### Quantum jump trajectories

Let us first have a look at single quantum jump trajectories. In Fig. 2.30 we present four single realisations of a quantum jump trajectory for one-dimensional systems with periodic boundary conditions. All four simulations were performed with time steps of  $\Delta t = 0.001$  for  $0 \leq t \leq 100$  and with a completely  $z$ -polarised initial state,  $|\Psi_0\rangle = |\uparrow\rangle$ . The system sizes were  $L = 2$  (A), 4 (B), 6 (C), and 8 (D) spins and the couplings were fixed at  $\sqrt{\kappa_P} = 1$  and  $\sqrt{\kappa_F} = 3$ . For each trajectory we measured the average  $z$ -polarisation (red line), namely  $\langle \Sigma^z \rangle = L^{-1} \sum_i \langle \sigma_i^z \rangle$ , and the nearest neighbour correlation  $\langle \sigma_1^z \sigma_2^z \rangle$  (light grey line). Below each plot we illustrate the occurrence of jumps with respect to time by impulses on the grey time line where blue and black marks represent paramagnetic and ferromagnetic jumps, respectively. Let us have a closer look:

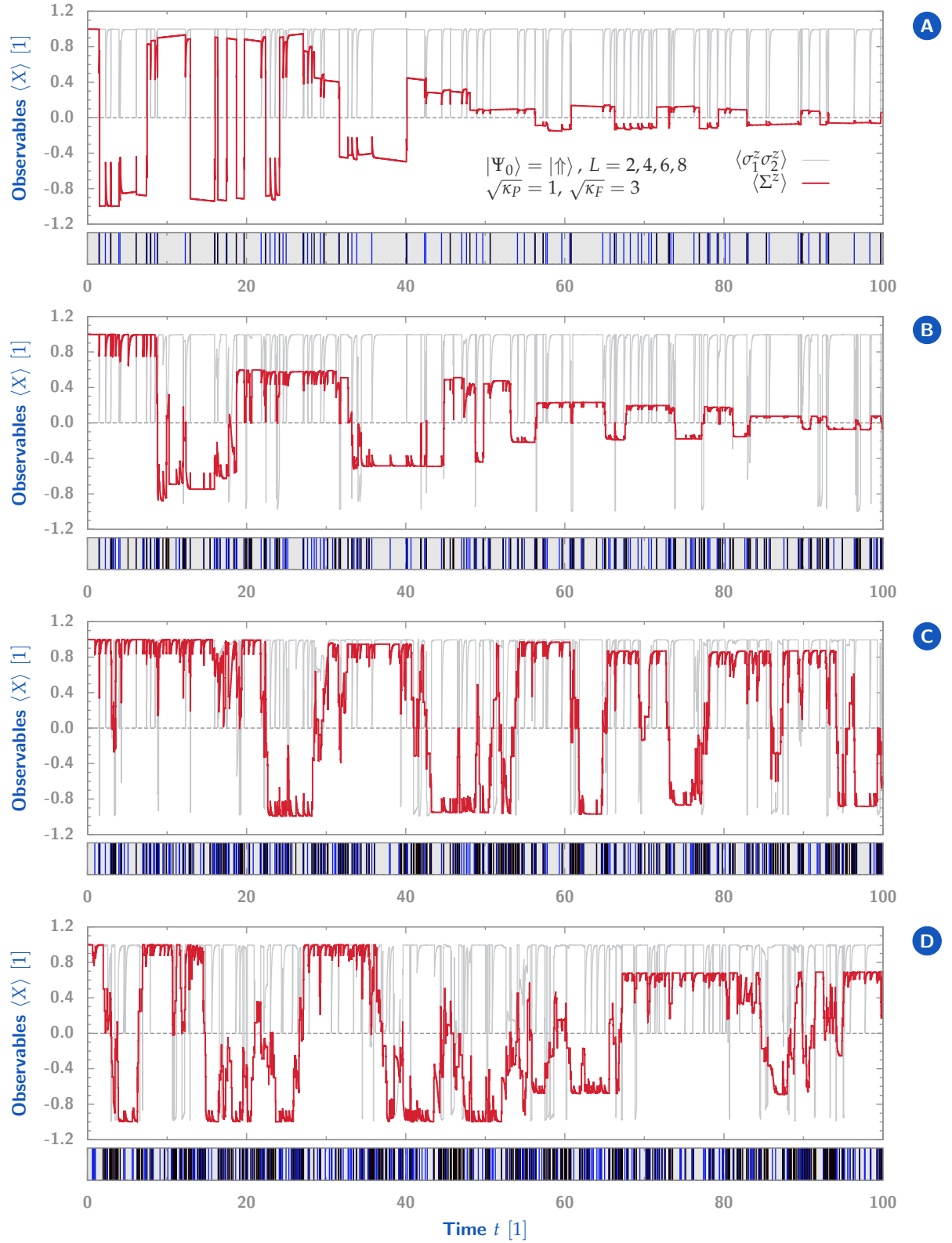
- The correlation remains positive and close to 1 most of the time, for all system sizes. A thorough inspection of the jump history reveals that the dents in the correlation plot go along with blue, that is, paramagnetic jumps. These paramagnetic jumps are often

<sup>48</sup>Not only for the reader but for the author as well.

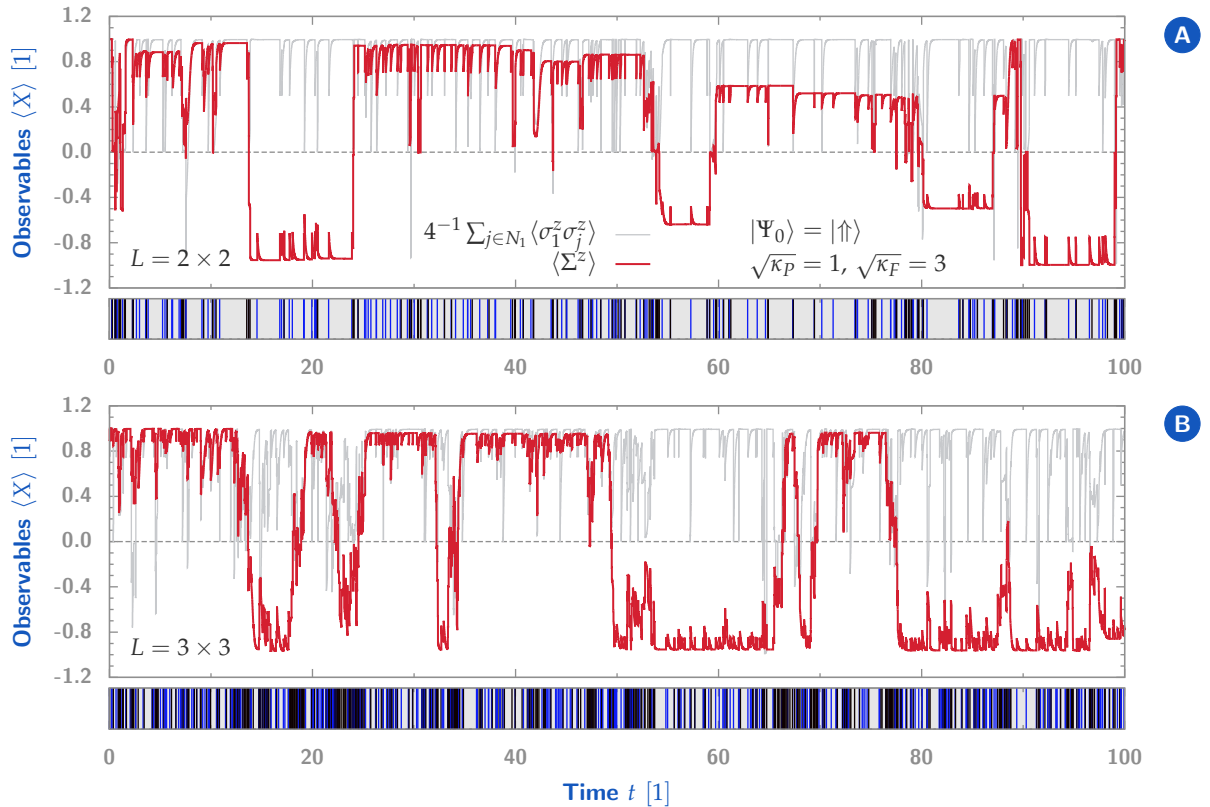
<sup>49</sup>To convey a feeling: Merely holding the matrix in the RAM in terms of complex doubles requires  $\sim 17$  terabytes of memory. Of course this a rough estimate that ignores the fact that (quasi-) locally coupled systems can be described by *sparse matrices* that require less storage capacity. This, however, does not affect the ultimate problem of an exponential scaling of resources.

<sup>50</sup> For comparison: The vector requires not more than 16 kilobytes and the matrix roughly 17 megabytes of RAM.





■ **Figure 2.30:** Quantum jump trajectories of the purely dissipative TIM for parameters  $\sqrt{\kappa_P} = 1$  and  $\sqrt{\kappa_F} = 3$  in one dimension. We simulated chains of size  $L = 2$  (A),  $L = 4$  (B),  $L = 6$  (C), and  $L = 8$  (D) and measured the nearest-neighbour correlation  $\langle \sigma_1^z \sigma_2^z \rangle$  and the average  $z$ -magnetisation  $\langle \Sigma^z \rangle$ . Impulses in the grey bar below each observable plot encode single quantum jumps (blue:  $d_i$ , black:  $c_i$ ). The initial state was completely polarised, namely  $|\Psi_0\rangle = |\uparrow\rangle$ . Details are given in the text.



■ **Figure 2.31:** Quantum jump trajectories of the purely dissipative TIM for parameters  $\sqrt{\kappa_P} = 1$  and  $\sqrt{\kappa_F} = 3$  in two dimensions. We simulated plaquettes of size  $L = 2 \times 2$  (A) and  $L = 3 \times 3$  (B) with PBC and measured the nearest-neighbour correlation  $\langle \sigma_1^z \sigma_j^z \rangle$  and the average z-magnetisation  $\langle \Sigma^z \rangle$ . Impulses in the grey bar below each observable plot encode single quantum jumps (blue:  $d_i$ , black:  $c_i$ ). The initial state was completely polarised, namely  $|\Psi_0\rangle = |\uparrow\rangle$ . Compare these trajectories to the one-dimensional results in Fig. 2.30. Details are given in the text.

followed by a subsequent ferromagnetic jump (most of the black impulses are actually combinations of a paramagnetic (blue) jump followed by a ferromagnetic (black) jump shortly after) which restores the correlation to unity. This mechanism, paramagnetic jumps followed by ferromagnetic ones which (try to) revert the actions of the preceding jump, is responsible for the typical evolution of the correlation function, that is, a horizontal line at 1 intermitted by sharp peaks.

- The total z-magnetisation starts at 1 due to the chosen initial state  $|\Psi_0\rangle = |\uparrow\rangle$ . What follows is an interesting evolution of long periods with almost constant magnetisation that repeatedly change sign almost instantaneously. This “metastability” of z-polarisation is a manifestation of the ferromagnetic jump operators and may be compared to the metastability of a *classical* two-dimensional and *finite* Ising system in the ferromagnetic phase just below the critical temperature. Let us try to reveal the mechanism that is responsible for the conversion by inspection of its first occurrence in plot (A). A closer look at the first impulse on the time line reveals that it is a typical combination of a blue line followed immediately by a black one, i.e. a paramagnetic jump followed by ferromagnetic one.

Then we can just write down what happened (let us assume that the first jump affected the first spin and omit normalisations):

$$|\uparrow\uparrow\rangle \xrightarrow{c_1=1/2\sigma_1^z(\mathbb{1}-\sigma_1^x)} |\uparrow\uparrow\rangle + |\downarrow\uparrow\rangle \xrightarrow{d_2=1/2\sigma_2^x(\mathbb{1}-\sigma_2^z\sigma_1^z)} |\downarrow\downarrow\rangle$$

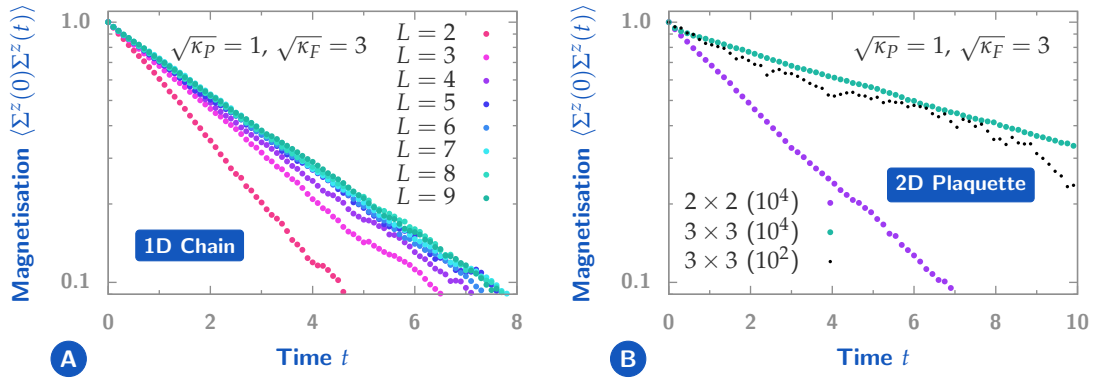
Note that the conversion was a coincidence since the (equiprobable) action of  $d_1$  would have reversed the effect of  $c_1$  completely. We realise that this characteristic behaviour of the average (or total)  $z$ -magnetisation is a *cooperative effect* of both, ferromagnetic and paramagnetic jumps: The conversions are *initiated* by paramagnetic jumps but *conducted* by the ferromagnetic operators. In the larger systems it becomes clear that not all initiated conversions actually succeed. Some reach a depolarised state ( $\langle \Sigma^z \rangle \approx 0$ ) but return to the previous sign afterwards, see (D) for instance. Clearly this is due to the requirement of a *sequence* of ferromagnetic jumps that traverses the complete system. In one dimension the diffusion of domain walls (i.e. adjacent spins with negative correlation) is equiprobable in both directions. Thus the retraction and subsequent annihilation of a domain with negative sign is not unlikely.

- There is another obvious effect concerning the the average  $z$ -magnetisation: Its amplitude decreases in time. The absolute value of the plateaus tends to zero for  $t \rightarrow \infty$  in stages and not continuously. Furthermore note that the correlation (see especially (A)) remains 1 although the magnetisation vanishes. That leads to the conclusion that a cooperative effect of jumps must be responsible for this effect as it creates *superpositions*  $\alpha |\uparrow\uparrow\rangle + \beta |\downarrow\downarrow\rangle$  of perfectly correlated states. Clearly this superposition is not symmetric, i.e.  $|\alpha| \neq |\beta|$ , since the magnetisation does not vanish completely (but it becomes more symmetric during in time). The basic jump sequence responsible for this effect is easily explained:

$$\begin{aligned} |\uparrow\uparrow\rangle &\xrightarrow{c_1} |\uparrow\uparrow\rangle + |\downarrow\uparrow\rangle \xrightarrow{\exp(-H_P\delta t)} \alpha |\uparrow\uparrow\rangle + \beta |\downarrow\uparrow\rangle \\ &\xrightarrow{c_2} \alpha |\uparrow\uparrow\rangle + \alpha |\uparrow\downarrow\rangle + \beta |\downarrow\uparrow\rangle + \beta |\downarrow\downarrow\rangle \\ &\xrightarrow{d_1} \alpha |\downarrow\downarrow\rangle + \beta |\uparrow\uparrow\rangle \end{aligned}$$

There are some comments in order: The completely symmetric state  $|\uparrow\uparrow\rangle + |\downarrow\downarrow\rangle$  can be reached by the (fast) sequence of jumps  $d_1 c_2 c_1$ . The plots however suggest that there are also superpositions with a residual magnetisation  $0 < |\langle \Sigma^z \rangle| < 1$  which requires an asymmetric superposition  $\alpha |\uparrow\uparrow\rangle + \beta |\downarrow\downarrow\rangle$ . This can be achieved by a modification of the *time span* between the first ( $c_1$ ) and the second ( $c_2$ ) jump where the system evolves non-unitarily according to the parent Hamiltonian  $H_P$ . For a dominant ferromagnetic bath its eigenstates are close to the eigenstates of  $\sigma_i^z$ ; hence the system evolves towards its ground state(s) which in our case read (approximately)  $|\uparrow\uparrow\rangle$  and  $|\downarrow\downarrow\rangle$ . Consequently we find  $|\alpha| > |\beta|$  after the time span  $\delta t$  which is responsible for the residual magnetisation in the end.

In a nutshell: A combination of paramagnetic and ferromagnetic jumps as well as the non-unitary evolution by the parent Hamiltonian are responsible for the successive loss of macroscopic magnetisation. That is, the system *symmetrises* asymmetric initial states for  $t \rightarrow \infty$ , essentially due to the action of paramagnetic jump operators, but nevertheless remains most of the time in a subspace with non-vanishing correlations (that in turn depend on the ratio of  $\kappa_P$  and  $\kappa_F$ ).



■ **Figure 2.32:** Relaxation of the z-magnetisation in a purely dissipative TIM in one (A) and two (B) dimension(s). All simulations were performed with PBC and the parameters  $\sqrt{\kappa_P} = 1$  and  $\sqrt{\kappa_F} = 3$ . The initial state was completely polarised,  $|\Psi_0\rangle = |\uparrow\rangle$ , and therefore the global magnetisation  $\langle \Sigma^z(t) \rangle$  equals the time correlation  $\langle \Sigma^z(0) \Sigma^z(t) \rangle$ . The simulations in one dimension (A) were performed on systems with  $L = 2, 3, \dots, 9$  spins; in two dimensions (B) plaquettes with dimensions  $L = 2 \times 2$  and  $L = 3 \times 3$  were examined. Note that the global magnetisation vanishes exponentially in both cases. In the one dimensional system this relaxation clearly remains exponential in the thermodynamic limit since results show a limiting behaviour for  $L \rightarrow \infty$ . In the two dimensional setup such a conclusion cannot be drawn due to a lack of different system sizes. However, it becomes evident that the  $L = 9$  spin *plaquette* loses its magnetisation much slower than the corresponding  $L = 9$  spin *chain*. Further comments are given in the text.

- The total jump density per time obviously increases with the system size as the jump sequences reveal. This is to be expected since the number of jumps *per site and time* remains constant. Since we mark any jump anywhere in the system with an impulse on the time line, the density of impulses increases for larger systems.

For comparison and to conclude this first part we simulated *two-dimensional* plaquettes with dimensions  $L = 2 \times 2$  (A) and  $L = 3 \times 3$  (B) in Fig. 2.31. The parameters were the same as for the one-dimensional systems above. Instead of the fixed correlation  $\langle \sigma_1^z \sigma_2^z \rangle$  we show the average correlation of spin 1 and its nearest neighbours,  $4^{-1} \sum_{j \in N_1} \langle \sigma_1^z \sigma_j^z \rangle$ .

The qualitative structure of the trajectories remains unaltered as a comparison with Fig. 2.30 reveals. The trajectory in (B) conveys the *clustering* of jumps at the points of time when a conversion of the average magnetisation takes place. These short periods of increased jump frequencies are separated by long periods of comparatively low jump rates where paramagnetic jumps are immediately followed by ferromagnetic jumps that revert the preceding actions. The regions of  $\langle \Sigma^z \rangle > 0$  and  $\langle \Sigma^z \rangle < 0$  can be considered as *dynamical phases* and the periods of increased jump rates qualify as *dynamical phase transitions* accordingly. Note that the vanishing of the magnetisation in the  $L = 3 \times 3$  setup seems to be suppressed. We cannot infer any *quantitative* changes from a single trajectory, though. To this end we analysed the relaxation of  $\langle \Sigma^z \rangle$  quantitatively in the following paragraph.

#### Relaxation of magnetisation

As the quantum trajectories suggest there are *two* reasons for the average magnetisation  $\langle \Sigma^z \rangle$  to vanish in time if one considers the time evolution of the *ensemble*  $\rho(t)$  (described by the Lindblad master equation):

1. The conversion of the quantum mechanical expectation value  $\langle \Sigma^z \rangle_\Psi$  as observed for single quantum trajectories  $|\Psi(t)\rangle$  causes a decay of the ensemble average  $\langle \Sigma^z \rangle_\rho$  for the complete evolution  $\rho(t)$  of the system. This would be the case even if the single trajectories were completely polarised,  $|\langle \Sigma^z \rangle_\Psi| = 1$ , for all times.
2. The vanishing of  $\langle \Sigma^z \rangle_\Psi$  for a single trajectory due to the action of the paramagnetic bath reduces the ensemble average  $\langle \Sigma^z \rangle_\rho$  further.

The combination of both effects results in an exponential decay of the average magnetisation for completely polarised initial states; this can be seen in Fig. 2.32 where we computed the time evolution of  $\langle \Sigma^z \rangle_\rho$  for the same parameters as before in one (A) and two (B) dimensions. We did this for various system sizes  $L = 2, \dots, 9$  (chain) and  $L = 2 \times 2, 3 \times 3$  (plaquette) and performed  $10^4$  samples for each of them to obtain results without too much statistical fluctuations<sup>51</sup>.

We have to point out that the  $2 \times 2$  plaquette and the 4-spin chain (both with PBC) are actually the *same* system. This explains why the plots of both systems in (A) and (B) coincide up to statistical fluctuations. This is not so much a bug as a feature since it provides us with a common reference system. There are two findings to be stressed:

- If one considers the change of the relaxation process in one dimension as the system size  $L$  increases, it becomes evident that there must be a *limiting curve* for the family of curves in the thermodynamic limit  $L \rightarrow \infty$ . This limit must be close to the  $L = 9$  curve since the shifting of the preceding curves for  $L = 6, 7$ , and  $8$  is already very small. We conclude that in *one dimension* the relaxation of the average magnetisation is exponential in the thermodynamic limit and for the chosen relative coupling  $\sqrt{\kappa} = 1/3$  (which describes a system of dominant ferromagnetic dissipation after all). There are two possible reasons for this behaviour which are not mutually exclusive: First, there is no dissipative phase transition in one dimension and the system remains in a paramagnetic phase for all finite  $\kappa$ . This is probably true as there is numerical evidence that the dissipative gap of the Lindbladian does not close in the thermodynamic limit in one dimension. Second, even in the presence of a genuine phase transition and in the ferromagnetic phase the magnetisation might decay over time due to second mechanism described above. In the end, the symmetry broken phase is indicated by a finite *correlation*  $\lim_{|i-j| \rightarrow \infty} \langle \sigma_i^z \sigma_j^z \rangle_\rho > 0$  in the ensemble description and not by a finite global magnetisation.
- Clearly there are not enough data sets available in (B) to draw analogous conclusions for the two-dimensional setup. As it is illusory to simulate  $L = 4 \times 4 = 16$  spins with the code and hardware at my disposal, there is no way to answer the question whether there is an analogous limiting curve with finite slope — at least not with the QTMC simulation. But we *can* infer that the relaxation, though exponential, is much slower in two dimensions than in one dimensional systems of similar size. Compare the slope of the  $L = 9 = 3 \times 3$  curves (green points) in that regard. This quantifies our previous impression that the height of the magnetisation plateaus of single trajectories decreases slower in two than in one dimensions. Note that the relaxation of the  $3 \times 3$  plaquette is already much slower than the suspected rate of the chain *in the thermodynamic limit*.

As we identified the correlation as *the* crucial quantity that indicates the phase transition in a statistical ensemble of quantum states<sup>52</sup>, it is natural to ask how  $\langle \sigma_1^z \sigma_j^z \rangle$  depends on the distance  $j$  and the relative coupling  $\kappa$ . So let us go into this matter.

<sup>51</sup>To demonstrate the effect of too few samples we included one of the first results with just 100 trajectories in plot (B).

<sup>52</sup>Which is given by the pseudo probability distribution  $\rho$ , i.e. the density matrix.

## Correlations

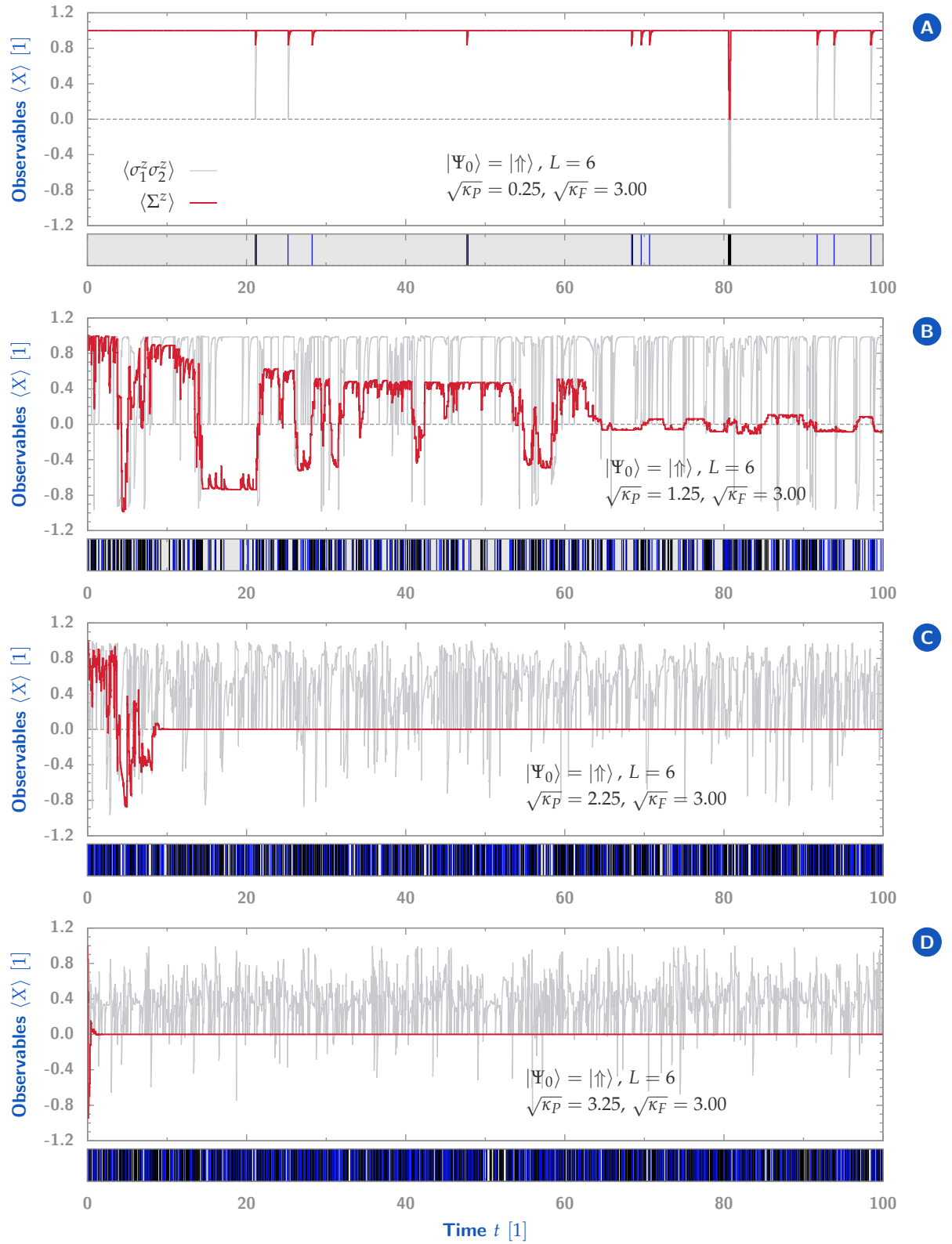
To conclude this section we examined the  $\kappa$ -dependence of both, single trajectories and the expectation values of spin-spin correlations in one and two dimensions. Let us start with the quantum jump trajectories shown in Fig. 2.33. They describe the dynamics of a  $L = 6$  spin chain with PBC and completely polarised initial state for fixed  $\sqrt{\kappa_F} = 3$  and varying  $\sqrt{\kappa_P} = 0.25, 1.25, 2.15$  and  $3.25$  (top down). Let us discuss the results:

- In (A) the ferromagnetic bath dominates the paramagnetic one completely. Both, the correlation and the magnetisation are 1 and constant up to few paramagnetic jumps. In the shown period of time their actions are either immediately reverted by a subsequent ferromagnetic jump (e.g. first jump from the left) or smoothed out by the non-unitary evolution of the parent Hamiltonian<sup>53</sup> (e.g. second and third jumps from the left).
- For larger  $\kappa_P$  the conversions of  $\langle \Sigma^z \rangle$  become visible within the shown time interval and the gradual relaxation of the plateaus is apparent (B). Due to the characteristic structure of the trajectories it seems natural to assume that the magnetisation decreases inevitably and *cannot* increase due to some restrictions of the jump operators. The trajectory in (B) disproves this assumption, cf. the magnetisations at  $t \sim 68$  and  $t \sim 98$ . The magnetisation *can* increase but our experience shows that this is rather unlikely. To cut the matter short: The decrease of magnetisation can be (partially) inverted for single trajectories — but it cannot for the *ensemble*.
- There actually *is* a “microscopically” irreversible process as the trajectories in (C) and (D) suggest: When the magnetisation vanishes identically at one point of time, it remains zero thereafter. This happens quite rapidly for strong paramagnetic couplings as (D) shows. We already figured out that fast sequences of paramagnetic and ferromagnetic jump operators can create states of vanishing magnetisation. For this effect we do not even require ferromagnetic operators: As there is a high *paramagnetic* jump density, it is not unlikely that the state ends up temporarily as  $|\Psi(t)\rangle = |+\rangle^{\otimes L}$ , that is, an eigenstate of  $X \equiv \prod_i \sigma_i^x$  with vanishing  $z$ -magnetisation.

It is important to keep in mind that this is *not* a dark state — there is none! This becomes also clear if one considers the correlation which keeps changing rapidly; obviously there are lots of jumps per time and the state is far from being stationary. Nevertheless the magnetisation remains identically zero which demands a symmetry argument. To this end note that our system features a (strong)  $\mathbb{Z}_2$  symmetry, namely the global spin-flip  $X$ . Assume that  $|\Psi(t)\rangle = |+\rangle^{\otimes L}$  at some point  $t$  of the trajectory. At a later time  $t + \delta t$  the state evolved according to some sequence of jumps ( $L_{i_k}$ ) with  $L_{i_k} \in \{d_j, c_j\}$  intermitted by periods of non-unitary evolution  $\exp(-H_P \Delta t_k)$  (up to normalisation). If we denote this evolution by  $U$ , it follows

$$\begin{aligned}
 \langle \Psi(t + \delta t) | \Sigma^z | \Psi(t + \delta t) \rangle &= \langle \Psi(t) | U^\dagger \Sigma^z U | \Psi(t) \rangle \\
 &= - \langle \Psi(t) | U^\dagger X^\dagger \Sigma^z X U | \Psi(t) \rangle \\
 &= - \langle \Psi(t) | X^\dagger U^\dagger \Sigma^z U X | \Psi(t) \rangle \\
 &= - \langle \Psi(t) | U^\dagger \Sigma^z U | \Psi(t) \rangle = - \langle \Psi(t + \delta t) | \Sigma^z | \Psi(t + \delta t) \rangle
 \end{aligned}$$

<sup>53</sup>Note that paramagnetic jumps preserve an overlap with the ferromagnetic dark states.



■ **Figure 2.33:** Quantum jump trajectories of the purely dissipative TIM for  $L = 6$  spins and different parameters  $\kappa_P$  (fixed  $\kappa_F = 3$ ) in one dimension with PBC. We simulated chains with increasing coupling to the paramagnetic bath, namely  $\sqrt{\kappa_P} = 0.25$  (A), 1.25 (B), 2.25 (C), and 3.25 (D) and measured the nearest-neighbour correlation  $\langle \sigma_1^z \sigma_2^z \rangle$  and the average  $z$ -magnetisation  $\langle \Sigma^z \rangle$ . Impulses in the grey bar below each observable plot encode single quantum jumps (blue:  $d_i$ , black:  $c_i$ ). The initial state was completely polarised, namely  $|\Psi_0\rangle = |\uparrow\rangle$ . Details are given in the text.

Here we used the strong symmetry of the dissipative process, namely  $[d_i, X] = 0$ ,  $\{c_i, X\} = 0$  and hence  $[H_P, X] = 0$  for all sites  $i$ . We conclude that  $\langle \Psi(t + \delta t) | \Sigma^z | \Psi(t + \delta t) \rangle = 0$  for all  $\delta t \geq 0$ . This is exactly what we observe in (C) and (D).

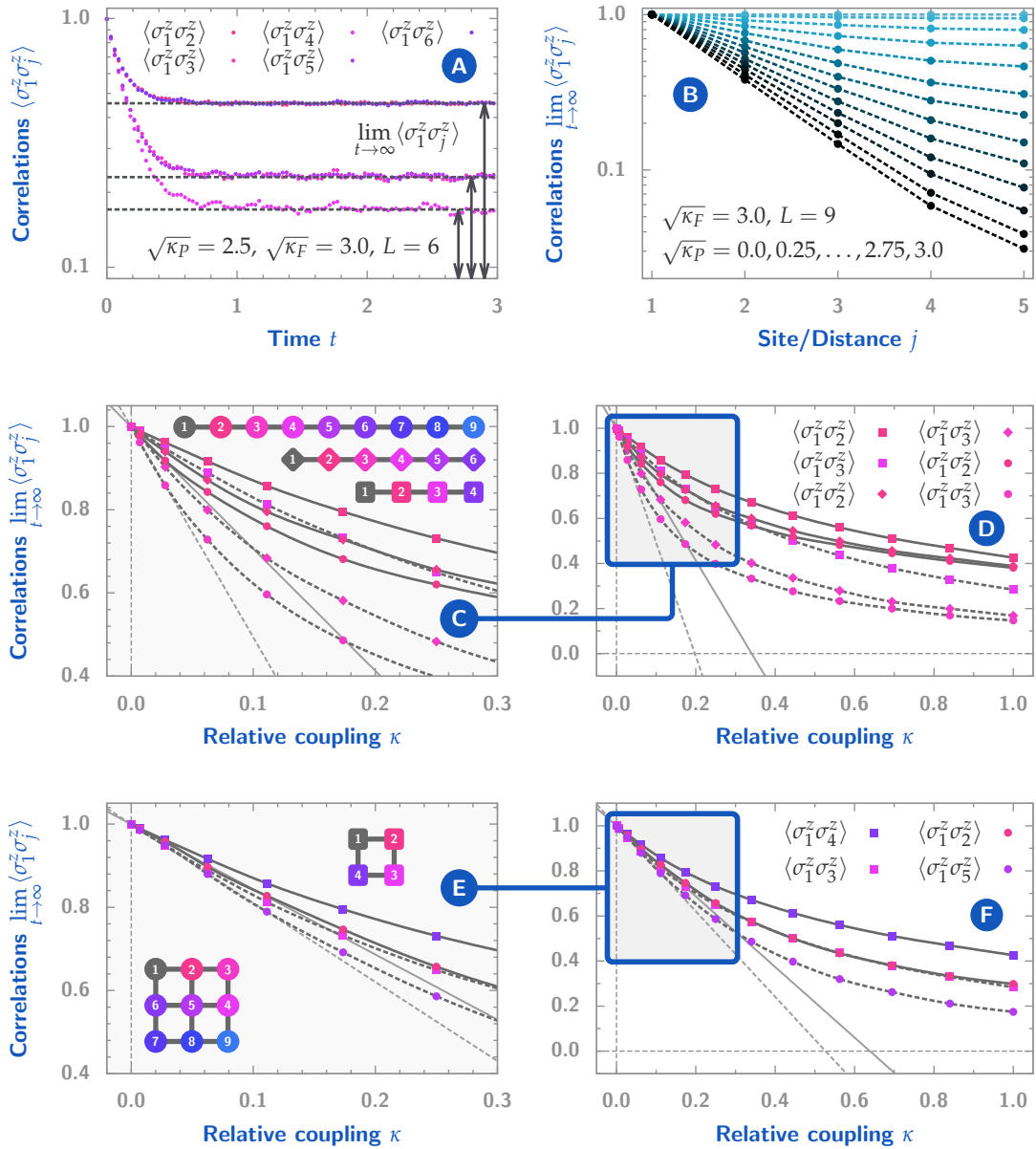
Let us now turn towards a quantitative analysis of the correlations and their dependence on the relative coupling  $\kappa$ .

In Fig. 2.34 we condense our results of a family of simulations for chains with  $L = 4, 6$  and 9 spins and plaquettes of size  $L = 2 \times 2$  and  $3 \times 3$ . The initial state was still completely polarised; this is irrelevant though as we are interested in the steady state correlations which are independent of the initial conditions. We measured the correlations  $\langle \sigma_1^z \sigma_j^z \rangle$  for  $j = 2, \dots, L$  for chains with time steps  $\Delta t = 0.001$  and  $0 \leq t \leq 3$ . This is shown in (A) exemplarily for a  $L = 6$  spin chain and with couplings  $\sqrt{\kappa_P} = 2.5$ ,  $\sqrt{\kappa_F} = 3.0$ . The correlations reach their steady state value  $\lim_{t \rightarrow \infty} \langle \sigma_1^z \sigma_j^z \rangle$  quickly and we extract their numerical value by horizontal fits denoted by dashed black lines. The same can be done for plaquettes where we measure the correlations  $\langle \sigma_1^z \sigma_j^z \rangle$  for  $j = 4, 3$  ( $L = 2 \times 2$  setup) and  $j = 2, 5$  ( $L = 3 \times 3$  setup). The spin labels refer to the pictorial illustrations of the simulated systems in (C) and (E). Note that due to the periodic boundary conditions there are just nearest and next-nearest neighbour correlations that can be measured in the small two-dimensional systems under investigation. As a consistency check we show all five possible correlations of the  $L = 6$  spin chain in (A). Evidently  $\langle \sigma_1^z \sigma_2^z \rangle = \langle \sigma_1^z \sigma_5^z \rangle$  and  $\langle \sigma_1^z \sigma_3^z \rangle = \langle \sigma_1^z \sigma_4^z \rangle$  which is to be expected due to the periodic boundary conditions. With the procedure described above we obtained values for the relevant correlations for varying relative couplings via  $\sqrt{\kappa_P} = 0, 0.25, \dots, 3.0$  (fixed  $\sqrt{\kappa_F} = 3$ ), different system sizes and geometries. We present the results in the remaining plots of Fig. 2.34, namely (B), (C), (D), (E), and (F):

- In (B) we show the steady state correlations  $\lim_{t \rightarrow \infty} \langle \sigma_1^z \sigma_j^z \rangle$  in dependence of  $j$  on a  $L = 9$  spin chain for varying  $\kappa$  as an array of curves. The dashed lines are drawn to keep track of the related points and bear no physical meaning. We conclude that the correlations decay exponentially with the distance in one dimensional systems. The rate of decay depends crucially on the relative couplings and increases with the strength of the paramagnetic bath. This is a typical behaviour for spatial correlations in quasilocal physical systems with a dissipative gap<sup>54</sup>. The reader may have noticed that the exponential decay is modified for  $j = 5$  where the correlations are larger as expected. This is a finite-size effect and caused by the periodic boundary conditions since the correlation at  $j = 6$  equals the one at  $j = 4$  and is therefore *larger* than the minimum at  $j = 5$ . This presumably lifts the correlation at  $j = 5$  above the exponential level. Note that this effect is also visible in (A) where one would expect equidistant gaps between the horizontal fits due to the logarithmic correlation axis.
- In the plots below, namely (D) and (F), we show the  $\kappa$ -dependence of the nearest and next-nearest neighbour correlation for the various system sizes. The plots (C) and (D) show the marked boxes of the corresponding plots in detail. The points of the nearest (next-nearest) neighbour correlations are connected by continuous (dashed) splines for clarity. We furthermore computed linear fits at the first few points of the  $L = 9 = 3 \times 3$  systems for small paramagnetic coupling  $\kappa < 0.1$  to emphasise the asymptotic behaviour for  $\kappa \rightarrow 0$ .
- As expected the correlations decrease for increasing  $\kappa$ . This is true for both, the nearest and next-nearest correlations, albeit the next-nearest neighbour correlations decrease faster for small couplings than the nearest neighbour correlations. Note that the curves for  $L = 4$  in

<sup>54</sup>As the system is finite, the spectrum is discrete and therefore trivially gapped. The question whether this behaviour (and the gap) survives in the *thermodynamic limit* cannot be inferred from this set of data.





■ **Figure 2.34:** QTM simulation of the purely dissipative TIM in one and two dimensions. In (A) we show exemplarily for  $\sqrt{\kappa_P} = 2.5$  and  $\sqrt{\kappa_F} = 3$  the time evolution of correlations  $\langle \sigma_1^z \sigma_j^z \rangle$  for  $j = 2, \dots, 6$  on a  $L = 6$  chain with PBC. The initial state is completely polarised,  $|\Psi_0\rangle = |\uparrow\rangle$ . The horizontal fits are used to extract the steady state correlations  $\lim_{t \rightarrow \infty} \langle \sigma_1^z \sigma_j^z \rangle$  as shown in the remaining plots. In (B) we show the steady state correlations for  $j = 1, \dots, 5$  of a  $L = 9$  chain in a logarithmic reference frame for varying  $\kappa$ . In (D) we show the nearest- (solid lines) and next-nearest- (dashed lines) neighbour correlations with respect to the relative coupling  $\kappa$  for chain sizes  $L = 4, 6, 9$ . Plot (C) shows in detail the marked box in plot (D). In (F) we show the nearest- and next-nearest neighbour correlations with respect to the relative coupling  $\kappa$  for plaquettes with dimensions  $L = 2 \times 2$  and  $L = 3 \times 3$ . Plot (E) shows in detail the marked box in plot (F). The solid (dashed) light-grey lines in (C), (D), (E), and (F) denote linear fits to the first few points of the shown nearest- (next-nearest-) neighbour correlations of the  $L = 9$  spin systems. The colour of the marks in the four plots (C), (D), (E), and (F) encodes  $j$  (in  $\langle \sigma_1^z \sigma_j^z \rangle$ ), their shape encodes the system size  $L$ ; see the pictorial illustration of the simulated systems printed as insets of (C) and (E). All systems were simulated with PBC. A detailed description is given in the text.

one and  $L = 2 \times 2$  in two dimensions coincide as these are the same systems. It is crucial to realise that the curves in both dimensions and for both, the nearest and next-nearest neighbour correlations, are bend down for larger systems. That this involves a change of shape and not just a shift towards smaller correlations can be seen from the data in (D). A manifestation of a genuine phase transition in the thermodynamic limit would be a curve that originates at 1 for  $\kappa = 0$  and decreases (presumably linearly<sup>55</sup>) until it hits the  $\kappa$ -axis at the critical value  $\kappa_c$ . For  $\kappa \geq \kappa_c$  one expects the correlation to vanish identically for  $j \rightarrow \infty$ . Such a behaviour cannot be observed for any finite system though. In these cases one would expect smooth curves that fit to the limiting curve from above in the limit  $L \rightarrow \infty$ . This tendency can be observed in (C) and (E). A non-trivial phase transition demands  $\kappa_c > 0$ . Unfortunately it is not possible to infer this without any doubt from the small systems depicted in (C) and (E). As we already suspected that  $\kappa_c = 0$  in *one dimension*, it seems reasonable that the curves for larger  $j$  and  $L$  fit asymptotically to the vertical correlation axis. This is *not* evident for the two dimensional system in (E) where, first, the difference in correlations to nearest and next-nearest neighbours is much smaller (cf. (C)), and second, the curves of the next-nearest neighbour correlations fit already quite convincing to straight lines (cf. (C)) with finite slope, as one would expect for  $\kappa_c \approx 0.5$  (see (F)).

To sum it up: The behaviour of the correlations supports our conjecture that there is no phase transition *in one dimension*. The behaviour for *two dimensional* systems is quantitatively different and does not rule out a phase transition, that is, a finite  $\kappa_c$ . As we cannot provide data for larger systems, it remains an open question whether the lower critical dimension  $d_c$  of the dissipative transverse field Ising model equals or exceeds 2.

This concludes our discussion of the QTMC results in particular and our discussion of the dissipative TIM in general — which played the role of a paradigmatic model after all. In the next chapter we turn towards more complex theories and possible dissipative analogues.

<sup>55</sup>Mean field theory suggests a square root behaviour for the magnetisation. Since  $\langle \sigma_1^z \sigma_j^z \rangle \sim m_z^2$  one would expect a linear behaviour for the correlation.

## Chapter 3

# A dissipative $\mathbb{Z}_2$ -Gauge-Higgs model

*“If you want to have good ideas you must have many ideas.  
Most of them will be wrong, and what you have to learn is  
which ones to throw away.”*

Linus Pauling

In Chapter 2 we introduced a *purely dissipative* version of the transverse field Ising model. Meaning: we contrived two competing baths, termed “ferromagnetic” and “paramagnetic” referring to its Hamiltonian counterparts, each of which drives the spin-system into one of the (pure) quantum phases of the Hamiltonian model. We then showed in mean field approximation that a purely dissipative phase transition takes place at a critical coupling where the  $\mathbb{Z}_2$ -symmetry is spontaneously broken.

In this chapter we show that the procedure to construct purely dissipative counterparts of Hamiltonian theories works also for more sophisticated models. In particular, we employ the  $\mathbb{Z}_2$ -Gauge-Higgs theory as our model Hamiltonian — for a review see Section 1.4 and especially paragraph 1.4.2 — and construct a purely dissipative version that (1) satisfies the local gauge symmetries and (2) reproduces the three characteristic phases of the Hamiltonian prototype; namely (A) the confined charge phase, (B) the free charge phase, and (C) the Higgs phase.

This chapter is structured as follows. In Section 3.1 we derive the mean field theory of the Hamiltonian model to compare the results with the dissipative ones. We derive two mean field theories, one without fixing the gauge degrees of freedom and with two mean fields (in 3.1.1), and a another in unitary gauge with fixed gauge degrees of freedom and a single mean field (in 3.1.2). In Section 3.2 we introduce our dissipative  $\mathbb{Z}_2$ -Gauge-Higgs model. The motivation is given in 3.2.1 and the steady states for important limiting cases are discussed in 3.2.2. In Section 3.3 we examine our theory in mean field approximation. The effective jump operators are presented in 3.3.1 and the steady states depending on the parameters are discussed in 3.3.2.

### 3.1 Mean field theory for the unitary theory

In Section 1.4 we mentioned that there are mean field approaches to approximate at least some of the features of the  $\mathbb{Z}_2$ -Gauge-Higgs model [102–104]. These approaches were commonly based on the classical version of the GHM formulated in terms of a gauge invariant action  $S$ . However, the quantum-classical correspondence [96, 101] for lattice spin models allows the transformation of  $D$ -dimensional classical theories to  $D - 1$ -dimensional quantum theories by means of the transfer matrix formalism (and vice versa). As a consequence, the results for classical models can be interpreted in terms of their corresponding quantum mechanical theories in one less spatial dimension. In the following two paragraphs we derive mean field theories for the quantum mechanical version of  $\mathbb{Z}_2$ -Gauge-Higgs model in  $D$  spatial dimensions. This is nothing new but we need these phase diagrams for comparison with our dissipative setup in Section 3.3.

As starting points we chose in 3.1.1 the GHM Hamiltonian in the common representation as given in Eq. (1.4.2) and in 3.1.2 the GHM in *unitary gauge* which results from the gauge fixing procedure we used to transform the GHM to the toric code (in two dimensions). For the first approach we assign separate mean fields to both the Higgs and the gauge field whereas the second approach gets along with a single mean field for the gauge field.

#### 3.1.1 Two mean fields and unphysical degrees of freedom

As mentioned above, here we derive the mean field theory of the GHM in the common gauge, namely

$$H_{\text{GHM}} = - \sum_e \tau_e^x - \sum_s \sigma_s^x - \lambda \sum_e I_e - \omega \sum_p B_p \quad (3.1)$$

with the additional gauge constraint  $\hat{A}_s |\Psi\rangle = |\Psi\rangle$ . This is equivalent to demand that physical states live in  $\mathcal{H}_{\text{GHM}}$ . Our straightforward mean field approach is based on the product ansatz

$$\rho = \prod_{e \in \mathbb{E}} \gamma_e \prod_{s \in \mathbb{S}} \pi_s \quad (3.2)$$

with density matrices  $\gamma_e$  for the gauge field and  $\pi_s$  for the Higgs field. The drawback of this approach is well-known [102]: This mean field approach cannot distinguish between *physical* and *unphysical* (gauge) degrees of freedom as we cannot enforce the gauge condition  $\hat{A}_s |\Psi\rangle = |\Psi\rangle$ . Although the theory takes into account unphysical degrees of freedom, it reveals some features of the phase diagram qualitatively.

So let us proceed with the partial trace of the VON NEUMANN equations to derive the dynamical mean field equations:

$$\dot{\pi}_s = \text{Tr}_s [\dot{\rho}] = -i \text{Tr}_s [[H_{\text{GHM}}, \rho]] \equiv -i [\tilde{h}_\pi^{\text{mf}}, \pi_s] \quad (3.3a)$$

$$\dot{\gamma}_e = \text{Tr}_e [\dot{\rho}] = -i \text{Tr}_e [[H_{\text{GHM}}, \rho]] \equiv -i [\tilde{h}_\gamma^{\text{mf}}, \gamma_e] \quad (3.3b)$$

A straightforward calculation yields the two mean field Hamiltonians

$$\tilde{h}_\pi^{\text{mf}} = -h_\pi^{\text{mf}} \sigma = - \begin{bmatrix} 1 & \\ & 0 \end{bmatrix} \cdot \sigma \quad \text{and} \quad \tilde{h}_\gamma^{\text{mf}} = -h_\gamma^{\text{mf}} \tau = - \begin{bmatrix} 1 & \\ & 0 \\ \lambda m_z^2 + 2\omega(d-1)g_z^3 & \end{bmatrix} \cdot \tau \quad (3.4)$$

where  $d \equiv D$  is the spatial dimension.  $m_k = \langle \sigma_s^k \rangle$  denotes the homogeneous Higgs field expectation values and  $g_k = \langle \tau_e^k \rangle$  the homogeneous gauge field expectation values for  $k = x, y, z$ . We already dropped the site and edge indices  $s$  and  $e$  and write  $\sigma$  and  $\tau$  for two representative spins coupled non-linearly by the mean fields. We can combine both Hamiltonians via a KRONECKER sum<sup>56</sup>

$$H_1^{\text{mf}} \equiv \tilde{h}_\pi^{\text{mf}} + \tilde{h}_\gamma^{\text{mf}} = - \begin{bmatrix} 1 \\ 0 \\ 2d\lambda m_z g_z \end{bmatrix} \cdot \sigma - \begin{bmatrix} 1 \\ 0 \\ \lambda m_z^2 + 2\omega(d-1)g_z^3 \end{bmatrix} \cdot \tau. \quad (3.5)$$

If we introduce the normalised mean fields  $\hat{h}_\pi^{\text{mf}}, \hat{h}_\gamma^{\text{mf}}$  and the absolute values  $h_\pi^{\text{mf}}, h_\gamma^{\text{mf}}$ , the self-consistency equations read

$$m_z = \hat{h}_{\pi,z}^{\text{mf}} \tanh \left[ \beta h_\pi^{\text{mf}} \right] \quad (3.6a)$$

$$g_z = \hat{h}_{\gamma,z}^{\text{mf}} \tanh \left[ \beta h_\gamma^{\text{mf}} \right] \quad (3.6b)$$

where  $\beta$  is the inverse temperature and

$$\hat{h}_{\pi,z}^{\text{mf}} = \frac{2d\lambda m_z g_z}{\sqrt{1 + (2d\lambda m_z g_z)^2}} \quad \text{and} \quad \hat{h}_{\gamma,z}^{\text{mf}} = \frac{\lambda m_z^2 + 2\omega(d-1)g_z^3}{\sqrt{1 + (\lambda m_z^2 + 2\omega(d-1)g_z^3)^2}}. \quad (3.7)$$

These are transcendental equations which cannot be solved analytically. Even numerical solutions are computationally expensive. As we are interested in a *qualitative* phase diagram, let us consider the boundary case of zero temperature, i.e  $\beta \rightarrow \infty$ . Then we find the simpler (algebraic) equations

$$(1 - g_z^2) \left[ \lambda \left( 1 - \frac{1}{4d^2 \lambda^2 g_z^2} \right) + 2\omega(d-1)g_z^3 \right]^2 = g_z^2 \quad \text{and} \quad m_z^2 = 1 - \frac{1}{4d^2 \lambda^2 g_z^2} \quad (3.8)$$

for a non-vanishing Higgs field  $m_z \neq 0$  and

$$4\omega^2(1 - g_z^2)(d-1)^2 g_z^4 = 1 \quad \vee \quad g_z = 0 \quad (3.9)$$

for a vanishing Higgs expectation value,  $m_z = 0$ . As these are polynomial equations of higher order, there are multiple solutions in most parameter regions. We choose the one(s) that minimise the energy expectation value

$$\begin{aligned} \langle H_1^{\text{mf}} \rangle &= \frac{1}{2} \text{Tr} \left[ \tilde{h}_\pi^{\text{mf}} (\mathbf{1} + \mathbf{m}\sigma) \right] + \frac{1}{2} \text{Tr} \left[ \tilde{h}_\gamma^{\text{mf}} (\mathbf{1} + \mathbf{g}\tau) \right] \\ &= \mp \sqrt{1 - m_z^2 - (2d\lambda m_z g_z)} m_z \mp \sqrt{1 - g_z^2 - (\lambda m_z^2 + 2\omega(d-1)g_z^3)} g_z \end{aligned} \quad (3.10)$$

where we used that  $m_y = 0 = g_y$  and  $m_x^2 + m_z^2 = 1 = g_x^2 + g_z^2$  since  $T = 0$ . Note that due to the structure of the mean field equations, we have to solve just for *one* variable, namely  $g_z$ , and can calculate the others via  $m_z^2 = 1 - (4d^2 \lambda^2 g_z^2)^{-1}$  and the aforementioned relations.

We illustrate the energy minimising solutions with positive expectation values in Fig. 3.1. In (A) we show the gauge field  $g_z = \langle \tau^z \rangle$ , in (B) the Higgs field  $m_z = \langle \sigma^z \rangle$ , and in (C) the quanti-

<sup>56</sup>That is,  $A \oplus B := A \otimes \mathbf{1} + \mathbf{1} \otimes B$ .

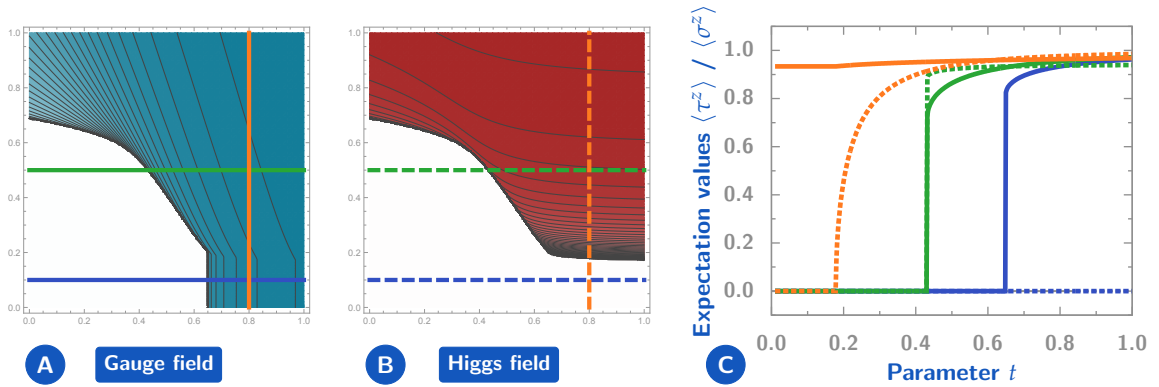


**Figure 3.1:** Mean field theory for the  $\mathbb{Z}_2$ -Gauge-Higgs model without gauge fixing. In (A) we show the colour-coded expectation value  $g_z = \langle \tau^z \rangle$  of the gauge field and in (B) the corresponding expectation value  $m_z = \langle \sigma^z \rangle$  for the Higgs field. The mean field theory identifies three distinct phases: The confined charge phase with  $g_z = 0 = m_z$ , the free charge phase with  $g_z > 0$  and  $m_z = 0$ , and the Higgs phase with  $g_z > 0$  and  $m_z > 0$ . The quantitative evaluation in (C) along the coloured paths in (A) and (B) reveals that the phase boundary separating the Higgs and the free charge phase is of second order whereas the phase boundaries between confined charge and Higgs phase and between confined and free charge phase are of first order. Note that in contrast to the correct phase diagram, the first order line that originates at the multicritical point ends at the (left)  $\lambda$ -axis.

tative results along the coloured parameter paths in (A) and (B). The mean field theory predicts three distinct phases: The confined charge phase with  $g_z = 0 = m_z$ , the free charge phase with  $g_z > 0$  and  $m_z = 0$ , and the Higgs phase with  $g_z > 0$  and  $m_z > 0$ . The phase transition between Higgs and free charge phase is correctly identified as a second order transition, the same holds for the first order transition between confined charge and Higgs phase; however, there are also two incorrect predictions: First, the phase boundary between confined and free charge phase is a *second order* transition and not of first order as the mean field theory makes us believe. And second, the first order transition that originates at the multicritical point does not meet the axis at  $\omega = 0$  — in contrast to the mean field theory result. In other words: The unphysical degrees of freedom taken unintentionally into account by the mean field theory cause the (provably correct) analyticity region to vanish. We conclude that the mean field approach at hand captures most of the characteristic features but fails at two of them.

### 3.1.2 A single mean field in unitary gauge

Here we pursue another mean field approach. As we could not enforce the gauge condition  $A_s$  during the mean field calculation above, it seem reasonable to look for a representation in which gauge fixing is simple and can be applied even in the mean field setting. To this end we employ the so called *unitary gauge* which is the  $d$ -dimensional generalisation of our GHM-TCM mapping discussed in 1.4.2. An application of the unitary transformation  $T$  (see subsection 1.4.2) yields the Hamiltonian

$$H_{\text{GHM}}^U \equiv T^\dagger H_{\text{GHM}} T = - \sum_e \tau_e^x - \lambda \sum_e \tau_e^z - \sum_s A_s - \omega \sum_p B_p \quad (3.11)$$

with the trivial gauge condition  $\sigma_s^x |\Psi\rangle = |\Psi\rangle$ . Note that  $H_{\text{GHM}}^U$  acts trivially on the Higgs field and can henceforth be restricted to the gauge field. Since the unphysical degrees of freedom

are no longer included in the dynamics, we can drop them. That is, we introduce a *single* mean field for the gauge degrees of freedom and the ansatz for the density matrix reads

$$\rho = \prod_{e \in \mathbb{E}} \gamma_e \quad (3.12)$$

with density matrices  $\gamma_e$  for the gauge field. The mean field Hamiltonian is defined by

$$\gamma_e = \text{Tr}_e [\rho] = -i \text{Tr}_e \left[ \left[ H_{\text{GHM}}^U, \rho \right] \right] \equiv -i \left[ \tilde{h}_\gamma^{\text{mf}}, \gamma_e \right] \quad (3.13)$$

and a straightforward calculation yields

$$H_2^{\text{mf}} \equiv \tilde{h}_\gamma^{\text{mf}} = -h_\gamma^{\text{mf}} \boldsymbol{\tau} = - \begin{bmatrix} 2g_x^{2d-1} + 1 \\ 0 \\ \lambda + 2\omega(d-1)g_z^3 \end{bmatrix} \cdot \boldsymbol{\tau}. \quad (3.14)$$

In contrast to the mean field theory above,  $g_x = \langle \tau_x^x \rangle$  occurs here explicitly in the expression for  $\tilde{h}_\gamma^{\text{mf}}$ . With the normalised mean field  $\hat{h}_\gamma^{\text{mf}}$  and the absolute value  $h_\gamma^{\text{mf}}$  the self-consistency equations read

$$g_x = \hat{h}_{\gamma,x}^{\text{mf}} \tanh \left[ \beta h_\gamma^{\text{mf}} \right] \quad (3.15a)$$

$$g_z = \hat{h}_{\gamma,z}^{\text{mf}} \tanh \left[ \beta h_\gamma^{\text{mf}} \right] \quad (3.15b)$$

where  $\beta$  is the inverse temperature and

$$\hat{h}_{\gamma,x}^{\text{mf}} = \frac{2g_x^{2d-1} + 1}{\sqrt{(2g_x^{2d-1} + 1)^2 + (\lambda + 2\omega(d-1)g_z^3)^2}} \quad \text{and} \quad (3.16)$$

$$\hat{h}_{\gamma,z}^{\text{mf}} = \frac{\lambda + 2\omega(d-1)g_z^3}{\sqrt{(2g_x^{2d-1} + 1)^2 + (\lambda + 2\omega(d-1)g_z^3)^2}}. \quad (3.17)$$

If we set again  $T = 0$ , that is, consider the limit  $\beta \rightarrow \infty$ , both self-consistency equations are related via  $g_x^2 + g_z^2 = 1$  since the states are pure and  $g_y = 0$ . Then there is just one non-trivial self-consistency equation left which reads

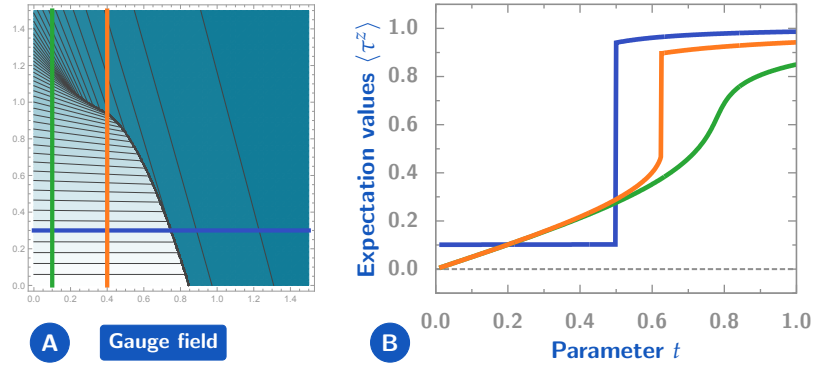
$$\left[ \lambda + 2\omega(d-1)g_z^3 \right]^2 (1 - g_z^2) = g_z^2 \left[ 2(1 - g_z^2)^{\frac{2d-1}{2}} + 1 \right]^2 \quad (3.18)$$

for arbitrary gauge fields  $g_x, g_z \in \mathbb{R}$ . As before, we choose the solutions that minimise the energy expectation value which reads here

$$\langle H_2^{\text{mf}} \rangle = \frac{1}{2} \text{Tr} \left[ \tilde{h}_\gamma^{\text{mf}} (\mathbb{1} + \mathbf{g}\boldsymbol{\tau}) \right] = \mp \sqrt{1 - g_z^2} \left[ \pm 2(1 - g_z^2)^{\frac{2d-1}{2}} + 1 \right] - g_z \left[ \lambda + 2\omega(d-1)g_z^3 \right]. \quad (3.19)$$

Once again we have to solve for one variable, namely  $g_z$ , and can derive  $g_x$  via  $g_x^2 = 1 - g_z^2$ .

We illustrate the energy minimising solutions with positive expectation values in Fig. 3.2. In (A) we show the gauge field  $g_z = \langle \tau^z \rangle$  and in (B) the quantitative results along the coloured parameter paths in (A). The differences to Fig. 3.2 are obvious: Formally there is just one phase as the lower region where  $g_z$  is small is smoothly connected to the upper region where  $g_z$  is

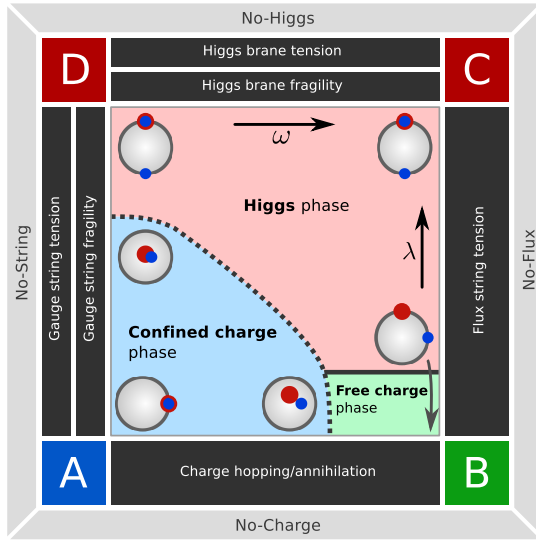


■ **Figure 3.2:** Unitary mean field theory for the  $\mathbb{Z}_2$ -Gauge-Higgs model in unitary gauge with a single mean field for the gauge degrees of freedom. In (A) we illustrate the expectation value  $g_z = \langle \tau^z \rangle$  of the gauge field and in (B) the quantitative results on the coloured lines in (A). There are two regions in the phase diagram with small (light) and large (dark)  $z$ -polarisation, respectively; they correspond to the confined charge and Higgs phase. For small values of  $\lambda$  both regions are separated by a first order transition as (B) reveals. This transition line ends at a critical point and thus allows for smooth paths that connect both phases. In contrast to Fig. 3.2 there is no separated deconfined phase in the lower right corner.

large by paths which stay close to the (left)  $\lambda$ -axis and avoid the first order transition. (B) shows clearly that this mean field theory reproduces the critical point (red disc in Fig. 1.14) where the first order line ends and the analyticity region starts. In this regard the mean field theory at hand is better than the first approach; however, it does not reproduce the free charge phase since there are no other (second order) phase transitions. Like the mean field theory before, this one does not predict the second order phase transition close to the (lower)  $\omega$ -axis.

To sum it up: Both mean field approximations yield different (correct) features of the phase diagram in Fig. 1.14. None of them succeeds completely in its qualitative approximation of the  $\mathbb{Z}_2$ -Gauge-Higgs model but *in combination* they provide all features but the second order line that separates the confined and free charge phase. The first approximation with two mean fields provides reasonable results in the small- $\lambda$  and large- $\omega$  regime whereas the second approximation in unitary gauge yields good results in the large- $\lambda$  and small- $\omega$  section of the parameter space. This is in agreement with the results presented in Ref. [102] (see p. 103 ff.) for the classical  $\mathbb{Z}_2$ -Gauge-Higgs model.





■ **Figure 3.3:** Qualitative mean field phase diagram for the  $\mathbb{Z}_2$ -Gauge-Higgs model motivated by the unitary result in Fig. 3.1. It approximates the (more) exact result in 1.14 and illustrates our expectations towards a mean field theory for a dissipative version of the GHM. The three phases are described in Sec. 1.4.2. The dark grey rectangles surrounding the phase diagram illustrate the dominant baths on the adjacent axis, see Table 3.1. Their (collective) goal is described verbally by the tags in the four light grey boxes. For instance, the gauge string tension in combination with their fragility seek for a string-free system, thus “No-String”. The four corners labeled by A-D denote the important limiting cases which are described in the text. The grey-framed circles depict cross sections of two superimposed Bloch balls (one for the gauge mean field and one for its Higgs counterpart). The red (blue) dot denotes the *expected* location of the dissipative steady state for the gauge (Higgs) mean field. We expect the steady states to become pure deep within each phase near the corners of the phase diagram and to be mixed close to the phase transitions.

## 3.2 The Setting

In Section 1.4.2 we presented the  $\mathbb{Z}_2$ -Gauge-Higgs model and in the previous Section 3.1 we derived two mean field theories for its unitary theory. As stated in the preliminary paragraph above, we aim at a purely dissipative counterpart of the Hamiltonian  $\mathbb{Z}_2$ -Gauge-Higgs model, that is, a lattice gauge theory defined by presumably several baths (given by their jump operators) and two parameters  $\omega$  and  $\lambda$  such that in the limiting cases the three pure quantum phases of the GHM are recovered. In a nutshell: We want to come up with a theory of quantum jumps — as we did in Chapter 2 for the paradigmatic but simple transverse field Ising model — that “mimics” the  $\mathbb{Z}_2$ -Gauge-Higgs model and features analogous phases and phase transitions.

### 3.2.1 Dissipative interpretation of a unitary theory

In Fig. 3.3 we sketch a qualitative mean field diagram motivated by the unitary mean field result in Fig. 3.1. This is what we aim at and what we hope to find as a dissipative mean field result. We will succeed qualitatively up to some subtleties as the mean field analysis reveals; but to reach this point we need to recall the phase diagram in Fig. 1.14 and the discussion of the phases in Subsec. 1.4.2 as we are looking for jump operators that drive the system into the phases of the four<sup>57</sup> corners of the phase diagram depicted in Fig. 3.3.

Our proposal comprises *six different jump operators* (or baths), each of which mimics a specific dynamical property of the original GHM. Their names, formal definitions and short descriptions can be found in Table 3.1. The dominant region for each bath is indicated on the boundaries of the (mean field) phase diagram in Fig. 3.3. At each corner denoted by A, B, C, and D the two or three baths on the adjacent edges dominate the dynamics of the system. This dominance is encoded directly into the definitions via the two parameters  $\omega$  and  $\kappa$ , see Tab. 3.1.

<sup>57</sup>Or at least the three “important” corners (A), (B) and (C) since (D) marks just the analytic transition region. | 193

Name	Jump Operator	Description
Gauge string tension	$F_p^{(1)} = \frac{1}{2} B_p \left( \mathbb{1} - \frac{1}{4} \sum_{e \in p} \tau_e^x \right)$	Causes fluctuation of gauge strings and contracts them.
Gauge string fragility	$F_e^{(2)} = \frac{1}{2} I_e (\mathbb{1} - \tau_e^x)$	Cuts gauge strings and creates a pair of charges at their ends.
Higgs brane tension	$D_s^{(1)} = \frac{1}{2} \sqrt{\lambda} \sigma_s^x \left( \mathbb{1} - \frac{1}{2d} \sum_{e \in s} I_e \right)$	Causes fluctuations of Higgs branes and contracts them.
Higgs brane fragility	$D_e^{(2)} = \frac{1}{2} \sqrt{\lambda} \tau_e^x (\mathbb{1} - I_e)$	Cuts Higgs branes and creates flux strings at their borders.
Charge hopping	$T_e = \frac{1}{2} I_e \left( \mathbb{1} - \frac{1}{2} \sum_{s \in e} \sigma_s^x \right)$	Causes diffusion of charges and their annihilation.
Flux string tension	$B_e = \frac{1}{2} \sqrt{\omega} \tau_e^x \left( \mathbb{1} - \frac{1}{2(d-1)} \sum_{p \in e} B_p \right)$	Causes fluctuations of flux strings and contracts them.

■ **Table 3.1:** The jump operators for the dissipative  $\mathbb{Z}_2$ -Gauge-Higgs model. Their action is described in the text.  $s$ ,  $e$  and  $p$  denote sites, edges and faces, respectively. Pictorial descriptions can be found in Figures 3.4, 3.5, and 3.6.

To get a better understanding of the proposed jump operators, let us shortly summarise the characteristic limiting cases:

- A** In the low  $\omega$  and  $\lambda$  regime the baths for charge hopping and annihilation as well as for gauge string tension and fragility dominate the dissipative dynamics. This is called the *confined charge* phase since two elementary charges are confined by a tense string of electric flux.
- B** In the low  $\lambda$  and high  $\omega$  regime the charge hopping and annihilation remain dominant. The gauge string tension and fragility is now superseded by the flux string tension which, in two dimensions, degenerates to hopping and annihilation of isolated magnetic fluxes. This phase is characterised by *free charges* since the electric flux lines connecting them lost their tension and fragility.
- C** In the high  $\lambda$  and  $\omega$  regime the flux string tension persists. The charge hopping and annihilation is superseded by two other baths, namely the Higgs brane tension and the Higgs brane fragility. This phase is called the *Higgs phase* and its elementary excitations are branes of Higgs excitations and closed loops of magnetic fluxes, both of which are equipped with a tension by the baths.
- D** In the low  $\omega$  and high  $\lambda$  phase the four baths for Higgs brane tension and fragility as well as gauge string tension and fragility determine the dynamics. We are not going to analyse this phase in more detail since it has no distinct features and (in the dissipative approach) it cannot be prepared as a pure state.

A detailed description of the action is given for each jump operator in the following subsection where we discuss the common steady and dark states of the bath combinations in the four corners. Before we proceed, let me once more stress the crucial point that characterises our

approach: The original Hamiltonian theory is governed by its *energy* which, at  $T = 0$ , is minimised. There is, to my knowledge, no such principle for the non-equilibrium setup. Whereas in the Hamiltonian theory, say, a gauge string contracts due to the fundamental urge to lower the total energy, there is no corresponding motivation for the same process in the dissipative setup *unless* we enforce it *by design*. To put it differently: In a Hamiltonian theory the contraction or breaking of a gauge string is an *implicit* effect motivated by energy minimisation. In the dissipative setup there is no such “deeper reason”; if we want a gauge string to contract or break, we have to provide suitable jump operators for this job. In this sense we are playing with Lego pieces and construct a theory according to some Hamiltonian model theory by mixing distinct ingredients in beneficial ratios.

There is second point worth mentioning: Obviously all six jump operators have a common structure. It is reasonable to think of them as very simple, quasilocal (quantum) computers with the atomic structure

$$\text{Jump operator} = \text{THEN} \cdot \text{IF} \quad (3.20)$$

where IF denotes an operator that checks whether a local condition is satisfied. As an example, this reads for the gauge string tension:

$$F_p^{(1)} = \frac{1}{2} B_p \left( \mathbb{1} - \frac{1}{4} \sum_{e \in p} \tau_e^x \right) \rightarrow \begin{cases} \text{IF} = \frac{1}{2} \left( \mathbb{1} - \frac{1}{4} \sum_{e \in p} \tau_e^x \right) \\ \text{THEN} = B_p \end{cases} \quad (3.21)$$

That is,  $F_p^{(1)}$  checks whether some gauge strings run along face  $p$  and redirects them with a certain amplitude depending on the local length of the string. We should point out that the summands in the *parent Hamiltonian* read

$$(\text{Jump operator})^\dagger (\text{Jump operator}) = \text{IF}^\dagger \cdot \text{THEN}^\dagger \cdot \text{THEN} \cdot \text{IF} = \text{IF}^\dagger \cdot \text{IF} \quad (3.22)$$

since the THEN-actions are unitary. That is, the parent Hamiltonian loses information about the *actions* triggered by the IF-statements. What  $H_p$  “knows” about a state is *that* an action has to take place but it is ignorant of the action *itself*. By the way, this point of view suggests potentially fruitful relations between quantum Markov processes described by quasilocal jump operators and (asynchronous) quantum cellular automata.

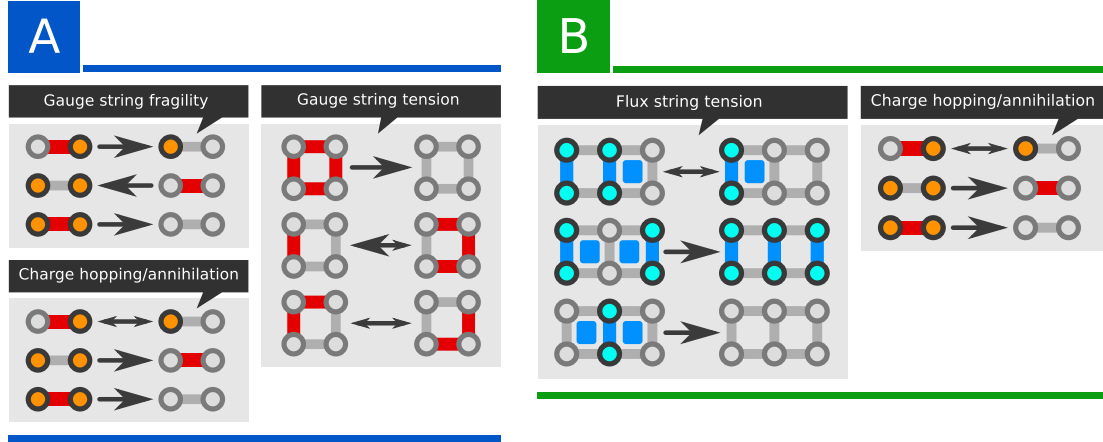
### 3.2.2 Steady states

Let us now investigate the steady states (especially the dark states) of certain combinations of the baths listed in Table 3.1. In order to determine the steady states of the theory, we restrict the possible states to the *gauge invariant* ones. Keep in mind that the quasilocal operators

$$\hat{A}_s = \sigma_s^x \prod_{e \in s} \tau_e^x = \sigma_s^x A_s \quad (3.23)$$

are strong symmetries of the dissipative process for all sites  $s$ , meaning that

$$[F_p^{(1)}, \hat{A}_s] = [F_e^{(2)}, \hat{A}_s] = [D_t^{(1)}, \hat{A}_s] = [D_e^{(2)}, \hat{A}_s] = [T_e, \hat{A}_s] = [B_e, \hat{A}_s] = 0 \quad (3.24)$$



■ **Figure 3.4:** **A** Schematic action of the jump operators which are dominant in the small  $\omega$  and  $\lambda$  regime denoted by **A** in Fig. 3.3. The three baths are responsible for the hopping and annihilation of charges, the fragility of gauge strings and their tension. This is the *confined phase*. **B** Schematic action of the jump operators which are dominant in the large  $\omega$  and small  $\lambda$  regime denoted by **B** in Fig. 3.3. The two baths are responsible for the hopping and annihilation of charges and fluxes. In three dimensions and above the flux hopping becomes a tension of flux strings. This is the *deconfined phase*. We indicate transitions which are more likely to occur in one than in the other direction by asymmetric arrows. The key reads: ■ = gauge string; ● = (electrical) charge; ●● = Higgs excitation; ■ = (magnetic) flux.

for all sites  $s, t$ , edges  $e$  and plaquettes  $p$ . This is evident since all jump operators are composites of gauge invariant terms. It is therefore legit to consider the dissipative process constrained to the linear subspace

$$\mathcal{H}_{\text{GHM}} = \{|\Psi\rangle \in \tilde{\mathcal{H}}_{\text{GHM}} \mid \forall_s : \hat{A}_s |\Psi\rangle = |\Psi\rangle\} \quad (3.25)$$

since there are no quantum jump trajectories which leave this space given the initial state lives in  $\mathcal{H}_{\text{GHM}}$ . A short reminder for the following paragraphs:  $\mathbb{S}$ ,  $\mathbb{E}$  and  $\mathbb{P}$  denote the sets of sites (vertices), edges and plaquettes (faces), respectively.

### ■ Confined phase (A)

In the *confined phase*, denoted by **A** in Fig. 3.3, the following three baths determine the steady states of the theory:

Name	Jump Operator	Description
Gauge string tension	$F_p^{(1)} = \frac{1}{2} B_p \left( \mathbb{1} - \frac{1}{4} \sum_{e \in p} \tau_e^x \right)$	Causes fluctuation of gauge strings and contracts them.
Gauge string fragility	$F_e^{(2)} = \frac{1}{2} I_e (\mathbb{1} - \tau_e^x)$	Cuts gauge strings and creates a pair of charges at their ends.
Charge hopping	$T_e = \frac{1}{2} I_e \left( \mathbb{1} - \frac{1}{2} \sum_{i \in e} \sigma_i^x \right)$	Causes diffusion of charges and their annihilation.

This corresponds to the fact that in the original theory gauge strings and charges are penalised and the system seeks a state devoid of these excitations. To get rid of strings and charges the latter need to be movable ( $T_e$ ) and the former must contract ( $F_p^{(1)}$ ). In systems with non-trivial

topology the strings must also be *fragile* ( $F_p^{(2)}$ ) — it must be possible to break them. Otherwise the steady state space decays into (mixed) disjoint topological sectors as single, homotopically non-trivial gauge strings cannot be contracted by quasilocal operations.

A dark state  $|D\rangle \in \mathcal{H}_{\text{GHM}}$  has to satisfy the three conditions  $F_p^{(1)}|D\rangle = 0$ ,  $F_e^{(2)}|D\rangle = 0$ , and  $T_e|D\rangle = 0$  for all edges  $e$  and plaquettes  $p$ . First, realise that  $B_p$  and  $I_e$  are unitary operators and thus it follows immediately

$$\frac{1}{4} \sum_{e \in p} \tau_e^x |D\rangle = |D\rangle \quad \text{and} \quad \tau_e^x |D\rangle = |D\rangle \quad \text{and} \quad \frac{1}{2} \sum_{i \in e} \sigma_i^x |D\rangle = |D\rangle. \quad (3.26)$$

Clearly, there is just one state satisfying all three constraints, namely the completely  $x$ -polarised state

$$|D_A\rangle = |+\rangle^{\mathbb{S}} |+\rangle^{\mathbb{E}} \quad (3.27)$$

Obviously this is also a physical state, i.e.  $|D_A\rangle \in \mathcal{H}_{\text{GHM}}$ . So we conclude that there is exactly *one* dark state in regime **A**. However, we have to rule out the possibility of additional *mixed* steady states. To this end we introduce a basis for  $\mathcal{H}_{\text{GHM}}$  which we term *string basis*<sup>58</sup>. Let  $\mathbf{s}$  be an arbitrary set of edges, i.e.  $\mathbf{s} \subseteq \mathbb{E}$ . We may equally consider it a collection of open and closed strings on the lattice. Then the *string states*

$$|\mathbf{s}\rangle \equiv \prod_{e \in \mathbf{s}} I_e |+\rangle^{\mathbb{S}} |+\rangle^{\mathbb{E}} \quad (3.28)$$

form an orthonormal basis of  $\mathcal{H}_{\text{GHM}}$  as they are a set of  $2^{|\mathbb{E}|}$  linearly independent states which clearly satisfy  $\hat{A}_s |\mathbf{s}\rangle = |\mathbf{s}\rangle$  by construction. Now let  $|\Psi\rangle = \sum_{\mathbf{s}} \Psi(\mathbf{s}) |\mathbf{s}\rangle \in \mathcal{H}_{\text{GHM}}$  be an arbitrary physical state. Choose an arbitrary string state  $|\tilde{\mathbf{s}}\rangle$  such that  $\Psi(\tilde{\mathbf{s}}) \neq 0$ . Then there is a polynomial  $P(\tilde{\mathbf{s}})$  in the jump operators  $\{F_p^{(1)}, F_e^{(2)}, T_e\}$  such that  $P(\tilde{\mathbf{s}}) |\tilde{\mathbf{s}}\rangle = |D_A\rangle$  is the string-free vacuum. Note that one needs  $F_e^{(2)}$  to break up strings which are homotopically non-trivial. Furthermore there are two possibilities to get rid of homotopically trivial loops: Either one breaks the loop by  $F_e^{(2)}$  and afterwards retracts it by  $F_e^{(2)}$  and  $T_e$ . Or one retracts it by  $F_p^{(1)}$  without breaking it altogether. Since  $P(\tilde{\mathbf{s}}) |\mathbf{s}\rangle$  for  $\mathbf{s} \neq \tilde{\mathbf{s}}$  cannot yield  $|D_A\rangle$ , we find that  $\langle D_A | P(\tilde{\mathbf{s}}) | \Psi \rangle \neq 0$  and consequently  $|D_A\rangle$  is the unique stationary state<sup>59</sup> of the dissipative process  $\{F_p^{(1)}, F_e^{(2)}, T_e\}$ .

<sup>58</sup>We already came across this basis during our preliminary discussions in Subsection 1.4.2.

<sup>59</sup>The observant reader may have noticed that the jump operators  $F_e^{(2)}$  are sufficient for the uniqueness of the steady state. However, to mimic the thermal behaviour of the excitations, the other two baths are necessary as well.

### ■ Free charge phase (B)

In the *free charge phase*, denoted by **B** in Fig. 3.3, the following two baths determine the steady states of the theory:

Name	Jump Operator	Description
Charge hopping	$T_e = \frac{1}{2} I_e \left( \mathbb{1} - \frac{1}{2} \sum_{s \in e} \sigma_s^x \right)$	Causes diffusion of charges and their annihilation.
Flux string tension	$B_e = \frac{1}{2} \sqrt{\omega} \tau_e^x \left( \mathbb{1} - \frac{1}{2(d-1)} \sum_{p \in e} B_p \right)$	Causes fluctuations of flux strings and contracts them.

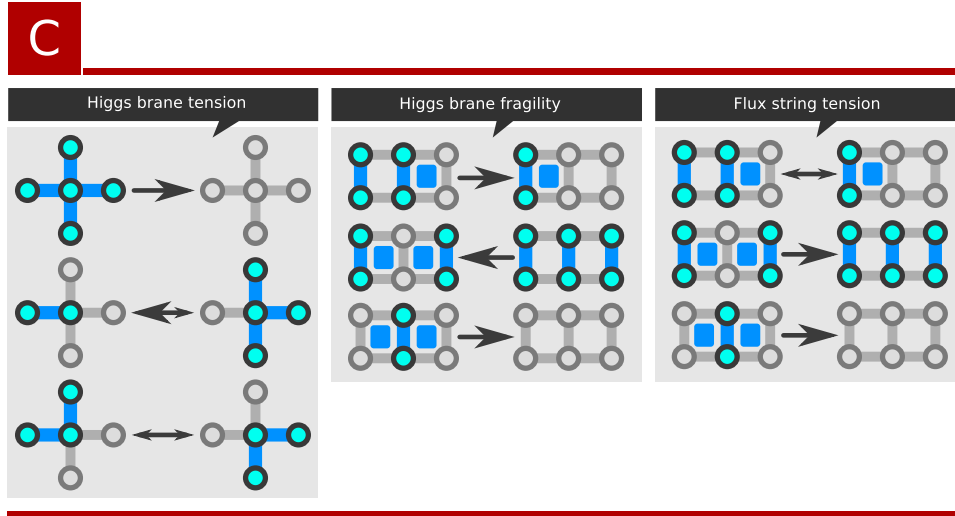
This choice accounts for the need to get rid of the unconfined charges via diffusion and pair annihilation ( $T_e$ ) and to do the same for magnetic monopoles in two dimensions ( $B_e$ ). In three and more dimensions  $B_e$  induces a fluctuation and contraction of closed flux *strings*.

A dark state  $|D\rangle \in \mathcal{H}_{\text{GHM}}$  has to satisfy the two conditions  $B_e |D\rangle = 0$  and  $T_e |D\rangle = 0$  for all edges  $e$ . As before they reduce to the eigenstate conditions

$$\frac{1}{2} \sum_{i \in e} \sigma_i^x |D\rangle = |D\rangle \quad \text{and} \quad \frac{1}{2(d-1)} \sum_{p \in e} B_p |D\rangle = |D\rangle \quad (3.29)$$

for all edges  $e$ . To satisfy the first condition, the dark state must be of the form  $|D\rangle = |+\rangle^S |D\rangle'$  where  $|D\rangle'$  is a pure gauge field state. Since our states live in  $\mathcal{H}_{\text{GHM}}$  where  $\hat{A}_s = \sigma_s^x A_s \equiv \mathbb{1}$ , the gauge constraint reads  $A_s |D\rangle' = |D\rangle'$  where  $A_s$  is the  $d$ -dimensional star operator known from the toric code. Since all star and plaquette operators  $A_s$  and  $B_p$  commute, there is (at least one) common eigenstate with eigenvalue one. If the topology of the manifold is non-trivial, there are several states with this property (cf. the ground states of the toric code). Thus there is a topology dependent dark state space  $\mathcal{D} \leq \mathcal{H}_{\text{GHM}}$  which is just the quantum code defined by the stabiliser  $\{A_s, B_p\}$ . Note that it is of crucial importance that the gauge string tension and fragility as well as the Higgs brane tension and fragility are no longer present since *deconfinement* and the *topologically ordered phases* of the toric code rely on the *invisibility* of the strings that connect pairs of particles.

That there are no mixed stationary states (but multiple dark states for non-trivial topologies) can be inferred from the effect of the jump operators. Let us exemplify this in two dimensions and in unitary gauge (see the next paragraph for a more formal treatment of this transformation): There one finds  $T_e = \frac{1}{2} \tau_e^z \left( \mathbb{1} - \frac{1}{2} \sum_{s \in e} A_s \right)$  for the charge hopping (and annihilation) and  $B_e = \frac{1}{2} \sqrt{\omega} \tau_e^x \left( \mathbb{1} - \frac{1}{2(d-1)} \sum_{p \in e} B_p \right)$  for the flux string tension which degenerates in two dimensions to magnetic monopole hopping (and annihilation). These jump operators cause free *diffusion* of electric charges and magnetic fluxes and *pair annihilation* whenever two particles of the same species meet. Clearly, this is enough to cool any initial state into a state devoid of excitations. The latter are non-unique for non-trivial topologies as straightforward calculations with the stabiliser formalism reveal. The actual dark state that is reached for  $t \rightarrow \infty$  depends on the topology of the particle trajectories.



■ **Figure 3.5:** **C** Schematic action of the jump operators which are dominant in the large  $\omega$  and  $\lambda$  regime denoted by **C** in Fig. 3.3. The three baths are responsible for the hopping and annihilation of fluxes, the fragility of Higgs branes and their tension. In three dimensions and above the flux hopping becomes a tension of flux strings. This is the *Higgs phase*. We indicate transitions which are more likely to occur in one than in the other direction by asymmetric arrows. The key reads:  $\bullet\text{---}\bullet$  = Higgs excitation;  $\blacksquare$  = (magnetic) flux.

### ■ Higgs phase (C)

In the *Higgs phase*, denoted by **C** in Fig. 3.3, the following three baths determine the steady states of the theory:

Name	Jump Operator	Description
Higgs brane tension	$D_s^{(1)} = \frac{1}{2}\sqrt{\lambda}\sigma_s^x \left( \mathbb{1} - \frac{1}{2d}\sum_{e\in s} I_e \right)$	Causes fluctuations of Higgs branes and contracts them.
Higgs brane fragility	$D_e^{(2)} = \frac{1}{2}\sqrt{\lambda}\tau_e^x (\mathbb{1} - I_e)$	Cuts Higgs branes and creates flux strings at their borders.
Flux string tension	$B_e = \frac{1}{2}\sqrt{\omega}\tau_e^x \left( \mathbb{1} - \frac{1}{2(d-1)}\sum_{p\in e} B_p \right)$	Causes fluctuations of flux strings and contracts them.

In two dimensions the flux string tension degenerates to a monopole diffusion ( $B_e$ ); in both cases  $B_e$  gets rid of magnetic fluxes. Note that magnetic flux lines ( $d > 2$ ) cannot end and form always closed loops<sup>60</sup>. In two dimensions the Higgs brane tension ( $D_s^{(1)}$ ) and fragility ( $D_e^{(2)}$ ) become the dual of the gauge string tension ( $F_p^{(1)}$ ) and fragility ( $F_e^{(2)}$ ) in the confined charge phase. The Higgs brane tension in two dimensions cuts (dual) Higgs strings and creates a pair of magnetic monopoles at their open ends. In higher dimensions the *pure* Higgs excitations form  $(d-1)$ -dimensional hyperplanes as there are  $2d$  Higgs excitations that surround a site  $s$  were  $\sigma_s^x$  has been applied. Higgs excitations created by  $\tau_e^x$  form strings that are paralleled by magnetic flux lines. The Higgs brane tension ( $D_s^{(1)}$ ) causes the hyperplanes to fluctuate and contracts them in

<sup>60</sup>To revive our analogy to electromagnetism, see Subsec. 1.4.2: There are no magnetic monopoles in dimensions  $d > 2$ .

the long time limit. The Higgs brane fragility ( $D_e^{(2)}$ ) tears holes in the hyperplanes and breaks strings and subsequently attaches magnetic flux lines to the created borders.

A dark state  $|D\rangle \in \mathcal{H}_{\text{GHM}}$  has to satisfy the three conditions  $D_s^{(1)} |D\rangle = 0$ ,  $D_e^{(2)} |D\rangle = 0$ , and  $B_e |D\rangle = 0$  for all edges  $e$  and sites  $i$ . As usually we find the eigenstate conditions

$$\frac{1}{2d} \sum_{e \in s} I_e |D\rangle = |D\rangle \quad \text{and} \quad I_e |D\rangle = |D\rangle \quad \text{and} \quad \frac{1}{2(d-1)} \sum_{p \in e} B_p |D\rangle = |D\rangle \quad (3.30)$$

for all edges  $e$ . As all operators  $I_e$ ,  $B_p$  and  $\hat{A}_s$  commute with each other, there is a common eigenstate with eigenvalue one. To derive this eigenstate, let us recast the system in unitary gauge by the transformation  $T$

$$T = \prod_e \left[ \frac{1}{2} (\mathbb{1} + \tau_e^x) + \frac{1}{2} \tilde{I}_e (\mathbb{1} - \tau_e^x) \right] \quad \text{where} \quad \tilde{I}_e = \sigma_s^z \sigma_j^z \quad \text{for} \quad e = (i, j) \quad (3.31)$$

which we already introduced and applied in Subsec. 1.4.2. There we also derived the transformation properties, namely

$$\begin{aligned} T \tau_e^z T^\dagger &= I_e \\ T \tau_e^x T^\dagger &= \tau_e^x \\ T \sigma_s^z T^\dagger &= \sigma_s^z \\ T \sigma_s^x T^\dagger &= \sigma_s^x A_s = \hat{A}_s. \end{aligned}$$

The back-transformed jump operators read then

$$\begin{aligned} T^\dagger D_s^{(1)} T &= \frac{1}{2} \sqrt{\lambda} A_s \left( \mathbb{1} - \frac{1}{2d} \sum_{e \in s} \tau_e^z \right) \\ T^\dagger D_e^{(2)} T &= \frac{1}{2} \sqrt{\lambda} \tau_e^x (\mathbb{1} - \tau_e^z) = \sqrt{\lambda} \tau_e^+ \\ T^\dagger B_e T &= \frac{1}{2} \sqrt{\omega} \tau_e^x \left( \mathbb{1} - \frac{1}{2(d-1)} \sum_{p \in e} B_p \right). \end{aligned}$$

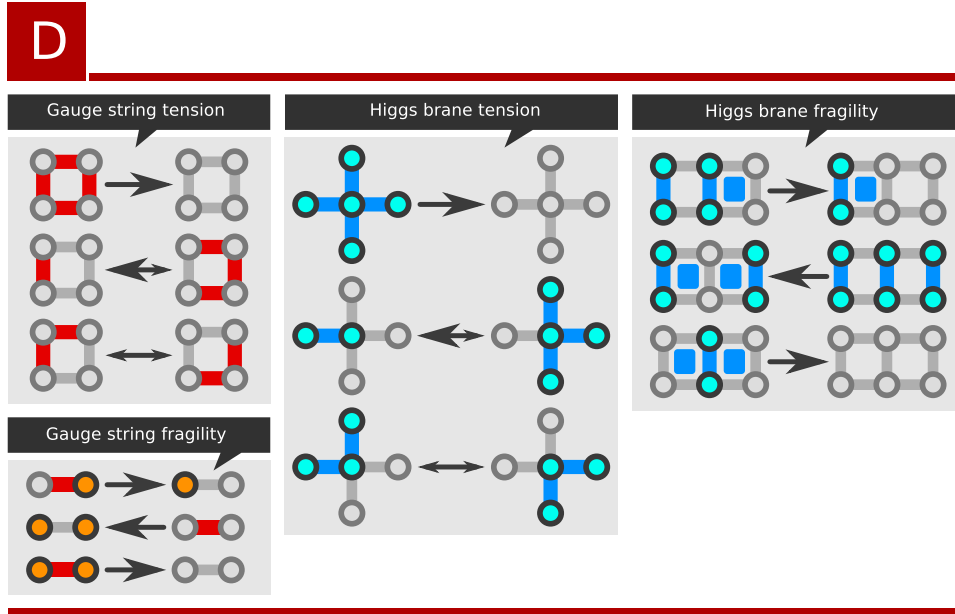
Recall that all physical states are now of the form  $|+\rangle^S |\Psi\rangle \in T^\dagger \mathcal{H}_{\text{GHM}}$  which corresponds to the fact, that the Higgs field no longer appears in the jump operators. In this subspace it is trivial to see that the unique steady state is the dark state

$$|D_C\rangle' = |+\rangle^V |\uparrow\rangle^E \quad (3.32)$$

and we note that the jump operators  $D_e^{(2)}$  alone are sufficient to drive into this dark state. The corresponding dual statement for the confined charge phase is that the gauge string fragility  $F_e^{(2)}$  is formally sufficient to get rid of all open and closed gauge strings.

We conclude that the unique dark state is just the completely  $z$ -polarised state in unitary gauge. Recall that we already discussed in Subsec. 1.4.2 that this state can be considered an equal-weight superposition of all open and closed string states with respect to the  $\tau^x$ -eigenbasis. The original dark state can now be obtained via  $T |D_C\rangle' = |D_C\rangle$  and one finds





■ **Figure 3.6:** **D** Schematic action of the jump operators which are dominant in the small  $\omega$  and large  $\lambda$  regime denoted by **D** in Fig. 3.3. The four baths are responsible for the fragility of gauge strings and their tension as well as the fragility and tension of Higgs branes. We indicate transitions which are more likely to occur in one than in the other direction by asymmetric arrows. The key reads: ■ = gauge string; ● = (electrical) charge; ● = Higgs excitation; ■ = (magnetic) flux.

$$|D_C\rangle = \frac{1}{\sqrt{|2^{\mathbb{E}}|}} \sum_{s \subseteq \mathbb{E}} |s\rangle = \frac{1}{\sqrt{|2^{\mathbb{E}}|}} \sum_{s \subseteq \mathbb{E}} \prod_{e \in s} I_e |+\rangle^s |+\rangle^{\mathbb{E}}. \quad (3.33)$$

where  $2^{\mathbb{E}}$  denotes the power set of  $\mathbb{E}$ . Therefore  $|D_C\rangle$  is the equal-weight superposition of all gauge-invariant charge configurations and all possible gauge string configurations.

#### ■ Confinement $\leftrightarrow$ Higgs phase (**D**)

In the transition region *Confinement*  $\leftrightarrow$  *Higgs phase*, denoted by **D** in Fig. 3.3, the following four baths determine the steady states of the theory:

Name	Jump Operator	Description
Gauge string tension	$F_p^{(1)} = \frac{1}{2} B_p \left( \mathbb{1} - \frac{1}{4} \sum_{e \in p} \tau_e^x \right)$	Causes fluctuation of gauge strings and contracts them.
Gauge string fragility	$F_e^{(2)} = \frac{1}{2} I_e (\mathbb{1} - \tau_e^x)$	Cuts gauge strings and creates a pair of charges at their ends.
Higgs brane tension	$D_i^{(1)} = \frac{1}{2} \sqrt{\lambda} \sigma_i^x \left( \mathbb{1} - \frac{1}{2d} \sum_{e \in i} I_e \right)$	Causes fluctuations of Higgs branes and contracts them.
Higgs brane fragility	$D_e^{(2)} = \frac{1}{2} \sqrt{\lambda} \tau_e^x (\mathbb{1} - I_e)$	Cuts Higgs branes and creates flux strings at their borders.

The transition region between confined charge and Higgs phase is not of particular interest as it constitutes no distinct phase with characteristic properties. Hence there is no deeper reason for the above combination of jump operators; the latter is rather a consequence of the other (required) combinations in the three distinct phases. The special status of **D** becomes apparent if we try derive dark states for this four-bath process:

A dark state  $|D\rangle \in \mathcal{H}_{\text{GHM}}$  has to satisfy the four conditions  $D_s^{(1)} |D\rangle = 0$ ,  $D_e^{(2)} |D\rangle = 0$ ,  $F_p^{(1)} |D\rangle = 0$ , and  $F_e^{(2)} |D\rangle = 0$  for all edges  $e$ , sites  $s$  and plaquettes  $p$ . We will now show that there is no such state. To this end, we recast the jump operators  $D_e^{(2)}$  and  $F_e^{(2)}$  in unitary gauge, i.e. we apply the unitary transformation  $T$ :

$$\begin{aligned} T^\dagger F_e^{(2)} T &= \frac{1}{2} \tau_e^z (\mathbb{1} - \tau_e^x) \\ T^\dagger D_e^{(2)} T &= \frac{1}{2} \sqrt{\lambda} \tau_e^x (\mathbb{1} - \tau_e^z) \end{aligned}$$

A dark state must satisfy

$$\tau_e^x |D\rangle = |D\rangle \quad \text{and} \quad \tau_e^z |D\rangle = |D\rangle \quad (3.34)$$

which immediately leads to  $|D\rangle = \tau_e^z \tau_e^x |D\rangle = -\tau_e^x \tau_e^z |D\rangle = -|D\rangle$  and therefore  $|D\rangle = 0$ . We conclude that in contrast to the three distinct phases **A**, **B** and **C**, there is no pure stationary state for  $\omega \rightarrow 0$  and  $\lambda \rightarrow \infty$ . We should not be too worried about this result as there are *three* distinct phases we are interested in. And these three (pure) phases can indeed be generated in the limits we discussed above.

Note that the previous result of a mixed steady state in **D** is not surprising: If we recast the theory in unitary gauge and restrict ourselves to the relevant spins on the edges, namely the gauge field, it becomes clear that the confined charge and Higgs phase correspond to the completely polarised phase in  $x$ - and  $z$ -direction, respectively. We already stressed this fact in Sec. 1.4.2 as a reason for the critical point and the analytic connection between confined charge and Higgs phase. There we realised that, in the unitary gauge, such analytic paths in the parameter space correspond to a spatial rotation of a dominant external magnetic field from  $x$ - to  $z$ -direction. Two baths drive into the limiting states by means of simple ladder operators

$$\begin{aligned} T^\dagger F_e^{(2)} T &= \frac{1}{2} \tau_e^z (\mathbb{1} - \tau_e^x) \propto \tau_e^{x,+} \\ T^\dagger D_e^{(2)} T &= \frac{1}{2} \sqrt{\lambda} \tau_e^x (\mathbb{1} - \tau_e^z) \propto \tau_e^{z,+} \end{aligned}$$

where  $\tau_e^{x,+}$  and  $\tau_e^{z,+}$  drive towards the completely  $x$ - and  $z$ -polarised state, respectively. But there is no simple *dissipative* process of two incoherent baths<sup>61</sup> which simulate a rotating magnetic field by following it with a *pure* stationary state. We already encountered this situation in the preliminaries, see 1.1.3, where we examined the stationary states of the competing ladder operators  $\tau_e^{x,+}$  and  $\tau_e^{z,+}$ . Consider also Fig. 1.1 in that regard.

<sup>61</sup>Certainly one could design jump operators that can be tuned *internally* by a parameter so that their stationary state remains pure and follows a rotating magnetic field (just transform  $\tau_e^{x,+}$  by the corresponding spin rotation). But this requires an active modification of the bath beyond the simple scaling of its strength. However, here we restrict ourselves to *fixed baths* since they require *fixed* local processes with no fine tuning degrees of freedom.

### 3.3 A short mean field analysis

In contrast to our detailed mean field analysis of the transverse field Ising model in Chapter 2, we present a rather short discussion of the mean field results for the dissipative  $\mathbb{Z}_2$ -Gauge-Higgs model. The primary purpose of this second model, introduced in the previous Section 3.2, is to demonstrate that the “dissipative translation”, introduced for the rather simple but paradigmatic TIM, may also yield interesting results for more complicated models. We already saw in Section 3.1 that the mean field approximations of the *Hamiltonian* GHM do not reproduce all characteristic features of the actual phase diagram. We therefore cannot expect to gain detailed insight into the phase structure of our proposed dissipative  $\mathbb{Z}_2$ -Gauge-Higgs model by a mean field analysis. However, as we will show in the following Section 3.3.2, the basic features of the mean field diagrams with and without gauge fixing can be reproduced in the dissipative mean field theory, although there are structural differences and some of the features change in the high-dimensional limit. Note that the existence and the behaviour of phase transitions may depend on the ratio and relative scaling of the six baths. This provides a multitude of free parameters, the choice of which may influence the phase diagrams drastically. We present here the straightforward results without further fine tuning of the bath ratios. A more detailed analysis is an open task for the future.

#### 3.3.1 Derivation of the mean field Lindblad superoperator

We perform mean field approximations for both representations: First, with the gauge conditions  $\hat{A}_s = \mathbb{1}$  which cannot be fixed in the mean field approach, and second, in the unitary gauge with the gauge conditions  $\sigma_s^x = \mathbb{1}$  and a single mean field. In the following we present the resulting effective jump operators without detailed derivations as they are straightforward but lengthy and provide no further insight. The reader may consider the analogous calculations for the dissipative TIM as a reference; see Section 2.3 for the condensed calculations and Appendix B for the detailed derivation.

Mean field theory without gauge fixing

We start with the jump operators given in Table 3.1 and a system that lives in the physical subspace  $\mathcal{H}_{\text{GHM}}$  with the gauge condition  $\hat{A}_s = \mathbb{1}$ . As for the Hamiltonian derivation in 3.1.1, we make the product ansatz

$$\rho = \prod_{e \in \mathbb{E}} \gamma_e \prod_{s \in \mathbb{S}} \pi_s \quad (3.35)$$

for the gauge ( $\gamma_e$ ) and Higgs ( $\pi_s$ ) fields. We discuss in Appendix A that the mean field jump operators can be derived by the partial trace

$$\begin{aligned} \partial_t \gamma_e &= \partial_t \text{Tr}_{\neq e} [\rho] = \sum_i \left[ \text{Tr}_{\neq e} [L_i \rho L_i^\dagger] - \frac{1}{2} \text{Tr}_{\neq e} [\{L_i^\dagger L_i, \rho\}] \right] \\ \partial_t \pi_s &= \partial_t \text{Tr}_{\neq s} [\rho] = \sum_i \left[ \text{Tr}_{\neq s} [L_i \rho L_i^\dagger] - \frac{1}{2} \text{Tr}_{\neq s} [\{L_i^\dagger L_i, \rho\}] \right] \end{aligned}$$

Name	Jump Operator	Mean Field Jump Operators
Gauge string tension	$F_p^{(1)} = \frac{1}{2} B_p \left( \mathbb{1} - \frac{1}{4} \sum_{e \in p} \tau_e^x \right)$	$f_1^{(1),\tau} = \frac{1}{2} \sqrt{\frac{2d-2}{d}} \tau^z \left( \mathbb{1} - \frac{3}{4} g_x - \frac{1}{4} \tau^x \right)$ $f_2^{(1),\tau} = \frac{1}{8} \sqrt{\frac{6d-6}{d}} \sqrt{1 - g_x^2} \tau^z$
Gauge string fragility	$F_e^{(2)} = \frac{1}{2} I_e \left( \mathbb{1} - \tau_e^x \right)$	$f_1^{(2),\tau} = \frac{1}{2\sqrt{d}} \tau^z \left( \mathbb{1} - \tau^x \right)$ $f_1^{(2),\sigma} = \frac{\sqrt{2}}{2} (1 - g_x) \sigma^z$ $f_2^{(2),\sigma} = \frac{\sqrt{2}}{2} \sqrt{1 - g_x^2} \sigma^z$
Higgs brane tension	$D_s^{(1)} = \frac{1}{2} \sqrt{\lambda} \sigma_s^x \left( \mathbb{1} - \frac{1}{2d} \sum_{e \in s} I_e \right)$	$d_1^{(1),\tau} = \frac{1}{2d} \sqrt{\frac{\lambda}{2}} \tau^z$ $d_1^{(1),\sigma} = \frac{\sqrt{\lambda}}{2} \sigma^x \left( \mathbb{1} - m_z g_z \sigma^z \right)$ $d_2^{(1),\sigma} = \frac{1}{2} \sqrt{\frac{\lambda}{2d}} \sqrt{1 - m_z^2 g_z^2} \sigma^x \sigma^z$ $d_3^{(1),\sigma} = \frac{1}{2} \sqrt{\frac{\lambda}{2d}} \sigma^z$
Higgs brane fragility	$D_e^{(2)} = \frac{1}{2} \sqrt{\lambda} \tau_e^x \left( \mathbb{1} - I_e \right)$	$d_1^{(2),\tau} = \frac{1}{2} \sqrt{\frac{\lambda}{d}} \tau^x \left( \mathbb{1} - m_z^2 \tau^z \right)$ $d_2^{(2),\tau} = \frac{1}{2} \sqrt{\frac{\lambda}{d}} \sqrt{1 - m_z^2} \tau^x \tau^z$ $d_1^{(2),\sigma} = \frac{\sqrt{2\lambda}}{2} \sigma^z$
Charge hopping	$T_e = \frac{1}{2} I_e \left( \mathbb{1} - \frac{1}{2} \sum_{s \in e} \sigma_s^x \right)$	$t_1^\tau = \frac{1}{2\sqrt{d}} (1 - m_x) \tau^z$ $t_2^\tau = \frac{1}{2\sqrt{2d}} \sqrt{1 - m_x^2} \tau^z$ $t_1^\sigma = \frac{\sqrt{2}}{2} \sigma^z \left( \mathbb{1} - \frac{1}{2} m_x - \frac{1}{2} \sigma^x \right)$ $t_2^\sigma = \frac{1}{2\sqrt{2}} \sqrt{1 - m_x^2} \sigma^z$
Flux string tension	$B_e = \frac{1}{2} \sqrt{\omega} \tau_e^x \left( \mathbb{1} - \frac{1}{2(d-1)} \sum_{p \in e} B_p \right)$	$b_1^\tau = \frac{\sqrt{\omega}}{2} \tau^x \left( \mathbb{1} - g_z^2 \tau^z \right)$ $b_2^\tau = \frac{1}{2} \sqrt{\frac{\omega}{2d-2}} \sqrt{1 - g_z^2} \tau^x \tau^z$ $b_3^\tau = \frac{1}{2} \sqrt{\frac{3\omega}{2d-2}} \tau^z$

■ **Table 3.2:** The rescaled mean field jump operators for the dissipative  $\mathbb{Z}_2$ -Gauge-Higgs model. The exact expression is given in the second row for comparison. In the third row all effective jump operators for the corresponding exact version are listed according to the labelling described in the text.

where  $\{L_i\} \equiv \{F_p^{(1)}, F_e^{(2)}, D_s^{(1)}, D_e^{(2)}, T_e, B_e\}$  denotes the complete dissipative process, that is, the combination of all six baths. If we assume a homogeneous system and drop the spatial indices  $s, e$  and  $p$ , this calculation yields two effective Lindblad equations (one for each mean field)

$$\begin{aligned} \partial_t \gamma &= \sum_l \sum_{\mu_l} \left[ l_{\mu_l}^\tau \gamma l_{\mu_l}^{\tau\dagger} - \frac{1}{2} \left\{ l_{\mu_l}^{\tau\dagger} l_{\mu_l}^\tau, \gamma \right\} \right] \\ \partial_t \pi &= \sum_l \sum_{\mu_l} \left[ l_{\mu_l}^\sigma \pi l_{\mu_l}^{\sigma\dagger} - \frac{1}{2} \left\{ l_{\mu_l}^{\sigma\dagger} l_{\mu_l}^\sigma, \pi \right\} \right] \end{aligned}$$

with the mean field jump operators  $\{l_{\mu_l}^\tau\}_{l, \mu_l}$  for the gauge field and  $\{l_{\mu_l}^\sigma\}_{l, \mu_l}$  for the Higgs field. Note that for each distinct interacting jump operator  $L$  (e.g.  $T_e$ ) one finds multiple effective jump operators  $l_1^\tau, \dots, l_q^\tau$  and  $l_1^\sigma, \dots, l_q^\sigma$  for each mean field (e.g.  $t_1^\tau, t_2^\tau$  and  $t_1^\sigma, t_2^\sigma$  for the charge hopping  $T_e$ ). All effective jump operators are listed in Table 3.2.

Note that we applied the rescaling

$$\omega \rightarrow \omega d \quad \text{and} \quad \lambda \rightarrow \lambda d \quad (3.36)$$

for the couplings and an overall rescaling (of time) via a global multiplication of the jump operators by  $\frac{1}{\sqrt{d}}$ .

Name	Jump Operator	Mean Field Jump Operators
Gauge string tension	$F_p^{(1)} = \frac{1}{2} B_p \left( \mathbb{1} - \frac{1}{4} \sum_{e \in p} \tau_e^x \right)$	$f_1^{(1),\tau} = \frac{\sqrt{2}}{2} \tau^z \left( \mathbb{1} - \frac{3}{4} g_x - \frac{1}{4} \tau^x \right)$ $f_2^{(1),\tau} = \frac{\sqrt{6}}{8} \sqrt{1 - g_x^2} \tau^z$
Gauge string fragility	$F_e^{(2)} = \frac{1}{2} I_e (\mathbb{1} - \tau_e^x)$	$f_1^{(2),\sigma} = \frac{\sqrt{2}}{2} (1 - g_x) \sigma^z$ $f_2^{(2),\sigma} = \frac{\sqrt{2}}{2} \sqrt{1 - g_x^2} \sigma^z$
Higgs brane tension	$D_s^{(1)} = \frac{1}{2} \sqrt{\lambda} \sigma_s^x \left( \mathbb{1} - \frac{1}{2d} \sum_{e \in s} I_e \right)$	$d_1^{(1),\sigma} = \frac{\sqrt{\lambda}}{2} \sigma^x (\mathbb{1} - m_z g_z \sigma^z)$
Higgs brane fragility	$D_e^{(2)} = \frac{1}{2} \sqrt{\lambda} \tau_e^x (\mathbb{1} - I_e)$	$d_1^{(2),\sigma} = \frac{\sqrt{2\lambda}}{2} \sigma^z$
Charge hopping	$T_e = \frac{1}{2} I_e \left( \mathbb{1} - \frac{1}{2} \sum_{s \in e} \sigma_s^x \right)$	$t_1^\sigma = \frac{\sqrt{2}}{2} \sigma^z \left( \mathbb{1} - \frac{1}{2} m_x - \frac{1}{2} \sigma^x \right)$ $t_2^\sigma = \frac{1}{2\sqrt{2}} \sqrt{1 - m_x^2} \sigma^z$
Flux string tension	$B_e = \frac{1}{2} \sqrt{\omega} \tau_e^x \left( \mathbb{1} - \frac{1}{2(d-1)} \sum_{p \in e} B_p \right)$	$b_1^\tau = \frac{\sqrt{\omega}}{2} \tau^x (\mathbb{1} - g_z^2 \tau^z)$

■ **Table 3.3:** The remaining mean field jump operators for the dissipative  $\mathbb{Z}_2$ -Gauge-Higgs model in the high-dimensional limit. The exact expression is given in the second row for comparison. In the third row the effective jump operators that survive the limit  $d \rightarrow \infty$  are listed. Note that mostly dephasing operators drop out, cf. Table 3.2.

Additionally the relative strength of the Higgs brane fragility must be modified according to

$$D_e^{(2)} = \frac{1}{2} \sqrt{\lambda} \tau_e^x (\mathbb{1} - I_e) \rightarrow \frac{1}{\sqrt{d}} \cdot \frac{1}{2} \sqrt{\lambda} \tau_e^x (\mathbb{1} - I_e) \quad (3.37)$$

This is necessary to obtain reasonable (that is, finite) jump operators in the high-dimensional limit  $d \rightarrow \infty$  but leaves the qualitative features of the phase diagram unaffected for finite  $d$ . The differences in the necessary rescaling arise since the numbers of (adjacent) sites, edges and faces scale differently with  $d$ . For instance, for each gauge spin there is *one* Higgs brane fragility operator  $D_e^{(2)}$  which acts non-trivially. In contrast, for each Higgs spin there are  $2d$  such non-trivial operators, namely  $D_e^{(2)}$  for all  $2d$  adjacent edges. This fact requires the additional rescaling of  $D_e^{(2)}$  in order to keep the action on Higgs spins finite. In Table 3.3 we list all effective jump operators that survive the  $d \rightarrow \infty$  limit. We use this reduced system to examine the phase diagram in the high-dimensional limit, see paragraph 3.3.2 below.

Mean field theory in unitary gauge

Let us now turn towards the second mean field approach. We have to transform the theory by the unitary  $T$

$$T = \prod_{e \in \mathbb{E}} [\mathbb{1}_e P_e^+ + \tilde{I}_e P_e^-] \quad (3.38)$$

into the subspace  $T^\dagger \mathcal{H}_{\text{GHM}}$ , see the preliminary discussions in Subsection 1.4.2. There the gauge condition becomes trivial, namely  $\sigma_s^x = \mathbb{1}$ , and we drop the Higgs spins for our mean field treatment. Then our ansatz reads once again

$$\rho = \prod_{e \in \mathbb{E}} \gamma_e \quad (3.39)$$

for the gauge field  $\gamma_e$ , just as for the Hamiltonian theory in 3.1.2. The transformed jump operators are listed in Table 3.4, together with the original jump operators for comparison.

Name	Gauge condition $\sigma_s^x A_s = \mathbb{1}$	Gauge condition $\sigma_s^x = \mathbb{1}$
Gauge string tension	$F_p^{(1)} = \frac{1}{2} B_p \left( \mathbb{1} - \frac{1}{4} \sum_{e \in p} \tau_e^x \right)$	$\tilde{F}_p^{(1)} = \frac{1}{2} B_p \left( \mathbb{1} - \frac{1}{4} \sum_{e \in p} \tau_e^x \right)$
Gauge string fragility	$F_e^{(2)} = \frac{1}{2} I_e (\mathbb{1} - \tau_e^x)$	$\tilde{F}_e^{(2)} = \frac{1}{2} \tau_e^z (\mathbb{1} - \tau_e^x)$
Higgs brane tension	$D_s^{(1)} = \frac{1}{2} \sqrt{\lambda} \sigma_s^x \left( \mathbb{1} - \frac{1}{2d} \sum_{e \in s} I_e \right)$	$\tilde{D}_s^{(1)} = \frac{1}{2} \sqrt{\lambda} A_s \left( \mathbb{1} - \frac{1}{2d} \sum_{e \in s} \tau_e^z \right)$
Higgs brane fragility	$D_e^{(2)} = \frac{1}{2} \sqrt{\lambda} \tau_e^x (\mathbb{1} - I_e)$	$\tilde{D}_e^{(2)} = \frac{1}{2} \sqrt{\lambda} \tau_e^x (\mathbb{1} - \tau_e^z)$
Charge hopping	$T_e = \frac{1}{2} I_e \left( \mathbb{1} - \frac{1}{2} \sum_{s \in e} \sigma_s^x \right)$	$\tilde{T}_e = \frac{1}{2} \tau_e^z \left( \mathbb{1} - \frac{1}{2} \sum_{s \in e} A_s \right)$
Flux string tension	$B_e = \frac{1}{2} \sqrt{\omega} \tau_e^x \left( \mathbb{1} - \frac{1}{2(d-1)} \sum_{p \in e} B_p \right)$	$\tilde{B}_e = \frac{1}{2} \sqrt{\omega} \tau_e^x \left( \mathbb{1} - \frac{1}{2(d-1)} \sum_{p \in e} B_p \right)$

■ **Table 3.4:** The jump operators for the dissipative  $\mathbb{Z}_2$ -Gauge-Higgs model in unitary gauge (right column). They can be derived from the original jump operators in the middle column, see also Table 3.1, by the unitary transformation  $T$  introduced in the preliminary Subsec. 1.4.2. Note that the Higgs field no longer appears in any of the jump operators.

Note that the gauge and flux string tension  $F_p^{(1)}$  and  $B_e$  are invariant under this transformation and we can reuse the mean field results found in the previous paragraph for them. Furthermore we find that the gauge string and Higgs brane fragility  $F_e^{(2)}$  and  $D_e^{(2)}$  become local operators and therefore remain unmodified by the mean field approximation. The only non-trivial mean field calculations remain to be done for the Higgs brane tension  $D_s^{(1)}$  and the charge hopping  $T_e$ . The results are shown in Table 3.5. To derive them, we applied the same rescaling as before; that is,  $\omega \rightarrow \omega d$ ,  $\lambda \rightarrow \lambda d$ ,  $\tilde{D}_e^{(2)} \rightarrow d^{-1/2} \tilde{D}_e^{(2)}$  and the global time scaling  $d^{-1/2}$ . The remaining effective jump operators in the high-dimensional limit are listed in Table 3.6. Please note that in this limit the gauge string and Higgs brane fragility vanish completely and only four baths are left. This is not really surprising since the previous result

Name	Jump Operator (Unitary Gauge)	Mean Field Jump Operators
Gauge string tension	$\tilde{F}_p^{(1)} = \frac{1}{2} B_p \left( \mathbb{1} - \frac{1}{4} \sum_{e \in p} \tau_e^x \right)$	$\tilde{f}_1^{(1),\tau} = \frac{1}{2} \sqrt{\frac{2d-2}{d}} \tau^z \left( \mathbb{1} - \frac{3}{4} g_x - \frac{1}{4} \tau^x \right)$ $\tilde{f}_2^{(1),\tau} = \frac{1}{8} \sqrt{\frac{6d-6}{d}} \sqrt{1 - g_x^2} \tau^z$
Gauge string fragility	$\tilde{F}_e^{(2)} = \frac{1}{2} \tau_e^z (\mathbb{1} - \tau_e^x)$	$\tilde{f}_1^{(2),\tau} = \frac{1}{2\sqrt{d}} \tau^z (\mathbb{1} - \tau^x)$
Higgs brane tension	$\tilde{D}_s^{(1)} = \frac{1}{2} \sqrt{\lambda} A_s \left( \mathbb{1} - \frac{1}{2d} \sum_{e \in s} \tau_e^z \right)$	$\tilde{d}_1^{(1),\tau} = \frac{\sqrt{2\lambda}}{2} \tau^x \left( \mathbb{1} - \frac{2d-1}{2d} g_z - \frac{1}{2d} \tau^z \right)$ $\tilde{d}_2^{(1),\tau} = \frac{\sqrt{2\lambda}}{2} \sqrt{\frac{2d-1}{2d}} \sqrt{1 - g_z^2} \tau^x$
Higgs brane fragility	$\tilde{D}_e^{(2)} = \frac{1}{2} \sqrt{\lambda} \tau_e^x (\mathbb{1} - \tau_e^z)$	$\tilde{d}_1^{(2),\tau} = \frac{1}{2} \sqrt{\frac{\lambda}{d}} \tau^x (\mathbb{1} - \tau^z)$
Charge hopping	$\tilde{T}_e = \frac{1}{2} \tau_e^z \left( \mathbb{1} - \frac{1}{2} \sum_{s \in e} A_s \right)$	$\tilde{t}_1^\tau = \frac{1}{2\sqrt{d}} \tau^z (\mathbb{1} - g_x^{2d-1} \tau^x)$ $\tilde{t}_2^\tau = \frac{1}{2\sqrt{2d}} \sqrt{1 - g_x^{2(2d-1)}} \tau^z \tau^x$ $\tilde{t}_3^\tau = \frac{1}{2} \sqrt{\frac{2d-1}{2d}} \tau^x$
Flux string tension	$\tilde{B}_e = \frac{1}{2} \sqrt{\omega} \tau_e^x \left( \mathbb{1} - \frac{1}{2(d-1)} \sum_{p \in e} B_p \right)$	$\tilde{b}_1^\tau = \frac{\sqrt{\omega}}{2} \tau^x (\mathbb{1} - g_z^3 \tau^z)$ $\tilde{b}_2^\tau = \frac{1}{2} \sqrt{\frac{\omega}{2d-2}} \sqrt{1 - g_z^2} \tau^x \tau^z$ $\tilde{b}_3^\tau = \frac{1}{2} \sqrt{\frac{3\omega}{2d-2}} \tau^z$

■ **Table 3.5:** The rescaled mean field jump operators for the dissipative  $\mathbb{Z}_2$ -Gauge-Higgs model in the unitary gauge. The exact expression is given in the second row for comparison. In the third row all effective jump operators for the corresponding exact version are listed.

Name	Jump Operator (Unitary Gauge)	Mean Field Jump Operators
Gauge string tension	$\tilde{F}_p^{(1)} = \frac{1}{2} B_p \left( \mathbb{1} - \frac{1}{4} \sum_{e \in p} \tau_e^x \right)$	$\tilde{f}_1^{(1),\tau} = \frac{\sqrt{2}}{2} \tau^z \left( \mathbb{1} - \frac{3}{4} g_x - \frac{1}{4} \tau^x \right)$ $\tilde{f}_2^{(1),\tau} = \frac{\sqrt{6}}{8} \sqrt{1 - g_x^2} \tau^z$
Higgs brane tension	$\tilde{D}_s^{(1)} = \frac{1}{2} \sqrt{\lambda} A_s \left( \mathbb{1} - \frac{1}{2d} \sum_{e \in s} \tau_e^z \right)$	$\tilde{d}_1^{(1),\tau} = \frac{\sqrt{2\lambda}}{2} \tau^x (\mathbb{1} - g_z)$
Charge hopping	$\tilde{T}_e = \frac{1}{2} \tau_e^z \left( \mathbb{1} - \frac{1}{2} \sum_{s \in e} A_s \right)$	$\tilde{t}_3^x = \frac{1}{2} \tau^x$
Flux string tension	$\tilde{B}_e = \frac{1}{2} \sqrt{\omega} \tau_e^x \left( \mathbb{1} - \frac{1}{2(d-1)} \sum_{p \in e} B_p \right)$	$\tilde{b}_1^\tau = \frac{\sqrt{\omega}}{2} \tau^x (\mathbb{1} - g_z^2 \tau^z)$

■ **Table 3.6:** The remaining mean field jump operators for the dissipative  $\mathbb{Z}_2$ -Gauge-Higgs model in the unitary gauge and in the high-dimensional limit. The exact expression is given in the second row for comparison. In the third row all effective jump operators that survive for  $d \rightarrow \infty$  are shown. Please note that the gauge string and Higgs brane fragility are no longer present in this limit.

for the other mean field approach, see Table 3.3, showed that the only remaining effect of both fragilities is a  $\sigma^z$ -dephasing on the Higgs field.

Now that all preparations were made, let us have a look at the solutions of the mean field equations for both theories and for finite dimensions  $d$  as well as in the high-dimensional limit.

### 3.3.2 Static solutions

In the following, we give a short analysis of the mean field stationary solutions depending on the parameters  $\omega$  and  $\lambda$ . To this end we consider the mean field jump operators with and without gauge fixing for finite dimensions and in the high dimensional limit and plug them into the steady state equations (A.26) that are derived in Appendix A and which read in our case

$$R^\sigma m^n = \epsilon^{ijn} I_{i,j}^\sigma + m^i R_{n,i}^\sigma \quad \text{and} \quad R^\tau g^n = \epsilon^{ijn} I_{i,j}^\tau + g^i R_{n,i}^\tau \quad (3.40)$$

without gauge fixing and just

$$\tilde{R}^\tau g^n = \epsilon^{ijn} \tilde{I}_{i,j}^\tau + g^i \tilde{R}_{n,i}^\tau \quad (3.41)$$

in unitary gauge with a single mean field. Here we parametrise the gauge and Higgs field density matrices

$$\gamma = \frac{1}{2} (\mathbb{1} + \mathbf{\Gamma} \boldsymbol{\tau}) \quad \text{and} \quad \pi = \frac{1}{2} (\mathbb{1} + \mathbf{\Lambda} \boldsymbol{\sigma}) \quad (3.42)$$

by means of two Bloch vectors  $\mathbf{\Gamma}$  and  $\mathbf{\Lambda}$ . Then the self-consistency conditions read  $\mathbf{\Gamma} = \mathbf{g}$  and  $\mathbf{\Lambda} = \mathbf{m}$ . The solutions of the mean field equations together with the self-consistency relations can be obtained numerically, even though they prove computationally demanding<sup>62</sup>. To simplify the calculations, one can exploit the fact that all physical stationary solutions have vanishing  $y$ -components, that is  $\Lambda_y = 0$  and  $\Gamma_y = 0$ . We already encountered this simplification in paragraph 2.3.2 where we examined the dissipative transverse field Ising model *without* unitary dynamics.

Finite dimensional system

Let us start with the mean field theories in finite dimensions  $d < \infty$ :

#### ■ Without gauge fixing

In Fig. 3.7 we show the results for the mean field theory without gauge fixing and in finite dimensions (here we set  $d = 5$ ). The expectation values  $g_z = \langle \tau^z \rangle$  for the gauge field and  $m_z = \langle \sigma^z \rangle$  for the Higgs field are shown colour-coded as functions of  $\omega$  (horizontal axis) and  $\lambda$  (vertical axis) in plots (B) and (C), respectively. The insets depict the small region around the multicritical point in detail. (A) shows the qualitative results on the coloured lines in (B) and (C). Please note that path 3 probes the phase transition between free charge and Higgs phase in detail (it runs vertically from  $\lambda = 0$  to  $\lambda = 1.5$ ) and is therefore only drawn in the insets. In (D) and (E) we show the well-known cross section of the Bloch balls with the dynamical mean field flux  $F$  which determines the flow of the Bloch vectors. In contrast to our previous analyses, here we have to deal with *two coupled* mean fields and thus two coupled Bloch vectors. That is, the dynamical flux is a true six-dimensional<sup>63</sup> vector field which cannot be illustrated without loosing information. Here we draw in (D) the Bloch ball for the gauge field and denote its *stable physical solutions* by bold and, if there are more than one, tiny dots. In (E) we do the same for the Higgs field. To draw the flux in one cross section, one has to define values of the Bloch coordinates in the other Bloch sphere and vice versa. Here we fix the Bloch coordinates of the

<sup>62</sup>At least for the finite dimensional theory with two coupled mean fields and in total 19 effective jump operators.

<sup>63</sup>Due to the trivial evolution in  $\Gamma_y$ - and  $\Lambda_y$ -direction, it can be reduced to a four-dimensional flux.



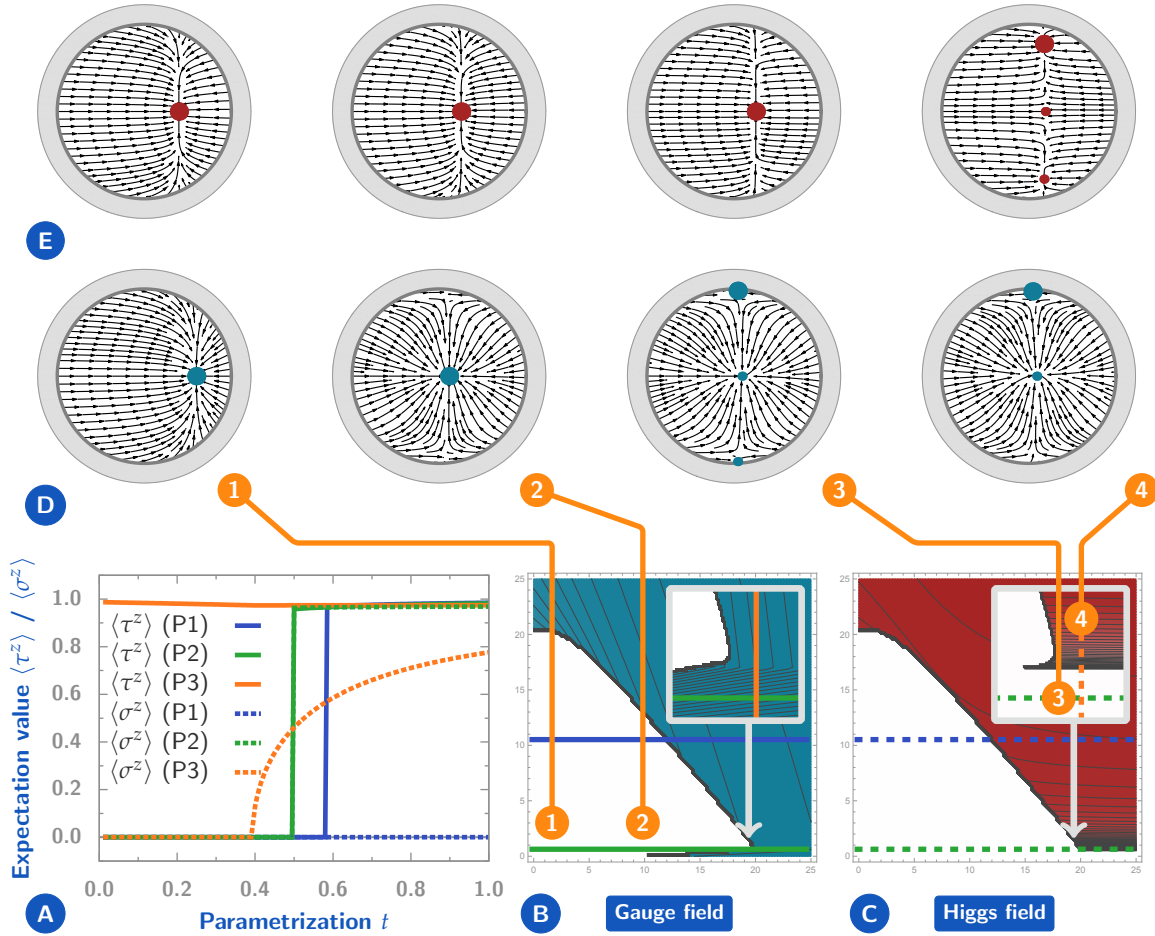


**Figure 3.7:** Mean field phase diagram for the dissipative  $\mathbb{Z}_2$ -Gauge-Higgs model with two separate mean fields for the gauge degrees of freedom and the Higgs field. In (B) we plot the maximal z-polarisation  $\langle \tau^z \rangle$  of all *stable physical steady states* for the gauge field colour-coded in the  $\omega$ - $\lambda$ -plane (light  $\rightarrow \langle \tau^z \rangle = 0$ , dark  $\rightarrow \langle \tau^z \rangle = 1$ ). (C) shows the same for the Higgs field, that is  $\langle \sigma^z \rangle$ . (A) depicts the quantitative results for  $\langle \tau^z \rangle$  (solid) and  $\langle \sigma^z \rangle$  (dashed) on the coloured paths in (B) and (C). (D) and (E) illustrate cross sections of the Bloch ball for the gauge (D) and Higgs field (E) with the dynamical mean field flux  $F$  as flux lines and the stable physical fixed points marked by discs. The corresponding parameters  $(\omega, \lambda)$  for each vertical pair of cross sections are highlighted by numbers in the 2D plots (B) and (C). The shown flux lines for the Bloch vector of one mean field depend on the Bloch vector of the other since the mean field equations couple all six degrees of freedom. Each depicted gauge field flux corresponds to a fixed point Bloch vector for the corresponding Higgs field and vice versa. Compare this mean field result with the Hamiltonian mean field theory in Fig. 3.1. A discussion of the results is given in the text.

*bold dots* in one Bloch ball and use these to draw the flux lines in the other Bloch ball. The shown flow therefore encodes the dynamics of one Bloch vector if we fix the other Bloch vector at the bold dot in the corresponding cross section. As a consequence, the flux lines cannot be used to infer the complete dynamics of the system; nevertheless they provide some insight into the stability of the stationary points and their relation to the other stationary solutions. The parameters for each vertical pair of cross sections are highlighted in the 2D plots by numbers.

We now turn towards the conclusions that can be drawn. To this end, compare Fig. 3.7 with the results for the Hamiltonian theory in Fig. 3.1. Let us emphasise the central results:

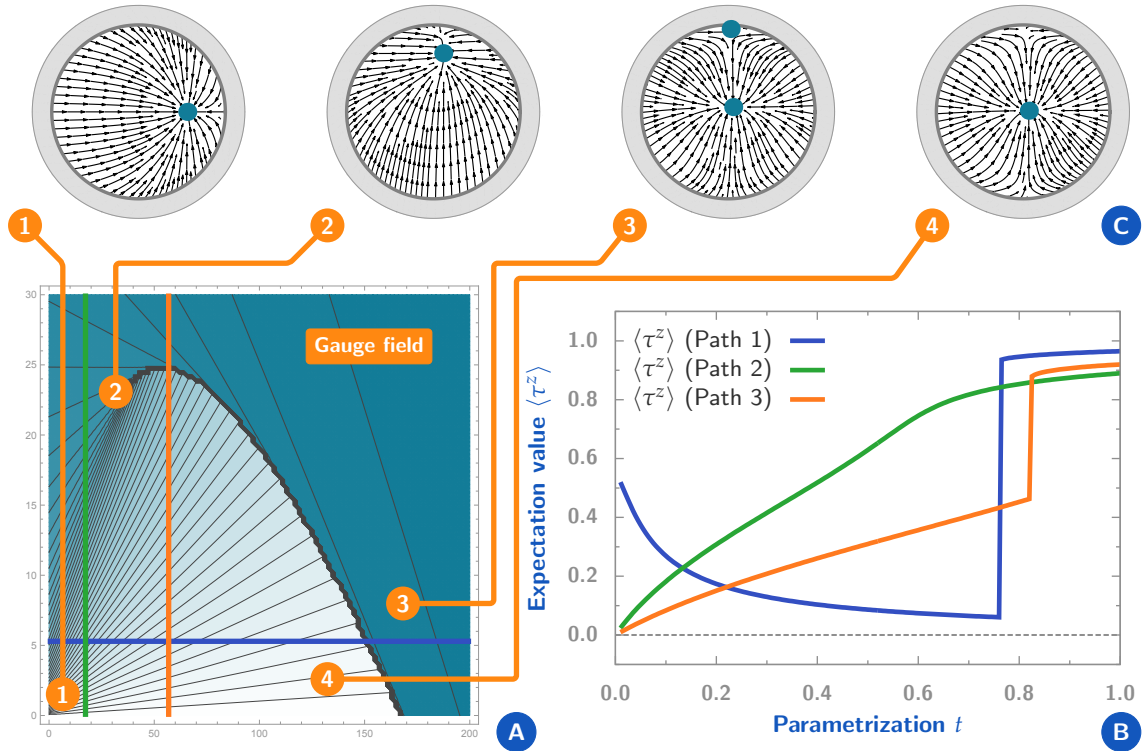
- We essentially succeeded: The plots in (B) and (C) as well as the qualitative results in (A) suggest the existence of three distinct phases which are characterised by  $g_z = 0$  and  $m_z = 0$  (confined charge phase),  $g_z > 0$  and  $m_z = 0$  (free charge phase), and  $g_z > 0$  and  $m_z > 0$  (Higgs phase) — just as in the Hamiltonian mean field theory.
- The phase transitions between confined and free charge phase as well as between confined charge and Higgs phase are of first order. Contrary to the transition separating free charge and Higgs phase which is obviously of second order as (A) reveals. This is also in accordance with the Hamiltonian mean field results.

However, there are also some drawbacks which may require a more carefully chosen relative strength of the six baths. Another reason for the deviations from our expected result (see Fig. 3.3) may be the break down of mean field theory which certainly does not take into account the subtle actions of the jump operators. Let us point out the most severe issues:

- As in the Hamiltonian mean field theory, in general one finds multiple solutions to the mean field equations. Whereas in the Hamiltonian framework we can employ the minimisation of energy to decide which solutions represents the actual ground state, there is no such principle for purely dissipative dynamics. In Fig. 3.7 (A)-(C) we choose always the solution which maximises the shown expectation values as this indicates successfully when new stable solutions appear. Although these solutions, highlighted in (D) and (E) by bold dots, are *stable*, we cannot conclude which of the multiple stable solutions in the free charge and Higgs phase correspond to the actual stationary states or whether they are competing, metastable solutions.
- We demanded that the stationary states in the three corners of the compactified parameter space become *pure dark states* since they represent the three distinct phases of the Hamiltonian  $\mathbb{Z}_2$ -Gauge-Higgs model. We *succeeded* for the Higgs phase as the cross sections in (D) and (E) reveal. In the free charge phase the gauge field becomes pure but the Higgs field remains mixed; not completely mixed, but mixed after all. In the confined charge phase both field remain mixed for  $\omega \rightarrow 0$  and  $\lambda \rightarrow 0$  where the gauge field is more pure than the Higgs field<sup>64</sup>. This is caused by the dephasings and could possibly be mended by a modification of the jump operators' relative strength.
- As (B) and the inset of (C) reveal, there is a *kink* at the multicritical point where the transition line to the free charge phase deviates from the Hamiltonian version which runs (more or less) vertically down to meet the  $\omega$ -axis. This, however, does not change the qualitative structure of the phase diagram.
- Note that the values of  $\omega$  and  $\lambda$  at which the first order transition occurs are rather large as compared to the value of  $\lambda$  where the second order transition takes place. This ratio may be tuned by modifications the relative bath strengths.

To sum it up: These first results of the mean field theory are promising but push forward several issues which require further inspection. Please note that the theory provides us with a large number of degrees of freedom (namely, the relative strengths of six baths) which allow for fine tuning. Since this theory is intended to show that there are more complicated structures that might feature purely dissipatively driven phase transitions — motivated by a model Hamiltonian theory — we are not going to have a closer look at the aforementioned issues and their possible mending. This is left open as a task for the future.

<sup>64</sup>Only for  $\omega = 0 = \lambda$  an unstable fixed point on the Bloch sphere at  $\Gamma_x = 1$  and  $\Lambda_x = 1$  appears.



■ **Figure 3.8:** Mean field phase diagram for the dissipative  $\mathbb{Z}_2$ -Gauge-Higgs model in unitary gauge with a single mean field for the gauge degrees of freedom. In (A) we plot the maximal  $z$ -polarisation  $\langle \tau^z \rangle$  of all *stable physical steady states* colour-coded in the  $\omega$ - $\lambda$ -plane (light  $\rightarrow \langle \tau^z \rangle = 0$ , dark  $\rightarrow \langle \tau^z \rangle = 1$ ). In (B) we show the quantitative results for  $\langle \tau^z \rangle$  on the coloured paths in (A). (C) illustrates four characteristic cross sections of the Bloch ball with the dynamical mean field flux  $F$  as flux lines and the stable physical fixed points marked by cyan discs. The corresponding parameters  $(\omega, \lambda)$  for each cross section are highlighted by numbers in the 2D plot (A). Compare this dissipative result with the Hamiltonian mean field theory in Fig. 3.2. A discussion of the results is given in the text.

### ■ With gauge fixing (Unitary gauge)

Let us now have a look at the corresponding theory in unitary gauge, the results of which are shown in Fig. 3.8. The basic structure of the illustration equals that of Fig. 3.7 which was described in detail above. The difference is that there is only a single mean field to be analysed. We compare these findings with the results for the Hamiltonian theory in Fig. 3.2:

- The result is obviously quite similar to the Hamiltonian theory. There is a region of small (but non-zero) gauge field expectation values  $g_z$  for small  $\omega$  and  $\lambda$  which represents the confined charge phase. Then there is a region for large  $\omega$  where  $g_z$  is close to 1 which corresponds to both the free charge and the Higgs phase. For small  $\lambda$ , both regions are separated by a first order transition that *ends* in a critical point close to (2). Beyond this critical point the transition between both phases is analytical, as can be inferred from the green curve in (B).
- Referring to the purity, we find pure stationary states in the Higgs phase limit  $\omega \rightarrow \infty$  and  $\lambda \rightarrow \infty$  as well as in the free charge limit  $\omega \rightarrow \infty$  and  $\lambda \rightarrow 0$ , the latter of which cannot be distinguished by a phase transition in this mean field theory (as in the Hamiltonian

counterpart). As before, in the confined charge limit  $\omega \rightarrow 0$  and  $\lambda \rightarrow 0$  the gauge field stationary state remains mixed as the cross section (1) demonstrates.

- The small- $g_z$  fixed point in the confined charge phase close to the first order line is almost completely mixed, see (4). When the phase boundary is traversed, a second stable solution close to the  $g_z = 1$ -pole of the Bloch ball appears, see (3). Please note that this almost pure solution is stable although the flux in (3) suggests otherwise. In fact, there is an unstable saddle point close to the pole and the stable solution lives within its attraction domain shaped like a pole cap.

We conclude that the mean field theory in unitary gauge yields the expected results up to the purity issue for small  $\omega$  and  $\lambda$ : Up to the scaling of  $\omega$  and  $\lambda$ , the phase diagram in Fig. 3.8 is close to its Hamiltonian counterpart in Fig. 3.2.

High-dimensional limit

We shall now turn towards the mean field theories in the high-dimensional limit:

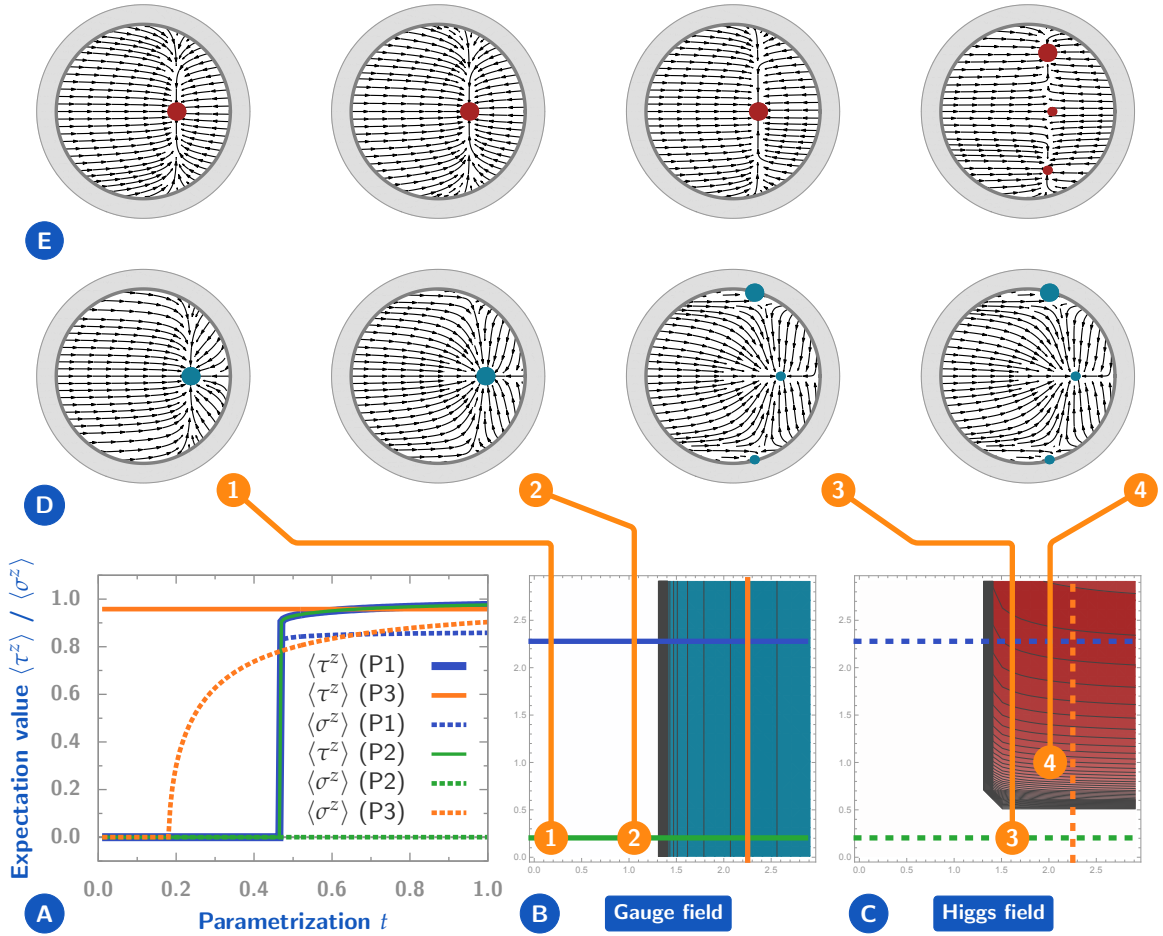
#### ■ Without gauge fixing

In Fig. 3.9 we present the results for the theory with two mean field degrees of freedom when we take into account only jump operators that survive in the  $d \rightarrow \infty$  limit. The structure of the illustration equals its finite- $d$  counterpart in Fig. 3.7. Compare these results with the findings for finite  $d$  in Fig. 3.7:

- If we have a look at (B) and (C), we find that there are still three distinct phases characterised by  $g_z = 0$  and  $m_z = 0$  (confined charge phase),  $g_z > 0$  and  $m_z = 0$  (free charge phase) and  $g_z > 0$  and  $m_z > 0$  (Higgs phase).
- The phase transitions that separate these phases remain of first and second order, respectively, see (A). We conclude that the key constituents of the mean field phase diagram survive in the high-dimensional limit.
- The cross sections in (D) and (E) are similar to those in 3.7 and we argue that the mathematical mechanisms that are responsible for the observed phase transitions remain unchanged. The only differences are, first, that the  $g_z = 0$  solution for the gauge field no longer shifts towards the completely mixed state in the centre of the Bloch ball but stays fixed halfway to the  $g_x = 1$ -pole, see (1)-(3). And second, that in the Higgs phase (4) there is another stable solution close to the  $g_z = -1$ -pole. A detailed inspection shows that this solution comes along with a *vanishing* Higgs field and is therefore *not equivalent* to the highlighted solution close to  $g_z = 1$ .

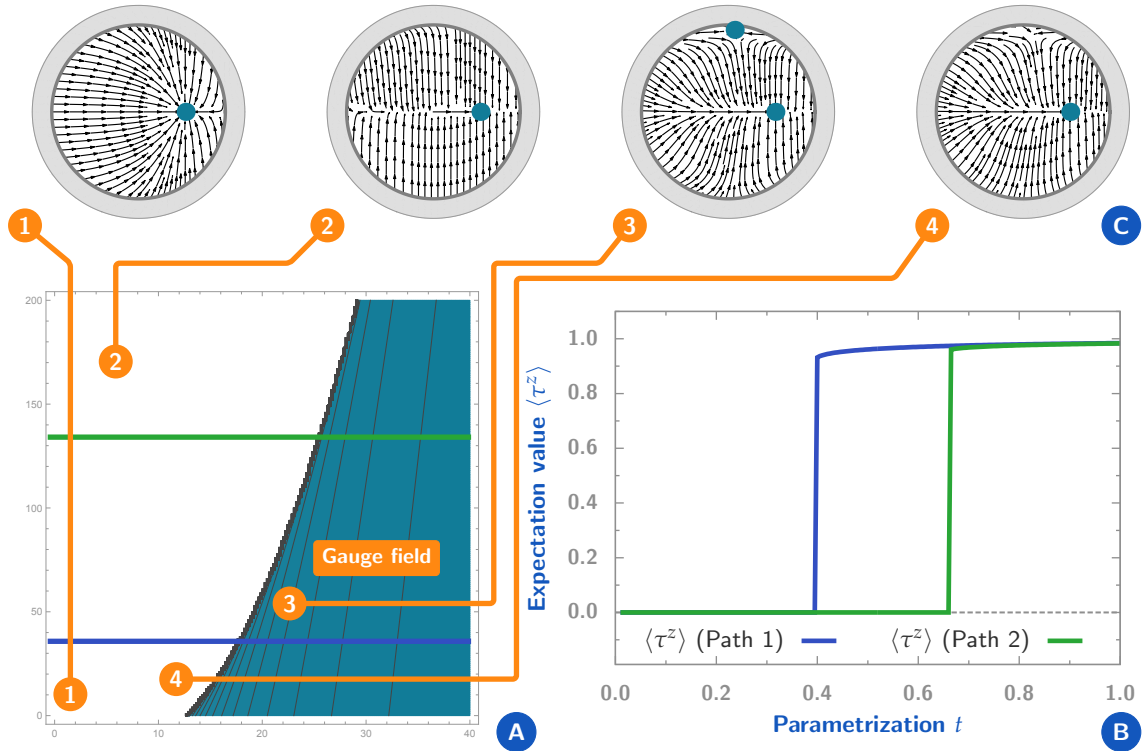
There are, however, some striking differences to the finite- $d$  phase diagram:

- The first order line separating confined charge and Higgs phase no longer terminates at the  $\lambda$  axis but runs off vertically towards infinity. This is a major drawback as it questions the existence of the analyticity region that connects confined charge and Higgs phase.
- Furthermore note that the irregular kink feature of the free charge phase below the multi-critical point is no longer present.



■ **Figure 3.9:** Mean field phase diagram for the dissipative  $\mathbb{Z}_2$ -Gauge-Higgs model with two separate mean fields for the gauge degrees of freedom and the Higgs field in the high-dimensional limit. In (B) we plot the maximal  $z$ -polarisation  $\langle \tau^z \rangle$  of all *stable physical steady states* for the gauge field colour-coded in the  $\omega$ - $\lambda$ -plane (light  $\rightarrow \langle \tau^z \rangle = 0$ , dark  $\rightarrow \langle \tau^z \rangle = 1$ ). (C) shows the same for the Higgs field, that is  $\langle \sigma^z \rangle$ . (A) depicts the quantitative results for  $\langle \tau^z \rangle$  (solid) and  $\langle \sigma^z \rangle$  (dashed) on the coloured paths in (B) and (C). (D) and (E) illustrate cross sections of the Bloch ball for the gauge (D) and Higgs field (E) with the dynamical mean field flux  $F$  as flux lines and the stable physical fixed points marked by discs. The corresponding parameters  $(\omega, \lambda)$  for each vertical pair of cross sections are highlighted by numbers in the 2D plots (B) and (C). The shown flux lines for the Bloch vector of one mean field depend on the Bloch vector of the other since the mean field equations couple all six degrees of freedom. Each depicted gauge field flux corresponds to a fixed point Bloch vector for the corresponding Higgs field and vice versa. Compare this result for  $d \rightarrow \infty$  with the mean field result for finite  $d < \infty$  in Fig. 3.7 and with the Hamiltonian mean field theory in Fig. 3.1. A discussion of the results is given in the text.

In this sense, the phase diagram for  $d \rightarrow \infty$  lost some of its peculiar and undesired features; but it lost also one of its characteristic features, namely the coincidence of first order line and  $\lambda$ -axis. The question that arises is whether this qualitative modification finds expression in the unitary gauge mean field theory.



■ **Figure 3.10:** Mean field phase diagram for the dissipative  $\mathbb{Z}_2$ -Gauge-Higgs model in unitary gauge with a single mean field for the gauge degrees of freedom in the high-dimensional limit. In (A) we plot the maximal  $z$ -polarisation  $\langle \tau^z \rangle$  of all *stable physical steady states* colour-coded in the  $\omega$ - $\lambda$ -plane (light  $\rightarrow \langle \tau^z \rangle = 0$ , dark  $\rightarrow \langle \tau^z \rangle = 1$ ). In (B) we show the quantitative results for  $\langle \tau^z \rangle$  on the coloured paths in (A). (C) illustrates four characteristic cross sections of the Bloch ball with the dynamical mean field flux  $F$  as flux lines and the stable physical fixed points marked by cyan discs. The corresponding parameters  $(\omega, \lambda)$  for each cross section are highlighted by numbers in the 2D plot (A). Compare this mean field result for  $d \rightarrow \infty$  with the corresponding result for  $d < \infty$  in Fig. 3.8 and with the Hamiltonian mean field theory in Fig. 3.2. A discussion of the results is given in the text.

#### ■ With gauge fixing (Unitary gauge)

In Fig. 3.10 we show the results for the mean field theory in unitary gauge in the limit  $d \rightarrow \infty$ . A comparison with the results for finite  $d$  in Fig. 3.8 yields immediately: *Yes*, the qualitative modification in Fig. 3.9 is also present in the unitary gauge:

- The two sections of *small*  $g_z$  and large  $g_z$  that were connected smoothly via the analyticity region are now completely separated since the first order transition runs off towards infinity. This corresponds to the the first order line in Fig. 3.8 that no longer terminates at a critical point on the  $\lambda$ -axis.
- As a consequence of this true first order separation, the expectation value  $g_z$  vanishes identically in the confined charge phase as (B) reveals.
- Note that the  $g_z = 0$ -solution remains fixed in the Bloch ball, see (1)-(4). In contrast to the finite- $d$  theory, see Fig. 3.8 (2), this solution no longer obtains any finite  $g_z$  value but remains attached to the  $\Gamma_x$ -axis. At the phase transition, the almost pure stationary solution at the  $g_z = 1$ -pole appears within its small but finite attraction domain.

We conclude that the results for the mean field theory in unitary gauge match our findings in the previous paragraph for the mean field theory without gauge fixing: Both lack the feature of a terminating first order line. Nevertheless, the first order transition and the two distinct phases survive in this limit. ■

In conclusion, our mean field analysis with and without gauge fixing revealed a qualitative resemblance with the Hamiltonian mean field results. The phases and phase transitions survive in the high-dimensional limit which supports their relevance for the actual physical system. Unfortunately, the termination of the first order line that separates confined charge and Higgs phase cannot be reproduced in this limit. This suggest either that the actual phase diagram of the dissipative  $\mathbb{Z}_2$ -Gauge-Higgs model features a qualitatively different phase structure than its Hamiltonian counterpart, or that the mean field theory breaks down and no longer reproduces the key features of the correct phases and phase transitions.

Answers to these questions cannot be given in the approximative framework that we applied here. As it is illusionary to hope for general analytical solutions, answering these questions demands for perturbative approaches or duality arguments. Since this thesis is already extensive enough and due to a lack of time, we leave these questions open as tasks for the future.





# The dissipative Majorana chain

*"I am a Quantum Engineer, but on Sundays I Have Principles."*

John Stewart Bell

The previous two chapters 2 and 3 represent the main part of this master thesis. There we introduced new models and analysed their properties in detail. This chapter is *different* as it is concerned with a model that was introduced recently by Diehl *et al.* in Ref. [1]. There a proposal for the purely *dissipative* implementation of the Majorana chain ground states was given. For a review of the *Hamiltonian* Majorana chain see Subsec. 1.3.4 in the preliminary chapter 1. The main part of the aforementioned publication is concerned with the identification and discussion of a topological invariant that is responsible for the stability of the dissipatively reached dark state space which comprises the degenerate edge modes known from Kitaev's Majorana chain. This analysis is based on non-interacting jump operators that equal the quasi particle annihilators of the Majorana chain at the ideal parameter point. However, as a *starting point* different jump operators are introduced for which an experimental realisation in terms of cold atoms is proposed. These jump operators are *interacting* and *number conserving*; the non-interacting and *parity violating* jump operators that are used for all theoretical conclusions are derived by a *mean field approximation* from the number conserving ones.

The calculations and investigations that we present in this chapter were motivated by this questionable transition from number conserving to parity violating jump operators. Here we are *not* concerned with the main results of Ref. [1] which are based on the non-interacting jump operators; due to some validating calculations we agree with these statements. However, we argue that the proposed *experimental realisation* in terms of number-conserving jump operators does not yield a dissipative counterpart of the Majorana chain in any finite setup that may be realised in the laboratory. To this end we analyse the structure of the exact dark states and compare them to the Majorana ground states. We furthermore give some detailed recalculations of the results presented in [1] and the supplementary information to gain a better understanding of the transition from number conserving to parity violating jump operators.

This chapter is structured as follows. In Section 4.1 we give a brief outline of the proposed setting. In Section 4.2 follows a detailed derivation of the exact (number conserving) dark states (Subsec. 4.2.2). We give a thorough treatment regarding the *uniqueness* of the steady states in each fixed number sector and provide a computer-assisted proof for up to 15 sites (Subsec. 4.2.3). In Section 4.3 we recalculate the mean field approximation of Ref. [1]. In Section 4.4 we compare the number conserving dark states with the Majorana ground states. We conclude this chapter with some final remarks in Section 4.5.

*Let me point out that — in contrast to the more or less self-contained chapters 5, 2 and 3 — it is crucial for the following calculations to be familiar with the original statements and calculations in Ref. [1]. It may be even advisable to read the supplementary information to gain a deeper understanding of this chapter.*

## 4.1 The Setting

The dissipative setup in [1] is *motivated* by Kitaev's Majorana chain [3] at the ideal point. In the preliminary review of the latter we found in Subsec. 1.3.4 the Hamiltonian

$$H = iw \sum_{i=1}^{L-1} c_{2i} c_{2i+1} = 2w \sum_{i=1}^{L-1} \left( \tilde{a}_i^\dagger \tilde{a}_i - \frac{1}{2} \right), \quad (4.1)$$

see Eq. (1.71) and (1.75). The elementary excitations  $\tilde{a}_i^\dagger$  are fermionic quasi particles with a flat dispersion at this ideal point. If one aims at a dissipative implementation of the above Hamiltonians ground state space, it is natural to choose the non-interacting jump operators

$$j_i = \tilde{a}_i = \frac{1}{2} \left( a_i + a_i^\dagger - a_{i+1} + a_{i+1}^\dagger \right) \quad \text{for } 1 \leq i < L; \quad (4.2)$$

that is, all fermionic annihilation operators but the edge mode  $\tilde{a}_L = b$  (which is non-local after all). Since these jump operators obey a fermionic Dirac algebra, it is trivial to see that the dark states coincide with the two degenerate ground states of (4.1) and that the coherent superpositions of the latter (and their mixtures) are the only steady states of the process. These are the jump operators that are used in [1] to derive a dissipative analogue of a *topological phase*. To this end a topological invariant (Chern number) is found that explains the stability of the dissipatively separated edge states against quenched disorder in the bath couplings.

The proposed experimental setup in terms of cold atoms however realises *not* the jump operators  $j_i$  but the *interacting* and *number conserving* jump operators

$$J_i = \frac{1}{4} \left( a_i^\dagger + a_{i+1}^\dagger \right) \left( a_i - a_{i+1} \right) = \frac{1}{4} \left( a_i^\dagger a_i + a_{i+1}^\dagger a_i - a_i^\dagger a_{i+1} - a_{i+1}^\dagger a_{i+1} \right) \quad (4.3)$$

for  $1 \leq i < L$ . Their dark states are not trivial to see nor is it trivial to proof their uniqueness in a fixed number sector of the Hilbert space. The authors of [1] then employ a mean field approximation of the  $J_i$  with a product ansatz of the density matrix in momentum space — which yields the above fermionic quasiparticle annihilators.

The relation between the dark states of  $J_i$  and  $j_i$  and the mentioned mean field approximation are the main topics of the following sections. We start with an analysis of the *exact* dark states for the number conserving jump operators and discuss their uniqueness as steady states of the dissipative process.

## 4.2 Steady states of the number conserving jump operators

In this section we derive the exact dark states of the number conserving process rigorously. We furthermore discuss the uniqueness of the latter as stationary states of the dissipative process in a fixed number sector of the Hilbert space and give a computer-assisted proof for  $L \leq 15$  sites. We conclude this section with a discussion of their parent Hamiltonian and some properties of the dark states.

### 4.2.1 Notation and some preliminary notes

Let us start with some remarks on notation and some facts about the jump operators  $\{J_i\}$ .

Description of the fermionic system

First, let us fix the notation. Let  $\mathfrak{F}_L$  be the abstract Fermion algebra on  $L$  generators, i.e.

$$\mathfrak{F}_L = \left\langle a_1, \dots, a_L, a_1^\dagger, \dots, a_L^\dagger \mid \{a_i, a_j\} = \{a_i^\dagger, a_j^\dagger\} = 0, \{a_i, a_j^\dagger\} = \delta_{ij}, 1 \leq i, j \leq L \right\rangle \quad (4.4)$$

with  $2^{2L}$  linearly independent, normal ordered basis elements  $a_{i_1}^\dagger \dots a_{i_n}^\dagger a_{j_1} \dots a_{j_m}$ , that is  $\dim \mathfrak{F}_L = 2^{2L}$  [121]. A commonly used representation of this algebra is obtained by a Jordan-Wigner transformation. To this end we choose the computational basis  $|0\rangle = (1, 0)^T$  and  $|1\rangle = (0, 1)^T$  such that  $\mathcal{H}_i = \text{span}\{|0\rangle_i, |1\rangle_i\}$ . Furthermore let  $\mathcal{H}_L = \otimes_i^L \mathcal{H}_i$  be spanned by  $\{|\mathbf{n}\rangle \mid \mathbf{n} \in \{0, 1\}^L\}$  which one usually calls *number states*. With this basis in mind, the representation  $\rho_L$  reads

$$\rho_L : \mathfrak{F}_L \longrightarrow \text{End } \mathcal{H}_L \cong \text{Mat}(\mathbb{C}, 2^L) \quad (4.5a)$$

$$a_j \mapsto \rho_L(a_j) = \left[ \prod_{k=1}^{j-1} \sigma_k^z \right] \sigma_j^+ \quad (4.5b)$$

$$a_j^\dagger \mapsto \rho_L(a_j^\dagger) = \left[ \prod_{k=1}^{j-1} \sigma_k^z \right] \sigma_j^- \quad (4.5c)$$

which is easily verified to be an algebra homomorphism. Since  $\rho_L$  provides an action of  $\mathfrak{F}_L$  on  $\mathcal{H}_L$ , the latter becomes a  $\mathfrak{F}_L$ -module. Here  $\sigma_i^{x,y,z}$  denotes the Pauli matrices acting on  $\mathcal{H}_i$  and  $\sigma_j^\pm = \frac{1}{2}(\sigma_j^x \pm i\sigma_j^y)$  the corresponding creation- and annihilation matrices. Note that  $\sigma_j^z |n\rangle_j = (-1)^n |n\rangle_j$ ,  $n \in \{0, 1\}$ . For simplicity we identify the abstract elements  $a_i \in \mathfrak{F}_L$  with their representations  $\rho_L(a_i)$ . Then we can write

$$|\mathbf{n}\rangle = |n_1, \dots, n_L\rangle = (a_1^\dagger)^{n_1} \dots (a_L^\dagger)^{n_L} |0, \dots, 0\rangle \quad (4.6)$$

and we find

$$a_i |n_1, \dots, n_i, \dots, n_L\rangle = \begin{cases} 0, & \text{if } n_i = 0 \\ (-1)^{n_1 + \dots + n_{i-1}} |n_1, \dots, 0, \dots, n_L\rangle, & \text{if } n_i = 1 \end{cases} \quad (4.7a)$$

and

$$a_i^\dagger |n_1, \dots, n_i, \dots, n_L\rangle = \begin{cases} (-1)^{n_1 + \dots + n_{i-1}} |n_1, \dots, 1, \dots, n_L\rangle, & \text{if } n_i = 0 \\ 0, & \text{if } n_i = 1 \end{cases} \quad (4.7b)$$

due to the anticommutation relation  $\{a_i, a_j\} = \delta_{ij}$ . As a result, it follows

$$a_i^\dagger a_i |n_1, \dots, n_i, \dots, n_L\rangle = n_i |n_1, \dots, n_i, \dots, n_L\rangle \quad (4.8a)$$

$$a_i^\dagger a_j |n_1, \dots, 0, \dots, 1, \dots, n_L\rangle = (-1)^{n_{i+1} + \dots + n_{j-1}} |n_1, \dots, 1, \dots, 0, \dots, n_L\rangle \quad (4.8b)$$

$$a_j^\dagger a_i |n_1, \dots, 1, \dots, 0, \dots, n_L\rangle = (-1)^{n_{i+1} + \dots + n_{j-1}} |n_1, \dots, 0, \dots, 1, \dots, n_L\rangle \quad (4.8c)$$

where  $N_i \equiv a_i^\dagger a_i$  is the one-site number operator and  $i < j$ .  $a_i^\dagger a_j$  performs a jump to the left, provided site  $i$  is vacant and site  $j$  is not. In the remaining cases, the state is annihilated. The same holds for the jump to the right,  $a_j^\dagger a_i$ .

We remind the reader of some special cases which will become important below:

$$a_i^\dagger a_{i+1} |n_1, \dots, 0, 1, \dots, n_L\rangle = |n_1, \dots, 1, 0, \dots, n_L\rangle \quad (4.9a)$$

$$a_{i+1}^\dagger a_i |n_1, \dots, 1, 0, \dots, n_L\rangle = |n_1, \dots, 0, 1, \dots, n_L\rangle \quad (4.9b)$$

$$a_1^\dagger a_L |0, \dots, 1\rangle = (-1)^{n_2 + \dots + n_{L-1}} |1, \dots, 0\rangle = (-1)^{N-1} |1, \dots, 0\rangle \quad (4.9c)$$

$$a_L^\dagger a_1 |1, \dots, 0\rangle = (-1)^{n_2 + \dots + n_{L-1}} |0, \dots, 1\rangle = (-1)^{N-1} |0, \dots, 1\rangle \quad (4.9d)$$

where  $N = \sum_{i=1}^L n_i$  denotes the total number of fermions.

## Description of the jump operators

The number conserving jump operators given above read

$$J_i = \frac{1}{4} (a_i^\dagger + a_{i+1}^\dagger) (a_i - a_{i+1}) = \frac{1}{4} (a_i^\dagger a_i + a_{i+1}^\dagger a_i - a_i^\dagger a_{i+1} - a_{i+1}^\dagger a_{i+1}) \quad (4.10)$$

for  $1 \leq i < L$ . In the following we give some preliminary notes on their Jordan-Wigner transformation and their algebra.

### ■ Jordan-Wigner transformation

In order to obtain numerical results (which may be employed for verification and inspiration), a matrix representation for the jump operators, and thus the fermionic algebra, is required. To this end, we insert the Jordan-Wigner transformed fermionic operators (as defined above) into the jump operators and obtain

$$\begin{aligned} \hat{J}_i &= \frac{1}{4} \left( \left[ \prod_{k=1}^{i-1} \sigma_k^z \right] \sigma_i^- + \left[ \prod_{k=1}^i \sigma_k^z \right] \sigma_{i+1}^- \right) \left( \left[ \prod_{k=1}^{i-1} \sigma_k^z \right] \sigma_i^+ - \left[ \prod_{k=1}^i \sigma_k^z \right] \sigma_{i+1}^+ \right) \\ &= \frac{1}{4} (\sigma_i^- + \sigma_i^z \sigma_{i+1}^-) (\sigma_i^+ - \sigma_i^z \sigma_{i+1}^+) \\ &= \frac{1}{4} (\sigma_i^- \sigma_i^+ + \sigma_i^z \sigma_{i+1}^- \sigma_i^+ - \sigma_i^- \sigma_i^z \sigma_{i+1}^+ - \sigma_i^z \sigma_{i+1}^- \sigma_i^z \sigma_{i+1}^+) \\ &= \frac{1}{4} \left[ \frac{1}{2} (\mathbb{1} - \sigma_i^z) - \frac{1}{2} (\mathbb{1} - \sigma_{i+1}^z) + \sigma_i^z (\sigma_{i+1}^- \sigma_i^+ + \sigma_i^- \sigma_{i+1}^+) \right] \\ &= \frac{1}{8} [\sigma_{i+1}^z - \sigma_i^z + 2\sigma_i^z (\sigma_{i+1}^- \sigma_i^+ + \sigma_i^- \sigma_{i+1}^+)] \\ &= \frac{1}{8} [\sigma_{i+1}^z - \sigma_i^z + i(\sigma_{i+1}^x \sigma_i^y - \sigma_{i+1}^y \sigma_i^x)] \end{aligned}$$

for  $1 \leq i \leq L-1$  where we used  $\sigma^z \sigma^+ = \sigma^+$  and  $\sigma^z \sigma^- = -\sigma^-$ . Obviously all jump operators in the open setup remain local after the Jordan-Wigner transformation. However, the additional jump operator  $J_L$  retains a non-local string which measures the parity of the bulk:

$$\begin{aligned} \hat{J}_L &= \frac{1}{4} \left( \left[ \prod_{k=1}^{L-1} \sigma_k^z \right] \sigma_L^- + \sigma_1^- \right) \left( \left[ \prod_{k=1}^{L-1} \sigma_k^z \right] \sigma_L^+ - \sigma_1^+ \right) \\ &= \frac{1}{4} (P' \sigma_1^z \sigma_L^- + \sigma_1^-) (P' \sigma_1^z \sigma_L^+ - \sigma_1^+) \\ &= \frac{1}{8} [\sigma_1^z - \sigma_L^z - 2P' \sigma_1^z (\sigma_1^- \sigma_L^+ + \sigma_L^- \sigma_1^+)] \\ &= \frac{1}{8} [\sigma_1^z - \sigma_L^z + iP' (\sigma_1^x \sigma_L^y - \sigma_1^y \sigma_L^x)] \end{aligned}$$

Where we introduced the bulk parity  $P' = \prod_{k=2}^{L-1} \sigma_k^z$ .

### ■ Action on the number basis

It obvious that  $J_i$  annihilates a number state if  $n_i = n_{i+1}$ . On the other hand, if  $n_i \neq n_{i+1}$ , either a left or a right jump is performed, along with a superposition with the previous state. In a pictorial representation this reads ( $i$  is the left fermionic site):

$$J_i |\square\square\rangle = 0 \quad (4.11a)$$

$$J_i |\square\blacksquare\rangle = -\frac{1}{4} [|\blacksquare\square\rangle + |\square\blacksquare\rangle] \quad (4.11b)$$

$$J_i |\blacksquare\square\rangle = \frac{1}{4} [|\square\blacksquare\rangle + |\blacksquare\square\rangle] \quad (4.11c)$$

$$J_i |\blacksquare\blacksquare\rangle = 0 \quad (4.11d)$$

It follows immediately that  $J_i^2$  annihilates every number state.

Note that the above discussion holds only for an *open chain*. Closing an open chain (i.e. introducing periodic boundary conditions) is described by an additional jump operator  $J_L$

$$J_L = \frac{1}{4} (a_L^\dagger a_L + a_1^\dagger a_L - a_L^\dagger a_1 - a_1^\dagger a_1) . \quad (4.12)$$

Whereas for the the other jump operators  $J_i$  with  $1 \leq i \leq L-1$  the previous arguments still apply, the new jump operator comes up with a peculiarity:

$$J_L |\square\dots\square\rangle = 0 \quad (4.13a)$$

$$J_L |\square\dots\blacksquare\rangle = -\frac{1}{4} [(-1)^{N-1} |\blacksquare\dots\square\rangle + |\square\dots\blacksquare\rangle] \quad (4.13b)$$

$$J_L |\blacksquare\dots\square\rangle = \frac{1}{4} [(-1)^{N-1} |\square\dots\blacksquare\rangle + |\blacksquare\dots\square\rangle] \quad (4.13c)$$

$$J_L |\blacksquare\dots\blacksquare\rangle = 0 \quad (4.13d)$$

We are now going to write the action of the jump operators on the number states in a more compact form. To this end, introduce the *local transposition*  $\tau_i$

$$\tau_i : \{0,1\}^L \longrightarrow \{0,1\}^L \quad (4.14a)$$

$$\mathbf{n} = (n_1, \dots, n_i, n_{i+1}, \dots, n_L)^T \mapsto \tau_i \mathbf{n} = (n_1, \dots, n_{i+1}, n_i, \dots, n_L)^T \quad (4.14b)$$

$$\tau_L : \{0,1\}^L \longrightarrow \{0,1\}^L \quad (4.14c)$$

$$\mathbf{n} = (n_1, \dots, n_L)^T \mapsto \tau_L \mathbf{n} = (n_L, \dots, n_1)^T, \quad (4.14d)$$

where  $1 \leq i \leq L-1$ . Furthermore the *local signum* is defined as

$$\sigma_i : \{0,1\}^L \longrightarrow \{-1,0,1\}, \quad \mathbf{n} \mapsto \sigma_i \mathbf{n} = \begin{cases} +1 & \Leftrightarrow n_i = 1 \wedge n_{i+1} = 0 \\ 0 & \Leftrightarrow n_i = n_{i+1} \\ -1 & \Leftrightarrow n_i = 0 \wedge n_{i+1} = 1 \end{cases} \quad (4.15)$$

where  $i$  is a variable modulo  $L$ . It is easy to verify that

$$\sigma_i \tau_j \mathbf{n} = \begin{cases} -\sigma_i \mathbf{n} & \Leftrightarrow |i-j| = 0 \\ \sigma_i \mathbf{n} + \sigma_j \mathbf{n} & \Leftrightarrow |i-j| = 1 \\ \sigma_i \mathbf{n} & \Leftrightarrow |i-j| > 1 \end{cases} . \quad (4.16)$$

We are now in the position to express the action of the jump operators as follows:

$$J_i |\mathbf{n}\rangle = \sigma_i \mathbf{n} (|\mathbf{n}\rangle + |\tau_i \mathbf{n}\rangle) \quad (4.17a)$$

$$J_L |\mathbf{n}\rangle = \sigma_L \mathbf{n} (|\mathbf{n}\rangle + (-1)^{N-1} |\tau_L \mathbf{n}\rangle) \quad (4.17b)$$

Set  $\|\mathbf{n}\| = \sum_{i=1}^L n_i$  and  $B_N = \{\mathbf{n} \in \{0, 1\}^L \mid \|\mathbf{n}\| = N\}$ . Then it is obvious that  $\tau_i B_N = B_N$  for all  $1 \leq i \leq L$  since  $\tau_i^2 = \mathbb{1}$ . This relates to the number preserving property of the jump operators.

### ■ The Temperley-Lieb algebra

The authors of Ref. [1] point out correctly that the jump operators  $J_i$  do not obey a simple *Dirac algebra* and thus the derivation of their dark states and a proof of the uniqueness as steady states is non-trivial [122]. Nevertheless, they obey another well-known algebra, namely the *Temperley-Lieb algebra*. This algebra was originally introduced in the context of statistical mechanics [123]. Today it is known that the range of its applications is much wider [124]. In particular, there are applications to quantum mechanical spin chains [125, 126] and there has been much progress with respect to its representation theory [127–129]. A comprehensible introduction is given in [128].

The Temperley-Lieb algebra and the *periodic* Temperley-Lieb algebra are defined as follows:

#### ► Definition 4.1: Temperley-Lieb algebra

Let  $\delta \in \mathbb{C}$  be an arbitrary but fixed complex parameter ( $\delta = 0$  allowed!).

- (i) The **Temperley-Lieb algebra (TLA)**  $TL_L(\delta)$  is the unital associative algebra over  $\mathbb{C}$  generated by  $\mathbb{1}, U_1, \dots, U_{L-1}$  with relations

$$U_i U_j = U_j U_i \quad \text{for all } |i - j| > 1, 1 \leq i, j \leq L - 1 \quad (4.18a)$$

$$U_i^2 = \delta U_i \quad \text{for all } 1 \leq i \leq L - 1 \quad (4.18b)$$

$$U_i U_{i+1} U_i = U_i \quad \text{for all } 1 \leq i \leq L - 2 \quad (4.18c)$$

$$U_i U_{i-1} U_i = U_i \quad \text{for all } 2 \leq i \leq L - 1. \quad (4.18d)$$

- (ii) The **Periodic Temperley-Lieb algebra (PTLA)**  $PTL_L(\delta)$  is the unital associative algebra over  $\mathbb{C}$  generated by  $\mathbb{1}, U_1, \dots, U_{L-1}, U_L$  with the relations of  $TL_L(\delta)$  and the additional relations

$$U_i U_L = U_L U_i \quad \text{for all } i \neq 1, L - 1 \quad (4.19a)$$

$$U_L^2 = \delta U_L \quad (4.19b)$$

$$U_L U_i U_i = U_L \quad \text{for } i = 1, L - 1 \quad (4.19c)$$

$$U_i U_L U_i = U_i \quad \text{for } i = 1, L - 1. \quad (4.19d)$$

The dimension of the TLA can be shown to be finite and it holds

$$\dim TL_L(\delta) = \binom{2L}{L} - \binom{2L}{L-1} = \frac{1}{L+1} \binom{2L}{L} \quad (4.20)$$

which is known from combinatorics as the *Catalan number*.

In contrast, the PTLA is infinite dimensional for  $L > 2$ , i.e.  $\dim PTL_L(\delta) = \infty$ . We are now going to show, that the particle conserving jump operators (up to a constant factor) constitute a representation of  $TL_L(0)$  and  $PTL_L(0)$  in the case of an open and closed chain, respectively. To this end, redefine the jump operators

$$J_j \longrightarrow 4iJ_j \quad (4.21)$$

and note that the factor 4 describes a rescaling of the system-bath coupling whereas the complex phase  $i$  has no physical relevance due to the global phase symmetry of the Lindblad superoperator. A straightforward but cumbersome calculation shows that the required relations hold:

$$\begin{aligned} J_i J_j &= J_j J_i \quad \text{for all } |i-j| > 1, 1 \leq i, j \leq L-1 \\ J_i^2 &= 0 \quad \text{for all } 1 \leq i \leq L-1 \\ J_i J_{i+1} J_i &= J_i \quad \text{for all } 1 \leq i \leq L-2 \\ J_i J_{i-1} J_i &= J_i \quad \text{for all } 2 \leq i \leq L-1. \end{aligned}$$

And in the closed chain the additional relations hold:

$$\begin{aligned} J_i J_L &= J_L J_i \quad \text{for all } i \neq 1, L-1 \\ J_L^2 &= 0 \\ J_L J_i J_L &= J_L \quad \text{for } i = 1, L-1 \\ J_i J_L J_i &= J_i \quad \text{for } i = 1, L-1. \end{aligned}$$

Here we employed the definition of  $J_i$  and the defining relations of the fermionic algebra  $\mathfrak{F}_L$ . In terms of spin  $S = \frac{1}{2}$  representations we find the representation (via the Jordan-Wigner transformation)

$$\rho_L : PTL_L(0) \longrightarrow \text{End} \bigotimes_{i=1}^L \mathbb{C}_i^2 \quad (4.22a)$$

$$U_i \mapsto \rho_L(U_i) = \frac{1}{2} \left[ i(\sigma_{i+1}^z - \sigma_i^z) + (\sigma_{i+1}^y \sigma_i^x - \sigma_{i+1}^x \sigma_i^y) \right] \quad (4.22b)$$

$$U_L \mapsto \rho_L(U_L) = \frac{1}{2} \left[ i(\sigma_1^z - \sigma_L^z) + P'(\sigma_1^y \sigma_L^x - \sigma_1^x \sigma_L^y) \right] \quad (4.22c)$$

where  $1 \leq i \leq L-1$ . This is consistent with recent findings in [129].

Although we will not use the Temperley-Lieb algebra explicitly, it might be helpful for future considerations of the dissipative process  $\{J_i\}$  and related jump operators to apply the machinery of representation theory that has been developed for the TLA and PTLA to gain a deeper understanding of the mathematics behind the theory. ■



### 4.2.2 Dark states

Let us now turn towards the dark states of the dissipative process  $\{J_i\}$ . In order to derive the dark state space, i.e. the linear subspace<sup>65</sup>  $\mathcal{D}_L = \{|\Psi\rangle \in \mathcal{H}_L \mid \forall_{1 \leq i \leq L-1} : J_i |\Psi\rangle = 0\}$ , we note that

$$\mathcal{H}_L = \mathcal{H}^{(L,0)} \oplus \mathcal{H}^{(L,1)} \oplus \dots \oplus \mathcal{H}^{(L,L)} \quad \text{where} \quad \mathcal{H}^{(L,N)} = \text{span} \{|\mathbf{n}\rangle \mid \mathbf{n} \in B_N\}. \quad (4.23)$$

The dimension of the number operator eigenspaces  $\mathcal{H}^{(L,N)}$  is  $\dim \mathcal{H}^{(L,N)} = \binom{L}{N}$ . We are going to show, that for each particle number  $N$  there is a (at most) one-dimensional dark state space  $\mathcal{D}^{(L,N)}$  such that

$$\mathcal{D}_L = \mathcal{D}^{(L,0)} \oplus \mathcal{D}^{(L,1)} \oplus \dots \oplus \mathcal{D}^{(L,L)}. \quad (4.24)$$

That is, every dark state is a unique superposition of fixed number dark states and the latter are unique in  $\mathcal{H}^{(L,N)}$ .

#### ■ Open Chain

In an open boundary setting, the jump operators  $J_i$  for  $1 \leq i \leq L-1$  must be considered. Let  $|\Psi\rangle = \sum_{\mathbf{n} \in B_N} \Psi(\mathbf{n}) |\mathbf{n}\rangle \in \mathcal{H}^{(L,N)}$  be an arbitrary state. Then we find

$$\begin{aligned} J_i |\Psi\rangle &= \sum_{\mathbf{n} \in B_N} \Psi(\mathbf{n}) J_i |\mathbf{n}\rangle = \sum_{\mathbf{n} \in B_N} \Psi(\mathbf{n}) \sigma_i \mathbf{n} (|\mathbf{n}\rangle + |\tau_i \mathbf{n}\rangle) \\ &= \frac{1}{2} \sum_{\mathbf{n} \in B_N} \Psi(\mathbf{n}) \sigma_i \mathbf{n} (|\mathbf{n}\rangle + |\tau_i \mathbf{n}\rangle) + \frac{1}{2} \sum_{\mathbf{n} \in B_N} \Psi(\tau_i \mathbf{n}) \sigma_i \tau_i \mathbf{n} (|\tau_i \mathbf{n}\rangle + |\mathbf{n}\rangle) \\ &= \frac{1}{2} \sum_{\mathbf{n} \in B_N} \Psi(\mathbf{n}) \sigma_i \mathbf{n} (|\mathbf{n}\rangle + |\tau_i \mathbf{n}\rangle) - \frac{1}{2} \sum_{\mathbf{n} \in B_N} \Psi(\tau_i \mathbf{n}) \sigma_i \mathbf{n} (|\mathbf{n}\rangle + |\tau_i \mathbf{n}\rangle) \\ &= \frac{1}{2} \sum_{\mathbf{n} \in B_N} [\Psi(\mathbf{n}) - \Psi(\tau_i \mathbf{n})] \sigma_i \mathbf{n} (|\mathbf{n}\rangle + |\tau_i \mathbf{n}\rangle) \stackrel{!}{=} 0 \end{aligned}$$

where we used  $\tau_i B_N = B_N$ ,  $\tau_i^2 = \mathbb{1}$  and  $\sigma_i \tau_i \mathbf{n} = -\sigma_i \mathbf{n}$ . Since  $\{|\mathbf{n}\rangle \mid \mathbf{n} \in B_N\}$  is a basis (and the summands appear in pairs with the same coefficients), this is equivalent to

$$[\Psi(\mathbf{n}) - \Psi(\tau_i \mathbf{n})] \sigma_i \mathbf{n} = 0 \quad \text{for all } 1 \leq i \leq L-1 \quad \text{and for all } \mathbf{n} \in B_N. \quad (4.25)$$

Note that  $\sigma_i \mathbf{n} = 0 \Leftrightarrow \tau_i \mathbf{n} = \mathbf{n}$  and the statement is trivial. Thus the only non trivial conditions read

$$\Psi(\mathbf{n}) = \Psi(\tau_i \mathbf{n}) \quad \text{for all } 1 \leq i \leq L-1 \quad \text{and for all } \mathbf{n} \in B_N. \quad (4.26)$$

It is clear that any two vectors  $\mathbf{n}, \mathbf{m} \in B_N$  may be converted into each other by a sequence of local transpositions  $\tau = \prod_k \tau_k$ :  $\tau \mathbf{m} = \mathbf{n}$ . Therefore the derived condition is satisfied if and only if  $\Psi(\mathbf{n}) = \text{const}$  for  $\mathbf{n} \in B_N$  and we find the unique fixed number dark state

$$|D, N\rangle = \mathcal{N}^{-1/2} \sum_{\mathbf{n} \in B_N} |\mathbf{n}\rangle \quad \text{where} \quad \mathcal{N} = \binom{L}{N} \quad \text{and} \quad \mathcal{D}^{(L,N)} = \text{span} \{|D, N\rangle\}. \quad (4.27)$$

Note that there is no condition on the particle number  $N$  whatsoever. ■

<sup>65</sup>If there is an additional Hamiltonian dynamics, the set of dark states (which have to be eigenstates of the Hamiltonian) is not a linear subspace in general. However, since we consider purely dissipative processes,  $\mathcal{D}_L$  is closed under summation.

### ■ Closed Chain

If we connect the two ends of the (finite) chain, the additional condition  $J_L |\Psi\rangle = 0$  for all  $|\Psi\rangle \in \overline{\mathcal{D}}^{(L,N)} = \{|\Psi\rangle \in \mathcal{H}^{(L,N)} \mid \forall_{1 \leq i \leq L} : J_i |\Psi\rangle = 0\}$  must hold. Since we derived a unique dark state for the reduced jump operator set ( $1 \leq i \leq L-1$ ), it remains to check, whether the additional jump operator  $J_L$  annihilates  $|D, N\rangle$ :

$$\begin{aligned} J_L |D, N\rangle &= \mathcal{N}^{-1/2} \sum_{\mathbf{n} \in B_N} J_L |\mathbf{n}\rangle = \mathcal{N}^{-1/2} \sum_{\mathbf{n} \in B_N} \sigma_L \mathbf{n} \left( |\mathbf{n}\rangle + (-1)^{N-1} |\tau_L \mathbf{n}\rangle \right) \\ &= \frac{\mathcal{N}^{-1/2}}{2} \sum_{\mathbf{n} \in B_N} \sigma_L \mathbf{n} \left[ |\mathbf{n}\rangle + (-1)^{N-1} |\tau_L \mathbf{n}\rangle - |\tau_L \mathbf{n}\rangle - (-1)^{N-1} |\mathbf{n}\rangle \right] \\ &= \begin{cases} 0 & \Leftrightarrow N \text{ odd or } N = 0, L \\ \mathcal{N}^{-1/2} \sum_{\mathbf{n} \in B_N} \sigma_L \mathbf{n} [|\mathbf{n}\rangle - |\tau_L \mathbf{n}\rangle] \neq 0 & \Leftrightarrow N \text{ even and } N \neq 0, L \end{cases} \end{aligned}$$

We conclude that for a PBC system with odd filling there is a unique dark state:  $\overline{\mathcal{D}}^{(L,N)} = \text{span}\{|D, N\rangle\}$ . However, for even numbers of particles the dark state space is trivial and there is no physical pure steady state:  $\overline{\mathcal{D}}^{(L,N)} = \{0\}$ . The absence of the even number (even parity) dark states corresponds to the absence of the boundary modes in the Majorana chain for PBC.

In Section 4.3.2 we derive the fixed number dark state for a periodic chain in momentum space. There we find

$$|\text{BCS}, N\rangle = \mathcal{N}_N^{-1/2} a_0^\dagger (G^\dagger)^N |0\rangle = \mathcal{N}_N^{-1/2} a_0^\dagger \left( \sum_{k>0} \varphi_k a_{-k}^\dagger a_k^\dagger \right)^N |0\rangle \quad (4.28)$$

which includes an odd number of fermions. This is consistent with our findings above. Since the dark state is unique, one can show  $|\text{BCS}, N\rangle = |D, 2N+1\rangle$  by combinatorial arguments. ■

Let us summarise our findings:

#### ► Result 4.1: Fixed number dark states

A System with  $L$  fermionic sites and  $N$  particles, driven by the dissipative process  $\{J_i\}$ , features the unique dark state

$$|D, N\rangle = \mathcal{N}^{-1/2} \sum_{\mathbf{n} \in B_N} |\mathbf{n}\rangle \quad \text{where} \quad \mathcal{N} = \binom{L}{N} \quad (4.29)$$

when *open boundary conditions* are inflicted. For *periodic systems*  $|D, N\rangle$  is the unique dark state only for *odd* fillings. In the case of *even* fillings there is no pure steady state.

Note that in the framework of spin-chains, the identification  $|n_1, \dots, n_L\rangle \leftrightarrow |\uparrow_{n_1}, \dots, \uparrow_{n_L}\rangle$  is made, where  $n_i = 1 \Leftrightarrow \uparrow_{n_i} = \downarrow$  and  $n_i = 0 \Leftrightarrow \uparrow_{n_i} = \uparrow$ . So we find the dark state  $|D, N\rangle_{\text{Spin}} = \mathcal{N}^{-1/2} \sum_{\mathbf{n} \in B_N} |\uparrow_{n_1}, \dots, \uparrow_{n_L}\rangle$ .

**4.2.3** Steady states

In the previous paragraph we showed the uniqueness of the dark state in the case of open and periodic boundary conditions. However, this does not guarantee that it is also the unique *steady state* of the system [130]. In the following we reformulate the criterion for the uniqueness of the steady state – as derived in [130] – in an more algebraic fashion and try to prove for the system at hand the uniqueness of the steady state rigorously. As a result, we find a purely mathematical statement in terms of recursively generated vectors that — if true — implies the uniqueness of the steady states. Computer-assisted results for this recursive set of vectors prove the uniqueness for up to 15 sites. We conjecture that the derived statement is generally true; finding a proof for this statement is left open as a task for the future.

Criterion for a unique steady dark state

We start with a quite general treatment of a (purely) dissipative dynamics governed by a Lindblad master equation and jump operators  $\{L_i\}_{i \in I}$  where  $I$  is some index set and  $L_i \in \mathcal{B}(\mathcal{H})$  are (usually non-Hermitian) bounded operators acting on the Hilbert space  $\mathcal{H}$ . Assume that the dark state  $|D\rangle$  is unique, i.e.  $\mathcal{D}$  is a one-dimensional linear subspace. Then it can be shown [130] that the following proposition holds.

**► Proposition 4.1: Uniqueness I**

If there exists no subspace  $S \leq \mathcal{H}$ ,  $S \perp \mathcal{D}$ , which is invariant under the action of the jump operator algebra,  $L_i S \subseteq S$  for all  $i \in I$ , then the dark state  $|D\rangle$  is the only steady state.

*Proof.* See Theorem 2 in Ref. [130]. ■

To recast this statement in a more practical form, we introduce the (abstract) unital jump operator algebra

$$\mathcal{A} = \langle \{L_i \mid i \in I\} \cup \{\mathbb{1}\} \rangle \tag{4.30}$$

which (in our case) is a subalgebra of  $\mathfrak{F}_L$ . Its intended action on  $\mathcal{H}$  is defined by a representation  $\rho : \mathcal{A} \rightarrow \text{End } \mathcal{H}$  which endows  $\mathcal{H}$  with the structure of an  $\mathcal{A}$ -module. Since  $\mathcal{A}$  is generated by  $\{J_i\}$  and the identity, every element  $A \in \mathcal{A}$  has the form of a complex polynomial in the jump operators. The proposition above now tells us that we have to rule out the possibility for an  $\mathcal{A}$ -invariant subspace which is orthogonal to the dark state  $|D\rangle$ . We are now going to prove the following proposition:

**► Proposition 4.2: Uniqueness II**

Given a unique dark state  $|D\rangle \in \mathcal{H}$  where  $\mathcal{H}$  is a (left)  $\mathcal{A}$ -module of the unital jump operator algebra  $\mathcal{A}$ . If the dual space  $\mathcal{H}^*$  is a cyclic (right)  $\mathcal{A}$ -module over  $\langle D|$ , then  $|D\rangle$  is the unique steady state. Formally this reads

$$\langle D| \mathcal{A} = \mathcal{H}^* \quad \Rightarrow \quad |D\rangle \text{ is the unique steady state} \tag{4.31}$$

*Proof.* We show the equivalence of the statement to proposition 4.1. To this end, it has to be shown that the non-existence of an  $\mathcal{A}$ -invariant subspace  $S$  which is orthogonal to  $|D\rangle$  is equivalent to  $\mathcal{H}^*$  being a cyclic  $\mathcal{A}$ -module over  $\langle D|$ :

- ( $\Rightarrow$ ) Assume that  $\langle D|\mathcal{A} \neq \mathcal{H}^*$ , i.e.  $\mathcal{H}^*$  is not cyclic over  $\langle D|$ . Since  $\langle D|\mathcal{A}$  is a (proper) linear subspace, its orthogonal complement  $V^\perp = (\langle D|\mathcal{A})^\perp \neq \{0\}$  is non-trivial. Choose an arbitrary vector  $|s\rangle \in V^\perp$  and define the subspace  $S = \mathcal{A}|s\rangle \leq \mathcal{H}$ .  $S$  is  $\mathcal{A}$ -invariant by construction and for every  $|\Psi\rangle = A_\Psi|s\rangle \in S$  we find  $\langle D|\Psi\rangle = \langle D|A_\Psi|s\rangle = 0$  since  $|s\rangle \in (\langle D|\mathcal{A})^\perp$ .
- ( $\Leftarrow$ ) Assume the opposite, i.e. there is an  $\mathcal{A}$ -invariant subspace  $S \leq \mathcal{H}$  which is orthogonal to  $|D\rangle$ . Choose  $|s\rangle \in S$  arbitrarily. Then we find  $\langle D|A|s\rangle = 0$  for every  $A \in \mathcal{A}$  since  $A|s\rangle \in S$  and  $S \perp |D\rangle$ . Consequently  $|s\rangle \notin \langle D|\mathcal{A}$  and thus  $\langle D|\mathcal{A} \neq \mathcal{H}^*$ . ■

A more convenient form of the statements 4.1 and 4.2 is the following:

► **Remark 4.1: Uniqueness I & II**

Let  $B$  be an arbitrary ONB of  $\mathcal{H}$ . The following statements are equivalent and sufficient for a unique dark state  $|D\rangle$  being the only steady state under the dissipative dynamics governed by the unital jump operator algebra  $\mathcal{A}$ :

- (i) For all states  $0 \neq |\Psi\rangle \in \mathcal{H}$  there is an operator  $A \in \mathcal{A}$  such that  $\langle D|A|\Psi\rangle \neq 0$ .
- (ii) There is a set  $\{A_1, \dots, A_n\} \subseteq \mathcal{A}$ ,  $n = \dim \mathcal{H}$ , such that  $\text{rank} \{A_i^\dagger|D\rangle \mid 1 \leq i \leq n\} = n$ .

*Proof.* We show the equivalence of the statements above to the premises of the previous two propositions (which are equivalent, as shown above).

- (i) Assume the statement holds. Then there is no  $\mathcal{A}$ -invariant subspace orthogonal to  $|D\rangle$ . Conversely, suppose there exists  $|\Psi\rangle \in \mathcal{H}$  such that for all  $A \in \mathcal{A}$  it holds  $\langle D|A|\Psi\rangle = 0$ . Then  $S := \mathcal{A}|\Psi\rangle$  is an  $\mathcal{A}$ -invariant subspace orthogonal to  $|D\rangle$ . Thus statement (i) is equivalent to the premise in proposition 4.1.
- (ii) Assume the statement holds. Then obviously  $\text{rank} \{\langle D|A_i \mid 1 \leq i \leq n\} = n$  and thus  $\langle D|\mathcal{A} = \mathcal{H}^*$ . Conversely, given  $\langle D|\mathcal{A} = \mathcal{H}^*$ , then the existence of a set  $\{A_1, \dots, A_n\} \subseteq \mathcal{A}$  with the demanded properties follows immediately. Thus statement (ii) is equivalent to the premise in proposition 4.2. ■

Criterion (i) implies the construction of a polynomial in the jump operators based on an arbitrary given state  $|\Psi\rangle \in \mathcal{H}$ . In contrast, criterion (ii) implies the construction of polynomials in the adjoint jump operators which generate the whole Hilbert space over the dark state.

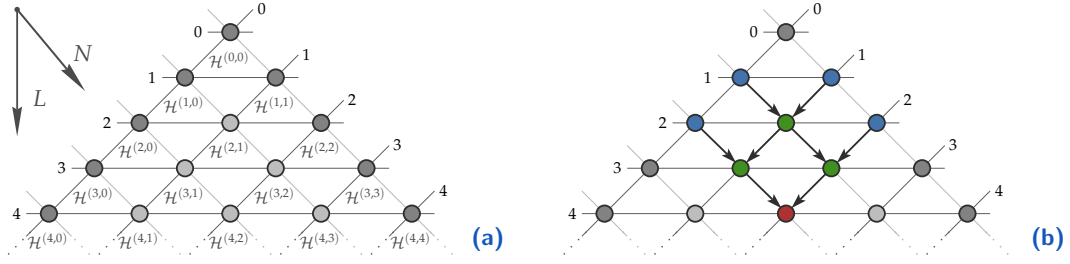


**Figure 4.1:** Schematic for the recursive generation of matrix representations for the jump operator algebra. **(a)** The system size  $L$  grows from top to bottom and the filling  $N$  from top left to down right. The vertices denote the  $\binom{L}{N}$ -dimensional  $\mathcal{A}_L$ -modules  $\mathcal{H}^{(L,N)}$  which coincide with the  $N$ -particle subspaces. The dimension as well as the recursion scheme motivate the arrangement as Pascal's triangle. **(b)** Example for the recursive construction of the representation  $\mathcal{H}^{(4,2)}$ , denoted by  $\bullet$ . Starting from the trivial, one-dimensional boundary representations – denoted by  $\bullet$  – one combines successively pairs of representations (denoted by  $\bullet$  and  $\bullet$ ) according to proposition 4.3. After four steps the target representation  $\bullet$  is reached.

Derivation of the statement

Consider an (open or closed) chain of  $L$  fermionic sites and a complete set of quasilocal jump operators  $\{a_i\}_{1 \leq i \leq L}$  which obey the fermionic algebra, i.e.  $\{a_i, a_j^\dagger\} = \delta_{ij}$  and so forth. Then the dark state  $|D\rangle$  is just the vacuum state (in general: a quasiparticle vacuum) which is unique due to the completeness of the jump operator algebra. In this case the criterion (ii) (Remark 4.1) is easily verified since  $\{a_i^\dagger\}_{1 \leq i \leq L}$  is just a complete set of creation operators which enables us to construct any number state from the quasiparticle vacuum  $|D\rangle$ .

In the case at hand, the jump operators  $\{J_i\}$  do not obey a fermionic algebra and thus the simple argument above is not valid. Nevertheless we are going to show the uniqueness of the dark states  $|D, N\rangle$  as steady states in the fixed particle number spaces  $\mathcal{H}^{(L,N)}$  by means of criterion (ii). This turns out to be quite complicated due to the complex jump operator algebra  $\mathcal{A}_L = TL_L(0)$ . Thus we start with some preliminary work first.

**Finite dimensional matrix representations**

Here we give a recursive construction for finite dimensional matrix representations of the jump operator algebra  $\mathcal{A}_L$ . Let  $\rho_L$  be the common matrix representation of  $\mathcal{A}_L$  on  $\mathcal{H}_L$  obtained by the Jordan Wigner transformation as described above. Due to the particle number preserving property of this representation, the  $\mathcal{A}_L$ -module  $\mathcal{H}_L$  is decomposable

$$\mathcal{H}_L = \mathcal{H}^{(L,0)} \oplus \mathcal{H}^{(L,1)} \oplus \dots \oplus \mathcal{H}^{(L,L)} \tag{4.32}$$

where each submodule  $\mathcal{H}^{(L,N)}$  is endowed with a  $\binom{L}{N}$ -dimensional subrepresentation  $\rho^{(L,N)}$  of  $\rho_L = \rho^{(L,0)} \oplus \rho^{(L,1)} \oplus \dots \oplus \rho^{(L,L)}$ . In the following, the abstract generators of the algebra are denoted by  $J_i$  whereas their matrix representation on  $\mathcal{H}^{(L,N)}$  is denoted by  $J_i^{(L,N)}$  (which is a  $\binom{L}{N} \times \binom{L}{N}$ -matrix). These  $\mathcal{A}_L$ -modules may be arranged as depicted in Fig. 4.1 (a) whose structure is motivated by Pascal's triangle due to the dimensions  $\binom{L}{N}$ .

In the following the number basis  $\mathcal{B}_N = \{|\mathbf{n}\rangle \mid \mathbf{n} \in B_N\}$  is furnished with a binary order where the least significant bit is located on the left hand side.

An example for  $L = 4$  and  $N = 2$  reads

$$|\blacksquare\blacksquare\blacksquare\blacksquare\rangle \quad |\blacksquare\blacksquare\blacksquare\rangle \quad |\blacksquare\blacksquare\blacksquare\rangle \quad |\blacksquare\blacksquare\blacksquare\rangle \quad |\blacksquare\blacksquare\blacksquare\rangle \quad |\blacksquare\blacksquare\blacksquare\rangle.$$

Such a basis can be generated recursively as follows: Let  $(|n_1\rangle, \dots, |n_p\rangle)$  and  $(|m_1\rangle, \dots, |m_q\rangle)$  be correctly ordered bases for  $\mathcal{H}^{(L, N-1)}$  and  $\mathcal{H}^{(L, N)}$ , respectively (so  $p = \binom{L}{N-1}$  and  $q = \binom{L}{N}$ ). Then the corresponding basis for  $\mathcal{H}^{(L+1, N)}$  reads  $(|m_1\rangle|0\rangle, \dots, |m_q\rangle|0\rangle, |n_1\rangle|1\rangle, \dots, |n_p\rangle|1\rangle)$ . With this in mind, we can show the following recursion:

► **Proposition 4.3: Recursive matrix representations for open chains**

Given  $L, N \in \mathbb{N}_0$  with  $0 \leq N \leq L$  and  $L \geq 1$  and the (abstract) generators  $\{J_i\}_{1 \leq i \leq L-1}$ . Then for each  $1 \leq i \leq L-1$  the matrix representation  $J_i^{(L+1, N)}$  is recursively given by

$$J_i^{(L+1, N)} = \begin{bmatrix} J_i^{(L, N)} & \mathbf{0} \\ \mathbf{0} & J_i^{(L, N-1)} \end{bmatrix} \quad \text{and} \quad J_L^{(L+1, N)} = \frac{1}{4} \begin{bmatrix} \mathbf{0}_1 & & & \\ & \mathbb{1}_2 & -\mathbb{1}_2 & \\ & \mathbb{1}_2 & -\mathbb{1}_2 & \\ & & & \mathbf{0}_3 \end{bmatrix} \quad (4.33)$$

where  $\mathbf{0}_1$  and  $\mathbf{0}_3$  denote the  $\binom{L-1}{N} \times \binom{L-1}{N}$ - and  $\binom{L-1}{N-2} \times \binom{L-1}{N-2}$ -zero matrix, respectively.  $\mathbb{1}_2$  is the  $\binom{L-1}{N-1} \times \binom{L-1}{N-1}$ -identity matrix. The identity is of course  $\mathbb{1}^{(L+1, N)} = \text{diag}\{1, \dots, 1\}$  with size  $\binom{L+1}{N} \times \binom{L+1}{N}$ . Note that

$$\binom{L+1}{N} = \binom{L}{N} + \binom{L}{N-1} = \binom{L-1}{N} + \binom{L-1}{N-1} + \binom{L-1}{N-1} + \binom{L-1}{N-2} \quad (4.34)$$

which is the proper dimension for  $\mathcal{H}^{(L+1, N)}$ . The boundary cases are  $N = 0$  and  $N = L$ . Then the representations are one-dimensional and read

$$\mathbb{1}^{(L, 0)} = [1], \quad J_i^{(L, 0)} = [0], \quad \text{and} \quad \mathbb{1}^{(L, L)} = [1], \quad J_i^{(L, L)} = [0]. \quad (4.35)$$

By means of these statements, recursive schemes along the lines of Fig. 4.1 (b) allow for the construction of representations for arbitrary  $L$  and  $N$ .

*Proof.* We start from the common representation defined by the action of the fermionic jump operators on  $\mathcal{H}_L$  and show that the matrices with respect to the binary ordered number basis  $\mathcal{B}_L$  take the claimed form.

First, consider the boundary representations, i.e.  $N = 0$  and  $N = L$ . The representations are one-dimensional since  $\dim \mathcal{H}^{(L, 0)} = \dim \mathcal{H}^{(L, L)} = 1$ . Furthermore we already saw that

$$J_i |\square\square\rangle = 0 \quad \text{and} \quad J_i |\blacksquare\blacksquare\rangle = 0 \quad (4.36)$$

which are the only basis states for  $N = 0$  and  $N = L$ , respectively. Thus we find  $J_i^{(L, 0)} = J_i^{(L, L)} = [0]$  for all  $1 \leq i \leq L-1$ .

Now assume that  $J_i^{(L,N-1)}$  and  $J_i^{(L,N)}$  are the correct representations on  $\mathcal{H}^{(L,N-1)}$  and  $\mathcal{H}^{(L,N)}$ , respectively. If we consider the new system with  $L + 1$  sites and  $N$  fermions, there are two possible states for the  $L + 1$ -th site. If it is empty, the  $N$  fermions have to be arranged on the “old” sites. These number states correspond to the left-hand side of the matrix (according to our convention) and are ordered in the same way as in  $\mathcal{H}^{(L,N)}$ . The same argument holds for the second case where the “new” site is occupied and there are  $N - 1$  fermions to be arranged on the “old” sites. These number states correspond to the right-hand side of the matrix. Furthermore we realise that the generators  $J_i$  do not operate on the  $L + 1$ -th site. Therefore their matrix representations remain unchanged. Since they cannot alter the state of the  $L + 1$ -th site, the new representation matrix is block diagonal, i.e.

$$J_i^{(L+1,N)} = \begin{bmatrix} J_i^{(L,N)} & \mathbf{0} \\ \mathbf{0} & J_i^{(L,N-1)} \end{bmatrix}. \quad (4.37)$$

The new jump operator  $J_L$  acts as follows on the number states:

$$J_L |\dots \square \square \rangle = 0 \quad (4.38a)$$

$$J_L |\dots \square \blacksquare \rangle = -\frac{1}{4} [|\dots \blacksquare \square \rangle + |\dots \square \blacksquare \rangle] \quad (4.38b)$$

$$J_L |\dots \blacksquare \square \rangle = \frac{1}{4} [|\dots \square \blacksquare \rangle + |\dots \blacksquare \square \rangle] \quad (4.38c)$$

$$J_L |\dots \blacksquare \blacksquare \rangle = 0 \quad (4.38d)$$

Due to our ordering the first  $\binom{L-1}{N}$  basis states are of the form  $|\dots \square \square \rangle$  whereas the last  $\binom{L-1}{N-2}$  states are of the form  $|\dots \blacksquare \blacksquare \rangle$ . Last but not least there are  $\binom{L-1}{N-1}$  basis states for each of the two forms  $|\dots \blacksquare \square \rangle$  and  $|\dots \square \blacksquare \rangle$  (in this order!). Finally we find

$$J_L^{(L+1,N)} = \frac{1}{4} \begin{bmatrix} \mathbf{0}_1 & & & & & & \\ & \mathbb{1}_2 & -\mathbb{1}_2 & & & & \\ & \mathbb{1}_2 & -\mathbb{1}_2 & & & & \\ & & & & & & \\ & & & & & & \mathbf{0}_3 \end{bmatrix} \quad (4.39)$$

with the block dimensions as claimed above. ■

#### ► Example on $\mathcal{H}^{(4,2)}$

As an example consider the  $\binom{4}{2} = 6$ -dimensional representation on  $\mathcal{H}^{(4,2)}$ . There the jump operators for  $\mathcal{A}_4$  read (Note the structure of  $J_3^{(4,2)}$ !)

$$J_1^{(4,2)} = \begin{bmatrix} 0 & 0 & 0 & 0 & 0 & 0 \\ 0 & 1 & -1 & 0 & 0 & 0 \\ 0 & 1 & -1 & 0 & 0 & 0 \\ 0 & 0 & 0 & 1 & -1 & 0 \\ 0 & 0 & 0 & 1 & -1 & 0 \\ 0 & 0 & 0 & 0 & 0 & 0 \end{bmatrix}, J_2^{(4,2)} = \begin{bmatrix} 1 & -1 & 0 & 0 & 0 & 0 \\ 1 & -1 & 0 & 0 & 0 & 0 \\ 0 & 0 & 0 & 0 & 0 & 0 \\ 0 & 0 & 0 & 0 & 0 & 0 \\ 0 & 0 & 0 & 0 & 1 & -1 \\ 0 & 0 & 0 & 0 & 1 & -1 \end{bmatrix}, J_3^{(4,2)} = \begin{bmatrix} 0 & 0 & 0 & 0 & 0 & 0 \\ 0 & 1 & 0 & -1 & 0 & 0 \\ 0 & 0 & 1 & 0 & -1 & 0 \\ 0 & 1 & 0 & -1 & 0 & 0 \\ 0 & 0 & 1 & 0 & -1 & 0 \\ 0 & 0 & 0 & 0 & 0 & 0 \end{bmatrix}.$$

It is easy to derive these matrices by hand if one employs the derivation depicted in Fig. 4.1 (b). For representations adjacent to the boundary (i.e.  $N = 1$  and  $N = L - 1$ ) there is a slight peculiarity, for binomial coefficients of the form  $\binom{L}{-1}$  and  $\binom{L-1}{L}$  occur. Such coefficients are defined to be equal zero and consequently some blocks in  $J_L^{(L+1,N)}$  vanish. ◀

#### ■ Cyclic matrix representations

We know that there is a unique dark state  $|D, N\rangle$  for each subspace  $\mathcal{H}^{(L,N)}$ . To show its uniqueness as a steady state, we have to show that the corresponding representation is cyclic over  $|D, N\rangle$ , see remark 4.1 (ii). To this end, note that

$$|D, N\rangle = \mathcal{N}^{-1/2} \sum_{\mathbf{n} \in B_N} |\mathbf{n}\rangle \Rightarrow (\langle \mathbf{n} | D, N \rangle) \propto (1 \ \dots \ 1)^T. \quad (4.40)$$

Thus we have to show that for each pair  $(L, N)$  there are elements  $\{A_1, \dots, A_n\} \subseteq \mathcal{A}$ ,  $n \geq \binom{L}{N}$ , such that

$$\text{rank} \left\{ \left( A_1^{(L,N)} \right)^\dagger \begin{pmatrix} 1 \\ \vdots \\ 1 \end{pmatrix}, \dots, \left( A_n^{(L,N)} \right)^\dagger \begin{pmatrix} 1 \\ \vdots \\ 1 \end{pmatrix} \right\} = \text{rank} \left\{ \varphi^{(L,N)}(A_1), \dots, \varphi^{(L,N)}(A_n) \right\} = \binom{L}{N}.$$

Here we introduced the homomorphism of vector spaces

$$\varphi^{(L,N)} : \mathcal{A}_L \longrightarrow \mathbb{C}^{\binom{L}{N}}, \quad A \mapsto \varphi^{(L,N)}(A) \equiv \left( \rho^{(L,N)}(A) \right)^\dagger \begin{bmatrix} 1 \\ \vdots \\ 1 \end{bmatrix} \quad (4.41)$$

which is easily seen to obey the relation  $\varphi^{(L,N)}(AB) = \hat{B}^\dagger \varphi^{(L,N)}(A)$  where  $\hat{B} \equiv \rho^{(L,N)}(B)$  and  $\varphi^{(L,N)}(\mathbf{1}) = [1 \ \dots \ 1]^T$ .  $\varphi^{(L+1,N)}(A)$  is a vector of size  $\binom{L+1}{N} = \binom{L}{N} + \binom{L}{N-1}$ . Then define the partition

$$\varphi^{(L+1,N)}(A) \equiv \begin{bmatrix} \varphi_\uparrow^{(L+1,N)}(A) \\ \varphi_\downarrow^{(L+1,N)}(A) \end{bmatrix} \quad \text{where} \quad \varphi_\uparrow^{(L+1,N)}(A) \in \mathbb{C}^{\binom{L}{N}} \quad \text{and} \quad \varphi_\downarrow^{(L+1,N)}(A) \in \mathbb{C}^{\binom{L}{N-1}}$$

where we assume<sup>66</sup>  $\binom{L}{N} \geq \binom{L}{N-1}$ .

<sup>66</sup>I.e. we confine ourselves to the left part of Pascal's triangle which will be no restriction due to the symmetry of the system with respect to fillings  $N \leftrightarrow L - N$ .



Let  $A \in \mathcal{A}_L$  be an arbitrary polynomial in the jump operators  $\{J_1, \dots, J_{L-1}\}$ . Recall that in  $\mathcal{H}^{(L+1,N)}$  the representation  $\rho^{(L+1,N)}(A)$  is block diagonal (See proposition 4.3) for such operators. Therefore we find

$$\varphi^{(L+1,N)}(A) = \hat{A}^\dagger \varphi^{(L+1,N)}(\mathbb{1}) = \begin{bmatrix} \varphi_\uparrow^{(L+1,N)}(A) \\ \varphi_\downarrow^{(L+1,N)}(A) \end{bmatrix} = \begin{bmatrix} \varphi^{(L,N)}(A) \\ \varphi^{(L,N-1)}(A) \end{bmatrix} = \begin{bmatrix} \varphi_\uparrow^{(L,N)}(A) \\ \varphi_\downarrow^{(L,N)}(A) \\ \varphi_\uparrow^{(L,N-1)}(A) \\ \varphi_\downarrow^{(L,N-1)}(A) \end{bmatrix}. \quad (4.42)$$

Now consider an operator of the form  $AJ_L \in \mathcal{A}_{L+1}$  where  $A \in \mathcal{A}_L$  is supported by the first  $L$  sites whereas  $J_L$  acts on the  $L$ -th and  $L+1$ -th site. Then it holds

$$\varphi^{(L+1,N)}(AJ_L) = \hat{J}_L^T \varphi^{(L+1,N)}(A) = \begin{bmatrix} \mathbf{0}_1 & & & \\ & \mathbb{1}_2 & \mathbb{1}_2 & \\ & -\mathbb{1}_2 & -\mathbb{1}_2 & \\ & & & \mathbf{0}_3 \end{bmatrix} \cdot \begin{bmatrix} \varphi_\uparrow^{(L,N)}(A) \\ \varphi_\downarrow^{(L,N)}(A) \\ \varphi_\uparrow^{(L,N-1)}(A) \\ \varphi_\downarrow^{(L,N-1)}(A) \end{bmatrix} \quad (4.43a)$$

$$= \begin{bmatrix} \mathbf{0} \\ \varphi_\downarrow^{(L,N)}(A) + \varphi_\uparrow^{(L,N-1)}(A) \\ -\varphi_\downarrow^{(L,N)}(A) - \varphi_\uparrow^{(L,N-1)}(A) \\ \mathbf{0} \end{bmatrix} \equiv \begin{bmatrix} \varphi_\uparrow^{(L+1,N)}(A) \\ \varphi_\downarrow^{(L+1,N)}(A) \end{bmatrix}. \quad (4.43b)$$

These observations motivate the definition of a recursive set of vectors which — as we shall prove — can be generated by monomials of jump operators:  $\leftrightarrow$

► Definition 4.2: Recursive generating system  $\mathcal{G}$

Let

$$\mathcal{G}(L, N) = \left( \left[ \begin{array}{c} \varphi_{\uparrow,1}^{(L,N)} \\ \varphi_{\downarrow,1}^{(L,N)} \end{array} \right], \dots, \left[ \begin{array}{c} \varphi_{\uparrow,2^{L-1}}^{(L,N)} \\ \varphi_{\downarrow,2^{L-1}}^{(L,N)} \end{array} \right] \right) \subseteq \mathbb{R}^{\binom{L}{N}}$$

be a finite set of vectors where  $\varphi_{\uparrow,i}^{(L,N)} \in \mathbb{R}^{\binom{L-1}{N}}$  and  $\varphi_{\downarrow,i}^{(L,N)} \in \mathbb{R}^{\binom{L-1}{N-1}}$ .

It is recursively defined as follows:

(i) The boundary sets, i.e.  $N = 0$  and  $N = L$ , are explicitly given as

$$\mathcal{G}(L, 0) = \left( \left[ \varphi_{\uparrow,1}^{(L,0)} \right], \dots, \left[ \varphi_{\uparrow,2^{L-1}}^{(L,0)} \right] \right) = \left( [1], [0], \dots, [0] \right) \quad (4.44)$$

$$\mathcal{G}(L, L) = \left( \left[ \varphi_{\downarrow,1}^{(L,L)} \right], \dots, \left[ \varphi_{\downarrow,2^{L-1}}^{(L,L)} \right] \right) = \left( [1], [0], \dots, [0] \right) \quad (4.45)$$

(ii) The recursion is defined as

$$\mathcal{G}(L+1, N) = \left( \left[ \begin{array}{c} \varphi_{\uparrow,1}^{(L+1,N)} \\ \varphi_{\downarrow,1}^{(L+1,N)} \end{array} \right], \dots, \left[ \begin{array}{c} \varphi_{\uparrow,2^{L-1}}^{(L+1,N)} \\ \varphi_{\downarrow,2^{L-1}}^{(L+1,N)} \end{array} \right], \left[ \begin{array}{c} \varphi_{\uparrow,2^{L-1}+1}^{(L+1,N)} \\ \varphi_{\downarrow,2^{L-1}+1}^{(L+1,N)} \end{array} \right], \dots, \left[ \begin{array}{c} \varphi_{\uparrow,2^L}^{(L+1,N)} \\ \varphi_{\downarrow,2^L}^{(L+1,N)} \end{array} \right] \right)$$

where for the first half ( $1 \leq i \leq 2^{L-1}$ ) it is

$$\varphi_{\uparrow,i}^{(L+1,N)} = \begin{bmatrix} \varphi_{\uparrow,i}^{(L,N)} \\ \varphi_{\downarrow,i}^{(L,N)} \end{bmatrix} \quad \text{and} \quad \varphi_{\downarrow,i}^{(L+1,N)} = \begin{bmatrix} \varphi_{\uparrow,i}^{(L,N-1)} \\ \varphi_{\downarrow,i}^{(L,N-1)} \end{bmatrix} \quad (4.46)$$

and for the second half ( $2^{L-1} + 1 \leq i \leq 2^L$ ) we define ( $i' = i - 2^{L-1}$ )

$$\varphi_{\uparrow,i}^{(L+1,N)} = \frac{1}{2} \begin{bmatrix} \mathbf{0} \\ \varphi_{\downarrow,i'}^{(L,N)} + \varphi_{\uparrow,i'}^{(L,N-1)} \end{bmatrix} \quad \text{and} \quad \varphi_{\downarrow,i}^{(L+1,N)} = \frac{1}{2} \begin{bmatrix} -\varphi_{\downarrow,i'}^{(L,N)} - \varphi_{\uparrow,i'}^{(L,N-1)} \\ \mathbf{0} \end{bmatrix}.$$

Therefore the set  $\mathcal{G}(L, N)$  has  $2^{L-1}$  elements.

This construction is performed easily by hand according to the scheme depicted in Fig. 4.1 (b). The first few sets read:

$$\begin{aligned} \mathcal{G}(1,0) = \left( [1] \right) \quad \text{and} \quad \mathcal{G}(1,1) = \left( [1] \right) &\quad \rightarrow \quad \mathcal{G}(2,1) = \left( \left[ \begin{array}{c} 1 \\ 1 \end{array} \right], \left[ \begin{array}{c} 1 \\ -1 \end{array} \right] \right) \\ \mathcal{G}(2,0) = \left( [1], [0] \right) \quad \text{and} \quad \mathcal{G}(2,1) &\quad \rightarrow \quad \mathcal{G}(3,1) = \left( \left[ \begin{array}{c} 1 \\ 1 \\ 1 \end{array} \right], \left[ \begin{array}{c} 1 \\ -1 \\ 0 \end{array} \right], \left[ \begin{array}{c} 0 \\ 1 \\ -1 \end{array} \right], \left[ \begin{array}{c} 0 \\ -1 \\ 1 \end{array} \right] \right) \\ \mathcal{G}(2,1) \quad \text{and} \quad \mathcal{G}(2,2) = \left( [1], [0] \right) &\quad \rightarrow \quad \mathcal{G}(3,2) = \left( \left[ \begin{array}{c} 1 \\ 1 \\ 1 \end{array} \right], \left[ \begin{array}{c} 0 \\ 1 \\ -1 \end{array} \right], \left[ \begin{array}{c} 1 \\ -1 \\ 0 \end{array} \right], \left[ \begin{array}{c} 1 \\ -1 \\ 0 \end{array} \right] \right) \end{aligned}$$

Obviously each of these sets has maximum rank, i.e. spans the whole space  $\mathbb{R}^{\binom{L}{N}}$ . ■

A computer-assisted generation of  $\mathcal{G}(L, N)$  up to  $L = 15$  and for every possible filling  $N$  suggests the following conjecture:

► **Conjecture 4.1: Maximum rank of  $\mathcal{G}$**

Given  $L, N \in \mathbb{N}_0$ ,  $0 \leq N \leq L$  and  $L \geq 1$ . Then  $\mathcal{G}(L, N)$  has the following properties:

(i) It has maximum rank, i.e.  $\text{rank } \mathcal{G}(L, N) = \binom{L}{N}$ .

(ii) There is a sequence  $(A_i)_{1 \leq i \leq 2^{L-1}} \subseteq \mathcal{A}$  such that  $\mathcal{G}(L, N) = \left( \varphi^{(L, N)}(A_i) \right)_{1 \leq i \leq 2^{L-1}}$ .

*Proof.* We prove the second part:

- (ii) Let  $\Lambda_L \subseteq \mathcal{A}_L$  be recursively defined as follows: Start with  $\Lambda_1 = (\mathbb{1})$ . Provided  $\Lambda_L$  is already known, set  $\Lambda_{L+1} = \Lambda_L \cup \Lambda_L J_L$  where  $\cup$  denotes the concatenation of sequences. Thus  $\Lambda_L$  contains all ordered sequences of jump operators up to length  $L - 1$  and we find  $|\Lambda_L| = 2^{L-1}$ . We claim that  $\Lambda_L$  is the sequence of operators we are looking for. We show this by induction: For the boundary cases  $N = 0$  and  $N = L$  we obviously get the correct sets  $\mathcal{G}(L, N)$  since the first element of  $\Lambda_L$  is  $\mathbb{1}$  which yields  $\begin{bmatrix} 1 \end{bmatrix}$  and the other elements are represented by  $1 \times 1$  zero-matrices which yield the remaining  $2^{L-1} - 1$  vectors  $\begin{bmatrix} 0 \end{bmatrix}$ . Now assume that  $\Lambda_L$  is the correct set for  $L$  and all  $0 \leq N \leq L$ . Then  $\Lambda_{L+1}$  yields via  $\varphi^{(L+1, N)}$  the correct vectors of  $\mathcal{G}(L+1, N)$  (in the correct order) as shown in Equations (4.42) and (4.43). ■

Unfortunately I was not able to find a general proof for (i) although it seems reasonable to tackle it by induction. Nevertheless we succeeded for small systems with  $L \leq 15$  as the computer-assisted generations show. Given a proof of (i) we would find as a corollary of Conjecture 4.1 and Remark 4.1 the desired statement for general  $L$  and  $N$ :

► **Corollary 4.1: Uniqueness of steady dark state**

Each  $\mathcal{A}_L$ -module  $\mathcal{H}^{(L, N)}$  is cyclic over  $|D, N\rangle$ .

The latter is the unique steady state of the dissipative dynamics  $\mathcal{A}_L$ .

#### 4.2.4 A parent Hamiltonian for the dark states

Let us now consider the parent Hamiltonian  $H_P = \sum_i J_i^\dagger J_i$  since its ground states with zero energy coincide with the dark states of the dissipative process. It is straightforward to show (up to a prefactor) that

$$H_{\text{OBC}} = \sum_{i=1}^{L-1} J_i^\dagger J_i = \frac{1}{2} \sum_{i=1}^{L-1} \left[ (n_i + n_{i+1} - 2n_i n_{i+1}) - (a_i^\dagger a_{i+1} + a_{i+1}^\dagger a_i) \right] \quad (4.47)$$

where  $n_i = a_i^\dagger a_i$  is the number operator on site  $i$ . The Hamiltonian  $H_{\text{OBC}}$  is called *parent Hamiltonian* for the process  $\{J_i\}$  (for open boundary conditions). For periodic boundary conditions the parent Hamiltonian reads

$$\begin{aligned} H_{\text{PBC}} &= \sum_{i=1}^L J_i^\dagger J_i = \frac{1}{2} \sum_{i=1}^{L-1} \left[ (n_i + n_{i+1} - 2n_i n_{i+1}) - (a_i^\dagger a_{i+1} + a_{i+1}^\dagger a_i) \right] \\ &\quad + \frac{1}{2} \left[ (n_L + n_1 - 2n_L n_1) - (a_L^\dagger a_1 + a_1^\dagger a_L) \right] \end{aligned} \quad (4.48)$$

where the additional term causes non-local operators after a Jordan-Wigner transformation (see below).

Their ground state spaces coincide with the dark state spaces  $\mathcal{D}$  if the latter is non-trivial. Recall that any operator  $A^\dagger A$  is positive semidefinite and that the sum of such operators is positive semidefinite as well. Therefore the spectrum of  $H_{\text{O/PBC}}$  is non-negative. Given any dark state  $|D\rangle \in \mathcal{D}$  then it is obviously  $H_{\text{O/PBC}} |D\rangle = 0$  and we conclude that  $|D\rangle$  is a ground state of  $H_{\text{O/PBC}}$ . Now assume that there is a ground state  $|G\rangle$  with  $H_{\text{O/PBC}} |G\rangle = 0$ . Then  $\langle G | H_{\text{O/PBC}} |G\rangle = \sum_i \langle G | J_i^\dagger J_i |G\rangle = 0$  and since  $J_i^\dagger J_i$  is positive semidefinite we conclude  $\langle G | J_i^\dagger J_i |G\rangle = \|J_i |G\rangle\|^2 = 0$  which implies  $J_i |G\rangle = 0$  for all  $1 \leq i \leq L-1$ .

Since we already know the dark state space  $\mathcal{D}$  we immediately conclude that the ground state space of  $H_{\text{OBC}}$  is  $L+1$ -times degenerate and spanned by the equal-weighted superpositions of number states  $|L, N\rangle$  with fixed particle number  $0 \leq N \leq L$ . For odd  $N$  and  $N=0$  or  $N=L$  we also can identify  $|L, N\rangle$  as the ground states of  $H_{\text{PBC}}$ . For  $N$  even (besides  $N=0$  and  $N=L$ , given  $L$  is even) we do not know the ground states since there are no dark states for the corresponding processes  $\{J_1, \dots, J_L\}$ . However, we can conclude that the ground state energy in these cases is strictly positive. The question is whether we can derive any properties of these states by analysing  $H_{\text{O/PBC}}$ .

To this end we employ the Jordan-Wigner transformation to recast  $H_{\text{O/PBC}}$  in terms of spin- $\frac{1}{2}$  sites. As is easily verified, this yields the well known *isotropic Heisenberg model* in one dimension and in the ferromagnetic regime. One easily verifies that

$$n_i \rightarrow \frac{1}{2} (\mathbb{1} - \sigma_i^z) \quad (4.49a)$$

$$a_i^\dagger a_{i+1} \rightarrow \frac{1}{4} \left( \sigma_i^x \sigma_{i+1}^x + i \sigma_i^x \sigma_{i+1}^y - i \sigma_i^y \sigma_{i+1}^x + \sigma_i^y \sigma_{i+1}^y \right) \quad (4.49b)$$

for  $1 \leq i \leq L-1$ .

This leads to

$$H_{\text{OBC}} = \frac{1}{4} \sum_{i=1}^{L-1} \left[ \mathbb{1} - \sigma_i^x \sigma_{i+1}^x - \sigma_i^y \sigma_{i+1}^y - \sigma_i^z \sigma_{i+1}^z \right] = \frac{L-1}{4} - \frac{1}{4} \sum_{i=1}^{L-1} \sigma_i \sigma_{i+1} = \frac{L-1}{4} - \sum_{i=1}^{L-1} S_i S_{i+1}$$

where  $S_i = \frac{1}{2} \sigma_i$  are the spin-operators for  $S = \frac{1}{2}$  and  $\hbar = 1$ . Clearly this is the ferromagnetic Heisenberg model (FHM), namely

$$H_{\text{1D-FHM,OBC}} = H_{\text{OBC}} - \frac{L-1}{4}$$

and we immediately identify our (Jordan-Wigner transformed) dark states  $|L, N\rangle$  as the ferromagnetic ground states with ground state energy  $E_0 = -\frac{L-1}{4}$ . The periodic boundary conditions lead to non-local string operators in the spin framework, that is

$$\begin{aligned} H_{\text{PBC}} &= \frac{1}{4} \sum_{i=1}^{L-1} \left[ \mathbb{1} - \sigma_i^x \sigma_{i+1}^x - \sigma_i^y \sigma_{i+1}^y - \sigma_i^z \sigma_{i+1}^z \right] + \frac{1}{4} \left[ \mathbb{1} - \sigma_L^z \sigma_1^z - P'(\sigma_L^x \sigma_1^x + \sigma_L^y \sigma_1^y) \right] \\ &= \frac{L}{4} - \sum_{i=1}^{L-1} S_i S_{i+1} - \frac{1}{4} \left[ \sigma_L^z \sigma_1^z + P'(\sigma_L^x \sigma_1^x + \sigma_L^y \sigma_1^y) \right] \end{aligned}$$

where  $P' = \prod_{i=2}^{L-1} \sigma_i^z$ . Since this Hamiltonian conserves the total z-magnetisation  $S_{\text{tot}}^z = \sum_{i=1}^L S_i^z$  we may restrict its action to subspaces of the Hilbert space with fixed number  $N$  of down spins<sup>67</sup>  $|\dots \downarrow \dots\rangle$ . In such subspaces  $P'$  measures the parity of  $N-1$  and we find

$$H_{\text{PBC}} = \frac{L}{4} - \sum_{i=1}^{L-1} S_i S_{i+1} - \frac{1}{4} \left[ \sigma_L^z \sigma_1^z + (-1)^{N-1} (\sigma_L^x \sigma_1^x + \sigma_L^y \sigma_1^y) \right] \stackrel{N \text{ odd}}{\equiv} \frac{L}{4} - \sum_{i=1}^{L-1} S_i S_{i+1}. \quad (4.50)$$

If we start from our fermionic theory with PBC and restrict the system to its odd parity supers-election sector, we obtain a mapping to the 1D-Heisenberg model with PBC via

$$H_{\text{1D-FHM,PBC}} = H_{\text{PBC}} - \frac{L}{4}$$

and therefore obtain the ground states  $|L, N\rangle$  with ground state energy  $E_0 = -\frac{L}{4}$  for the odd  $N$  sector. This is compatible with the well known results due to the Bethe ansatz, see e.g. [131] (set  $J = 1$ ). For  $N$  even the mapping is not valid; however, in these cases there are no dark states and we could not have derived the ground states anyway. These result are compatible with the observation that there are quasilocal operators such that their correlations decay algebraically (and *not* exponentially). E.g.

$$\begin{aligned} \langle a_i^\dagger a_{i+1}^\dagger a_j a_{j+1} \rangle &= \mathcal{N}_N^{-1} \sum_{\mathbf{n}, \mathbf{m} \in B_N} \langle \mathbf{n} | a_i^\dagger a_{i+1}^\dagger a_j a_{j+1} | \mathbf{m} \rangle = - \binom{L-4}{N-2} \binom{L}{N}^{-1} \\ &= - \frac{N(N-1) \cdot (L-N)(L-N-1)}{L^4 + \mathcal{O}(L^3)} \\ &= - \frac{\alpha L(\alpha L-1) \cdot (L-\alpha L)(L-\alpha L-1)}{L^4 + \mathcal{O}(L^3)} \xrightarrow{L \rightarrow \infty} -\alpha^2(1-\alpha)^2 \\ &\neq \langle a_i^\dagger a_{i+1}^\dagger \rangle \langle a_j a_{j+1} \rangle = 0 \end{aligned} \quad (4.51)$$

<sup>67</sup>Which correspond to occupied fermionic sites in our original theory.

which is even a non-decaying correlation independent of  $|j - i| \neq 0$  ( $\alpha = \frac{N}{L}$  is the particle density and kept constant in the thermodynamic limit). That  $\langle a_i^\dagger a_{i+1}^\dagger \rangle = \langle a_j a_{j+1} \rangle = 0$  follows since  $|L, N\rangle$  is characterised by a fixed particle number. According to [132, 133] the connected correlation function  $\langle a_i^\dagger a_{i+1}^\dagger a_j a_{j+1} \rangle - \langle a_i^\dagger a_{i+1}^\dagger \rangle \langle a_j a_{j+1} \rangle$  would decay exponentially for  $|i - j| \rightarrow \infty$  provided the dark states were ground states of some *gapped* Hamiltonian (since  $a_i^\dagger a_{i+1}^\dagger$  and  $a_j a_{j+1}$  commute). Therefore we conclude that the considered dark states cannot be described as a gapped phase and cannot be classified within the context of gapped topological phases [20].

## 4.3 A mean field theory for late times

Here we recalculate and evaluate the mean field theory that is used in Ref. [1] to obtain the effective jump operators  $j_i$  in the thermodynamic limit and close to the steady state, that is at late times. This is done to obtain a better understanding of the relation between the number-conserving jump operators  $J_i$  and their parity violating counterparts  $j_i$ . Please note that a few months after this paragraph has been written, the authors of [1] published a review of their results in [122] where they give a more detailed account of the mean field approximation in the appendix (as compared with the discussions in the supplementary information of [1]).

### 4.3.1 Derivation of the mean field theory

Let us start with the derivation of the mean field jump operators in momentum space.

Definitions and notation

In the following, we consider a finite system of  $L$  spinless, fermionic sites with periodic boundary conditions. The Hilbert space  $\mathcal{H} = \langle \mathcal{B} \rangle$  (Fock space) is spanned by the fermionic number states

$$\mathcal{B} = \{|n_1, \dots, n_L\rangle \mid n_1, \dots, n_L \in \{0, 1\}\}$$

and thus  $\dim \mathcal{H} = 2^L$ . The fermionic ladder operators obey the usual anticommutation relations

$$\{a_i, a_j\} = \{a_i^\dagger, a_j^\dagger\} = 0 \quad \text{and} \quad \{a_i, a_j^\dagger\} = \delta_{ij} \quad \text{for all } i, j \in \{1, \dots, L\} \quad (4.52)$$

where  $a_i$  acts on the  $i$ -th site.

We start with number conserving jump operators  $J_i := C_i^\dagger A_i$  where

$$C_i^\dagger := \sum_{j=1}^L v_{i-j} a_j^\dagger \quad \text{and} \quad A_i := \sum_{j=1}^L u_{i-j} a_j \quad (4.53)$$

with position space functions  $u, v : \mathbb{Z} \rightarrow \mathbb{C}$ ,  $i \mapsto u_i, v_i$  which obey the periodic boundary conditions, i.e.  $u_{i+L}, v_{i+L} = u_i, v_i$ .

Since we will do the calculations in momentum space, let us fix the notation first. For any sequence  $(X_i)_{i \in \{1, \dots, L\}}$  of operators in the operator algebra  $\mathcal{L}(\mathcal{H})$  on  $\mathcal{H}$ , we define the discrete Fourier transform (DFT) and the inverse discrete Fourier transform (iDFT) as follows:

$$\hat{X}_m \equiv \mathcal{F}(X)_m := \frac{1}{\sqrt{L}} \sum_{j=1}^L X_j e^{-i\frac{2\pi}{L}m \cdot j} \quad \text{where } m \in \{1, \dots, L\} \quad (4.54a)$$

$$X_j \equiv \mathcal{F}^{-1}(\hat{X})_j := \frac{1}{\sqrt{L}} \sum_{m=1}^L \hat{X}_m e^{i\frac{2\pi}{L}m \cdot j} \quad \text{where } j \in \{1, \dots, L\} \quad (4.54b)$$

For the sake of simplicity, we write  $X_k \equiv \hat{X}_m$  with  $k = \frac{2\pi}{L}m$ .

Furthermore define the abbreviations

$$\sum_k \equiv \sum_{k=\frac{2\pi}{L}}^{2\pi} = \sum_{m=1}^L \quad \text{Full Brillouin zone} \quad (4.55a)$$

$$\sum_{k>0} \equiv \sum_{k=\frac{2\pi}{L}}^{\frac{2\pi}{L} \lfloor \frac{L-1}{2} \rfloor} = \sum_{m=1}^{\lfloor \frac{L-1}{2} \rfloor} \quad \text{Half Brillouin zone.} \quad (4.55b)$$

Note that the sum over the half Brillouin zone excludes  $k = 0$  and (given  $L$  is even)  $k = \pi$ .

Thus we find

$$\sum_k X_k = \sum_{k>0} [X_k + X_{-k}] + X_{k=0} (+X_{k=\pi}) \quad \text{for } L \text{ odd (even)}. \quad (4.56)$$

Finally, we set  $\sum_j \equiv \sum_{j=1}^L$ . Furthermore we write  $\mathbf{BZ} := \{\frac{2\pi}{L}, \dots, 2\pi\}$  for the full Brillouin zone.

Master equation in momentum space

We aim at a mean field approximation of the Lindblad master equation

$$\partial_t \rho = \kappa \sum_j \left[ J_j \rho J_j^\dagger - \frac{1}{2} \{ J_j^\dagger J_j, \rho \} \right] \equiv \mathcal{L}(\{J_j\})[\rho] \quad (4.57)$$

in momentum space. Let us begin with the DFT of  $J$ , that is

$$\begin{aligned} J_k &= \frac{1}{\sqrt{L}} \sum_j J_j e^{-ikj} = \frac{1}{\sqrt{L}} \sum_j C_j^\dagger A_j e^{-ikj} = \frac{1}{L^{3/2}} \sum_j \sum_{k_1, k_2} C_{k_1}^\dagger e^{-ik_1 j} A_{k_2} e^{ik_2 j} e^{-ikj} \\ &= \frac{1}{L^{3/2}} \sum_{k_1, k_2} C_{k_1}^\dagger A_{k_2} \sum_j e^{i(k_2 - k - k_1)j} = \frac{1}{\sqrt{L}} \sum_{k_1, k_2} C_{k_1}^\dagger A_{k_2} \delta_{k_2, k_1 + k} \\ &= \frac{1}{\sqrt{L}} \sum_q C_q^\dagger A_{q+k} = \frac{1}{\sqrt{L}} \sum_q C_{q-k}^\dagger A_q \end{aligned}$$

The DFTs of the creation and annihilation parts read

$$C_k^\dagger = \frac{1}{\sqrt{L}} \sum_j C_j^\dagger e^{ikj} = \frac{1}{\sqrt{L}} \sum_{j,n} v_{j-n} a_n^\dagger e^{ikj} = \frac{1}{\sqrt{L}} \sum_n a_n^\dagger e^{ikn} \sum_j v_{j-n} e^{ik(j-n)} = \sqrt{L} v_{-k} a_k^\dagger \quad (4.58a)$$

$$A_k = \frac{1}{\sqrt{L}} \sum_j A_j e^{-ikj} = \frac{1}{\sqrt{L}} \sum_{j,n} u_{j-n} a_n e^{-ikj} = \frac{1}{\sqrt{L}} \sum_n a_n e^{-ikn} \sum_j u_{j-n} e^{-ik(j-n)} = \sqrt{L} u_k a_k \quad (4.58b)$$

and thus we find  $J_k = \frac{1}{\sqrt{L}} \sum_q C_{q-k}^\dagger A_q = \sqrt{L} \sum_q v_{k-q} u_q a_{q-k}^\dagger a_q$ . Using Parseval's identity  $\sum_j X_j X_j^\dagger = \sum_{k_1, k_2} X_{k_1} X_{k_2}^\dagger \frac{1}{L} \sum_j e^{ij(k_1 - k_2)} = \sum_k X_k X_k^\dagger$  we obtain for the Lindblad equation in momentum space

► Remark 4.2: Lindblad equation in momentum space

$$\partial_t \rho = \kappa L \sum_{k,q,p} \left( v_{k-q} u_q v_{k-p}^* u_p^* \right) \left[ a_{q-k}^\dagger a_q \rho a_p^\dagger a_{p-k} - \frac{1}{2} \left\{ a_p^\dagger a_{p-k} a_{q-k}^\dagger a_q, \rho \right\} \right]. \quad (4.59)$$



Note that Eq. (4.59) is invariant with respect to transformations of the form  $u_k \rightarrow e^{\alpha k + \beta} u_k$  and  $v_k \rightarrow e^{\alpha k + \gamma} v_k$  where  $\alpha, \beta, \gamma \in \mathbb{R}$ . In our case, we have

$$\begin{aligned} J_j = \frac{1}{4} (a_j^\dagger + a_{j+1}^\dagger) (a_j - a_{j+1}) &\Rightarrow C_j^\dagger = \frac{1}{2} (a_j^\dagger + a_{j+1}^\dagger), \quad A_j = \frac{1}{2} (a_j - a_{j+1}) \\ &\Rightarrow v_j = \frac{1}{2} (\delta_{j,0} + \delta_{j+1,0}) \quad u_j = \frac{1}{2} (\delta_{j,0} - \delta_{j+1,0}) \end{aligned}$$

where  $j \in \mathbb{Z}_L$  is an integer modulo  $L$ . The DFTs therefore read

$$v_k = \frac{1}{2\sqrt{L}} \sum_j (\delta_{j,0} + \delta_{j+1,0}) e^{-ijk} = \frac{1}{2\sqrt{L}} (1 + e^{ik}) = \frac{e^{i\frac{k}{2}}}{\sqrt{L}} \cos \frac{k}{2} \quad (4.60a)$$

$$u_k = \frac{1}{2\sqrt{L}} \sum_j (\delta_{j,0} - \delta_{j+1,0}) e^{-ijk} = \frac{1}{2\sqrt{L}} (1 - e^{ik}) = -i \frac{e^{i\frac{k}{2}}}{\sqrt{L}} \sin \frac{k}{2}. \quad (4.60b)$$

Due to the invariance mentioned above, we may neglect the phases, i.e.  $v_k = \frac{1}{\sqrt{L}} \cos \frac{k}{2}$  and  $u_k = \frac{1}{\sqrt{L}} \sin \frac{k}{2}$ . Therefore we assume in the following  $u_{-k} = \pm u_k$  and  $v_{-k} = \mp v_k$ .

Mean field approximation

We normalised the mode operators  $a_k$  so that

$$\{a_k, a_q\} = \{a_k^\dagger, a_q^\dagger\} = 0 \quad \text{and} \quad \{a_k, a_q^\dagger\} = \delta_{kq} \quad \text{for all } k, q \in \mathbf{BZ}. \quad (4.61)$$

Thus we find a new decomposition  $\mathcal{H} = \mathcal{H}_0 \otimes \bigotimes_{k>0} \mathcal{H}_{\pm k} (\otimes \mathcal{H}_\pi)$  with the mode-pair Hilbert spaces  $\mathcal{H}_\pm$  and the corresponding ladder operators  $a_{-k}$  and  $a_k$ . Let

$$\mathcal{H}_{\pm k} = \langle \{ |0,0\rangle_{\pm k}, |0,1\rangle_{\pm k}, |1,0\rangle_{\pm k}, |1,1\rangle_{\pm k} \} \rangle \quad (4.62)$$

where the first (second) entry denotes the occupation of the  $-k(k)$ -mode. Then we define

$$\rho_k := \mathcal{N}^{-1} (u_k + \alpha v_k a_{-k}^\dagger a_k^\dagger) |0,0\rangle_{\pm k} \langle 0,0| (u_k^* + \alpha^* v_k^* a_k a_{-k}) \in \mathcal{L}(\mathcal{H}_{\pm k}) \quad \text{for } 0 < k < \pi \quad (4.63)$$

where  $\mathcal{N} := |u_k|^2 + |\alpha v_k|^2$  ensures that  $\rho_k$  is a density operator on  $\mathcal{H}_{\pm k}$  and  $\alpha = |\alpha| e^{i\theta}$ . For the sake of simplicity, we will assume that  $L$  is odd (i.e., there is no  $k = \pi$  mode) as well as  $u_0 = 0$  and  $v_0 \neq 0$  (as derived above). Then one employs the ansatz  $\rho_0 := |1\rangle_0 \langle 1|$ .

Now consider the product ansatz for the density matrix

$$\rho = \rho_0 \otimes \bigotimes_{k>0} \rho_k (\otimes \rho_\pi) \equiv \prod_{k \geq 0} \rho_k \quad (4.64)$$

and insert it into Eq. (4.59):

$$\partial_t \prod_{k \geq 0} \rho_k = \kappa L \sum_{k,q,p} (v_{k-q} u_q v_{k-p}^* u_p^*) \left[ a_{q-k}^\dagger a_q \prod_{k \geq 0} \rho_k a_p^\dagger a_{p-k} - \frac{1}{2} \left\{ a_p^\dagger a_{p-k} a_{q-k}^\dagger a_q, \prod_{k \geq 0} \rho_k \right\} \right]. \quad (4.65)$$

To obtain the time evolution for the  $\pm k$ -pairs, we trace over the remaining degrees of freedom, i.e.  $\text{Tr}_r [\rho] \equiv \text{Tr}_{\neq \pm r} [\rho] = \rho_r$ ,

$$\partial_t \rho_r = \kappa L \sum_{k,q,p} \left( v_{k-q} u_q v_{k-p}^* u_p^* \right) \left[ \text{Tr}_r \left[ a_{q-k}^\dagger a_q \tilde{\rho} a_p^\dagger a_{p-k} \right] - \frac{1}{2} \text{Tr}_r \left[ \left\{ a_p^\dagger a_{p-k} a_{q-k}^\dagger a_q, \tilde{\rho} \right\} \right] \right]. \quad (4.66)$$

Here  $\tilde{\rho} = \rho_{q-k} \rho_q \rho_p \rho_{p-k}$  (given the four momenta are distinct) and  $0 \leq r < \pi$ . In the following we focus on the first part  $\sum_{k,q,p} \left( v_{k-q} u_q v_{k-p}^* u_p^* \right) \text{Tr}_r \left[ a_{q-k}^\dagger a_q \tilde{\rho} a_p^\dagger a_{p-k} \right]$  (since the second one follows then straightforwardly). To evaluate this sum, note the following: Each summand in Eq. (4.66) with  $k - q, q, k - p, p \neq \pm r$  vanishes due to the cyclic property of the trace. Therefore we need to consider only summands with at least one occurrence of  $\pm r$ . There are four cases:

► **One occurrence of  $\pm r$ :** Let  $\alpha, \beta, \gamma \in \mathbf{BZ}$  and  $\alpha, \beta, \gamma \neq r$ . Then the partial trace is of the form  $\text{Tr}_r \left[ a_r^\dagger a_\alpha \rho a_\beta^\dagger a_\gamma \right]$  (and permutations thereof). Obviously

$$\text{Tr}_r \left[ a_r^\dagger a_\alpha \rho a_\beta^\dagger a_\gamma \right] = a_r^\dagger \rho_r \text{Tr}_r \left[ a_\alpha \rho' a_\beta^\dagger a_\gamma \right] = - \text{Tr}_r \left[ a_\alpha \rho' a_\beta^\dagger a_\gamma \right] a_r^\dagger \rho_r \quad (4.67)$$

and it follows  $\text{Tr}_r \left[ a_r^\dagger a_\alpha \rho a_\beta^\dagger a_\gamma \right] = 0$ . The same argument holds for the anticommutator in the equation above.

► **Two occurrences of  $\pm r$ :** There are two cases to be considered separately.

–  *$r$ 's on the same site of the density matrix:* That is, we have  $\text{Tr}_r \left[ a_r^\dagger a_r \rho a_\alpha^\dagger a_\beta \right]$  where  $\alpha, \beta \in \mathbf{BZ}$  and  $\alpha, \beta \neq r$  (on one side of the density matrix the signs must coincide, see below). If  $\alpha \neq \beta$ , the trace vanishes. Therefore assume  $\alpha = \beta$  and we find  $\text{Tr}_r \left[ a_r^\dagger a_r \rho a_\alpha^\dagger a_\alpha \right] - \frac{1}{2} \text{Tr}_r \left[ \left\{ a_\alpha^\dagger a_\alpha a_r^\dagger a_r, \rho \right\} \right] + \text{Tr}_r \left[ a_\alpha^\dagger a_\alpha \rho a_r^\dagger a_r \right] - \frac{1}{2} \text{Tr}_r \left[ \left\{ a_r^\dagger a_r a_\alpha^\dagger a_\alpha, \rho \right\} \right] = 0$  by employing the cyclic property of the trace. Thus there is no contribution due to this case.

–  *$r$ 's on opposite sites of the density matrix:* Given on each side of the density matrix one ladder operators acts on the  $\pm r$ -th mode. Then we end up with traces of the form  $\text{Tr}_r \left[ a_\alpha^{(\dagger)} \rho' a_\beta^{(\dagger)} \right]$  where  $\rho'$  denotes the product density matrix save  $\rho_r$ . It is clear that  $|\alpha| \neq |\beta|$  implies  $\text{Tr}_r \left[ a_\alpha^{(\dagger)} \rho' a_\beta^{(\dagger)} \right] = 0$ . Thus we consider the cases where  $\alpha = \pm \beta$ .

A straightforward calculation shows that there are just eight non-vanishing traces, viz.  $\text{Tr}_r \left[ a_{\pm \alpha} \rho_\alpha a_{\pm \alpha}^\dagger \right]$ ,  $\text{Tr}_r \left[ a_{\pm \alpha} \rho_\alpha a_{\mp \alpha} \right]$ ,  $\text{Tr}_r \left[ a_{\pm \alpha}^\dagger \rho_\alpha a_{\pm \alpha} \right]$ , and  $\text{Tr}_r \left[ a_{\pm \alpha}^\dagger \rho_\alpha a_{\mp \alpha} \right]$  where  $\alpha \in \mathbf{BZ}$  and  $\alpha \neq r$ . Combining this with Eq. (4.66), we find eight corresponding relations for  $p, q$ , and  $k$  which reduce the triple sum to a simple sum over  $k$ :

- (i)  $p - k = q - k = \pm r \Leftrightarrow p = q = \pm r + k$
- (ii)  $p = k - q = \pm r \Leftrightarrow p - k = -q = \pm r - k$
- (iii)  $p = q = \pm r \Leftrightarrow p - k = q - k = \pm r - k$
- (iv)  $p - k = -q = \pm r \Leftrightarrow p = k - q = \pm r + k$

► **Three occurrences of  $\pm r$ :** Three occurrences of  $r$  would imply (on one side of the density matrix the signs must coincide, see below)  $p - k = p = r \Leftrightarrow k = 0 \Leftrightarrow q - k = q = r$  and we end up in the next case.

► **Four occurrences of  $\pm r$ :** Here the partial trace reads  $\text{Tr}_r \left[ a_{\pm r}^\dagger a_{\pm r} \rho a_{\pm r}^\dagger a_{\pm r} \right]$ . One verifies easily that  $\text{Tr}_r \left[ a_{\sigma r}^\dagger a_{\sigma r} \rho a_{\kappa r}^\dagger a_{\kappa r} \right] = a_r^\dagger a_r \rho_r a_r^\dagger a_r$  for  $\sigma, \kappa \in \{+, -\}$ . On the other hand one finds  $a_r^\dagger a_{-r} \rho_r = a_{-r}^\dagger a_r \rho_r = 0$ , so the other partial traces with different signs of  $r$  on one side vanish.

Conclusively, we have to consider all summands with two and four occurrences of  $\pm r$ , whereas in the case of two occurrences further conditions apply. Combining these results yields the following expression for the triple sum:

$$\sum_{k,q,p} = \underbrace{\sum_{p-k=q-k=\pm r}}_{(i)} + \underbrace{\sum_{p=k-q=\pm r}}_{(ii)} + \underbrace{\sum_{p=q=\pm r}}_{(iii)} + \underbrace{\sum_{p-k=-q=\pm r}}_{(iv)} - \sum_{p=q=\pm r, k=0} - \sum_{q=-p=\pm r, k=0}$$

Note that the summands for  $(p, q, k) = (\pm r, \pm r, 0)$  and  $(p, q, k) = (\mp r, \pm r, 0)$  appear twice in the first four sums. Thus we subtract them at the end (as it will turn out, this is not necessary, for the sum of the additional terms vanishes).

There are some special cases in the sum  $\sum_{k,q,p} (v_{k-q} u_q v_{k-p}^* u_p^*) \text{Tr}_r [a_{q-k}^\dagger a_q \tilde{\rho} a_p^\dagger a_{p-k}]$  which require a separate treatment in the evaluations below:

$$\begin{aligned} k=0: & \quad \text{Tr}_r [a_r^\dagger a_r \tilde{\rho} a_r^\dagger a_r] = \text{Tr}_r [a_{-r}^\dagger a_{-r} \tilde{\rho} a_r^\dagger a_r] = \text{Tr}_r [a_r^\dagger a_r \tilde{\rho} a_{-r}^\dagger a_{-r}] = a_r^\dagger a_r \rho_r a_r^\dagger a_r \\ k=\pm 2r: & \quad \text{Tr}_r [a_{-r}^\dagger a_r \tilde{\rho} a_r^\dagger a_{-r}] = \text{Tr}_r [a_r^\dagger a_{-r} \tilde{\rho} a_{-r}^\dagger a_r] = 0 \quad (r \neq 0) \end{aligned}$$

Let us start with the evaluation of the eight non-trivial sums<sup>68</sup>:

■  $p = q = \pm r$

Without loss of generality let  $p = q = r$ . Then we find

$$\begin{aligned} \sum_k (v_{k-r} u_r v_{k-r}^* u_r^*) \text{Tr}_r [a_{r-k}^\dagger a_r \tilde{\rho} a_r^\dagger a_{r-k}] &= \sum_{k \neq 0, k \neq 2r} |v_{k-r} u_r|^2 a_r \rho_r a_r^\dagger \frac{|u_{r-k}|^2}{|u_{r-k}|^2 + |\alpha v_{r-k}|^2} + \mathcal{R} \\ &= |u_r|^2 a_r \rho_r a_r^\dagger \sum_{|q| \neq r} \frac{|u_q v_q|^2}{|u_q|^2 + |\alpha v_q|^2} + \mathcal{R} \end{aligned}$$

where  $\mathcal{R} = |v_r u_r|^2 a_r^\dagger a_r \rho_r a_r^\dagger a_r$ . Note that for  $r = 0$  this term vanishes.

■  $p - k = q - k = \pm r$

Without loss of generality let  $p - k = q - k = r$ . Then we find

$$\begin{aligned} \sum_k (v_{-r} u_{r+k} v_{-r}^* u_{r+k}^*) \text{Tr}_r [a_r^\dagger a_{r+k} \tilde{\rho} a_{r+k}^\dagger a_r] &= \sum_{k \neq 0, k \neq -2r} |v_{-r} u_{r+k}|^2 a_r^\dagger \rho_r a_r \frac{|\alpha v_{r+k}|^2}{|u_{r+k}|^2 + |\alpha v_{r+k}|^2} + \mathcal{R} \\ &= |\alpha v_r|^2 a_r^\dagger \rho_r a_r \sum_{|q| \neq r} \frac{|u_q v_q|^2}{|u_q|^2 + |\alpha v_q|^2} + \mathcal{R} \end{aligned}$$

where  $\mathcal{R} = |v_r u_r|^2 a_r^\dagger a_r \rho_r a_r^\dagger a_r$ . ■

<sup>68</sup>Due to the symmetry regarding  $\pm r$  we evaluate just four of them

$$\blacksquare p - k = -q = \pm r$$

Without loss of generality let  $p - k = -q = r$ . Then we find

$$\begin{aligned} & \sum_k (v_{k+r} u_{-r} v_{-r}^* u_{r+k}^*) \text{Tr}_r \left[ a_{-r-k}^\dagger a_{-r} \tilde{\rho} a_{r+k}^\dagger a_r \right] \\ &= - \sum_{k \neq 0, k \neq -2r} (v_{k+r} u_{-r} v_{-r}^* u_{r+k}^*) a_{-r} \rho_r a_r \text{Tr}_r \left[ a_{-(r+k)}^\dagger \rho_{r+k} a_{r+k}^\dagger \right] - \mathcal{R} \\ &= - \sum_{k \neq 0, k \neq -2r} (v_{k+r} u_{-r} v_{-r}^* u_{r+k}^*) a_{-r} \rho_r a_r \frac{-\alpha^* v_{r+k}^* u_{r+k}}{|u_{k+r}|^2 + |\alpha v_{k+r}|^2} - \mathcal{R} \\ &= \alpha^* u_{-r} v_{-r}^* a_{-r} \rho_r a_r \sum_{|q| \neq r} \frac{|v_q u_q|^2}{|u_q|^2 + |\alpha v_q|^2} - \mathcal{R} \end{aligned}$$

where  $\mathcal{R} = |v_r u_r|^2 a_{-r}^\dagger a_{-r} \rho_r a_r^\dagger a_r = |v_r u_r|^2 a_r^\dagger a_r \rho_r a_r^\dagger a_r$ . Concerning the minus before  $\mathcal{R}$ , we used the fact that  $u_{-r} v_{-r}^* = -v_r u_r^*$ . Note that for  $r = 0$  this term vanishes.

$$\blacksquare q - k = -p = \pm r$$

Without loss of generality let  $q - k = -p = r$ . Then we find

$$\begin{aligned} & \sum_k (v_{-r} u_{r+k} v_{k+r}^* u_{-r}^*) \text{Tr}_r \left[ a_r^\dagger a_{r+k} \tilde{\rho} a_{-r}^\dagger a_{-r-k} \right] \\ &= - \sum_{k \neq 0, k \neq -2r} (v_{-r} u_{r+k} v_{k+r}^* u_{-r}^*) a_r^\dagger \rho_r a_{-r}^\dagger \text{Tr}_r \left[ a_{r+k} \rho_{r+k} a_{-(r+k)} \right] - \mathcal{R} \\ &= - \sum_{k \neq 0, k \neq -2r} (v_{-r} u_{r+k} v_{k+r}^* u_{-r}^*) a_r^\dagger \rho_r a_{-r}^\dagger \frac{-\alpha v_{r+k} u_{r+k}^*}{|u_{k+r}|^2 + |\alpha v_{k+r}|^2} - \mathcal{R} \\ &= \alpha u_{-r}^* v_{-r} a_r^\dagger \rho_r a_{-r}^\dagger \sum_{|q| \neq r} \frac{|v_q u_q|^2}{|u_q|^2 + |\alpha v_q|^2} - \mathcal{R} \end{aligned}$$

where  $\mathcal{R} = |v_r u_r|^2 a_r^\dagger a_r \rho_r a_{-r}^\dagger a_{-r} = |v_r u_r|^2 a_r^\dagger a_r \rho_r a_r^\dagger a_r$ . Concerning the minus before  $\mathcal{R}$ , we used the fact that  $u_{-r}^* v_{-r} = -v_r^* u_r$ . Note that for  $r = 0$  this term vanishes.  $\blacksquare$

If we define

$$\kappa_r := \kappa \sum_{|q| \neq r} \frac{|v_q u_q|^2}{|u_q|^2 + |\alpha v_q|^2} \quad (4.68)$$

it follows

$$\begin{aligned} & \kappa \sum_{k,q,p} (v_{k-q} u_q v_{k-p}^* u_p^*) \text{Tr}_r \left[ a_{q-k}^\dagger a_q \rho a_p^\dagger a_{p-k} \right] \\ &= \kappa \left( \sum_{p=q=\pm r} + \sum_{p-k=q-k=\pm r} + \sum_{p-k=-q=\pm r} + \sum_{q-k=-p=\pm r} - \sum_{p=q=\pm r, k=0} - \sum_{q=-p=\pm r, k=0} \right) [\dots] \\ &= \frac{\kappa_r}{L} \left[ j_r \rho_r j_r^\dagger + j_{-r} \rho_r j_{-r}^\dagger \right] \equiv \frac{\kappa_r}{L} \sum_{\sigma=\pm} j_{\sigma r} \rho_r j_{\sigma r}^\dagger \quad (4.69) \end{aligned}$$

where we defined the mean field jump operators

$$j_k := \sqrt{L}u_k a_k + \sqrt{L}\alpha v_k a_{-k}^\dagger = A_k + \alpha C_{-k}^\dagger. \quad (4.70)$$

In the case  $r = 0$  one finds

$$\kappa \sum_{k,q,p} \left( v_{k-q} u_q v_{k-p}^* u_p^* \right) \text{Tr}_0 \left[ a_{q-k}^\dagger a_q \rho a_p^\dagger a_{p-k} \right] = \frac{\kappa_0}{L} j_0 \rho_0 j_0^\dagger = \kappa_0 |\alpha v_0|^2 a_0^\dagger \rho_0 a_0 \quad (4.71)$$

which is consistent with the equation for  $j_k$  above and the assumption that  $u_0 = 0$ .

Then it follows immediately:

#### ► Result 4.2: Mean field Lindblad equation

In mean field approximation the Lindblad master equation reads

$$\partial_t \rho_k = \kappa_k \sum_{\sigma=\pm} \left[ j_{\sigma k} \rho_k j_{\sigma k}^\dagger - \frac{1}{2} \left\{ j_{\sigma k}^\dagger j_{\sigma k}, \rho_k \right\} \right] \quad (4.72a)$$

with the jump operators

$$j_k = \sqrt{L}u_k a_k + \sqrt{L}\alpha v_k a_{-k}^\dagger = A_k + \alpha C_{-k}^\dagger \quad (4.72b)$$

and the new bath coupling

$$\kappa_k = \kappa \sum_{|q| \neq k} \frac{|v_q u_q|^2}{|u_q|^2 + |\alpha v_q|^2}. \quad (4.72c)$$

The new jump operators form (up to a normalisation) a Dirac algebra, that is

$$\left\{ j_k^\dagger, j_q^\dagger \right\} = \left\{ j_k, j_q \right\} = L \left\{ u_k a_k + \alpha v_k a_{-k}^\dagger, u_q a_q + \alpha v_q a_{-q}^\dagger \right\} = 0 \quad \text{and} \quad (4.73a)$$

$$\left\{ j_k, j_q^\dagger \right\} = L \left\{ u_k a_k + \alpha v_k a_{-k}^\dagger, u_q^* a_q^\dagger + \alpha^* v_q^* a_{-q} \right\} = L \left( |u_k|^2 + |\alpha v_k|^2 \right) \delta_{k,q}. \quad (4.73b)$$

Note that to show the first equation, we used  $u_{-k} = \pm u_k$  and  $v_{-k} = \mp v_k$  for  $k = -q$ . In order to get a proper Dirac algebra, we introduce the normalised jump operators

$$\tilde{j}_k := \frac{1}{\sqrt{L(|u_k|^2 + |\alpha v_k|^2)}} j_k \quad (4.74)$$

and the new mode coupling

$$\tilde{\kappa}_k := \kappa_k L \left( |u_k|^2 + |\alpha v_k|^2 \right). \quad (4.75)$$

With the new defined operators, the master equation for  $\rho_k$  reads

$$\partial_t \rho_k = \sum_{q=\pm k} \tilde{\kappa}_q \left[ \tilde{j}_q \rho_k \tilde{j}_q^\dagger - \frac{1}{2} \left\{ \tilde{j}_q^\dagger \tilde{j}_q, \rho_k \right\} \right]. \quad (4.76)$$

Recall that  $[j_{\pm k}, \rho_q] = 0$  ( $k \neq q$ ) and multiply the master equation by  $\prod_{p \geq 0, p \neq k} \rho_p$ :

$$\partial_t \rho_k \prod_{p \geq 0, p \neq k} \rho_p = \sum_{q = \pm k} \tilde{\kappa}_q \left[ \tilde{j}_q \rho \tilde{j}_q^\dagger - \frac{1}{2} \left\{ \tilde{j}_q^\dagger \tilde{j}_q, \rho \right\} \right] \quad (4.77)$$

A summation over  $k \geq 0$  finally yields

$$\partial_t \rho = \sum_{k \geq 0} \left[ \partial_t \rho_k \prod_{p \geq 0, p \neq k} \rho_p \right] = \sum_q \tilde{\kappa}_q \left[ \tilde{j}_q \rho \tilde{j}_q^\dagger - \frac{1}{2} \left\{ \tilde{j}_q^\dagger \tilde{j}_q, \rho \right\} \right]. \quad (4.78)$$

To sum it up, the mean field Lindblad master equation in momentum space reads

► **Remark 4.3: Linblad equation in momentum space**

$$\partial_t \rho = \sum_k \tilde{\kappa}_k \left[ \tilde{j}_k \rho \tilde{j}_k^\dagger - \frac{1}{2} \left\{ \tilde{j}_k^\dagger \tilde{j}_k, \rho \right\} \right] = \sum_k \kappa_k \left[ j_k \rho j_k^\dagger - \frac{1}{2} \left\{ j_k^\dagger j_k, \rho \right\} \right]. \quad (4.79)$$

Back in position space we find for the jump operators

$$j_j = \frac{1}{\sqrt{L}} \sum_k j_k e^{ijk} = \frac{1}{\sqrt{L}} \sum_k A_k e^{ijk} + \alpha \frac{1}{\sqrt{L}} \sum_k C_{-k}^\dagger e^{ijk} = A_j + \alpha C_j^\dagger. \quad (4.80)$$

In our case, this reads  $j_i = \frac{1}{2} (a_i^\dagger + a_{i+1}^\dagger + a_i - a_{i+1})$  where  $\alpha = 1$ .

### 4.3.2 Some properties of the quadratic mean field theory

In [1] the quasi particle vacuum of the Majorana chain with PBC is referred to as *fixed phase state*  $|\text{BCS}, \alpha\rangle$  whereas the dark state of the exact jump operators  $J_i$  is termed *fixed number state*  $|\text{BCS}, N\rangle$ . Here  $\alpha = |\alpha| e^{i\theta}$  encodes the fixed phase  $\theta$  and the particle density  $|\alpha|$  of the coherent state  $|\text{BCS}, \alpha\rangle$ . This is motivated by analogy to the mean field approach in BCS theory. Here we stick to this terminology: In the following we prove the dark state property for the fixed phase (number) state  $|\text{BCS}, \alpha\rangle$  ( $|\text{BCS}, N\rangle$ ). Furthermore we derive a relation between  $\langle \hat{N} \rangle$  and  $\alpha$ .

Fixed phase dark state  $|\text{BCS}, \alpha\rangle$

Since the  $j_j$  (and  $j_k$ ) jump operators form a complete Dirac algebra (that is, they are the Bogoliubov quasiparticle operators of a Hamiltonian theory), the Hamiltonian ground state — the quasiparticle vacuum — coincides with the unique dark state of the dissipative dynamics described by the Lindblad superoperator  $\mathcal{L}(\{j_i\})$ . That is

$$\begin{aligned} |\text{BCS}, \alpha\rangle &\propto \prod_k j_k |0\rangle \propto j_0 \prod_{k>0} j_k j_{-k} |0\rangle \\ &\propto a_0^\dagger \prod_{k>0} \left( u_k a_k + \alpha v_k a_{-k}^\dagger \right) \left( u_{-k} a_{-k} + \alpha v_{-k} a_k^\dagger \right) |0\rangle \\ &\propto a_0^\dagger \prod_{k>0} \left( u_k + \alpha v_k a_{-k}^\dagger a_k^\dagger \right) |0\rangle \end{aligned} \quad (4.81)$$

where we used the fact that pairs  $j_k j_{-k}$  of fermionic operators commute and  $a_k |0\rangle = 0$ . This is the (unique) dark state described by  $\mathcal{L}(\{j_i\})$  since

$$j_k |\text{BCS}, \alpha\rangle = j_k \prod_q j_q |0\rangle = 0 \quad \forall k \in \mathbf{BZ} \quad \Leftrightarrow \quad j_i |\text{BCS}, \alpha\rangle = 0 \quad \forall i \in \{1, \dots, L\} \quad (4.82)$$

holds by construction. This is consistent with the ansatz  $\rho = |\text{BCS}, \alpha\rangle \langle \text{BCS}, \alpha|$  for the density matrix used to derive the mean field jump operators, given  $|\text{BCS}, \alpha\rangle$  is properly normalised:

► **Result 4.3: Fixed phase dark state  $|\text{BCS}, \alpha\rangle$**

$$|\text{BCS}, \alpha\rangle = N_\alpha^{-\frac{1}{2}} a_0^\dagger \prod_{k>0} (u_k + \alpha v_k a_{-k}^\dagger a_k^\dagger) |0\rangle \quad \text{where} \quad N_\alpha = \prod_{k>0} (|u_k|^2 + |\alpha v_k|^2) \quad (4.83)$$

If we define<sup>69</sup>  $\varphi_k := \frac{v_k}{u_k}$ , we may rewrite (up to a sign) the fixed phase state as follows:

$$|\text{BCS}, \alpha\rangle = \tilde{N}_\alpha^{-\frac{1}{2}} a_0^\dagger \prod_{k>0} (1 + \alpha \varphi_k a_{-k}^\dagger a_k^\dagger) |0\rangle \quad \text{where} \quad \tilde{N}_\alpha = \prod_{k>0} (1 + |\alpha \varphi_k|^2) \quad (4.84)$$

Now let  $G^\dagger = \sum_{k>0} \varphi_k a_{-k}^\dagger a_k^\dagger$  and recall that  $a_k^2 = 0 = (a_k^\dagger)^2$ . Then it follows easily that

$$\begin{aligned} |\text{BCS}, \alpha\rangle &= \tilde{N}_\alpha^{-\frac{1}{2}} a_0^\dagger \prod_{k>0} \left[ 1 + \alpha \varphi_k a_{-k}^\dagger a_k^\dagger + \frac{1}{2!} (\alpha \varphi_k a_{-k}^\dagger a_k^\dagger)^2 + \dots \right] |0\rangle \\ &= \tilde{N}_\alpha^{-\frac{1}{2}} a_0^\dagger \prod_{k>0} \exp \left[ \alpha \varphi_k a_{-k}^\dagger a_k^\dagger \right] |0\rangle = \tilde{N}_\alpha^{-\frac{1}{2}} a_0^\dagger \exp \left[ \alpha \sum_{k>0} \varphi_k a_{-k}^\dagger a_k^\dagger \right] |0\rangle \\ &= \tilde{N}_\alpha^{-\frac{1}{2}} a_0^\dagger \exp \left( \alpha G^\dagger \right) |0\rangle \end{aligned} \quad (4.85)$$

where we used the fact that  $[a_{-k}^\dagger a_k^\dagger, a_{-q}^\dagger a_q^\dagger] = 0$  for all  $k, q \in \mathbf{BZ}$ .

Fixed number dark state  $|\text{BCS}, N\rangle$

Consider now the number preserving jump operators  $J_i = C_i^\dagger A_i$  and  $J_k = \frac{1}{\sqrt{L}} \sum_q C_{q-k}^\dagger A_q = \sqrt{L} \sum_q v_{k-q} u_q a_{q-k}^\dagger a_q$ , respectively. The corresponding dark state is the fixed number state  $|\text{BCS}, N\rangle$  which is given by

$$|\text{BCS}, N\rangle = N_N^{-\frac{1}{2}} a_0^\dagger (G^\dagger)^N |0\rangle \quad (4.86)$$

with an appropriate normalisation  $N_N$ . We don not give an explicit expression for  $N_N$  since there is no need for it (and it is rather unattractive in the momentum space formulation anyway). Note that in [1] the  $a_0^\dagger$ -mode was erroneously neglected. This mode, however, is crucial for the dark state property as we will see immediately. Recall that we found in 4.2.2 that the only dark states for  $J_i$  with PBC contain *odd* numbers of fermions. This corresponds to the fact that the quasi particle vacuum of the Majorana chain has *odd* parity. From this point of view it is clear that the  $a_0^\dagger$ -mode in the above expression for  $|\text{BCS}, N\rangle$  is necessary as  $G^\dagger = \sum_{k>0} \varphi_k a_{-k}^\dagger a_k^\dagger$  generates even parity states from the physical vacuum  $|0\rangle$ . Please note that  $|\text{BCS}, N\rangle$  contains  $2N + 1$  fermions.

<sup>69</sup>Note that, since  $u_k \propto \sin \frac{k}{2}$ ,  $u_k$  cannot vanish except for  $k = 0$ . E.g.  $\varphi_k$  is well defined except for  $k = 0$ .

We are now going to derive the dark state property, i.e.  $J_i |\text{BCS}, N\rangle = J_k |\text{BCS}, N\rangle = 0$ . We show that  $[J_k, a_0^\dagger (G^\dagger)^N] = 0$  for all  $k \in \mathbf{BZ}$ . In combination with  $J_k \propto \sum_q v_{k-q} u_q a_{q-k}^\dagger a_q$ , this yields immediately  $J_k a_0^\dagger (G^\dagger)^N |0\rangle = a_0^\dagger (G^\dagger)^N J_k |0\rangle = 0$ . To this end, we compute

$$[J_k, G^\dagger] = \left[ \sum_q v_{k-q} u_q a_{q-k}^\dagger a_q, \sum_{p>0} \varphi_p a_{-p}^\dagger a_p^\dagger \right] = \sum_q \sum_{p>0} \varphi_p v_{k-q} u_q [a_{q-k}^\dagger a_q, a_{-p}^\dagger a_p^\dagger]. \quad (4.87)$$

The evaluation of the commutator yields

$$\begin{aligned} [a_{q-k}^\dagger a_q, a_{-p}^\dagger a_p^\dagger] &= a_{q-k}^\dagger [a_q, a_{-p}^\dagger] a_p^\dagger + a_{q-k}^\dagger a_{-p}^\dagger [a_q, a_p^\dagger] \\ &= a_{q-k}^\dagger (2a_q a_{-p}^\dagger - \delta_{q,-p}) a_p^\dagger + a_{q-k}^\dagger a_{-p}^\dagger (2a_q a_p^\dagger - \delta_{q,p}) \\ &= -a_{q-k}^\dagger a_p^\dagger \delta_{q,-p} - a_{q-k}^\dagger a_{-p}^\dagger \delta_{q,p} + 2(a_{q-k}^\dagger a_q a_{-p}^\dagger a_p^\dagger + a_{q-k}^\dagger a_{-p}^\dagger a_q a_p^\dagger) \\ &= a_{q-k}^\dagger a_p^\dagger \delta_{q,-p} - a_{q-k}^\dagger a_{-p}^\dagger \delta_{q,p} \end{aligned} \quad (4.88)$$

Now assume that  $\varphi_k = \frac{v_k}{u_k}$  and recall that  $u_{-k} = -u_k$ ,  $v_{-k} = v_k$  and  $u_{k+2\pi} = u_k$ ,  $v_k = v_{k+2\pi}$ . The form of  $\varphi_k$  is *postulated*. We show in the following that this is indeed the correct choice. With this in mind, we find

$$\begin{aligned} [J_k, G^\dagger] &= \sum_q \sum_{p>0} \varphi_p v_{k-q} u_q [a_{q-k}^\dagger a_p^\dagger \delta_{q,-p} - a_{q-k}^\dagger a_{-p}^\dagger \delta_{q,p}] \\ &= \sum_{p>0} [\varphi_p v_{k+p} u_{-p} a_{-p-k}^\dagger a_p^\dagger - \varphi_p v_{k-p} u_p a_{p-k}^\dagger a_{-p}^\dagger] \\ &= -\sum_{p>0} v_p v_{k+p} a_{-p-k}^\dagger a_p^\dagger - \sum_{p>0} v_p v_{k-p} a_{p-k}^\dagger a_{-p}^\dagger \\ &= -\sum_{p<0} v_p v_{k-p} a_{p-k}^\dagger a_{-p}^\dagger - \sum_{p>0} v_p v_{k-p} a_{p-k}^\dagger a_{-p}^\dagger \\ &= -\sum_{p<0, p>0} v_p v_{k-p} a_{p-k}^\dagger a_{-p}^\dagger \end{aligned} \quad (4.89)$$

To get a sum over the full Brillouin zone, we add the  $p = 0$ -term  $v_0 v_k a_{-k}^\dagger a_0^\dagger$ , that is

$$[J_k, G^\dagger] = -\sum_p v_p v_{k-p} a_{p-k}^\dagger a_{-p}^\dagger + v_0 v_k a_{-k}^\dagger a_0^\dagger. \quad (4.90)$$

To show that the first term vanishes, apply the index shift  $-q := p - k$  where  $q$  is the new summation index that runs over the full Brillouin zone. This yields

$$-\sum_p v_p v_{k-p} a_{p-k}^\dagger a_{-p}^\dagger = -\frac{1}{2} \left[ \sum_p v_p v_{k-p} a_{p-k}^\dagger a_{-p}^\dagger + \sum_q v_{k-q} v_q a_{-q}^\dagger a_{q-k}^\dagger \right] = 0. \quad (4.91)$$

So we are left with  $[J_k, G^\dagger] = v_0 v_k a_{-k}^\dagger a_0^\dagger$ . Recall that  $[J_i, a_0^\dagger] = 0 = [J_k, a_0^\dagger]$  since in  $J_k = \sqrt{L} \sum_q v_{k-q} u_q a_{q-k}^\dagger a_q$  the  $q = 0$  term is not present due to  $u_0 = 0$  (which is, on the other hand, the reason for the occurrence of  $a_0^\dagger$  anyway). Then it is clear that

$$[J_k, a_0^\dagger G^\dagger] = a_0^\dagger [J_k, G^\dagger] = v_0 v_k a_0^\dagger a_{-k}^\dagger a_0^\dagger = 0. \quad (4.92)$$



Now assume that  $[J_k, a_0^\dagger (G^\dagger)^{N-1}] = 0$  for some  $N \in \mathbb{N}$ . Then it follows by induction

$$\left[ J_k, a_0^\dagger (G^\dagger)^N \right] = G^\dagger \left[ J_k, a_0^\dagger (G^\dagger)^{N-1} \right] + [J_k, a_0^\dagger G^\dagger] (G^\dagger)^{N-1} = 0 + 0 = 0 \quad (4.93)$$

where we used that  $[a_0^\dagger, G^\dagger] = 0$ . This is exactly what we wanted to show and we conclude:

► **Result 4.4: Fixed number dark state  $|\text{BCS}, N\rangle$**

The momentum space representation of the fixed number dark states reads

$$|\text{BCS}, N\rangle = N_N^{-\frac{1}{2}} a_0^\dagger (G^\dagger)^N |0\rangle \quad (4.94)$$

for an state with  $2N + 1$  fermions.

Note that in contrast to the fixed phase state  $|\text{BCS}, \alpha\rangle$ , the fixed number state  $|\text{BCS}, N\rangle$  has no product form in momentum space. We may express the fixed phase state as a superposition of fixed number states<sup>70</sup>:

$$|\text{BCS}, \alpha\rangle \propto a_0^\dagger \exp(\alpha G^\dagger) |0\rangle = a_0^\dagger \sum_{N=0}^{\infty} \frac{\alpha^N}{N!} (G^\dagger)^N |0\rangle \propto \sum_{N=0}^{\infty} \frac{\alpha^N}{N!} |\text{BCS}, N\rangle \quad (4.95)$$

The sum is actually finite since  $(G^\dagger)^N = 0$  for  $N > \frac{L-1}{2}$  ( $L$  odd) which follows from a nice application of the pigeon hole principle. Now it is evident that

$$J_i |\text{BCS}, \alpha\rangle \propto \sum_{N=0}^{\infty} \frac{\alpha^N}{N!} J_i |\text{BCS}, N\rangle = 0 \quad \text{for all } i \in \{1, \dots, L\}. \quad (4.96)$$

That is, the fixed phase state  $|\text{BCS}, \alpha\rangle$  is also dark state of the *number conserving* jump operators and not just of  $J_i$ . The above calculation shows why:  $|\text{BCS}, \alpha\rangle$  is the coherent state of all fixed number dark states.

Expectation value of the particle number

Since  $|\text{BCS}, \alpha\rangle$  is not an eigenstate of the number operator

$$\hat{N} := \sum_k a_k^\dagger a_k = a_0^\dagger a_0 + \sum_{k>0} (a_k^\dagger a_k + a_{-k}^\dagger a_{-k}) \quad (4.97)$$

we may give an expression for its expectation value (or rather, the particle density).

<sup>70</sup>This is due to the fact that  $|\text{BCS}, \alpha\rangle$  is a coherent state.

This yields

$$\begin{aligned}
n &= \frac{\langle \text{BCS}, \alpha | \hat{N} | \text{BCS}, \alpha \rangle}{L} \\
&= (LN_\alpha)^{-1} \langle 0 | \prod_{k>0} (u_k^* + \alpha^* v_k^* a_k a_{-k}) a_0 \left[ a_0^\dagger a_0 + \sum_{q>0} (a_q^\dagger a_q + a_{-q}^\dagger a_{-q}) \right] a_0^\dagger \prod_{k>0} (u_k + \alpha v_k a_{-k}^\dagger a_k^\dagger) | 0 \rangle \\
&= \frac{1}{L} + L^{-1} \sum_{q>0} \frac{-q, q \langle 0 | (u_q^* + \alpha^* v_q^* a_q a_{-q}) (a_q^\dagger a_q + a_{-q}^\dagger a_{-q}) (u_q + \alpha v_q a_{-q}^\dagger a_q^\dagger) | 0 \rangle_{-q, q}}{-q, q \langle 0 | (u_q^* + \alpha^* v_q^* a_q a_{-q}) (u_q + \alpha v_q a_{-q}^\dagger a_q^\dagger) | 0 \rangle_{-q, q}} \\
&= \frac{1}{L} + L^{-1} \sum_{q>0} \frac{-q, q \langle 0 | (u_q^* + \alpha^* v_q^* a_q a_{-q}) (2\alpha v_q a_{-q}^\dagger a_q^\dagger) | 0 \rangle_{-q, q}}{-q, q \langle 0 | (u_q^* + \alpha^* v_q^* a_q a_{-q}) (u_q + \alpha v_q a_{-q}^\dagger a_q^\dagger) | 0 \rangle_{-q, q}} \\
&= \frac{1}{L} + L^{-1} \sum_{q>0} \frac{2|\alpha v_q|^2}{|u_q|^2 + |\alpha v_q|^2} = \frac{1}{L} \sum_q \frac{|\alpha v_q|^2}{|u_q|^2 + |\alpha v_q|^2} \tag{4.98}
\end{aligned}$$

Here we used  $u_0 = 0$  in the last step. Recall that  $\alpha = |\alpha|e^{i\theta}$ , i.e. the modulus  $|\alpha|$  determines the filling  $n$  of the system. To encapsulate the result:

► **Result 4.5: Particle number density**

The particle number density of the system in a fixed phase state  $|\text{BCS}, \alpha\rangle$  is given by

$$n(|\alpha|) = \frac{1}{L} \sum_q \frac{|\alpha v_q|^2}{|u_q|^2 + |\alpha v_q|^2}. \tag{4.99}$$

This concludes our recalculation and analysis of the mean field theory that is used in [1] to make the transition from the number conserving and experimentally proposed jump operators  $J_i$  to the parity violating operators  $j_i$ . Up to some technical details, we verified the results outlined in the supplementary information of [1]. We give some critical remarks on the assumptions that were used for these derivations in the concluding section 4.5. In the next section we once again consider the exact (number conserving) dark states and compare their entanglement structure to the exact ground states of the Majorana chain.

## 4.4 Topology as local indistinguishability

Here we consider a characteristic property of topologically ordered states, namely the operational notion of *local indistinguishability* of quantum states as put forward in [134] and developed further in [71, 72]. Let me stress that this property refers to topologically ordered states and is *a priori* unrelated to the concept of topological invariants used for the characterisation of *topological phases* (for the Majorana chain, see 1.3.4 in the preliminaries).

One of the principal characteristics of topologically ordered states is their quasilocal equality, i.e. a state  $|\Psi_1\rangle$  is topologically ordered if there is another (necessarily orthogonal) state  $|\Psi_2\rangle$  such that there is no quasilocal observable which discriminates them and there is no quasilocal operator which creates a finite overlap between these states. The motivation of this definition is quite obvious: Realistic operations (controlled or not) can safely assumed to be quasilocal. Consequently there is no environmental process which rotates one topologically ordered state onto the other. To put it differently: Given a superposition of two topologically ordered states, then there is no quasilocal decoherence process which destroys the encoded quantum information.

In the following we consider structure graph induced interaction systems  $\mathcal{I}$  as defined in Appendix E.2. Thus we talk about Hilbert spaces  $\mathcal{H} = \otimes_i \mathcal{H}_i$  composed of subsystem Hilbert spaces  $\mathcal{H}_i$  and impose a spatial meta-structure on  $\mathcal{H}$  by identification of subsystems with a structure graph  $S$  which is connected and becomes a metric space with the usual geodesic distance.  $\mathcal{B}_C(\mathcal{H})$  denotes the set of bounded operators on  $\mathcal{H}$  such that the diameter of their support (i.e. region of non-trivial action) is bounded by  $C \in \mathbb{N}$ . Formally

$$\mathcal{B}_C(\mathcal{H}) = \{\mathcal{O} \in \mathcal{B}(\mathcal{H}) \mid \text{diam}_S(\text{supp}(\mathcal{O})) \leq C\}$$

where the diameter is defined with respect to the geodesic metric on the underlying structure graph  $S$ . We may now define topological ordered states on  $\mathcal{H}$  with respect to  $S$  as follows [58]:

► **Definition 4.3: Topological Quantum Order (TQO) with  $(R, \varepsilon)$ -error**

Consider a Hilbert space  $\mathcal{H} = \otimes_i \mathcal{H}_i$  furnished with a spatial meta-structure due to a given structure graph  $S$ . A set  $\{|\Psi_i\rangle\}_{1 \leq i \leq M}$  of states is termed *topologically ordered with  $(R, \varepsilon)$ -error* iff for all  $R$ -local operators  $\mathcal{O}_{\text{loc}} \in \mathcal{B}_R(\mathcal{H})$  and all  $1 \leq i, j \leq M$  it holds

$$|\langle \Psi_i | \mathcal{O}_{\text{loc}} | \Psi_j \rangle| \leq \varepsilon \|\mathcal{O}_{\text{loc}}\| \quad \text{for } i \neq j \quad \text{and} \quad |\langle \Psi_i | \mathcal{O}_{\text{loc}} | \Psi_i \rangle - \langle \Psi_j | \mathcal{O}_{\text{loc}} | \Psi_j \rangle| \leq \varepsilon \|\mathcal{O}_{\text{loc}}\|$$

where  $\|\bullet\|$  denotes the operator norm on  $\mathcal{B}(\mathcal{H})$ . We say that the set of states shows *symmetry protected topological quantum order (STQO) with  $(R, \varepsilon)$ -error* if the above condition holds just for operators  $\mathcal{O}_{\text{loc}} \in \mathcal{B}_R(\mathcal{H})$  that respect a given symmetry.

That is to say, topologically ordered states are *locally indistinguishable* (at least up to some error  $\varepsilon$ ). There are two remarks in order:

1. As pointed out in Appendix E.1 there is a notorious difficulty to come up with canonical definitions for intuitive physical properties such as “quasilocality” or here “topological order” for *single instances* of physical systems. If one tries to do so, one usually ends up with parameter dependent definitions where there is no canonical choice for the parameter(s). The definition of  $(R, \varepsilon)$ -TQO exemplifies this situation. Obviously there is no canonical choice for

$R$  and  $\varepsilon$  for which we could safely call the states in question “topologically ordered”. Clearly we require  $R$  to be of the order of the system size and  $\varepsilon \ll 1$  to be small. However, this is not a definition but rather a vague abstraction of a even more vague physical concept. The concept of templates sometimes provides a way to get rid of such parameters.

2. According to the previous definition, TQO is the property of a *set* of (at least two) states. However, one can “project” the property of TQO on single states by requiring the existence of another state which is locally indistinguishable in the above sense.

We apply this definition of STQO in the following to (1) the pair of Majorana chain ground states and (2) to the dark states of the number conserving dissipative process  $\{J_i\}$ . As we are concerned with fermionic systems, it is reasonable to demand parity symmetry for all admissible physical operators.

#### Majorana chain ground states

In this chapter we encountered the ground state of the Majorana chain with PBC in momentum space. As we are interested in local indistinguishability, we need to compare the *two* degenerate ground states of the Majorana chain with OBC. In Section 5.2 of Chapter 5 we derive the number state representation of these states rigorously. It turns out that they correspond to equal-weight superpositions of number states with fixed parity:

$$|\Psi^\pm\rangle = \mathcal{N}_L^{-1/2} \sum_{n \in \mathbb{P}_L^\pm} |n\rangle \quad \text{with} \quad \mathcal{N}_L = 2^{L-1} \quad (4.100)$$

We first show that the states  $\{\Psi^\pm\}$  are *not* topologically ordered without symmetry protection. To this end consider the matrix element<sup>71</sup>

$$\langle \Psi^+ | a_1^\dagger | \Psi^- \rangle = \mathcal{N}_L^{-1} \sum_{n \in \mathbb{P}_L^+, m \in \mathbb{P}_L^-} \langle n | a_1^\dagger | m \rangle. \quad (4.101)$$

and note that

$$\sum_{n \in \mathbb{P}_L^\pm} |n\rangle = \sum_{n \in \mathbb{P}_{L-1}^\pm} |0, n\rangle + \sum_{n \in \mathbb{P}_{L-1}^\mp} |1, n\rangle. \quad (4.102)$$

Therefore we find

$$\langle \Psi^+ | a_1^\dagger | \Psi^- \rangle = \mathcal{N}_L^{-1} \sum_{n \in \mathbb{P}_{L-1}^-, m \in \mathbb{P}_{L-1}^-} \langle n | m \rangle = \frac{2^{L-1-1}}{2^{L-1}} = \frac{1}{2}, \quad (4.103)$$

i.e.  $\varepsilon \geq \frac{1}{2}$  even for  $R = 1$  since  $\|a_1\| = 1$ . Even though we did not give a precise definition of (parameterless) TQO so far, it is clear that we do not want states with  $(R \leq 1, \varepsilon \geq 1/2)$ -error termed “topologically ordered” since  $R$  doesn’t scale with the system size  $L$  and  $\varepsilon$  cannot be made small.

Let us now turn towards the distinguishability of  $\{\Psi^\pm\}$ . Clearly

$$|\langle \Psi^+ | P | \Psi^+ \rangle - \langle \Psi^- | P | \Psi^- \rangle| = 2 \quad (4.104)$$

<sup>71</sup>It is no coincidence that we choose  $a_1^\dagger$  to live on the *edge* of the chain. Only there the ground states can be distinguished reliably.

where the parity operator has range  $L$  and thus the states *can* be distinguished by operators acting on all  $L$  sites. Let us show that this is not true for any  $R < L$ . Let  $\mathcal{O}_{\text{loc}} \in \mathcal{B}_R(\mathcal{H})$  where  $R < L$ . We denote the set of systems (or vertices in  $S$ ) on which  $\mathcal{O}_{\text{loc}}$  acts non-trivially by  $O$  and its complement by  $E$ . Then the Schmidt decomposition of  $\Psi^\pm$  with respect to the bipartition  $OE$  reads

$$|\Psi^+\rangle = \frac{1}{\sqrt{2}} (|\Psi^+\rangle_O |\Psi^+\rangle_E + |\Psi^-\rangle_O |\Psi^-\rangle_E) \quad (4.105a)$$

$$|\Psi^-\rangle = \frac{1}{\sqrt{2}} (|\Psi^-\rangle_O |\Psi^+\rangle_E + |\Psi^+\rangle_O |\Psi^-\rangle_E) \quad (4.105b)$$

and we obtain

$$\begin{aligned} |\langle \Psi^+ | \mathcal{O}_{\text{loc}} | \Psi^+ \rangle - \langle \Psi^- | \mathcal{O}_{\text{loc}} | \Psi^- \rangle| &= \frac{1}{2} |(\langle \Psi^+_O \Psi^+_E | + \langle \Psi^-_O \Psi^-_E |) \mathcal{O}_{\text{loc}} (|\Psi^+_O \Psi^+_E\rangle + |\Psi^-_O \Psi^-_E\rangle) \\ &\quad - (\langle \Psi^-_O \Psi^+_E | + \langle \Psi^+_O \Psi^-_E |) \mathcal{O}_{\text{loc}} (|\Psi^-_O \Psi^+_E\rangle + |\Psi^+_O \Psi^-_E\rangle)| \\ &= \frac{1}{2} |\langle \Psi^+_O | \mathcal{O}_{\text{loc}} | \Psi^+_O \rangle + \langle \Psi^-_O | \mathcal{O}_{\text{loc}} | \Psi^-_O \rangle \\ &\quad - \langle \Psi^-_O | \mathcal{O}_{\text{loc}} | \Psi^-_O \rangle - \langle \Psi^+_O | \mathcal{O}_{\text{loc}} | \Psi^+_O \rangle| \\ &= 0. \end{aligned} \quad (4.106)$$

This result holds for any operator with range  $R < L$ , irrespective of its symmetries. So the unprotected TQO is destroyed due to the  $R = 1$  operators  $a_1^\dagger$  and  $a_L^\dagger$  as shown above and not due to distinguishability.

Let us now consider a system where parity is strictly conserved (say, due to fermionic superselection rules). Then the conditions of Def. 4.3 must be satisfied only for  $R$ -local operators  $\mathcal{O}_{\text{loc}}$  such that  $[\mathcal{O}_{\text{loc}}, P] = 0$  where  $P$  denotes the parity operator. Since  $\{\Psi^\pm\}$  are parity eigenstates, it follows trivially that  $\langle \Psi^+ | \mathcal{O}_{\text{loc}} | \Psi^- \rangle = 0$  for parity conserving operators (for arbitrary  $1 \leq R \leq L$ ). Combined with the second condition from above, this yields STQO for the Majorana chain ground states with optimal error  $(L - 1, 0)$  which obviously is consistent with our vague notion of (parameterless) STQO. This result is consistent with the findings in [135] for the two ground states of the Majorana chain.

Number conserving dark states

Let us now proceed with the number conserving dark states. Here the  $L + 1$  dark states are characterised by their particle number  $0 \leq N \leq L$  and given by the equal-weight superposition of number states with fixed particle number (as derived in 4.2.2):

$$|L, N\rangle = \mathcal{N}_{N,L}^{-1/2} \sum_{\mathbf{n} \in \mathcal{B}_N} |\mathbf{n}\rangle \quad \text{with} \quad \mathcal{N}_{N,L} = \binom{L}{N}$$

For any bipartition  $OE$  we can use the Schmidt decomposition

$$|L, N\rangle = \sum_{M=0}^{\min\{O,N\}} e^{-\frac{\lambda_{L,N}(M)}{2}} |O, M\rangle_O |E, N - M\rangle_E \quad (4.107)$$

with the entanglement spectrum  $\lambda$  given as  $e^{-\frac{\lambda_{L,N}(M)}{2}} = \binom{L}{N}^{-1/2} \binom{O}{M}^{1/2} \binom{E}{N-M}^{1/2}$ . Here we write  $O$  for both, the system as subset of subsystems and its size, i.e. the number of subsystems. Let  $\mathcal{O}_{\text{loc}} \in \mathcal{B}_R(\mathcal{H})$  be an arbitrary operator with support  $O$  and range  $O = R < L$ . Then we can calculate  $|\langle L, N_1 | \mathcal{O}_{\text{loc}} | L, N_1 \rangle - \langle L, N_2 | \mathcal{O}_{\text{loc}} | L, N_2 \rangle|$  for  $0 \leq N_1, N_2 \leq L$  and obtain

$$\left| \sum_{M, M'} e^{-\frac{\lambda_{L, N_1}(M) + \lambda_{L, N_1}(M')}{2}} \langle O, M |_O \langle E, N_1 - M |_E \mathcal{O}_{\text{loc}} | O, M' \rangle_O | E, N_1 - M' \rangle_E \right. \\ \left. - \sum_{M, M'} e^{-\frac{\lambda_{L, N_2}(M) + \lambda_{L, N_2}(M')}{2}} \langle O, M |_O \langle E, N_2 - M |_E \mathcal{O}_{\text{loc}} | O, M' \rangle_O | E, N_2 - M' \rangle_E \right|.$$

Using  $\langle O, M |_O \langle E, N - M |_E \mathcal{O}_{\text{loc}} | O, M' \rangle_O | E, N - M' \rangle_E = \delta_{M, M'} \langle O, M | \mathcal{O}_{\text{loc}} | O, M \rangle$  yields

$$|\langle L, N_1 | \mathcal{O}_{\text{loc}} | L, N_1 \rangle - \langle L, N_2 | \mathcal{O}_{\text{loc}} | L, N_2 \rangle| = \left| \sum_M \left[ e^{-\lambda_{L, N_1}(M)} - e^{-\lambda_{L, N_2}(M)} \right] \langle O, M | \mathcal{O}_{\text{loc}} | O, M \rangle \right|$$

An application of the triangle inequality and the CAUCHY-SCHWARZ inequality

$$|\langle O, M | \mathcal{O}_{\text{loc}} | O, M \rangle| \leq \| |O, M\rangle \| \cdot \| \mathcal{O}_{\text{loc}} |O, M\rangle \| \leq \| \mathcal{O}_{\text{loc}} \|$$

yields

$$|\langle L, N_1 | \mathcal{O}_{\text{loc}} | L, N_1 \rangle - \langle L, N_2 | \mathcal{O}_{\text{loc}} | L, N_2 \rangle| \leq \sum_M \left| e^{-\lambda_{L, N_1}(M)} - e^{-\lambda_{L, N_2}(M)} \right| \cdot \| \mathcal{O}_{\text{loc}} \| . \quad (4.108)$$

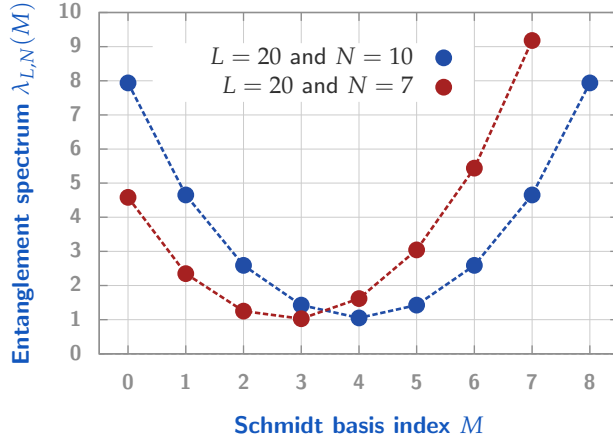
This gives an upper bound for  $\varepsilon$ , namely

$$\varepsilon \leq C_L(N_1, N_2) \equiv \sum_M \left| e^{-\lambda_{L, N_1}(M)} - e^{-\lambda_{L, N_2}(M)} \right| . \quad (4.109)$$

Unfortunately, this cannot be used to prove STQO since  $C_L(N_1, N_2)$  becomes only zero for  $|N_1 - N_2| \rightarrow 0$  and remains finite otherwise. There is a reason for that: It is rather simple to *refute* STQO by providing a quasilocal operator that distinguishes states for different particle numbers  $N$ . To this end, consider any *local* particle number operator  $n_j = a_j^\dagger a_j$ . We find

$$\langle L, N | n_j | L, N \rangle = \binom{L}{N}^{-1} \sum_{\mathbf{n}, \mathbf{m} \in B_N} \langle \mathbf{n} | n_j | \mathbf{m} \rangle = \binom{L}{N}^{-1} \binom{L-1}{N-1} = \frac{N}{L} = \alpha \quad (4.110)$$

with the particle density  $\alpha$ . Therefore we find  $N = L \langle L, N | n_j | L, N \rangle$  which allows to distinguish states for different  $N$  by a quasilocal measurement with  $R = 2$ . As the only sensible thermodynamic limit can be defined via fixed particle *densities*, this distinguishability remains valid for  $L \rightarrow \infty$  (it is exactly the particle density that can be locally measured after all). We conclude that the fixed number dark states do *not* show STQO in our reading.



■ **Figure 4.2:** We show the entanglement spectrum for the *fixed number dark state* with  $L = 20$  sites and bipartition  $O = 8$ ,  $E = L - O = 12$  at half filling  $N = 10$  (blue) and away from half filling  $N = 7$  (red). There is a pairwise degeneracy at half filling. However, away from half filling there is no degeneracy left (save for accidental degeneracies). We conclude that there is no *general* stable degeneracy in the entanglement spectrum.

Comparison of entanglement spectra

The so called *entanglement spectrum*  $\{\lambda\}$  that we computed above for the fixed number dark states via the Schmidt decomposition

$$|L, N\rangle = \sum_{M=0}^{\min\{O, N\}} e^{-\frac{\lambda_{L,N}(M)}{2}} |O, M\rangle_O |E, N - M\rangle_E \quad (4.111)$$

with

$$e^{-\frac{\lambda_{L,N}(M)}{2}} = \binom{L}{N}^{-1/2} \binom{O}{M}^{1/2} \binom{E}{N - M}^{1/2} \quad (4.112)$$

is a well-known indicator for both topological phases [135, 136] and topological order [137]. Stable degeneracies of the entanglement spectrum are usually related to states with topological order. To compare the entanglement spectrum of the fixed number dark states with the entanglement spectrum of the Majorana chain ground states, we have to derive the latter by a *Schmidt* decomposition. We already derived the decomposition above and it reads

$$|\Psi^+\rangle = \frac{1}{\sqrt{2}} (|\Psi^+\rangle_O |\Psi^+\rangle_E + |\Psi^-\rangle_O |\Psi^-\rangle_E) = \sum_{\sigma=\pm} e^{-\frac{\lambda_\sigma}{2}} |\Psi^\sigma\rangle_O |\Psi^\sigma\rangle_E \quad (4.113)$$

for the ground state  $|\Psi^+\rangle$  with positive parity (the negative parity state  $|\Psi^-\rangle$  yields obviously the same result for  $\lambda_\pm$ ). Then we find for the entanglement spectrum of the Majorana chain ground states

$$e^{-\frac{\lambda_\sigma}{2}} = \begin{cases} 2^{-\frac{1}{2}} & \sigma = + \\ 2^{-\frac{1}{2}} & \sigma = - \end{cases} \quad (4.114)$$

and  $\lambda = \infty$  for all other Schmidt basis vectors on  $O$  and  $E$ , respectively<sup>72</sup>.

<sup>72</sup>For each decomposition there is a complete Schmidt ONB for the subsystems  $O$  and  $E$ . Since the sum comprises only *two* orthonormal summands, the remaining coefficients are zero — which is equivalent to  $\lambda = \infty$ .

We conclude that the entanglement spectrum of the two ground states is *two-fold degenerate* and independent of both the system size  $L$  and the (non-trivial) bipartition  $OE$ . This characterises the topological phase of the Majorana chain.

In contrast, the entanglement spectrum  $\lambda_{L,N}(M)$  for the fixed number dark states exhibits no general stable degeneracies: In Fig. 4.2 we illustrate the entanglement spectrum of Eq. (4.111) exemplarily for a chain of  $L = 20$  sites and the bipartition  $O = 8$ ,  $E = L - O = 12$  for half filling  $N = 10$  (blue) and away from half filling  $N = 7$  (red). The Schmidt basis index  $M$  denotes the filling of  $|O, M\rangle_O$  and thus can be viewed as a label for the Schmidt basis. The spectrum  $\lambda_{L,N}(M)$  has a discrete parabola form — which is not surprising since the binomial coefficients are closely related to Gaussian functions. Away from the special case of half filling, there are generally *no* degeneracies as the blue points in Fig. 4.2 show (save for accidental or approximate ones for large systems). Furthermore the spectrum depends crucially on the bipartition  $OE$ .

This shows that there are no distinct features of a topological phase present in the fixed number dark states which is in line with our previous findings that these states can be locally distinguished. This is in clear contrast to the two-fold degeneracy — that is even independent of  $OE$  — for the Majorana chain ground states. All in all we arrive at the conclusion the the fixed number dark states show *no* definite features of (1) topological phases and (2) topologically ordered states.



## 4.5 Some concluding remarks

This is a rather technical chapter with lots of details but few results. Let us make some conclusive remarks:

- In the first part we derived the dark states of the number conserving process and provided evidence for the uniqueness as a steady state in a fixed number sector. We furthermore revealed that the jump operators constitute a representation of the Temperley-Lieb algebra on the Fock space.
- We showed that the number conserving dark states feature non-vanishing correlations and consequently cannot be classified in the framework of gapped quantum phases — in contrast to the Majorana chain ground states.
- We recalculated the mean field theory of [1] and verified their results up to some technical subtleties. However, it is highly questionable whether the applied mean field approximation yields any relevant relation between the exact dark states and the approximate ones. There are two points I want to stress: First, the ansatz

$$\rho_k = \mathcal{N}^{-1}(u_k + \alpha v_k a_{-k}^\dagger a_k^\dagger) |0, 0\rangle_{\pm k} \langle 0, 0| (u_k^* + \alpha^* v_k^* a_k a_{-k})$$

for the density matrix in momentum space is extremely restrictive and implements the result that is aimed at *a priori* into the mean field theory. Furthermore,  $u_k$  and  $v_k$  are predefined by the exact jump operator  $J$  and are not determined by a self-consistency equation. And secondly, the number fluctuations of the mean field steady state are of absolute order  $\sqrt{N}$ . Although the *relative* fluctuations vanish in the thermodynamic limit, the crucial properties of Majorana physics are related to *parity* which corresponds to number fluctuations of order  $\sim 1$ .

- In the last section we compared the exact (number conserving) dark states and the Majorana ground states in terms of their local indistinguishability and their entanglement spectrum. Both are known as indicators for topological phases but may also be applied to topologically ordered states. The comparison revealed that the number conserving dark states exhibit no topology related characteristics: They can be locally distinguished and the entanglement spectrum is not degenerate in general — in contrast to the Majorana chain ground states.
- Let us point out that these results are consistent with the well-known fact regarding *Hamiltonian* theories that *particle conserving* Hamiltonians do *not* feature Majorana modes [135].

Finally, I want to stress once more that this criticism applies only to the experimental proposal in [1] and its connection to the theory that follows. The main part, namely the identification and discussion of a topological invariant for the parity violating dissipative process is not affected by our conclusions.



# Dissipatively driven topological quantum error correction

*“The theory of computation has traditionally been studied almost entirely in the abstract, as a topic in pure mathematics. This is to miss the point of it. Computers are physical objects, and computations are physical processes. What computers can or cannot compute is determined by the laws of physics alone, and not by pure mathematics.”*

David Deutsch

This is a short concluding chapter where we discuss some aspects of *physically restricted* error correction schemes, both classical and quantum mechanical. It is basically motivated by the previous chapter 4 where we scrutinised some aspects of a recent proposal [1] to implement a dissipative version of Kitaev’s Majorana chain [3] by incoherent interactions with a tailored environment. We came to the conclusion that the proposed *number conserving* jump operators do not drive the system into a dark state space with topologically protected edge states that could serve as a code space for the storage of a topologically protected qubit. The mean field versions of these jump operators were shown to equal the fermionic quasiparticle annihilators [1,122] (see also Subsection 4.3 of Chapter 4) and drive into the degenerate code space of the Majorana chain. In this chapter we argue that the quasiparticle annihilators cannot be used as jump operators of a dissipatively self-stabilised quantum memory and propose alternative operators that drive towards the Majorana code space. Unfortunately (but not unexpectedly) numerical simulations suggest that our natural jump operators do not provide a reliable quantum memory with enhanced fidelity.

This chapter is structured as follows. In Section 5.1 we discuss the abstract concept of both classical and quantum mechanical *local* error correction. This can be considered as the theoretical foundation of dissipative error self-correction. In Section 5.2 we introduce our alternative jump operators and derive their dark states rigorously. Thereby we find also the number state representation of the Majorana chain ground states and derive relations to the number conserving jump operators in Ref. [1]. In Subsection 5.2.3 we present results of a straightforward quantum trajectory Monte Carlo simulation which indicate that there is no improvement of fidelity due to our proposed jump operators. Finally, in Section 5.3, we discuss briefly some ideas that came along with our treatment of the dissipative Majorana chain.

## 5.1 Algorithmic error correction and locality

In order to embed the dissipative Majorana chain — which will be introduced as we go along — into a more general framework, we introduce the notion of *local error correction* and *statistical error correction* in the following paragraphs. The basic idea is to impose physically motivated *locality conditions* on algorithmic (quantum) error correction procedures. This is closely related to the concept of error self-correction where the ground states of physical (that is, quasilocal) systems are considered as code spaces for the storage of (quantum) information.

### 5.1.1 Classical error correction: An abstract point of view

Let us start with a quite general description of *classical* error correction algorithms. Imagine we want to protect a register of  $N$  logical bits (denote it by  $\mathbf{l} \in \{0,1\}^N$ ) against a certain set of noise  $\mathcal{E}$  or “errors” by encoding them in a register  $\mathbf{c} \in \{0,1\}^L$  of  $L > N$  physical bits. This encoding is performed by a Turing machine  $M_{\downarrow} \equiv M_{\downarrow}(\mathcal{E}, L, N)$  which maps the logical bits to a certain combination of physical bits, i.e.

$$M_{\downarrow}\mathbf{l} = \mathbf{c}(\mathbf{l}) \equiv \langle \mathbf{l} \rangle. \quad (5.1)$$

Each element  $e \in \mathcal{E}$  may be considered as a function  $e : \{0,1\}^L \rightarrow \{0,1\}^L$ . Assume there is another Turing machine  $M_{\uparrow} \equiv M_{\uparrow}(\mathcal{E}, L, N)$  which recovers the logical bits from the physical ones via

$$M_{\uparrow}\mathbf{c}(\mathbf{l}) = M_{\uparrow}M_{\downarrow}\mathbf{l} = \mathbf{l}. \quad (5.2)$$

This is usually termed *decoding* and the action of  $M_{\downarrow}$  is correspondingly referred to as *encoding*. Now let  $\mathbf{c}(\mathbf{l})$  be the state of a physical register with a piece  $\mathbf{l}$  of encoded information and expose it to the noise  $\mathcal{E}$ . After some time the content of the register reads

$$\mathbf{c}(\mathbf{l}) \xrightarrow{\mathcal{E}} e\mathbf{c}(\mathbf{l}) \quad (5.3)$$

with some (random) error function  $e \in \mathcal{E}$ . Assume there is a third Turing machine  $\hat{M}_{\mathcal{E}}$  with the property

$$\forall e \in \mathcal{E} \forall \mathbf{l} \in \{0,1\}^N : \hat{M}_{\mathcal{E}}eM_{\downarrow}\mathbf{l} = \mathbf{l}. \quad (5.4)$$

That is, even if an arbitrary error  $e \in \mathcal{E}$  was applied to the physical register, the logical bit  $\mathbf{l}$  is not lost and can be recovered by  $\hat{M}_{\mathcal{E}}$ . We say that  $\hat{M}_{\mathcal{E}}$  corrects for the errors in  $\mathcal{E}$  and call the tuple  $\mathcal{I} = (M_{\downarrow}, \hat{M}_{\mathcal{E}}, N, L, \mathcal{E})$  an *information preserving structure* that protects  $N$  logical bits against the errors  $\mathcal{E}$  by means of  $L$  physical bits.

Note that at this general point  $\mathcal{E}$  features *no* non-trivial closure properties (e.g. against concatenation of errors). Now let  $M_{\mathcal{E}} \equiv M_{\downarrow}\hat{M}_{\mathcal{E}}$  be the Turing machine that recovers the physical register of  $L$  bits for each error in  $\mathcal{E}$ . That is, for each error  $e \in \mathcal{E}$  and each *valid* code  $\mathbf{c}$  we have  $M_{\mathcal{E}}e\mathbf{c} = M_{\downarrow}\hat{M}_{\mathcal{E}}eM_{\downarrow}\mathbf{l} = M_{\downarrow}\mathbf{l} = \mathbf{c}$ . Please note that  $M_{\mathcal{E}}$  reconstructs  $\mathbf{c}$  from the spoiled register  $e\mathbf{c}$  in absence of any constraints. Particularly it is possible for  $M_{\mathcal{E}}$  to choose its actions on  $e\mathbf{c}$  based on the knowledge of  $e\mathbf{c}$  as a whole.

Pictorially:



This is a simple repetition code that encodes  $N = 1$  logical bit in  $L = 6$  physical bits and performs error correction by a majority vote. In this representation a Turing machine is rather a *physical realisation* of an apparatus which is Turing complete (except for the infinite storage of course). Therefore the act of correcting the physical register is rather a sequence of *measuring* the register, *processing* the retrieved information, and *writing* the output of the error correction algorithm to the register. At this stage there are two points to consider:

1. It is reasonable to demand that the physical system which performs the error correction is reverted to its initial state after the error correction has finished. During this reset procedure, the measurement outcome has to be deleted. According to LANDAUER’S principle [138] any deleted bit is accompanied by an entropy ejection of  $k_B \ln 2$ . This is necessary to ensure that the second law of thermodynamics remains valid (since  $e$  is unknown, the entropy of the physical system raised during this process).
2. The Turing machine  $M_E$  gains immediate knowledge of the *whole* register  $ec$ : There is *one* measurement, *one* computation, and subsequently *one* reset process which takes care of the entropy transferred to the Turing machine due to the measurement and correction process.

This is a quite powerful procedure (actually, there is no constraint at all but the general framework) and it is clear that any such error correction procedure may be implemented by means of classical computers since the latter are Turing complete. However, it would be appealing if  $M_E$  – which usually is just a computer – could be realised on a more fundamental level. That is, it would be great if we could implement the chain of measuring, running  $M_E$ , and correcting the register by a simple *physical process* instead of using a full-fledged computer (which, in most cases, is just a waste of resources). Such an information preserving structure is capable of *error self-correction*.

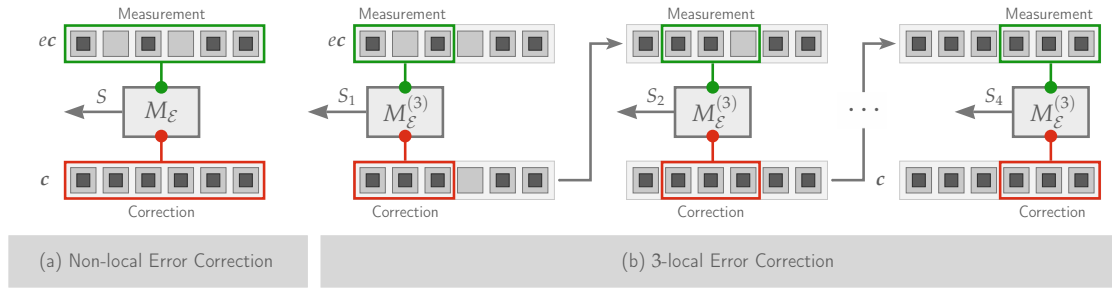
However, there is no generic distinction between “normal” error correction procedures and systems capable of error self-correction. This is due to the fact that a computer (which implements  $M_E$ ) actually *is* a well defined (in case of a classical computer: deterministic) physical system. Therefore a mathematician would be inclined to call “normal” error correction procedures “trivially self-correcting procedures”. Nevertheless it is clear that the pivotal characteristics of error self-correction is the *simplicity* of the physical realisation of  $M_E$ . E.g. we could demand that the correction of the physical register is performed by a quasilocal stochastic process. The notions of *quasilocality* and *stochasticity* lead us to a more restrictive model of error correction, which, on the contrary, is more suitable for fundamental physical implementations:

### 5.1.2 Classical local error correction

In order to derive a more restrictive model of classical error correction, let us state the physical requirements which have to be met for a simple physical realisation of the correction process<sup>73</sup>:

1. The physical register hosting  $ec$  is a spatially distributed structure of local physical subsystems, each of which features (at least) two inner degrees of freedom. For the sake of simplicity, assume a finite linear chain of “spins” which may point up and downward.

<sup>73</sup>We are not going to deal with the encoding and decoding process ( $M_d$  and  $M_r$ ) since this is an unrelated story.

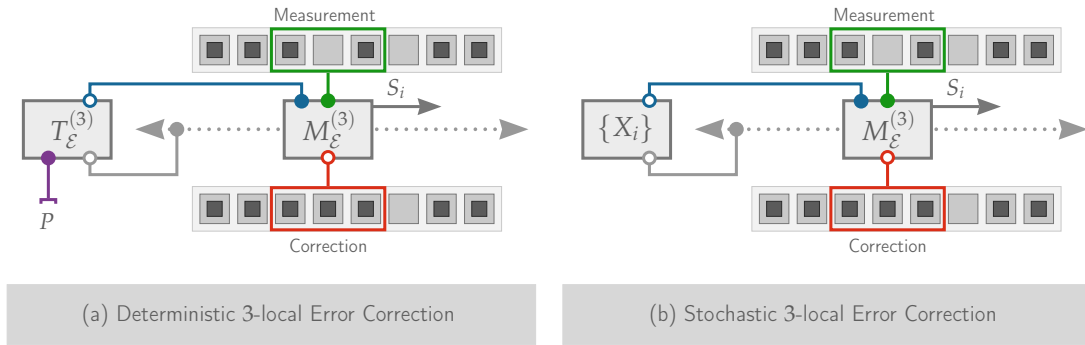


■ **Figure 5.1:** Illustration of classical error correction schemes. The physical bits are labelled by (un)filled grey squares and form a register which holds the encoded logical bit(s). Here we show a simple repetition code: The *logical* bit 1 is encoded by six *physical* bits in the same state. The paradigmatic *algorithmic* error correction is illustrated in (a). The (corrupted) register  $ec$  is measured and the complete result is used as input for a computing device (symbolised by a Turing machine)  $M_{\mathcal{E}}$  which computes the appropriate operations to restore the encoded logical bit. For the shown repetition code this is just a majority vote. In (b) we illustrate the concept of *local* error correction (here 3-local). The device measures only 3 adjacent physical bits at once and subsequently starts the Turing machine to receive instructions how to modify the 3 measured bits in order to revert the local errors. Subsequently the machine is reset and thereby ejects an amount  $S_i$  of entropy. The shown (two) errors can still be correct by a 3-local majority vote.

2. The measuring process  $X$  should affect only a finite, spatially compact set  $K_X$  of subsystems (regardless of the system size  $L$ ).
3. Any process  $Y$  operating on the physical register which features correlations between subsystems should affect only a finite, spatially compact set  $K_Y$  of subsystems (regardless of the system size  $L$ ).
4. For any process  $Y$  which is caused by a preceding measurement  $X$  we demand  $K_Y \subseteq K_X$ . This requirement encodes the assumption, that a subsystem which can be operated on can also be measured.

These conditions lead to the notion of classical *local* error correction, the basic concept of which is exemplified and compared with “normal” non-local error correction in Fig. 5.1: In (a) we show the classical error correction scheme by means of a simple repetition code on six physical bits (grey boxes). The state of bits is indicated by filled and blank boxes. The physical register is shown twice, before (upper row) and after (lower row) the error correction. The logical bit is encoded by six identical copies of its state. The corrupted register  $ec$  is illustrated in the upper row. In the first step, the states of all physical bits are measured (green box). The result (error syndrome) is used as input for some computing device (symbolised by a Turing machine  $M_{\mathcal{E}}$ ) that derives the appropriate countermeasures on the physical bits to revert the errors. In the last step the output of  $M_{\mathcal{E}}$  is applied to the physical bits (red box). For the repetition code this is a simple majority vote. Note that for the computation of the subsequent error correcting actions, the *complete* error syndrome is available

In contrast, (b) illustrates the more constrained scheme of *local* error correction (here the 3-local repetition code as an example). The major constraint being the restriction of both measurement and correction range on a bounded set of adjacent physical bits. Here the Turing machine  $M_{\mathcal{E}}$  is initialised several times with the measurement results of three adjacent bits. Based on this limited information, it computes appropriate countermeasures that are subsequently applied to the *same* bits that were measured before. After each local correction procedure (measurement  $\rightarrow$  computation  $\rightarrow$  correction) the Turing machine is *reset*, that is, its tape and final state is *erased*.



■ **Figure 5.2:** Here we illustrate our extended concept of classical local error correction. (a) shows the scheme for *deterministic* 3-local error correction with a trivial repetition code on 8 physical bits. The local combination of measurement device (green box), computing machine ( $M_{\mathcal{E}}^{(3)}$ ) and correction device (red box) — the *operator* — is controlled externally by a *supervisor*  $T_{\mathcal{E}}^{(3)}$  (another Turing machine) which controls (1) the position of the operator and (2) its mode (type and initialisation of the local error correction procedure). The supervisor can be triggered deterministically by the external input  $P$ . The crucial point is that the supervisor cannot obtain information on the measured error syndrome as there is no feedback channel from  $M_{\mathcal{E}}^{(3)}$  to  $T_{\mathcal{E}}^{(3)}$ . Once triggered, a local measurement is performed,  $M_{\mathcal{E}}^{(3)}$  runs its program on the measurement result and subsequently resets its tape (and thereby ejects the entropy  $S_i$ ). In (b) the concept of *stochastic* local error correction is illustrated. There the supervisor is replaced by a stochastic process (symbolised by a set of random variables  $\{X_i\}$ ) and determines the position of the operator and its initialisation randomly via realisations of  $X_i$ .

As mentioned above, this requires the ejection of a certain amount of entropy  $S_i$  after each step  $i$  according to LANDAUER’s principle [138]. The shown repetition code is trivial and was chosen for illustrative purposes. Clearly the constraints in (b) reduce the number of errors that can be corrected considerably (however, the shown error can still be corrected).

Let us refine this notion further. In Fig. 5.2 we illustrate two concepts of local error correction that differ by additional constraints on the *coordination* of the local error correction procedures: In (a) we illustrate the scheme of *deterministic* local error correction. There are two computing (or Turing) machines, the *operator* denoted by  $M_{\mathcal{E}}$  that computes the local error correction actions (red box) based on the limited local error syndrome (green box), and the *supervisor*  $T_{\mathcal{E}}$  that controls the position and initialisation of the operator. The supervisor can be triggered by an external input  $P$ . As before, the local error correction is completed by a reset procedure on the operator which results in an entropy ejection  $S_i$ . The crucial point is that the supervisor cannot gain knowledge on the measured error syndromes as there is no feedback channel from the operator to the supervisor (otherwise this would be equivalent to the “normal” non-local error correction).

In (b) the supervisor is replaced by a stochastic process denoted by the set of random variables  $\{X_i\}$ . Both the position and initialisation of the operator are controlled by realisations of these random variables. Clearly this is even more restrictive than the deterministic scheme in (a) where the local error corrections can still build on each other according to some global master plan (even if they cannot communicate). Nevertheless this is the concept which seems to be most convenient to formalise what a dissipative, quasilocal physical process can achieve — at least in the Markovian regime.

### 5.1.3 Local quantum error correction

Our actual motivation for thinking about quasilocal error correction is the notion of *dissipative quantum error correction*. So far we were concerned with classical error correction. We do not give a *formal* treatment of *local quantum error correction* as its development is beyond the scope of this thesis. So let us just briefly discuss *possible* translations of the classical concepts developed above to the quantum realm.

The central difference surely is the exchange of the bits by, say, two-level quantum systems (i.e. qubits). There are two different possibilities to translate the actions of the operator: First, the operator could be kept as “classical” as possible, meaning the *measurement* becomes a measurement of some local observable (for instance, a stabiliser) with a subsequent projection into the corresponding eigenspace. Then the Turing machine  $M_{\mathcal{E}}$  remains classical as its input is a classical bit string. The correction operations that are controlled by its output should be replaced by an arbitrary local quantum operation, that is, a CPTP map with local support. As  $M_{\mathcal{E}}$  remains classical, it is consistent to keep the supervisor  $T_{\mathcal{E}}$  as a classical Turing machine as well.

The second translation is more “quantum mechanical”: We could still keep the supervisor as a classical deterministic  $T_{\mathcal{E}}$  Turing machine or a stochastic process  $\{X_i\}$ . But now the whole action of the operator becomes quantum mechanical. That is, the chain “measurement  $\rightarrow$  computation  $\rightarrow$  correction” is contracted to a single, composite operation that may be described in the most general case as a quantum channel with local support. This concept then allows for *coherent* processes in the course of the error correction.

The reader may have noticed that these concepts are closely related to quantum cellular automata (QCA); especially the latter one. This insight motivated some of the remarks and definitions presented in the concluding section 5.3.



## 5.2 Error correction and the dissipative Majorana chain

After these rather abstract preliminary remarks — which were intended to convey an intuition of error self-correction isolated from specific physical realisations — we now return to a concrete and familiar model: the (dissipative) Majorana chain.

To this end, we consider an open chain of  $L$  fermionic sites associated with the fermion algebra  $\mathfrak{F}_L$  spanned by physical creation and annihilation operators  $a_i^\dagger$  and  $a_i$ ,  $1 \leq i \leq L$ . Each physical site splits into two Majorana modes  $c_{2j-1}$  and  $c_{2j}$  which may be recombined to form new fermionic algebras. As long as the recombination remains *quasilocal* in a physical sense, the resulting fermionic modes can be considered as *quasiparticles*. We will be concerned with the following fermionic modes:

$$a_j = \frac{1}{2}(c_{2j} - ic_{2j-1}) \Leftrightarrow c_{2j} = a_j + a_j^\dagger \quad \text{and} \quad c_{2j-1} = i(a_j - a_j^\dagger) \quad (5.5a)$$

$$\tilde{a}_j = \frac{1}{2}(c_{2j} + ic_{2j+1}) \Leftrightarrow c_{2j} = \tilde{a}_j + \tilde{a}_j^\dagger \quad \text{and} \quad c_{2j+1} = i(\tilde{a}_j^\dagger - \tilde{a}_j) \quad (5.5b)$$

where the physical fermions  $a_j$  are defined for  $1 \leq j \leq L$  and the quasiparticles  $\tilde{a}_j$  are located “between” two adjacent physical sites, i.e.  $1 \leq j \leq L-1$ . The unpaired Majorana edge modes  $c_1$  and  $c_{2L}$  form a macroscopically delocalised fermionic boundary mode  $b \equiv \tilde{a}_L = \frac{1}{2}(c_{2L} + ic_1)$ . Based on the relations above, it is straightforward to show

$$\tilde{a}_j = \frac{1}{2}(a_j + a_j^\dagger - a_{j+1} + a_{j+1}^\dagger) \quad \text{and} \quad a_j = \frac{1}{2}(\tilde{a}_j + \tilde{a}_j^\dagger - \tilde{a}_{j-1} + \tilde{a}_{j-1}^\dagger).$$

We aim at a dissipative realisation of the Majorana chain, meaning, we are looking for jump operators that drive the open chain of fermionic sites into the degenerate ground state space of Kitaev’s Majorana chain which can be used as a topological quantum memory. The hope is that excitations (i.e. errors) can be eliminated by the jump operators before they traverse the system and cause logical errors (see Subsec. 1.3.4 for a review of the Majorana chain as a quantum memory). In the following we discuss two of the simplest sets of jump operators that drive the system into the code space:

### 5.2.1 A naïve approach: Dissipative dynamics with parity violation

In [1] the effective jump operators obtained by a mean field approximation of the number conserving jump operators read

$$L_j = \tilde{a}_j = \frac{1}{2}(c_{2j} + ic_{2j+1}) = \frac{1}{2}(a_j + a_j^\dagger - a_{j+1} + a_{j+1}^\dagger) \quad (5.6)$$

which are exactly the quasiparticle annihilators. It is evident that the dissipative process  $\{L_j\}$  features a two dimensional dark state space  $\mathcal{PS}$  which coincides with the code space of the quantum error correction code, see 1.3.4. What happens if we boldly propose these jump operators from the beginning as a possible realisation of a dissipative quantum memory? In the preliminaries 1.3.4 we pointed out that the quantum error correction code which is realised by the ground state space of the Majorana chain — and which we wish to realise by quasilocal jump operators — *cannot* correct odd bit-flip errors, that is, parity violating fermionic operations. We

are immediately led to the conclusion that the above *parity violating* jump operators introduce *new* errors which cannot even be corrected by the manual error correction procedure.

This becomes apparent if we recall that the *logical*  $Z$ -operator corresponds to the quasiparticle parity

$$\tilde{P} = \prod_{j=1}^{L-1} (-ic_{2j}c_{2j+1}) \cdot (-ic_{2L}c_1) = \prod_{j=1}^{L-1} (-1)^{\tilde{a}_j^\dagger \tilde{a}_j} \cdot (-1)^{b^\dagger b}$$

with the boundary mode  $b^\dagger$ . That is,  $P|\tilde{0}\rangle = |\tilde{0}\rangle$  and  $P|\tilde{1}\rangle = -|\tilde{1}\rangle$ . A logical *phase* error then corresponds to a chain of elementary errors  $E_j$  that traverses the whole chain. We already saw that and how such errors can be corrected. But the above jump operators correspond to *logical*  $X$ -errors<sup>74</sup> as  $\{P, L_j\} = 0$ ; and the error correction scheme in 1.3.4 cannot cope with such errors. In the Hamiltonian setting this reads as follows: The last paragraph of 1.3.4 showed that away from the ideal point, there appear terms which couple the boundary mode to the quasiparticles near the endpoints of the chain. If somewhere in the bulk a *physical*  $X$ -error, say a single  $\tilde{a}_j^\dagger$ , occurred, the non-trivial dynamics of the quasiparticles can transfer this excitation into the boundary mode and thereby lift it to a *logical* bit-flip error.

We conclude that the above parity violating jump operators do more harm than good; at least if the spectrum is not flat and the quasiparticles can diffuse across the system (which is to be expected in any experimental realisation to some degree).

### 5.2.2 A second approach: Dissipative dynamics with parity conservation

According to the previous discussion, we need *parity conserving* jump operators if we wish to reproduce the quantum error correction code in a dissipative setting. The most straightforward approach certainly is the following:

$$L_{j,c} \equiv \frac{1}{2}E_{j+c} (1 - S_j) = \frac{i}{2}c_{2(j+c)}c_{2(j+c)-1} (1 + ic_{2j}c_{2j+1}) = \begin{cases} -\tilde{a}_{j-1}^\dagger \tilde{a}_j + \tilde{a}_{j-1} \tilde{a}_j, & (c = 0) \\ \tilde{a}_{j+1}^\dagger \tilde{a}_j + \tilde{a}_{j+1} \tilde{a}_j, & (c = 1) \end{cases}. \quad (5.7)$$

These jumps push the excitations (that is, physical errors) across the system and annihilate pairs of adjacent excitations. Contrary to the parity violating jump operators, the parity conserving versions are *interacting*. However, due to their quasilocal nature, a physical realisation is not beyond the realms of possibility. Since  $c$  takes the values 0 and 1, there are  $2L - 2$  independent jump operators whose action on the quasiparticle number-states can be illustrated as follows (sites  $j - 1, j$  and  $j + 1$  are depicted):

$$\begin{array}{ll} L_{j,0} |\square \blacksquare \square\rangle = -|\blacksquare \square \square\rangle & L_{j,1} |\square \blacksquare \square\rangle = |\square \square \blacksquare\rangle \\ L_{j,0} |\square \blacksquare \blacksquare\rangle = -|\blacksquare \blacksquare \square\rangle & L_{j,1} |\square \square \blacksquare\rangle = |\square \square \square\rangle \\ L_{j,0} |\blacksquare \square \square\rangle = -|\square \square \square\rangle & L_{j,1} |\blacksquare \square \square\rangle = |\blacksquare \blacksquare \square\rangle \\ L_{j,0} |\blacksquare \blacksquare \square\rangle = -|\square \square \blacksquare\rangle & L_{j,1} |\blacksquare \blacksquare \square\rangle = |\blacksquare \square \square\rangle \end{array}$$

If the corresponding site  $j$  is unoccupied, the jump operators annihilate the state:

$$L_{j,0/1} |\square \square \square\rangle = L_{j,0/1} |\blacksquare \square \square\rangle = L_{j,0/1} |\square \blacksquare \square\rangle = L_{j,0/1} |\blacksquare \blacksquare \square\rangle = 0$$

<sup>74</sup>In the spin representation that we obtained by a Jordan-Wigner transformation, such errors appear as *non-local* string operators.

That is, the jump operators simulate a *diffusion* and *annihilation* process on the quasiparticle excitations. In the original (physical) fermion basis we find

$$L_{j,c} = \frac{1}{2} \begin{cases} -\left(1 - 2a_j^\dagger a_j - a_j a_{j+1} - a_j^\dagger a_{j+1}^\dagger\right) - a_j^\dagger a_{j+1} + a_{j+1}^\dagger a_j, & \text{for } c = 0 \\ \left(1 - 2a_{j+1}^\dagger a_{j+1} - a_j a_{j+1} - a_j^\dagger a_{j+1}^\dagger\right) - a_j^\dagger a_{j+1} + a_{j+1}^\dagger a_j, & \text{for } c = 1 \end{cases}. \quad (5.8)$$

Interestingly enough, we can recover the particle conserving jump operators from Chapter 4 by adding the jump operators for  $c = 0$  and  $c = 1$ , i.e.

$$L_{j,0} + L_{j,1} = a_j^\dagger a_j - a_{j+1}^\dagger a_{j+1} + a_{j+1}^\dagger a_j - a_j^\dagger a_{j+1} \propto J_j \quad (5.9)$$

and we conclude that any dark state of  $\{L_{j,c}\}$ ,  $1 \leq j \leq L-1$  and  $c \in \{0,1\}$ , is automatically a dark state of the number conserving dynamics  $\{J_j\}$ . Now define additionally

$$F_j \equiv L_{j,0} - L_{j,1} = a_j^\dagger a_j + a_{j+1}^\dagger a_{j+1} - \mathbb{1} + a_j a_{j+1} + a_j^\dagger a_{j+1}^\dagger. \quad (5.10)$$

Since  $J_j = L_{j,0} + L_{j,1}$  and  $F_j = L_{j,0} - L_{j,1}$  define a nonsingular linear transformation of operators, it follows that the two dissipative processes  $\{J_j, F_j\}$  and  $\{L_{j,0}, L_{j,1}\}$  stabilise the same dark states.

This can be formulated more generally:

► **Lemma 5.1: Transformation of jump operators**

Consider an arbitrary set of jump operators  $\{A_i\}_{1 \leq i \leq L}$  that defines a dissipative process such that the only steady states are described by the dark state space  $\mathcal{D}$ . Let  $M \in \text{GL}(L, \mathbb{C})$  be an arbitrary nonsingular matrix. Then the new set of jump operators  $\{B_j\}_{1 \leq j \leq L}$  defined via

$$B_j \equiv \sum_{i=1}^L M_j^i A_i \equiv M_j^i A_i \quad (5.11)$$

constitutes a dissipative process with the same dark states  $\mathcal{D}$ .

*Proof.* Let  $\bar{M}$  be the inverse of  $M$ . For any state  $|D\rangle \in \mathcal{H}$  it holds

$$\forall_j : B_j |D\rangle = 0 \quad \Leftrightarrow \quad \forall_j : M_j^i A_i |D\rangle = 0 \quad \Leftrightarrow \quad \forall_l : \bar{M}_l^j M_j^i A_i |D\rangle = 0 \quad \Leftrightarrow \quad \forall_l : A_l |D\rangle = 0$$

so that the dark state space of the new dissipative process remains  $\mathcal{D}$ . To show that these are the only steady states assume that there is a subspace  $\mathcal{S} \leq \mathcal{H}$ ,  $\mathcal{S} \perp \mathcal{D}$ , such that  $\forall_{1 \leq j \leq L} : A_j \mathcal{S} \subseteq \mathcal{S}$ . Let  $|\Psi\rangle$  be an arbitrary state in  $\mathcal{S}$ , i.e.  $\forall_{1 \leq j \leq L} : A_j |\Psi\rangle \in \mathcal{S}$ . Then it follows immediately (due to the subspace property of  $\mathcal{S}$ ) that  $\forall_{1 \leq i \leq L} : B_i |\Psi\rangle = M_i^j A_j |\Psi\rangle \in \mathcal{S}$ . Since  $\mathcal{D}$  is also the dark state space of the new process, this shows that the condition of Proposition 4.1 remains true (or false) under the transformation  $M$ . ■

■ **Derivation of the dark states**

We will now *derive* the dark states for the process  $\{J_j, F_j\}$  from scratch and conclude immediately, that these dark states are stabilised by the equivalent process  $\{L_{j,0}, L_{j,1}\}$ . However, it is clear that the dark states for the dissipative process  $\{\tilde{a}_j\}_{1 \leq j \leq L-1}$  are also dark states for e.g.  $\{L_{j,1}\}$

since  $L_{j,1} = \tilde{a}_{j+1}^\dagger \tilde{a}_j + \tilde{a}_{j+1} \tilde{a}_j$ . Conversely, assume that  $L_{j,1} |D\rangle = 0$  for some state  $|D\rangle \in \mathcal{H}$ . Recall that for any state  $|\Psi\rangle$  and site  $l$  it holds  $(\tilde{a}_l^\dagger + \tilde{a}_l) |\Psi\rangle = 0 \Rightarrow |\Psi\rangle = 0$ . Set  $l = j+1$  and it follows  $\tilde{a}_j |D\rangle = 0$ .

Hence all three dissipative processes  $\{J_j, F_j\}$ ,  $\{L_{j,0}, L_{j,1}\}$ , and  $\{\tilde{a}_j\}$  stabilise the *same* dark states. So let us construct the dark states for  $\{J_j, F_j\}$  which coincide with the topologically ordered Majorana chain ground states. We shall use the superselection sectors of even and odd parity. Therefore define

$$\mathbb{P}_L^+ \equiv \bigcup_{i=0}^{\lfloor L/2 \rfloor} B_{2i} \quad \text{and} \quad \mathbb{P}_L^- \equiv \bigcup_{i=0}^{\lfloor L/2 \rfloor} B_{2i+1}. \quad (5.12)$$

Thus  $\mathbb{P}_L^\pm$  is the set of all binary vectors  $\mathbf{n} \in \{0,1\}^L$  with even (+) and odd (−) occupancy and the superselection sectors in  $\mathcal{H}_L$  read  $\mathcal{H}_L^\pm = \text{span} \{|\mathbf{n}\rangle \mid \mathbf{n} \in \mathbb{P}_L^\pm\}$ . That is, relative phases between states of these superselection sectors are physically unobservable and any (mathematical) superposition of such vectors degenerates (physically) to a statistical mixture (see paragraph 1.3.4 in the preliminaries for some remarks on superselection).

We first want to express the action of  $J_j$  and  $F_j$  in terms of binary transformations. To this end let  $\epsilon_j$  be the binary addition of 11 on sites  $j$  and  $j+1$ , that is

$$\epsilon_j \mathbf{n} = \epsilon_j (n_1, \dots, n_j, n_{j+1}, \dots, n_L) \equiv (n_1, \dots, n_j \oplus 1, n_{j+1} \oplus 1, \dots, n_L). \quad (5.13)$$

Furthermore recall the definition of  $\sigma_j$ :

$$\sigma_j : \{0,1\}^L \longrightarrow \{-1,0,1\}, \quad \mathbf{n} \mapsto \sigma_j \mathbf{n} = \begin{cases} +1 & \Leftrightarrow n_j = 1 \wedge n_{j+1} = 0 \\ 0 & \Leftrightarrow n_j = n_{j+1} \\ -1 & \Leftrightarrow n_j = 0 \wedge n_{j+1} = 1 \end{cases} \quad (5.14)$$

where  $j$  is a variable modulo  $L$  and it holds  $\sigma_j \epsilon_j \mathbf{n} = -\sigma_j \mathbf{n}$ . Analogously we define

$$\mu_j : \{0,1\}^L \longrightarrow \{-1,0,1\}, \quad \mathbf{n} \mapsto \mu_j \mathbf{n} = \begin{cases} +1 & \Leftrightarrow n_j = 1 = n_{j+1} \\ 0 & \Leftrightarrow n_j \neq n_{j+1} \\ -1 & \Leftrightarrow n_j = 0 = n_{j+1} \end{cases} \quad (5.15)$$

where  $j$  is a variable modulo  $L$ . Obviously  $\mu_j \epsilon_j \mathbf{n} = -\mu_j \mathbf{n}$ .

Now recall the action of  $J_j$  on the number basis:

$$\begin{aligned} J_j |\square\square\rangle &= 0 & J_j |\blacksquare\square\rangle &= |\square\blacksquare\rangle + |\blacksquare\square\rangle \\ J_j |\square\blacksquare\rangle &= -|\blacksquare\square\rangle - |\square\blacksquare\rangle & J_j |\blacksquare\blacksquare\rangle &= 0 \end{aligned}$$

For the new operators  $F_j$  we find a similar structure:

$$\begin{aligned} F_j |\square\square\rangle &= |\blacksquare\square\rangle - |\square\square\rangle & F_j |\blacksquare\square\rangle &= 0 \\ F_j |\square\blacksquare\rangle &= 0 & F_j |\blacksquare\blacksquare\rangle &= |\blacksquare\blacksquare\rangle - |\square\square\rangle \end{aligned}$$

Using the previously introduced symbols  $\epsilon_j$ ,  $\sigma_j$  and  $\mu_j$  this can be written in the compact form

$$J_j |\mathbf{n}\rangle = \sigma_j \mathbf{n} [|\mathbf{n}\rangle + |\epsilon_j \mathbf{n}\rangle] \quad (5.16)$$

$$F_j |\mathbf{n}\rangle = \mu_j \mathbf{n} [|\mathbf{n}\rangle - |\epsilon_j \mathbf{n}\rangle] . \quad (5.17)$$

Now let  $|\Psi^\pm\rangle = \sum_{\mathbf{n} \in \mathbb{P}_L^\pm} \Psi^\pm(\mathbf{n}) |\mathbf{n}\rangle \in \mathcal{H}_L^\pm$  be an arbitrary state of defined parity. We rewrite this state in terms of sectors of constant particle number, namely

$$|\Psi^+\rangle = \sum_{\mathbf{n} \in \mathbb{P}_L^+} \Psi^+(\mathbf{n}) |\mathbf{n}\rangle = \sum_{i=0}^{\lfloor L/2 \rfloor} \sum_{\mathbf{n} \in B_{2i}} \Psi^+(\mathbf{n}) |\mathbf{n}\rangle . \quad (5.18)$$

Here we considered w.l.o.g. an even parity state  $|\Psi^+\rangle$ . Demanding  $J_j |\Psi^+\rangle = 0$  for all  $1 \leq j \leq L-1$  is equivalent to the condition  $J_j \sum_{\mathbf{n} \in B_{2i}} \Psi^+(\mathbf{n}) |\mathbf{n}\rangle = 0$  since vectors  $|\mathbf{n}\rangle$  and  $|\mathbf{m}\rangle$  are linearly independent for  $\mathbf{n} \in B_l$  and  $\mathbf{m} \in B_k$  if  $l \neq k$  and the subspaces  $\mathcal{H}^{(L,N)}$  of fixed particle number are invariant with respect to all  $J_j$  jump operators. However, this condition has already been solved previously (see 4.2.2) and we find  $\Psi^+(\mathbf{n}) = \Psi_{2i}^+ = \text{const}$  for each sector  $|\mathbf{n}| = 2i$  of constant particle numbers which leads us to

$$|\Psi^+\rangle = \sum_{i=0}^{\lfloor L/2 \rfloor} \Psi_{2i}^+ \sum_{\mathbf{n} \in B_{2i}} |\mathbf{n}\rangle = \sum_{i=0}^{\lfloor L/2 \rfloor} \Psi_{2i}^+ \binom{L}{2i}^{1/2} |L, 2i\rangle = \sum_{\mathbf{n} \in \mathbb{P}_L^+} \Psi_{|\mathbf{n}|}^+ |\mathbf{n}\rangle \quad (5.19)$$

where  $|L, 2i\rangle$  denotes the well known dark states of the  $\{J_j\}$  process. Now the additional conditions  $F_j |\Psi^+\rangle = 0$  must be satisfied for all  $1 \leq j \leq L-1$  which means

$$\begin{aligned} F_j |\Psi^+\rangle &= \sum_{\mathbf{n} \in \mathbb{P}_L^+} \Psi_{|\mathbf{n}|}^+ F_j |\mathbf{n}\rangle = \sum_{\mathbf{n} \in \mathbb{P}_L^+} \Psi_{|\mathbf{n}|}^+ \mu_j \mathbf{n} [|\mathbf{n}\rangle - |\epsilon_j \mathbf{n}\rangle] \\ &= \frac{1}{2} \sum_{\mathbf{n} \in \mathbb{P}_L^+} \Psi_{|\mathbf{n}|}^+ \mu_j \mathbf{n} [|\mathbf{n}\rangle - |\epsilon_j \mathbf{n}\rangle] + \frac{1}{2} \sum_{\mathbf{n} \in \mathbb{P}_L^+} \Psi_{|\epsilon_j \mathbf{n}|}^+ \mu_j \epsilon_j \mathbf{n} [|\epsilon_j \mathbf{n}\rangle - |\mathbf{n}\rangle] \\ &= \frac{1}{2} \sum_{\mathbf{n} \in \mathbb{P}_L^+} \Psi_{|\mathbf{n}|}^+ \mu_j \mathbf{n} [|\mathbf{n}\rangle - |\epsilon_j \mathbf{n}\rangle] + \frac{1}{2} \sum_{\mathbf{n} \in \mathbb{P}_L^+} \Psi_{|\epsilon_j \mathbf{n}|}^+ \mu_j \mathbf{n} [|\mathbf{n}\rangle - |\epsilon_j \mathbf{n}\rangle] \\ &= \frac{1}{2} \sum_{\mathbf{n} \in \mathbb{P}_L^+} [\Psi_{|\mathbf{n}|}^+ + \Psi_{|\epsilon_j \mathbf{n}|}^+] \mu_j \mathbf{n} [|\mathbf{n}\rangle - |\epsilon_j \mathbf{n}\rangle] \stackrel{!}{=} 0 \end{aligned}$$

where we used the fact that  $\epsilon_j^2 = \mathbb{1}$ ,  $\epsilon_j \mathbb{P}_L^\pm \subseteq \mathbb{P}_L^\pm$  and hence  $\epsilon_j \mathbb{P}_L^\pm = \mathbb{P}_L^\pm$ . Note that for  $\mu_j \mathbf{n} = 0$  no additional constraint is obtained. However, due to the linear independence we find

$$\Psi_{|\mathbf{n}|}^+ + \Psi_{|\epsilon_j \mathbf{n}|}^+ = 0 \quad \Leftrightarrow \quad \Psi_{|\mathbf{n}|}^+ = -\Psi_{|\mathbf{n}| \mp 2}^+ \quad \text{if } \mu_j \mathbf{n} = \pm 1 \quad (5.20)$$

since clearly  $|\epsilon_j \mathbf{n}| = |\mathbf{n}| - 2\mu_j \mathbf{n}$ . That is, we get the alternating structure

$$|\Psi^+\rangle = \mathcal{N}_L^{-1/2} \sum_{i=0}^{\lfloor L/2 \rfloor} (-1)^i \binom{L}{2i}^{1/2} |L, 2i\rangle \quad \text{and} \quad (5.21a)$$

$$|\Psi^-\rangle = \mathcal{N}_L^{-1/2} \sum_{i=0}^{\lfloor L/2 \rfloor} (-1)^i \binom{L}{2i+1}^{1/2} |L, 2i+1\rangle \quad (5.21b)$$

which is the equal-weight and alternating-phase superposition of all even (odd) parity number states. We conclude that the dark states of the fermionic process  $\{\tilde{a}_j\}_{1 \leq j \leq L-1}$  are unique in each superselection sector  $\mathcal{H}_L^\pm$ .

The reader might have noticed that we actually did not use the fact that  $F_j |\Psi^\pm\rangle = 0$  for all  $1 \leq j \leq L-1$ . The above argument applies even if we just demand that there exists one  $j^*$  such that  $F_{j^*} |\Psi^\pm\rangle = 0$ . This shows that already the process  $\{F_1, J_j\}_{1 \leq j \leq L-1}$  (one may replace  $F_1$  by some other  $F_j$ ) drives the system to the Majorana chain dark states  $|\Psi^\pm\rangle$  (depending on the superselection sector). This is intuitively accessible as follows: The  $\{J_j\}$  process fixes the relative phases and weights within each fixed particle number sector  $\mathcal{H}^{(L,N)}$ . Then it is sufficient so fix the relative phases and weights between these sectors at an arbitrary position by means of a single jump operator  $F_{j^*}$  to fix everything. Pictorially this is a ‘‘hole’’ in the system where fermion pairs can be injected and ejected. It is straightforward to show by induction over the quasiparticle sites that being a dark state of  $\{F_1, J_j\}_{1 \leq j \leq L-1}$  implies being a dark state of  $\{\tilde{a}_j\}_{1 \leq j \leq L-1}$ .

Since the operators  $\tilde{a}_j$  obey a fermionic algebra for  $1 \leq j \leq L$ , there is a unique quasiparticle vacuum  $|L, -\rangle \equiv |\text{Vac}\rangle = \prod_{j=1}^L \tilde{a}_j |0\rangle$  for  $L$  odd and  $|L, -\rangle \equiv |\text{Vac}\rangle = \prod_{j=1}^{L-1} \tilde{a}_j |0\rangle$  for  $L$  even<sup>75</sup> such that  $\tilde{a}_j |L, -\rangle = 0$  for all  $1 \leq j \leq L$ . Due to the uniqueness of the dark state (as derived above) it follows immediately (up to a global phase)

$$|L, +\rangle = \tilde{a}_L^\dagger |L, -\rangle = |\Psi^+\rangle \quad \text{and} \quad |L, -\rangle = |\Psi^-\rangle. \quad (5.22)$$

Note that  $\tilde{a}_L^\dagger = \frac{1}{2}(c_{2L} - ic_1)$  is a non-local fermionic mode located at the edges of the system.

Let us give a short summary: We know that all three processes  $\{J_j, F_j\}$ ,  $\{L_{j,0}, L_{j,1}\}$  and  $\{\tilde{a}_j\}$  have the same dark states and we derived these dark states rigorously. Thereby we found the above number state representation for the two degenerate Majorana chain ground states which belong to different parity superselection sectors  $\mathcal{H}_L^\pm$ .

<sup>75</sup>Note that the quasiparticle vacuum has in any case odd parity as derived previously. That, provided  $L$  is even,  $\tilde{a}_L |L, -\rangle = \tilde{a}_L \prod_{j=1}^{L-1} \tilde{a}_j |0\rangle = 0$  can be seen as follows:  $\prod_{j=1}^L \tilde{a}_j |0\rangle$  has even parity since  $L$  is even. Obviously  $\tilde{a}_i \prod_{j=1}^L \tilde{a}_j |0\rangle = 0$  for all  $1 \leq i \leq L$ . However, we proved already that  $|\text{Vac}\rangle$  has odd parity. By combining these facts with the uniqueness of the fermionic vacuum it follows immediately that  $\tilde{a}_L \prod_{j=1}^{L-1} \tilde{a}_j |0\rangle = 0$ .

### ■ Gauging the dark states

The alternating sign  $(-1)^i$  in Eq. (5.21a) is unfortunate — at least from an aesthetic point of view. Let us get rid of it. To this end note that the physical content of the theory remains unaltered by a *gauge transformation* defined via

$$a_j \rightarrow a'_j := e^{-i\chi(j)} a_j \quad \Leftrightarrow \quad a_j = e^{i\chi(j)} a'_j \quad (5.23)$$

where  $\chi : \mathbb{Z} \rightarrow \mathbb{R}$  is an arbitrary real-valued function. The local unitary transformation  $T_\chi$  describing such a gauge transformation is easily obtained via

$$\begin{aligned} |\mathbf{n}\rangle &= (a_1^\dagger)^{n_1} \dots (a_L^\dagger)^{n_L} |\mathbf{0}\rangle = (e^{-i\chi(1)} a_1'^\dagger)^{n_1} \dots (e^{-i\chi(L)} a_L'^\dagger)^{n_L} |\mathbf{0}\rangle \\ &= e^{-i\sum_{j=1}^L \chi(j) n_j} (a_1'^\dagger)^{n_1} \dots (a_L'^\dagger)^{n_L} |\mathbf{0}\rangle = e^{-i\sum_{j=1}^L \chi(j) \hat{n}_j} |\mathbf{n}'\rangle \end{aligned} \quad (5.24)$$

and we find

$$T_\chi = e^{i\sum_{j=1}^L \chi(j) \hat{n}_j} \quad \text{such that} \quad |\Psi'\rangle = T_\chi |\Psi\rangle \quad (5.25)$$

where  $\hat{n}_j = a_j^\dagger a_j = a_j'^\dagger a_j'$  denotes the one-site particle number operator (in contrast to its quantum numbers  $n_j$ ). It is then easy to show that

$$a'_n = T_\chi a_n T_\chi^\dagger = e^{i\chi(n)} a_n^\dagger a_n e^{-i\chi(n)} a_n^\dagger a_n = \left[ \mathbb{1} - i\chi(n) + \frac{(-i\chi(n))^2}{2!} + \dots \right] a_n = e^{-i\chi(n)} a_n$$

where we applied the Hadamard lemma. In context of our parity-conserving dissipative dynamics we obtain the transformed jump operators

$$J'_j = T_\chi J_j T_\chi^\dagger = a_j'^\dagger a'_j - a_{j+1}'^\dagger a'_{j+1} + a_{j+1}'^\dagger a'_j - a_j'^\dagger a'_{j+1} \quad (5.26a)$$

$$F'_j = T_\chi F_j T_\chi^\dagger = a_j'^\dagger a'_j + a_{j+1}'^\dagger a'_{j+1} - \mathbb{1} + a_j' a'_{j+1} + a_j'^\dagger a'_{j+1} \quad (5.26b)$$

and the transformed dark states

$$|\Psi^+\rangle' = \mathcal{N}_L^{-1/2} \sum_{i=0}^{\lfloor L/2 \rfloor} (-1)^i \binom{L}{2i}^{1/2} T_\chi |L, 2i\rangle \quad \text{and} \quad (5.27a)$$

$$|\Psi^-\rangle' = \mathcal{N}_L^{-1/2} \sum_{i=0}^{\lfloor L/2 \rfloor} (-1)^i \binom{L}{2i+1}^{1/2} T_\chi |L, 2i+1\rangle. \quad (5.27b)$$

Let us choose  $\chi(j) \equiv \frac{\pi}{2}$  constant. Constrained to a fixed particle sector  $\mathcal{H}^{(L,N)}$ , the gauge transformation reads  $T_\chi = e^{i\frac{\pi}{2} \sum_{j=1}^L \hat{n}_j} = e^{i\frac{\pi}{2} N} = i^N$ . Since  $|L, 2i\rangle \in \mathcal{H}^{(L,2i)}$  and  $|L, 2i+1\rangle \in \mathcal{H}^{(L,2i+1)}$  we find  $T_\chi |L, 2i\rangle = i^{2i} |L, 2i\rangle = (-1)^i |L, 2i\rangle$  and  $T_\chi |L, 2i+1\rangle = i(-1)^i |L, 2i+1\rangle$ . Therefore

$$|\Psi^+\rangle' = \mathcal{N}_L^{-1/2} \sum_{i=0}^{\lfloor L/2 \rfloor} \binom{L}{2i}^{1/2} |L, 2i\rangle \quad \text{and} \quad (5.28a)$$

$$|\Psi^-\rangle' = \mathcal{N}_L^{-1/2} \sum_{i=0}^{\lfloor L/2 \rfloor} \binom{L}{2i+1}^{1/2} |L, 2i+1\rangle \quad (5.28b)$$

(up to a global phase) which is the *equal-weight superposition* of all number states with fixed parity. We see: the alternating factor  $(-1)^i$  can be gauged away. ■

### 5.2.3 QTMC simulation

The original motivation for the parity conserving jump operators  $L_{j,c} = \frac{1}{2}E_{j+c}(1 - S_j)$  for left ( $c = 0$ ) and right jumps ( $c = 1$ ) of elementary errors was *quantum error correction*. As we outlined in 5.1.2, the basic idea is that of a *dissipative self-correcting quantum memory*: The dark state space  $\mathcal{D}$  of the dissipative process  $\{L_{j,c}\}$  corresponds to the two-fold degenerate ground state space of the Majorana chain which, in turn, is a quantum code.

Suppose that we start in a logical state  $|\Psi\rangle \in \mathcal{PS}$ . If errors occur, the logical state is corrupted and leaves the dark state space. Subsequently the jump operators push the errors randomly across the system and annihilate pairs of them whenever two errors meet. When the noise is switched off but the bath coupling remains finite, the system is cooled back into the dark state space, that is, the code space. The question is, whether the final dark state equals the initial state or if the dissipative process caused two excitations to traverse the system and annihilated them in the boundary mode — which corresponds to a logical phase error.

In short, is this dissipative process a self-correcting quantum memory? What is the fidelity as a function of the noise level and the system size? Let us first discuss heuristically what we should expect. To this end (and for the QTMC simulation that we apply to compute the fidelity numerically) it proves advantageous to recast the dissipative process on a spin chain by mean of a Jordan-Wigner transformation. We already found in 1.3.4 that the fundamental errors  $E_j$  and stabilisers  $S_j$  read  $E_j = \sigma_j^z$  and  $S_j = \sigma_j^x \sigma_{j+1}^x$  on the spin- $\frac{1}{2}$  chain. Therefore we find

$$L_{j,c} = \frac{1}{2}\sigma_{j+c}^z \left(1 - \sigma_j^x \sigma_{j+1}^x\right) \quad (5.29)$$

for the proposed jump operators. To simplify the QTMC implementation and to recast the theory in the more familiar  $\sigma^z$ -eigenbasis, we perform an additional  $\frac{\pi}{2}$ -rotation about the  $\sigma^y$ -axis, namely  $U = \prod_j \exp\left(-i\frac{\pi}{4}\sigma_j^y\right)$  which yields  $U\sigma^x U^\dagger = -\sigma^z$  and  $U\sigma^z U^\dagger = \sigma^x$ . In this basis, the jump operators read

$$L_{j,c} = \frac{1}{2}\sigma_{j+c}^x \left(1 - \sigma_j^z \sigma_{j+1}^z\right). \quad (5.30)$$

This is enlightening as it reveals immediately that the two-fold degeneracy of the Majorana code space corresponds to the two-fold degeneracy of the quantum Ising model: The dark states read  $|\bar{0}\rangle = |\uparrow \dots \uparrow\rangle$  and  $|\bar{1}\rangle = |\downarrow \dots \downarrow\rangle$  and our jump operators reach them by shifting the *domain walls* (which correspond to quasiparticles  $\tilde{a}_i^\dagger$ ) across the system. Elementary errors  $E_j = \sigma_j^x$  flip the spin at site  $j$  and create a pair of domain walls on the adjacent dual sites (which corresponds to a parity conserving pair creation process of quasiparticles). When an elementary error occurs, there are two possibilities for the dissipative process to get rid of the domain walls. First, the domain walls meet again in the bulk and “annihilate”. Thereby the total  $z$ -polarisation is preserved which corresponds to a successful error correction. Second, the domain walls meet the opposite ends of the chain and vanish there (one can imagine that they annihilate “outside” the chain). As a consequence, the total  $z$ -polarisation is *inverted* which corresponds to a *phase error* in the fermionic setting.

This is a nice result as it closes the circle with Chapter 2 where we contrived similar jump operators (that could be applied here, too) to drive into the ground state manifold of the transverse field Ising model for vanishing magnetic field.



We are now ready to establish an unpleasant conjecture. A local error correction would be successful (in most cases) if the jump operators annihilated the excitations according to the minimum weight decoding algorithm introduced in 1.3.4. However, there the actor who performs the error correction knows the *complete* error syndrome and derives the appropriate error correction operator in accordance with this information. But the jump operators are *quasilocal operators* that know only about the *local* error syndrome. And in *one* dimension this is a problem. It is impossible to decide *locally* in which direction (that is,  $c = 0$  or  $c = 1$ ) the domain wall must be shifted in order to annihilate it with its appropriate partner. This is not true for strings in two and branes in higher dimensions as the *local curvature* allows the contraction of such objects based solely on local decisions. That is, our proposed jump operators cannot “know” which is the correct action and therefore we expect our dissipative system to fail as a self-correcting quantum memory. This would even be true if we employed the jump operators that we proposed for the transverse field Ising model<sup>76</sup>.

The attentive reader may have noticed that there is a close connection to phase transitions in *classical* Ising models. The above argumentation can be adapted one-on-one to these systems for finite temperatures (which corresponds to errors): Since there is no method to decide how to contract domains in one-dimensional systems most efficiently, there is no phase transition in the one-dimensional Ising model. As stated above, this is not true in higher dimension where the Ising model exhibits thermal phase transitions after all.

Before we conclude this section with a negative result, let us have a look at two characteristic realisations of quantum trajectories. To this end, we simulate the local spin-flip errors  $E_j$  by jump operators  $L_j^E = \sqrt{\kappa}\sigma_j^x$  with the noise strength  $\kappa$ . We start with a random initial state  $|\Psi_0\rangle$  in the code space, that is

$$|\Psi_0\rangle = \cos\left(\frac{\phi}{2}\right) |\uparrow\rangle^{\otimes L} + \sin\left(\frac{\phi}{2}\right) e^{i\theta} |\downarrow\rangle^{\otimes L} \quad (5.31)$$

where we choose  $\theta = 2\pi u$  and  $\phi = \arccos(2v - 1)$  with uniformly distributed random variables  $u, v \in \mathcal{U}(0, 1)$ <sup>77</sup>. Then we activate both baths,  $\{L_{j,c}\}$  and  $\{L_j^E\}$ , for a time period  $\Delta t_1$  where errors occur and the jump operators try to get rid of them at the same time. Usually this is not successful at the end of  $\Delta t_1$ . Therefore we append a second period  $\Delta t_2$  without noise but with the error correction operators to annihilate all remaining excitations and to drive the system back into the code space. During the simulation, we record the type of jumps ( $L_{j,c}$  and  $L_j^E$ ) and their location  $j$ . We furthermore measure the code space projector

$$P(t) \equiv \langle \Psi(t) | \hat{P} | \Psi(t) \rangle \quad \text{with} \quad \hat{P} = |\uparrow \dots \uparrow\rangle \langle \uparrow \dots \uparrow| + |\downarrow \dots \downarrow\rangle \langle \downarrow \dots \downarrow| \quad (5.32)$$

as a function of time to indicate when the state leaves the code space. To test whether the final state in the code space coincides with the initial state, we measure the time evolution of the overlap (or *fidelity*), that is

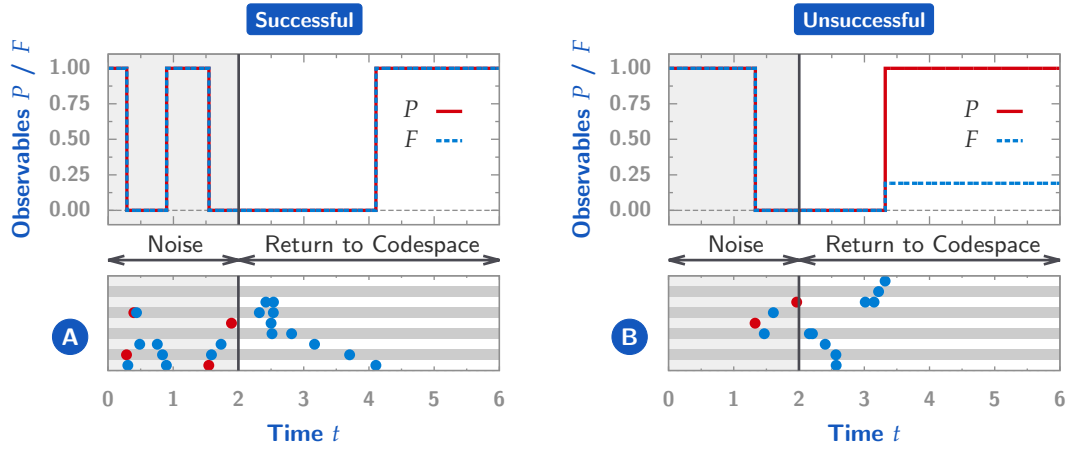
$$F(t) \equiv |\langle \Psi_0 | \Psi(t) \rangle| \quad (5.33)$$

These quantities are shown in Fig. 5.3 for two characteristic quantum jump trajectories. The lower part of each plot represents a space-time diagram of the chain<sup>78</sup> with errors and error

<sup>76</sup>Recall that they perform an *average* over the adjacent correlations; in two dimensions they read  $d_j = \sigma_j^x \left( \mathbb{1} - \frac{1}{2}\sigma_j^z \sigma_{j+1}^z - \frac{1}{2}\sigma_j^z \sigma_{j-1}^z \right)$ . Yet they cannot know about the correct direction.

<sup>77</sup>This is necessary to obtain a uniform distribution of Bloch vectors on the Bloch sphere.

<sup>78</sup>The chain lies parallel to the vertical axis and evolves in time along the horizontal axis



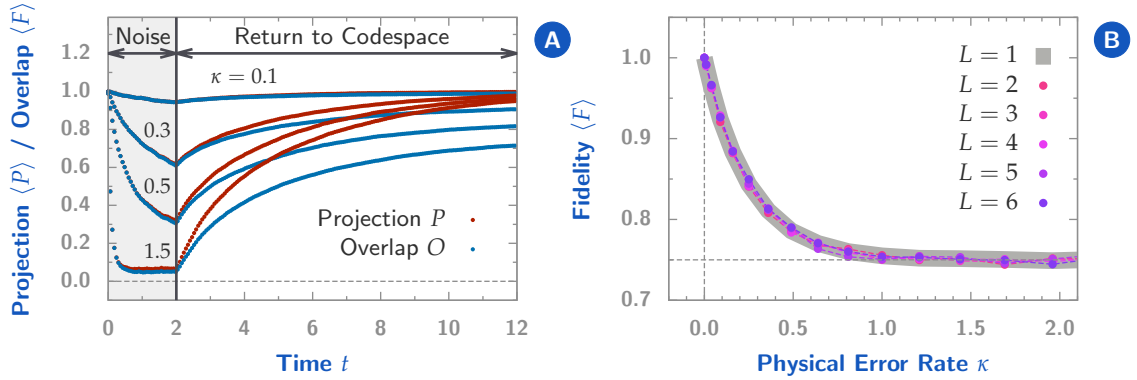
■ **Figure 5.3:** Single realizations of quantum jump trajectories for the dissipative Majorana Chain. In the upper part of each plot we show the time evolution of the expectation value  $P(t) = \langle \Psi(t) | \hat{P} | \Psi(t) \rangle$  of the code space projector  $\hat{P}$  (red solid) and the overlap  $F(t) = |\langle \Psi(0) | \Psi(t) \rangle|$  with the initial state (blue dashed). In the lower part a time-space diagram of the chain shows the jump history of the trajectory. The white/grey stripes denote world lines of the single spins of the chain. Red dots encode  $L_j^E$  jumps (i.e. errors), blue dots encode  $L_{i,c}$  jumps (i.e. error corrections). In (A) we show a history of a successful error correction: The domain walls caused by the errors in the noise regime do *not* traverse the whole chain as they never reach the upper end. In (B) an unsuccessful error correction is illustrated: The domain walls of both errors merge in the middle while their counterparts reach opposite ends of the chain. The polarization is flipped and a *logical error* is introduced. Note that in both cases the state ends up back in the code space ( $P = 1$  in the end) whereas the initial state is lost in (B) since  $O < 1$  after elimination of all domain walls.

correction operators labeled by red and blue dots, respectively. The grey region denotes the first time period  $\Delta t_1$  where errors occur, the subsequent white region corresponds to the cooling process.

In (A) we show a history with a successful error correction: There occur four errors during  $\Delta t_1$ ; two of them are immediately annihilated. The other two errors start a diffusion process across the system which can be followed by its “path” of error correction operators. A single excitation (its partner is attached the lower end of the chain) survives for a little while during the cooling period  $\Delta t_2$  but reaches the lower end at  $t \approx 4$ . Please note that during the existence of the excitations the state is orthogonal to the code space as  $P$  reveals. When the system is once again in a dark state, the projector jumps to 1 — along with the fidelity! We conclude that the qubit was restored successfully. Note that no excitation traversed the system during the evolution.

In (B) we show a history with an unsuccessful error correction: The two errors create four domain walls, two of which join between them. The remaining two domain walls are driven towards the *opposite* chain boundaries, as can be seen from the error correction paths. When the last excitation vanishes, the system returns to the code space. Unfortunately, the fidelity does not reach unity and the original logical qubit is corrupted. The reason is that during the evolution excitations traversed the whole system and thereby inflicted a phase error on the logical qubit. These results illustrate our previous discussions explicitly.

To conclude this section and to substantiate our previous arguments, we computed statistical averages  $\langle P \rangle$  and  $\langle F \rangle$  over  $N = 10000$  trajectories with random initial states for varying noise



■ **Figure 5.4:** QTMC simulations of the dissipatively implemented Majorana chain. In (A) we show the statistical averages  $\langle P \rangle$  and  $\langle F \rangle$  for the code space projector  $P$  and overlap (fidelity)  $F$  as functions of time. The results were obtained as averages over  $N = 10000$  trajectories with random initial states and with  $\Delta t_1 = 2$  and  $\Delta t_2 = 10$  as noise and cooling period, respectively. Depending on the noise rate  $\kappa$  both the code space projection and the overlap decrease when the  $\sigma^x$ -dephasing is switched on. Subsequently the system returns to the code space due to the cooling, i.e.  $\langle P(t) \rangle \rightarrow 1$  for  $t \rightarrow \infty$ . However, the fidelity reaches values  $\lim_{t \rightarrow \infty} \langle F(t) \rangle < 1$  that decrease for increasing noise  $\kappa$ . In (B) we show the averaged fidelity  $\langle F \rangle$  for trajectories that returned to the code space after the cooling interval  $\Delta t_2$ , i.e.  $P(\Delta t_1 + \Delta t_2) = 1$ , as function of the noise rate  $\kappa$  and for different system sizes. For comparison we computed the fidelity for a single qubit without error correction that was exposed to the same  $\sigma^x$ -dephasing for the same period of time  $\Delta t_1$ . Obviously the dissipative Majorana chain does not provide an enhanced coherence time compared to the single, uncorrected qubit. Further details are given in the text.

rates  $\kappa$  and system sizes  $L = 2, 3, 4, 5, 6$ . We set  $\Delta t_1 = 2$  and  $\Delta t_2 = 10$  with time steps  $\delta t = 0.001$ . The results are shown in Fig. 5.4.

In (A) we show the statistical averages of the expectation values  $\langle P \rangle$  and  $\langle F \rangle$  for different noise rates  $\kappa$  and a fixed system size  $L = 6$ . The stronger the  $x$ -dephasing the faster the system leaves the code space. For large rates  $\kappa \gtrsim 1$  there is a saturation behaviour observable. In the cooling regime, most systems return to the code space within  $\Delta t_2 \approx 10$  as the red curves indicate. In contrast, the asymptotic fidelity that is reached for  $t \rightarrow \infty$  depends crucially on the noise rate  $\kappa$  and does not reach unity for  $\kappa > 0$ . This is illustrated quantitatively in (B) where we computed statistical averages  $\langle F \rangle$  for the fidelity as functions of the error rate  $\kappa$  and for different system sizes. For the computation of  $\langle F \rangle$  we took into account all trajectories that reached the code space at the end of the cooling interval  $\Delta t_2$ , that is, all trajectories with  $P(\Delta t_1 + \Delta t_2) = 1$ . Depending on the rate  $\kappa$ , more than  $\sim 8000$  trajectories contributed to each average of  $\langle F \rangle$ . For comparison, we simulated also a *single spin* ( $L = 1$ ) with the same parameters (but obviously without the error correction bath). The results verify our conjecture: There seems to be *no effect at all* due to the storage of the qubit in the quantum code. The fidelities drop exponentially with  $\kappa$  and are independent of the system size.

Thus we argue that this straightforward dissipative implementation of the Majorana chain does not yield a convenient *self-correcting quantum memory*. It is, in fact, not even more resilient to noise than a single qubit without any error correction. This result is unfortunate but not unexpected for four reasons:

1. *Hamiltonian* self-correcting quantum memories are notoriously hard to find, at least in  $D \leq 3$  dimensions. For instance, the toric code is completely unstable in 2D [71, 72] and becomes only partially stable in 3D [73] (for finite temperatures). However it *is* stable at finite temperatures in four spatial dimensions [49] which, of course, is a useless fact if one seeks a realisation in our three-dimensional world.
2. It is known that the Hamiltonian theory of the Majorana chain does *not* provide a considerable improvement in coherence time [69] in noisy environments.
3. There was an earlier approach to contrive self-correcting quantum memories via dissipation based on spin systems in Ref. [55]. However, their results experience more or less the same restrictions as for Hamiltonian theories: They provide a *four-dimensional* self-correcting theory and a *two-dimensional* theory which provides protection against purely depolarising noise, that is, no full-fledged self-correcting quantum memory in less than four dimensions.
4. We realised that there seems to be a close relation to *classical* phase transitions if one considers only one type of error (which is tolerable for the Majorana chain thanks to parity superselection). But there are, to the best of my knowledge, no Hamiltonian systems *in one dimension* that feature a phase transition at finite temperature.

This concludes our treatment of the dissipative Majorana chain. In the remaining paragraphs of this chapter we give some additional remarks and present some ideas that came along with our treatment of dissipative systems.

## 5.3 Some asides: QCA and localisation of observables

We conclude this short chapter with two concepts that came to my mind during the work on Section 5.1 and 5.2. They are rather unrelated to the concept of quantum error correction but are more or less closely linked to quasilocal dissipative processes on physical lattice systems. There are neither answers nor specific questions related to these concepts; they might just be interesting to think about.

### 5.3.1 A physically motivated definition of quantum cellular automata

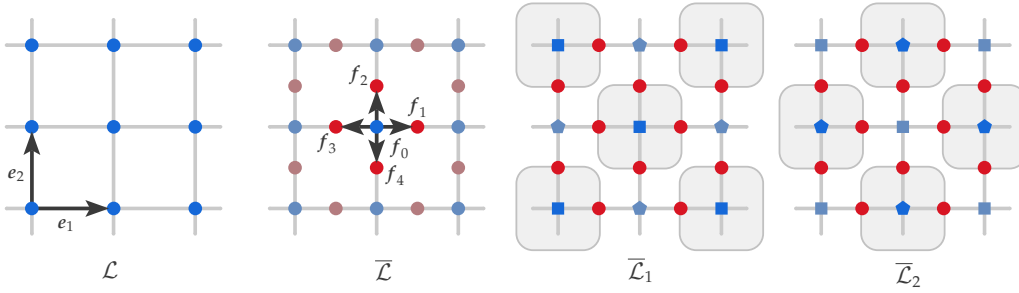
As a byproduct of Section 5.1, I first came into contact with classical cellular automata (CA) [139–148] and subsequently with quantum cellular automata (QCA) [149–155]. There are various different (equivalent and non-equivalent) concepts of QCAs [153, 154] and most of them are reversible.

Here we give a quite general definition of a quantum cellular automata (QCA), extending the definition of unitary (thus reversible) QCAs in [154] and of non-unitary QCAs in [150]. Our definition is operational and physically motivated and consequently based upon general quasilocal quantum operations (i.e. CPTP maps). To motivate the definitions below, let us sketch the physical requirements that should be met for any realisable many-body dynamics:

1. Operations may be unitary (reversible) and non-unitary (irreversible); where the latter occurs due to environmental couplings. A general quantum operation  $\mathcal{O}$  is described by a completely positive and trace preserving (CPTP) map acting as a superoperator on the convex set of density matrices  $\mathcal{D}(\mathcal{H}) \subseteq \mathcal{B}(\mathcal{H})$ .
2. Physically realisable operations are quasi-local, i.e. their support is bounded by a constant in the thermodynamic limit.
3. These operations should be translation invariant in *space* to allow for compact descriptions.
4. These operations should also be translation invariant in *time*. One may soften this requirement to describe processes whose physical rules change in time.

We aim at a *formalisation* of these requirements in terms of a quantum cellular automaton. Let me stress that the fascinating property of cellular automata in general is the emergence of complex behaviour from simple microscopic (and thus *local*) rules. But this very statement could also be made about *physical systems* that describe the emergence of collective phenomena (such as phase transitions) from simple constituents and local interactions. It is therefore natural to think of physical (lattice) systems as quantum cellular automata.

To this end we need some operational definitions to describe the objects we are interested in:



■ **Figure 5.5:** We show an example for a physical lattice system  $\mathfrak{P}$  as defined in Def. 5.1. The leftmost figure illustrates the *structure lattice*  $\mathcal{L}$  with basis vectors  $e_1$  and  $e_2$ . The blue vertices denote the structure lattice sites. The next figure from the left shows the *site lattice*  $\bar{\mathcal{L}}$  (marked by blue and red dots) as it can be constructed from  $\mathcal{L}$  and the shown vectors  $f_0 = 0$  and  $f_1, \dots, f_4 \neq 0$ . The *family*  $\mathcal{F}_x$  of the centred blue site is marked by arrows. Note that the (blue) structure lattice site becomes a site of the *site lattice* only if  $f_0 = 0$  is used for the construction of the latter. For example, this site lattice could be used for the  $\mathbb{Z}_2$ -Gauge-Higgs model in Chapter 3 in two dimensions. The remaining two plots on the right-hand side illustrate a possible *layer set*  $\mathcal{I}$  consisting of the two layers  $\bar{\mathcal{L}}_1$  and  $\bar{\mathcal{L}}_2$ . Note that the *families* of both layers are not necessarily disjoint.

► **Definition 5.1: Physical Lattice System (PLS)**

- (i) Let  $\mathcal{L}$  be a  $D$ -dimensional lattice in  $\mathbb{R}^D$  spanned by the basis  $\mathcal{B} = \{e_i\}_{1 \leq i \leq D}$ , i.e.  $\mathcal{L} = \left\{x = \sum_{i=1}^D x_i e_i \mid x_j \in \mathbb{Z}, 1 \leq j \leq D\right\}$ . We will call  $\mathcal{L}$  the *structure lattice* henceforth.
- (ii) Let  $\mathcal{F} = \{f_i\}_{1 \leq i \leq f}$  be an arbitrary set of vectors in  $\mathbb{R}^D$ . For any  $x \in \mathcal{L}$  we call  $\mathcal{F}_x \equiv x + \mathcal{F} \equiv \{x + f \mid f \in \mathcal{F}\}$  the *family* of  $x$ .
- (iii) The *site lattice*  $\bar{\mathcal{L}}$  is defined as union of all families, i.e.

$$\bar{\mathcal{L}} \equiv \mathcal{L} + \mathcal{F} = \bigcup_{x \in \mathcal{L}} \mathcal{F}_x. \quad (5.34)$$

Note that there may be common sites to different families,  $\mathcal{F}_x \cap \mathcal{F}_y \neq \emptyset$ .

- (iv) Now attach a finite dimensional Hilbert space  $\mathcal{H}_s \cong \mathbb{C}^d$  to each site  $s \in \bar{\mathcal{L}}$  and define the complete Hilbert space as

$$\mathcal{H}_{\bar{\mathcal{L}}} \equiv \bigotimes_{s \in \bar{\mathcal{L}}} \mathcal{H}_s. \quad (5.35)$$

Then we call the triple  $\mathfrak{P} = (\mathcal{H}_{\bar{\mathcal{L}}}, \mathcal{L}, \mathcal{F})$  the *physical lattice system (PLS)*  $\mathfrak{P}$ .

- (v)  $\mathfrak{P}$  is a *local* physical lattice system if  $\max\{|f| \mid f \in \mathcal{F}\}$  is of the same order as  $\max\{|e| \mid e \in \mathcal{B}\}$ . From now on all PLS will be considered local.
- (vi) A *layer set*  $\mathcal{I}$  is defined as a finite tuple of disjoint sublattices  $(\mathcal{L}_1, \dots, \mathcal{L}_I)$  such that

$$\mathcal{L} = \bigcup_{1 \leq i \leq I} \mathcal{L}_i \quad \text{and} \quad \forall_{1 \leq i \leq I} \forall_{x, y \in \mathcal{L}_i} : \mathcal{F}_x \cap \mathcal{F}_y = \emptyset. \quad (5.36)$$

$\bar{\mathcal{L}}_i \equiv \mathcal{L}_i + \mathcal{F}$  is then called the *ith layer*. Obviously  $\bar{\mathcal{L}} = \bigcup_{1 \leq i \leq I} \bar{\mathcal{L}}_i$ .

An example of a physical lattice system is depicted in Fig. 5.5.

We are now in the position to define our quantum cellular automaton which describes the time-discrete evolution of states in  $\mathcal{H}_{\mathcal{L}}$ :

► **Definition 5.2: Deterministic Quantum Cellular Automaton (D-QCA)**

(i) Let  $\mathfrak{P}$  be a PLS with family template  $\mathcal{F}$ . Given a quantum channel template  $\mathcal{R}$  operating on the density matrix space template  $\mathcal{D}(\mathcal{H}_{\mathcal{F}}) \equiv \mathcal{D}\left(\bigotimes_{f \in \mathcal{F}} \mathcal{H}_f\right)$  via its Kraus representation  $\mathcal{R}[\rho] = \sum_i K_i \rho K_i^\dagger$ , define for each structure lattice site  $x \in \mathcal{L}$  the generic embedding  $\mathcal{R}_x$  which operates as  $\mathcal{R}$  on  $\mathcal{D}\left(\bigotimes_{f \in \mathcal{F}_x} \mathcal{H}_f\right)$  where  $\rho \in \mathcal{D}(\mathcal{H}_{\mathcal{F}_x})$ .

(ii) Let  $\mathcal{I}$  be a layer set of  $\mathfrak{P}$ . Then we define the *transition channel*  $C_{\mathcal{R}}$  as

$$C_{\mathcal{R}} : \mathcal{D}(\mathcal{H}_{\mathcal{L}}) \longrightarrow \mathcal{D}(\mathcal{H}_{\mathcal{L}}), \quad \rho \mapsto C_{\mathcal{R}}[\rho] = \prod_{i=1, \dots, I} \bigotimes_{x \in \mathcal{L}_i} \mathcal{R}_x[\rho] \quad (5.37)$$

which describes the transition of the PLS  $\rho_t \mapsto \rho_{t+1} = C_{\mathcal{R}}[\rho_t]$  for each time step.

(iii) The triple  $(\mathfrak{P}, \mathcal{I}, \mathcal{R})$  is called *deterministic I-layer quantum cellular automaton*. We always assume that  $I$  is minimal, i.e. there is no layer set  $\mathcal{I}'$  with fewer layers than  $I$ .

Note that due to the definition of the layer set  $\mathcal{I}$ , the support of two quantum channels  $\mathcal{R}_x$  and  $\mathcal{R}_y$  for  $x, y \in \mathcal{L}_i$ ,  $x \neq y$ , is disjoint. Therefore they can be implemented simultaneously. It is natural to demand a minimal layer set  $\mathcal{I}$  to reduce the time for the implementation of  $C_{\mathcal{R}}$ .

As stated before, this definition of a QCA is physically motivated to provide a formally rigorous framework of *quasilocal* physical systems (see Appendix E for some notes on the term “quasilocal”). From an operational point of view, Def. 5.1 describes the stroboscopic evolution of a physical lattice with finite dimensional local quantum systems. The local operations are *not* restricted to unitary operations but to the most general *physical* quantum operations, namely CPTP maps. In particular this includes local projective measurements and non-unitary dissipative evolutions. Please note that this is closely related to the concept of *quantum simulation* [156]. For instance, in [157] a stroboscopic quantum simulator for both unitary and dissipative dynamics is described by means of Rydberg atoms. There synchronous time-discrete local operations on sublayers (as illustrated in Fig. 5.5) are employed to simulate the time evolution of general Lindblad master equations.

### 5.3.2 An new concept: Localisable observables

While deriving the dark states in Section 5.2 (which are equal-weight superpositions of states in fixed number or parity sectors) the following definition came about:

#### ► Definition 5.3: Localizable Observable

Consider a Hilbert space template  $\hat{\mathcal{H}} = \otimes_i \hat{\mathcal{H}}_i$  with subsystems  $\hat{\mathcal{H}}_i$  and structure graph template  $\hat{S}$  with diameter  $\hat{L} = \text{diam } \hat{S}$ . A (global) observable  $\hat{O}$  with  $|\text{supp } (\hat{O})| \in \Omega(\hat{L})$  is termed *dissipatively localisable* iff there is a (quasilocal) observable  $\hat{O}_{\text{loc}}$  with  $|\text{supp } (\hat{O}_{\text{loc}})| \in \mathcal{O}(1)$  and a quasilocal dissipative process  $\{\hat{L}_i\}$  such that

$$\langle O \rangle = \text{Tr} [O\rho] = \text{Tr} \left[ O_{\text{loc}} \lim_{t \rightarrow \infty} e^{\mathcal{L}t} \rho \right] \quad \text{with} \quad \mathcal{L} = \mathcal{L}(\{L_i\}) \quad (5.38)$$

for any state  $\rho \in \mathcal{D}(\mathcal{H})$  and for each instance  $N \in \mathbb{N}$  of the template.

For explanations concerning the concept of templates, see Appendix E. Here are two straightforward examples for localisable observables:

#### ■ Example 1: Parity

Consider a one-dimensional chain of  $L$  fermionic sites. A typical global observable of this setting is the fermion parity

$$P = \prod_{i=1}^L (-1)^{a_i^\dagger a_i} \quad (5.39)$$

where  $P$  is a global or non-local operator since obviously  $\text{supp}(P) = L$ . The parity is dissipatively localisable via the parity-conserving jump operators

$$L_i = \frac{1}{\sqrt{2}} (a_{i+1}^\dagger a_i + a_{i+1} a_i) \quad \text{for} \quad 1 \leq i \leq L-1.$$

To see this, note that the dark states are  $|D^+\rangle = |\square \dots \square\rangle$  and  $|D^-\rangle = |\square \dots \blacksquare\rangle$  according to the parity sector the system initially started from. Here is an example for  $L = 10$ :

$$\begin{aligned} |\Psi_0\rangle &= |\blacksquare \blacksquare \blacksquare \blacksquare \blacksquare \blacksquare \blacksquare \blacksquare \blacksquare \blacksquare\rangle & \xrightarrow{t \rightarrow \infty} & |D^-\rangle = |\square \square \square \square \square \square \square \square \square \square\rangle \\ |\Psi_0\rangle &= |\square \blacksquare \square \blacksquare \square \blacksquare \square \blacksquare \square \blacksquare\rangle & \xrightarrow{t \rightarrow \infty} & |D^+\rangle = |\square \square \square \square \square \square \square \square \square \square\rangle \\ |\Psi_0\rangle &= |\blacksquare \blacksquare \blacksquare \blacksquare \square \square \square \square \square \square\rangle & \xrightarrow{t \rightarrow \infty} & |D^-\rangle = |\square \square \square \square \square \square \square \square \square \blacksquare\rangle \\ |\Psi_0\rangle &= |\square \blacksquare \blacksquare \blacksquare \blacksquare \blacksquare \blacksquare \blacksquare \square \square\rangle & \xrightarrow{t \rightarrow \infty} & |D^+\rangle = |\square \square \square \square \square \square \square \square \square \square\rangle \end{aligned}$$

The formerly nonlocal property of parity can now be measured locally by means of  $n_L = a_L^\dagger a_L$  or  $p_L = (-1)^{a_L^\dagger a_L}$ . If we assume that any pure physical state is a parity eigenstate, it follows immediately

$$\text{Tr} [P\rho] = \text{Tr} \left[ p_L \lim_{t \rightarrow \infty} e^{\mathcal{L}t} \rho \right] \quad (5.40)$$

since there are exactly two dark states, one for each parity sector. ■



### ■ Example 2: Particle number

We stay with our one-dimensional chain of  $L$  fermionic sites. Another well known non-local observable is the total particle number

$$N = \sum_{i=1}^L n_i = \sum_{i=1}^L a_i^\dagger a_i \quad (5.41)$$

where obviously  $\text{supp}(N) = L$ . For general states there is no possibility to deduce  $\langle N \rangle$  by any local measurement. However, recall that the number-conserving jump operators

$$J_i = \frac{1}{2} (a_i^\dagger + a_{i+1}^\dagger) (a_i - a_{i+1}) \quad \text{for } 1 \leq i \leq L-1$$

drive any eigenstate of the number operator  $N$  to an equal weighted superposition of all number states with the same particle number, namely

$$|L, N\rangle = \mathcal{N}_{N,L}^{-1/2} \sum_{\mathbf{n} \in B_N} |\mathbf{n}\rangle .$$

It is now straightforward to show that the total particle number may be derived from the *local* particle density

$$n = \frac{N}{L} = \langle n_i \rangle = \langle a_i^\dagger a_i \rangle \quad \text{for any } 1 \leq i \leq L .$$

So we find that

$$\text{Tr}[N\rho] = \text{Tr} \left[ L n_i \lim_{t \rightarrow \infty} e^{\mathcal{L}t} \rho \right] \quad (5.42)$$

which yields a dissipative localisation of the particle number. ■

These are two simple examples with the purpose to illustrate the main idea of localisable observables. But it is conceivable that there might be more complex and more intriguing setups. The basic idea is simple: There are properties of scalable systems that are *nonlocal* in a classical perception as they require non-trivial actions or measurements on large parts of the systems, such as e.g. the parity or the total particle number. And we ask for quasilocal dissipative processes that “collect” such quantities and make them locally available. This concept can be extended to global properties of the system such as the *topology*. In that regard we may ask whether there are quasilocal dissipative processes that localise information about the global topology of the system, say the genus of the system’s spatial manifold.



# Conclusion

In this thesis we covered various topics with the focus on dissipative counterparts of well-known Hamiltonian theories that feature quantum phase transitions and topological phases. We also considered aspects of quantum information theory in terms of a dissipative version of the Majorana chain. Let us give a brief summary of the preceding chapters:

In Chapter 1 we introduced some of the *theoretical basics* that were required for the discussions of this thesis. Besides rather short outlines of the mathematical framework and the field of quantum phases, we provided detailed discussions and examples for the crucial topics, including *the quantum trajectory approach to Markovian dynamics* (Subsec. 1.1.3), the Hamiltonian *Majorana chain* (Subsec. 1.3.4) and *lattice gauge theories with Higgs fields* in Section 1.4.

In the most comprehensive Chapter 2 we investigated *spontaneous symmetry breaking by dissipation* by means of a paradigmatic example, namely the dissipative transverse field Ising model. We pursued *a mean field approach* in Section 2.3 and provided a thorough analysis of the *static solutions* in Subsec. 2.3.2. We concluded that the mean field theory of the dissipative TIM features a second order non-equilibrium phase transition. In Subsec. 2.3.3 we examined the *dynamic evolution* described by the mean field theory and found a critical slowing down near the phase transition. In Section 2.4 we proceeded with a *comparison of the dissipative and Hamiltonian mean field theories* and found a relation between dissipative and thermal phase transitions of the parent Hamiltonian in mean field approximation. In Section 2.5 we discussed the *exact solutions of a minimal instance* for the dissipative TIM for didactical reasons and as reference solutions for the subsequent Section 2.6 where we performed straightforward *quantum trajectory Monte Carlo simulations* of small one and two-dimensional systems. Thereby we found a characteristic metastability of magnetisation in systems with strong ferromagnetic driving.

In Chapter 3 we expanded the construction of dissipative theories that feature non-equilibrium phase transitions by means of Hamiltonian prototypes. To this end we introduced a *dissipative  $\mathbb{Z}_2$ -Gauge-Higgs model*. For comparison we derived first the *mean field theory for the unitary theory* in Section 3.1. Then we introduced our dissipative  $\mathbb{Z}_2$ -Gauge-Higgs model in Section 3.2, followed by a discussion of the *steady states* 3.2.2 for particular limits of the parameters. We argued that these dark states coincide with the pure ground states of the Hamiltonian prototype. We concluded the chapter with *a short mean field analysis* in Section 3.3 and discussed their *static solutions* in Subsec. 3.3.2. Our findings revealed considerable similarities to the Hamiltonian mean field theory and suggested non-trivial dissipatively driven phase transitions (there are also differences, though).

In the second part of this master thesis we were concerned with dissipative versions of the Majorana chain and their error correction capabilities. In Chapter 4 we discussed and recalculated some results regarding the *dissipative Majorana chain* proposed in Ref. [1]. We started with a rigorous treatment of the *steady states of the number conserving jump operators* in Section 4.2: In Subsec. 4.2.2 we derived the *dark states* rigorously and concluded that these are equal-weight superpositions of number states with fixed particle number. We also provided evidence for their uniqueness as *steady states* in a fixed number sector in Subsec. 4.2.3; there we proved rigorously the uniqueness for systems up to 15 sites. In Subsec. 4.3 we recalculated the *mean field theory for late times* on which the statements in [1] rely. Up to some technical subtleties we verified their results. In Section 4.4 we examined the *local indistinguishability* and the *entanglement spectrum* of both the fixed number dark states and the Majorana ground states and came to the conclusion that the former do not show signatures of a topological phase. Finally we made *some concluding remarks* in Section 4.5 where we argued that the proposed number conserving jump operators are not suitable for experimental setups if one aims at unpaired Majorana fermions on the system edges.

In the short last Chapter 5 we deepened aspects of the dissipative Majorana chain regarding *dissipatively driven topological quantum error correction*. We started with a few general remarks on *algorithmic error correction and locality* in Section 5.1. In the subsequent Section 5.2 we proposed alternative jump operators that drive the chain into the code space and provided a rigorous derivation of the Majorana chain ground states in terms of number states. We substantiated our conjectures regarding the applicability as a *dissipatively driven self-correcting quantum memory* by quantum trajectory Monte Carlo simulations in 5.2.3 and found evidence that the straightforward dissipative realisation of the Majorana chain does not yield a self-correcting quantum memory. Finally we presented some loosely related concepts in the last Section 5.3 concerning *quantum cellular automata and localisation of observables*.

In the Appendices we give some *auxiliary calculations* in D, remarks on the *implementation of the QTMC simulation* in C, a detailed derivation of the *mean field jump operators for the dissipative TIM* in B, and a formal treatment of *non-equilibrium steady states in mean field approximation* in A. Appendix E is somewhat different. There we introduce and discuss some topics on *locality in lattice systems* which are only loosely related to the main topics of this thesis.

# Non-equilibrium steady states in mean field approximation

For both models, the dissipative transverse field Ising model in Chapter 2 and the dissipative  $\mathbb{Z}_2$ -Gauge-Higgs model in Chapter 3, we are interested in the steady state solutions of a Lindblad equation. Thus it is natural to ask whether there is a *compact formulation* of the steady state equation which clearly reads

$$\sum_i L_i \rho L_i^\dagger = \frac{1}{2} \{H_P, \rho\} \quad \text{where} \quad H_P = \sum_i L_i^\dagger L_i. \quad (\text{A.1})$$

Here  $\{L_i\}$  denotes the exact jump operators which determine the dissipative part of the dynamics completely. We use mean field approximation in order to catch the structure of steady states in the thermodynamic limit roughly (at least in the high-dimensional limit).

## Mean field approximation

.....

The system's state is described by the  $N$ -spin Hilbert space  $\mathcal{H}_N = \otimes_{i=1}^N \mathbb{C}_i^2$ . We choose the ansatz  $\rho = \otimes_l \rho_l$  where  $\rho_l$  is the density matrix of a single spin degree of freedom. As a generic case, assume that there are  $1 \leq M \leq N$  independent mean fields. For  $M = 1$  we end up with a completely homogeneous system;  $M = N$  describes a system of  $N$  distinguished spins. Usually one will choose  $\mathcal{O}(1)$  mean fields to assign a distinct mean field to all distinguished fields in the exact theory<sup>79</sup>.

Given  $M$  mean fields, the density matrix reads  $\rho^{\text{mf}} = \otimes_{\alpha=1}^M \tilde{\rho}_\alpha$  where  $\tilde{\rho}_\alpha$  describes the (homogeneous)  $\alpha$ -th mean field. The effective jump operators are obtained by tracing out selectively all degrees of freedom but one, meaning

$$\partial_t \tilde{\rho}_\alpha = \partial_t \text{Tr}_{\neq m} [\rho] = \sum_i \text{Tr}_{\neq m} [L_i \rho L_i^\dagger] - \frac{1}{2} \text{Tr}_{\neq m} [\{H_P, \rho\}] \quad (\text{A.2})$$

<sup>79</sup>For instance, consider the  $\mathbb{Z}_2$ -Gauge-Higgs model. Here one naturally introduces two mean fields for the gauge and the Higgs field, respectively.

where  $1 \leq m \leq N$  is a physical spin which represents the field of type  $\alpha$ . The dynamics of the  $\{\tilde{\rho}_\alpha\}$  is described by effective Lindblad equations (one for each mean field)

$$\partial_t \tilde{\rho}_\alpha = \sum_i \sum_{\mu_i} \left[ l_{i,\mu_i}^\alpha \tilde{\rho}_\alpha l_{i,\mu_i}^{\alpha\dagger} - \frac{1}{2} \left\{ l_{i,\mu_i}^\alpha \tilde{\rho}_\alpha l_{i,\mu_i}^{\alpha\dagger} + l_{i,\mu_i}^{\alpha\dagger} \tilde{\rho}_\alpha l_{i,\mu_i}^\alpha \right\} \right] \quad (\text{A.3})$$

where one has to keep in mind that these equations are *non-linear* due to the mean fields included in the effective jump operators:

$$L_i \xrightarrow{\alpha} \left\{ l_{i,\mu_i}^\alpha \right\}_{\mu_i} = \left\{ l_{i,\mu_i}^\alpha \left( \left\{ m_\beta^k \right\} \right) \right\}_{\mu_i} \quad (\text{A.4})$$

Here  $m_\beta^k \equiv \langle \sigma_\beta^k \rangle = \text{Tr} \left[ \sigma_\beta^k \tilde{\rho}_\beta \right]$  denotes the  $k$ -th component of the  $\beta$ -th mean field. Furthermore notice that for each exact jump operator  $L_i$  there may be several effective jump operators  $l_{i,\mu_i}^\alpha$  with  $\mu_i = 1, 2, 3, \dots$  for each mean field  $\alpha$ .

For the sake of simplicity we employ a resummation and redefinition of the effective jump operators to get rid of duplicates (which usually occur due to structural symmetries of the lattice). So let us write

$$\partial_t \tilde{\rho}_\alpha = \sum_\mu \left[ l_\mu^\alpha \tilde{\rho}_\alpha l_\mu^{\alpha\dagger} - \frac{1}{2} \left\{ l_\mu^{\alpha\dagger} l_\mu^\alpha \tilde{\rho}_\alpha + \tilde{\rho}_\alpha l_\mu^\alpha l_\mu^{\alpha\dagger} \right\} \right] \quad (\text{A.5})$$

for the effective Markovian dynamics. The number of effective jump operators  $\{l_\mu^\alpha\}$  is bounded and does not depend on the system size  $N$  (otherwise a mean field approximation would hardly be legitimate). This is our starting point for the analysis of non-equilibrium steady states.

Parent Hamiltonian

The most generic form of a given mean field jump operator certainly is

$$l_\mu^\alpha = \sum_{\lambda=0}^3 l_{\mu,\lambda}^\alpha \sigma_\alpha^\lambda \equiv l_{\mu,\lambda}^\alpha \sigma_\alpha^\lambda \quad (\text{A.6})$$

where we introduced the complex-valued functions  $l_{\mu,\lambda}^\alpha = l_{\mu,\lambda}^\alpha \left( \left\{ m_\beta^k \right\} \right)$ . We use Einstein's convention for Latin indices but not for Greek indices. In the most generic case, jump operators are not traceless, i.e.  $l_{\mu,0}^\alpha \neq 0$  (recall that  $\sigma_\alpha^0 = \mathbb{1}_\alpha$ ). However, in the models we consider below these components vanish altogether and thus we assume  $l_{\mu,0}^\alpha = 0$  henceforth. To make this clear, we switch to Latin indices  $i, j, k, \dots$  which run over  $1, 2, 3$  (whereas Greek indices run over  $0, 1, 2, 3$  except for  $\mu$  which indicates the different jump operators).

So we are given a set of mean field jump operators of the form  $l_\mu^\alpha = l_{\mu,i}^\alpha \sigma_\alpha^i$ . Let us first express the parent Hamiltonian in the  $l_{\mu,\lambda}^\alpha$ -functions:

$$H_P^\alpha \equiv \sum_\mu l_\mu^{\alpha\dagger} l_\mu^\alpha = \sum_\mu \overline{l_{\mu,i}^\alpha} l_{\mu,j}^\alpha \sigma_\alpha^i \sigma_\alpha^j \quad (\text{A.7})$$

Let us introduce the three-index function

$$L_{i,j}^\alpha \equiv R_{i,j}^\alpha + iI_{i,j}^\alpha \equiv \sum_\mu \overline{I_{\mu,i}^\alpha} I_{\mu,j}^\alpha \quad \text{where} \quad R_{i,j}^\alpha = \text{Re} L_{i,j}^\alpha \quad \text{and} \quad I_{i,j}^\alpha = \text{Im} L_{i,j}^\alpha \quad (\text{A.8})$$

which is a Hermitian matrix in for every fixed  $\alpha$ ; consequently  $R_{i,j}^\alpha = R_{j,i}^\alpha$  and  $I_{i,j}^\alpha = -I_{j,i}^\alpha$ . Applying the well-known relation  $\sigma^i \sigma^j = i\epsilon^{ijk} \sigma^k + \delta^{ij} \mathbb{1}$  yields

$$H_P^\alpha = L_{i,j}^\alpha \sigma_\alpha^i \sigma_\alpha^j = L_{i,j}^\alpha \left( i\epsilon^{ijk} \sigma_\alpha^k + \delta^{ij} \mathbb{1}_\alpha \right) = i\epsilon^{ijk} L_{i,j}^\alpha \sigma_\alpha^k + L_{i,i}^\alpha \mathbb{1}_\alpha. \quad (\text{A.9})$$

The quantity  $h_\alpha^k \equiv i\epsilon^{ijk} L_{i,j}^\alpha$  is the  $k$ -th component of the Hamiltonian mean field  $\alpha$ ;  $L^\alpha \equiv L_{i,i}^\alpha$  is just the trace of the *system matrix*  $L_{i,j}^\alpha$ . So we end up with the mean field parent Hamiltonian

$$H_P^\alpha = h_\alpha^k \sigma_\alpha^k + L^\alpha \mathbb{1}_\alpha \quad \text{where} \quad h_\alpha^k \equiv i\epsilon^{ijk} L_{i,j}^\alpha. \quad (\text{A.10})$$

Note that  $\overline{h_\alpha^k} = -i\epsilon^{ijk} \overline{L_{i,j}^\alpha} = i\epsilon^{jik} L_{j,i}^\alpha = h_\alpha^k$  is a real field; the same holds for  $L^\alpha \equiv L_{i,i}^\alpha = R_{i,i}^\alpha$ .

Thermal states

The thermal equilibrium states of the (mean field) parent Hamiltonian are given by the Gibbs ensemble

$$\rho_{\text{th}}(\beta) = \mathcal{Z}^{-1} e^{-\beta \sum_\alpha H_P^\alpha} = \mathcal{Z}^{-1} \prod_\alpha e^{-\beta H_P^\alpha} \quad \text{where} \quad \mathcal{Z} = \text{Tr} \left[ e^{-\beta \sum_\alpha H_P^\alpha} \right]. \quad (\text{A.11})$$

Here the sum has to be understood as a **KRONECKER** sum. The thermal state solutions are now determined by the self-consistency relation

$$m_\beta^k = \text{Tr} \left[ \sigma_\beta^k \rho(\beta) \right] = \mathcal{Z}^{-1} \text{Tr} \left[ \sigma_\beta^k \prod_\alpha e^{-\beta H_P^\alpha} \right]. \quad (\text{A.12})$$

Since the mean field Hamiltonians  $H_P^\alpha$  act on distinct subsystems for each  $\alpha$ , the trace factorises and we get

$$m_\beta^k = \mathcal{Z}^{-1} \text{Tr} \left[ \sigma_\beta^k e^{-\beta H_P^\beta} \right] \quad (\text{A.13})$$

where we used  $\mathcal{Z} = \text{Tr} \left[ e^{-\beta \sum_\alpha H_P^\alpha} \right] = \prod_\alpha \text{Tr} \left[ e^{-\beta H_P^\alpha} \right] \equiv \prod_\alpha \mathcal{Z}_\alpha$ . If we insert the result of Eq. (A.10) for  $H_P^\beta$  the constant part of the Hamiltonian drops out, therefore

$$m_\beta^k = \tilde{\mathcal{Z}}_\beta^{-1} \text{Tr} \left[ \sigma_\beta^k e^{-\beta h_\beta^k \sigma_\beta^k} \right] \quad \text{with} \quad \tilde{\mathcal{Z}}_\beta = \text{Tr} \left[ e^{-\beta h_\beta^k \sigma_\beta^k} \right]. \quad (\text{A.14})$$

Let us introduce the norm of the mean field  $h_\alpha^2 \equiv \sum_{k=1}^3 h_\alpha^k{}^2$ . We remind the reader of the useful relation

$$e^{-\beta h_\beta^k \sigma_\beta^k} = \mathbb{1}_\beta \cosh(\beta h_\beta) - h_\beta^{-1} h_\beta^k \sigma_\beta^k \sinh(\beta h_\beta)$$

and thus  $\tilde{Z}_\beta = \text{Tr} \left[ e^{-\beta h_\beta^k \sigma_\beta^k} \right] = 2 \cosh(\beta h_\beta)$ . It follows

$$\rho_{\text{th}}(\beta) = \prod_{\alpha=1}^M \mathcal{Z}_\alpha^{-1} e^{-\beta h_\alpha^k \sigma_\alpha^k} = \frac{1}{2^M} \prod_{\alpha=1}^M \left( \mathbb{1}_\alpha - \tanh(\beta h_\alpha) h_\alpha^{-1} h_\alpha^k \sigma_\alpha^k \right) \quad (\text{A.15})$$

for the thermal density matrix. Now the self-consistency takes the simple form

$$m_\alpha^k = -h_\alpha^{-1} h_\alpha^k \tanh(\beta h_\alpha) \Leftrightarrow h_\alpha m_\alpha^k + h_\alpha^k \tanh(\beta h_\alpha) = 0 \quad (\text{A.16})$$

for all  $k = 1, 2, 3$  and  $\alpha = 1, 2, \dots, M$ . To conclude this paragraph, let us express the self-consistency equation in terms of mean field jump operators. We already know that  $h_\alpha^k = \iota \epsilon^{ijk} L_{i,j}^\alpha$ , so

$$h_\alpha m_\alpha^k + \iota \epsilon^{ijk} L_{i,j}^\alpha \tanh(\beta h_\alpha) = 0. \quad (\text{A.17})$$

The mean field yields

$$\begin{aligned} h_\alpha^2 &= \sum_k h_\alpha^{k2} = -\sum_k \epsilon^{ijk} \epsilon^{lmk} L_{i,j}^\alpha L_{l,m}^\alpha = \sum_k \epsilon^{ijk} \epsilon^{lmk} I_{i,j}^\alpha I_{l,m}^\alpha \\ &= I_{i,j}^\alpha I_{l,m}^\alpha \left( \delta^{il} \delta^{jm} - \delta^{im} \delta^{jl} \right) = I_{i,j}^\alpha I_{i,j}^\alpha - I_{i,j}^\alpha I_{j,i}^\alpha \\ &= 2I_{i,j}^\alpha I_{i,j}^\alpha. \end{aligned}$$

Conclusively, the mean field is given by  $h_\alpha = \sqrt{2I_{i,j}^\alpha I_{i,j}^\alpha}$ . So the self-consistency equations reads

$$m_\alpha^k \sqrt{2I_{i,j}^\alpha I_{i,j}^\alpha} = \epsilon^{ijk} I_{i,j}^\alpha \tanh\left(\beta \sqrt{2I_{i,j}^\alpha I_{i,j}^\alpha}\right) \quad \text{with } k = 1, 2, 3; \alpha = 1, 2, \dots, M \quad (\text{A.18})$$

where we realise that the thermal properties of the parent Hamiltonian are solely determined by the *imaginary part* of the mean field matrix.

### Steady states

Due to the product structure of  $\rho^{\text{mf}} = \otimes_{\alpha=1}^M \tilde{\rho}_\alpha$  we may parametrise each mean field density matrix as  $\tilde{\rho}_\alpha = \frac{1}{2} \left( \mathbb{1}_\alpha + a_\alpha^k \sigma_\alpha^k \right)$ . Clearly, self-consistency requires

$$m_\alpha^k = \text{Tr} \left[ \sigma_\alpha^k \tilde{\rho}_\alpha \right] = a_\alpha^k \quad (\text{A.19})$$

so we can just substitute  $a_\alpha^k$  by the expectation value  $m_\alpha^k$ :  $\tilde{\rho}_\alpha = \frac{1}{2} \left( \mathbb{1}_\alpha + m_\alpha^k \sigma_\alpha^k \right)$ . Then steady states  $\tilde{\rho}_\alpha^{\text{NESS}}$  are given by solutions  $\{\hat{m}_\alpha^k\}$  ( $k = 1, 2, 3$  and  $\alpha = 1, 2, \dots, M$ ) for the set of non-linear equations

$$\sum_\mu I_\mu^\alpha \tilde{\rho}_\alpha I_\mu^{\alpha\dagger} = \frac{1}{2} \left\{ \sum_\mu I_\mu^{\alpha\dagger} I_\mu^\alpha \tilde{\rho}_\alpha \right\} = \frac{1}{2} \{ H_P^\alpha, \tilde{\rho}_\alpha \}. \quad (\text{A.20})$$

Inserting the parametrisation and the result for  $H_P^\alpha$  yields

$$\sum_\mu I_\mu^\alpha I_\mu^{\alpha\dagger} + m_\alpha^k \sum_\mu I_\mu^\alpha \sigma_\alpha^k I_\mu^{\alpha\dagger} = h_\alpha^k \sigma_\alpha^k + \frac{1}{2} h_\alpha^k m_\alpha^l \{ \sigma_\alpha^k, \sigma_\alpha^l \} + L^\alpha \left( \mathbb{1}_\alpha + m_\alpha^k \sigma_\alpha^k \right). \quad (\text{A.21})$$



Recall that  $l_\mu^\alpha = l_{\mu,i}^\alpha \sigma_\alpha^i$  and  $\{\sigma_\alpha^k, \sigma_\alpha^l\} = 2\delta^{kl} \mathbb{1}_\alpha$ , so the equation above reads

$$\sum_\mu l_{\mu,i}^\alpha \overline{l_{\mu,j}^\alpha} \sigma_\alpha^i \sigma_\alpha^j + m_\alpha^k \sum_\mu l_{\mu,i}^\alpha \overline{l_{\mu,j}^\alpha} \sigma_\alpha^i \sigma_\alpha^k \sigma_\alpha^j = h_\alpha^k \sigma_\alpha^k + h_\alpha^k m_\alpha^l \delta^{kl} \mathbb{1}_\alpha + L^\alpha \mathbb{1}_\alpha + L^\alpha m_\alpha^k \sigma_\alpha^k. \quad (\text{A.22})$$

It is now easy to see that the condition  $0 \stackrel{!}{=} \partial_t \tilde{\rho}_\alpha = \mathcal{L}[\tilde{\rho}_\alpha]$  is equivalent to three independent conditions, namely  $0 \stackrel{!}{=} \partial_t m_\alpha^n = \text{Tr}[\sigma_\alpha^n \partial_t \tilde{\rho}_\alpha] = \text{Tr}[\sigma_\alpha^n \mathcal{L}[\tilde{\rho}_\alpha]]$ , which follows in a straightforward calculation from the parametrisation  $\tilde{\rho}_\alpha = \frac{1}{2} (\mathbb{1}_\alpha + m_\alpha^k \sigma_\alpha^k)$ . Therefore multiply Eq. (A.22) by  $\sigma_\alpha^n$  and take the trace:

$$\begin{aligned} \sum_\mu l_{\mu,i}^\alpha \overline{l_{\mu,j}^\alpha} \text{Tr}[\sigma_\alpha^n \sigma_\alpha^i \sigma_\alpha^j] + m_\alpha^k \sum_\mu l_{\mu,i}^\alpha \overline{l_{\mu,j}^\alpha} \text{Tr}[\sigma_\alpha^n \sigma_\alpha^i \sigma_\alpha^k \sigma_\alpha^j] = \\ h_\alpha^k \text{Tr}[\sigma_\alpha^n \sigma_\alpha^k] + h_\alpha^k m_\alpha^l \delta^{kl} \text{Tr}[\sigma_\alpha^n] + L^\alpha \text{Tr}[\sigma_\alpha^n] + L^\alpha m_\alpha^k \text{Tr}[\sigma_\alpha^n \sigma_\alpha^k]. \end{aligned}$$

We immediately realise that  $\text{Tr}[\sigma_\alpha^n] = 0$  and  $\text{Tr}[\sigma_\alpha^n \sigma_\alpha^k] = 2\delta^{nk}$  and furthermore  $\sum_\mu l_{\mu,i}^\alpha \overline{l_{\mu,j}^\alpha} = L_{j,i}^\alpha$  which simplifies the expression to

$$L_{j,i}^\alpha \text{Tr}[\sigma_\alpha^n \sigma_\alpha^i \sigma_\alpha^j] + m_\alpha^k L_{j,i}^\alpha \text{Tr}[\sigma_\alpha^n \sigma_\alpha^i \sigma_\alpha^k \sigma_\alpha^j] = 2h_\alpha^n + 2L^\alpha m_\alpha^n. \quad (\text{A.23})$$

In order to resolve the two remaining traces we use the well-known relations  $\epsilon^{ijk} \epsilon^{ilm} = \delta^{jl} \delta^{km} - \delta^{jm} \delta^{kl}$  and  $\sigma^i \sigma^j = i\epsilon^{ijk} \sigma^k + \delta^{ij} \mathbb{1}$  which yield

$$\begin{aligned} \text{Tr}[\sigma_\alpha^n \sigma_\alpha^i \sigma_\alpha^k \sigma_\alpha^j] &= i\epsilon^{nip} \text{Tr}[\sigma_\alpha^p \sigma_\alpha^k \sigma_\alpha^j] + 2\delta^{ni} \delta^{kj} \\ &= -\epsilon^{nip} \epsilon^{pkq} \text{Tr}[\sigma_\alpha^q \sigma_\alpha^j] + i\epsilon^{nip} \delta^{pk} \text{Tr}[\sigma_\alpha^j] + 2\delta^{ni} \delta^{kj} \\ &= -2\delta^{qj} (\delta^{nk} \delta^{iq} - \delta^{nq} \delta^{ik}) + 2\delta^{ni} \delta^{kj} \\ &= 2(\delta^{nj} \delta^{ik} - \delta^{nk} \delta^{ij} + \delta^{ni} \delta^{kj}) \end{aligned}$$

and analogously

$$\text{Tr}[\sigma_\alpha^n \sigma_\alpha^i \sigma_\alpha^j] = i\epsilon^{nik} \text{Tr}[\sigma_\alpha^k \sigma_\alpha^j] + \delta^{ni} \text{Tr}[\sigma_\alpha^j] = 2i\epsilon^{nik} \delta^{kj} = 2i\epsilon^{nij}.$$

Applied to Eq. (A.23) leads us to

$$2i\epsilon^{nij} L_{j,i}^\alpha + 2(\delta^{nj} \delta^{ik} - \delta^{nk} \delta^{ij} + \delta^{ni} \delta^{kj}) m_\alpha^k L_{j,i}^\alpha = 2h_\alpha^n + 2L^\alpha m_\alpha^n \quad (\text{A.24})$$

which finally yields

$$i\epsilon^{ijn} \overline{L_{i,j}^\alpha} + m_\alpha^k L_{n,k}^\alpha - m_\alpha^n L_{i,i}^\alpha + m_\alpha^k \overline{L_{n,k}^\alpha} = i\epsilon^{ijn} L_{i,j}^\alpha + L^\alpha m_\alpha^n. \quad (\text{A.25})$$

If we recall the properties of  $L_{i,j}^\alpha$  this can be simplified to

$$R^\alpha m_\alpha^n = \epsilon^{ijn} I_{i,j}^\alpha + m_\alpha^i R_{n,i}^\alpha \quad (\text{A.26})$$

where we used the fact that  $L^\alpha = L_{i,i}^\alpha = R_{i,i}^\alpha = R^\alpha$ . We conclude that the matrices  $L^\alpha = (L_{i,j}^\alpha)_{ij}$  determine the dynamics and the steady states of the mean field theory completely.

Some extensions

Here we present more general versions of the steady state equations and extend them to the *dynamical* mean field equations:

### ■ General jump operators

Let now the jump operators be of the most generic form, i.e.

$$l_\mu^\alpha = l_{\mu,\lambda}^\alpha \sigma_\alpha^\lambda = l_{\mu,0}^\alpha \mathbb{1}_\alpha + l_{\mu,1}^\alpha \sigma_\alpha^1 \equiv l_{\mu,0}^\alpha \mathbb{1}_\alpha + A_\mu. \quad (\text{A.27})$$

Then the Lindblad equation for mean field  $\alpha$  reads

$$\partial_t \tilde{\rho}_\alpha = \sum_\mu \left[ \left( l_{\mu,0}^\alpha \mathbb{1}_\alpha + A_\mu \right) \tilde{\rho}_\alpha \left( \overline{l_{\mu,0}^\alpha} \mathbb{1}_\alpha + A_\mu^\dagger \right) - \frac{1}{2} \left\{ \left( \overline{l_{\mu,0}^\alpha} \mathbb{1}_\alpha + A_\mu^\dagger \right) \left( l_{\mu,0}^\alpha \mathbb{1}_\alpha + A_\mu \right), \tilde{\rho}_\alpha \right\} \right]. \quad (\text{A.28})$$

A straightforward calculation yields

$$\partial_t \tilde{\rho}_\alpha = -i \left[ \frac{i}{2} \sum_\mu \left( \overline{l_{\mu,0}^\alpha} A_\mu - l_{\mu,0}^\alpha A_\mu^\dagger \right), \tilde{\rho}_\alpha \right] + \sum_\mu \left( A_\mu \tilde{\rho}_\alpha A_\mu^\dagger - \frac{1}{2} \left\{ A_\mu^\dagger A_\mu, \tilde{\rho}_\alpha \right\} \right). \quad (\text{A.29})$$

We see that the identity component in the jump operators gives rise to an effective *unitary dynamics* governed by the Hamiltonian

$$H_{\text{eff}}^\alpha = \frac{i}{2} \sum_\mu \left( \overline{l_{\mu,0}^\alpha} A_\mu - l_{\mu,0}^\alpha A_\mu^\dagger \right) \quad (\text{A.30})$$

which is obviously Hermitian.

### ■ Unitary dynamics

What happens if an additional unitary dynamics described by a mean field Hamiltonian  $H^{\text{mf}} = \sum_\alpha h_\alpha^{\text{mf},i} \sigma_\alpha^i$  is present? Then the full Lindblad master equation reads

$$\partial_t \tilde{\rho}_\alpha = -i \left[ h_\alpha^{\text{mf},i} \sigma_\alpha^i, \tilde{\rho}_\alpha \right] + \sum_\mu \left[ l_\mu^\alpha \tilde{\rho}_\alpha l_\mu^{\alpha\dagger} - \frac{1}{2} \left\{ l_\mu^{\alpha\dagger} l_\mu^\alpha, \tilde{\rho}_\alpha \right\} \right] \quad (\text{A.31})$$

and we find the additional contribution

$$-i \left[ h_\alpha^{\text{mf},i} \sigma_\alpha^i, \tilde{\rho}_\alpha \right] = -\frac{i}{2} h_\alpha^{\text{mf},i} m_\alpha^j \left[ \sigma_\alpha^i, \sigma_\alpha^j \right] = \epsilon^{ijk} h_\alpha^{\text{mf},i} m_\alpha^j \sigma_\alpha^k.$$

Multiplication by  $\sigma_\alpha^n$  and taking the trace yields

$$\text{Tr} \left[ \epsilon^{ijk} h_\alpha^{\text{mf},i} m_\alpha^j \sigma_\alpha^n \sigma_\alpha^k \right] = 2\delta^{nk} \epsilon^{ijk} h_\alpha^{\text{mf},i} m_\alpha^j = 2 \left( \mathbf{h}_\alpha^{\text{mf}} \times \mathbf{m}_\alpha \right)_n$$

which describes a rotation of  $m_\alpha$  about  $h_\alpha^{\text{mf}}$  given the latter does not depend on  $m_\alpha^i$ . We have to add this new term to the left-hand side<sup>80</sup> of Eq. (A.24) which yields

$$2\epsilon^{ijn} h_\alpha^{\text{mf},i} m_\alpha^j + \iota \epsilon^{nij} L_{j,i}^\alpha + \left( \delta^{nj} \delta^{ik} - \delta^{nk} \delta^{ij} + \delta^{ni} \delta^{kj} \right) m_\alpha^k L_{j,i}^\alpha = h_\alpha^n + L^\alpha m_\alpha^n \quad (\text{A.32})$$

and consequently

$$2\epsilon^{ijn} h_\alpha^{\text{mf},i} m_\alpha^j + \iota \epsilon^{ijn} \overline{L_{i,j}^\alpha} + m_\alpha^k L_{n,k}^\alpha - m_\alpha^n L_{i,i}^\alpha + m_\alpha^k \overline{L_{n,k}^\alpha} = \iota \epsilon^{ijn} L_{i,j}^\alpha + L^\alpha m_\alpha^n. \quad (\text{A.33})$$

With the same simplifications as above we find

$$R^\alpha m_\alpha^n = \epsilon^{ijn} I_{i,j}^\alpha + m_\alpha^i R_{n,i}^\alpha + \epsilon^{ijn} h_\alpha^{\text{mf},i} m_\alpha^j = \epsilon^{ijn} \left[ I_{i,j}^\alpha + h_\alpha^{\text{mf},i} m_\alpha^j \right] + m_\alpha^i R_{n,i}^\alpha \quad (\text{A.34})$$

which describes the stationary states with both, dissipative *and* unitary dynamics.

### ■ The dynamical equations

In the paragraphs above we were only concerned with the *stationary states* of the Lindblad equation. If we are interested in the *dynamics* of the mean field theory, we have to keep the left-hand side of the Lindblad equation arbitrary (meaning: we cannot set it to zero as above). Then Eq. (A.32) reads

$$2\epsilon^{ijn} h_\alpha^{\text{mf},i} m_\alpha^j + \iota \epsilon^{nij} L_{j,i}^\alpha + \left( \delta^{nj} \delta^{ik} - \delta^{nk} \delta^{ij} + \delta^{ni} \delta^{kj} \right) m_\alpha^k L_{j,i}^\alpha - h_\alpha^n - L^\alpha m_\alpha^n = \partial_t m_\alpha^n \quad (\text{A.35})$$

and therefore

$$2\epsilon^{ijn} h_\alpha^{\text{mf},i} m_\alpha^j + \iota \epsilon^{ijn} \overline{L_{i,j}^\alpha} + m_\alpha^k L_{n,k}^\alpha - m_\alpha^n L_{i,i}^\alpha + m_\alpha^k \overline{L_{n,k}^\alpha} - \iota \epsilon^{ijn} L_{i,j}^\alpha - L^\alpha m_\alpha^n = \partial_t m_\alpha^n. \quad (\text{A.36})$$

Further simplifications yield finally

$$\partial_t m_\alpha^n = 2\epsilon^{ijn} \left[ I_{i,j}^\alpha + h_\alpha^{\text{mf},i} m_\alpha^j \right] + 2 \left( R_{n,i}^\alpha - R^\alpha \delta_{ni} \right) m_\alpha^i \quad (\text{A.37})$$

which describes the dynamics of the complete mean field Lindblad equation. If we consider all  $m_\alpha^n$  ( $\alpha = 1, \dots, M$  and  $n = 1, 2, 3$ ) as independent real coordinates in  $\mathbb{R}^{3M}$ , it is convenient to define the vector field

$$\left[ F \left( \{m_\beta^i\} \right) \right]_{(\alpha,n)} := 2\epsilon^{ijn} \left[ I_{i,j}^\alpha + h_\alpha^{\text{mf},i} m_\alpha^j \right] + 2 \left( R_{n,i}^\alpha - R^\alpha \delta_{ni} \right) m_\alpha^i \quad (\text{A.38})$$

which is the flux that determines the time evolution of the mean field theory via the dynamical system

$$\partial_t \mathbf{M} = \mathbf{F}. \quad (\text{A.39})$$

Here we introduced the vector  $\mathbf{M} \equiv \left( m_\alpha^i \right)_{(\alpha,i)}$  which comprises all mean fields. ■

<sup>80</sup>Note that we have to insert an additional factor of  $\frac{1}{2}$  that was cancelled in Eq. (A.21) but has to be kept for the present calculations.



## Dissipative TIM: Mean field jump operators

In Chapter 2 we introduced the dissipative transverse field Ising model. To examine its phase structure we employed a detailed mean field analysis in Section 2.3. To keep the line of thought as clear as possible, we present in paragraph 2.3.1 only a compactified version of the calculations that were necessary to derive the effective mean field jump operators. Here we expand this derivation and provide detailed calculations for the sake of completeness.

A short summary

.....

To provide a self-contained discussion, let us first summarise the most important points: The unitary dynamics of the transverse field Ising model is described by the Hamiltonian

$$H_{\text{TIM}} = -J \sum_{\langle n,m \rangle} \sigma_n^z \sigma_m^z - h \sum_n \sigma_n^x \quad (\text{B.1})$$

where  $J$  and  $h$  denote the nearest neighbour coupling strength and the (transverse) magnetic field, respectively. Recall that we use the convention

$$\sum_{\langle n,m \rangle} \equiv \frac{1}{2} \sum_{n=1}^N \sum_{m \in N_n} . \quad (\text{B.2})$$

for sums over nearest-neighbour pairs  $\langle n,m \rangle$ . In the following, we consider two independent dissipative processes described by the jump operators

$$c_j = \frac{1}{2} (\sigma_j^z - i\sigma_j^y) \quad (\text{B.3a})$$

$$d_j = \sigma_j^x \left[ \frac{1}{q} \sum_{m \in N_j} \sigma_m^z \sigma_j^z - 1 \right] = -\frac{i}{q} \sum_{m \in N_j} \sigma_m^z \sigma_j^y - \sigma_j^x . \quad (\text{B.3b})$$

The dynamics (unitary and dissipative) is described by a master equation in Lindblad form

$$\partial_t \rho = -i [H_{\text{TIM}}, \rho] + \kappa_P \sum_j \left[ c_j \rho c_j^\dagger - \frac{1}{2} \{c_j^\dagger c_j, \rho\} \right] + \kappa_F \sum_j \left[ d_j \rho d_j^\dagger - \frac{1}{2} \{d_j^\dagger d_j, \rho\} \right] \quad (\text{B.4a})$$

$$\equiv -i [H_{\text{TIM}}, \rho] + \mathcal{L}[\rho] \quad (\text{B.4b})$$

where  $\kappa_P, \kappa_F \geq 0$  describe the strength of the coupling to the external baths and  $\mathcal{L}[\bullet]$  denotes the Lindblad superoperator.

Each spin  $i$  is described by its two-dimensional Hilbert space  $\mathcal{H}_i = \mathbb{C}_i^2$ , therefore the systems Hilbert space is  $\mathcal{H} = \otimes_j \mathcal{H}_j$ . In the following we write  $\overline{\mathcal{H}}_i = \otimes_{j,j \neq i} \mathcal{H}_j$  and  $\text{Tr}_i [X] \equiv \text{Tr}_{\overline{\mathcal{H}}_i} [X]$  for tracing out the whole system except the  $i$ th spin.

Derivation of the mean field equation

In self-consistent field theory (or mean field theory, MFT) the nearest neighbour couplings are replaced by the interaction with an effective mean field arising from the spin environment. To this end, the product ansatz

$$\rho = \prod_{l=1}^N \rho_l \quad (\text{B.5})$$

is inserted into the master equation, where  $\rho_l$  operates on  $\mathcal{H}_l$ . We note that now  $\text{Tr}_i [\rho] = \rho_i$ . Due to the product ansatz above, the master equation decouples into  $N$  independent differential equations for  $\{\rho_i\}_{1 \leq i \leq N}$ . That is

$$\underbrace{\text{Tr}_i [\partial_t \rho]}_{\text{Derivative}} = \underbrace{-i \text{Tr}_i [[H, \rho]]}_{\text{Unitary term}} + \underbrace{\kappa_P \sum_j \text{Tr}_i \left[ c_j \rho c_j^\dagger - \frac{1}{2} \{c_j^\dagger c_j, \rho\} \right]}_{\text{Paramagnetic term}} + \underbrace{\kappa_F \sum_j \text{Tr}_i \left[ d_j \rho d_j^\dagger - \frac{1}{2} \{d_j^\dagger d_j, \rho\} \right]}_{\text{Ferromagnetic term}}$$

is expected to be of the form

$$\partial_t \rho_i = -i [H_i^{\text{mf}}, \rho_i] + \mathcal{L}_i^{\text{mf}}[\rho_i] \quad (\text{B.6})$$

where  $H_i^{\text{mf}}$  and  $\mathcal{L}_i^{\text{mf}}$  denote the local mean field versions of the Hamiltonian and the Lindbladian, respectively. In the next paragraphs the exact form of  $H_i^{\text{mf}}$  and  $\mathcal{L}_i^{\text{mf}}$  is derived.

### ■ Derivative

It is trivial to see that

$$\text{Tr}_i [\partial_t \rho] = \partial_t \text{Tr}_i \left[ \prod_{l=1}^N \rho_l \right] = \partial_t \rho_i \quad (\text{B.7})$$

holds for the left-hand side of the master equation.

■ Unitary term

The mean field solution for the transverse field Ising model is given by

$$-i \text{Tr}_i [[H, \rho]] = -i \text{Tr}_i \left[ \left[ -J \sum_{\langle n,m \rangle} \sigma_n^z \sigma_m^z - h \sum_n \sigma_n^x, \rho \right] \right] \quad (\text{B.8a})$$

$$= iJ \sum_{\langle n,m \rangle} \text{Tr}_i [[\sigma_n^z \sigma_m^z, \rho]] + ih \sum_n \text{Tr}_i [[\sigma_n^x, \rho]] \quad (\text{B.8b})$$

$$= iJ \underbrace{\sum_{\substack{\langle n,m \rangle \\ n \neq i \wedge m \neq i}} \text{Tr}_i [[\sigma_n^z \sigma_m^z, \rho]]}_{=0} + ih \underbrace{\sum_{n, n \neq i} \text{Tr}_i [[\sigma_n^x, \rho]]}_{=0} \quad (\text{B.8c})$$

$$+ iJ \sum_{\substack{\langle n,m \rangle \\ n=i \vee m=i}} \text{Tr}_i [[\sigma_n^z \sigma_m^z, \rho]] + ih \text{Tr}_i [[\sigma_i^x, \rho]] \quad (\text{B.8d})$$

$$= iJ \sum_{\substack{\langle n,m \rangle \\ n=i \vee m=i}} \text{Tr}_i [[\sigma_n^z \sigma_m^z, \rho]] + ih \text{Tr}_i [[\sigma_i^x, \rho]] \quad (\text{B.8e})$$

$$= iJ \sum_{\substack{\langle n,m \rangle \\ n=i \vee m=i}} m_z [\sigma_i^z, \rho_i] + ih [\sigma_i^x, \rho] \quad (\text{B.8f})$$

$$= iJ q m_z [\sigma_i^z, \rho_i] + ih [\sigma_i^x, \rho] = -i [-J q m_z \sigma_i^z - h \sigma_i^x, \rho_i] \quad (\text{B.8g})$$

Here we used that  $\text{Tr}_i [[X, \rho]] = \text{Tr}_i [X\rho] - \text{Tr}_i [\rho X] = \rho_i (\langle X \rangle - \langle X \rangle) = 0$  if  $X$  acts nontrivially on  $\overline{\mathcal{H}}_i$  only and assumed a homogeneous system; that is,  $m_z \equiv \langle \sigma_n^z \rangle = \text{Tr}_i [\sigma_n^z \rho_n]$  is independent of  $n (\neq i)$ . Therefore the mean field Hamiltonian reads

$$H_i^{\text{mf}} = -J q m_z \sigma_i^z - h \sigma_i^x = -\mathbf{h}_{\text{mf}} \sigma_i \quad (\text{B.9})$$

where  $\sigma_i = [\sigma_i^x, \sigma_i^y, \sigma_i^z]^T$  and  $\mathbf{h}_{\text{mf}} = -(h, 0, J q m_z)^T$  denotes the *mean field*. This is a well-known result for the transverse field Ising model.

■ Paramagnetic term

Since

$$c_j = \frac{1}{2} (\sigma_j^z - i \sigma_j^y) \quad (\text{B.10})$$

acts non-trivially on  $\mathcal{H}_i$  only, we find immediately

$$\text{Tr}_i [c_i \rho c_i^\dagger] = c_i \rho_i c_i^\dagger \quad (\text{B.11a})$$

$$\text{Tr}_i [c_i^\dagger c_i \rho] = c_i^\dagger c_i \rho_i \quad (\text{B.11b})$$

$$\text{Tr}_i [\rho c_i^\dagger c_i] = \rho_i c_i^\dagger c_i \quad (\text{B.11c})$$

and for  $j \neq i$

$$\text{Tr}_i [c_j \rho c_j^\dagger] = \text{Tr}_i [c_j^\dagger c_j \rho] = \text{Tr}_i [\rho c_j^\dagger c_j] = \rho_i \langle c_j^\dagger c_j \rangle. \quad (\text{B.12})$$

Therefore we obtain for the paramagnetic term

$$\kappa_P \sum_j \text{Tr}_i \left[ c_j \rho c_j^\dagger - \frac{1}{2} \{c_j^\dagger c_j, \rho\} \right] = \kappa_P \sum_j \left\{ \text{Tr}_i [c_j \rho c_j^\dagger] - \frac{1}{2} \text{Tr}_i [\{c_j^\dagger c_j, \rho\}] \right\} \quad (\text{B.13a})$$

$$= \kappa_P \underbrace{\sum_{j,j \neq i} \left\{ \text{Tr}_i [c_j \rho c_j^\dagger] - \frac{1}{2} \text{Tr}_i [\{c_j^\dagger c_j, \rho\}] \right\}}_{=0} \quad (\text{B.13b})$$

$$+ \kappa_P \left\{ \text{Tr}_i [c_i \rho c_i^\dagger] - \frac{1}{2} \text{Tr}_i [\{c_i^\dagger c_i, \rho\}] \right\} \quad (\text{B.13c})$$

$$= \kappa_P \left( c_i \rho_i c_i^\dagger - \frac{1}{2} \{c_i^\dagger c_i, \rho_i\} \right). \quad (\text{B.13d})$$

Or for short

$$\kappa_P \sum_j \text{Tr}_i \left[ c_j \rho c_j^\dagger - \frac{1}{2} \{c_j^\dagger c_j, \rho\} \right] = \kappa_P \mathcal{L}(c_i) [\rho_i] \quad (\text{B.14})$$

which was expected since the paramagnetic jump operators  $c_j$  act locally and are independent of their neighbours  $N_j$ .

#### ■ Ferromagnetic term

The ferromagnetic term is the most complicated one since the jump operators  $d_j$  act on spin  $j$  and its neighbours  $N_j$ . First we note that for  $j \notin N_i \cup \{i\}$

$$\text{Tr}_i [d_j \rho d_j^\dagger] = \text{Tr}_i [d_j^\dagger d_j \rho] = \text{Tr}_i [\rho d_j^\dagger d_j] = \rho_i \langle d_j^\dagger d_j \rangle. \quad (\text{B.15})$$

and thus

$$\kappa_F \sum_{j,j \notin N_i \cup \{i\}} \text{Tr}_i \left[ d_j \rho d_j^\dagger - \frac{1}{2} \{d_j^\dagger d_j, \rho\} \right] = \kappa_F \sum_{j,j \notin N_i \cup \{i\}} \left\{ \text{Tr}_i [d_j \rho d_j^\dagger] - \frac{1}{2} \text{Tr}_i [\{d_j^\dagger d_j, \rho\}] \right\} = 0$$

vanishes. Therefore the sum reduces to

$$\kappa_F \sum_j \text{Tr}_i \left[ d_j \rho d_j^\dagger - \frac{1}{2} \{d_j^\dagger d_j, \rho\} \right] = \underbrace{\kappa_F \sum_{j,j \in N_i} \left\{ \text{Tr}_i [d_j \rho d_j^\dagger] - \frac{1}{2} \text{Tr}_i [\{d_j^\dagger d_j, \rho\}] \right\}}_{\text{Nearest neighbours (NN)}} \quad (\text{B.16a})$$

$$+ \kappa_F \underbrace{\left( \text{Tr}_i [d_i \rho d_i^\dagger] - \frac{1}{2} \text{Tr}_i [\{d_i^\dagger d_i, \rho\}] \right)}_{\text{Spin } i \text{ (Si)}} \quad (\text{B.16b})$$

which comprises  $2d + 1$  summands for a  $d$ -dimensional lattice.



The terms expand to

$$d_j \rho d_j^\dagger = \left[ -\frac{i}{q} \sum_{m \in N_j} \sigma_m^z \sigma_j^y - \sigma_j^x \right] \rho \left[ \frac{i}{q} \sum_{n \in N_j} \sigma_n^z \sigma_j^y - \sigma_j^x \right] \quad (\text{B.17a})$$

$$= \frac{1}{q^2} \sum_{m, n \in N_j} \sigma_m^z \sigma_j^y \rho \sigma_n^z \sigma_j^y + \frac{i}{q} \sum_{m \in N_j} \sigma_m^z \sigma_j^y \rho \sigma_j^x - \frac{i}{q} \sum_{n \in N_j} \sigma_j^x \rho \sigma_n^z \sigma_j^y + \sigma_j^x \rho \sigma_j^x \quad (\text{B.17b})$$

and

$$d_j^\dagger d_j = \left[ \frac{i}{q} \sum_{m \in N_j} \sigma_m^z \sigma_j^y - \sigma_j^x \right] \left[ -\frac{i}{q} \sum_{n \in N_j} \sigma_n^z \sigma_j^y - \sigma_j^x \right] \quad (\text{B.18a})$$

$$= \frac{1}{q^2} \sum_{m, n \in N_j} \sigma_m^z \sigma_j^y \sigma_n^z \sigma_j^y - \frac{i}{q} \sum_{m \in N_j} \sigma_m^z \sigma_j^y \sigma_j^x + \frac{i}{q} \sum_{n \in N_j} \sigma_j^x \sigma_n^z \sigma_j^y + \mathbb{1}. \quad (\text{B.18b})$$

In the following we calculate the partial traces for the nearest neighbours (NN) and the spin itself (Si).

► Nearest neighbours (NN)

Let us first consider the case where  $j \in N_i \Leftrightarrow i \in N_j (\Rightarrow i \neq j)$ . For simplicity, introduce  $\bar{\rho}_j := \prod_{l, l \neq j} \rho_l$ . Then we find

$$\begin{aligned} \text{Tr}_i [d_j \rho d_j^\dagger] &= \frac{1}{q^2} \sum_{m, n \in N_j} \text{Tr}_i [\sigma_m^z \bar{\rho}_j \sigma_n^z] \langle \sigma_j^y \sigma_j^y \rangle + \frac{i}{q} \sum_{m \in N_j} \text{Tr}_i [\sigma_m^z \bar{\rho}_j] \langle \sigma_j^x \sigma_j^y \rangle \\ &\quad - \frac{i}{q} \sum_{n \in N_j} \text{Tr}_i [\bar{\rho}_j \sigma_n^z] \langle \sigma_j^y \sigma_j^x \rangle + \langle \sigma_j^x \sigma_j^x \rangle \rho_i \\ &= \frac{1}{q^2} \sum_{m, n \in N_j} \text{Tr}_i [\sigma_m^z \bar{\rho}_j \sigma_n^z] - \frac{1}{q} \sum_{m \in N_j} \text{Tr}_i [\sigma_m^z \bar{\rho}_j] m_z - \frac{1}{q} \sum_{n \in N_j} \text{Tr}_i [\bar{\rho}_j \sigma_n^z] m_z + \rho_i \\ &= \frac{1}{q^2} \sum_{m, n \in N_j} \text{Tr}_i [\sigma_m^z \bar{\rho}_j \sigma_n^z] - \frac{m_z}{q} \sum_{m \in N_j} \text{Tr}_i [\{\sigma_m^z, \bar{\rho}_j\}] + \rho_i \\ &= \frac{1}{q^2} \left[ \left( \sum_{m, n \in N_j; m, n \neq i} + \sum_{m, n \in N_j; m \neq i; n = i} + \sum_{m, n \in N_j; m = i; n \neq i} \right) \text{Tr}_i [\sigma_m^z \bar{\rho}_j \sigma_n^z] + \text{Tr}_i [\sigma_i^z \bar{\rho}_j \sigma_i^z] \right] \\ &\quad - \frac{m_z}{q} \left[ \sum_{m \in N_j, m \neq i} \text{Tr}_i [\{\sigma_m^z, \bar{\rho}_j\}] + \text{Tr}_i [\{\sigma_i^z, \bar{\rho}_j\}] \right] + \rho_i \\ &= \frac{1}{q^2} [(C(q, m_z) \rho_i + (q-1) m_z \rho_i \sigma_i^z + (q-1) m_z \sigma_i^z \rho_i) + \sigma_i^z \rho_i \sigma_i^z] \\ &\quad - \frac{m_z}{q} [(q-1) 2 m_z \rho_i + \{\sigma_i^z, \rho_i\}] + \rho_i \\ &= \frac{1}{q^2} [C(q, m_z) \rho_i + (q-1) m_z \{\sigma_i^z, \rho_i\} + \sigma_i^z \rho_i \sigma_i^z] - \frac{m_z}{q} [(q-1) 2 m_z \rho_i + \{\sigma_i^z, \rho_i\}] + \rho_i. \end{aligned}$$

And for the other term

$$\begin{aligned}
\mathrm{Tr}_i [d_j^\dagger d_j \rho] &= \frac{1}{q^2} \sum_{m,n \in N_j} \mathrm{Tr}_i [\sigma_m^z \sigma_n^z \bar{\rho}_j] \langle \sigma_j^y \sigma_j^y \rangle - \frac{i}{q} \sum_{m \in N_j} \mathrm{Tr}_i [\sigma_m^z \bar{\rho}_j] \langle \sigma_j^y \sigma_j^x \rangle \\
&\quad + \frac{i}{q} \sum_{n \in N_j} \mathrm{Tr}_i [\sigma_n^z \bar{\rho}_j] \langle \sigma_j^x \sigma_j^y \rangle + \rho_i \\
&= \frac{1}{q^2} \sum_{m,n \in N_j} \mathrm{Tr}_i [\sigma_m^z \sigma_n^z \bar{\rho}_j] - \frac{1}{q} \sum_{m \in N_j} \mathrm{Tr}_i [\sigma_m^z \bar{\rho}_j] m_z - \frac{1}{q} \sum_{n \in N_j} \mathrm{Tr}_i [\sigma_n^z \bar{\rho}_j] m_z + \rho_i \\
&= \frac{1}{q^2} \sum_{m,n \in N_j} \mathrm{Tr}_i [\sigma_m^z \sigma_n^z \bar{\rho}_j] - \frac{2m_z}{q} \sum_{m \in N_j} \mathrm{Tr}_i [\sigma_m^z \bar{\rho}_j] + \rho_i \\
&= \frac{1}{q^2} \left[ \left( \sum_{m,n \in N_j; m,n \neq i} + \sum_{m,n \in N_j; m \neq i; n=i} + \sum_{m,n \in N_j; m=i; n \neq i} \right) \mathrm{Tr}_i [\sigma_m^z \sigma_n^z \bar{\rho}_j] + \sigma_i^z \sigma_i^z \rho_i \right] \\
&\quad - \frac{2m_z}{q} [(q-1)m_z \rho_i + \sigma_i^z \rho_i] + \rho_i \\
&= \frac{1}{q^2} [(C(q, m_z) \rho_i + (q-1)m_z \sigma_i^z \rho_i + (q-1)m_z \sigma_i^z \rho_i) + \sigma_i^z \sigma_i^z \rho_i] \\
&\quad - \frac{2m_z}{q} [(q-1)m_z \rho_i + \sigma_i^z \rho_i] + \rho_i \\
&= \frac{1}{q^2} [C(q, m_z) \rho_i + 2(q-1)m_z \sigma_i^z \rho_i + \sigma_i^z \sigma_i^z \rho_i] - \frac{2m_z}{q} [(q-1)m_z \rho_i + \sigma_i^z \rho_i] + \rho_i.
\end{aligned}$$

By symmetry it follows

$$\mathrm{Tr}_i [\rho d_j^\dagger d_j] = \frac{1}{q^2} [C(q, m_z) \rho_i + 2(q-1)m_z \rho_i \sigma_i^z + \rho_i \sigma_i^z \sigma_i^z] - \frac{2m_z}{q} [(q-1)m_z \rho_i + \rho_i \sigma_i^z] + \rho_i.$$

Combining these results yields

$$\begin{aligned}
&\kappa_F \sum_{j,j \in N_i} \left\{ \mathrm{Tr}_i [d_j \rho d_j^\dagger] - \frac{1}{2} \mathrm{Tr}_i [\{d_j^\dagger d_j, \rho\}] \right\} \\
&= \kappa_F q \left\{ \frac{1}{q^2} [C(q, m_z) \rho_i + (q-1)m_z \{\sigma_i^z, \rho_i\} + \sigma_i^z \rho_i \sigma_i^z] - \frac{m_z}{q} [(q-1)2m_z \rho_i + \{\sigma_i^z, \rho_i\}] + \rho_i \right. \\
&\quad - \frac{1}{2} \left[ \frac{1}{q^2} [C(q, m_z) \rho_i + 2(q-1)m_z \sigma_i^z \rho_i + \sigma_i^z \sigma_i^z \rho_i] - \frac{2m_z}{q} [(q-1)m_z \rho_i + \sigma_i^z \rho_i] + \rho_i \right] \\
&\quad \left. - \frac{1}{2} \left[ \frac{1}{q^2} [C(q, m_z) \rho_i + 2(q-1)m_z \rho_i \sigma_i^z + \rho_i \sigma_i^z \sigma_i^z] - \frac{2m_z}{q} [(q-1)m_z \rho_i + \rho_i \sigma_i^z] + \rho_i \right] \right\} \\
&= \kappa_F q \left\{ \frac{1}{q^2} \sigma_i^z \rho_i \sigma_i^z - \frac{1}{2q^2} \sigma_i^z \sigma_i^z \rho_i - \frac{1}{2q^2} \rho_i \sigma_i^z \sigma_i^z \right\} \\
&= \frac{\kappa_F}{q} \left( \sigma_i^z \rho_i \sigma_i^z - \frac{1}{2} \{\sigma_i^z \sigma_i^z, \rho_i\} \right).
\end{aligned}$$

Thus we found as additional mean field jump operator the  $\sigma^z$ -dephasing

$$\bar{v}_j := \frac{1}{\sqrt{q}} \sigma_j^z. \tag{B.23}$$

► Spin  $i$  ( $S_i$ )

For the special case  $j = i$ , we find

$$\begin{aligned}
\text{Tr}_i [d_i \rho d_i^\dagger] &= \frac{1}{q^2} \sum_{m,n \in N_i} \langle \sigma_m^z \sigma_n^z \rangle \sigma_i^y \rho_i \sigma_i^y + \frac{i}{q} \sum_{m \in N_i} \langle \sigma_m^z \rangle \sigma_i^y \rho_i \sigma_i^x - \frac{i}{q} \sum_{n \in N_i} \langle \sigma_n^z \rangle \sigma_i^x \rho_i \sigma_i^y + \sigma_i^x \rho_i \sigma_i^x \\
&= \frac{1}{q^2} [(q^2 - q)m_z^2 + q] \sigma_i^y \rho_i \sigma_i^y + \frac{i}{q} q m_z \sigma_i^y \rho_i \sigma_i^x - \frac{i}{q} q m_z \sigma_i^x \rho_i \sigma_i^y + \sigma_i^x \rho_i \sigma_i^x \\
&= \frac{1}{q} (1 - m_z^2) \sigma_i^y \rho_i \sigma_i^y + m_z^2 \sigma_i^y \rho_i \sigma_i^y + m_z i \sigma_i^y \rho_i \sigma_i^x - m_z \sigma_i^x \rho_i \sigma_i^y + \sigma_i^x \rho_i \sigma_i^x \\
&= \frac{1}{q} (1 - m_z^2) \sigma_i^y \rho_i \sigma_i^y + (-i m_z \sigma_i^y - \sigma_i^x) \rho_i (i m_z \sigma_i^y - \sigma_i^x) \\
&= \bar{b}_i \rho_i \bar{b}_i^\dagger + \bar{d}_i \rho_i \bar{d}_i^\dagger
\end{aligned}$$

where we introduced the mean field jump operators

$$\bar{d}_j := (-i m_z \sigma_j^y - \sigma_j^x) = \sigma_j^x (m_z \sigma_j^z - \mathbb{1}) \quad (\text{B.25a})$$

$$\bar{b}_j := \frac{1}{\sqrt{q}} \sqrt{1 - m_z^2} \sigma_j^y. \quad (\text{B.25b})$$

For the second term it follows

$$\begin{aligned}
\text{Tr}_i [d_i^\dagger d_i \rho] &= \frac{1}{q^2} \sum_{m,n \in N_i} \langle \sigma_m^z \sigma_n^z \rangle \sigma_i^y \sigma_i^y \rho_i - \frac{i}{q} \sum_{m \in N_i} \langle \sigma_m^z \rangle \sigma_i^y \sigma_i^x \rho_i + \frac{i}{q} \sum_{n \in N_i} \langle \sigma_n^z \rangle \sigma_i^x \sigma_i^y \rho_i + \rho_i \\
&= \frac{1}{q^2} [(q^2 - q)m_z^2 + q] \sigma_i^y \sigma_i^y \rho_i - \frac{i}{q} q m_z \sigma_i^y \sigma_i^x \rho_i + \frac{i}{q} q m_z \sigma_i^x \sigma_i^y \rho_i + \rho_i \\
&= \frac{1}{q} (1 - m_z^2) (\sigma_i^y)^\dagger \sigma_i^y \rho_i + (i m_z \sigma_i^y - \sigma_i^x) (-i m_z \sigma_i^y - \sigma_i^x) \rho_i \\
&= \bar{b}_i^\dagger \bar{b}_i \rho_i + \bar{d}_i^\dagger \bar{d}_i \rho_i
\end{aligned}$$

and subsequently

$$\text{Tr}_i [\{d_i^\dagger d_i, \rho\}] = \{\bar{b}_i^\dagger \bar{b}_i, \rho_i\} + \{\bar{d}_i^\dagger \bar{d}_i, \rho_i\}. \quad (\text{B.27})$$

Finally we have

$$\text{Tr}_i [d_i \rho d_i^\dagger] - \frac{1}{2} \text{Tr}_i [\{d_i^\dagger d_i, \rho\}] = [\bar{d}_i \rho_i \bar{d}_i^\dagger - \frac{1}{2} \{\bar{d}_i^\dagger \bar{d}_i, \rho_i\}] + [\bar{b}_i \rho_i \bar{b}_i^\dagger - \frac{1}{2} \{\bar{b}_i^\dagger \bar{b}_i, \rho_i\}] \quad (\text{B.28})$$

with the new mean field jump operators  $\bar{b}_j$  and  $\bar{d}_j$ . ◀

The total contributions due the ferromagnetic jump operators  $d_j$  in mean field approximation therefore read

$$\kappa_F \sum_j \text{Tr}_i [d_j \rho d_j^\dagger - \frac{1}{2} \{d_j^\dagger d_j, \rho\}] = \kappa_F \mathcal{L}(\bar{d}_i) [\rho_i] + \kappa_F \mathcal{L}(\bar{b}_i) [\rho_i] + \kappa_F \mathcal{L}(\bar{v}_i) [\rho_i] \quad (\text{B.29})$$

with the three superoperators

$$\mathcal{L}(\bar{d}_i) [\rho_i] = \bar{d}_i \rho_i \bar{d}_i^\dagger - \frac{1}{2} \{ \bar{d}_i^\dagger \bar{d}_i, \rho_i \} \quad (\text{B.30a})$$

$$\mathcal{L}(\bar{b}_i) [\rho_i] = \bar{b}_i \rho_i \bar{b}_i^\dagger - \frac{1}{2} \{ \bar{b}_i^\dagger \bar{b}_i, \rho_i \} \quad (\text{B.30b})$$

$$\mathcal{L}(\bar{o}_i) [\rho_i] = \bar{o}_i \rho_i \bar{o}_i^\dagger - \frac{1}{2} \{ \bar{o}_i^\dagger \bar{o}_i, \rho_i \} \quad (\text{B.30c})$$

and the jump operators  $\bar{d}_j$ ,  $\bar{b}_j$  and  $\bar{o}_j$  as defined above. ■

By combining the results derived above, we finally arrive at the mean field version of the master equation:

► **Result B.1: Mean field Lindblad equation for dissipative TIM**

The mean field version of the Lindblad master equation for the dissipative TIM reads

$$\partial_t \rho_i = -i [H_i^{\text{mf}}, \rho_i] + \kappa_P \mathcal{L}(c_i) [\rho_i] + \kappa_F \mathcal{L}(\bar{d}_i) [\rho_i] + \kappa_F \mathcal{L}(\bar{b}_i) [\rho_i] + \kappa_F \mathcal{L}(\bar{o}_i) [\rho_i]$$

with the four effective jump operators

$$\bar{d}_j = \sigma_j^x (m_z \sigma_j^z - \mathbb{1}) \quad (\text{B.31a})$$

$$\bar{b}_j = \frac{1}{\sqrt{q}} \sqrt{1 - m_z^2} \sigma_j^y \quad (\text{B.31b})$$

$$\bar{o}_j = \frac{1}{\sqrt{q}} \sigma_j^z \quad (\text{B.31c})$$

$$c_j = \frac{1}{2} (\sigma_j^z - i \sigma_j^y) \quad (\text{B.31d})$$

and the mean field Hamiltonian

$$H_i^{\text{mf}} = -Jq m_z \sigma_i^z - h \sigma_i^x = -\mathbf{h}_{\text{mf}} \sigma_i. \quad (\text{B.31e})$$

for the unitary evolution of the transverse field Ising model.

This is the result presented at the end of paragraph 2.3.1 upon which the whole mean field analysis in 2.3.2 and 2.3.3 is based.

## QTMC simulation: Implementation

In Chapter 2 we introduced the dissipative transverse field Ising model and in Section 2.6 we applied a quantum trajectory Monte Carlo simulation to simulate this model. In Chapter 5 we proposed a dissipative process to implement the Majorana chain. In paragraph 5.2.3 we applied the QTMC simulation to obtain fidelities for the dissipative Majorana chain. We discussed the QTMC algorithm theoretically in paragraph 2.6.1. Here provide the actual source code (at least the crucial parts) that we used to perform these simulations.

Our implementation is written in C++ and we utilise several open source libraries, namely

- Boost for managing threads and parsing system configurations via regular expressions.
- OpenBLAS as BLAS implementation (mostly BLAS Level 2 operations, namely matrix-vector multiplications).
- Armadillo as wrapper for BLAS functions.

OpenBLAS was compiled manually to take full advantage of its optimisation for the Intel Sandy-Bridge architecture. In the following we describe the most important loops that constitute the core of the simulation. The code runs parallelized on `ncores` cores, in our case `ncores = 8`.

**Listing C.1: Run over many trajectories**

```
1 arma::cx_vec cs = arma::zeros<arma::cx_vec>(ndimension);
2 arma::cx_vec buf = arma::zeros<arma::cx_vec>(ndimension);
3
4 for (int t=1; t<=nsamples/ncores; t++)
5 {
```

The simulation loop starts in C.1 with a definition of local variables which hold the quantum state that we want to evolve in time. Then the code enters the outer loop which runs over all `nsamples` trajectories (split between `ncores` cores).

**Listing C.2: Choose initial state**

```

6     double rnd = unif(eng), cmp = 0;
7     for (int i=0; i<(int)start.size(); i++)
8     {
9         cmp += startProb[i];
10        if (rnd <= cmp)
11        {
12            cs = start[i];
13            spin::Normalize(&cs);
14            break;
15        }
16    }

```

Subsequently we choose the initial state for the current trajectory  $t$ . This is done in C.2 by choosing a random variable `rnd` and comparing it with predefined probabilities in `startProb`. These probabilities and the corresponding initial states in `start` are given by the initial density matrix as input.

**Listing C.3: Run over time steps**

```

17    for (int s=1; s<=nsteps; s++)
18    {

```

In C.3 the program enters the inner loop which evolves the state in time for `nsteps` time intervals `dt`.

**Listing C.4: Check if jump occurs**

```

19        double rnd2 = unif(eng), cmp2 = 0;
20        bool jmp = false;
21
22        for (vector<arma::cx_mat>::iterator it = jops.begin();
23             it != jops.end(); ++it)
24        {
25            buf = (*it)*cs;
26            double nrm = arma::norm(buf,2);
27            cmp2 += dt*pow(nrm,2);

```

For each time step  $s$  we check whether a quantum jump occurs or not. This is done in C.4 by choosing another random variable `rnd2` and comparing it with the cumulative norms of states in `buf` where all jump operators in `it` have been applied to tentatively.

**Listing C.5: Apply jump operator**

```

28        if (rnd2 <= cmp2)
29        {
30            cs = buf/nrm;
31            jmp = true;
32            break;
33        }
34    }

```

If a jump occurs, the new state in `buf` is renormalised and stored in `cs`. Otherwise the state in `cs` remains unmodified; this is done in C.5.

**Listing C.6: Apply discrete time evolution operator**

```
35     if (!jump)
36     {
37         cs = cs - dt*heff*cs;
38         spin::Normalize(&cs);
39     }
```

The code in C.6 is responsible for the discrete time evolution if in C.5 *no* jump occurred. To this end the non-Hermitian effective Hamiltonian in `heff` is applied to `cs`, multiplied by the time interval `dt` and subtracted from `cs` (first order expansion of the non-unitary time evolution). Subsequently the state is renormalised which is necessary as `heff` is not Hermitian.

**Listing C.7: Perform measurements**

```
40     if (!((s-1)%(nsteps/npoints)))
41     {
42         int mp = (s-1)/(nsteps/npoints);
43
44         for (int o=0; o<nobs; o++)
45         {
46             av[o][mp] += spin::ExpValue(obs[o],cs);
47             sq[o][mp] += spin::ExpValue(sqobs[o],cs);
48         }
49     }
50 }
51 }
```

Depending on the time step  $s$ , a measurement is performed in C.7. The variable `npoints` specifies how many measurements are performed in the course of one trajectory. For each measurement the expectation values of all observables in `obs` (first moment) and their squares `sqobs` (second moment) are computed and stored in `av` and `sq`, respectively. Subsequently the time evolution loop starts all over again. When the latter is done, the outer trajectory loop starts with another trajectory. The ensemble averages of the observables are computed afterwards when all cores finished their trajectories and their results can be merged.





## Auxiliary calculations

### ■ Trace distance of single-site density matrices

The trace distance of two density matrices is defined as the trace norm of their difference, i.e.

$$\text{TD}[\rho_a, \rho_b] := \frac{1}{2} \|\rho_a - \rho_b\|_1 = \frac{1}{2} \text{Tr} \left[ \sqrt{(\rho_a - \rho_b)^\dagger (\rho_a - \rho_b)} \right] \quad (\text{D.1})$$

which simplifies to

$$\text{TD}[\rho_a, \rho_b] = \frac{1}{2} \text{Tr} \left[ \sqrt{(\rho_a - \rho_b)^2} \right] = \frac{1}{2} \sum_i |\lambda_i| \quad (\text{D.2})$$

since  $\rho = \rho^\dagger$ . Here  $\{\lambda_i\}$  are the eigenvalues of the self-adjoint (but not necessarily positive) operator  $\rho_a - \rho_b$ . Considering density matrices of a single site (i.e. one-qubit density matrices), it is convenient to describe such states by Bloch vectors, namely

$$\rho_a = \frac{1}{2} (\mathbb{1} + \mathbf{a}\boldsymbol{\sigma}) \quad \text{where } \mathbf{a} \in \mathbb{R}^3, |\mathbf{a}| \leq 1 \quad (\text{D.3})$$

and  $\boldsymbol{\sigma}$  denotes the vector of Pauli matrices. Inserting this into the expression for the trace distance yields

$$\text{TD}[\rho_a, \rho_b] = \frac{1}{4} \text{Tr} \left[ \sqrt{[(\mathbf{a} - \mathbf{b})\boldsymbol{\sigma}]^2} \right] \quad (\text{D.4})$$

and after a straightforward calculation we end up with  $-|\mathbf{a} - \mathbf{b}|$  and  $+|\mathbf{a} - \mathbf{b}|$  for the eigenvalues of  $[(\mathbf{a} - \mathbf{b})\boldsymbol{\sigma}]$ . Thus we find

$$\text{TD}[\rho_a, \rho_b] = \frac{1}{2} |\mathbf{a} - \mathbf{b}|. \quad (\text{D.5})$$

Note that for  $\mathbf{a} = \mathbf{b}$  the trace distance vanishes,  $\text{TD}[\rho_a, \rho_b] = 0$ , whereas for  $\mathbf{a} = -\mathbf{b}$  and  $|\mathbf{a}| = 1$  it takes its maximum value  $\text{TD}[\rho_a, \rho_b] = 1$ . ■

### ■ Von Neumann entropy of single-site density matrices

The VON NEUMANN entropy  $S$  for a given state  $\rho$  is defined as

$$S[\rho] := -\text{Tr}[\rho \log \rho] = -\sum_i \lambda_i \log \lambda_i \quad (\text{D.6})$$

where  $\{\lambda_i\}$  are the eigenvalues of  $\rho$ . For a one-qubit density matrix  $\rho_a = \frac{1}{2}(\mathbb{1} + a\sigma)$  these are given by  $\frac{1}{2}(1-a)$  and  $\frac{1}{2}(1+a)$  as one easily verifies (here we introduced  $a = |a|$ ). Then it follows

$$S[\rho_a] = -\frac{1-a}{2} \log \frac{1-a}{2} - \frac{1+a}{2} \log \frac{1+a}{2} = -\frac{1}{2} \log \left[ \frac{1-a^2}{4} \cdot \left( \frac{1+a}{1-a} \right)^a \right]. \quad (\text{D.7})$$

As a check of consistency, consider the limiting cases  $a \rightarrow 0$  and  $a \rightarrow 1$ . It follows easily  $\lim_{a \rightarrow 0} \left[ \frac{1-a^2}{4} \cdot \left( \frac{1+a}{1-a} \right)^a \right] = \frac{1}{4}$ . On the other hand it follows

$$\lim_{a \rightarrow 1} \left[ \frac{1-a^2}{4} \cdot \left( \frac{1+a}{1-a} \right)^a \right] = \frac{1}{4} \lim_{a \rightarrow 1} [(1-a)(1+a) \cdot (1+a)^a \cdot (1-a)^{-a}] = \lim_{a \rightarrow 1} (1-a)^{1-a} = 1$$

which follows by L'HOSPITAL'S rule. Thus we conclude

$$\lim_{a \rightarrow 0} S[\rho_a] = \log 2 \quad (\text{D.8a})$$

$$\lim_{a \rightarrow 1} S[\rho_a] = 0 \quad (\text{D.8b})$$

which lives up to our expectations. ■

## Some Asides: Locality in lattice systems

The notion of locality is ubiquitous in condensed matter physics. For instance, the definition and classification of (topological) quantum phases is based on local unitary evolutions [22] that require a spatial structure and some kind of metric on the subsystems of the Hilbert space. Other results such as the famous LIEB-ROBINSON bounds [11, 134, 158–160] rely on concepts of adjacency and spatial distances. The dynamics, stability and realisability of dissipative quantum systems is closely related to spatial structures of the underlying lattice [11, 133, 161, 162]. It is therefore natural to ask for a precise operational definition of terms like “quasilocal operator” and “lattice dimension”.

Unfortunately, physicists tend to describe systems imprecisely, at least from a mathematically rigorous point of view. Even theoretical physicists avoid unambiguous definitions of the objects their theories are concerned with. This is often encouraged by the circumstances: Due to the simplicity of interesting models, it is often obvious what is implied if we say “quasilocal operator” or “dimension of the lattice” — although a general definition is not given. Here we give an account on some of these subtleties involved in the discussions of this thesis.

### E.1 Templates and instances

A typical question of theoretical physics reads: *Has object  $X$  property  $A$ ?* In this context it proves advantageous to consider a property  $A$  as a total mapping  $P_A$  from a well defined set of objects  $\mathcal{X}$  into the binary set  $\{0, 1\}$ . We then tag object  $X \in \mathcal{X}$  with property  $A$  iff  $P_A(X) = 1$ . We say that  $X$  does not possess property  $A$  iff  $P_A(X) = 0$ . Here some examples:

- Let  $X = \langle \text{RED APPLE} \rangle$  and  $R = \langle \text{IS RED} \rangle$ ,  $B = \langle \text{IS BLUE} \rangle$ . Then obviously  $P_R(X) = 1$  and  $P_B(X) = 0$ .
- Let  $\mathcal{X} = \langle \text{APPLES} \rangle$  and  $F = \langle \text{IS FRUIT} \rangle$ ,  $B = \langle \text{IS BEAN} \rangle$ ,  $G = \langle \text{IS GREEN} \rangle$ . Then we have  $P_F(X) = 1$  and  $P_B(X) = 0$  for all  $X \in \mathcal{X}$  but  $P_G(X) = 1$  and  $P_G(Y) = 0$  for some  $X, Y \in \mathcal{X}$ .

The last example motivates the following definition:

► **Definition E.1: Trivial properties**

Given a set of objects  $\mathcal{X}$  and properties  $C$ ,  $G$  and  $N$ . Then we say that

- (i)  $C$  is a *common property* of  $\mathcal{X}$  iff  $\forall_{X \in \mathcal{X}} : P_C(X) = 1$ .
- (ii)  $G$  is a *genuine property* of  $\mathcal{X}$  iff  $\exists_{X, Y \in \mathcal{X}} : P_G(X) = 1 \wedge P_G(Y) = 0$ .
- (iii)  $N$  is *not a property* of  $\mathcal{X}$  iff  $\forall_{X \in \mathcal{X}} : P_N(X) = 0$ .

What we are aiming at are linguistic inaccuracies which are common in scientific literature but prove disastrous in the context of didactics as they not only prevent clear and precise comprehension of the matter but also proliferate uncontrollably through scientific communities thereby establishing a dangerous standard of inexactness and veiling ignorance.

Typical statements in that regard are the following:

- Given two many-body states  $|\Psi\rangle$  and  $|\Phi\rangle$ . Are  $|\Psi\rangle$  and  $|\Phi\rangle$  equivalent with respect to quasilocal unitary operations?
- Given a Hamiltonian  $H$ . Is the spectrum  $\sigma(H)$  gapped?

As long as we are considering physical (i.e. finite) systems, both questions are to some extent senseless or ill-defined. This can be seen quite easily: Given two states  $|\Psi\rangle$  and  $|\Phi\rangle$  on a *fixed* Hilbert space  $\mathcal{H}$ . Can you imagine a procedure to answer the question of quasilocal unitary equivalence? *No, you cant!* Given any fixed Hamiltonian  $H$  on a finite dimensional Hilbert space  $\mathcal{H}$ . Can you decide whether it is gapped or not? *No, you cant!* One may object that given e.g. the Heisenberg Hamiltonian

$$H = -J \sum_{i=1}^N \mathbf{S}_i \mathbf{S}_{i+1} \quad (\text{E.1})$$

one can show (even analytically) that for  $J > 0$  there is no spectral gap *in the thermodynamic limit*. But that is the hitch: “Thermodynamic limit” means  $N \rightarrow \infty$ . That is to say, being gapless is *not* the property of a Hamiltonian  $H$  but of a *series of Hamiltonians*  $(H_N)$ . In this context it becomes clear that by writing  $H = -J \sum_{i=1}^N \mathbf{S}_i \mathbf{S}_{i+1}$  one usually refers to the *function*  $H_N : \mathbb{N} \rightarrow \mathcal{B}(\mathcal{H})$  rather than to its values, i.e. a specific Hamiltonian  $H_N$  for  $N \in \mathbb{N}$ . This distinction seems to be trivial at least on the level of applications; it is certainly not as trivial if we consider the rigorous framework of physical theories. To the best of my belief, obliterating such differences is one reason for the difficulties encountered in learning and teaching physics.

Let us try to give a more precise account on that subject:

► **Definition E.2: Templates and Instances**

The following functions  $* : \mathbb{N} \rightarrow \cdot$  are all required to be *computable*<sup>a</sup>:

- (i) Let  $\mathcal{H}(\cdot)$  be a function on  $\mathbb{N}$  such that  $\mathcal{H}(N)$  is a finite dimensional Hilbert space for any  $N \in \mathbb{N}$ . We call  $\mathcal{H}(\cdot)$  a *Hilbert space template*.
- (ii) Given a Hilbert space template  $\mathcal{H}(\cdot)$ . A function  $A(\cdot) : \mathbb{N} \rightarrow \bigcup_{N \in \mathbb{N}} \mathcal{B}(\mathcal{H}(N))$  with  $A(N) \in \mathcal{B}(\mathcal{H}(N))$  is called an *operator template* on  $\mathcal{H}(\cdot)$ . If additionally  $A(N)^\dagger = A(N)$  for all  $N \in \mathbb{N}$  it is called a *self-adjoint operator template*. If we intend to interpret a self-adjoint operator template  $A(\cdot)$  as Hamiltonians on  $\mathcal{H}(\cdot)$  it is called a *Hamiltonian template* and usually denoted by  $H(\cdot)$ .
- (iii) Given a Hilbert space template  $\mathcal{H}(\cdot)$ . A function  $\Psi(\cdot) : \mathbb{N} \rightarrow \bigcup_{N \in \mathbb{N}} \mathcal{H}(N)$  with  $\Psi(N) \equiv |\Psi(N)\rangle \in \mathcal{H}(N)$  is called a *state template* on  $\mathcal{H}(\cdot)$ .

Given any template  $*(\cdot)$ . Then  $*(N)$  is denoted an *instance* thereof for all  $N \in \mathbb{N}$ .

<sup>a</sup>A function  $f$  on  $\mathbb{N}$  is called *computable* if there is a Turing Machine  $M$  which – given an encoding  $\langle N \rangle$  of  $N \in \mathbb{N}$  – halts and outputs an encoding  $\langle f(N) \rangle$  for  $f(N)$ . To put it simply: One can implement an algorithm in any Turing complete programming language which computes  $f$ .

We illustrate these definitions by reinterpretations of the properties discussed above:

- Given two state templates  $\Psi(\cdot)$  and  $\Phi(\cdot)$  over a Hilbert space template  $\mathcal{H}(\cdot)$ . They are called *equivalent under quasilocal unitary operations (QLU-equivalent)* iff

$$\exists C \in \mathbb{N} \forall N \in \mathbb{N} \exists U = \otimes_{i \in I} U_i \in \mathcal{U}(\mathcal{H}(N)) : \forall i \in I \text{diam}(\text{supp}(U_i)) \leq C \wedge |\Psi(N)\rangle = U |\Phi(N)\rangle. \quad (\text{E.2})$$

Here  $\text{diam}(\cdot)$  denotes the diameter of a subset of the underlying spatial structure of the considered system (usually a lattice) with respect to an appropriate metric on this structure. In this case we write  $P_{\text{QLU}}(|\Psi\rangle(\cdot), |\Phi\rangle(\cdot)) = 1$  or  $\Psi(\cdot) \sim_{\text{QLU}} \Phi(\cdot)$ . Thus QLU is a *genuine property of state templates* (more precisely: of pairs of state templates) but it is *not a property of (pairs of) states*.

- In contrast consider two states  $|\Psi\rangle$  and  $|\Phi\rangle$  over a Hilbert space  $\mathcal{H}$ . They are called *equivalent under local unitary operations (LU-equivalent)* iff

$$\exists U = \otimes_{i \in I} U_i \in \mathcal{U}(\mathcal{H}) : \forall i \in I |\text{supp}(U_i)| = 1 \wedge |\Psi\rangle = U |\Phi\rangle. \quad (\text{E.3})$$

That is,  $|\Psi\rangle$  and  $|\Phi\rangle$  are LU-equivalent in the usual sense; write  $P_{\text{LU}}(|\Psi\rangle, |\Phi\rangle) = 1$  or  $|\Psi\rangle \sim_{\text{LU}} |\Phi\rangle$ . We conclude that LU-equivalence, as defined above, is a *genuine property of states* and *not a property of state templates*<sup>81</sup>.

<sup>81</sup> Note that it is straightforward to extend the notion of LU-equivalence to state templates. Such a new property would then be a genuine property of the latter

- Along the same lines we identify “gapped Hamiltonians” as a genuine property of Hamiltonian templates: Let  $H(\cdot)$  be a Hamiltonian template on the Hilbert space template  $\mathcal{H}(\cdot)$ . We call  $H(\cdot)$  *gapped*, write  $P_{\text{GAP}}(H(\cdot)) = 1$ , iff

$$\exists_{\Delta E \in \mathbb{R}^+} \forall_{N \in \mathbb{N}} \forall_{E_0 \in \min \sigma(H(N))} \forall_{E_1 \notin \min \sigma(H(N))} : |E_0 - E_1| \geq \Delta E. \quad (\text{E.4})$$

Note that an analogous definition for *Hamiltonians* over finite dimensional Hilbert spaces  $\mathcal{H}(N)$  does not make any sense.

## E.2 Realisability and locality

Physical systems can be described by mathematical means. E.g. consider some finite lattice system, then the corresponding mathematical structure is its Hilbert space which is obtained by tensoring the Hilbert spaces of the local subsystems. The question is which mathematical structures may be called “physical” or “physically realisable”. The point we are heading at is the notion of *locality* which is *a priori* not included in mathematical structures such as Hilbert spaces and their operator algebras. Physicists speaking of the Hilbert space  $\mathcal{H}$  of some lattice system implicitly furnish this abstract object with some kind of “spatial meta-structure”, meaning that there is a distinguished representation in terms of a tensor product  $\mathcal{H} = \otimes_i \mathcal{H}_i$  where  $\mathcal{H}_i$  denotes the Hilbert space of a physically point like structure. However note that there is no such distinguished meta-structure from a mathematical point of view, which can be seen from the fact that by means of e.g. discrete Fourier transformations the new representation  $\mathcal{H} = \otimes_k \mathcal{H}_k$  in terms of wave vectors  $k$  can be obtained. That is to say, physical systems (at least in quantum mechanics) are described by some kind of “spatial structure” from which a Hilbert space can be derived. Only in this framework notions such as “quasilocal interactions” or “long range entanglement” are well defined properties. In the following we propose a formal treatment of this subject in order to clarify several notions used throughout this thesis. Actually, without the following (seemingly trivial) definitions, technical terms such as “topological order” or “gapped systems” are ill defined or at least remain vague concepts. The latter may be no obstacle for specialists in the field but renders the didactics much more cumbersome.

### E.2.1 Spatial structures

In this subsection we introduce concepts of “spatial structures” which are physically motivated. Their formulation in terms of graph theory remains purely abstract, though.

#### Physical systems and interaction graphs

Here we introduce our notion of interaction systems starting from a purely abstract description in terms of Hilbert spaces and bounded linear operators. We then derive from such abstract descriptions the concept of interaction and locality. Then the question arises, whether the proposed interaction system is “local” in a sense that has to be defined with thought. This procedure yields a rigorously defined notion of “physicality” as property of a given *sequence* of interaction systems (termed *interaction templates*).

We begin with the definition of a single interaction system:

► **Definition E.3: Interaction system**

Consider a finite set of Hilbert spaces  $\{\mathcal{H}_i\}_{1 \leq i \leq N}$  and let  $\mathcal{B}(\mathcal{H}_i)$  be the set of bounded linear operators on  $\mathcal{H}_i$ . Now set  $\mathcal{H} = \otimes_{i=1}^N \mathcal{H}_i$  and  $\mathcal{B}(\mathcal{H}) = \otimes_{i=1}^N \mathcal{B}(\mathcal{H}_i)$ . Given any operator of the form

$$H = \sum_{j \in \mathbb{N}} \bigotimes_{i=1}^N L_{ij} \in \mathcal{B}(\mathcal{H}) \quad (\text{E.5})$$

where  $L_{ij} \in \mathcal{B}(\mathcal{H}_i)$  and  $L_{ij} \neq \mathbb{1}$  for finitely many  $i$  and  $j$ . Then  $\mathcal{I} \equiv (H, \{\mathcal{H}_i\}_{1 \leq i \leq N})$  is called an *(abstract) interaction system*.

The physical interpretation is as follows: A finite physical system can be seen as a collection of point-like subsystems  $i$ , each with internal degrees of freedom described by the subsystems Hilbert space  $\mathcal{H}_i$ . A *physical theory* or *physical system* is described by some operator  $H$  acting on  $\mathcal{H}$  which defines the dynamics of states in  $\mathcal{H}$ . In most cases  $H$  will be a Hamiltonian, but we may also consider Markovian dynamics described by a Lindblad superoperator  $\mathcal{L}$  or another form of operational description. One then interprets each summand in  $H$  as an *interaction term*  $\bigotimes_{i=1}^N L_{ij}$  which involves multipartite interactions between the subsystems for which  $L_{ij}$  describes a non-trivial operation on  $\mathcal{H}_i$ , i.e.  $L_{ij} \neq \mathbb{1}$ .

In order to contrive a precise definition of “local interactions”, we need some basic definitions from graph theory. The crucial notion is that of a *hypergraph* which is extensively studied in the fields of graph theory, computational geometry, combinatorics, network theory etc.:

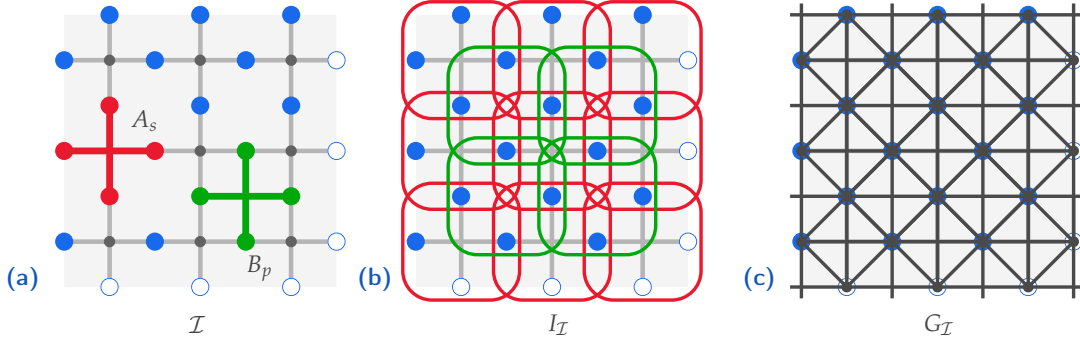
► **Definition E.4: Hypergraph and Primal graphs**

- (i) Let  $V$  be a finite set and  $E \subseteq \mathcal{P}(V) \setminus \{\emptyset\}$  an arbitrary set of non-empty subsets of  $V$ . Then  $H = (V, E)$  is called *hypergraph* with *nodes*  $V$  and *hyperedges*  $E$ . In the field of computational geometry  $H$  is sometimes referred to as *range space*.
- (ii) Given a hypergraph  $H = (V, E)$ . The simple graph  $G(H) = (V_H, E_H)$  defined by  $V_H \equiv V$  and  $E_H \equiv \{\{p, q\} \mid p, q \in V \wedge p \neq q \wedge \exists e \in E : p, q \in e\}$  is called *primal graph* of  $H$  and features a clique for each hyperedge of  $H$ .
- (iii) Given a hypergraph  $H$  and its primal graph  $G(H)$ .  $H$  is termed *conformal* iff every maximal clique of  $G(H)$  is a hyperedge of  $H$ .

It is now rather obvious how to proceed: Each interaction term in  $H$  defines a hyperedge on the set of subsystems. Therefore the following

► **Definition E.5: Interaction hypergraph and interaction graph**

Given an abstract interaction system  $\mathcal{I} \equiv (H, \{\mathcal{H}_i\}_{1 \leq i \leq N})$  with  $H = \sum_{j \in \mathbb{N}} \bigotimes_{i=1}^N L_{ij} \in \mathcal{B}(\mathcal{H})$ . Let  $V = \{s_1, \dots, s_N\}$  be a set of  $N$  distinct elements where  $s_i$  labels subsystem  $i$  described by  $\mathcal{H}_i$ . For each  $j$  let  $e_j \in \mathcal{P}(V) \setminus \{\emptyset\}$  be the set of all system-labels  $s_i$  such that  $L_{ij} \neq \mathbb{1}$  and collect all  $e_j$  in  $E$ . We will refer to  $I_{\mathcal{I}} = (V, E)$  as the *interaction hypergraph*. Its primal graph  $G_{\mathcal{I}} \equiv G(I_{\mathcal{I}})$  is termed *interaction graph* of  $\mathcal{I}$ .



■ **Figure E.1:** The interaction system  $\mathcal{I} = \text{TCM}$  of the toric code is schematically illustrated in (a). Spins and their local Hilbert spaces  $\mathcal{H}_i$  are attached to edges of the lattice. The Hamiltonian defines interactions via *star operators*  $A_s$  on sites  $s$  and *plaquette operators*  $B_p$  on faces  $p$ . Each summand in the Hamiltonian describes interactions between four spins. This defines the *interaction hypergraph*  $I_{\mathcal{I}} = I_{\text{TCM}}$  in (b) where the colours of hyperedges correspond to the operators in (a). Note that we omit the hyperedges on the boundary for convenience. The *primal graph* of  $I_{\mathcal{I}}$ , termed *interaction graph*  $G_{\mathcal{I}} = G_{\text{TCM}}$  is depicted in (c) with grey lines. Pairs of spins that are connected by an edge of  $G_{\mathcal{I}}$  are close with respect to the spatial meta-structure induced by the toric code Hamiltonian  $H_{\text{TCM}}$ . For a physical system this usually implies that they have to be close in terms of the metric of space as well.

Let us give an example in terms of the famous toric code, see 1.3.3 in the preliminaries. To this end consider a finite square lattice of extension  $L$  embedded into the torus with a spin  $S = \frac{1}{2}$  attached to each edge. That is there are  $L^2$  subsystems, each described by the qubit Hilbert space  $\mathcal{H}_i = \mathbb{C}_i^2$ . The toric code Hamiltonian reads

$$H_{\text{TCM}} = -J_A \sum_s A_s - J_B \sum_p B_p \quad (\text{E.6})$$

where  $s$  runs over all vertices and  $p$  over all faces of the embedded lattice and the quasilocal stabiliser operators are defined as  $A_s = \otimes_{i \in s} \sigma_i^x$  and  $B_p = \otimes_{i \in p} \sigma_i^z$ . Here  $i \in s$  denotes all edges  $i$  originating from vertex  $s$  and  $i \in p$  denotes all edges bounding face  $p$ . The derived interaction hypergraph  $I_{\text{TCM}}$  and the vicinity graph  $G_{\text{TCM}}$  are depicted in Fig. E.1.

#### Graph embeddings

A finite<sup>82</sup> *physical* system consists of  $N$  point-like subsystems which are localised in a  $d$ -dimensional euclidean space  $\mathbb{R}^d$ . However, usually the exact positions of subsystems are irrelevant (and experimentally unobservable) due to descriptions in terms of effective theories. Then the crucial point is the *scaling* of distances with respect to the scaling of the system size. For instance: If we define a quantum Ising system the relevant spatial information is not the exact position of the spins in space but rather the lattice type and its dimension.

So far we derived a purely graph theoretic description from an abstract model of interactions between certain subsystems in terms of its vicinity graph. The former is an abstract graph without any *a priori* connection to the euclidean space where the actual physics takes place. As to say, we may position each subsystem  $s_i$  arbitrarily in space. Depending on this spatial meta-structure imposed on  $\mathcal{H}$ , some interaction terms in  $H$  may be long-ranged whereas others couple only nearby subsystems. The interesting question is, whether there are spatial configurations

<sup>82</sup>Infinite systems are inherently unphysical although their description often simplifies their treatment from a mathematical point of view (e.g. in the case of thermodynamic limits).



rendering *all* interaction terms in  $H$  quasilocal (which still has to be defined). To this end, we have to consider embeddings of abstract graphs into the  $d$ -dimensional real euclidean space  $\mathbb{R}^d$ :

► **Definition E.6: Simple graphs and graph embeddings**

- (i) Given a finite set  $V = \{v_1, \dots, v_N\}$  of *vertices* and finite set  $E \subseteq \{\{v, w\} \mid v, w \in V \wedge v \neq w\}$  of *edges*. The pair  $G = (V, E)$  is called *simple graph*. If for each pair of vertices  $s, f \in V$  there is a path of edges in  $E$  connecting  $s$  and  $f$ ,  $G$  is called *connected*. From now on all graphs will be simple and connected.
- (ii) A *graph embedding* ( $E$ )  $\Gamma_G$  of  $G$  in  $d$ -dimensions is – informally speaking – a drawing of  $G$  in  $\mathbb{R}^d$  *without intersecting edges*. By a slight abuse of notation we will interpret  $\Gamma_G : V \rightarrow \mathbb{R}^d$  as the mapping which maps an abstract vertex  $v \in V$  to its real-space representation  $\Gamma_G(v) \equiv \mathbf{v} \in \mathbb{R}^d$ . If crossing of edges is allowed, the embedding is called *crossing embedding* (GE).
- (iii) A graph embedding is called *straight line embedding* (SE) if for all  $e = \{v, w\} \in E$  and for all  $t \in (0, 1)$  it holds  $t\mathbf{v} + (1-t)\mathbf{w} \notin \Gamma(V)$ , i.e. if the edges  $E$  can be drawn as straight lines. If crossing of edges is allowed, the embedding is called *crossing straight line embedding* (CSE).
- (iv) A graph  $G$  which can be embedded into  $\mathbb{R}^2$  is called *planar*.

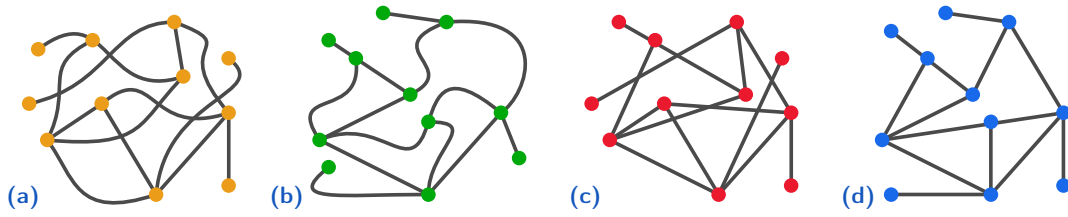
There are several theorems known in graph theory providing statements about possible embeddings of simple graphs. Here we give some of the most important statements:

► **Proposition E.1: Graph embeddings**

Let  $G = (V, E)$  be an arbitrary connected simple graph.

- (i) **Kuratowski's theorem:**  $G$  is planar if and only if it does not contain a subgraph that is a subdivision of  $K_5$  (the complete graph on five vertices) or  $K_{3,3}$  (the complete bipartite graph on six vertices).
- (ii) **Fáry's theorem:** Every planar graph  $G$  has a straight line embedding in  $\mathbb{R}^2$ .
- (iii) **3D-embedding theorem:** Every graph  $G$  has a straight line embedding in  $\mathbb{R}^3$ .

We see: Any graph may be embedded with straight lines in three dimensional space but there are graphs which cannot be embedded in the plane (not even with bent edges). However, if a graph can be embedded in the plane, then we can do so with straight lines. Further information on graph theory can be found in Ref. [163].



■ **Figure E.2:** Examples for graph embeddings in two dimensions. We show four different embeddings for the same graph in the plane: (a) is a crossing embedding with bent edges; (b) is an embedding with bent edges devoid of crossings; (c) is a crossing straight line embedding and (d) is a straight line embedding devoid of crossings. The embeddings (b) and (d) qualify the shown graph as *planar*.

### ■ Constrained embeddings

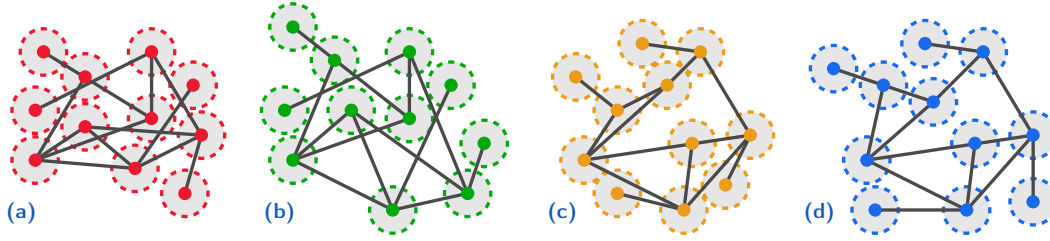
As we will see, we have to impose additional constraints on the embeddings of our vicinity graphs (and hence physical subsystems) in order to capture the notion of a physically realisable system appropriately. Let us first introduce some characteristic length scales and parameters defined for a given graph embedding  $\Gamma_G$  ( $E, CE, SE, CSE$ ):

#### ► Definition E.7: Distances

Let  $G = (V, E)$  be an arbitrary connected simple graph and  $\Gamma_G$  be an embedding in  $d$ -dimensional space  $\mathbb{R}^d$ .

- (i) We call  $L(\Gamma_G) = \max \{ |v - v'| \mid v, v' \in V \}$  the *(linear) size* of the embedding.
- (ii) We call  $N(G) = |V|$  the *order* of the graph.
- (iii) We call  $\epsilon(\Gamma_G) = \max \{ |v - v'| \mid \{v, v'\} \in E \}$  the *intrinsic distance* of the embedding.
- (iv) We call  $\delta(\Gamma_G) = \min \{ |v - v'| \mid v, v' \in V \}$  the *intrinsic isolation* of the embedding.

The meaning of these quantities should be quite intuitive. In Fig. E.2 the four types of embeddings are illustrated for a graph  $G$  with  $N = 11$ . In the case of a vicinity graph the lines symbolise two particle interactions. Since elementary *through-space* interactions between two subsystems usually depend on the euclidean distance between both parties, they can be represented by straight lines appropriately. Therefore we will constrain our considerations in the following to straight line embeddings where one may think of the edges as paths of mediators.



■ **Figure E.3:** Examples for constrained graph embeddings in two dimensions. We show four different straight line embeddings of the same graph. (a) is a Type-1 embedding (with crossings and  $\Delta$ -balls may intersect edges); (b) is a Type-2 embedding (with crossings and  $\Delta$ -balls free of edges); (c) is a Type-3 embedding (without crossings and  $\Delta$ -balls may intersect edges) and (d) is a Type-4 embedding (without crossings and  $\Delta$ -balls free of edges).

Let us now introduce a class of constrained embeddings which will become relevant below:

► **Definition E.8: Civilized Embeddings, Quasi Unit-Disc Embeddings**

Let  $G = (V, E)$  be an arbitrary connected simple graph and  $\Gamma_G$  be a straight line embedding (SE or CSE) in  $d$ -dimensional space  $\mathbb{R}^d$ .

- (i)  $\Gamma_G$  is called  *$\Delta$ -civilised embedding* ( $\Delta c$ ) iff  $\delta(\Gamma_G) \geq \Delta$  for some  $\Delta > 0$ .
- (ii)  $\Gamma_G$  is called *quasi unit-disc embedding* (qUDE) iff  $\epsilon(\Gamma_G) \leq 1$ .
- (iii)  $\Gamma_G$  is called *Type-1 embedding* iff it is a  $\Delta c$  qUDE for some  $\Delta > 0$  and crossings are allowed.
- (iv)  $\Gamma_G$  is called *Type-2 embedding* iff it is a  $\Delta c$  qUDE for some  $\Delta > 0$ , crossings are allowed and there is no edge within a  $\Delta$ -ball<sup>a</sup> of any vertex which is not its origin.
- (v)  $\Gamma_G$  is called *Type-3 embedding* iff it is a  $\Delta c$  qUDE for some  $\Delta > 0$  without crossings.
- (vi)  $\Gamma_G$  is called *Type-4 embedding* iff it is a  $\Delta c$  qUDE for some  $\Delta > 0$  without crossings and there is no edge within a  $\Delta$ -ball of any vertex which is not its origin.

A graph  $G$  is of Type- $n$  in  $d$ -dimensions iff there is a Type- $n$  embedding  $\Gamma_G$  in  $\mathbb{R}^d$ .

<sup>a</sup>A  $\Delta$ -ball is defined with respect to the euclidean metric  $d_E$  as  $B_\Delta(r) = \{x \in \mathbb{R}^d \mid d_E(x, r) < \Delta\}$ .

Type-1,2,3 and 4 embeddings of the same graph  $G$  as above are depicted in Fig. E.3. Clearly, any Type-2,3,4 embedding is of Type-1 and any Type-4 embedding is of Type-2 and 3. However, general Type-2 and 3 embeddings are not comparable. Some remarks:

- All graphs are of Type-1,2,3,4 for some  $\Delta > 0$  in  $d \geq 3$ .
- All planar graphs are of Type-1,2,3,4 for some  $\Delta > 0$  in  $d = 2$ .
- All graphs are of Type-1,2 for some  $\Delta > 0$  in  $d = 2$ .
- For  $\Delta > \frac{1}{2}$  no non-trivial graph (i.e. with at least one edge) is of Type-1,2,3,4 in any dimension  $d$ .

Due to this findings the function

$$\Theta_d^{(n)}(G) \equiv \sup \left\{ \Delta \in \mathbb{R}^+ \mid \exists \Gamma_G \text{ in } \mathbb{R}^d \text{ which is Type-}n \text{ for } \Delta \right\} \quad (\text{E.7})$$

is well-defined if  $n = 1, 2, 3, 4$  and  $d \geq 3$  ( $d = 2$  and  $n = 3, 4$  requires  $G$  to be planar). It is an interesting question whether  $\Theta$  can be computed efficiently. ■

Locality in interacting systems - a first approach

We turn now towards physical applications of these abstract notions. Here we introduce a first definition for “locality” in interacting systems. However, as it turns out this allows long range interactions and therefore renders some “local” systems unphysical. In the next subsection this caveat will be cured.

The motivation reads as follows: A physical system of  $N$  point-like subsystems features interactions between these subsystems (described by e.g. operators in a Hamiltonian). Assume that by some description (Hamiltonian, Lindblad equation etc.) it can be deduced which subsystems must be able to interact in order to implement the system<sup>83</sup>. Each subsystem may be identified with a vertex  $v \in V$ . If two subsystems  $v$  and  $v'$  interact, this is encoded by an edge  $\{v, v'\} \in E$ . To summarise: Given  $N$  subsystems, each identified with a vertex  $v \in V$  and physically described by a Hilbert space  $\mathcal{H}_v$ , the hole system (identified with  $V$ ) is physically described by  $\mathcal{H} = \otimes_{v \in V} \mathcal{H}_v$  and some equation<sup>84</sup>  $H$  defined over  $\mathcal{H}$  (e.g. a Hamiltonian). Then we can derive a graph  $G = (V, E)$  from the interactions encoded in  $H$  with respect to the partition  $\mathcal{H} = \otimes_{v \in V} \mathcal{H}_v$ . Note that at this point there is no restriction on  $H$  whatsoever.

We now revive the notion of *templates* as introduced before and denote them by a hat. A general template  $\hat{\bullet}$  is a *computable* function

$$\hat{\bullet} : \mathbb{N} \longrightarrow X$$

defined over the natural numbers which returns for each  $n \in \mathbb{N}$  an object  $\hat{\bullet}(n) \in X$  – called an *instance*. In the following we consider *graph templates*  $\hat{G}$  which are infinite sequences of arbitrary (simple and connected) graphs  $\hat{G}(n)$  and corresponding templates of embeddings  $\hat{\gamma}_G$ . Why are templates necessary? Well, imagine a graph  $G$  describing the interactions of some proposed Hamiltonian. We can now ask, whether the proposal is “physical” in the sense that there is an embedding  $\Gamma_G$  in  $\mathbb{R}^3$  such that all subsystems are within a certain range of their interacting neighbours. This requirement is motivated by the fact that the controlled interaction between two (or more) subsystems usually requires them to be spatially close to each other (where the maximum distance depends on the methods available in the lab). But then it is clear that, given any *fixed* and *finite* system, we can just shrink any embedding  $\Gamma_G$  in  $\mathbb{R}^3$  such that  $\epsilon(\Gamma_G)$  becomes small enough. To put it differently: There is no well defined notion of “locality” for a single *instance* of a physical system. But there is one for templates:

<sup>83</sup>Note that this does not imply any spatial structure yet! This is a property of the mathematical structure alone.

<sup>84</sup>We just write  $H$  for any dynamical description of the system in terms of operators acting on  $\mathcal{H}$ . I.e.  $H$  is not necessarily a Hamiltonian.

► **Definition E.9: Locality I - Weak locality**

Given a straight line embedding template  $\hat{\Gamma}_G$  in  $\mathbb{R}^d$ . We call  $\hat{\Gamma}_G$  *weakly local* in  $d$  dimensions iff

$$\lim_{n \rightarrow \infty} \frac{\epsilon(\hat{\Gamma}_G(n))}{L(\hat{\Gamma}_G(n))} = 0 \quad (\text{E.8})$$

or  $\epsilon \in o(L)$  for short. A graph template  $\hat{G}$  is called *weakly local* iff there exists a weakly local straight line embedding  $\hat{\Gamma}_G$ .

A physical system template  $(\hat{H}, \hat{\mathcal{H}})$  – defined by some equation templates  $\hat{H}$  and a Hilbert space template  $\hat{\mathcal{H}}$  – is thus *weakly local* iff its induced interaction graph  $\hat{G}$  is weakly local.

Note that this definition is explicitly scale invariant, i.e. rescaling (“shrinking”) each instance  $\hat{\Gamma}_G(n)$  separately by some factor  $\lambda_n$  (write  $\lambda_n \hat{\Gamma}_G(n)$ ) has no effect at all on the property of locality since  $L(\lambda_n \hat{\Gamma}_G(n)) = \lambda_n L(\hat{\Gamma}_G(n))$  and  $\epsilon(\lambda_n \hat{\Gamma}_G(n)) = \lambda_n \epsilon(\hat{\Gamma}_G(n))$ . This definition is kind of canonical if we restrict ourselves to the characteristic length scales  $L(\hat{\Gamma}_G(n))$  and  $\epsilon(\hat{\Gamma}_G(n))$ . The question is whether it is physical.

Consider as an example for  $\hat{\Gamma}_G$  a square lattice (i.e.  $d = 2$ ) with lattice constant  $a$  and length/width  $n \cdot a$ . Then obviously

$$\begin{aligned} L(\hat{\Gamma}_G(n)) &= \sqrt{(a \cdot n)^2 + (a \cdot n)^2} = \sqrt{2}a \cdot n \\ N(\hat{\Gamma}_G(n)) &= (n+1)^2 \\ \epsilon(\hat{\Gamma}_G(n)) &= a \\ \delta(\hat{\Gamma}_G(n)) &= a \end{aligned}$$

and it follows easily  $\lim_{n \rightarrow \infty} \frac{\epsilon(\hat{\Gamma}_G(n))}{L(\hat{\Gamma}_G(n))} = \lim_{n \rightarrow \infty} \frac{a}{\sqrt{2}a \cdot n} = 0$ . However it is clear that we may contrive templates such that the intrinsic distance (or interaction range)  $\epsilon$  grows when the system grows; for instance  $\epsilon(\hat{\Gamma}_G(n)) \propto \sqrt{n}$  and  $L(\hat{\Gamma}_G(n)) \propto n$ . That is, the notion of weak locality qualifies systems which become “more and more” local when the system grows. However from a physical point of view this usually is still experimentally intractable. To see this note that the usual projection of a four dimensional hypercubic lattice of edge length  $a \cdot n$  into a  $d < 4$ -dimensional space requires edges of length  $(a \cdot n)^{\frac{4-d}{d}}$  [51]. For  $d = 3$  we find  $\lim_{n \rightarrow \infty} \frac{\epsilon(\hat{\Gamma}_G(n))}{L(\hat{\Gamma}_G(n))} = \lim_{n \rightarrow \infty} \frac{(a \cdot n)^{\frac{4-d}{d}}}{2a \cdot n} = 0$  which renders the four dimensional hypercubic lattice weakly local in three dimensions.

It seems as if a more physical requirement would be that  $\epsilon \in \mathcal{O}(1)$  is bounded by some constant  $C > 0$  and  $\lim_{n \rightarrow \infty} L(\hat{\Gamma}_G(n)) = \infty$ , i.e. the system grows unbounded in linear size. However this yields the *same* class of weakly local systems as defined above: First, if a graph template  $\hat{G}$  features a straight line embedding template  $\hat{\Gamma}_G$  with bounded intrinsic distance and unbounded linear size, it is clear that  $\lim_{n \rightarrow \infty} \frac{\epsilon(\hat{\Gamma}_G(n))}{L(\hat{\Gamma}_G(n))} = 0$ . Conversely, given a template  $\hat{\Gamma}_G$  with  $\lim_{n \rightarrow \infty} \frac{\epsilon(\hat{\Gamma}_G(n))}{L(\hat{\Gamma}_G(n))} = 0$ . Define the rescaled template  $\hat{\Gamma}'_G(n) = \lambda_n \hat{\Gamma}_G(n)$  where  $\lambda_n = \epsilon(\hat{\Gamma}_G(n))^{-1} \in (0, \infty)$ . Then obviously  $\epsilon(\hat{\Gamma}'_G(n)) = 1 \leq 1 \equiv C$  and furthermore  $\lim_{n \rightarrow \infty} L(\hat{\Gamma}'_G(n)) = \lim_{n \rightarrow \infty} \frac{L(\hat{\Gamma}_G(n))}{\epsilon(\hat{\Gamma}_G(n))} = \infty$ .

## Graph templates and the geometric gap

In order to obtain a more appropriate abstraction of physical locality let us use the previously introduced theory of Type- $n$  embeddings. A graph template is a sequence  $\hat{G}$  of graphs  $\hat{G}(N)$  for  $N \in \mathbb{N}$  which is recursively enumerable. If we are not interested in the sequential properties of  $\hat{G}$  we interpret the sequence as set  $\{\hat{G}(N)\}_{N \in \mathbb{N}}$ . We may now introduce the notion of a *geometrically gapped graph template*:

## ► Definition E.10: Geometric gap

Let  $\hat{G}$  be a graph template. We call

$$\theta_d^{(n)}(\hat{G}) \equiv \inf_{G \in \hat{G}} \Theta_d^{(n)}(G) \geq 0 \quad (\text{E.9})$$

the *type- $n$  geometric gap* of  $\hat{G}$  in  $d$  dimensions. Provided  $\theta_d^{(n)}(\hat{G}) > 0$ ,  $\hat{G}$  is called *gapped graph template*. We will write  $\theta_d \equiv \theta_d^{(1)}$  for short.

Pictorially, a gapped graph template is a set of graphs such that each graph can be embedded into  $\mathbb{R}^d$  by means of a type- $n$  embedding with parameter  $\Delta \geq \theta$ . Note that since  $\Theta_d^{(n)}(G) \geq 0$  for all graphs  $G$ ,  $\theta$  is well defined. Clearly  $0 \leq \theta \leq \frac{1}{2}$ . It is straightforward to see that for gapped templates  $\hat{G}$  it is necessary for the maximum degree  $\Delta(G) = \max \{\deg(v) \mid v \in V\}$  to be bounded over  $\hat{G}$ , i.e.  $\sup_{G \in \hat{G}} \Delta(G) \leq C$  for some  $C > 0$ . This implies the necessary condition of bounded clique sizes over  $\hat{G}$  as well.

There is a quite useful condition to show that a given graph template is *not* gapped by means of appropriately chosen subgraphs. Given a graph template  $\hat{G}$ , a *subsequence*<sup>85</sup>  $\hat{G}' \subseteq \hat{G}$  is defined as a sequence of connected subgraphs  $\hat{G}'(N) \subseteq \hat{G}(N)$  with  $\text{rank } \hat{G}'(N) \geq 2$  for all  $N \in \mathbb{N}$ . We may now state the following

## ► Lemma E.1: Ungapped templates

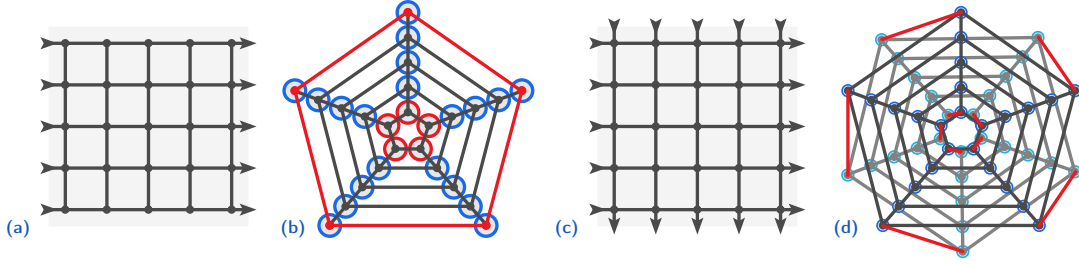
Let  $\hat{G}$  be a graph template and  $d \in \mathbb{N}$ . If there is a non-trivial subsequence  $\hat{G}' \subseteq \hat{G}$  such that

$$\lim_{N \rightarrow \infty} \frac{\text{diam}^d(\hat{G}'(N))}{\text{rank}(\hat{G}'(N))} = 0 \quad (\text{E.10})$$

then  $\theta_d^{(n)} = 0$  for  $n = 1, 2, 3, 4$ .

*Proof.* Given the subsequence  $\hat{G}' \subseteq \hat{G}$  with  $\lim_{N \rightarrow \infty} \frac{\text{diam}^d(\hat{G}'(N))}{\text{rank}(\hat{G}'(N))} = 0$ . Clearly  $\Theta_d^{(n)}(\hat{G}'(N)) \geq \Theta_d^{(n)}(\hat{G}(N))$  since  $\hat{G}'(N) \subseteq \hat{G}(N)$ . Thus if we show  $\lim_{N \rightarrow \infty} \Theta_d^{(n)}(\hat{G}'(N)) = 0$  it immediately follows  $\theta_d^{(n)}(\hat{G}) = 0$ . To this end note that all type- $n$  embeddings  $\hat{\Gamma}_{G'}(N)$  can be enclosed by a sphere with radius proportional to  $\text{diam}(\hat{G}'(N))$  and volume proportional to  $\text{diam}^d(\hat{G}'(N))$ .

<sup>85</sup>Note that this sequence is not necessarily computable and thus not termed "template".



■ **Figure E.4:** Examples for geometrically gapped graph embeddings. In (a) we show a rectangular lattice embedded into a cylinder with periodic boundary conditions in one and open boundary conditions in the other direction. A Type-4 embedding of this lattice is shown in (b). The toroidal square lattice in (c) is embedded via a Type-1 embedding in (d). These are two twisted and connected copies of the cylindrical embedding in (b).

Then the maximal volume  $V_{\max}(N)$  of the spheres separating vertices is bounded from above by

$$V_{\max}(N) \leq \frac{\text{diam}^d(\hat{G}'(N))}{\text{rank}(\hat{G}'(N))} \tag{E.11}$$

since  $\text{rank}(\hat{G}'(N))$  is just the number of separating spheres. Therefore we find  $\lim_{N \rightarrow \infty} V_{\min}(N) = 0$  and  $\hat{G}$  is ungapped. ■

We are now going to give some examples of gapped and ungapped graph templates.

■ **Example 1: (Hyper-)Cubic lattices**

Consider the graph  $\hat{C}(N)$  of a cubic lattice of side length  $N$  in each direction. The sequence of all such cubic lattices for  $N = 1, 2, \dots$  constitutes a graph template  $\hat{C}$ . For  $d = 3$  it is easy to see that  $\Theta_3^{(4)}(\hat{C}(N)) = \frac{1}{2}$  for any  $N \in \mathbb{N}$  if we chose the usual embedding of the cubic lattice in  $\mathbb{R}^3$  and thus  $\theta_3^{(4)}(\hat{C}) = \frac{1}{2}$ . Consequently  $\theta_3^{(n)}(\hat{C}) = \frac{1}{2}$  for  $n = 1, 2, 3, 4$  and  $\hat{C}$  is gapped for all  $n$  in three dimensions. For  $d = 2$  we note that  $\text{diam}(\hat{C}(N)) = 3N$  and  $\text{rank}(\hat{C}(N)) \sim N^3$  and therefore  $\lim_{N \rightarrow \infty} \frac{\text{diam}^2(\hat{C}'(N))}{\text{rank}(\hat{C}'(N))} = 0$ . Thus  $\theta_2^{(n)}(\hat{C}) = 0$  and the cubic lattice is ungapped in two dimensions.

Now consider the graph  $\hat{H}(N)$  of a (four-dimensional) hypercubic lattice of side length  $N$  in each direction and the corresponding template  $\hat{H}$ . With the same arguments above it follows  $\theta_4^{(n)}(\hat{H}) = \frac{1}{2}$  and  $\hat{H}$  is gapped in four dimensions. However, for  $d = 3$  we find  $\text{diam}(\hat{H}(N)) = 4N$  and  $\text{rank}(\hat{H}(N)) \sim N^4$  and therefore  $\lim_{N \rightarrow \infty} \frac{\text{diam}^3(\hat{H}'(N))}{\text{rank}(\hat{H}'(N))} = 0$ . Thus  $\theta_3^{(n)}(\hat{H}) = 0$  and the hypercubic lattice is ungapped in three dimensions. Clearly, the same holds for  $d = 2$ . ■

■ **Example 2: The cylindrical square lattice**

Consider a square lattice of size  $N$  in each direction embedded into a cylinder (i.e. with periodic boundary conditions in one direction). Let  $\hat{S}$  denote the corresponding graph template. If we chose the usual rectangular embedding it is clear that  $\theta_3^{(4)}(\hat{S}) = \frac{1}{2}$  and thus  $\theta_3^{(n)}(\hat{S}) = \frac{1}{2}$  for all  $n$ . It is now interesting to ask whether  $\hat{S}$  is gapped for  $d = 2$ . Lemma E.1 cannot be applied beneficially since the quotient becomes independent of  $N$ . Indeed, we can show that  $\theta_3^{(n)}(\hat{S}) > 0$

and  $\hat{S}$  is gapped in two dimensions. To this end consider the embedding of the cylindrical lattice in Fig. E.4 (a) as depicted in Fig. E.4 (b).

There the lattice is projected onto the plane along the symmetry axis of the cylinder. The circumference of the outer polygon cycle is bounded from above by the maximum length of the edges whereas the inner polygon cycles length is bounded by the separation condition. We have to show that the separating distance  $\Delta$  can be chosen  $N$ -independent. Clearly, the minimum inner radius is determined by  $2\pi R_i = 2\Delta \cdot N$  and the maximum outer radius by  $2\pi R_o = 1 \cdot N$ . The length of the spokes is then  $R_o - R_i = \left(\frac{1}{2} - \Delta\right) \frac{N}{\pi}$ . If the separating spheres are in contact with each other on the spokes, we find (for large  $N$ )  $R_o - R_i = 2\Delta N$ . That is,

$$\left(\frac{1}{2} - \Delta\right) \frac{N}{\pi} = 2\Delta N \quad \Rightarrow \quad \Delta^* = \frac{1}{2 + 4\pi}. \quad (\text{E.12})$$

So there is a type-4 embedding for each  $\hat{S}(N)$  in  $d = 2$  with  $\Delta \geq \frac{1}{2+4\pi}$  and we conclude  $\Theta_2^{(n)}(\hat{S}(N)) \geq \Delta^*$ . Consequently  $\theta_2^{(n)} \geq \Delta^* > 0$  and the square lattice with periodic boundary conditions in one direction is gapped in two dimensions. ■

### ■ Example 3: The toroidal square lattice

Consider a square lattice of size  $N$  in each direction embedded into a torus (i.e. with periodic boundary conditions in both directions). Let  $\hat{T}$  denote the corresponding graph template. If we chose the usual rectangular embedding it is clear that  $\theta_3^{(4)}(\hat{T}) = \frac{1}{2}$  and thus  $\theta_3^{(n)}(\hat{T}) = \frac{1}{2}$  for all  $n$ . Surprisingly we find that this graph template remains gapped in two dimensions. To this end consider the embedding of the toroidal lattice in Fig. E.4 (c) as depicted in Fig. E.4 (d) which is derived from two copies of the cylindrical embedding we introduced above. Note that this is just a twisted and flattened version of the toroidal lattice in two dimensions. We obtain a lower bound for the separating radius by shrinking the separating spheres of the cylindrical embedding by one half. Then the copy of the cylindrical square lattice can be rotated slightly to fit in the resulting “holes” on the inner polygon cycle. The straight line edges connecting both copies at their perimeter are short enough since the outer edges have length 1. So there is a type-1 embedding for each  $\hat{T}(N)$  in  $d = 2$  with  $\Delta \geq \frac{1}{4+8\pi}$  and we conclude  $\Theta_2^{(1)}(\hat{T}(N)) \geq \frac{\Delta^*}{2}$ . Consequently  $\theta_2^{(1)} \geq \frac{\Delta^*}{2} > 0$  and the square lattice with periodic boundary conditions in both directions is gapped in two dimensions. Note that due to the crossings between edges and spheres we derived a type-1 embedding. However, it may be possible to modify the proposed embedding to obtain more powerful results in terms of type-2, 3, 4 embeddings. ■

Locality in interacting systems - a second approach

Above we used the fact that, even when the intrinsic distance  $\epsilon$  is unbounded, we may *shrink* the system so that the maximum interaction range remains bounded. At this point it becomes evident where the “unphysicality” enters: A physical system cannot be shrunken arbitrarily without loosing its structure of distinct subsystems. More graphically, to control the interaction between two subsystems, there are *two independent* restrictions we have to take care of:

1. *Interacting subsystems* have to be within the interaction range of each other.
2. *All subsystems* have to be separated at least by some finite “buffer range”.



The last condition prevents us from shrinking the system arbitrarily and thus leads to a more restrictive notion of locality.

It is clear that by combining the notion of gapped graph templates with the concept of interaction graphs we end up with a quite reasonable abstraction of “quasilocal physical systems” or what we would deem a “realisable theory”. At this point we do not fix a type of embedding yet, though it seems to be reasonable that type-1 embeddings are at least a good basis for the most general characterisation of quasilocal theories. Besides, they are easier to handle from a geometric point of view.

Let us give the definition and discuss some implications afterwards:

► **Definition E.11: Locality II - Strong locality**

Given an abstract interaction system template  $\hat{\mathcal{I}} \equiv (\hat{H}, \{\hat{\mathcal{H}}_i\})$  and its derived interaction graph template  $\hat{G}_{\hat{\mathcal{I}}}$ . We call  $\hat{\mathcal{I}}$  *quasilocal, strongly local* or *geometrically gapped* iff  $\hat{G}_{\hat{\mathcal{I}}}$  is geometrically gapped.

Here an *interaction system template*  $\hat{\mathcal{I}}$  is defined as usual: There is an algorithm such that for every  $N \in \mathbb{N}$  we can compute an instance  $\hat{\mathcal{I}}(N)$  which is an interaction system as defined above. It is important that quasilocality is the property of an interaction system template and *not* of one of its instances. This is analogous to the definition of gapped Hamiltonians; we may ask whether the interaction graph of a given interaction system is of type- $n$  in  $d$  dimensions *with parameter*  $\Delta > 0$ . For an actual implementation this can be quite important since  $\Theta_d^{(n)}(G_{\mathcal{I}})$  tells us something about the relation between the distance and the spatial precision of interactions which have to be realised. However, there is no “canonical” choice of  $\Delta > 0$  which renders it unfeasible to define the notion of quasilocality for a single instance. To get rid of such parameter-dependent definitions it proves handy to step back and consider templates instead of instances where we hope to flesh out the crucial ideas behind “locality”.

■ **Structure graphs and locality**

Often the interaction system itself is derived from some underlying spatial structure, i.e. a graph (usually a lattice). We start with some graph template  $\hat{S}$  – from now on called *structure graph (template)* – and attach physical subsystems to its vertices. The interaction operator template  $\hat{H}$  is then defined for each instance  $\hat{H}(N) = \sum_{j \in \mathbb{N}} \otimes_{i=1}^N L_{ij}$  via its quasilocal interaction terms  $L_{ij}$ .

► **Definition E.12: Abstract locality**

We say that an interaction system template  $\hat{\mathcal{I}}$  residing on a structure graph template  $\hat{S}$  is *abstract local* iff there is a constant  $C > 0$  such that for all  $i$  and  $j$  and for all instances  $\hat{\mathcal{I}}(N)$  and  $\hat{S}(N)$

$$\text{supp}(L_{ij}) \subseteq B_C(s_i) \quad (\text{E.13})$$

where  $s_i$  denotes the vertices in  $\mathbb{V}(\hat{S}(N))$  and  $B_C(s_i)$  is the ball of vertices around  $s_i$  in  $\hat{S}(N)$  with geodesic radius  $C$ .

This is the formalisation of the usually applied notion of “quasilocality” in discrete physical systems. Here the underlying structure graph  $\hat{S}$  provides its own notion of locality defined by

its edge-based adjacency relation. For simple lattices as structure graph, this is a reasonable way to speak of quasilocal systems. However, if we allow arbitrary graph templates  $\hat{S}$  it is not granted that a system can be implemented quasilocally if  $\hat{S}$  itself is not geometrically gapped. We can show the following:

► **Lemma E.2: Structure graphs and Interaction graphs**

Given an abstract local, structure graph induced interaction system template  $\hat{\mathcal{I}}$  with constant  $C > 0$  (as defined above). If the structure graph template  $\hat{S}$  is geometrically gapped, then the interaction graph template  $\hat{G}_{\mathcal{I}}$  is type-1 geometrically gapped and the interaction system is type-1 quasilocal.

*Proof.* Consider a sequence of embeddings  $\hat{\Gamma}_S$  of arbitrary type with parameters  $\delta(\hat{\Gamma}_S(N)) \geq \theta_d^{(n)}(\hat{S}) > 0$  (this is possible since  $\hat{S}$  is geometrically gapped). That is, for all  $N \in \mathbb{N}$  we have  $\epsilon(\hat{\Gamma}_S(N)) \leq 1$  and  $\delta(\hat{\Gamma}_S(N)) \geq \theta_d^{(n)}(\hat{S}) > 0$ . Now define the rescaled embeddings  $\hat{\Gamma}_{G_{\mathcal{I}}} := \frac{1}{2C}\hat{\Gamma}_S$ . Clearly for all  $N \in \mathbb{N}$  we have  $\delta(\hat{\Gamma}_{G_{\mathcal{I}}}(N)) \geq \frac{\theta_d^{(n)}(\hat{S})}{2C} > 0$  and thus the separation condition is satisfied. Furthermore, all edges  $e \in \mathbb{E}(\hat{G}_{\mathcal{I}}(N))$  connect vertices within a ball  $B_C(v)$  around some vertex  $v \in \mathbb{V}(\hat{G}_{\mathcal{I}}(N))$  (due to the abstract locality condition). Since all edges in  $\hat{S}(N)$  have maximum length 1 and the maximum geodesic distance within a ball  $B_C(v)$  is  $2C$ , the maximum distance of connected vertices in  $\hat{G}_{\mathcal{I}}(N)$  is  $2C$  times the rescaling of  $(2C)^{-1}$ . We conclude that  $\epsilon(\hat{G}_{\mathcal{I}}(N)) \leq 1$  for all  $N \in \mathbb{N}$ . ■

Dimension of graph templates

Given a discrete physical system, there is usually a intuitive notion of its spatial dimension. E.g. the Ising model on the square lattice is “obviously” two-dimensional, the “same” model on the cubic lattice is three-dimensional and so on. If one tries to generalise the concept of spatial dimension to arbitrary interaction systems, two problems arise:

1. There seems to be no canonical method to derive a spatial dimension for finite systems (Why should one consider an Ising system on a  $4 \times 4$  square lattice two dimensional?).
2. If the system is defined on a aperiodic graph without any canonical embedding in euclidean space, there seems to be no relation between the graph and the dimension of its embedding space. (Any graph can be embedded with straight lines and without crossings in  $\mathbb{R}^d$ ).

Both problems should seem familiar to us as we faced such obstacles before. Clearly we can get rid of them by using templates instead of instances. We cannot assign a spatial dimension to finite interaction systems in an abstract and canonical way. However, for interaction system templates this should be possible generically:

► **Definition E.13: Spatial dimension**

The *spatial dimension*  $\dim(\hat{G})$  of a graph template  $\hat{G}$  is the minimal dimension  $d$  required to render it geometrically gapped. The *spatial dimension*  $\dim(\hat{\mathcal{I}})$  of an interaction system template is the spatial dimension of its interaction graph template  $\hat{G}_{\mathcal{I}}$ . We call  $\hat{\mathcal{I}}$  *realistic* iff its spatial dimension is less or equal to three.

According to this definition (recall the examples from above) the *graph* of a square lattice is indeed two-dimensional as expected whereas the graph for a hypercubic lattice is four-dimensional. Interestingly, the dimension of square lattices with periodic boundary conditions (in one or two directions) is now well defined; we already proved that such graphs are two-dimensional.

**E.2.2** An application: Local quantum circuits and quantum complexity theory

If one thinks about quantum circuits as a paradigmatic model for quantum computation in quantum information theory, it is natural to consider *gates* as interactions between the qubits of the bus on which the gate acts non-trivially. This motivates the following definition of the complexity class “Scalable **BQP**” which is a (seemingly) more restricted version of the well-known **BQP**:

► **Definition E.14: Scalable BQP**

A language  $L$  is in  $\mathbf{S}_d\mathbf{BQP}$  (Scalable **BQP** in  $d$  dimensions) iff there exists a *polynomial-time uniform* family of quantum circuits  $\{Q_n\}_{n \in \mathbb{N}}$  with *geometrically gapped* interaction graphs  $\{G_n \equiv G(Q_n)\}_{n \in \mathbb{N}}$  in  $d$  dimensions, such that

- for each  $n \in \mathbb{N}$ ,  $Q_n$  is a  $n$ -qubit quantum circuit with dedicated output qubit.
- for all  $x \in L$ ,  $\Pr(Q_{|x|}(x) = 1) \geq \frac{2}{3}$ .
- for all  $x \notin L$ ,  $\Pr(Q_{|x|}(x) = 0) \geq \frac{2}{3}$ .

We call the problems/languages in  $\mathbf{S}_3\mathbf{BQP}$  *realistic*.

Here  $\Pr(Q_{|x|}(x) = 0, 1)$  denotes the probability of measuring 0, 1 for the output qubit if  $Q_{|x|}$  runs on input  $x$ .  $G_n = G(Q_n)$  is the interaction graph between the  $n$  qubits defined by the gates of the quantum circuit  $Q_n$ . The above definition may suggest, that, given  $\mathbf{S}_3\mathbf{BQP} \subsetneq \mathbf{BQP}$ , there are problems for which no *scalable* quantum algorithm exists which could be implemented on a “static quantum computer”<sup>86</sup>. However, there are two arguments against this presumed restriction: First, even if the physical subsystems encoding the qubits are fixed in space (e.g. Nitrogen vacancy centres or atoms in optical lattices) there is always the possibility of teleportation between distant sites as long as there are quasilocal mechanisms to synthesise long-range entanglement (and it is not hard to think of such processes). And second, we may simplify each quantum circuit  $Q_n \rightarrow \tilde{Q}_n$  such that  $\tilde{Q}_n$  is composed of local unitaries/measurements and *nearest-neighbour* CNOT-gates, rendering the sequence  $\{\tilde{Q}_n\}$  quasilocal even in one dimension.

<sup>86</sup>I.e. a quantum computer which supports no flying qubits over arbitrary distances.

That is:

► Lemma E.3: Scalable BQP equals BQP

$$\mathbf{S}_d\mathbf{BQP} = \mathbf{BQP} \quad \text{for all } d \in \mathbb{N} \quad (\text{E.14})$$

*Proof.* The proof is almost trivial. It is a well known fact that any quantum circuit  $Q_n$  can be decomposed in terms of arbitrary one-qubit unitaries<sup>87</sup> and two-qubit CNOT-gates. Therefore the only edges in the derived interaction graph  $G(Q_n)$  stem from CNOT-gates. It is easy to show that two-qubit SWAP-gates may be composed of three subsequent CNOT-gates. Now consider a linear chain of  $n$  qubits. One may replace each non-nearest-neighbour CNOT-gate by a sequence of SWAP-gates and a nearest neighbour CNOT-gate followed by the reversed sequence of SWAP-gates. Clearly the overhead by expanding non-nearest-neighbour CNOT-gates is in  $\mathcal{O}(n)$  and thus the new quantum circuit  $\tilde{Q}_n$  can be computed in polynomial time and contains only nearest-neighbour CNOT-gates (if we replace the SWAP-gates by CNOT-gates). The new interaction graphs  $G(\tilde{Q}_n)$  are obviously chain-graphs and thus trivially gapped in all dimensions. ■

As an alternative proof for  $d \geq 2$  one may employ the concept of *measurement-based quantum computation on cluster states* [164]. Since it is known that two-dimensional cluster states are a resource for universal quantum computation [165] and the creation of the latter requires just conditioned phase gates on adjacent qubits on a square lattice, it is clear that there are always scalable quasilocal quantum algorithms in 2D.

So we find that the physically motivated notion of local quantum circuits is actually no restriction at all; which we should be glad about, since there is no loss of computational power if we restrict ourselves to spatially fixed qubits and short range interactions (and thus exclude flying qubits).

<sup>87</sup>Note that this in general requires an uncountable number of local unitaries which certainly is not realistic. Fortunately it is possible to approximate any one-qubit unitary, to arbitrary precision, by a discrete set of unitaries, see [37] for further explanations. This is not important for our point, though.





# List of Figures

1.1	Illustration of single spin dissipative dynamics: Cross-sections of the Bloch sphere.	29
1.2	Contribution of finite jump trajectories in Dyson series. . . . .	31
1.3	Approximation of dissipative dynamics by finite number jump trajectories. . . . .	32
1.4	Toric Code: The setting used for the toric code model as proposed by Kitaev. . . . .	39
1.5	Repairing of the Majorana modes as proposed by Kitaev. . . . .	42
1.6	Fermion and hole densities for different parameters and modes. . . . .	49
1.7	Spectrum of the Majorana chain for different parameters. . . . .	50
1.8	Ground state energy of the Majorana edge modes in dependence of the system size.	50
1.9	Spectrum of Majorana chain with static disorder for varying chemical potential. . . . .	51
1.10	Edge mode energy of the Majorana chain with static noise as a function of the chemical potential. . . . .	52
1.11	Exact spectrum and gap of the Majorana chain as function of the parameters. . . . .	55
1.12	Dynamics of the quasiparticles in non-ideal Majorana chain. . . . .	59
1.13	Illustration of the winding number in the trivial and topological phase. . . . .	61
1.14	Qualitative phase diagram of the $\mathbb{Z}_2$ -Gauge-Higgs model in $(2 + 1)$ dimensions. . . . .	78
2.1	Classification of solutions of the mean field equations (physical solutions). . . . .	100
2.2	Classification of solutions of the mean field equations (stable solutions). . . . .	102
2.3	Steady states of dissipative TIM in mean field approximation (Overview). . . . .	104
2.4	Steady states of dissipative TIM in mean field approximation (purely dissipative). . . . .	105
2.5	Classification of solutions for the purely dissipative system (physical and stable solutions). . . . .	106
2.6	Illustration of mean field dynamics in cross section of Bloch ball for purely dissipative system. . . . .	107
2.7	Phase diagram of purely dissipative TIM in mean field approximation. . . . .	109
2.8	Illustration of mean field dynamics in cross section of Bloch ball for purely dissipative system ( $q = \infty$ ). . . . .	110
2.9	Phase diagram of purely dissipative TIM in mean field approximation ( $q = \infty$ ). . . . .	111
2.10	Steady states of dissipative TIM with unitary dynamics (detail). . . . .	113
2.11	Phase diagram of dissipative TIM with unitary dynamics (ferromagnetic island). . . . .	115
2.12	Phase diagram of dissipative TIM with unitary dynamics (first order transition). . . . .	117
2.13	Classification of solutions of the mean field equations (high-dimensional limit). . . . .	119
2.14	Steady states of dissipative TIM with unitary contributions (high-dimensional limit). . . . .	121
2.15	Phase diagram of dissipative TIM with unitary dynamics (high-dimensional limit). . . . .	123
2.16	Dynamics of purely dissipative TIM in mean field approximation for late times. . . . .	127

2.17	Dynamics of purely dissipative TIM in mean field approximation at the critical point. . . . .	130
2.18	Spectrum of Jacobian matrix and critical slowing down of relaxation in purely dissipative system. . . . .	132
2.19	Dynamics of inhomogeneous dissipative TIM in one dimension above, at and below the critical coupling. . . . .	138
2.20	Dynamics of inhomogeneous dissipative TIM in two dimensions above, at and below the critical coupling. . . . .	140
2.21	Comparison of dissipative TIM with thermal TIM in mean field approximation. . . . .	154
2.22	Purity, concurrence and $x$ -magnetisation for the 2-spin instance of the dissipative TIM as functions of $\kappa_F$ and $\kappa_P$ . . . . .	159
2.23	Steady states of 2-spin dissipative TIM with unitary dynamics for $\kappa_P = 0$ and $h \neq 0$ . . . . .	162
2.24	Trace distance between unique and non-unique steady states for the 2-spin dissipative TIM as function of $\kappa_F$ and $\lambda$ . . . . .	163
2.25	Steady states of 2-spin TIM with unitary dynamics for $\kappa_P = 0$ and $h = 0$ . . . . .	165
2.26	Examples of the exact time evolution of the 2-spin dissipative TIM. . . . .	166
2.27	QTMC simulation of generic 2-spin TIM with unitary dynamics and different initial states. . . . .	171
2.28	QTMC simulation of 2-spin TIM with unitary dynamics and non-unique steady states. . . . .	173
2.29	Realizations of quantum jump trajectories for the 2-spin TIM for different parameters. . . . .	175
2.30	Realizations of quantum jump trajectories of the purely dissipative TIM for different system sizes in one dimension. . . . .	177
2.31	Realizations of quantum jump trajectories of the purely dissipative TIM for different system sizes in two dimensions. . . . .	178
2.32	Relaxation of $z$ -magnetisation in purely dissipative TIM in one and two dimensions. . . . .	180
2.33	Realizations of quantum jump trajectories of the purely dissipative TIM for different couplings in one dimension. . . . .	183
2.34	QTMC simulation of the dissipative TIM: Correlations in dependence of $\kappa$ . . . . .	185
3.1	Unitary mean field theory for the $\mathbb{Z}_2$ -Gauge-Higgs model without gauge fixing. . . . .	190
3.2	Unitary mean field theory for the $\mathbb{Z}_2$ -Gauge-Higgs model in unitary gauge. . . . .	192
3.3	Qualitative mean field phase diagram for the $\mathbb{Z}_2$ -Gauge-Higgs model. . . . .	193
3.4	Schematic action of the jump operators for the dissipative $\mathbb{Z}_2$ -Gauge-Higgs model (A and B). . . . .	196
3.5	Schematic action of the jump operators for the dissipative $\mathbb{Z}_2$ -Gauge-Higgs model (C). . . . .	199
3.6	Schematic action of the jump operators for the dissipative $\mathbb{Z}_2$ -Gauge-Higgs model (D). . . . .	201
3.7	Mean field phase diagram for dissipative $\mathbb{Z}_2$ -Gauge-Higgs model. . . . .	209
3.8	Mean field phase diagram for dissipative $\mathbb{Z}_2$ -Gauge-Higgs model in unitary gauge. . . . .	211
3.9	Mean field phase diagram for dissipative $\mathbb{Z}_2$ -Gauge-Higgs model in the high-dimensional limit. . . . .	213
3.10	Mean field phase diagram for dissipative $\mathbb{Z}_2$ -Gauge-Higgs model in unitary gauge in the high-dimensional limit. . . . .	214



4.1	Schematic for the recursive generation of matrix representations for the jump operator algebra. . . . .	229
4.2	Entanglement spectrum of fixed number dark states. . . . .	255
5.1	Schematic illustration for deterministic, classical non-local and local error correction. . . . .	262
5.2	Schematic illustration for deterministic and stochastic, classical local error correction. . . . .	263
5.3	Quantum jump trajectories of (un)successful error correction in the Majorana Chain.	274
5.4	QTMC simulation of the dissipative Majorana chain (dissipative quantum error correction). . . . .	275
5.5	Example for physical lattice system used for the definition of a QCA. . . . .	278
E.1	The Toric Code: Example for interaction hypergraphs and vicinity graphs. . . . .	312
E.2	Examples for graph embeddings in two dimensions. . . . .	314
E.3	Examples for constrained graph embeddings in two dimensions. . . . .	315
E.4	Examples for geometrically gapped graph embeddings. . . . .	319



# Bibliography

- [1] Diehl, S., Rico, E., Baranov, M. A. & Zoller, P. Topology by dissipation in atomic quantum wires. *Nature Physics* **7**, 971–977 (2011).  
■ <http://www.nature.com/doi/10.1038/nphys2106>.
- [2] Fradkin, E. & Shenker, S. Phase diagrams of lattice gauge theories with Higgs fields. *Physical Review D* **19**, 3682 (1979).  
■ [http://prd.aps.org/abstract/PRD/v19/i12/p3682\\_1](http://prd.aps.org/abstract/PRD/v19/i12/p3682_1).
- [3] Kitaev, A. Unpaired Majorana fermions in quantum wires. *Physics-Uspokhi* **131** (2007).  
■ <http://iopscience.iop.org/1063-7869/44/10S/S29>.
- [4] Wolf, M. Quantum channels & operations: Guided tour. *Lecture notes* (2012).  
■ <http://sunmaph6.ma.tum.de/foswiki/pub/M5/Allgemeines/MichaelWolf/QChannelLecture.pdf>.
- [5] Lindblad, G. On the generators of quantum dynamical semigroups. *Communications in Mathematical Physics* **48**, 119–130 (1976).  
■ <http://www.springerlink.com/index/10.1007/BF01608499>.
- [6] Adler, S. L. Derivation of the lindblad generator structure by use of the itô stochastic calculus. *Physics Letters A* **265**, 58 – 61 (2000).  
■ <http://www.sciencedirect.com/science/article/pii/S0375960199008476>.
- [7] Pearle, P. Simple derivation of the Lindblad equation. *European Journal of Physics* **33**, 805–822 (2012).  
■ <http://stacks.iop.org/0143-0807/33/i=4/a=805>.
- [8] Majenz, C., Albash, T., Breuer, H. & Lidar, D. Coarse-Graining Can Beat the Rotating Wave Approximation in Quantum Markovian Master Equations. *arXiv preprint arXiv:1303.6580* **012103** (2013).  
■ <http://arxiv.org/abs/1303.6580>.
- [9] Gardiner, C. & Zoller, P. *Quantum Noise: A Handbook of Markovian and Non-Markovian Quantum Stochastic Methods with Applications to Quantum Optics*. Springer Series in Synergetics (Springer, 2004).
- [10] Alicki, R. & Lendi, K. *Quantum Dynamical Semigroups and Applications*. Lecture Notes in Physics (Springer, 2007).
- [11] Poulin, D. Lieb-Robinson Bound and Locality for General Markovian Quantum Dynamics. *Physical Review Letters* **104**, 190401 (2010).  
■ <http://link.aps.org/doi/10.1103/PhysRevLett.104.190401>.
- [12] Foss-Feig, M. & Hazzard, K. Non-equilibrium dynamics of Ising models with decoherence: an exact solution. *arXiv preprint arXiv: ...* 1–8 (2012).  
■ <http://arxiv.org/abs/1209.5795>. [arXiv:1209.5795v2](https://arxiv.org/abs/1209.5795v2).
- [13] Lucas, F. & Hornberger, K. Adaptive Resummation of Markovian Quantum Dynamics. *Physical Review Letters* **110**, 240401 (2013).  
■ <http://link.aps.org/doi/10.1103/PhysRevLett.110.240401>.
- [14] Sachdev, S. *Quantum Phase Transitions* (Cambridge University Press, 2011), 2 edn.
- [15] Wen, X.-G. *Quantum Field Theory of Many-body Systems: From the Origin of Sound to an Origin of Light and Electrons (Oxford Graduate Texts)* (Oxford University Press, USA, 2007), reissue edn.
- [16] Schnyder, A., Ryu, S., Furusaki, A. & Ludwig, A. Classification of topological insulators and superconductors in three spatial dimensions. *Physical Review B* **78**, 195125 (2008).  
■ <http://link.aps.org/doi/10.1103/PhysRevB.78.195125>.
- [17] Kitaev, A., Lebedev, V. & Feigel'man, M. Periodic table for topological insulators and superconductors. *AIP Conference Proceedings* **22**, 22–30 (2009).  
■ <http://link.aip.org/link/APCPCS/v1134/i1/p22/s1&Agg=doi>.

- [18] Fidkowski, L. & Kitaev, A. Effects of interactions on the topological classification of free fermion systems. *Physical Review B* **81**, 134509 (2010).  
 ■ <http://link.aps.org/doi/10.1103/PhysRevB.81.134509>.
- [19] Chen, X., Gu, Z.-C. & Wen, X.-G. Classification of gapped symmetric phases in one-dimensional spin systems. *Physical Review B* **83**, 035107 (2011).  
 ■ <http://link.aps.org/doi/10.1103/PhysRevB.83.035107>.
- [20] Chen, X., Gu, Z.-C. & Wen, X.-G. Complete classification of one-dimensional gapped quantum phases in interacting spin systems. *Physical Review B* **84**, 235128 (2011).  
 ■ <http://link.aps.org/doi/10.1103/PhysRevB.84.235128>.
- [21] Schuch, N., Pérez-García, D. & Cirac, I. Classifying quantum phases using matrix product states and projected entangled pair states. *Physical Review B* **84**, 165139 (2011).  
 ■ <http://link.aps.org/doi/10.1103/PhysRevB.84.165139>.
- [22] Chen, X., Gu, Z.-C. & Wen, X.-G. Local unitary transformation, long-range quantum entanglement, wave function renormalization, and topological order. *Physical Review B* **82**, 155138 (2010).  
 ■ <http://link.aps.org/doi/10.1103/PhysRevB.82.155138>.
- [23] Verstraete, F., Cirac, J., Latorre, J., Rico, E. & Wolf, M. Renormalization-Group Transformations on Quantum States. *Physical Review Letters* **94**, 140601 (2005).  
 ■ <http://link.aps.org/doi/10.1103/PhysRevLett.94.140601>.
- [24] Huang, C.-y., Chen, X. & Lin, F.-I. Symmetry Protected Quantum State Renormalization. *arXiv preprint* 1–13 (2013).  
 ■ <http://arxiv.org/abs/1303.4190>.
- [25] Prosen, T. & Pižorn, I. Quantum Phase Transition in a Far-from-Equilibrium Steady State of an XY Spin Chain. *Physical Review Letters* **101**, 105701 (2008).  
 ■ <http://link.aps.org/doi/10.1103/PhysRevLett.101.105701>.
- [26] Diehl, S., Tomadin, A., Micheli, A., Fazio, R. & Zoller, P. Dynamical Phase Transitions and Instabilities in Open Atomic Many-Body Systems. *Physical Review Letters* **105**, 015702 (2010).  
 ■ <http://link.aps.org/doi/10.1103/PhysRevLett.105.015702>.
- [27] Eisert, J. & Prosen, T. Noise-driven quantum criticality. *arXiv preprint arXiv:1012.5013* 1–5 (2010).  
 ■ <http://arxiv.org/abs/1012.5013>. [arXiv:1012.5013v1](http://arxiv.org/abs/1012.5013v1).
- [28] Nagy, D., Szirmai, G. & Domokos, P. Critical exponent of a quantum-noise-driven phase transition: The open-system Dicke model. *Physical Review A* **84**, 043637 (2011).  
 ■ <http://link.aps.org/doi/10.1103/PhysRevA.84.043637>.
- [29] Tomadin, A., Diehl, S. & Zoller, P. Nonequilibrium phase diagram of a driven and dissipative many-body system. *Physical Review A* **83**, 013611 (2011).  
 ■ <http://link.aps.org/doi/10.1103/PhysRevA.83.013611>.
- [30] Ates, C., Olmos, B., Garrahan, J. P. & Lesanovsky, I. Dynamical phases and intermittency of the dissipative quantum Ising model. *Physical Review A* **85**, 043620 (2012).  
 ■ <http://link.aps.org/doi/10.1103/PhysRevA.85.043620>.
- [31] Kessler, E. M. *et al.* Dissipative phase transition in a central spin system. *Physical Review A* **86**, 012116 (2012).  
 ■ <http://link.aps.org/doi/10.1103/PhysRevA.86.012116>.
- [32] Birman, J., Nazmitdinov, R. & Yukalov, V. Effects of symmetry breaking in finite quantum systems. *Physics Reports* **526**, 1 – 91 (2013).  
 ■ <http://www.sciencedirect.com/science/article/pii/S0370157312004127>.
- [33] Shirai, T., Mori, T. & Miyashita, S. Novel symmetry-broken phase in a cavity system. *arXiv preprint* 10 (2012).  
 ■ <http://arxiv.org/abs/1204.5516>.
- [34] Banchi, L., Giorda, P. & Zanardi, P. Quantum information-geometry of dissipative quantum phase transitions. *arXiv preprint* 4 (2013).  
 ■ <http://arxiv.org/abs/1305.4527>.
- [35] Lesanovsky, I., van Horssen, M., Guță, M. & Garrahan, J. P. Characterization of Dynamical Phase Transitions in Quantum Jump Trajectories Beyond the Properties of the Stationary State. *Physical Review Letters* **110**, 150401 (2013).  
 ■ <http://link.aps.org/doi/10.1103/PhysRevLett.110.150401>.

- [36] Shor, P. Scheme for reducing decoherence in quantum computer memory. *Physical review A* **52**, 2493–2496 (1995).  
 ■ <http://pra.aps.org/abstract/PRA/v52/i4/pR2493.1>.
- [37] Nielsen, M. A. & Chuang, I. L. *Quantum Computation and Quantum Information* (Cambridge University Press, 2010), 10th anniv edn.
- [38] Paz, J. P. & Zurek, W. H. Continuous error correction. *Proceedings of the Royal Society A: Mathematical, Physical and Engineering Sciences* **454**, 355–364 (1998).  
 ■ <http://rspa.royalsocietypublishing.org/cgi/doi/10.1098/rspa.1998.0165>.
- [39] Devitt, S. J., Munro, W. J. & Nemoto, K. Quantum error correction for beginners. *Reports on Progress in Physics* **76**, 076001 (2013).  
 ■ <http://stacks.iop.org/0034-4885/76/i=7/a=076001>.
- [40] Lidar, D., Chuang, I. & Whaley, K. Decoherence-Free Subspaces for Quantum Computation. *Physical Review Letters* **81**, 2594–2597 (1998).  
 ■ <http://link.aps.org/doi/10.1103/PhysRevLett.81.2594>.
- [41] Beige, a., Braun, D., Tregenna, B. & Knight, P. Quantum computing using dissipation to remain in a decoherence-free subspace. *Physical review letters* **85**, 1762–5 (2000).  
 ■ <http://www.ncbi.nlm.nih.gov/pubmed/10970608>.
- [42] Bacon, D. Operator quantum error-correcting subsystems for self-correcting quantum memories. *Physical Review A* **73**, 012340 (2006).  
 ■ <http://link.aps.org/doi/10.1103/PhysRevA.73.012340>.
- [43] Poulin, D. Stabilizer Formalism for Operator Quantum Error Correction. *Physical Review Letters* **95**, 230504 (2005).  
 ■ <http://link.aps.org/doi/10.1103/PhysRevLett.95.230504>.
- [44] Bravyi, S., Poulin, D. & Terhal, B. Tradeoffs for Reliable Quantum Information Storage in 2D Systems. *Physical Review Letters* **104**, 050503 (2010).  
 ■ <http://link.aps.org/doi/10.1103/PhysRevLett.104.050503>.
- [45] Alicki, R. Quantum Memory as a Perpetuum Mobile? Stability vs. Reversibility of Information Processing. *Open Systems & Information Dynamics* **19**, 1250016 (2012).  
 ■ <http://www.worldscientific.com/doi/abs/10.1142/S1230161212500163>.
- [46] Terhal, B. The fragility of quantum information? *Theory and Practice of Natural Computing* 1–10 (2012).  
 ■ <http://link.springer.com/chapter/10.1007/978-3-642-33860-1.5>. arXiv:1305.4004v2.
- [47] van Dam, W. & Nguyen, H. D. Minimum Energy Surface Required by Quantum Memory Devices. *Physical Review Letters* **110**, 250502 (2013).  
 ■ <http://link.aps.org/doi/10.1103/PhysRevLett.110.250502>.
- [48] Bravyi, S. & Terhal, B. A no-go theorem for a two-dimensional self-correcting quantum memory based on stabilizer codes. *New Journal of Physics* **043029** (2009).  
 ■ <http://iopscience.iop.org/1367-2630/11/4/043029>.
- [49] Alicki, R. & Horodecki, M. On thermal stability of topological qubit in Kitaev's 4D model. *Open Systems & ...* (2010).  
 ■ <http://www.worldscientific.com/doi/abs/10.1142/S1230161210000023>. arXiv:0811.0033v1.
- [50] Haah, J. Local stabilizer codes in three dimensions without string logical operators. *Physical Review A* **83**, 042330 (2011).  
 ■ <http://link.aps.org/doi/10.1103/PhysRevA.83.042330>.
- [51] Dennis, E., Kitaev, A., Landahl, A. & Preskill, J. Topological quantum memory. *Journal of Mathematical Physics* **43**, 4452 (2002).  
 ■ <http://link.aip.org/link/JMAPAQ/v43/i9/p4452/s1&Agg=doi>.
- [52] Bravyi, S. & Koenig, R. Disorder-assisted error correction in Majorana chains. *arXiv preprint arXiv:1108.3845* (2011).  
 ■ <http://arxiv.org/abs/1108.3845>. arXiv:1108.3845v1.
- [53] Bravyi, S., Terhal, B. B. M. & Leemhuis, B. Majorana fermion codes. *New Journal of Physics* **12**, 083039 (2010).  
 ■ <http://stacks.iop.org/1367-2630/12/i=8/a=083039>. arXiv:1004.3791v2.
- [54] Yoshida, B. Feasibility of self-correcting quantum memory and thermal stability of topological order. *Annals of Physics* **326**, 2566–2633 (2011).  
 ■ <http://linkinghub.elsevier.com/retrieve/pii/S0003491611001023>.

- [55] Pastawski, F., Clemente, L. & Cirac, J. I. Quantum memories based on engineered dissipation. *Physical Review A* **83**, 012304 (2011).  
 ■ <http://link.aps.org/doi/10.1103/PhysRevA.83.012304>.
- [56] Ahn, C., Doherty, A. & Landahl, A. Continuous quantum error correction via quantum feedback control. *Physical Review A* **65**, 042301 (2002).  
 ■ <http://link.aps.org/doi/10.1103/PhysRevA.65.042301>.
- [57] Wootton, J. R. A witness for topological order and stable quantum memories in Abelian anyonic systems. *Journal of Physics A: Mathematical and Theoretical* **45**, 395301 (2012).  
 ■ <http://stacks.iop.org/1751-8121/45/i=39/a=395301>.
- [58] Kim, I. H. Long-range entanglement is necessary for a topological storage of quantum information. *arXiv preprint* 1–6 (2013). [arXiv:1304.3925v1](https://arxiv.org/abs/1304.3925v1).
- [59] Bravyi, S. & König, R. Classification of Topologically Protected Gates for Local Stabilizer Codes. *Physical Review Letters* **110**, 170503 (2013).  
 ■ <http://link.aps.org/doi/10.1103/PhysRevLett.110.170503>.
- [60] Michnicki, K. 3-d quantum stabilizer codes with a power law energy barrier. *arXiv preprint arXiv:1208.3496* 1–19 (2012).  
 ■ <http://arxiv.org/abs/1208.3496>. [arXiv:1208.3496v1](https://arxiv.org/abs/1208.3496v1).
- [61] Duclos-Cianci, G. & Poulin, D. Fast Decoders for Topological Quantum Codes. *Physical Review Letters* **104**, 050504 (2010).  
 ■ <http://link.aps.org/doi/10.1103/PhysRevLett.104.050504>.
- [62] Duclos-Cianci, G. & Poulin, D. Kitaev's  $Z_2$ -code threshold estimates. *Physical Review A* **87**, 062338 (2013).  
 ■ <http://link.aps.org/doi/10.1103/PhysRevA.87.062338>.
- [63] Nickerson, N. H., Li, Y. & Benjamin, S. C. Topological quantum computing with a very noisy network and local error rates approaching one percent. *Nature Communications* **4**, 1756 (2013).  
 ■ <http://www.nature.com/doi/10.1038/ncomms2773>. [arXiv:1211.2217v3](https://arxiv.org/abs/1211.2217v3).
- [64] Kim, I. Exactly solvable 3D quantum model with finite temperature topological order. *arXiv preprint arXiv:1012.0859* 1–6 (2010).  
 ■ <http://arxiv.org/abs/1012.0859>. [arXiv:1012.0859v3](https://arxiv.org/abs/1012.0859v3).
- [65] Becker, D., Tanamoto, T. & Hutter, A. Dynamic Generation of Topologically Protected Self-Correcting Quantum Memory. *arXiv preprint arXiv: ...* **042340**, 1–10 (2013).  
 ■ <http://arxiv.org/abs/1302.3998>.
- [66] Hamma, A., Castelnovo, C. & Chamon, C. Toric-boson model: Toward a topological quantum memory at finite temperature. *Physical Review B* **79**, 245122 (2009).  
 ■ <http://link.aps.org/doi/10.1103/PhysRevB.79.245122>.
- [67] Wootton, J. R. Novel Topological Phases and Self-Correcting Memories in Interacting Anyon Systems. *arXiv preprint* 5 (2013).  
 ■ <http://arxiv.org/abs/1305.1808>. [1305.1808](https://arxiv.org/abs/1305.1808).
- [68] Bombin, H., Chhajlany, R. W., Horodecki, M. & Martin-Delgado, M. a. Self-correcting quantum computers. *New Journal of Physics* **15**, 055023 (2013).  
 ■ <http://stacks.iop.org/1367-2630/15/i=5/a=055023>.
- [69] Kongschelle, F. m. c. & Hassler, F. Effects of nonequilibrium noise on a quantum memory encoded in majorana zero modes. *Phys. Rev. B* **88**, 075431 (2013).  
 ■ <http://link.aps.org/doi/10.1103/PhysRevB.88.075431>.
- [70] Kitaev, A. Fault-tolerant quantum computation by anyons. *Annals of Physics* **303**, 2–30 (2003).  
 ■ <http://www.sciencedirect.com/science/article/pii/S0003491602000180>.
- [71] Nussinov, Z. & Ortiz, G. Autocorrelations and thermal fragility of anyonic loops in topologically quantum ordered systems. *Physical Review B* **77**, 064302 (2008).  
 ■ <http://link.aps.org/doi/10.1103/PhysRevB.77.064302>.
- [72] Nussinov, Z. & Ortiz, G. A symmetry principle for topological quantum order. *Annals of Physics* **324**, 977 – 1057 (2009).  
 ■ <http://www.sciencedirect.com/science/article/pii/S0003491608001711>.
- [73] Castelnovo, C. & Chamon, C. Topological order in a three-dimensional toric code at finite temperature. *Physical Review B* **78**, 155120 (2008).  
 ■ <http://link.aps.org/doi/10.1103/PhysRevB.78.155120>.

- [74] Tupitsyn, I. S., Kitaev, a., Prokof'ev, N. V. & Stamp, P. C. E. Topological multicritical point in the phase diagram of the toric code model and three-dimensional lattice gauge Higgs model. *Physical Review B* **82**, 085114 (2010).  
 ■ <http://link.aps.org/doi/10.1103/PhysRevB.82.085114>.
- [75] Wilczek, F. Majorana returns. *Nature Physics* **5**, 614–618 (2009).  
 ■ <http://www.nature.com/doi/10.1038/nphys1380>.
- [76] Budich, J. C. & Ardonne, E. Equivalent topological invariants for one-dimensional majorana wires in symmetry class *d*. *Phys. Rev. B* **88**, 075419 (2013).  
 ■ <http://link.aps.org/doi/10.1103/PhysRevB.88.075419>.
- [77] Kitaev, A. & Laumann, C. Topological phases and quantum computation. *arXiv preprint arXiv:0904.2771* (2009).  
 ■ <http://arxiv.org/abs/0904.2771>. arXiv:0904.2771v1.
- [78] Wen, X.-G. Quantum order from string-net condensations and the origin of light and massless fermions. *Physical Review D* **68**, 065003 (2003).  
 ■ <http://link.aps.org/doi/10.1103/PhysRevD.68.065003>.
- [79] Levin, M. & Wen, X.-G. Quantum ether: Photons and electrons from a rotor model. *Physical Review B* **73**, 035122 (2006).  
 ■ <http://link.aps.org/doi/10.1103/PhysRevB.73.035122>.
- [80] Mourik, V. *et al.* Signatures of Majorana fermions in hybrid superconductor-semiconductor nanowire devices. *Science (New York, N.Y.)* **336**, 1003–7 (2012).  
 ■ <http://www.ncbi.nlm.nih.gov/pubmed/22499805>.
- [81] Wick, G., Wightman, A. & Wigner, E. The Intrinsic Parity of Elementary Particles. *Physical Review* **88**, 101–105 (1952).  
 ■ <http://link.aps.org/doi/10.1103/PhysRev.88.101>.
- [82] Wightman, A. Superselection rules; old and new. *Il Nuovo Cimento B (1971-1996)* **110**, 751–769 (1995).  
 ■ <http://www.springerlink.com/index/N24439H86601X418.pdf>.
- [83] Aharonov, Y. & Susskind, L. Charge superselection rule. *Phys. Rev.* **155**, 1428–1431 (1967).  
 ■ <http://link.aps.org/doi/10.1103/PhysRev.155.1428>.
- [84] Bartlett, S. & Wiseman, H. Entanglement Constrained by Superselection Rules. *Physical Review Letters* **91**, 097903 (2003).  
 ■ <http://link.aps.org/doi/10.1103/PhysRevLett.91.097903>.
- [85] Kitaev, A., Mayers, D. & Preskill, J. Superselection rules and quantum protocols. *Physical Review A* **69**, 052326 (2004).  
 ■ <http://link.aps.org/doi/10.1103/PhysRevA.69.052326>.
- [86] Tanimura, S. Superselection Rules from Measurement Theory. *arXiv preprint arXiv:1112.5701* 1–19 (2011).  
 ■ <http://arxiv.org/abs/1112.5701>. arXiv:1112.5701v1.
- [87] Bartlett, S., Rudolph, T. & Spekkens, R. Reference frames, superselection rules, and quantum information. *Reviews of Modern Physics* **79**, 555–609 (2007).  
 ■ [http://rmp.aps.org/abstract/RMP/v79/i2/p555\\_1](http://rmp.aps.org/abstract/RMP/v79/i2/p555_1).
- [88] Alicea, J. *et al.* Non-Abelian statistics and topological quantum information processing in 1D wire networks. *Nature Physics* **7**, 27–30 (2011).  
 ■ <http://dx.doi.org/10.1038/nphys1915>. arXiv:1006.4395v2.
- [89] Burnell, F. J., Shnirman, A. & Oreg, Y. Measuring fermion parity correlations and relaxation rates in 1D topological superconducting wires. *arXiv preprint* 1–12 (2013).  
 ■ <http://arxiv.org/abs/1306.6622>. 1306.6622.
- [90] Alba, E., Pachos, J., Lahtinen, V. & Garcia-Ripoll, J. Seeing Majorana fermions in time-of-flight images of staggered spinless fermions coupled by s-wave pairing. *Bulletin of the American ...* 1–13 (2013).  
 ■ <http://meeting.aps.org/Meeting/MAR13/Event/183720>. arXiv:1209.5115v2.
- [91] Fregoso, B. M., Lobos, A. M. & Sarma, S. D. Electrical detection of topological phase transitions in disordered Majorana nanowires. *arXiv preprint* 5 (2013).  
 ■ <http://arxiv.org/abs/1307.3505>. 1307.3505.
- [92] Mezzacapo, a., Casanova, J., Lamata, L. & Solano, E. Topological qubits with Majorana fermions in trapped ions. *New Journal of Physics* **15**, 033005 (2013).  
 ■ <http://stacks.iop.org/1367-2630/15/i=3/a=033005>.

- [93] Rodrigo, J. G., Crespo, V., Suderow, H., Vieira, S. & Guinea, F. Topological superconductivity in metallic nanowires fabricated with a scanning tunneling microscope. *New Journal of Physics* **15**, 055020 (2013).  
 ■ <http://stacks.iop.org/1367-2630/15/i=5/a=055020>.
- [94] Kogut, J. An introduction to lattice gauge theory and spin systems. *Reviews of Modern Physics* (1979).  
 ■ <http://rmp.aps.org/abstract/RMP/v51/i4/p659-1>.
- [95] Wegner, F. J. Duality in Generalized Ising Models and Phase Transitions without Local Order Parameters. *Journal of Mathematical Physics* **12**, 2259 (1971).  
 ■ <http://link.aip.org/link/?JMP/12/2259/1&Agg=doi>.
- [96] Fradkin, E. & Susskind, L. Order and disorder in gauge systems and magnets. *Physical Review D* **17**, 2637 (1978).  
 ■ <http://adsabs.harvard.edu/abs/1978PhRvD..17.2637F>.
- [97] Elitzur, S. Impossibility of spontaneously breaking local symmetries. *Phys. Rev., D, v. 12, no. 12, pp. 3978-3982* (1975).  
 ■ [http://www.osti.gov/energycitations/product.biblio.jsp?osti\\_id=4037412](http://www.osti.gov/energycitations/product.biblio.jsp?osti_id=4037412).
- [98] Caudy, W. & Greensite, J. Ambiguity of spontaneously broken gauge symmetry. *Physical Review D* **78**, 025018 (2008).  
 ■ <http://link.aps.org/doi/10.1103/PhysRevD.78.025018>.
- [99] Buchmüller, W., Fodor, Z. & Hebecker, A. Gauge invariant treatment of the electroweak phase transition. *Physics Letters B* **331**, 131–136 (1994).  
 ■ <http://www.sciencedirect.com/science/article/pii/0370269394909539>.
- [100] Friederich, S. Gauge symmetry breaking in gauge theories—in search of clarification. *European Journal for Philosophy of Science* 1–30 (2011).  
 ■ <http://link.springer.com/article/10.1007/s13194-012-0061-y>. arXiv:1107.4664v2.
- [101] Hsieh, T. H. From d-dimensional Quantum to d + 1-dimensional Classical Systems. *Public notes* 1–4 (2012).
- [102] Drouffe, J. & Zuber, J. Strong Coupling and Mean Field Methods in Lattice Gauge Theories. *Physics Reports* (1983).  
 ■ <http://adsabs.harvard.edu/abs/1983PhR...102....1D>.
- [103] Alvarez, J. & Socolovsky, H. Mean-field approximation for ZN lattice gauge theory coupled to matter. *Il Nuovo Cimento A (1971-1996)* **93**, 31–38 (1986).  
 ■ <http://www.springerlink.com/index/j4563863k6p36177.pdf>.
- [104] Dagotto, E. An improved Mean-Field Calculation for the Z(2) Higgs Model. *Physics Letters B* **136**, 3–6 (1984).  
 ■ <http://www.sciencedirect.com/science/article/pii/0370269384920562>.
- [105] Brezin, E. & Drouffe, J. Continuum limit of AZ 2 lattice gauge theory. *Nuclear Physics B* 93–106 (1982).  
 ■ <http://www.sciencedirect.com/science/article/pii/0550321382900608>.
- [106] Jongeward, G., Stack, J. & Jayaprakash, C. Monte Carlo calculations on Z2 gauge-Higgs theories. *Physical Review D* **21**, 3360 (1980).  
 ■ <http://prd.aps.org/abstract/PRD/v21/i12/p3360-1>.
- [107] Genovese, L., Gliozzi, F., Rago, A. & Torrero, C. The phase diagram of the three-dimensional Z2 gauge Higgs system at zero and finite temperature. *Nuclear Physics B - Proceedings Supplements* **119**, 894–899 (2003).  
 ■ <http://linkinghub.elsevier.com/retrieve/pii/S0920563203017134>.
- [108] Vidal, J., Dusuel, S. & Schmidt, K. Low-energy effective theory of the toric code model in a parallel magnetic field. *Physical Review B* **79**, 033109 (2009).  
 ■ <http://link.aps.org/doi/10.1103/PhysRevB.79.033109>.
- [109] Zohar, E., Cirac, J. I. & Reznik, B. Quantum simulations of gauge theories with ultracold atoms: Local gauge invariance from angular-momentum conservation. *Phys. Rev. A* **88**, 023617 (2013).  
 ■ <http://link.aps.org/doi/10.1103/PhysRevA.88.023617>.
- [110] Yokomizo, N. & Teotonio-Sobrinho, P. GL (2, Bbb R) dualities in generalised Z (2) gauge theories and Ising models. *Journal of High Energy ...* 1–29 (2007).  
 ■ <http://iopscience.iop.org/1126-6708/2007/03/081.0701075v1>.
- [111] Chew, W. C. Electromagnetic theory on a lattice. *Journal of Applied Physics* **75**, 4843 (1994).  
 ■ <http://link.aip.org/link/JAPIAU/v75/i10/p4843/s1&Agg=doi>.
- [112] Buca, B. & Prosen, T. A note on symmetry reductions of the Lindblad equation: transport in constrained open spin chains. *New Journal of Physics* (2012).  
 ■ <http://iopscience.iop.org/1367-2630/14/7/073007>. arXiv:1203.0943v1.



- [113] Murnaghan, F. On a convenient system of parameters for the unitary group. *Proceedings of the National Academy of Sciences of ...* **38**, 127–129 (1952).  
 ■ <http://www.jstor.org/stable/10.2307/88614>.
- [114] Rieger, H. & Uimin, G. The one-dimensional ANNNI model in a transverse field: analytic and numerical study of effective Hamiltonians. *Zeitschrift für Physik B Condensed Matter* **101**, 597–611 (1996).  
 ■ <http://www.springerlink.com/openurl.asp?genre=article&id=doi:10.1007/s002570050252>.
- [115] Plenio, M. & Virmani, S. An introduction to entanglement measures. *arXiv preprint quant-ph/0504163* (2005).  
 ■ <http://arxiv.org/abs/quant-ph/0504163>. 0504163v3.
- [116] Amico, L., Osterloh, A. & Vedral, V. Entanglement in many-body systems. *Reviews of Modern Physics* **80**, 517–576 (2008).  
 ■ <http://link.aps.org/doi/10.1103/RevModPhys.80.517>.
- [117] Hill, S. & Wootters, W. Entanglement of a Pair of Quantum Bits. *Physical Review Letters* **78**, 5022–5025 (1997).  
 ■ <http://link.aps.org/doi/10.1103/PhysRevLett.78.5022>.
- [118] Dalibard, J., Castin, Y. & Mølmer, K. Wave-Function Approach to Dissipative Process in Quantum Optics. *Physical review letters* **68**, 580–583 (1992).  
 ■ <http://prl.aps.org/abstract/PRL/v68/i5/p580-1>.
- [119] Dum, R., Zoller, P. & Ritsch, H. Monte Carlo simulation of the atomic master equation for spontaneous emission. *Physical Review A* **45**, 4879–4887 (1992).  
 ■ <http://pra.aps.org/abstract/PRA/v45/i7/p4879-1>.
- [120] Plenio, M. B. & Knight, P. L. The quantum-jump approach to dissipative dynamics in quantum optics. *Reviews of Modern Physics* **70**, 101–144 (1998).  
 ■ <http://link.aps.org/doi/10.1103/RevModPhys.70.101>.
- [121] Bose, a. K. Decomposition of the finite-dimensional fermion algebra into irreducible spaces. *Journal of Mathematical Physics* **23**, 2229 (1982).  
 ■ <http://link.aip.org/link/?JMP/23/2229/1&Agg=doi>.
- [122] Bardyn, C., Baranov, M. & Kraus, C. Topology by dissipation. *arXiv preprint arXiv: ...* 1–61 (2013).  
 ■ <http://arxiv.org/abs/1302.5135>. arXiv:1302.5135v1.
- [123] Temperley, H. & Lieb, E. Relations between the ‘percolation’ and ‘colouring’ problem and other graph-theoretical problems associated with regular planar lattices: some exact results for the ‘percolation’ problem. *... of the Royal ...* (1971).  
 ■ <http://rspa.royalsocietypublishing.org/content/322/1549/251.short>.
- [124] Abramsky, S. Temperley-Lieb Algebra: From Knot Theory to Logic and Computation via Quantum Mechanics **5**, 293–508 (1984).
- [125] Korff, C. PT symmetry of the non-Hermitian XX spin-chain: non-local bulk interaction from complex boundary fields. *Journal of Physics A: Mathematical and Theoretical* (2008).  
 ■ <http://iopscience.iop.org/1751-8121/41/29/295206>. arXiv:0803.4500v1.
- [126] Aufgebauer, B. & Klümper, A. Quantum spin chains of Temperley–Lieb type: periodic boundary conditions, spectral multiplicities and finite temperature. *Journal of Statistical Mechanics: Theory and Experiment* **2010**, P05018 (2010).
- [127] Westbury, B. W. The representation theory of the Temperley-Lieb algebras. *Science (New York, N.Y.)* **52**, 155 (1920).  
 ■ <http://www.ncbi.nlm.nih.gov/pubmed/17788632>.
- [128] Ridout, D. & Saint-Aubin, Y. Standard Modules, Induction and the Structure of the Temperley-Lieb Algebra (2012).  
 ■ <http://people.physics.anu.edu.au/~drt105/papers/RSA1204.4505.pdf>. arXiv:1204.4505v2.
- [129] Morin-duchesne, A. & Saint-aubin, Y. A homomorphism between link and XXZ modules over the periodic Temperley-Lieb algebra (2013). arXiv:1203.4996v3.
- [130] Kraus, B. *et al.* Preparation of entangled states by quantum Markov processes. *Physical Review A* **78**, 042307 (2008).  
 ■ <http://link.aps.org/doi/10.1103/PhysRevA.78.042307>.
- [131] Karbach, M. & Müller, G. Introduction to the Bethe ansatz I **8** (1998).  
 ■ <http://arxiv.org/abs/cond-mat/9809162>. 9809162.
- [132] Hastings, M. B. & Koma, T. Spectral Gap and Exponential Decay of Correlations. *Communications in Mathematical Physics* **265**, 781–804 (2006).  
 ■ <http://link.springer.com/10.1007/s00220-006-0030-4>.

- [133] Hastings, M. Locality in Quantum and Markov Dynamics on Lattices and Networks. *Physical Review Letters* **93**, 140402 (2004).  
 ■ <http://link.aps.org/doi/10.1103/PhysRevLett.93.140402>.
- [134] Bravyi, S., Hastings, M. & Verstraete, F. Lieb-Robinson Bounds and the Generation of Correlations and Topological Quantum Order. *Physical Review Letters* **97**, 050401 (2006).  
 ■ <http://link.aps.org/doi/10.1103/PhysRevLett.97.050401>.
- [135] Turner, A. M., Pollmann, F. & Berg, E. Topological phases of one-dimensional fermions: An entanglement point of view. *Physical Review B* **83**, 075102 (2011).  
 ■ <http://link.aps.org/doi/10.1103/PhysRevB.83.075102>.
- [136] Pollmann, F., Turner, A. M., Berg, E. & Oshikawa, M. Entanglement spectrum of a topological phase in one dimension. *Physical Review B* **81**, 064439 (2010).  
 ■ <http://link.aps.org/doi/10.1103/PhysRevB.81.064439>.
- [137] Li, H. & Haldane, F. Entanglement Spectrum as a Generalization of Entanglement Entropy: Identification of Topological Order in Non-Abelian Fractional Quantum Hall Effect States. *Physical Review Letters* **101**, 010504 (2008).  
 ■ <http://link.aps.org/doi/10.1103/PhysRevLett.101.010504>.
- [138] Landauer, R. Irreversibility and Heat Generation in the Computing Process. *IBM Journal of Research and Development* **5**, 183–191 (1961).  
 ■ <http://ieeexplore.ieee.org/lpdocs/epic03/wrapper.htm?arnumber=5392446>.
- [139] Nishio, H. & Kobuchi, Y. Fault tolerant cellular spaces. *Journal of Computer and System Sciences* **11**, 150–170 (1975).  
 ■ <http://linkinghub.elsevier.com/retrieve/pii/S0022000075800651>.
- [140] Toom, A. Stable and attractive trajectories in multicomponent systems. *Multicomponent Systems* (1980).
- [141] Gács, P. Reliable computation with cellular automata. *Journal of Computer and System Sciences* **78**, 15–78 (1986).  
 ■ <http://www.sciencedirect.com/science/article/pii/0022000086900024>.
- [142] Gács, P. & Reif, J. A simple three-dimensional real-time reliable cellular array. *Journal of Computer and System Sciences* **36**, 125–147 (1988).  
 ■ <http://linkinghub.elsevier.com/retrieve/pii/0022000088900244>.
- [143] Chowdhury, D. & Basu, S. Design of CAECC-Cellular automata based error correcting code. ... *IEEE Transactions on* **43** (1994).  
 ■ <http://ieeexplore.ieee.org/xpls/abs.all.jsp?arnumber=286310>.
- [144] Pippenger, N. Symmetry in self-correcting cellular automata. *Journal of Computer and System Sciences* **49**, 83–95 (1994).  
 ■ <http://linkinghub.elsevier.com/retrieve/pii/S002200000580087X>.
- [145] Gács, P. Reliable cellular automata with self-organization. *Journal of Statistical Physics* **103** (2001).  
 ■ <http://link.springer.com/article/10.1023/A:1004823720305>.
- [146] Gray, L. A Reader's Guide to Gacs's "Positive Rates" Paper. *Journal of Statistical Physics* **103**, 1–44 (2001).  
 ■ <http://link.springer.com/article/10.1023/A:1004824203467>.
- [147] McCann, M. & Pippenger, N. Fault tolerance in cellular automata at high fault rates. *Journal of Computer and System Sciences* **74**, 910–918 (2008).  
 ■ <http://linkinghub.elsevier.com/retrieve/pii/S0022000008000172>.
- [148] McCann, M. & Pippenger, N. Fault tolerance in cellular automata at low fault rates. *Journal of Computer and System Sciences* **1**, 1–18 (2013).  
 ■ <http://linkinghub.elsevier.com/retrieve/pii/S0022000013000482>.
- [149] Richter, S. & Werner, R. Ergodicity of quantum cellular automata. *Journal of statistical physics* **82**, 963–998 (1996).  
 ■ <http://link.springer.com/article/10.1007/BF02179798>.
- [150] Brennen, G. & Williams, J. Entanglement dynamics in one-dimensional quantum cellular automata. *Physical Review A* **68**, 042311 (2003).  
 ■ <http://link.aps.org/doi/10.1103/PhysRevA.68.042311>.
- [151] Schumacher, B. & Werner, R. Reversible quantum cellular automata. *arXiv preprint quant-ph/0405174* (2004).  
 ■ <http://arxiv.org/abs/quant-ph/0405174>. 0405174v1.
- [152] Harrington, J. Analysis of quantum error-correcting codes: symplectic lattice codes and toric codes. *PhD Thesis 2004* (2004).  
 ■ <http://citeseerx.ist.psu.edu/viewdoc/download?doi=10.1.1.83.6167&rep=rep1&type=pdf>.

- [153] Wiesner, K. Quantum Cellular Automata. *arXiv preprint* (2008).  
 ■ <http://arxiv.org/abs/0808.0679>. 0808.0679.
- [154] Arrighi, P. & Grattage, J. Intrinsically universal n-dimensional quantum cellular automata. *Journal of Computer and System Sciences* **78**, 1883–1898 (2012).  
 ■ <http://linkinghub.elsevier.com/retrieve/pii/S002200001100153X>.
- [155] Hastings, M. B. Classifying Quantum Phases With The Torus Trick. *arXiv preprint* **7**, 23 (2013).  
 ■ <http://arxiv.org/abs/1305.6625>. 1305.6625.
- [156] Lloyd, S. Universal quantum simulators. *SCIENCE-NEW YORK THEN ...* (1996).  
 ■ <http://research.physics.illinois.edu/demarco/lloyd96paper.pdf>.
- [157] Weimer, H., Müller, M., Lesanovsky, I., Zoller, P. & Büchler, H. P. A Rydberg quantum simulator. *Nature Physics* **6**, 382–388 (2010). 0907.1657.
- [158] Koochakie, M. M. R., Alipour, S. & Reza khani, A. T. Lieb-Robinson Bound and Adiabatic Evolution 1–5 (2013).  
 ■ <http://arxiv.org/abs/1307.3726>. 1307.3726.
- [159] Descamps, B. Asymptotically decreasing lieb-robinson velocity for a class of dissipative quantum dynamics. *Journal of Mathematical Physics* **54**, 092202 (2013).  
 ■ <http://link.aip.org/link/?JMP/54/092202/1>.
- [160] Kliesch, M., Gogolin, C. & Eisert, J. Lieb-Robinson bounds and the simulation of time evolution of local observables in lattice systems 14 (2013).  
 ■ <http://arxiv.org/abs/1306.0716>. 1306.0716.
- [161] Cubitt, T. S. *et al.* Stability of local quantum dissipative systems 1–39 (2013).  
 ■ <http://arxiv.org/abs/1303.4744>. arXiv:1303.4744v1.
- [162] Barthel, T. & Kliesch, M. Quasilocalilty and Efficient Simulation of Markovian Quantum Dynamics. *Physical Review Letters* **108**, 230504 (2012).  
 ■ <http://link.aps.org/doi/10.1103/PhysRevLett.108.230504>.
- [163] Diestel, R. *Graph Theory (Graduate Texts in Mathematics)* (Springer, 2010), 4th ed. 2010. corr. 3rd printing 2012 edn.
- [164] Raussendorf, R. & Briegel, H. Computational model underlying the one-way quantum computer. *Quantum Information & Computation* (2002).  
 ■ <http://dl.acm.org/citation.cfm?id=2011495>. 0108067v2.
- [165] Raussendorf, R., Browne, D. & Briegel, H. Measurement-based quantum computation on cluster states. *Physical Review A* 1–32 (2003).  
 ■ <http://pra.aps.org/abstract/PRA/v68/i2/e022312>.



# Corrigenda

Please let me know about errors; both contentual and orthographical criticism is appreciated:

 [nicolai@itp3.uni-stuttgart.de](mailto:nicolai@itp3.uni-stuttgart.de).